

NASA CR-143642

22296-6001-RU-02

1 OCTOBER 1974

FINAL  
REPORT

3

DESIGN/COST  
TRADEOFF STUDIES  
APPENDIX A.  
SUPPORTING ANALYSES  
AND TRADEOFFS

BOOK 1

(NASA-CR-143642) DESIGN/COST TRADEOFF  
STUDIES. APPENDIX A. SUPPORTING ANALYSES  
AND TRADEOFFS, BOOK 1. EARTH OBSERVATORY  
SATELLITE SYSTEM DEFINITION STUDY (EOS)

N75-15688

Final Report (TRW Systems Group) 488 p HC G3/18 09225

Unclass

EARTH OBSERVATORY SATELLITE  
SYSTEM DEFINITION STUDY (EOS)

PREPARED FOR

NATIONAL AERONAUTICS AND SPACE ADMINISTRATION  
GODDARD SPACE FLIGHT CENTER

IN RESPONSE TO  
CONTRACT NAS5-20519



**TRW**  
SYSTEMS GROUP

ONE SPACE PARK • REDONDO BEACH, CALIFORNIA 90278

22296-6001-RU-02

1 OCTOBER 1974

**FINAL  
REPORT**

**3**

**DESIGN/COST  
TRADEOFF STUDIES**

**APPENDIX A.  
SUPPORTING ANALYSES  
AND TRADEOFFS**

**BOOK 1**

**EARTH OBSERVATORY SATELLITE  
SYSTEM DEFINITION STUDY (EOS)**

PREPARED FOR

**NATIONAL AERONAUTICS AND SPACE ADMINISTRATION  
GODDARD SPACE FLIGHT CENTER**

IN RESPONSE TO  
CONTRACT NAS5-20519

**TRW**  
SYSTEMS GROUP

ONE SPACE PARK • REDONDO BEACH, CALIFORNIA 90278

# CONTENTS

	Page
1. MISSION ANALYSIS	1-1
1.1 Mission Definition	1-1
1.1.1 Candidate Missions	1-1
1.1.2 Study Methodology	1-1
1.1.3 Study Results	1-2
1.1.4 Later Payloads	1-11
1.1.5 Future Mission Analysis Data	1-11
2. ORBIT ANALYSIS	2-1
2.1 Orbit Selection and Characterization	2-1
2.1.1 Problem Discussion	2-1
2.1.2 Analysis	2-4
2.1.3 Conclusions	2-12
2.2 Orbit Transfer Requirements	2-20
2.3 Multiple Spacecraft Servicing	2-23
2.3.1 Analysis	2-23
2.3.2 Conclusions	2-27
3. SHUTTLE INTERFACES	3-1
3.1 MEMS Applicability	3-1
3.1.1 Discussion	3-1
3.1.2 Assumptions	3-4
3.1.3 Areas of Concern	3-4
3.1.4 Tradeoff and Decisions	3-6
3.1.5 Description of Conceptual End Effector	3-6
3.2 Shuttle Interfaces	3-13
4. PAYLOADS	4-1
4.1 TM Status and Interface Review	4-1
4.1.1 Development Status	4-1
4.1.2 Characteristics Comparison	4-2
4.1.3 Data Buffering Requirements	4-5
4.2 High-Resolution Pointable Imager	4-9
4.2.1 HRPI Status and Interface Review	4-9
4.2.2 HRPI Design Improvements	4-18
4.2.3 HRPI Offset Pointing Options	4-20
4.3 Data Collection System	4-28
4.3.1 DCS Configuration	4-30
4.3.2 Link Analysis	4-36
4.3.3 Concluding Remarks	4-44
4.3.4 Platform Capacity of the Data Collection Subsystem	4-48

## CONTENTS

	Page
4. 4    Synthetic Aperture Radar	4-54
4. 4. 1    Comparison of Westinghouse and Goodyear Designs	4-54
4. 4. 2    Extended X- and L-Band Designs	4-59
4. 4. 3    Spacecraft Attitude Requirements for SAR	4-59
4. 4. 4    Electromagnetic Interference	4-61
4. 4. 5    Cost	4-61
4. 5    Passive Multichannel Microwave Radiometer	4-63
4. 5. 1    PMMR Conceptual Design — Phased Array Antenna	4-63
4. 5. 2    Comparison of Conceptual Designs	4-65
4. 5. 3    Compatibility with EOS Modularity Concept	4-68
4. 5. 4    Cost	4-69
4. 6    Wideband Communications and Data Handling	4-70
4. 6. 1    EOS-A Data Handling	4-70
4. 6. 2    Wideband Tape Recorder	4-79
4. 6. 3    Wideband Data Handling Design	4-83
4. 6. 4    High-Speed Buffer	4-98
4. 6. 5    Wideband Communication System	4-130
5.    SPACECRAFT STUDIES	5-1
5. 1    Communications and Data Handling	5-1
5. 1. 1    Communication System Definition	5-1
5. 1. 2    Polarization Diversity Systems for EOS	5-36
5. 1. 3    Communication Equipment Design	5-127
5. 1. 4    Computer Tradeoffs	5-159
5. 1. 5    Downlink Telemetry Carrier Phase Modulation Index Optimization	5-165
5. 1. 6    Command and Telemetry Autonomy	5-171
5. 1. 7    Data Handling Subsystem	5-174



## 1. MISSION ANALYSIS

### 1.1 MISSION DEFINITION

#### 1.1.1 Candidate Missions

A complete listing of EOS candidate missions has been developed (Figure 1-1) and will be used as a baseline for describing EOS payloads through 1991. The rationale used for development of this listing has been documented in EOS-52, Subject: Mission Model, dated 9 May 1974.

Missions have been identified in terms of first-generation payloads (A, B, C), second-generation payloads (A', B', C'), and third-generation payloads (A'', B'', C''). The following letter assignments have been used:

- EOS-A/A'/A'' are the earth resources missions.
- EOS-B/B'/B'' are the environmental-pollution missions.
- EOS-C/C'/C'' are the oceanographic/meteorological (O/M) missions.
- SEOS-A/B/C/D are missions in geostationary orbit. These missions are dedicated to all earth observations targets: earth resources, pollution, oceanography and meteorology. It should be noted that the SEOS mission will involve multiple spacecraft (e.g., two) with similar payloads. Thus, SEOS-A and SEOS-B will carry first-generation payloads, and SEOS-C and SEOS-D will carry second-generation payloads.
- SEASAT-A and -B are the first-generation and second-generation missions devoted to physical properties of the oceans.
- SMM is the Solar Maximum Mission defined by GSFC.
- Gap Filler is the 5-band MSS successor to ERTS.

#### 1.1.2 Study Methodology

This mission analysis has been conducted by use of the following procedures and data sources:

- A logical schedule of missions (Attachment 1) has been developed, considering NASA documentation, the scientific disciplines involved, anticipated NASA budgets, and predicted technological rate of progress in sensors.
- First-generation payloads were generally based on NASA documentation, e.g., the Thematic Mapper, HRPI and DCS for EOS-A.
- Second-generation and third-generation payloads are based on surveys of scientific literature, discussions with TRW scientific and engineering people, and on recent TRW studies.
- Payload-support requirements have been developed on the basis of engineering judgement, recent studies and NASA documentation.

### 1.1.3 Study Results

#### 1.1.3.1 EOS-A

This mission has been well defined, both by NASA and by TRW investigations.

Payload:	Thematic Mapper HRPI DCS
Weight:	- (Titan) 1277 lbs (Ref. Table 6.1 of TRW proposal). - (Delta w/914 km orbit) 697 lbs (Ref. Table 6.1 of TRW proposal). - (Delta w/583 km orbit) 573 lbs (Ref. Table 6.1 of TRW proposal).
Volume:	164" of modules above above transition ring for Titan (Ref. TRW proposal, Figure 6.1-2); this value applies to antenna-deployed condition.
Power:	495 watts maximum for payload (Ref. Figure 6.2 of TRW proposal).
Orbit:	315-494 nmi, sun-synchronous (Ref. Table 6.1 of TRW proposal).
Pointing Requirements:	0.01° pointing; $10^{-6}$ deg/sec; 0.0006 deg for $t = 20$ Min/Jitter (Ref. Figure 8.6 of TRW proposal).

Data Rate:	Total 200 MB/S (Ref. TRW proposal Figure 7.2)
Mission Peculiars:	Data-storage devices or TDRSS compatibility (Ref. TRW proposal Figure 7.2); compatibility with low cost ground stations (Ref. Section 7.2 of TRW proposal); radiation cooler required (Ref. Figure 7.4 of TRW proposal). Highly susceptible to contamination on optical surfaces and radiation cooler.

#### 1.1.3.2 EOS-B

An environmental-pollution payload has been postulated for EOS-B. This choice has been made because of the strong backing for this mission within government, the scientific community and by the general public; the "Report of the Advanced Imager and Scanners Working Group, 11-15 December 1972" is an example of this influence. Further, the inclusion of such a payload will drive out payload-support requirements for EOS which are different from those of earth resources and oceanography/meteorology.

Payload data have been developed from on-going and planned AAFE programs, TRW studies, NASA planning for Nimbus-G, and the Final Report of the Earth Observatory Satellite Mission Review Group, dated November 1971.

Payload:	<ul style="list-style-type: none"> <li>- Particulate-measuring sensor (Ref. TRW Modes of Data Handling).</li> <li>- Gas -measuring sensor for CO<sub>2</sub>, SO<sub>2</sub>, CO, O<sub>3</sub> (Ref. TRW Modes of Data Handling).</li> <li>- Water pollution sensor (color) (Ref. TRW Modes of Data Handling).</li> <li>- Vertical Temperature Sounder (Ref. TRW Modes of Data Handling).</li> <li>- Very high resolution radiometer (Ref. TRW Modes of Data Handling).</li> <li>- Side Looking Radar (Ref. EOSMRG)</li> <li>- Data Collection System (Ref. EOSMRG)</li> </ul>
Payload Weight:	1100 lbs. (Ref. Modes of Data Handling by TRW).

Payload Volume:	10 ft <sup>3</sup> plus antenna 2.5 x 1 x 27 ft. (Ref. TRW Modes of Data Handling).
Payload Power:	1.7 kw (Ref. TRW Modes of Data Handling).
Payload Orbit:	64° retrograde or 72°; posigrade; sun-synchronous; 300 nm alt. (Ref. EOSMRG, Appendix D).
Data Rate:	Payload total 200 MB/S (Ref. TRW Proposal Figure 7.2).
Pointing Requirements:	+0.25° all axes.
Mission Peculiars:	Coolers for detectors (passive or active TBD); data-storage devices or TDRSS compatibility; earth-viewing clearance for all sensors.

#### 1.1.3.3 EOS-C

The EOS family of spacecraft will perform the missions previously assigned to Nimbus. Oceanography and meteorology are the principal disciplines involved, and EOS-C is devoted to these disciplines.

The major sources of payload data are the TRW Study of Mission Requirements for an EOS Emphasizing Meteorology, the EOS Mission Review Group, the TRW Tradeoff Analysis of Modes of Data Handling Study, and the NASA Imagers and Scanner Work Group.

Payload:	<ul style="list-style-type: none"> <li>- Advanced atmospheric sounder (Ref. TRW Modes of Data Handling).</li> <li>- Oceanic Scanning Spectrophotometer (Ref. TRW Modes of Data Handling).</li> <li>- Sea Surface Temperature Imaging Radiometer (Ref. TRW Modes of Data Handling).</li> <li>- Passive Multichannel Microwave Radiometer (Ref. TRW Modes of Data Handling).</li> <li>- Constant Resolution Meteorological Scanner (Ref. TRW Modes of Data Handling).</li> <li>- Cloud Physics Radiometer (Ref. EOSMRG).</li> <li>- Data Collection System</li> </ul>
Payload Weight:	Approximately 500 lbs (including estimated 100 lbs for cloud physics radiometer).

Payload Volume:	Approximately 12 ft <sup>3</sup> (including 1 ft <sup>3</sup> estimate for cloud physics radiometer).
Payload Power:	450 W (including 75 w estimate for cloud physics radiometer).
Orbit:	700-1000 nmi; sun synchronous; 0900-1500 local sun time equatorial crossing).
Pointing Requirements:	+0.25° all axes.
Mission Peculiars:	Data-storage devices or TDRSS compatibility; detector cooling (passive or active TBD); 6 x 8 ft parabolic antenna with conical scan 40 degrees from nadir.
Data Rate:	1 MB/S total

#### 1.1.3.4 SEOS-A

This spacecraft will replace the SMS as a NASA R&D vehicle for geostationary earth observations. The mission will include observations of earth resources, oceanography and meteorology.

The payload will consist of a large telescope (e. g. , approximately 1.5 m optics) plus a data collection system. Two parallel Phase-A studies for telescope definition are currently underway; the Perkin-Elmer/TRW study is used as one source of data for the payload. Also, GSFC has provided payload data in EOS-L-204.

Payload:	- Large Earth Survey Telescope (LEST) - DCS
Payload Weight:	2640 lbs (Ref. GSFC Data; see EOS-L-204).
Payload Volume:	351 ft <sup>3</sup> (13 m <sup>3</sup> ) (Ref. GSFC Data; see EOS-L-204).
Payload Power:	145 w peak
Orbit:	Geostationary at about 100° W.
Pointing Requirements:	+28 μrad pointing; hold pointing to 0.7 μrad.
Mission Peculiars:	Data rates 50-60 MB/S; spacecraft slewing for scanning at 0.028 rad/min; detector coolers (passive or active TBD); extremely severe contamination constraints on optics (e. g. , covers needed). Severe thermal constraints on structure and telescope.

#### 1.1.3.5 SEASAT-A

The SEASAT program is designed to measure the physical characteristics of the world's oceans. Definition of the program is not yet complete, e.g., it is not known which NASA center will manage the program. Data presented here are from TRW involvement in SEASAT as a contractor to JPL, one of the NASA centers competing for the program and from EOS-L-204.

Principal parameters to be measured by SEASAT are the ocean's height and slope, wave profiles, surface winds, tides, currents and temperatures.

Payload:	Ocean sensors (undefined; Ref. GSFC input, see EOS-L-204).
Payload weight:	500 lb (EOS-L-204).
Payload Volume:	600 ft <sup>3</sup> (EOS-L-204). (Note: this must include antenna volumes)
Payload Power:	500 w (EOS-L-204).
Orbit:	725 km; 82° (non-sun synchronous).
Pointing Requirements:	0.25° all axes.
Data Rate:	0.5K-10M B/S
Mission Peculiars:	Data-Storage (10 <sup>8</sup> -10 <sup>9</sup> bits) devices or TDRSS compatibility; detector coolers (active or passive TBD); tracking beacon (probable); laser tracking STDN/USB; thermal constraints on antennas with variable sun angle 180 degrees turn of spacecraft or rotatable solar array.

Note: This payload may be modified by 15 June 1974.

#### 1.1 3.6 Solar Max Mission (SMM)

The SMM has been given top priority by the Space Science Board of the NAS, following its July 1973 meeting at Woods Hole. SMM is aimed at the 1977-79 period of maximum solar activity. A wide range of instruments will be carried to cover the electromagnetic spectrum (from the visible through several MeV). GSFC tells us (Ref. EOS-L-204) that Delta will be used for a launch in 1978, and Shuttle for payloads in the 1980's. Data below are from the GSFC documents (EOS-L-204).

Payload:	Unnamed sensors (EOS-L-204)
Payload Weight:	1431 lb
Payload Volume:	13.5 ft <sup>3</sup>
Payload Power:	174 w
Orbit:	300 nmi; 33°
Pointing Requirements:	5 arcsecond pointing; 5 min. stability; 1 arcsecond accuracy
Data Rate:	5 KB/S
Mission Peculiars:	Sun pointing attitude for payload; data-storage devices or TDRSS compatibility; severe contamination constraints on optics. Payload must point at the sun.

#### 1.1.3.7 Gap Filler (5-band MSS)

This mission is to be an interim solution to the gap between ERTS and EOS-A. The primary objective will be to survey earth resources. Our best information is from the GSFC documentation in EOS-L-204.

Payload:	5-band MSS.
Payload Weight:	160-610 lb
Payload Volume:	12-42 ft <sup>3</sup>
Payload Power:	55-125 W.
Orbit:	920 km; 99°; sun synchronous
Pointing Requirements:	0.25° nadir pointing accuracy; 0.0005°/sec rate; 5-8° off nadir requirements are same as nadir-pointing requirements.
Data Rate:	30 MB/S total.
Mission Peculiars:	Data-storage devices or TDRSS compatibility will probably be required.

Note: GSFC has given us three alternate payloads (EOS-L-204), which accounts for the wide variation in payload weight, volume and power.

#### 1.1.3.8 EOS-A'

This mission is expected about 1984. It will be a second-generation earth resources mission. Payload data are taken from the TRW Tradeoff Analysis of Modes of Data Handling for Earth Resources Study, for which upgraded EOS payloads were developed.

Payload:	- High Resolution Multispectral Point Scanner (HRMPS) - Pointable Imager (PI) - Synthetic Aperture Radar (SAR) - DCS
Payload Weight:	2170 lb
Payload Volume:	92 Ft <sup>3</sup> plus antenna 2.5 x 1 x 27 ft. min.
Payload Power:	2360 w
Orbit:	480-500 nmi; sun synchronous.
Pointing Requirements:	0.005°; 10 <sup>-7</sup> deg/sec (TRW estimates).
Data Rate:	HRMPS and PI 368 MB/S SAR 300 MB/S
Mission Peculiarities:	Data-storage devices or TDRSS compatibility (Ref. TRW proposal Figure 7.2); compatibility with low cost ground stations (Ref. Section 7.2 of TRW proposal); radiation cooler required (Ref. Figure 7.4 of TRW proposal). Highly susceptible to contamination on optical surfaces and radiation cooler.

#### 1.1.3.9 EOS-B'

Payload for EOS-B' will be an upgraded environmental-pollution set of instruments. Launch expected about 1985. The payload has been extrapolated from the state of current technology by TRW; little documented information is available.

Payload:	- Laser particulate sensor. - Laser planckton profiler (water pollution) - Multispectral polarimeter (gaseous air pollution).
Payload Weight:	1400 lb (TRW estimate)
Payload Volume:	12 ft <sup>3</sup> Antenna 2.5 x 1 x 27 ft.



Payload Power:	2.4 kw
Orbit:	64° retrograde or 72° posigrade; sun synchronous; 300 nmi alt. (Ref. EOSMRG, Appendix D).
Pointing Requirements:	$\pm 0.1^\circ$ all axes
Data Rate:	Total 300 MB/S
Mission Peculiars:	Coolers for detectors; data storage devices or TDRSS compatible; earth-viewing clearances for all sensors.

#### 1.1.3.10 EOS-C'

EOS-C' will be an oceanography-meteorology mission. The payload described below is based on TRW data developed in the Tradeoff Analysis of Modes of Data Handling for Earth Resources Study. It is likely that this generation of O/M payloads will be slanted toward microwave, lasers, radar and IR sensors which use active coolers.

Payload:	<ul style="list-style-type: none"> <li>(1) Advanced Atmospheric Sounder</li> <li>(2) Advanced Oceanic Scanning Spectrophotometer</li> <li>(3) Advanced Passive Multichannel Microwave Radiometer.</li> <li>(4) Advanced Constant Resolution Met Scanner Laser Backscatter Wind Sensor</li> <li>(5) Advanced Data Collection System.</li> </ul>
Payload Weight:	1500 lb (estimated from 1075 lbs for sensors 1, 2, 3 and 4, plus 100 lbs for DCS and 325 lbs for Laser sensor).
Payload Volume:	26 ft <sup>3</sup> (18 ft <sup>3</sup> for sensors 1, 2, 3 and 4 plus 8 ft <sup>3</sup> for laser and DCS).
Payload Power:	2 kw (1800 w for 1, 2, 3 and 4 plus 200 w for laser and DCS).
Orbit:	700-1000 nmi; sun synchronous; 0900-1500 local sun time equatorial crossing.
Pointing Requirements:	0.1° (TRW estimate).
Data Rate:	2 MB/S
Mission Peculiars:	10-20 m PMMR antenna, with conical scan about Z axis; TDRSS for data link; active cooling for IR detectors.

#### 1.1.3.11 SEOS-B

This spacecraft is in the same time frame as SEOS-A. The payload will be similar to that of SEOS-A, since there is no appreciable time between the two missions for development of a second-generation sensor. The two spacecraft (SEOS-A and -B) will be positioned to monitor the Pacific and Atlantic plus dual coverage of the United States.

#### 1.1.3.12 SEASAT-B

SEASAT-B will carry a second-generation payload. There is no documentation on which to base the SEASAT-B payload, so this payload is extrapolated from SEASAT-A requirements and the payload for that mission.

Payload:	- Multi-frequency Microwave Radiometer - Side Looking Synthetic Aperture Radar - Advanced Altimeter - Advanced Scatterometer - Advanced DCS.
Payload Weight:	Approximately 1500 lbs
Payload Volume:	1000 ft <sup>3</sup>
Payload Power:	1.5 kw
Orbit:	725 km; non-sun synchronous.
Pointing Requirements:	0.1° all axes
Data Rate:	50 MB/S
Mission Peculiars:	Multiple antennas; SLR antenna approximately 60 ft long, with rotation about X-axis; TDRSS data links; high-rate data handling for SAR; active coolers for IR detectors; thermal control and power vs variable sun angle.

#### 1.1.3.13 SMM (Advanced)

This payload is as defined in GSFC documentation (EOS-L-204).

Payload:	No specific sensors are identified
Payload Weight:	6800 lb
Payload Volume:	343 ft <sup>3</sup>

Payload Power:	600 W
Orbit:	300 nmi; 33° inclination
Pointing Requirements:	2 arcsecond pointing; 5 min pointing stability; 0.22 arcsecond accuracy.
Data Rate:	3 MB/S
Mission Peculiars:	TDRSS links; severe contamination constraint for optical surfaces. Payload must point at the sun.

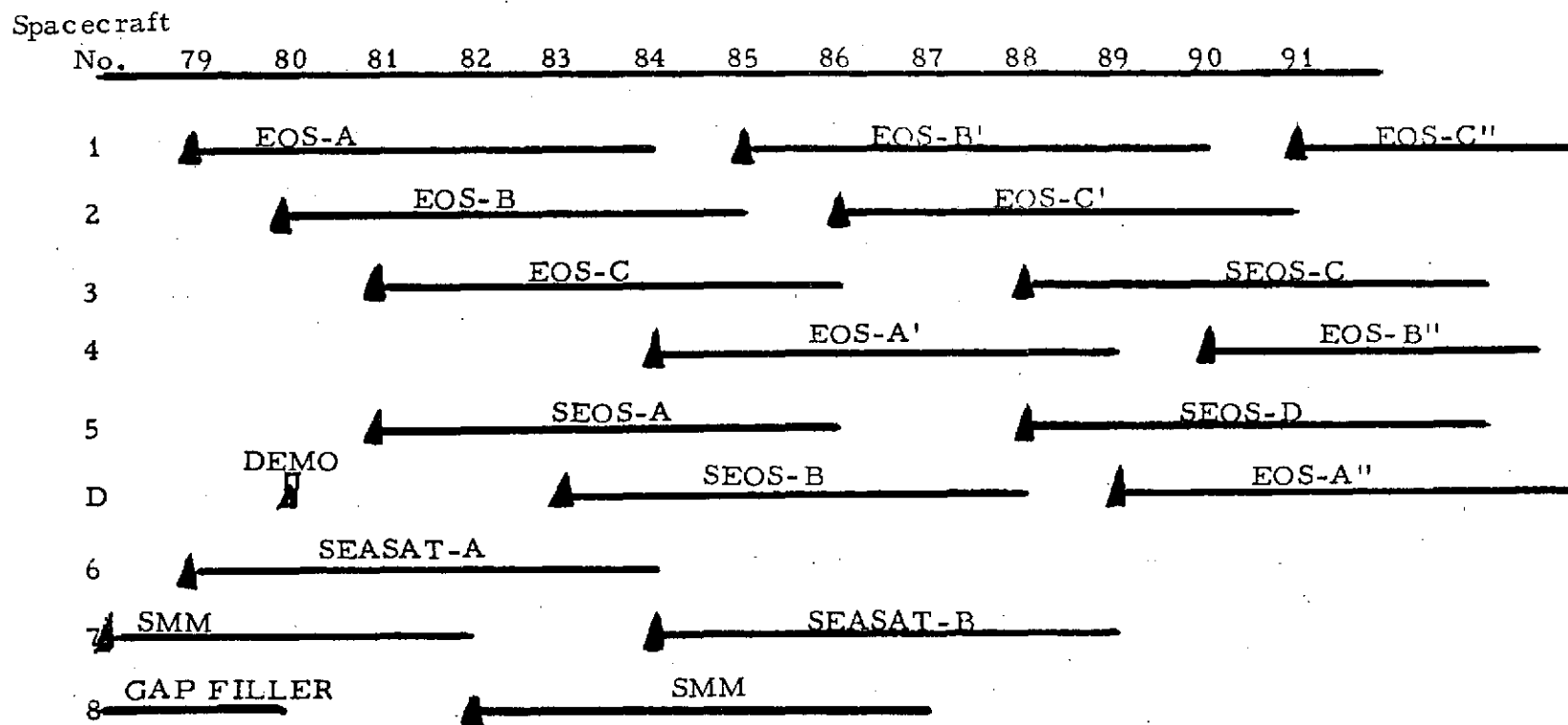
#### 1.1.4 Later Payloads

Payloads beyond the mid-1980's can only be characterized, rather than defined. The following guidelines are recommended for consideration in scaling EOS to fit these later payloads:

- Because higher resolution (spatial and spectral) is a driving function in EOS-related disciplines, it is likely that data rates will increase.
- Command systems should be expected to increase in capacity and flexibility. This trend will be caused by scientists' desire to be more selective in their observational requirements.
- Off-track pointing of sensors will become a stronger requirement because of scientists' desires to view targets on a more selective basis.
- Contamination of optical systems will be an increasing problem as optical systems increase in size.
- Microwave and side-looking radars will require larger antennas, often with pointing or rotation required of the antennas.
- Tighter pointing and stabilization requirements will be imposed on the spacecraft because of the sensors' higher spatial resolution.
- Orbits will deviate from the sun synchronous as scientists choose to look at other diurnal regimes. For example, terminator orbits and SEASAT-type orbits will be selected.

#### 1.1.5 Future Mission Analysis Data

It is anticipated that the SEASAT payload may be redefined by the NASA Headquarters SEASAT program manager. When the information becomes available, a revision to this report will be prepared.



- This model supports EOS, SEOS, SEASAT, and SMM with nine new spacecraft buys and six refurbishment cycles, plus development/acquisition of 15 payloads.
- Five-year retrieval/replacement cycles based on best estimates for development cycles for new payloads. This estimate considers budget constraints and technology-development times. (Five years probably on the low side.)

Figure 1-1. EOS Candidate Missions

#### 1.1.5.1 Mission Operations

##### 1.1.5.1.1 Mission Objectives

Major mission events are detailed for three possible EOS mission segments:

- From liftoff through operational orbit insertion
- From operational orbit through capture by the Shuttle through resupply and repair through redeployment and reestablishment of the operational orbit
- From operational orbit to capture, storage and Shuttle deorbit.

The operations are given in as much detail as is practical at this stage of the EOS mission(s) development. Emphasis is placed on those events that set the mission profile or place requirements on spacecraft hardware or ground systems. In many cases the relative timing (spacing) of the events presented is not known in detail; however, the order of presentation is considered accurate. No attempt is made to consider unplanned contingencies; only nominal operations and planned contingencies (resupply, retrieval) are considered.

##### a. Liftoff to Operational Orbit Insertion (Circularization Maneuver Required)

Figure 1-2 defines the major operations that must be performed in order to inject EOS into its operational orbit in the desired attitude configuration. The general case where a circularization burn is required after insertion is presented.

At a specified time after separation the pyrotechnic devices that hold down the solar array are activated and the array extends (deployment takes about two minutes). Immediately after the array is deployed, reorientation of the spacecraft to the sun pointing attitude is initiated. When sun pointing is achieved, the spacecraft negative yaw axis (-Z) points at the center of the sun and holds. The yaw rate is zero. The solar array is then driven into the yaw plane. With the spacecraft -Z axis holding on the sun and the yaw rate damped, the star trackers will each lock on stars and the magnetometer output will stabilize. These data (magnetometer readings

➔ Means the time is known

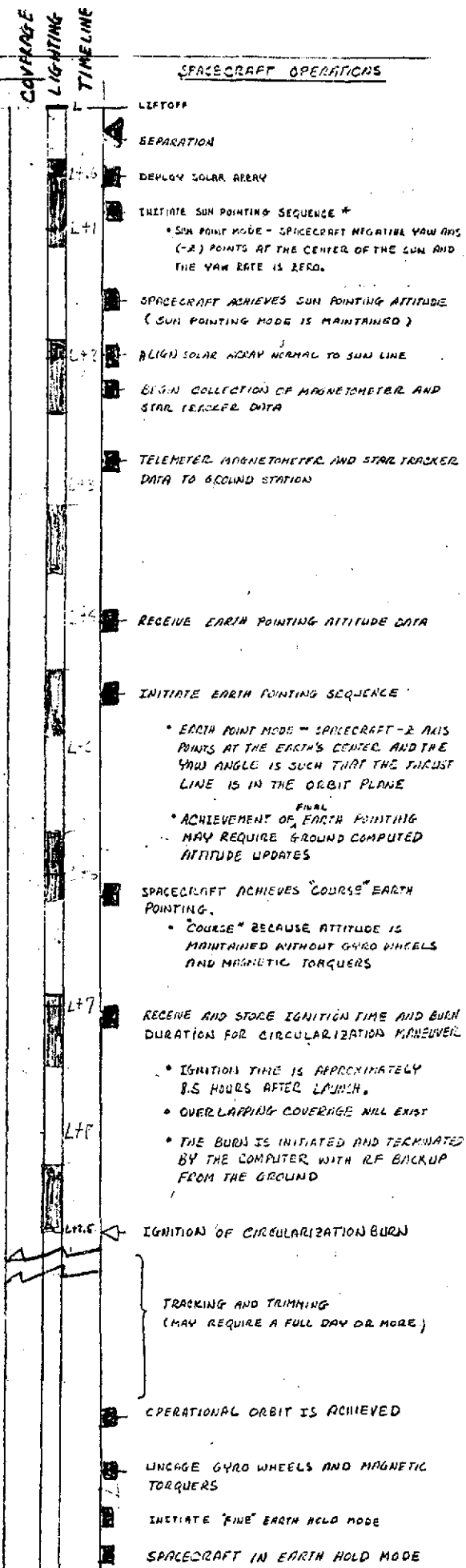
█ The existence and order of the events is assured but the time is unknown

COMPUTE EARTH HOLD  
ATTITUDE COMMANDS  
FROM MAGNETOMETER  
READINGS AND STAR  
TRACKER COORDINATES

COMPUTE CIRCULARIZATION  
BURN DATA

ORIGINAL PAGE IS  
OF POOR QUALITY

Figure 1-2. Launch to Operational Orbit Insertion (Circularization Burn Required)



and star tracker coordinates) are transmitted to the ground where the attitude commands that will reorient the spacecraft to the Earth pointing attitude are computed.

As soon as possible, the ground computed attitude commands are telemetered to the spacecraft and reorientation to the Earth Hold Mode is initiated. The Earth pointing attitude is then trimmed using onboard spacecraft ephemeris data and star tables until a "coarse" earth-hold attitude is achieved.\* In the earth hold mode the spacecraft orbits the earth with its -Z axis pointing at the center of the earth and the pitch axis in the orbit plane. The ground now tracks the spacecraft until an accurate burn time\*\* and burn duration is computed and at the earliest opportunity these data are telemetered to the spacecraft and stored. The burn time and duration are refined on the ground and transmitted to the spacecraft as required until the burn is executed. After execution of the circularization burn the spacecraft is again tracked and orbit trim maneuvers are computed, transmitted, stored and executed until the desired operational orbit is achieved. At this point the gyro wheels and magnetic torquers are uncaged and the spacecraft is put in the operational Earth Hold Mode (i.e., the earth pointing attitude is maintained using the gyro wheels and magnetic torquers rather than the gas jets). Now, the experiment covers are removed and the wideband antennas are uncaged and nominal on-orbit operation commence.

The ground station coverage during the first nine hours of a sun-synchronous mission is given in Figure 1-3. The figure shows that the first few orbits are covered only by Alaska. It is not until approximately 8.5 hours after insertion that apogee has full and overlapping coverage. It is during this apogee coverage period that the circularization burn is planned. This leaves about eight hours to command the spacecraft to the earth hold mode, track the vehicle to obtain a good state vector and compute and store the circularization burn maneuver.

---

\*"Coarse" refers to the fact that the attitude is maintained with gas jets rather than gyro wheels and magnetic torquers as will be the case after injection into the operational orbit is achieved.

\*\*The burn time will correspond approximately to the first apogee that has adequate ground coverage. This will be about 8.5 hours after launch (see Figure 1-3).

PERIOD = 93.5941 min

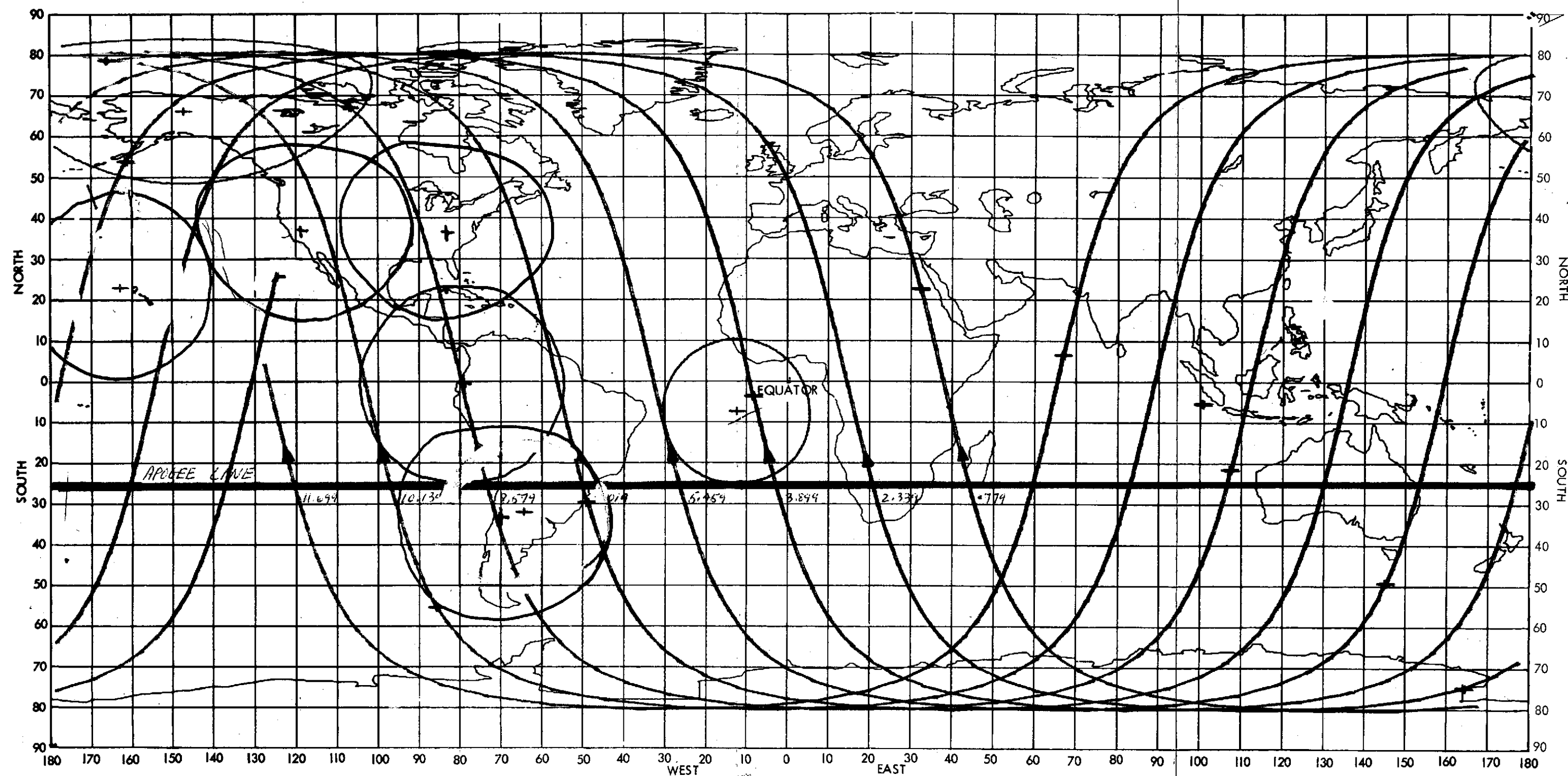


Figure 1-3. Ground Coverage During the First Nine Hours of the EOS Mission

ORIGINAL PAGE IS  
OF POOR QUALITY

PRECEDING PAGE BLANK NOT FILMED

FOLDOUT PAGE 1

1-17

FOLDOUT FRAME 17



Trajectory lighting, unlike ground station coverage, is a function of local launch time. For launches between 10 a.m. and 2 p.m. local time, first darkness occurs about 25 minutes after insertion and the duration of the eclipse is about 37 minutes. The lighting for an 11 a.m. launch is shown on Figures 1-2 and 1-3.

b. Liftoff to Operational Orbit Insertion  
(No Circularization Burn Required)

Figure 1-4 gives the major mission operations for the case where no circularization burn is required to achieve the desired operational orbit. This case is identical to the above case except that the burn related operations are deleted.

c. Resupply Mission (Servicing Orbit Required)

Figure 1-5 defines the sequence of major operations (for EOS, Shuttle and the ground) for an in-orbit resupply mission. The general case where EOS is required to inject into an intermediate servicing orbit, accessible to the Shuttle, is presented.

The sequence begins when EOS receives and stores the operational-orbit-to-servicing-orbit maneuver data. Implicit in this transmission is Shuttle launch readiness. From the EOS standpoint the constraints on the operational orbit-to-service-orbit-back-to-operational orbit maneuver sequence are that: 1) the burns be done over a ground station — preferably over overlapping ground coverage, and 2)\* the relationship between the EOS orbit node and the solar right ascension that exists prior to the service orbit burn be restored within a specified tolerance when EOS regains its operational orbit. Except for these two EOS requirements the maneuvers may be chosen so as to optimize Shuttle operations.

After completion of the service orbit injection maneuver a period of tracking and trimming ensues. When an acceptable servicing orbit is achieved the Shuttle is launched and a sequence of Shuttle rendezvous maneuvers\*\* are carried out. When the Shuttle achieves stationkeeping

---

\* This constraint is removed in the retrieval case.

\*\* EOS is passive during rendezvous.

Note:

✈ Means the time is known

□ The existence and order of the events is assured but the time is unknown

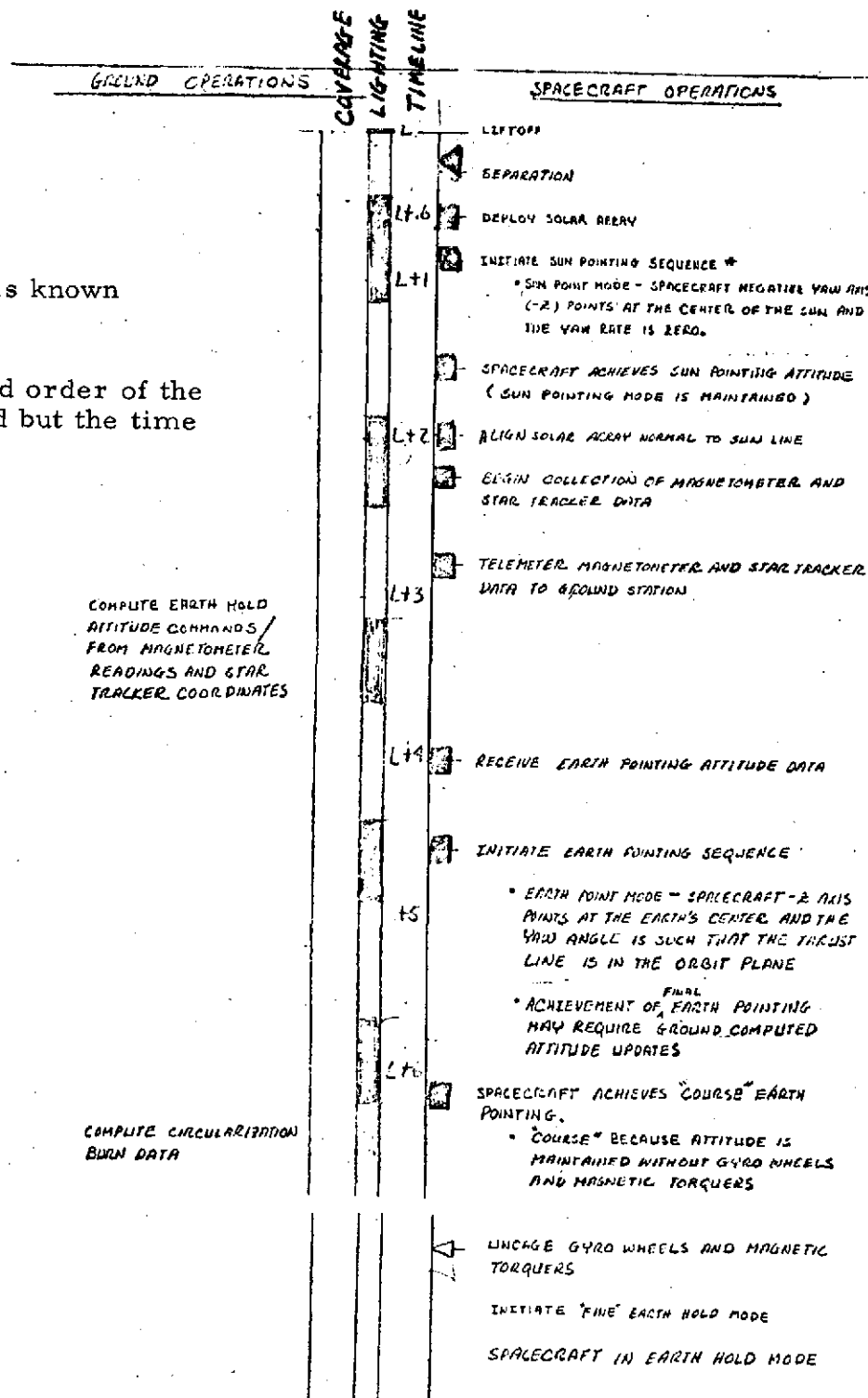


Figure 1-4. Launch to Operational Orbit Insertion (No Circularization Burn Required)

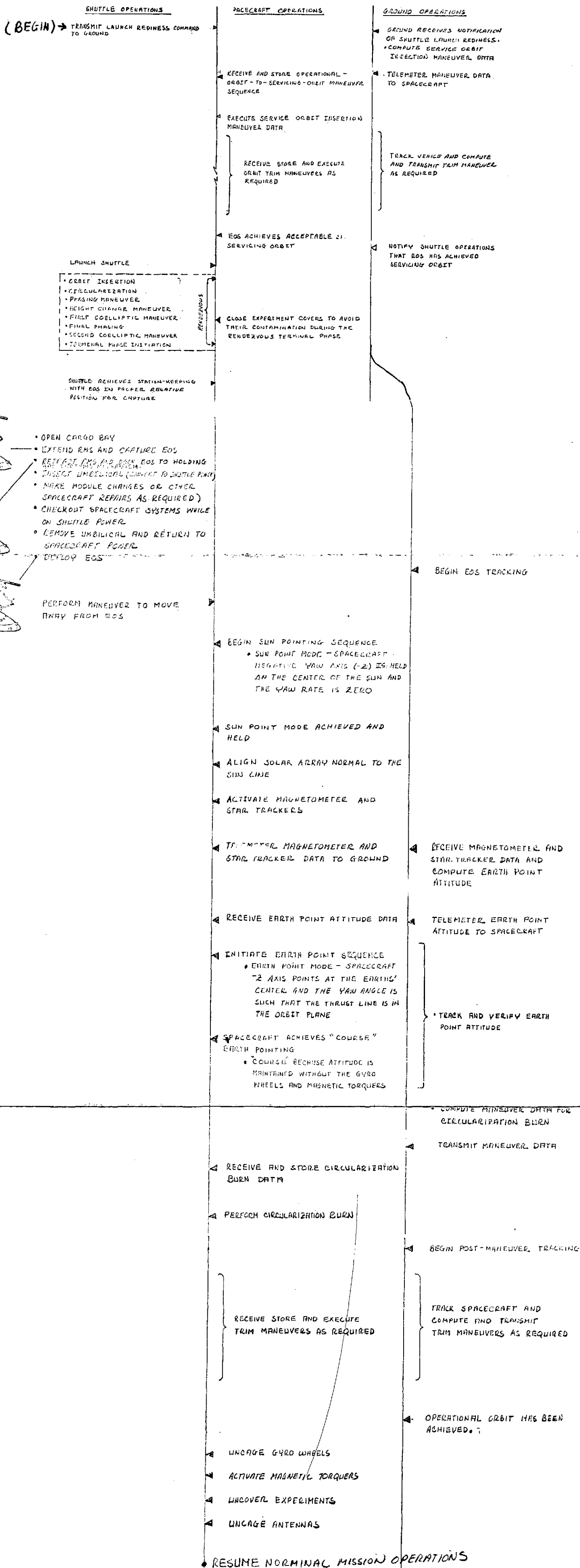


Figure 1-5. Resupply Mission Operation (Intermediate Servicing Orbit Required)

with EOS it maneuvers to the proper relative position for capture. The EOS/Shuttle interface (i.e., capture through redeployment) is well established. It is described and partially illustrated in Figure 1-5 and further illustrated in Figure 1-6.

After EOS is redeployed the Shuttle will perform a small maneuver to separate it from EOS. At this point the sequence of EOS operations necessary to reestablish the operational orbit are virtually identical to the separation-to-operational orbit insertion operation discussed above. The required sequence is given in Figure 1-5.

d. Resupply Mission (No Servicing Orbit Required)

If EOS resupply can be carried out in the operational orbit the mission is greatly simplified (as compared with resupply when an intermediate servicing orbit is required). The required operations are specified in Figure 1-7; they represent a small subset of the more general service-orbit-required case outlined in Figure 1-5.

e. Retrieval Mission

An EOS retrieval mission, whether an intermediate servicing orbit is required or not, is identical, up to a point, with the corresponding resupply case. However, in the retrieval case the mission effectively ends when the spacecraft is docked with the Shuttle. After docking instead of module exchange, redeployment, etc., the solar array is retracted — the docking mechanism folds putting EOS into a special retention device — the docking mechanism is then released leaving the spacecraft totally supported by the retention mechanism. The cargo bay is closed and the Shuttle deorbits and lands. The list of operations for the two retrieval cases are given in Figures 1-8 and 1-9.

PRECEDING PAGE BLANK NOT FILMED

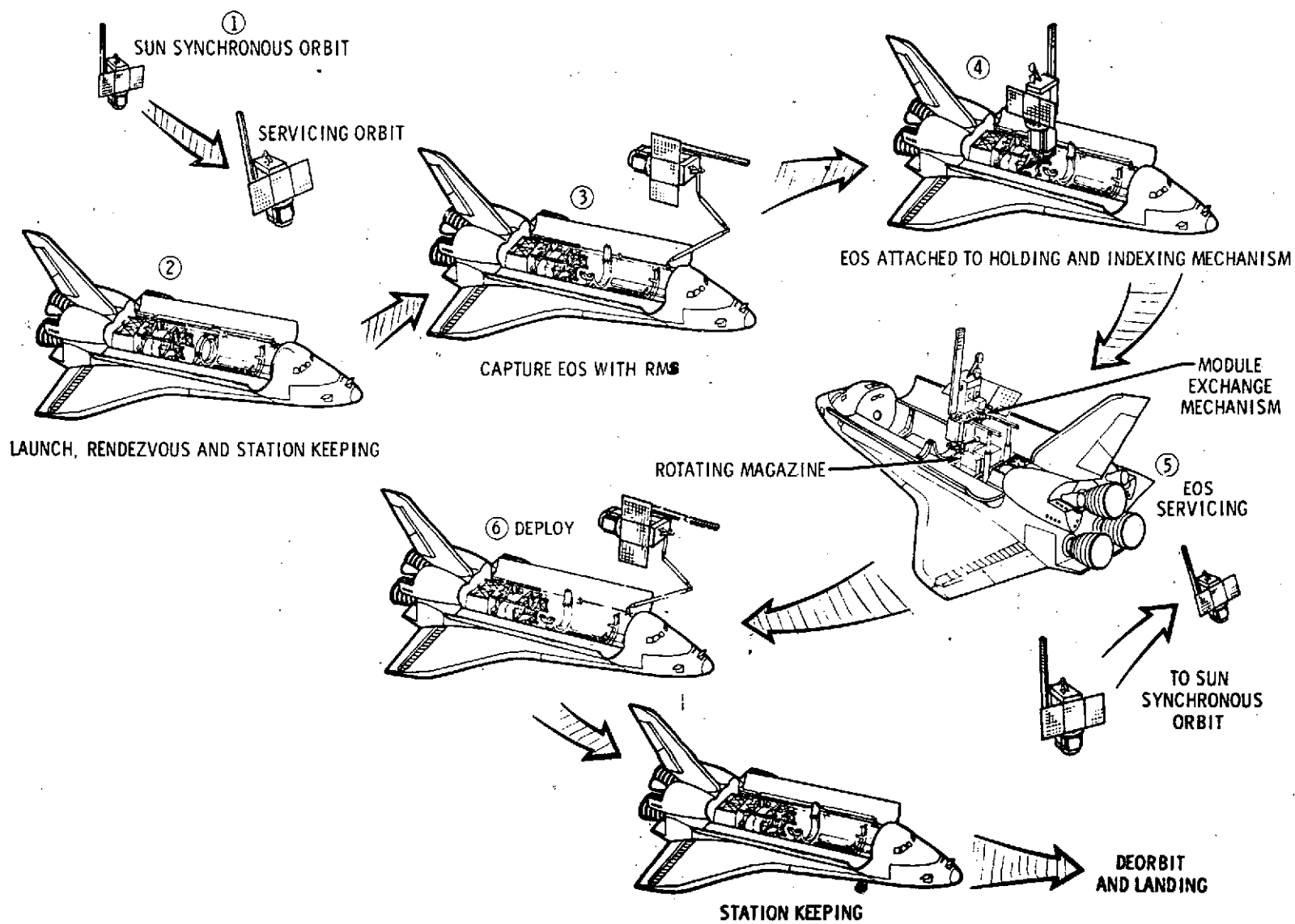


Figure 1-6. EOS Orbit Servicing Operations

### SHUTTLE OPERATIONS

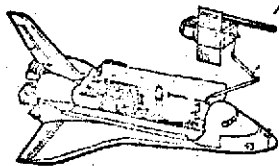
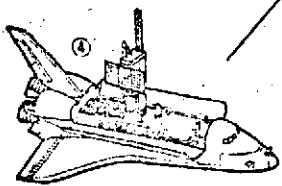
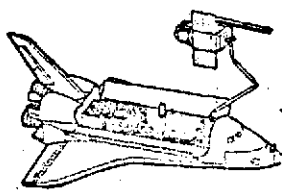
TRANSMIT LAUNCH REDINESS COMMAND TO GROUND

#### LAUNCH SHUTTLE

- ORBIT INSERTION
- CIRCULARIZATION
- PHASING MANEUVER
- HEIGHT CHANGE MANEUVER
- FIRST COELLIPTIC MANEUVER
- FINAL PHASING
- SECOND COELLIPTIC MANEUVER
- TERMINAL PHASE INITIATION

RENDEZVOUS

SHUTTLE ACHIEVES STATION-KEEPING WITH EOS IN PROPER RELATIVE



- OPEN CARGO BAY
- EXTEND RMS AND CAPTURE EOS
- RETRACT RMS AND BACK EOS TO HOLDING AND LINGERING MECHANISM
- INSERT UMBILICAL (CONNECT TO SHUTTLE POWER)
- MAKE MODULE CHANGES OR OTHER SPACECRAFT REPAIRS AS REQUIRED
- CHECKOUT SPACECRAFT SYSTEMS WHILE ON SHUTTLE POWER
- REMOVE UMBILICAL AND RETURN TO SPACECRAFT POWER
- DEPLOY EOS

PERFORM MANEUVER TO MOVE AWAY FROM EOS

### SPACECRAFT OPERATIONS

CLOSE EXPERIMENT COVERS TO AVOID THEIR CONTAMINATION DURING THE RENDEZVOUS TERMINAL PHASE

### GROUND OPERATIONS

BEGIN EOS TRACKING

BEGIN SUN POINTING SEQUENCE

- SUN POINT MODE - SPACECRAFT NEGATIVE YAW AXIS (-Z) IS HELD ON THE CENTER OF THE SUN AND THE YAW RATE IS ZERO

SUN POINT MODE ACHIEVED AND HELD

ALIGN SOLAR ARRAY NORMAL TO THE SUN LINE

ACTIVATE MAGNETOMETER AND STAR TRACKERS

TELEMETER MAGNETOMETER AND STAR TRACKER DATA TO GROUND

RECEIVE MAGNETOMETER AND STAR TRACKER DATA AND COMPUTE EARTH POINT ATTITUDE

RECEIVE EARTH POINT ATTITUDE DATA

TELEMETER EARTH POINT ATTITUDE TO SPACECRAFT

INITIATE EARTH POINT SEQUENCE

- EARTH POINT MODE - SPACECRAFT -Z AXIS POINTS AT THE EARTH'S CENTER AND THE YAW ANGLE IS SUCH THAT THE THRUST LINE IS IN THE ORBIT PLANE

TRACK AND VERIFY EARTH POINT ATTITUDE

SPACECRAFT ACHIEVES "COURSE" EARTH POINTING

- "COURSE" BECAUSE ATTITUDE IS MAINTAINED WITHOUT THE GYRO WHEELS AND MAGNETIC TORQUERS

UNCAGE GYRO WHEELS

ACTIVATE MAGNETIC TORQUERS

UNCOVER EXPERIMENTS

UNCAGE ANTENNAS

Figure 1-7. EOS Resupply (No Intermediate Service Orbit Required)

FOLDOUT PAGE 1

ORIGINAL PAGE IS OF POOR QUALITY

FOLDOUT PAGE 2

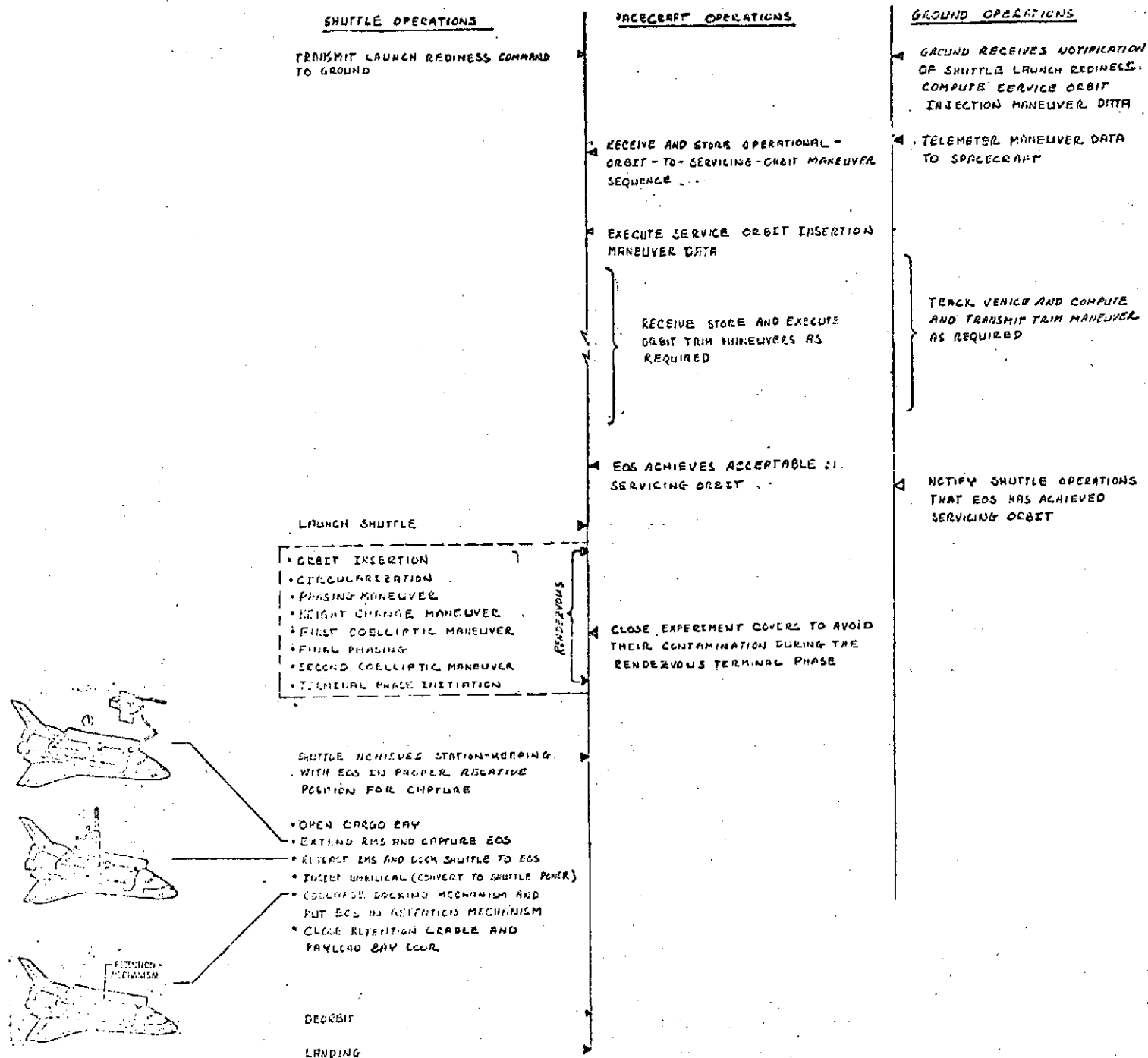


Figure 1-8. EOS Retrieval Mission Operations (Intermediate Service Orbit Required)

PRECEDING PAGE BLANK NOT FILMED

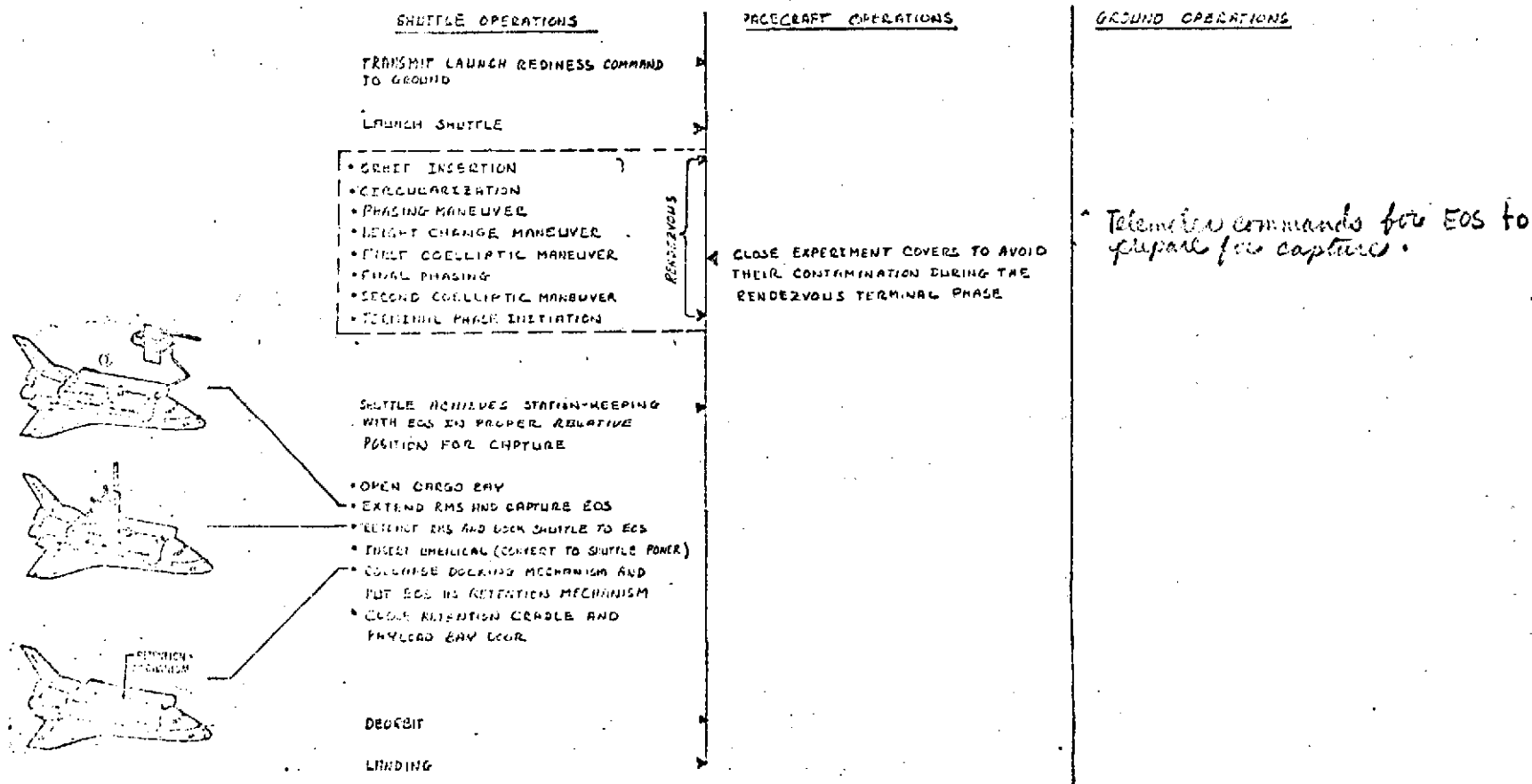


Figure 1-9. EOS Retrieval Mission Operations  
(No Intermediate Service Orbit Required)



#### 1.1.5.1.2 Yaw Turn Considerations

This task is required to identify the need for a yaw turn capability and assess the impact on instrument payload and support subsystems of orientation of the +X axis either in the direction of the velocity vector or opposed to it. The attitude control system can function equally well in either orientation.

The basic spacecraft platform, as conceptually configured in this study, takes advantage of the sun synchronous orbit required for EOS-A and locates the power module containing the batteries on the anti-sun side, the solar array module on the sun side, and directs the fixed star sensors toward the anti-sun side. Additionally, the TM and HRPI instrument payloads for EOS-A are configured to take advantage of the cooling available on the anti-sun side. The task briefly addresses the impact of this constraint on how the mission can be flown and still satisfy the constraint.

#### EOS-A

##### Requirements and Constraints:

- The baseline EOS-A orbit is sun synchronous, therefore, the sun remains on one side of the orbit plane throughout any one mission.
- The instrument payload design concept requires that one side of the instrument payload points nominally away from the sun side of the orbit plane for cooling.
- The orbit nodes must be capable of being placed anywhere from the 6 am subpoint position to the 6 pm subpoint position and will remain fixed (at the selected time) during any one mission.

##### Alternative Implementations:

There are three alternative implementations for satisfying the above requirements. These are:

- 1) Assuming that the baseline is configured with the sun on the -Y side with +X in the direction of the velocity vector, the ascending node can be positioned within the sector of 6 am to noon subpoint positions (see Figure 1-10)

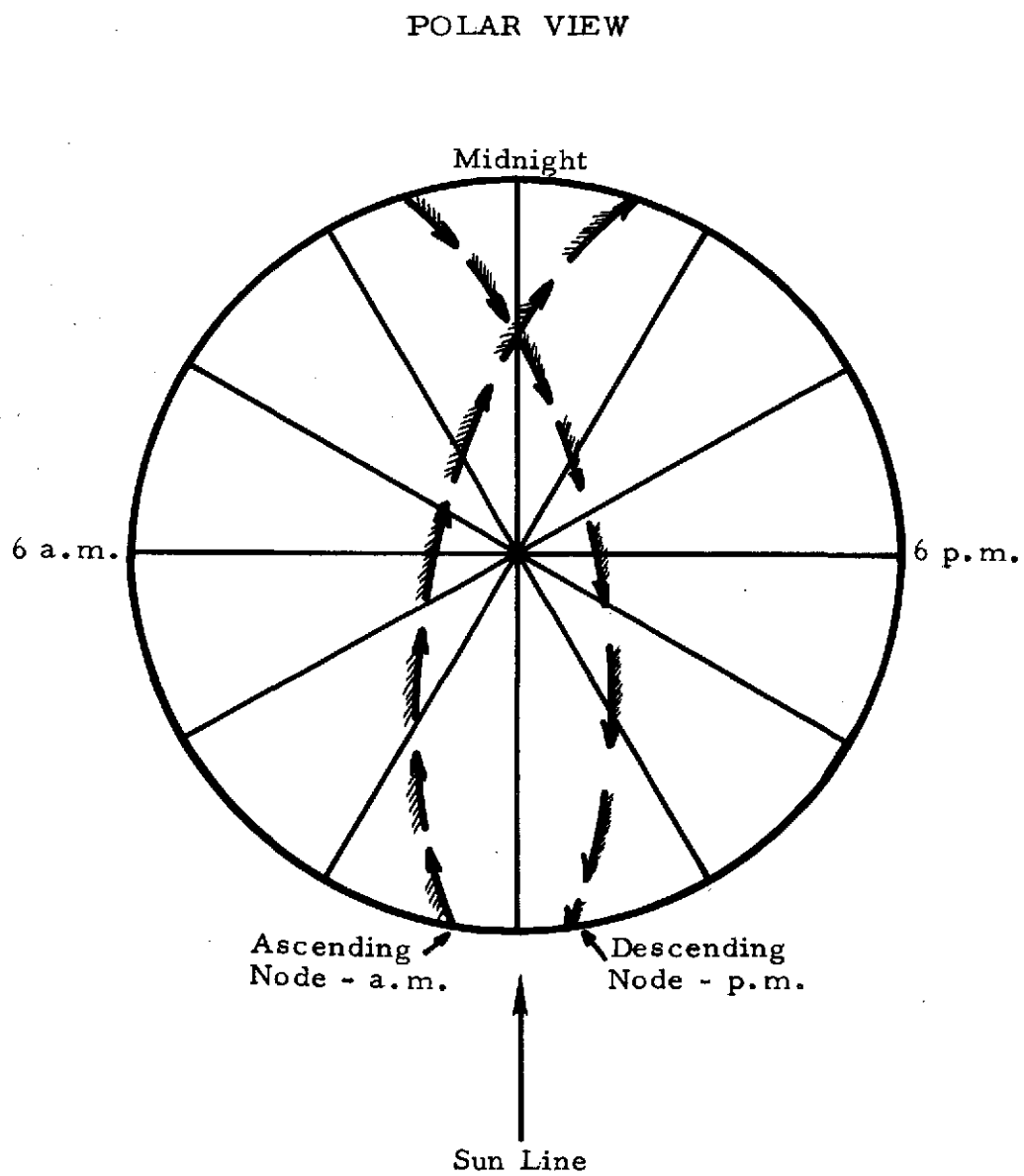


Figure 1-10. EOS-A Orbit Concept to Avoid Yaw Turns  
for Drag Makeup  $\Delta V$  Thrusting

or the descending node may be positioned within the sector of noon to 6 pm subpoint positions. No yaw turn is required for this configuration and there are no configuration changes.

- 2) This alternative is similar to (1) above in which the descending node is positioned in the am sector or an ascending node is positioned in the pm sector. No yaw turn is required in this configuration however, "right" and "left" hand wiring harnesses are required for the reversal instrument, power, and attitude determination, and solar array and drive modules, and some structural changes are required to accommodate the "reversed hand" configuration. Adjustment of instrument alignment is also required to accommodate the reversed attitude with regard to apparent direction of travel and earth rotation effects. Some additional cost for fabrication of right and left-handed assemblies and possibly conversion of replacement instruments to opposite direction operation would be incurred if both am and pm missions using this alternative are flown.
- 3) This alternative is similar to (1) above for am ascending nodes but would require operation with the -X axis in the direction of the velocity vector for ascending nodes in the pm. The  $\Delta V$  operation mode would require a  $180^\circ$  yaw turn for orbit maintenance plus additional propellant gas for the yaw maneuvers.  $\Delta V$  thrusting may be required for initial orbit circularization and subsequently at intervals of every 17 days for the 387 nm altitude baseline case. The  $\Delta V$  burn attitude can probably be referenced to gyro sensing only and performed during instrument "off" periods. The  $180^\circ$  maneuver and settling time would require about one-half hour to return to data-taking attitude control constraints. As in the case of alternative (2), instrument alignment is required to accommodate the reverse direction traverse. This alternative will have a slight additional cost and weight for the increased gas required.

All cases will require at least one yaw maneuver for either initial orbit circularization or deboost thrusting for rendezvous.

#### Recommendation for EOS-A:

The first alternative above, i.e., 6 am to noon ascending node or noon to 6 pm descending node is recommended for EOS-A because the observatory

design is identical for either case. If afternoon ascending nodes are required, the least design change (lowest cost) would result from the third alternative wherein the -X axis is in the direction of the velocity vector. In this case, instrument re-alignment is required to accommodate the reverse traverse and yaw turns are required for the orbit makeup  $\Delta V$  burns every 17 days which can probably be performed without mission interference.

#### OTHER MISSIONS

##### EOS-B and EOS-C:

Similar to EOS-A.

##### SEASAT:

This low altitude non-synchronous orbit will regress relative to the sun line and as in the case of EOS-A, it will be necessary to keep the sun on one side of the satellite for thermal management and to illuminate the solar array without shadowing. The best way to do this will be to perform a yaw turn and reverse the +X axis relative to the velocity vector at each  $180^\circ$  rotation of the sun line relative to the orbit plane. Review of the tentative instrument payload indicates that the sensors can operate equally well in either orientation if the ground data processing is adjusted to the change in orientation mode. For example, with a 725 km,  $82^\circ$  inclination orbit the relative sun line regression would require a  $180^\circ$  yaw maneuver approximately every 93 days. This maneuver will require approximately one-half hour and could be performed during a no-data-taking period without mission interference.

##### SEOS-A:

Since this orbit is geostationary the observatory must accommodate only the seasonal north/south sun excursion. In this case, thermal control can be accommodated with either a sun shade or a  $180^\circ$  roll re-orientation every six months.

##### SOLAR MAX:

Since the observatory is sun pointing in this mission, thermal control is manageable.

#### 1.1.5.1.3 Antenna and Ephemeris Autonomy

Ground operational requirements are affected by the manner in which the On-Board Computer is used to implement ephemeris modelling and antenna pointing.

The detailed design of both on-board ephemeris and antenna pointing equations are the subject of attitude determination and control studies. Guidelines to these studies have been developed under this task. These guidelines have resulted from evaluation of performance and operational requirements.

Some degree of on-board ephemeris modelling is required for EOS, in order to earth-point the spacecraft based on data from a stellar-inertial attitude determination system. The type of modelling is selected (see attitude determination design) based on pointing accuracy requirements, ground update frequency constraints, and on-board computer requirements. The presence of this on-board ephemeris model will not simplify ground ephemeris prediction; however, the manner of its implementation can affect the volume and frequency of ground update commands.

A cursory analysis indicates that the on-board ephemeris data will be adequate to permit open-loop command pointing of the LCGS and CDPF narrow beam antennas.\* Such an on-board antenna pointing requirement is needed if we assume possible servicing of LCGS users while not in communication with the OCC. Given on-board ephemeris and data specifying the location of the ground stations (and a specification of their sequence), the gimbal commands can be generated in the OBC via rather simple analytic expressions. Slew commands can also be generated on board according to re-targeting requirements. Development of these pointing equations is part of the attitude control design activity.

---

\* Beamwidths for the LCGS/CDPF antenna will be in the neighborhood of 5 degrees, requiring control to within 0.25 - 0.50 deg. The TDRS data link (at 14 GHz) would have a beam width of about one degree.

## 2. ORBIT ANALYSIS

### 2.1 ORBIT SELECTION AND CHARACTERIZATION

#### 2.1.1 Problem Discussion

The EOS-A mission is to be flown in a low-altitude (300 to 900 n mi), circular sun-synchronous orbit. This establishes the only free variable as the orbital altitude. The selection of the orbital altitude is governed by the frequency and pattern of earth surface coverage desired, payload capability of the launch vehicle, ground station coverage and pass time, and maintenance required to compensate for altitude caused by atmospheric drag.

##### 2.1.1.1 Earth Coverage Consideration

To determine the nature, extent, and frequency of coverage of features on the earth's surface, it is necessary to examine its trace pattern. The trace repetition parameter  $Q$  is the number of satellite revolutions that occur during one rotation of the earth relative to the osculating orbit plane. In general,  $Q$  is expressed as an integer plus a fraction  $n/d$  where  $n$  and  $d$  are relative prime integers. The denominator  $d$  is the whole number of rotations the earth must make relative to the orbit plane before the trace closes, i.e.,  $d$  is the duration in days of the coverage pattern cycle. The numerator  $n$  determines the order in which the trace pattern develops. For circular, sun-synchronous orbits, the trace parameter  $Q$  is given as a function of altitude in Figure 2-1. Note that suitable values of  $Q$  for the altitude range specified (300 to 900 n mi) are between 12 and 15 orbits per day.

The minimum swathwidth required for full earth coverage is directly related to the number of days required to achieve global coverage. Figure 2-2 shows the minimum swath width required for full earth coverage for various repeat cycles as a function of  $Q$ . Note that for the specified swathwidth value of 100 n mi, the repeat cycle must be at least 18 days for the higher altitudes (low  $Q$ ) and at least 15 days for the lower altitudes (high  $Q$ ).

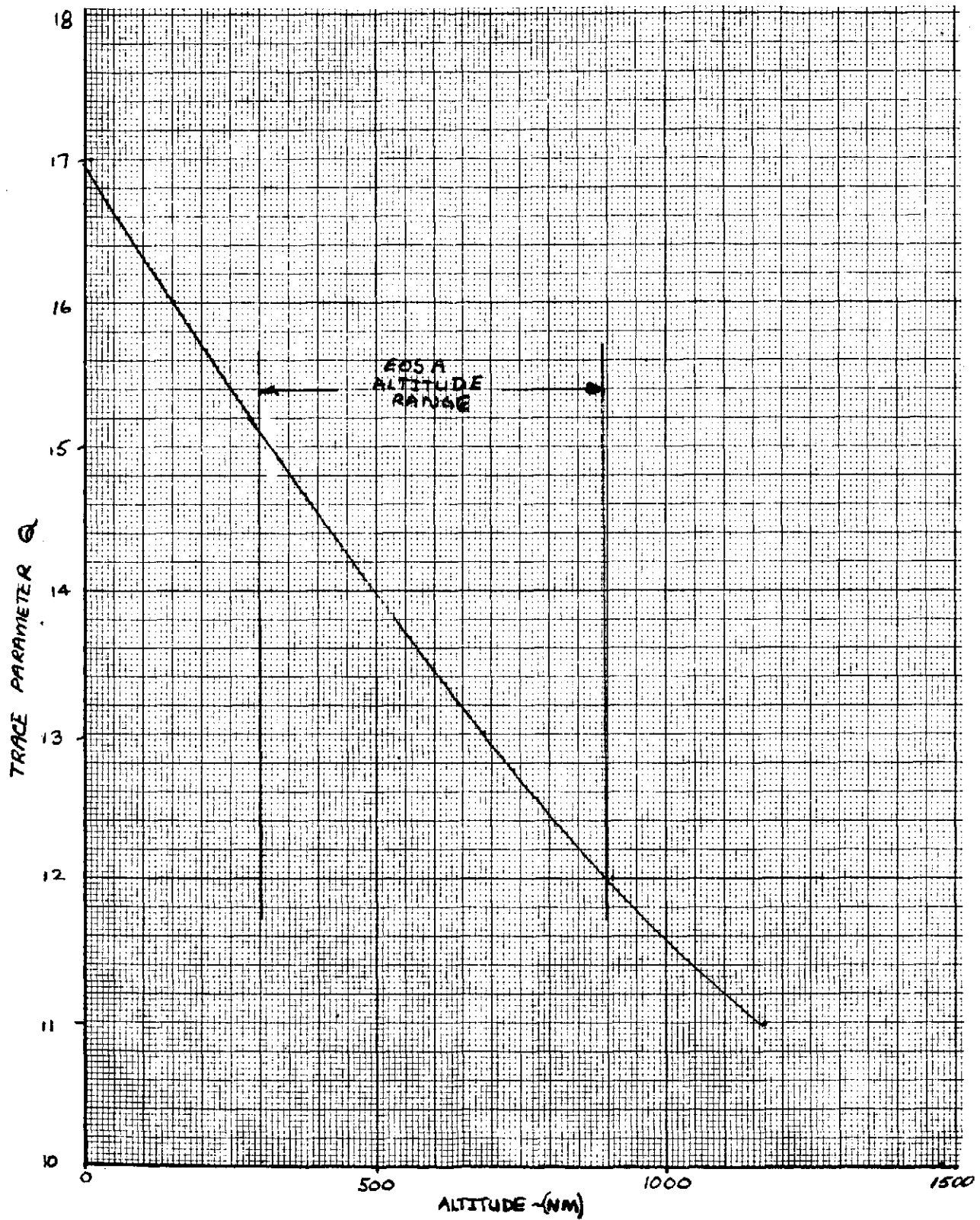


Figure 2-1. Trace Parameter Q versus Altitude

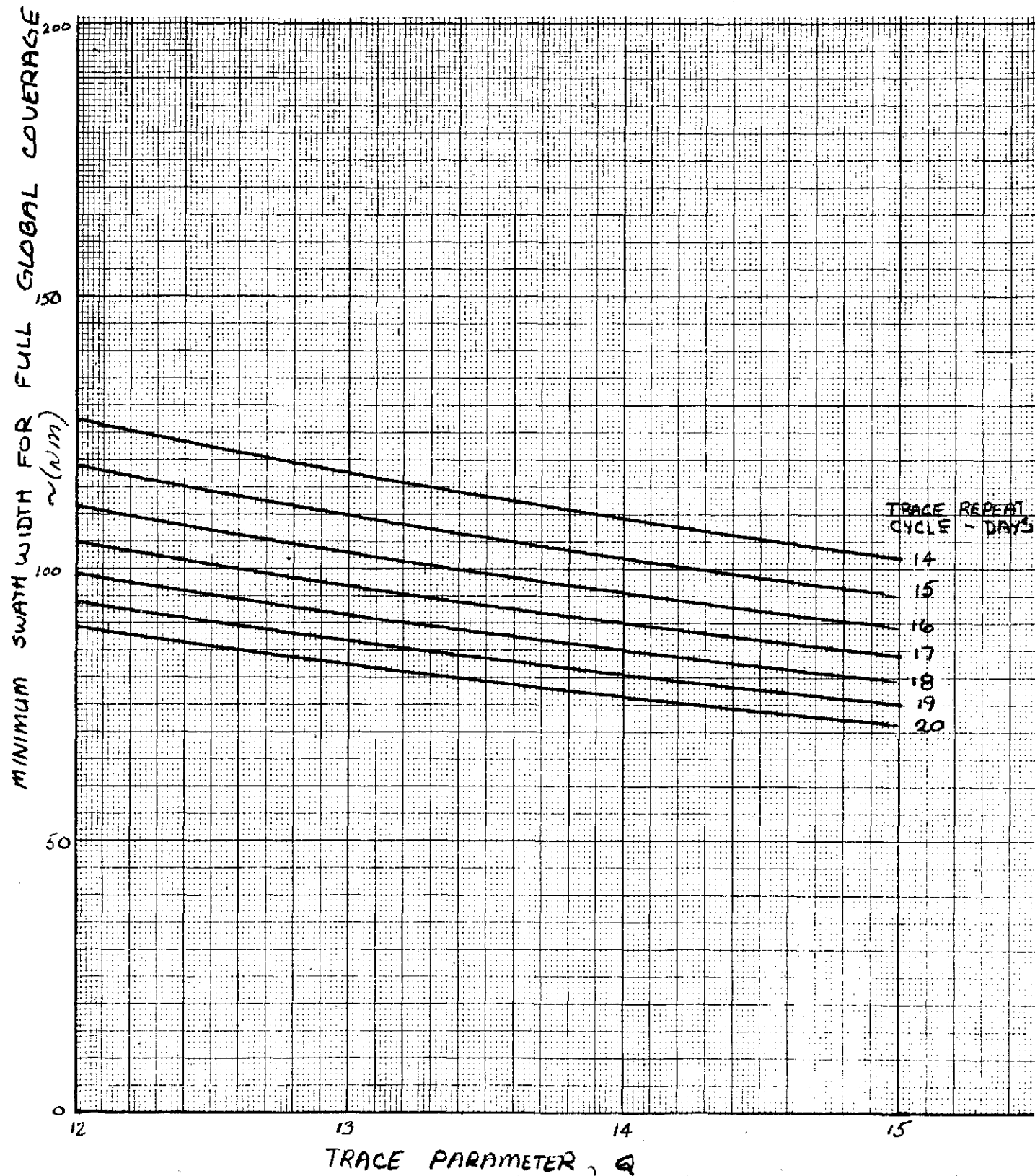


Figure 2-2. Swath Width Requirements for Full Earth Coverage



#### 2.1.1.2 Launch Vehicle Considerations

The launch vehicle payload characteristics establish the upper altitude limits for specified payload weights. The payload characteristics for the candidate launch vehicles are presented in Figure 2-3. Current estimates for the EOS-A mission limit altitude to 480 n mi. The Shuttle ability to achieve this circular altitude for servicing missions was a factor in this limit.

#### 2.1.1.3 Orbit Maintenance

Requirements for minimum swath overlap place specific tolerances on orbital period. The most significant perturbation on the orbit is from atmospheric drag which causes altitude decay, and therefore, period variations. The frequency and magnitude of the orbit maintenance to correct for atmospheric drag is a function of the spacecraft ballistic parameter ( $M/C_D A$ ) and the allowable swath overlap. Presented in Figures 2-4 and 2-5 are estimates of the frequency and magnitude of orbit maintenance as a function of altitude and ballistic parameter.

#### 2.1.2 Analysis

The selection of orbital altitude not only governs the frequency of earth surface coverage but also the pattern of coverage. As stated above, the numerator,  $n$ , of the fractional part of a  $Q$  determines the trace pattern. Considering 16 and 17-day repeat cycles, Figure 2-6 indicates the relationship between altitude and the quantity  $n$ . Figures 2-7 and 2-8 present the trace patterns for all values of  $n$  for a 17-day repeat cycle.

A primary factor in the selection of a trace pattern was the optimum utilization of the ability of the high-resolution pointable image (HRPI) to be offset up to  $\pm 30$  degrees from the down nadir direction ( $\pm 45$  degrees offset should also be considered). This capability is essentially the same as providing an effective increase in the swathwidth and with proper selection of the trace pattern can permit full global coverage in a significantly shorter time than the repeat cycle.\* For example, consider  $Q$  equal  $14 \frac{6}{17}$  and  $14 \frac{11}{17}$ . Figure 2-9 illustrates this case with the 100 nm swath and an offset of 30 degrees (the HRPI swathwidth is 25.9 n mi). Note that the

---

\* The capability to observe any point on the globe, not to collect data from each point.

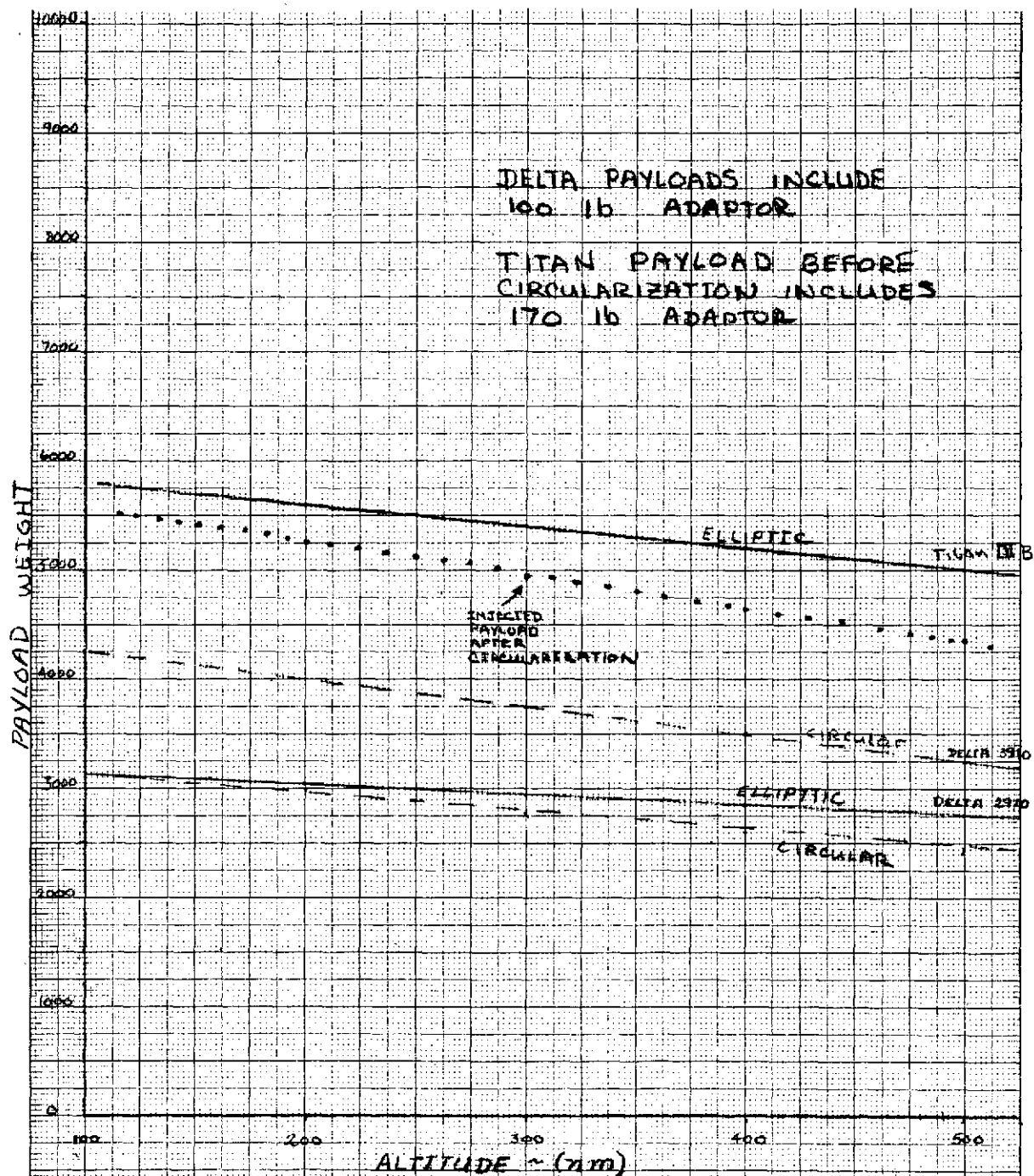


Figure 2-3. Launch Vehicle Payload Capability

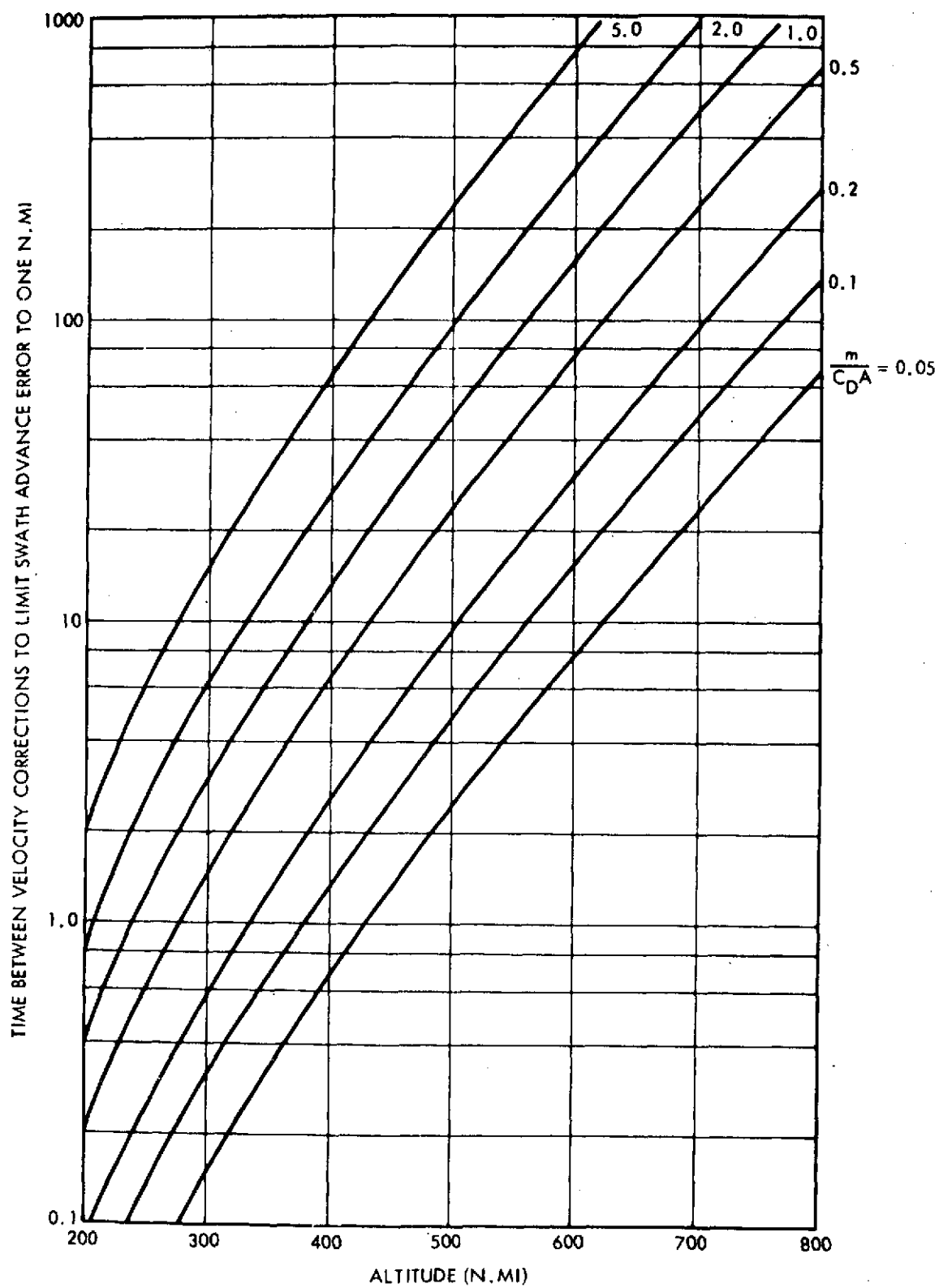


Figure 2-4. Frequency of Velocity Corrections Per Nautical Mile Swath Advance Error

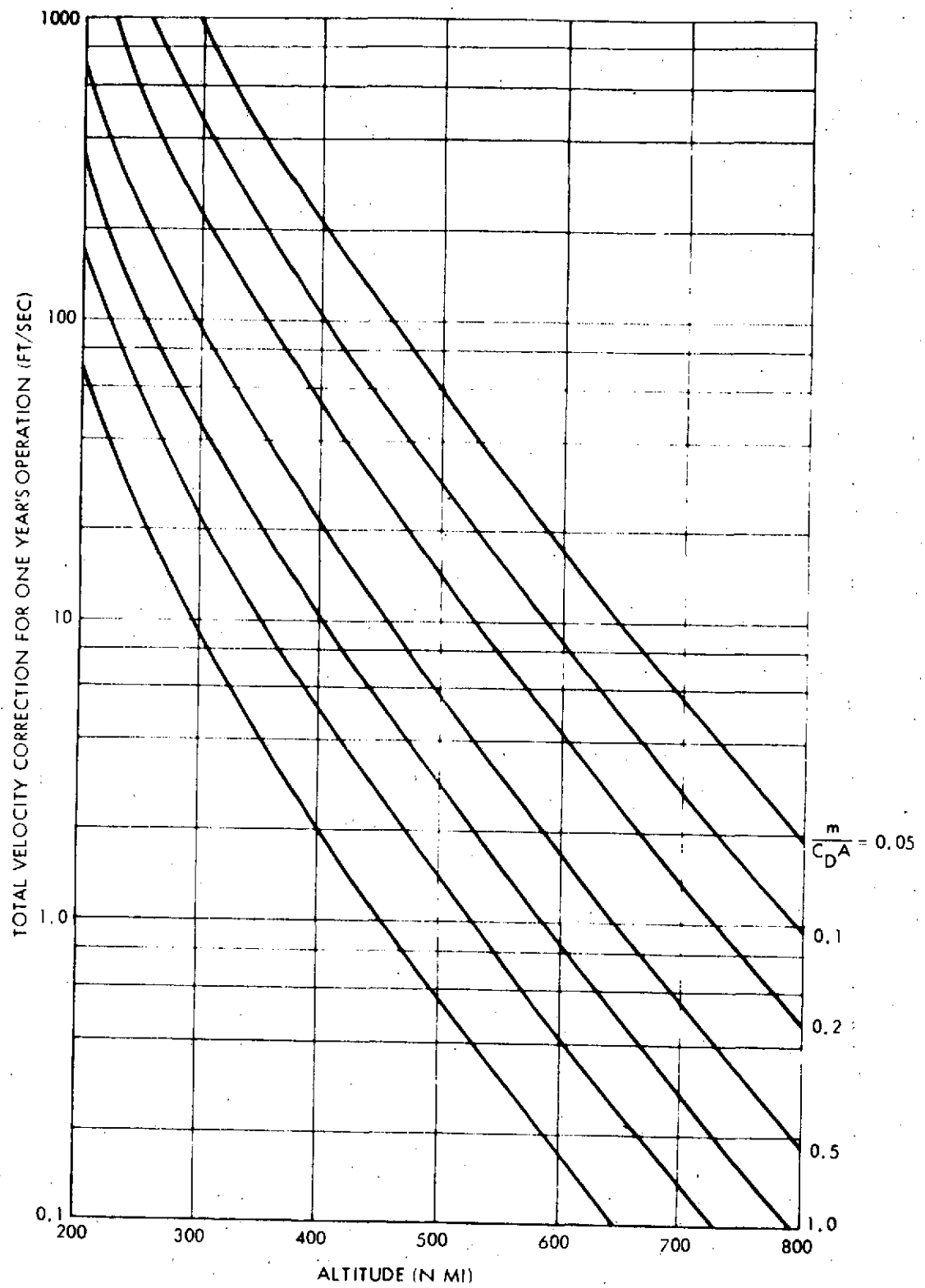


Figure 2-5. Total Velocity Correction Required for One Year's Operation

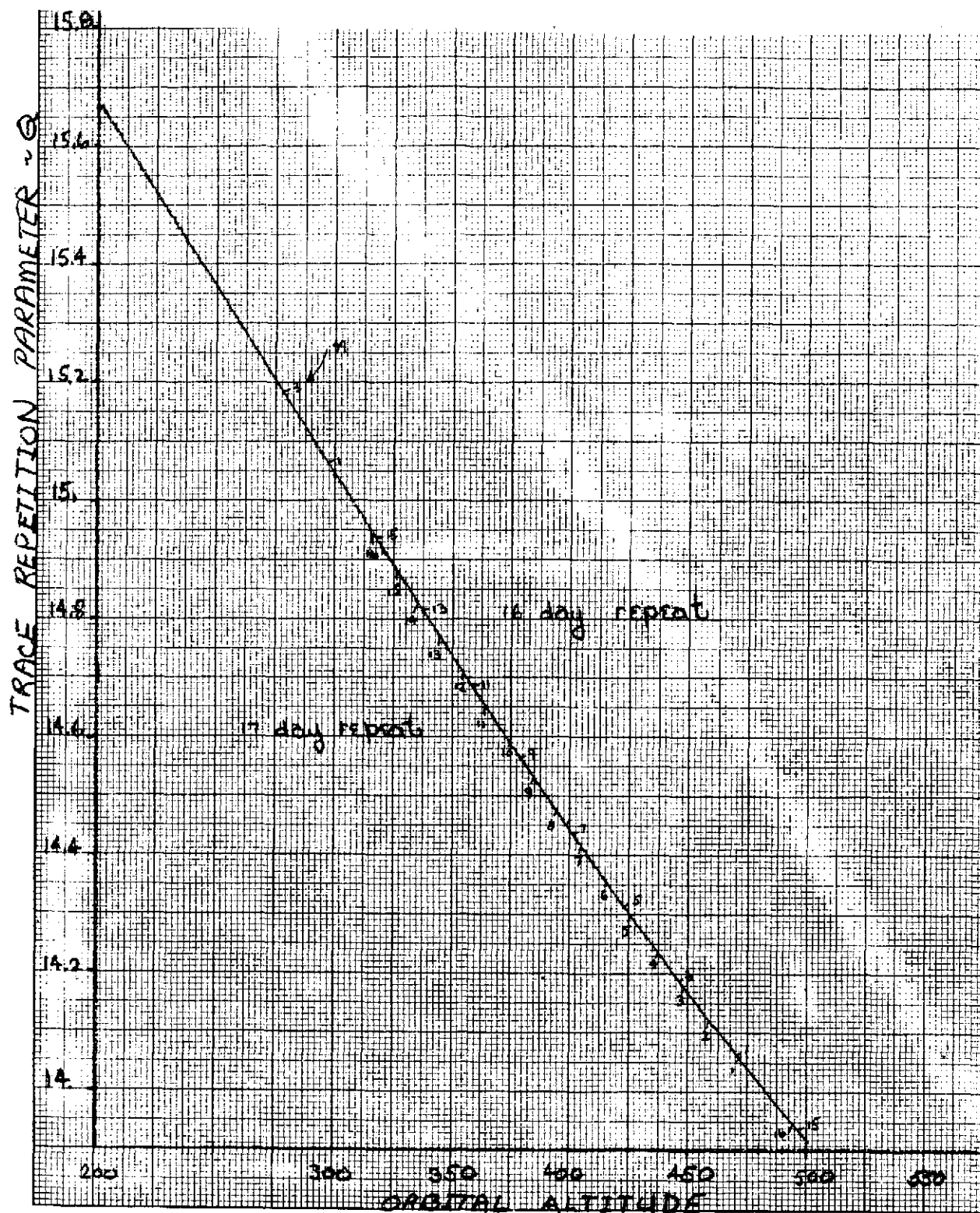


Figure 2-6. Trace Parameter for 16 and 17 Repeat Cycles

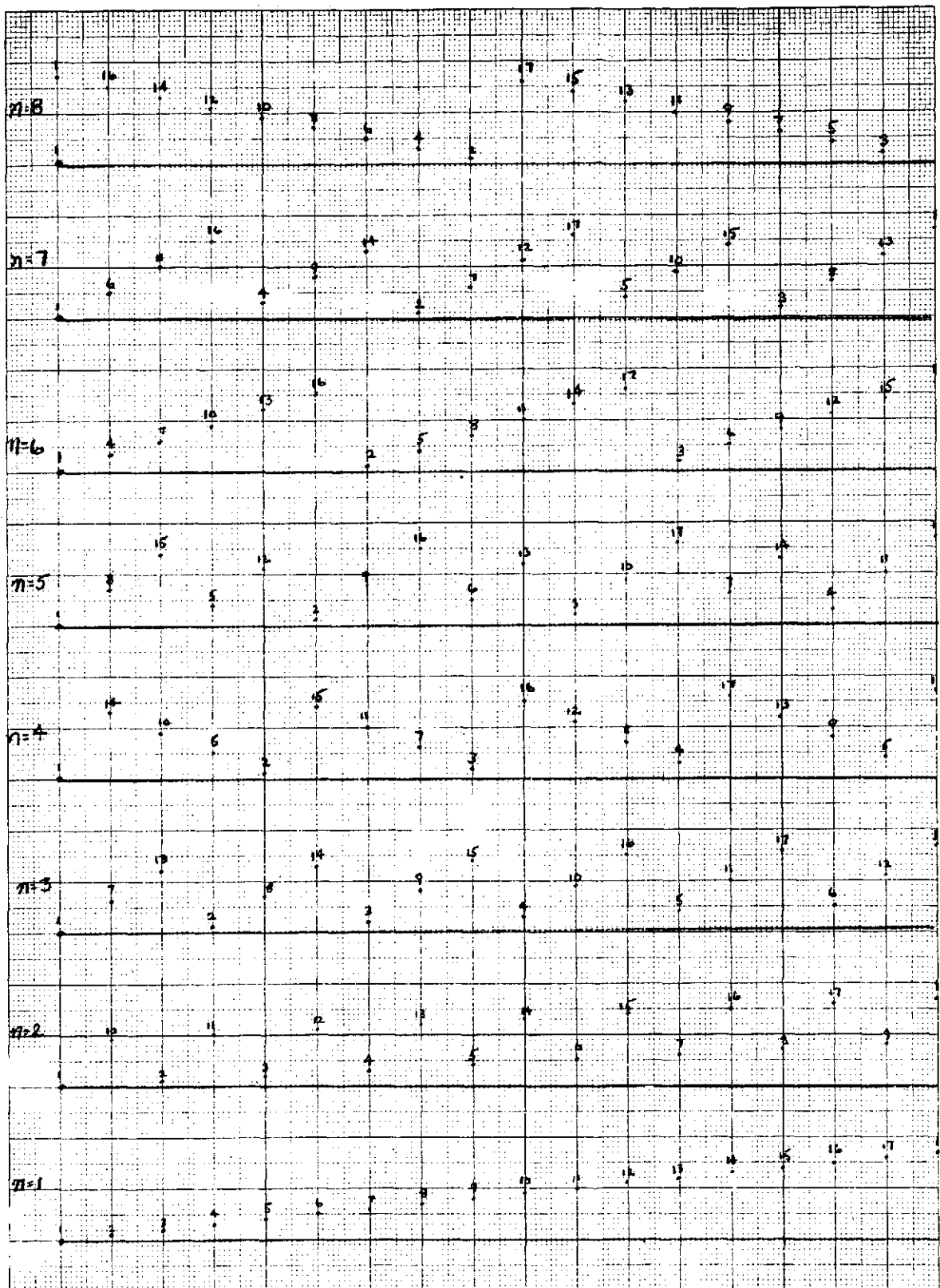


Figure 2-7. Trace Pattern

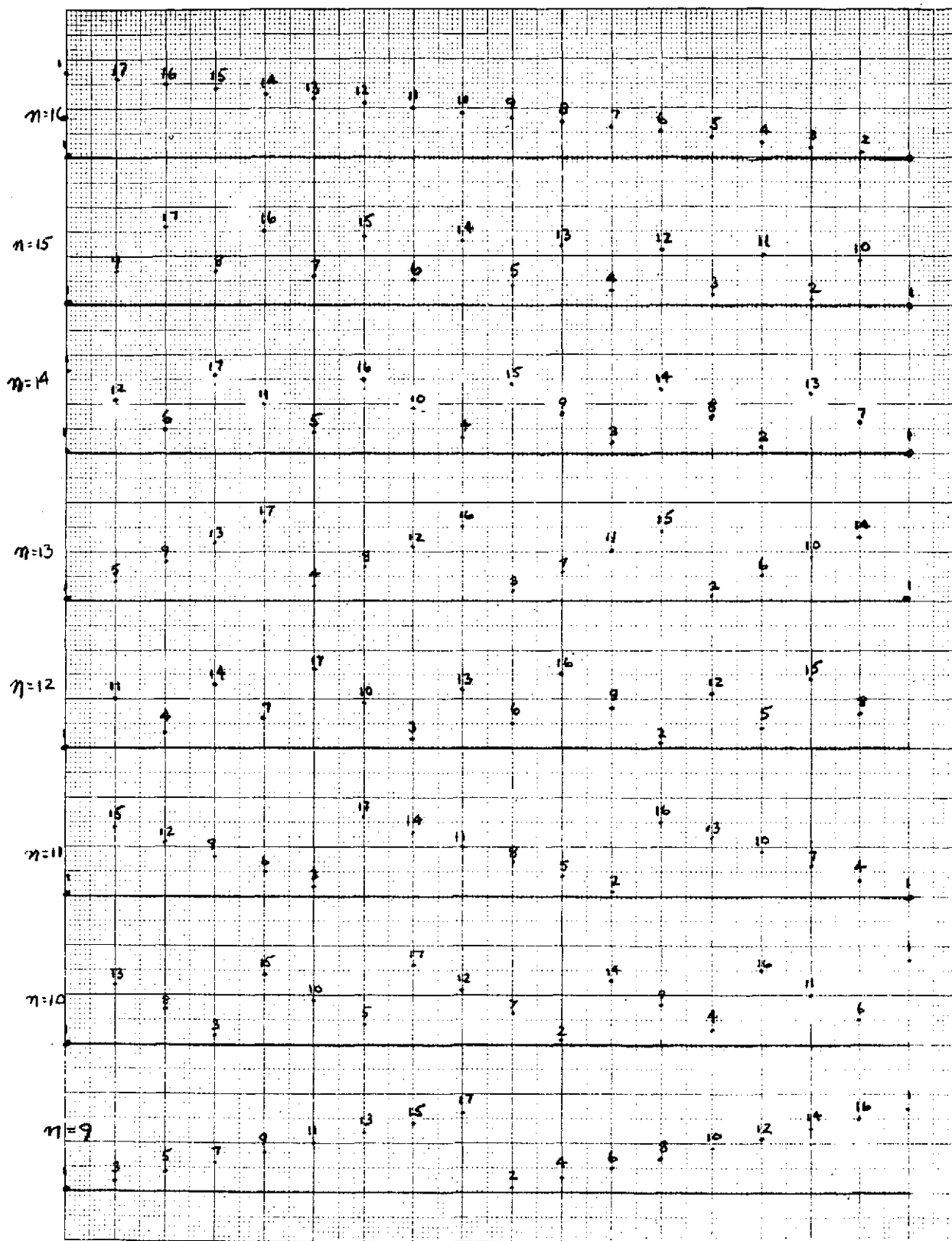


Figure 2-8. Trace Pattern

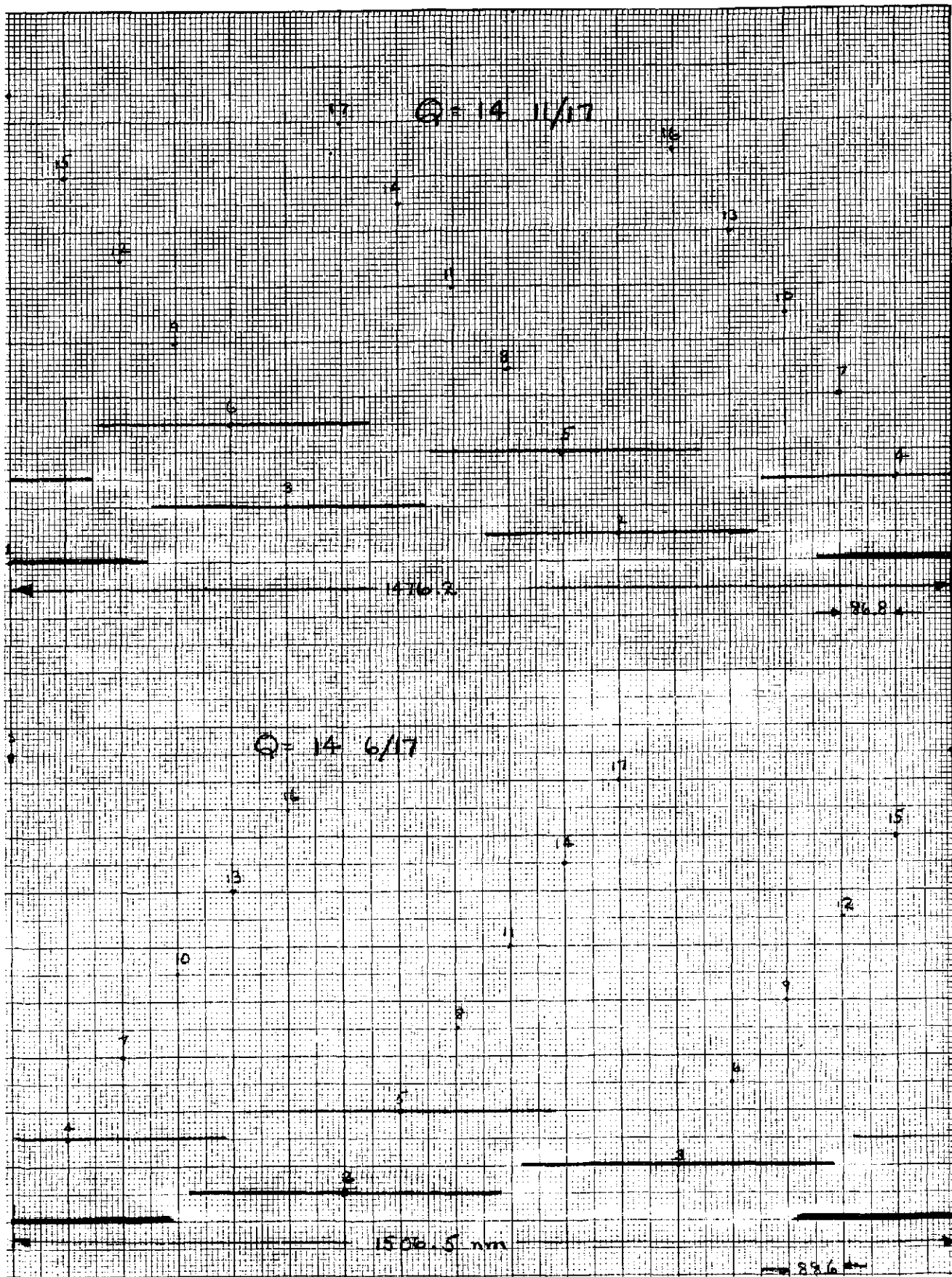


Figure 2-9. HRPI Offset Considerations



offset capability can permit full coverage in 5 days for  $n = 6$  and 6 days for  $n = 11$ . Table 2-1 presents the time required for full coverage for 17-day repeat cycle trace patterns for both a 30- and 45-degree offset.

For  $n$  equals 9 and a 45-degree offset, coverage is permitted every 2 days, as shown in Figure 2-10. Reducing the offset to 30 degrees permits coverage every 9 days. However, by moving the offset to a value slightly greater than 30 degrees, the full coverage could be obtained in 5 days.

Table 2-1. Reduction in Coverage Time for 17 Day Cycle by HRPI Offset

n	Days for Full Coverage -Offset-		Altitude (nm)
	30°	45°	
1	12	7	471.0
2	7	4	460.1
3	5	4	449.3
4	4	3	438.6
5	4	3	427.9
6	5	3	417.3
7	5	3	406.8
8	9	3	396.4
9	9	2	386.0
10	4	3	375.7
11	6	3	365.5
12	7	3	355.3
13	5	4	345.2
14	6	4	335.2
15	8	6	325.2
16	14	11	315.3

### 2.1.3 Conclusions

The two primary criteria for the selection of a baseline EOS-A mission orbital altitude are the launch vehicle capabilities and the global coverage characteristics. An additional factor which does enter into the selection process is the ability of the Shuttle to reach the orbital altitude for in-orbit maintenance. Because of the large difference in launch vehicle performance characteristics, both a Delta and Titan EOS configuration was considered.

The Delta baseline orbit will be limited to altitudes below 350 n mi. A baseline altitude of 335.2 n mi was selected since coverage could be reduced to 6 days with a 30-degree HRPI offset.

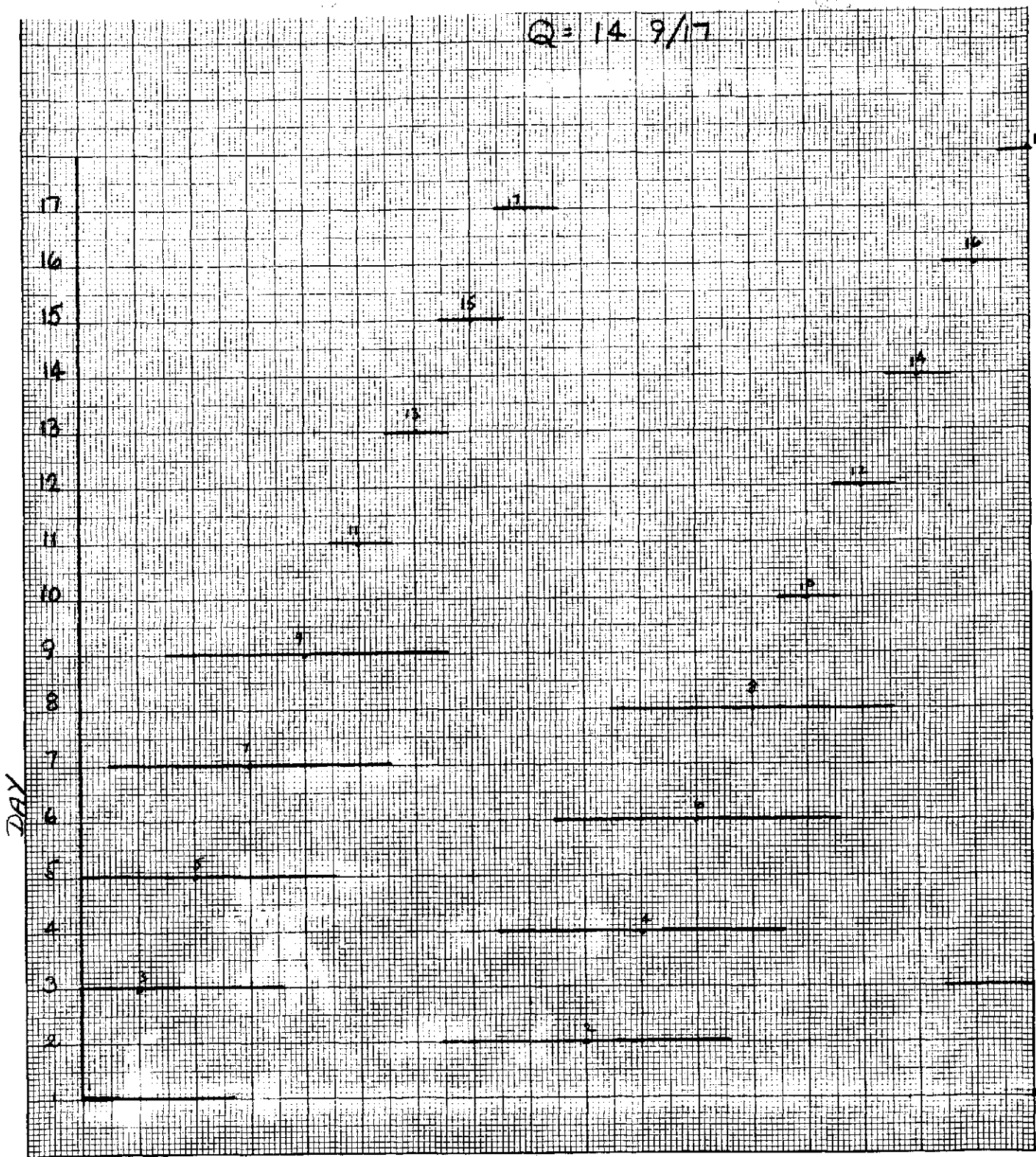


Figure 2-10. Coverage for 30° HRPI Offset

The Titan baseline orbital altitude is 386 n mi because of the possible 2-day coverage ability with a 45-degree HRPI offset. It should be noted, however, that relatively small changes in altitude about the baseline can change the coverage pattern significantly as indicated in Table 2-1. Therefore, the data presented for the baseline orbits such as ground station coverage and illumination are representative of the various trace patterns available in the same altitude range.

A sun-synchronous orbit is one that maintains a constant angle between the mean sun and the orbit plane of the spacecraft. Therefore, sun-synchronous orbits have the desirable property of minimizing variations in the angle between the sun and the local vertical at the subsatellite point (the solar illumination angle) at a given altitude throughout the year. Variations of this angle at a given latitude arise because of ellipticity of the earth's orbit about the sun and the angle of the axis of rotation of the earth with the ecliptic plane. The selection of the orbital node relative to the mean sun will dictate the solar illumination angle. Current user requirements have established the relative node at -15 degrees (referred to as an 11:00 a.m. orbit). Slight variations in solar illumination angle history occur depending on whether the node is ascending (northbound) or descending (southbound). Both cases are presented.

Table 2-2 presents the orbital data for each of the two EOS configurations. Figures 2-11 and 2-12 present the solar illumination angle variations for the Delta configuration. Figure 2-12 illustrates the orbital ground trace for a typical day for the Titan configuration. Also indicated are the visibility contours for the Goldstone and Goddard ground stations.

Figure 2-13 presents the orbital maintenance data for ballistic parameters corresponding to the Titan and Delta configurations.

It should be noted that if drag decay orbit maintenance maneuvers were made every 17 days, this maneuver would ensure precise repeat coverage every cycle.

Table 2-2. Baseline Orbits

	Titan	Delta
Altitude (nm)	386	335.2
Inclination (deg)	98.25	97.7
Trace Parameter	14 9/17	14 14/17
Node (deg)	11:00 A.M.	11:00 A.M.
Period (hours)	1.652	1.659
Orbit Achievement $\Delta V$ (ft/sec)	480.9	0.
S/C weight (lbs)	5000	2750
Area (ft <sup>2</sup> )	145	50
$C_D$	2.4	2.4
Orbit Maintenance		
total $\Delta V$ (ft/sec)	29	34
frequency $\frac{\text{days}}{\text{sw error allowed}}$	2.4	3.8

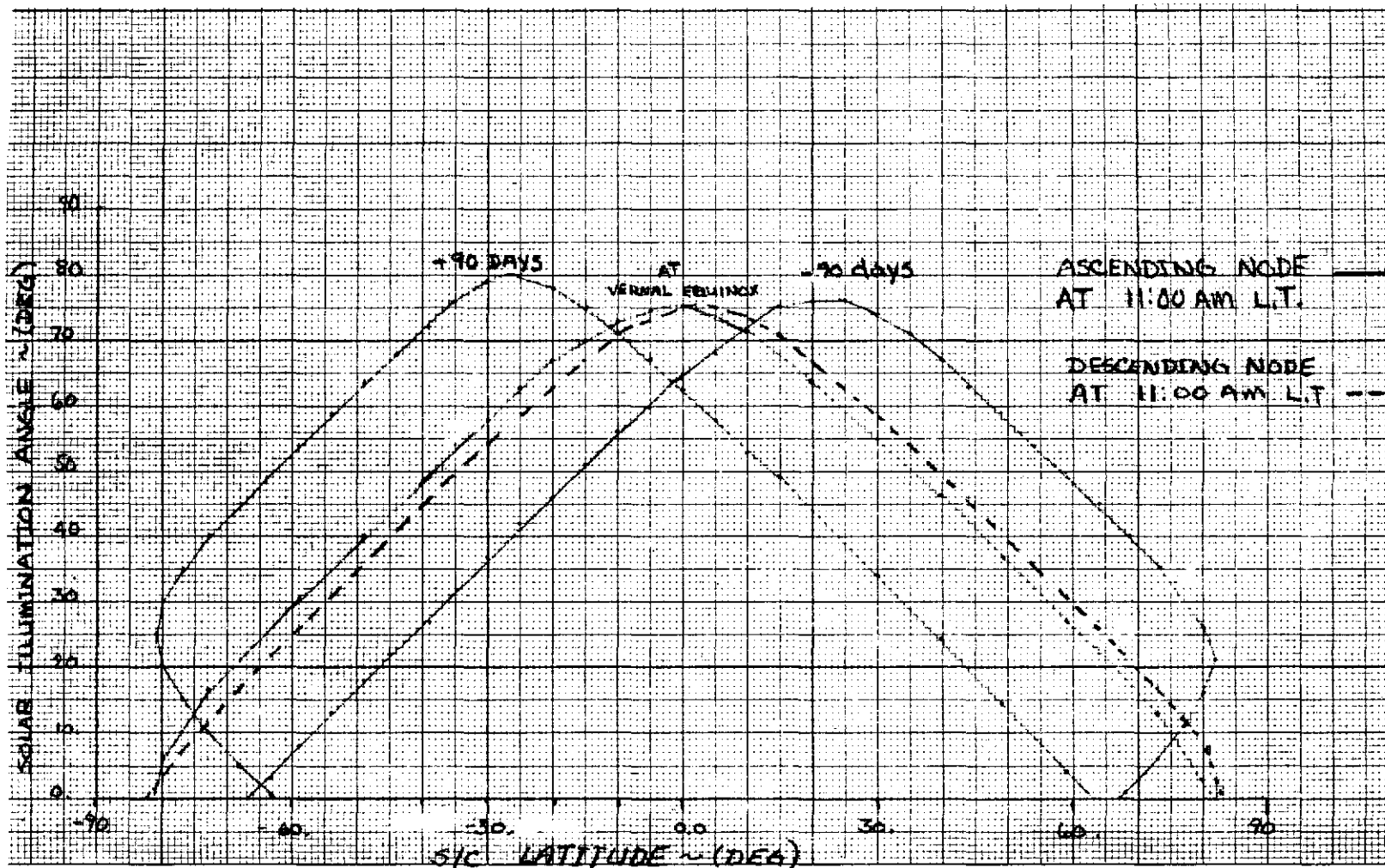


Figure 2-11. Solar Illumination for 11 a.m. Orbit

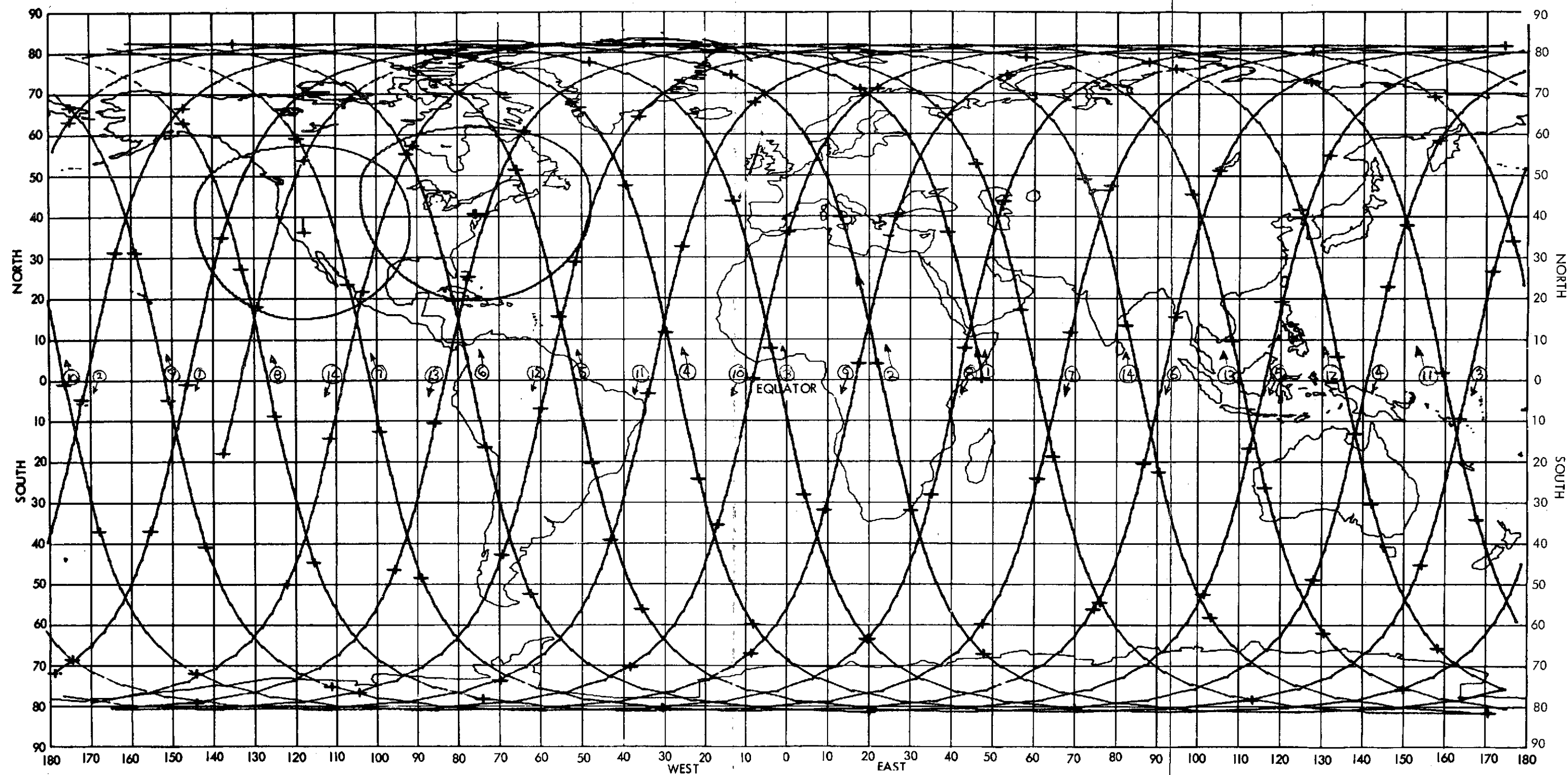


Figure 2-12. Typical EOS Daily Ground Trace

FOLDOUT FRAME 1

ORIGINAL PAGE IS  
OF POOR QUALITY

FOLDOUT FRAME 2

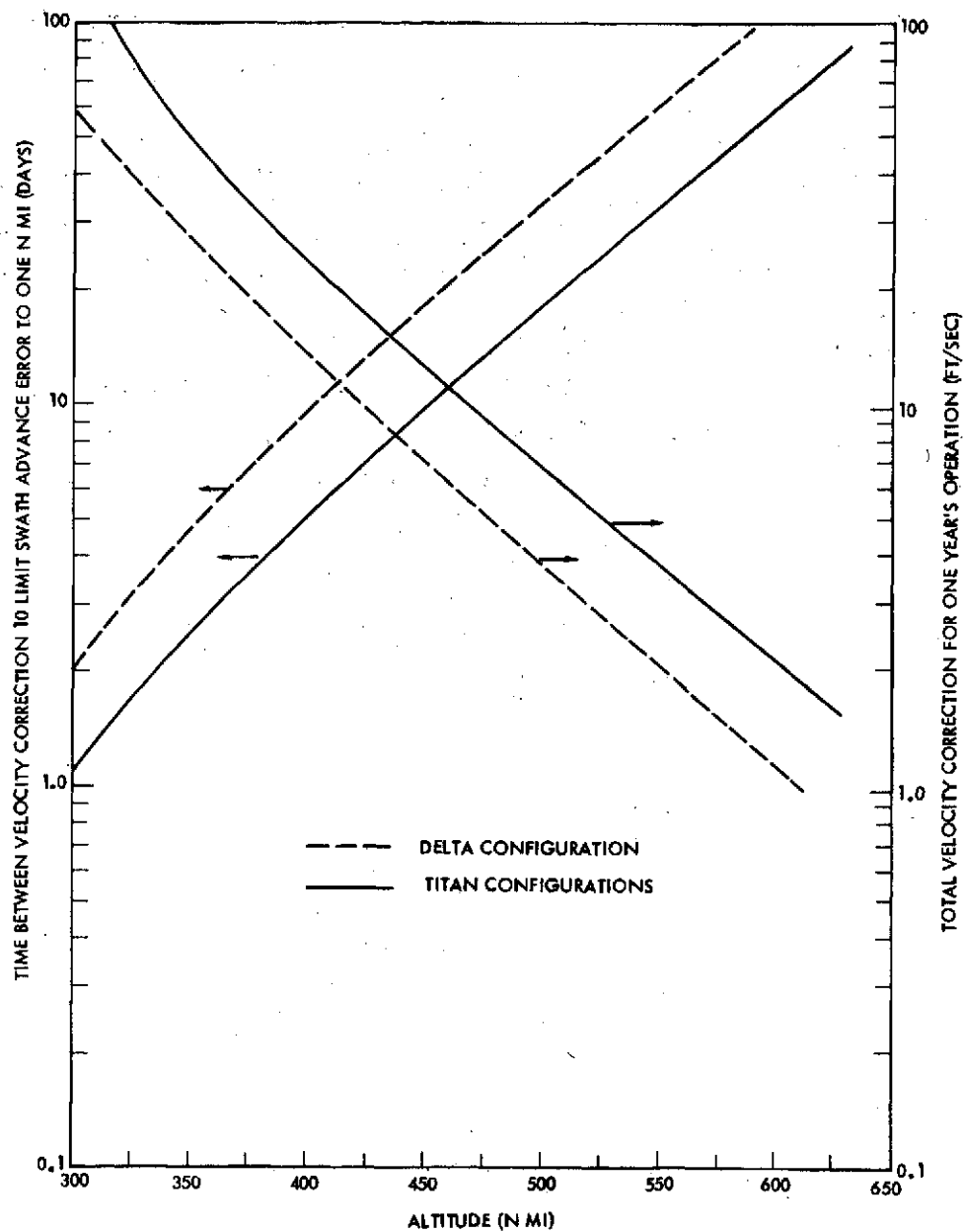


Figure 2-13. Orbit Maintenance

PRECEDING PAGE BLANK NOT FILMED

## 2.2 ORBIT TRANSFER REQUIREMENTS

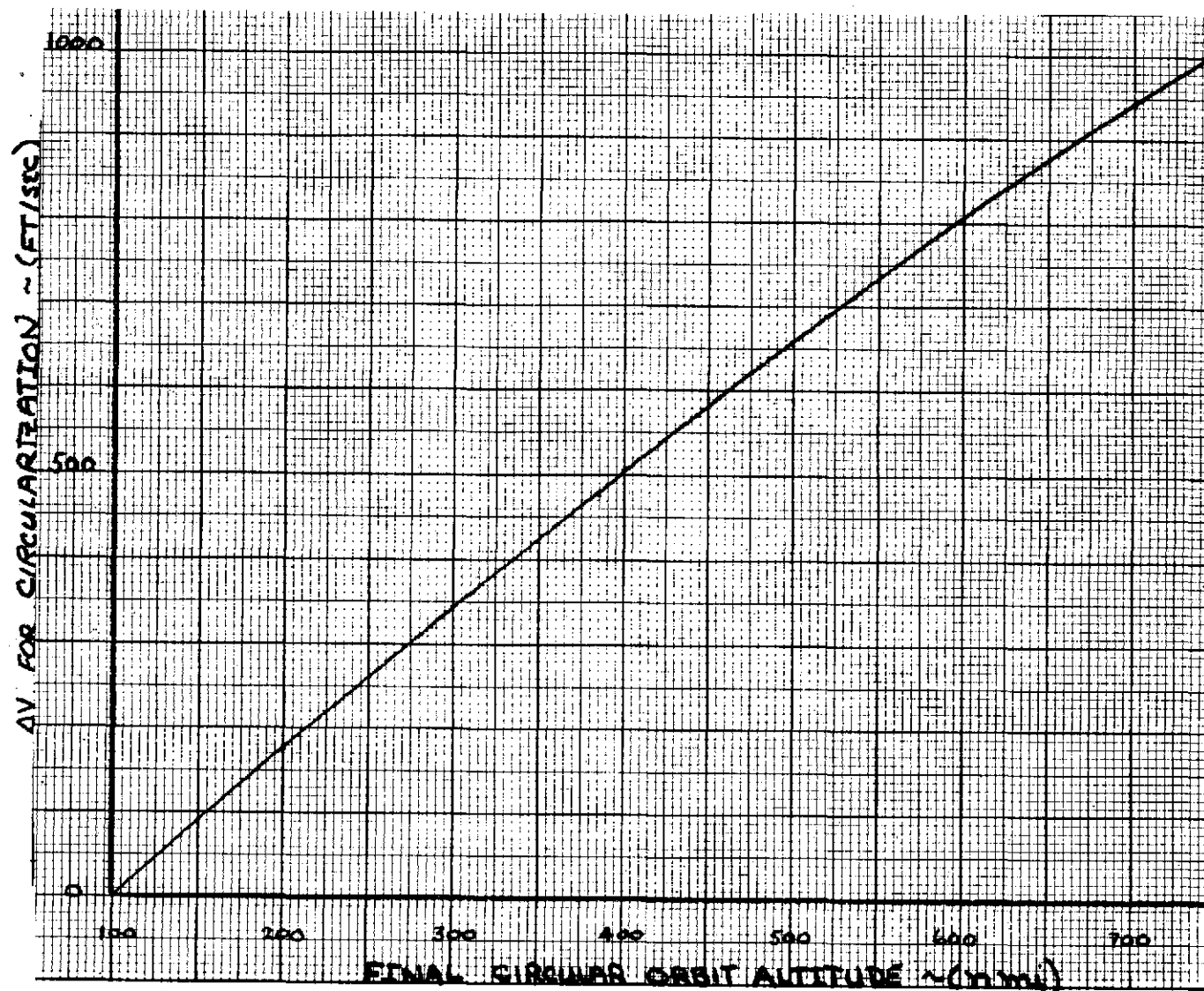
The inability of the Titan and Shuttle launch systems to place the EOS into circular orbits places the requirement on the EOS to provide the impulse to circularize the insertion elliptical orbit. In addition, the spacecraft may also be required to provide the impulse to deorbit from the circular orbit to an elliptical orbit on which the Shuttle can effect rendezvous for maintenance and refurbishment.

The impulsive  $\Delta V$  required to circularize an elliptical orbit at its apogee altitude (perigee at 100 nm) is given in Figure 2-14. The same  $\Delta V$  is required to deboost the spacecraft from the circular orbit to an elliptical servicing orbit with an apogee altitude equivalent to the circular altitude.

While in an elliptical servicing orbit the relative nodal rates will change the orientation of the original and servicing orbital planes. The  $\Delta V$  to correct the node error per day of drift is given in Figure 2-15.



BEE 20x20 TO INCH

Figure 2-14. Circularization  $\Delta V$  Requirements

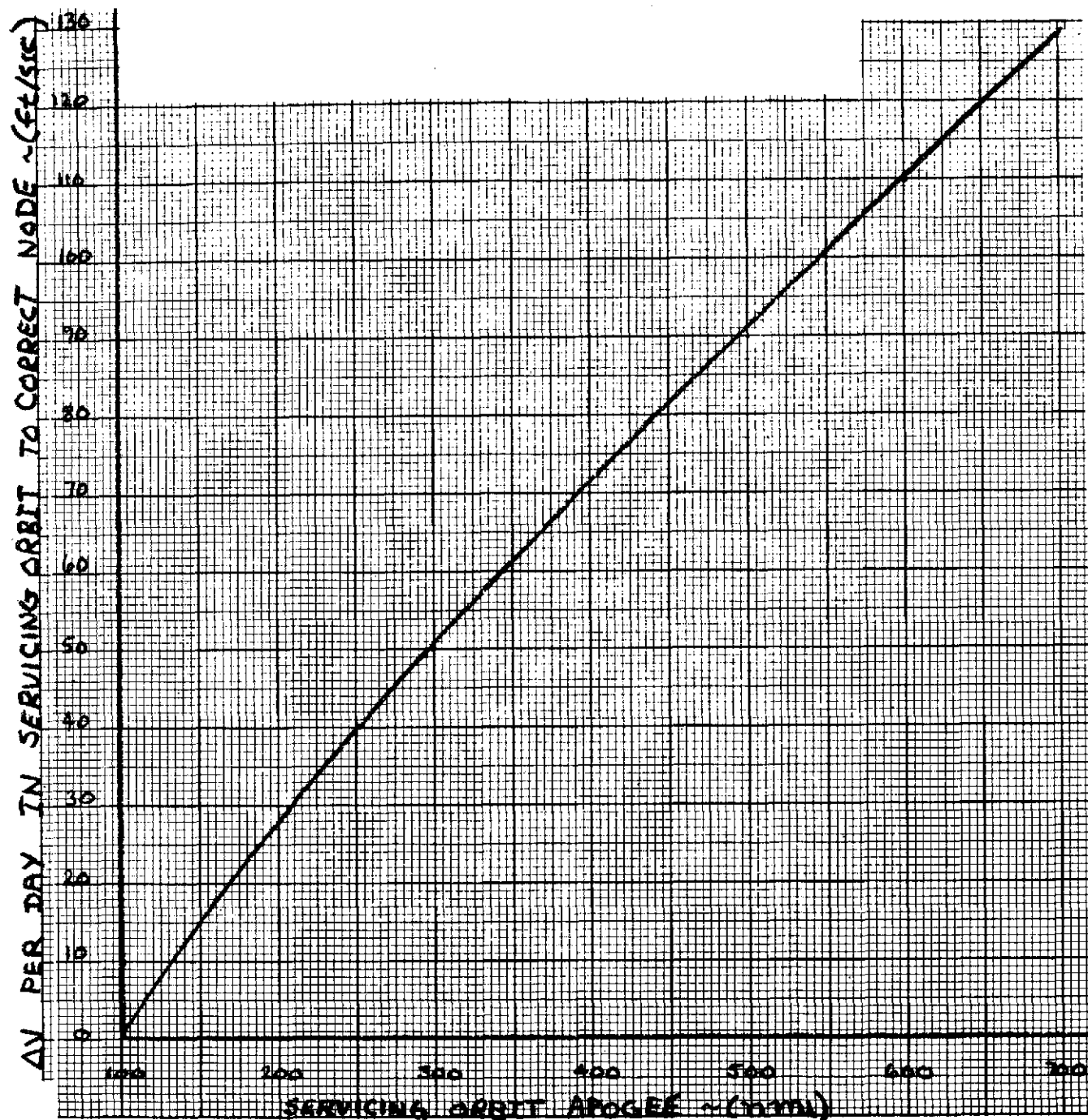


Figure 2-15. Node Drift Correction  $\Delta V$

## 2.3 MULTIPLE SPACECRAFT SERVICING

The ability of the Shuttle to service more than one spacecraft during a single flight is determined by the  $\Delta V$  capability available. If required, the spacecraft to be serviced by the Shuttle will provide the impulse to transfer into an elliptical servicing orbit if the Shuttle cannot achieve the operational circular orbit. The Shuttle must then perform all additional maneuvers required for rendezvous. The maximum total on-orbit Shuttle  $\Delta V$  capability for servicing missions was assumed to be 2500 ft/sec.

This capability dictates the classes of orbit transfers available for servicing for EOS missions.

- Transfer between two sun synchronous orbits at different altitudes with no node difference
- Transfer between two sun synchronous orbits at same altitude and with a node difference
- Removal of phase angle between two spacecraft in same sun synchronous orbit

### 2.3.1 Analysis

Since the inclination of a sun synchronous orbit is a function of the orbital altitude, transfer between sun synchronous orbits includes both an altitude and inclination change. The  $\Delta V$  requirements for transfer between sun synchronous orbits with the same node are presented in Figure 2-16. The data indicate that approximately 300 nmi altitude changes are possible with the Shuttle  $\Delta V$  capability. The  $\Delta V$  required for orbit plane changes are presented in Figure 2-17. The maximum node change (with no inclination change) for  $\Delta V$  capability is six degrees (24 minutes change in local time of equator crossing). An alternate approach to node change maneuvers directly would be an altitude change to modify the nodal rate caused by the earth's oblateness. The difference in node rates between the two orbits would cause the nodes to drift and decrease (or increase) their relative difference. Figure 2-18 presents the relative drift rates between various apogee altitude elliptical orbits with 100 nm perigee and sun synchronous orbits. The data indicate that for a 500 nm apogee, a one degree drift is obtained every five days. Time restrictions imposed on Shuttle mission duration limits the node reduction available by this method.

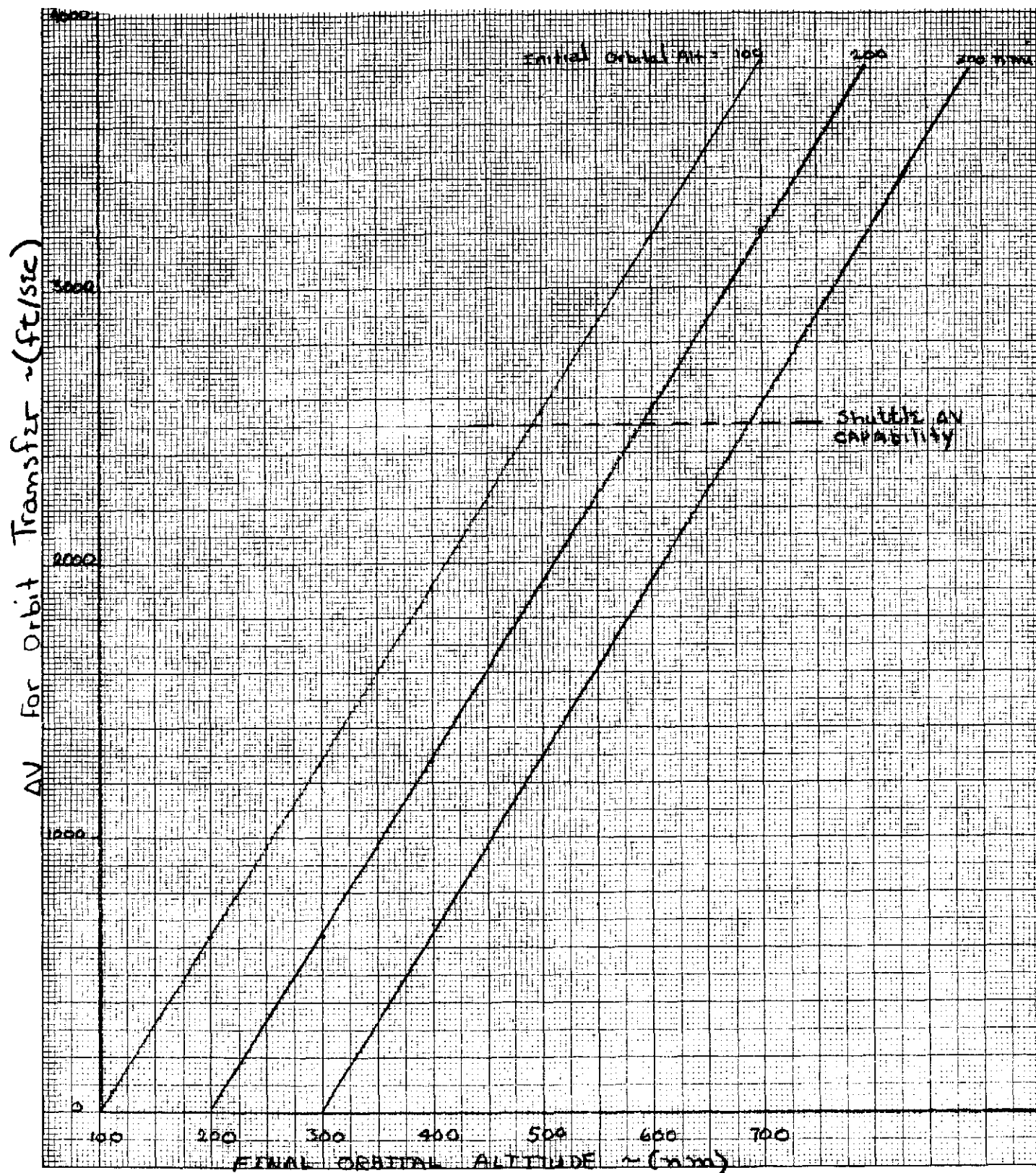


Figure 2-16. Transfer Between Sun-Synchronous Orbits

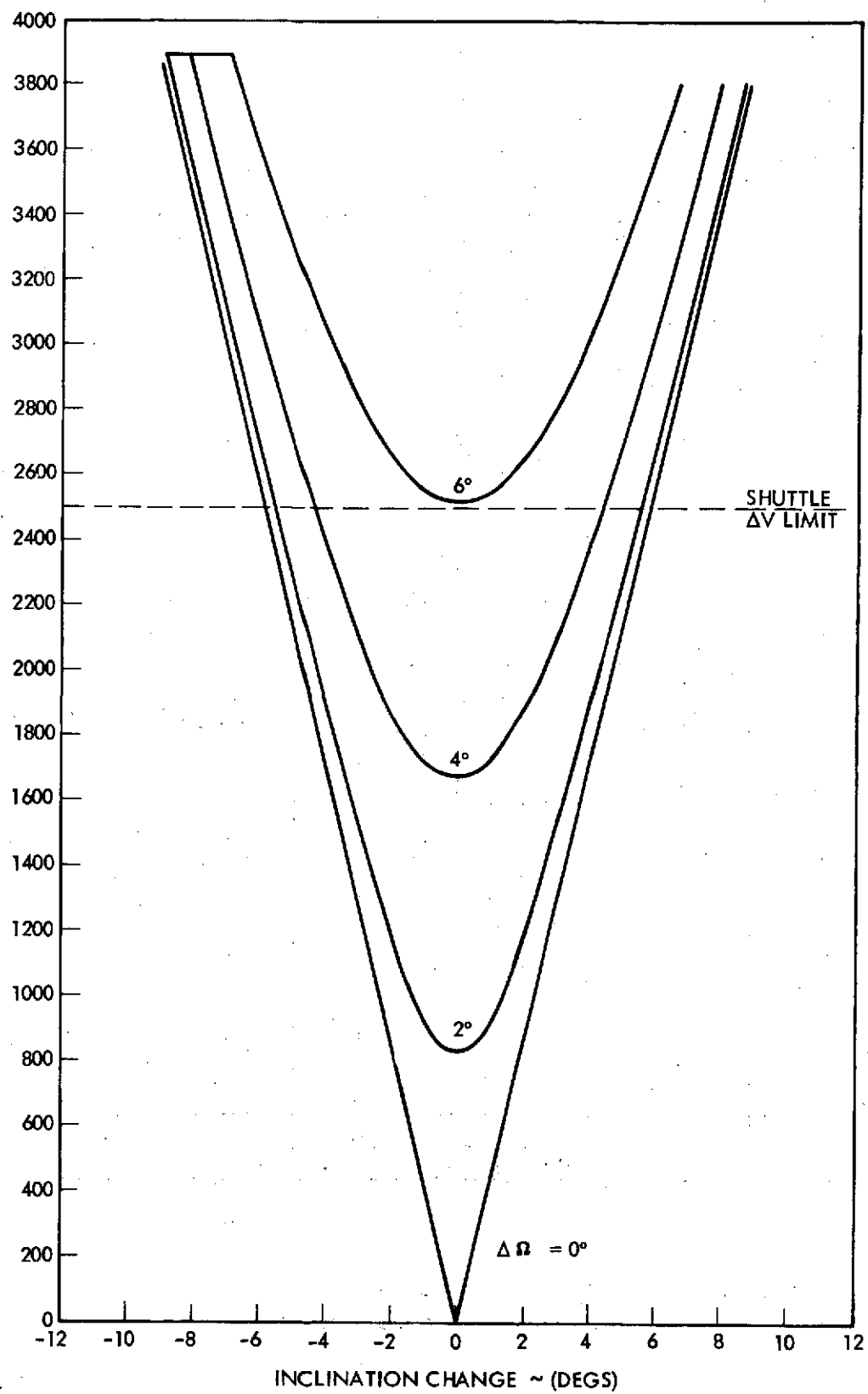


Figure 2-17.  $\Delta V$  Requirements for Plane Change

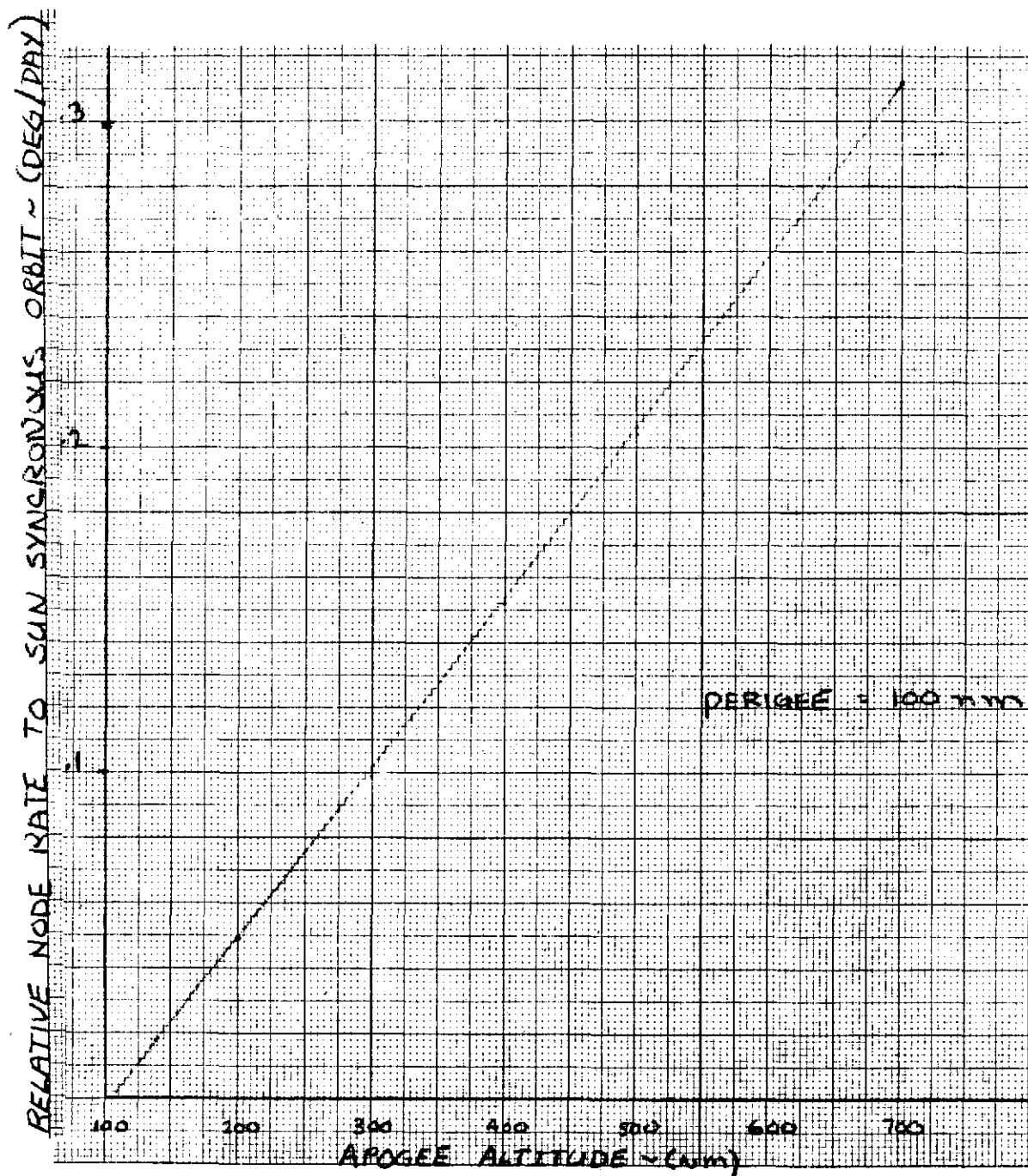


Figure 2-18. Node Drift Rates Relative to Sun-Synchronous Orbits

Multiple spacecraft servicing could also be carried out with two spacecraft in the same orbit but placed at different positions relative to each other. The Shuttle would then be required to transfer to an intermediate phasing orbit and then return to the servicing orbit and rendezvous with the second spacecraft. Figure 2-19 presents the  $\Delta V$  required to perform these maneuvers as a function of the phase angle reduction per day.

### 2.3.2 Conclusions

The Shuttle  $\Delta V$  capability limits the orbital maneuvers between two orbits to the following missions:

- Two sun synchronous orbits at same altitude (and thus inclination) and an equator crossing time difference of 24 minutes
- Two sun synchronous orbits with same equator crossing time and an altitude difference of 300 nm
- Two spacecraft in the same orbit with any phase difference.

The probability of any of the above missions existing is small and does not justify further examination of multiple spacecraft Shuttle servicing at this time.

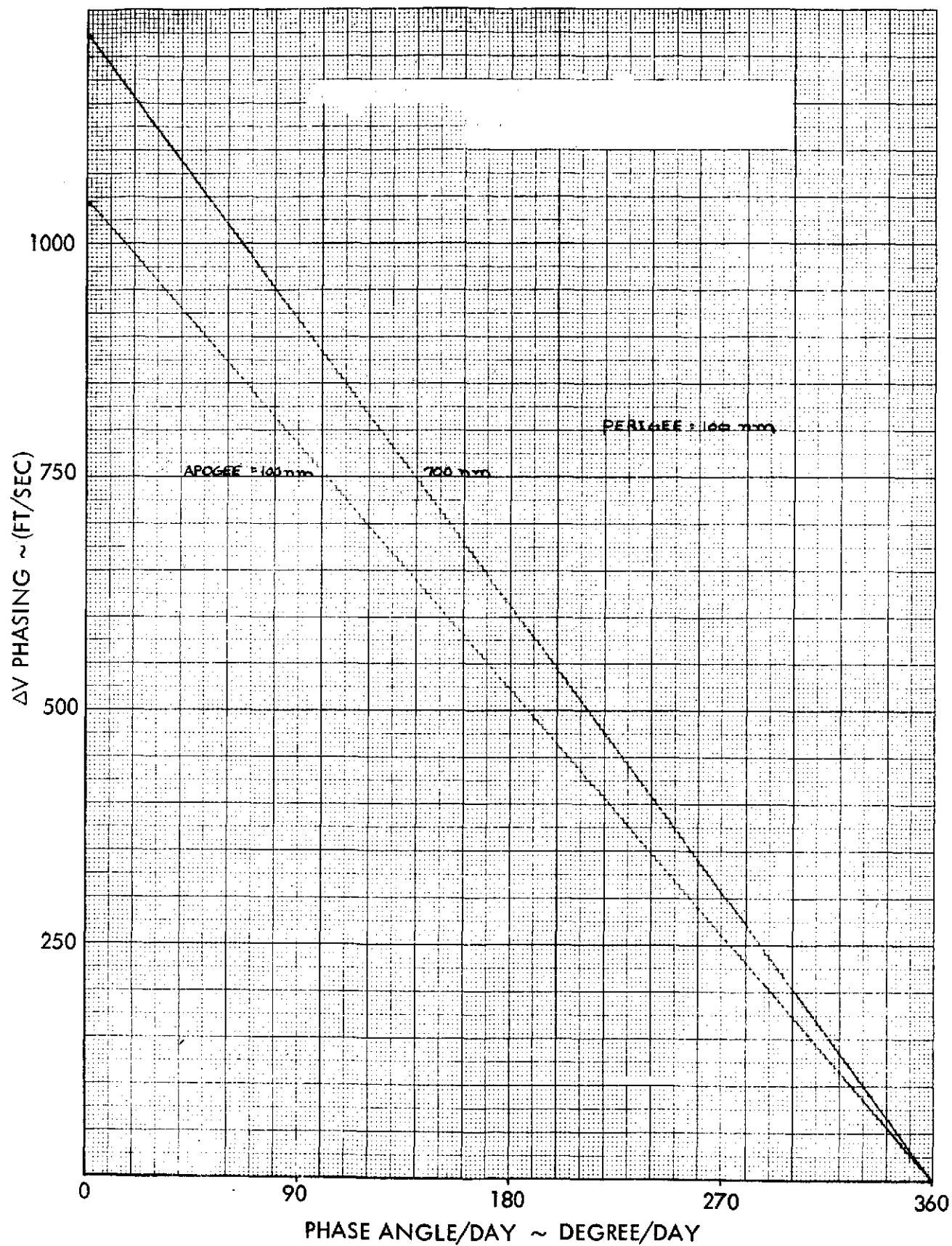


Figure 2-19.  $\Delta V$  Required for Phase Angle Reduction



### 3. SHUTTLE INTERFACES

#### 3.1 MEMS APPLICABILITY

EOS interface with the MEM (Module Exchange Mechanism, also SPMS, Special Purpose Manipulator System) is critical to the whole concept of on-orbit replacement of spacecraft modules. MEM is well along in development by the SPAR Canadian Consortium, with a working mock-up to be completed soon. Several inconsistencies must be resolved by us (together with Rockwell and SPAR) within the immediate future to assure compatibility.

##### 3.1.1 Discussion

The MEM is a fairly rigid manipulator system (see Figure 3-1), which grasps modules, operates their latches, and exchanges new for old between EOS and the storage magazine. The most recent philosophies (from SPAR) are:

- Four "Arms" to simultaneously grab and operate four latches at the corners of a module.
- A second set of arms such that MEM can hold two modules at once (alleviating the requirement for temporary storage).
- MEM must now operate in 1 g (with some counterbalancing) probably accounting for the four arms as opposed to two or one.
- SPAR intends to use a single motor size (with different gear boxes) for all functions.
- MEM Specifications -- Notice the  $\pm 0.25$ -inch precision (No. 5) in positioning of a module for replacement.
- The movements of MEM will now be semi-automatic. That is, the astronaut/operator will be required to "juggle" MEM during the last few inches in all degrees of freedom to account for the 0.25 inch misalignment of module to EOS during insertion (grasping, removal, etc.). Gross movements, traversing from EOS to magazine, etc., will be automatic, controlled by software, initiated by a command, and over-rideable.

1.	Classification	High Force, High Precision Orthogonal Axis Module Exchange System, Man-In- The-Loop
2.	Working Stroke	130 in. in X-Axis 214 in. in Z-Axis 40 in. in Y-Axis
3.	Tip Force	300 lbs through 18 in. Travel
4.	Stiffness of Structure	230 lbs./in. (At Full Extension)
5.	Precision (No Load)	$\pm 0.25$ in.
6.	Speed of Operation	1 in./sec. (Unloaded) 0.10 in./sec. Module Engage Under 300 lb. load
7.	Stopping Distance	0.25 in. at 1 in./sec. with 900 lb. Mass
8.	Dexterity & Control	4 DOF, Force Feedback Control, Visual Position Sensing
9.	Storage Capacity	Up to 9 Spacecraft & Instrument Modules
10.	Weight	2840 Lbs. (Appendix C)
11.	Operational Power	250 Watts
12.	Cycle Time	15 Minutes Nominal
13.	Flight Environments	Shuttle Launch and Orbit

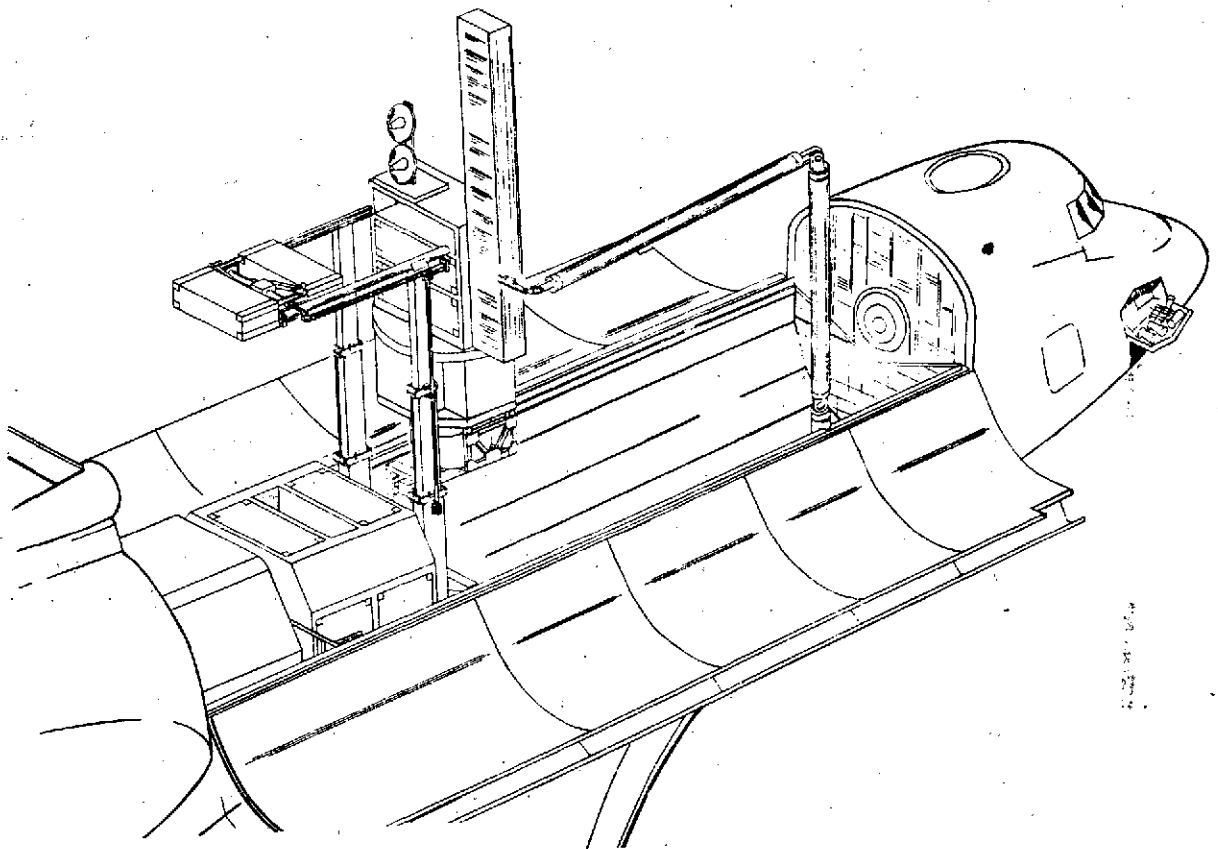


Figure 3-1. The MEM System Shown Exchanging an EOS Module

### 3.1.2 Assumptions

It is assumed that astronaut controlled motions during "fit-up" will not induce excessive stresses in either module or EOS. (Not a brute force insertion, requiring him to have visual aids (TV), proximity indicators, tactile feedback, or some combination). This will be confirmed with Goddard or SPAR. It is also assumed that the MEM design will remain flexible enough to accommodate our recommendations and requirements such as latch operation (presently envisioned as a bolt torquing operation; refer to paragraph 3.1.5), ability to handle somewhat different module sizes (see below) and latching sequence command formats.

### 3.1.3 Areas of Concern

- Wideband communications module with antennas and propulsion/attitude actuation module compatibility with MEMS appears to be generally feasible, but further definition of their configurations is required for detailed analysis.
- Figure 3-2 depicts a discrepancy between our module sizes and MEM capability. This must be resolved with SPAR.
- The grappling, insertion, and latching operations are generally of concern with respect to tolerancing, thermal, and stress interaction. We must generate a specification of our own for MEM interface following module detailed design.
- The exchange between MEM and SAMS of special modules, (i. e., solar array) for forward bay storage is rather loosely defined. This is of concern to us since module latching and grappling are involved.

ORIGINAL PAGE IS  
OF POOR QUALITY

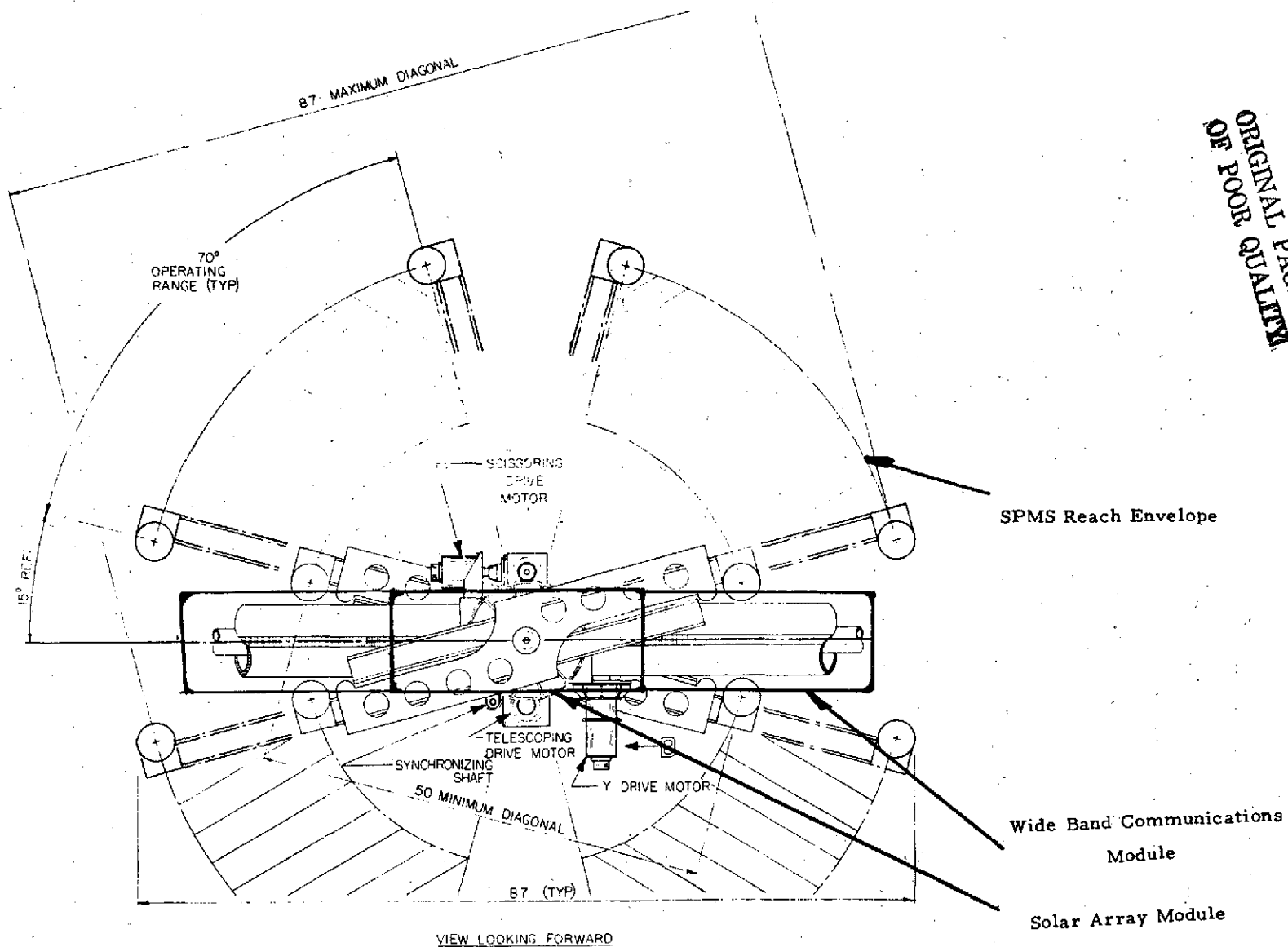


Figure 3-2. An Example of Two EOS Modules (Heavy Rectangles) Which are Outside Reach Envelope of Current SPMS

#### 3.1.4 Tradeoff and Decisions

It has become evident during initial configuration efforts that cantilivered modules, particularly those with long overhang such as wideband communication and data collection will require bolted (as opposed to spring preloaded) latches. This implies the MEM have the capability for rather significant latch torquing motion (around 125 - 140 ft-lb) which is probably easier to produce than the push-pull of early Goddard designs. It is also evident that a meeting with SPAR is required to resolve our interface and assure no future incompatibilities, particularly ; since the MEM system is advancing rapidly (a working mock-up, which mates the Goddard EOS version is currently under development).

#### 3.1.5 Description of Conceptual End Effector

Figure 3-3 shows a conceptual approach to a power driven latch design. It also presents an alternate system of captive attach bolt retention.

##### Latching System

The latching function is independent from the bolt driving function. Latching interface consists of an annular groove on the module, and a pair of latch dogs on the SPMS. The latch dogs are operated by double links which are attached to trunions on a recirculating ball nut. The ball nut is restrained from rotation by the links. The mating ball screw is attached to a bevel gear which is driven by a matching pinion providing a reduction ratio of 2.8. The latch drive motors are mounted such that they become extensions to the length of the telescoping tubes of the SPMS where clearance of other mechanisms is available. Limit switches are envisioned for each end of the ball nut travel to provide stop/start control for the latch drive motor.

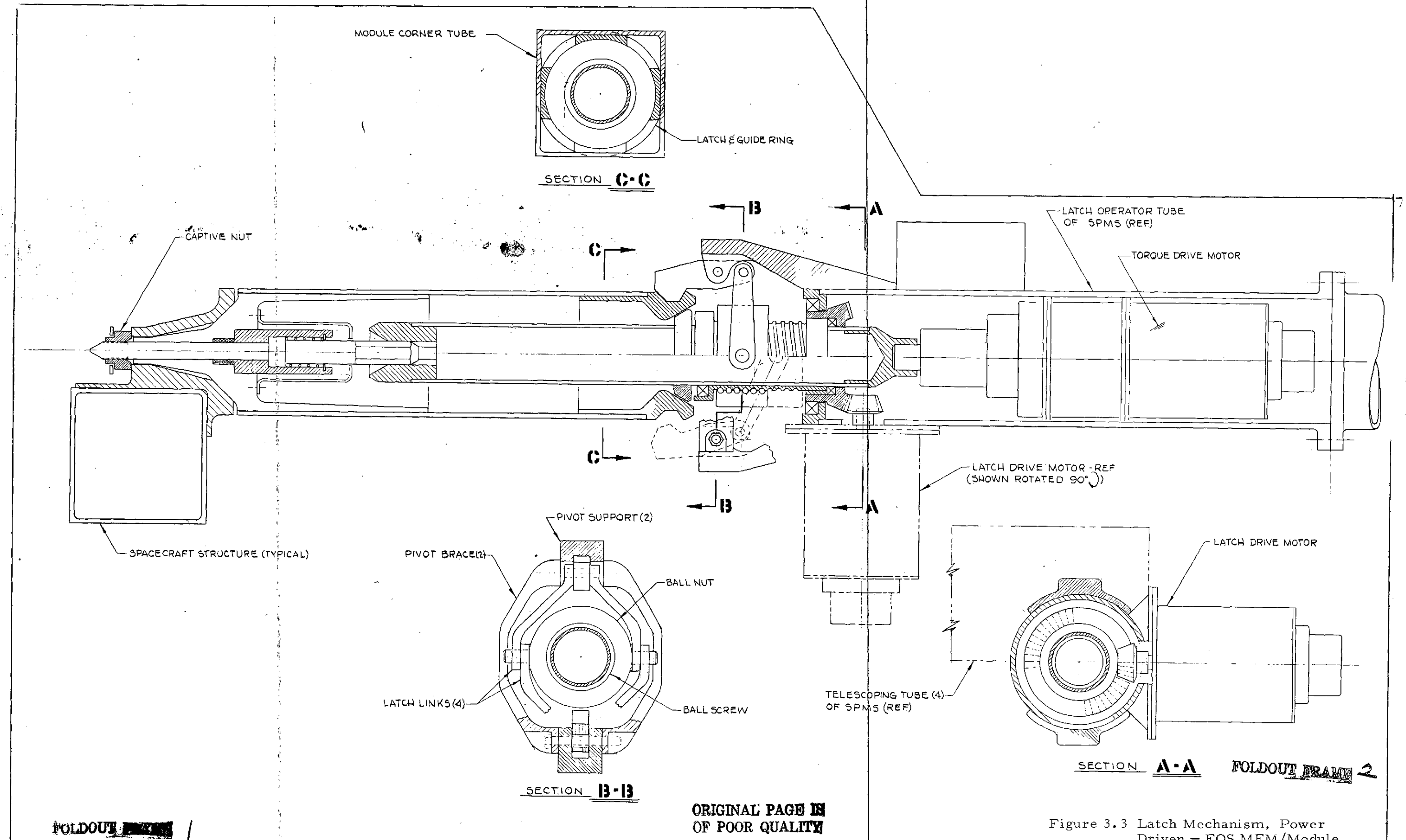


Figure 3.3 Latch Mechanism, Power Driven - EOS MEM/Module Interface

An engaged/disengaged sensor is also required to inform the latch drive system that the module and SPMS are in position for latch operation.

#### Bolt Torque System

The socket probe on the torque tube engages the captive bolt in the module corner tube. An indexing device (not shown) is required to align the socket with the bolt flats. The bolt is contained by a cylindrical carrier which permits a spring to provide soft but positive engagement of the bolt threads in the spacecraft captive nut. The bolt carrier is sprung in the opposite direction to assist withdrawal and to maintain static fixity of the bolt/carrier combination when the bolt is free at both ends. The torque tube is spline connected directly to the torque drive motor through a two stage gear reduction system. Counter torque is reacted through keys between the gear housings and the latch operator tube of the SPMS. A torque sensing device is required to switch off the motor when the bolt preload (500 inch pound min) has been achieved. Also, the reverse (withdrawal) rotation should continue until the latching system is disengaged and the socket probe is free of the bolt.

Figure 3-4 shows an alternate method of providing the latching function. The bolt torque system is identical to that shown in Figure 3-3.

Internal latch arms (3) are actuated by a positive two directional cam system, driven by a ball nut and screw arrangement similar to that used in Figure 3-3. The alignment funnel shown may also be incorporated into various module corner tube configurations depicted in Figure 3-3. Limit switching and control functions are also similar to those described above for the external latching concept.

**PRECEDING PAGE BLANK NOT FILMED**



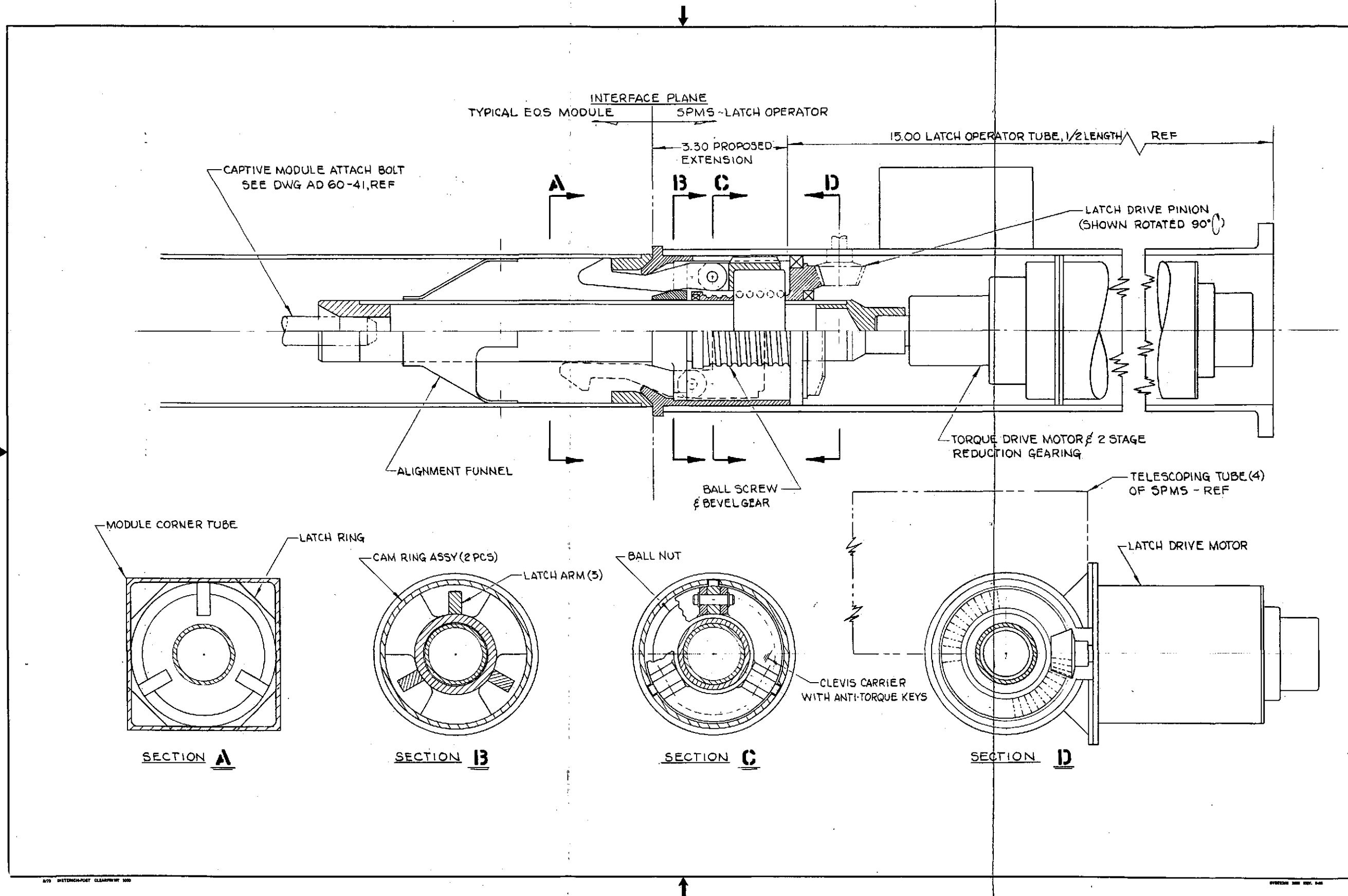


Figure 3-4. Latch Mechanism, Power Driven Internal Concept

### 3.2 SHUTTLE INTERFACES

The Shuttle orbiter will be used to support the EOS Program for launches (after the initial EOS-A flight), on-orbit servicing (module exchange), and return of the entire observatory to earth (retrieval). The physical interface between EOS and Shuttle generally involves three mechanisms: The transition Ring Cradle (essentially an adapter for securing EOS in the Shuttle Bay during launch and retrieval by means of its transition ring), the Docking Adapter (provides support and positioning of EOS during module exchange and EOS release and capture operations) and the SAMS (Shuttle Attached Manipulator Subsystem - grapples EOS at initial rendezvous, and aids peculiar module stowage and appendage erection). \* There is also the Module Exchange Mechanism and its magazine, discussed in Section 3.1. Figure 3-5 depicts these mechanisms.

#### Docking Adapter

Each EOS spacecraft will be equipped with four docking drogue probes and hard mounted at the base of the EOS structure as shown in Figure 3-6 (three for the Thor-Delta). \*\* The docking adapter contains mechanisms, which when activated, capture and secure each docking Drogue upon insertion when triggered by proximity sensors in the Docking Adapter. The ability to account for Drogue misalignment due to thermal differences without inducing excessive stress in the spacecraft structure is the responsibility of the Docking Adapter. This will be done with heaters in the adapter. With EOS docked, the Docking

\* North American Rockwell, Seal Beach, is contracted with Goddard for the transition ring cradle and docking platform. No contractor has yet been selected for SAMS. Rockwell has the overall integration responsibility for the Flight Support System (FSS) which includes these enumerated items.

\*\* No attempt has been made to make Delta and IIID versions identical per discussions with Rockwell.

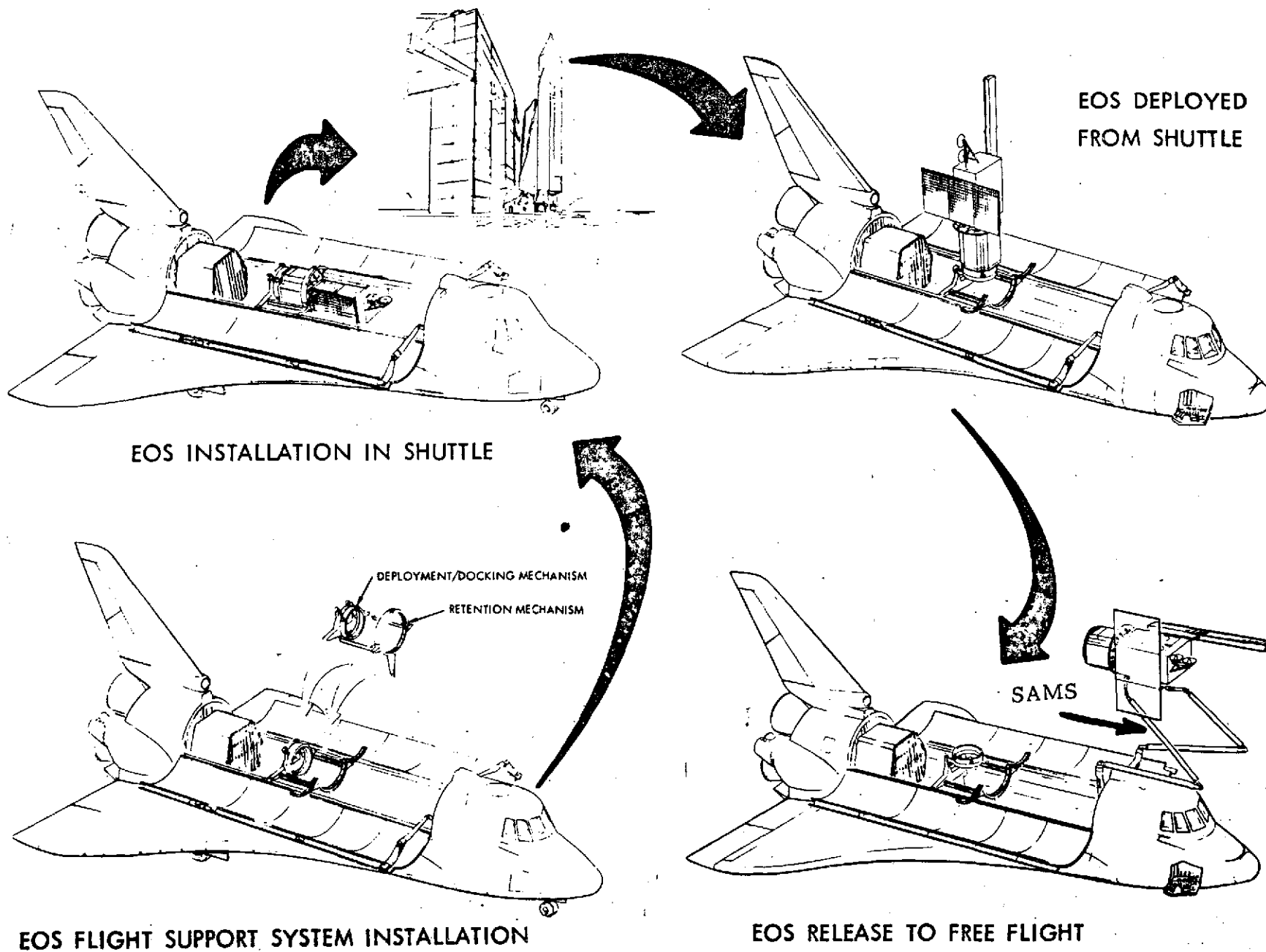


Figure 3-5. Shuttle Interface Elements

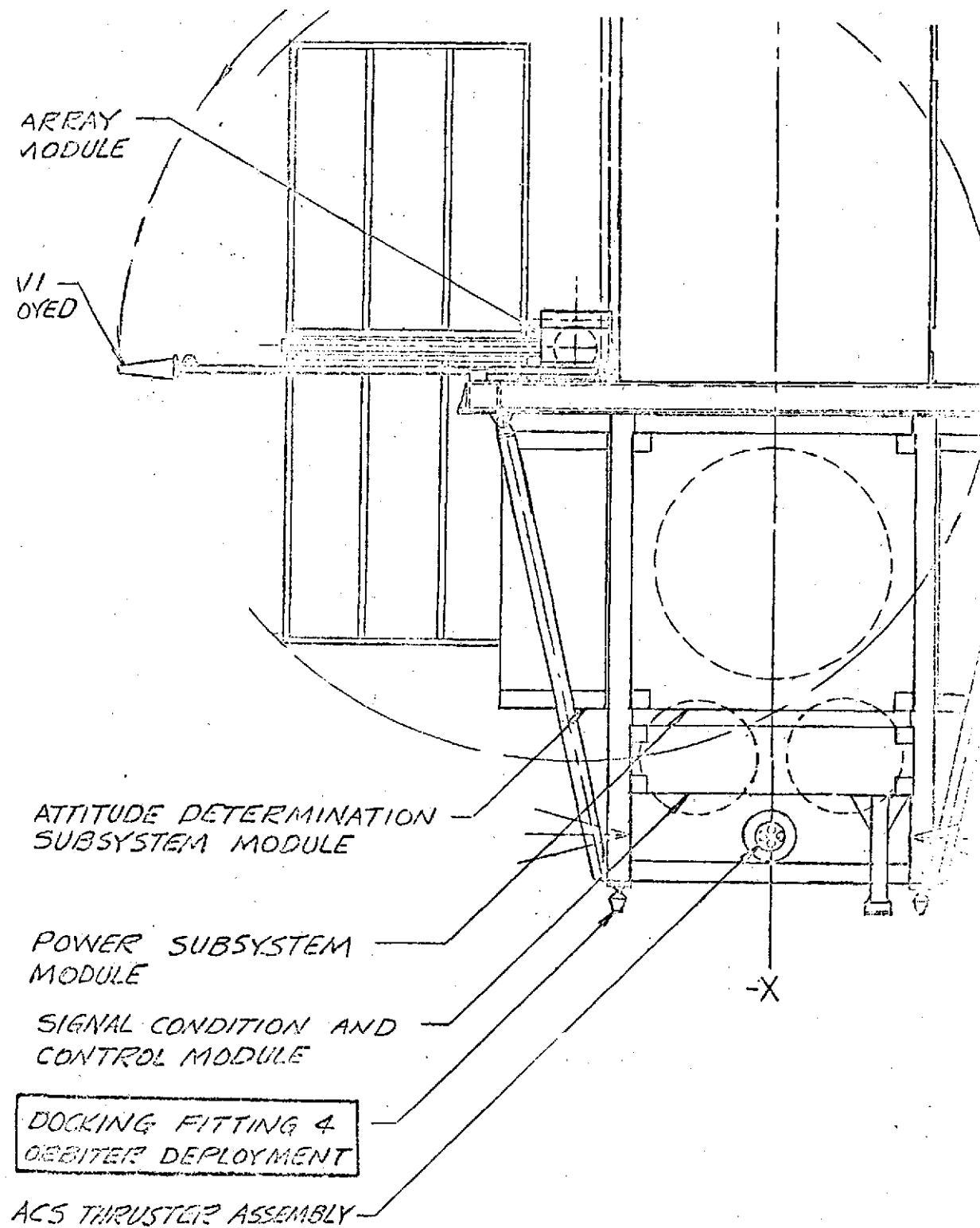


Figure 3-6. Docking Drogue Mounting

Adapter can erect the spacecraft to a vertical position, (presently requiring an initial vertical motion to clear the transition ring cradle), rotate it for module accession by SPMS, and release and move back to provide clearance from EOS during Shuttle flight. As presently envisioned, these motions, following discussions with Rockwell International, Seal Beach, are controlled by detents and are not available for coordinated motion with the SPMS (to jockey a peculiarly shaped propulsion module into position, for example). Figure 3-7 details the docking adapter motions.

### SAMS

The Shuttle Attached Manipulator Subsystem (SAMS) is utilized for the initial grappling of EOS upon rendezvous and to position the spacecraft on the docking platform. SAMS will also be used to retrieve peculiar modules (i.e., solar array and SAR antenna) from forward stowage positions in the Shuttle Bay. This may require a special end effector on SAMS. Another function of SAMS may be to deploy and collapse appendages such as antennas and the solar array if required. In conventional spacecraft such deployments are normally done with pyrotechnic pin pullers and spring-loaded hinges (as will EOS with conventional launch). EOS retrieval (and some module exchange operations) will necessitate retraction.

Our present philosophy is to utilize SAMS for this function with simple mechanical hinges rather than incorporate automatic mechanisms internal to EOS, which would increase EOS cost, complexity, and weight.

### Transition Ring Cradle

This assembly secures EOS to Shuttle during Shuttle launch and return. It was originally conceived as a large clamping ring which contacts the transition ring around its periphery, distributing loads uniformly. An alternate approach under consideration by ourselves and Rockwell would secure EOS with three hard points as indicated in Figure 3-8. The following advantages of the latter are apparent:

- Alleviation of the "raising" motion of the docking adapter to clear the transition ring (fewer actuators and complexity).

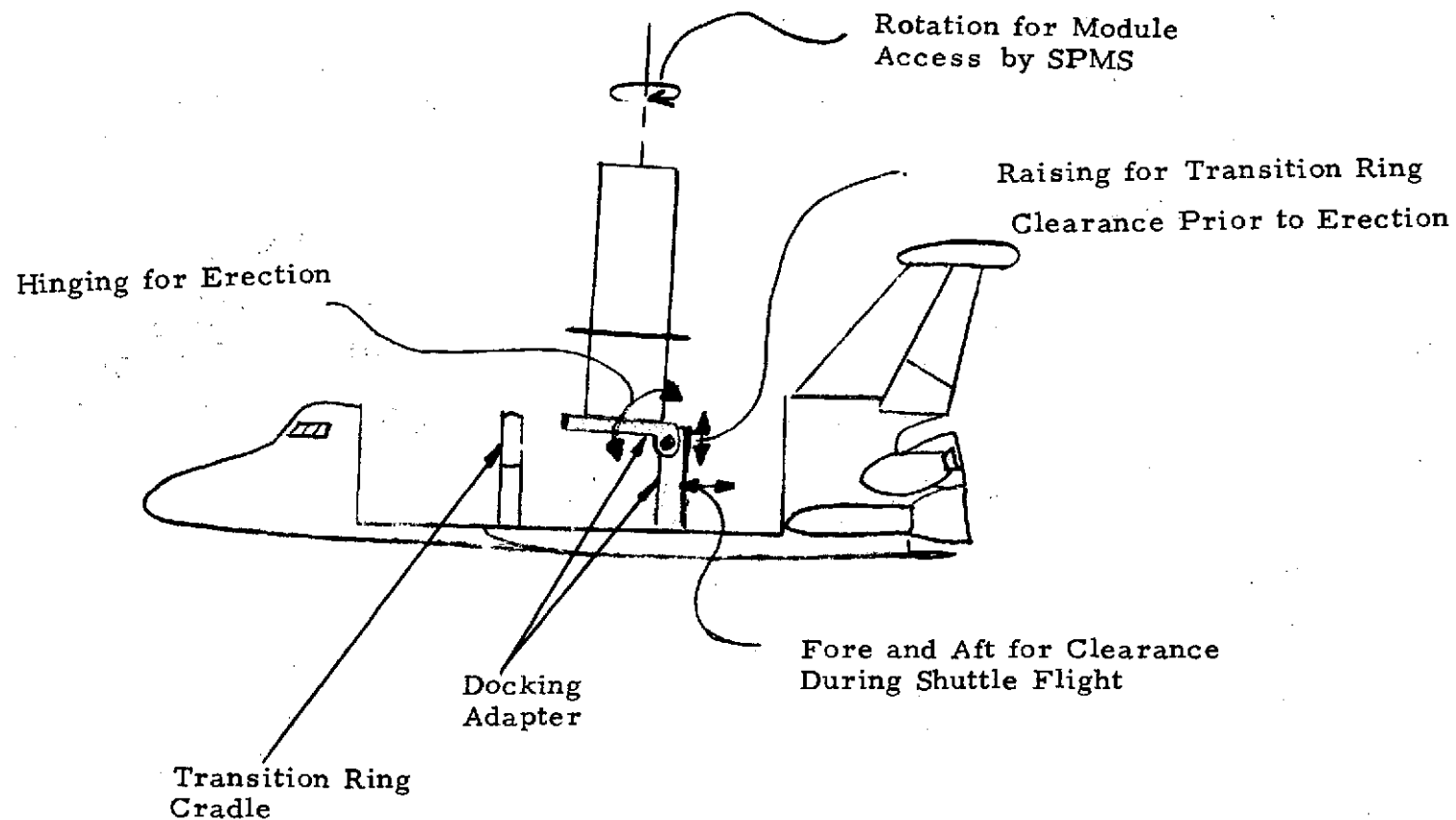
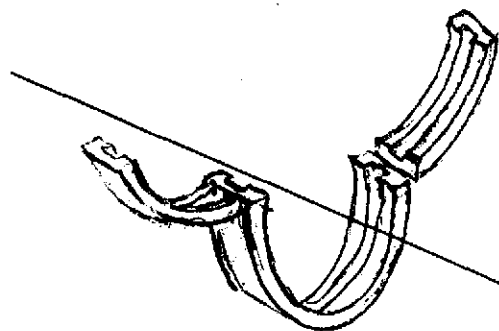
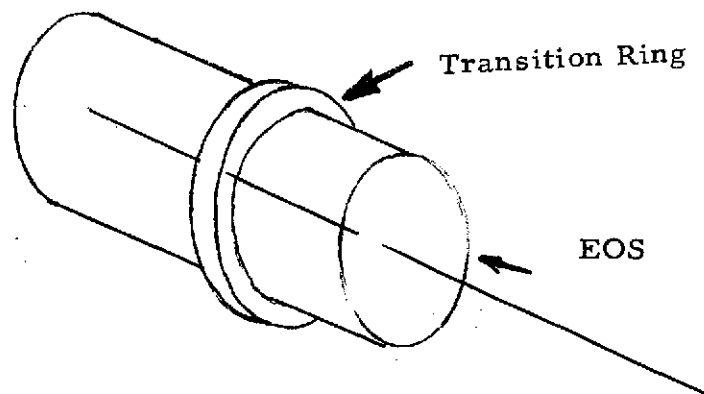
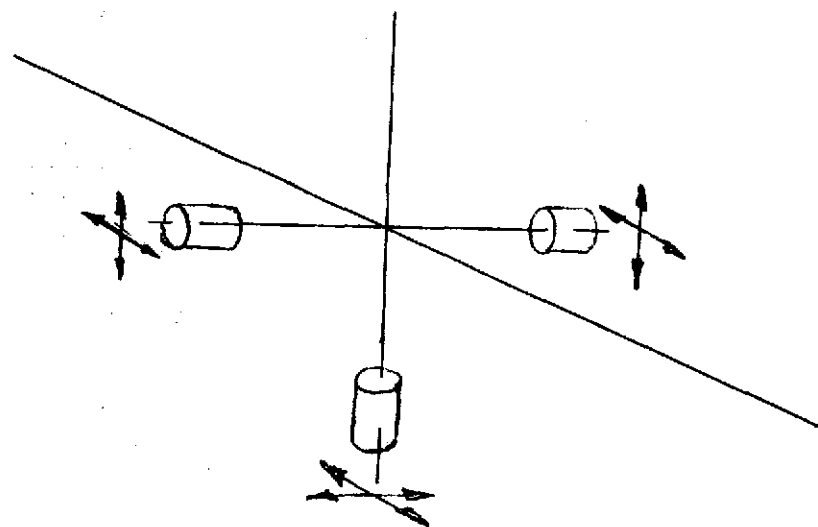


Figure 3-7. Docking Adapter Motions



Clam Shell Cradle



3-Point

Figure 3-8. "Clam Shell" vs 3-Point Transition Ring Retention

- Significant (values will be defined as work progresses) weight savings in the cradle assembly and transition ring.
- Less thermal and tolerance interplay between EOS and its securing assembly.

The form of the transition ring will be the subject of another memo.

#### Stowage for Peculiar Modules

The Solar Array Module and SAR antenna must be stowed in the forward bay of Shuttle. Their large sizes precludes stowage in the module magazine. Exchange of these modules will be more complex than the standard modules since SAMS must be manually directed by an astronaut. The SAMS will operate the module attachment mechanisms conventionally, with SAMS used to move the array (antenna, etc.), to and from its stowed position. Areas of concern presently identified but as yet unresolved, awaiting further system specifics are:

- The latching scheme for holding the modules in the Shuttle bay must be operable with SAMS or Shuttle-operated.
- Additional tie points will probably be required at the ends of the appendages (as during launch, when mounted to the observatory).
- During exchange, the replacement array (etc.), must be temporarily stored somewhere while the original is exchanged, or the "old" one discarded, or two stowage positions provided in Shuttle bay.
- The Solar Array Module connector may be "hot" if the array is sunlit.
- EOS may be required to be placed in the transition ring cradle in order to allow SAMS to reach the SPMS.

#### Safety

This area will require more study as requirements are defined. The following topics have been identified as critical:

- No possibility of causing Shuttle bay doors to be impaired from closing - entire payload jettisonable if necessary to assure safe return.
- Dumping of dangerous fluids if launch is aborted; possible overdesign of pressure vessels and associated piping and joints.



- Pyrotechnic constraints
- Special battery safety requirements - discharge prior to rendezvous, etc.

### Contamination

Based on discussions with Rockwell, the Shuttle bay will be a fairly "dirty" environment, particularly after Shuttle has flown a few missions since there is no practical way to clean it effectively. One approach which has been considered for EOS launch is a tent-like cocoon, kept at a slight positive pressure by dry nitrogen purge, which surrounds EOS during ground handling and launch. This of course, would not be effective during resupply. Lubricant outgassing is also an important consideration near optics, and the SPMS, for example, has many wet lubricated mechanisms (although sealed). References B and C relate to the optics/contamination problem. For our baseline approach, it is assumed that each critical element (payload optics, radiative cooler, star tracker, etc.), has its own commandable cover to protect it during Shuttle proximity.

### REFERENCES

- A. Final Report, Shuttle/Typical Payload Interface Study, Space Division, Rockwell International, EOS-L-70.
- B. "Control of Contaminants on Sensors," W. Hovis, et.al., October 1973, GSFC.
- C. "Partial Performance Degradation of a Remote Sensor in a Space Environment, and Some Probable Causes," John J. Horman, et.al., Applied Optics, Vol. 13, No. 5, May 14, P. 1230.

## 4. PAYLOADS

### 4.1 TM STATUS AND INTERFACE REVIEW

The designs of three versions of the thematic mapper have been reviewed. At this point in time, all three designs are being seriously considered. Concurrent breadboard development and test contracts are being funded by NASA to the three contractors: Te Company, Hughes Aircraft Company, and Honeywell Company. Key differences between the three approaches are discussed, stressing impact on spacecraft interfaces as appropriate.

#### 4.1.1 Development Status

Honeywell is the furthest along in the development of the thematic mapper. Their S192 instrument for the Skylab program demonstrated that an operational sensor, employing conical image plane scanning, could be realized. They have also fabricated a breadboard sensor, that includes critical elements of their proposed thematic mapper sensor. Preliminary test results on their seven-band scanner breadboard show that the measured scanner stability and optical quality is consistent with thematic mapper requirements. Subsequent testing will evaluate the performance of the deflectors and electronics.

The multispectral scanner, built by Hughes Aircraft for the ERTS program, successfully demonstrated the application of their object plane scanner concept in a space-qualified instrument. The next development effort, not yet underway, is to fabricate and test a larger scan mirror and scan assembly sized to satisfy the thematic mapper application.

The Te Company version of the thematic mapper is the least developed of the three. Extensive analysis and significant detailed design have been performed that supports the design concept. A breadboard version of the scan wheel and optics will be built in the near future. During fabrication, assembly, alignment, and test of the breadboard, the practicality and performance capability of the concept will be demonstrated. Not until this state of development is reached should we choose the Te Company design approach over the other two thematic mapper candidates.

#### 4.1.2 Characteristics Comparison

A summary of key parameters for the alternate design concepts is presented in Table 4-1. Discussions relating to the various table entries follows.

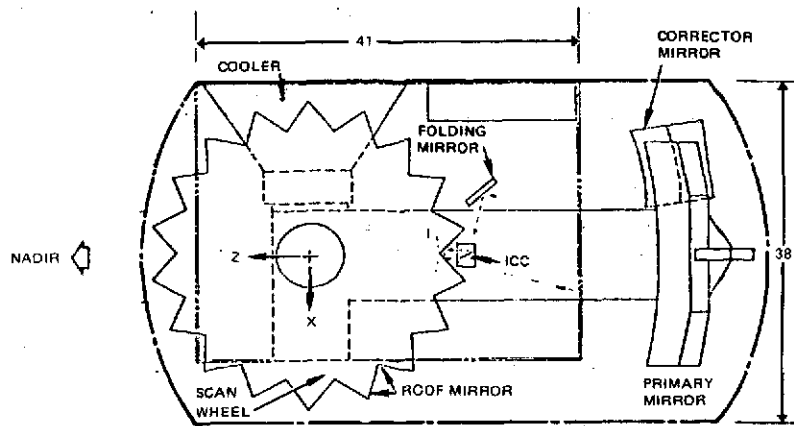
Te Company's version of the thematic mapper is shown conceptually in Figure 4-1a. An image (I) of the scene below the spacecraft is developed by the primary mirror. Image plane scanning is accomplished by rotating a roof mirror in front of the image plane. This mirror motion directs light from different areas of the image into the spectrometer portion of the instrument. A secondary effect of this type of image plane scan is that the cone of light leaving the second mirror surface is tilted as a function of scan angle. Oscillating mirror ICC compensates for this tilt such that the light distribution at the corrector mirror is constant with scan angle. The Aft-Schmidt corrector mirror achieves acceptable imagery over the total  $\pm 7.38$  degree scan field. In order to simplify the spectrometer optics and minimize the optics losses, the Te design requires spatial separation of the field of view for Bands 1 through 6 detectors. The 7th band detector straddles the field of view of the detectors for Bands 5 and 6. This latter feature was achieved by splitting the light at a dichroic beam splitter and directing it to the respective Band 7 detectors and Bands 5 through 6 detectors.

Honeywell's optical configuration is also shown in Figure 4-1b. The primary mirror images the ground scene on to a small area at the periphery of the scan wheel. Six flat mirror segments are positioned on the periphery of the wheel. As it rotates, light from different points in the image plane are directed to the latter elements of the optical train. A conical scan of the image plane results from the mirror motion. Successive arcs are swept as each mirror segment passes through the image plane. Spherical relay mirror M2 and aspheric mirror M3 transfer the light to the spectrometer portion of the optics, and corrects the final imagery over the total scanned field. Band 1 through 6 detectors simultaneously receive light from the same point in the image plane. This feature is accomplished by dispersing the light through a prism and

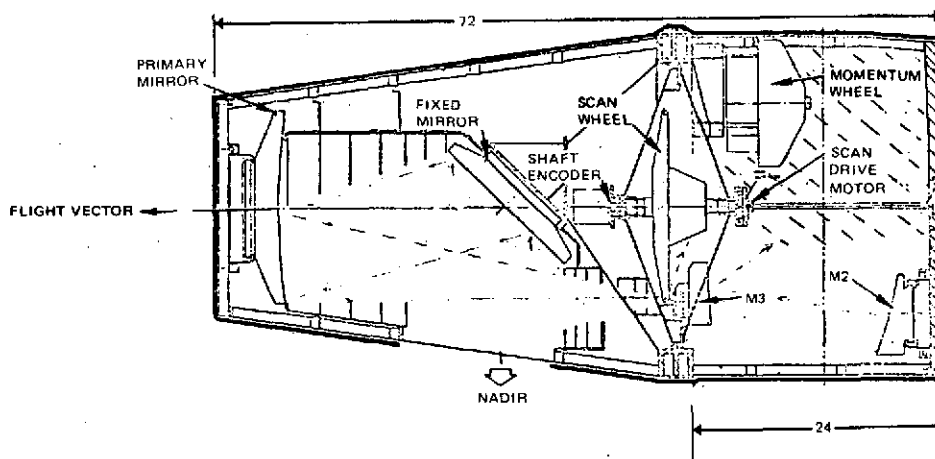
Table 4-1. Thematic Mapper Instrument Comparison

Parameter	Te	Hughes	Honeywell
Development status			
Technology basis	Analysis	ERTS MSS	Skylab S192
Breadboard	Scanner and optics fabrication to start soon	Scanner and drive fabrication to start soon	In-test
Configuration			
Scan concept	Linear scan of image plane	Object plane scanning	Conical scan of image plane
Band separation scheme			
1 to 3	Filter	Prism and fiber opt	Prism and fiber opt
4	Filter	Filter	Prism and fiber opt
5 to 6	Filter	Filter	Prism and fiber opt
7	Filter	Filter	Filter
Radiative cooler	ITT or AD Little contract	Modified MSS design	ITT or AD Little contract
Electronics (bands 1 to 7)	Cooled FET Post-amp 5-pole Butterworth	FET preamp Post-amp 5-pole Bessel	FET preamp Post-amp 2-pole Butterworth
Collecting aperture	700 cm <sup>2</sup>	990 cm <sup>2</sup>	950 cm <sup>2</sup>
Electrical Interface			
Number of channels	93	100	100
Signal frequency for 30 meter/half cycle tgt	54.4 kHz	113 kHz	50 kHz
Power (average)	110 watts	55 watts	210 watts
Mechanical interface			
Size	38 x 40 x 67 in	21 x 36 x 67 in	36 dia x 72 in
Weight	365 lb	320 lb	600 lb
Performance *			
Altitude	914 km	717 km	900 km
Instantaneous field 1 to 6	33 $\mu$ rad	30 $\mu$ rad	33 $\mu$ rad
S/N (Band 1)	8.7	12.3	11.5
S/N (Band 6)	6.5	1.9	2.0
NE $\Delta$ T (Band 7)	0.3	0.97	0.3

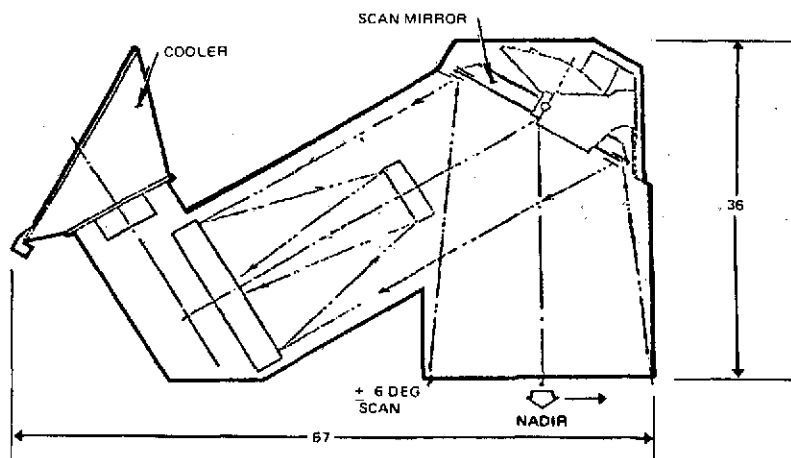
\* Numbers excerpted from NASA correspondence "Thematic Mapper Descriptive Parameters," file number 17986, 18 June 1974, R. W. Stroup.



a) Te Company Thematic Mapper



b) Honeywell Company Thematic Mapper



c) Hughes Aircraft Company Thematic Mapper

Figure 4-1. Candidate Versions of EOS Thematic Mapper

then intercepting the proper wavelength band by various fiber bundles, which relay the energy to the respective detectors. The fields of view of the Band 7 detectors are slightly displaced from those for the other six bands.

The Hughes thematic mapper is the only version that employs object plane scanning. The scan mirror rotates through  $\pm 3.69$  degrees of mechanical motion to produce a  $\pm 7.38$  degree optical deflection. Light from this mirror is directed into a 16-inch aperture, Richey-Chretien telescope. With this scanning concept, the rays entering the telescope are all essentially "on-axis" ( $\pm 0.05$  degree) thus simplifying the telescope optical design and making near diffraction limited performance achievable. Light for Bands 1 through 3 detectors are intercepted by fiber optics bundles, after being dispersed by a prism. Detectors for the other bands each view slightly displaced points in the field of view. Each detector for these bands is preceded by an appropriate spectral filter.

A detailed comparison of the three thematic mapper concepts in terms of weight and swathwidth capability is given in Report 1, Section 4.1

#### 4.1.3 Data Buffering Requirements

This section compares the data buffering requirements of each of the three thematic mappers on a parametric basis.

Due to the conical scan pattern of the Honeywell scanner, linear film writers cannot be used to print data images or existing algorithms used to process data unless adequate data buffering is provided to rearrange the data in a linear format. Figure 4-2 illustrates the geometry of the problem. The simplest approach is to buffer the whole block LW and readout lines sequentially from the bottom. However, some storage can be saved by storing only that portion of the area shown double-hatched and reading in and out in a carefully planned sequence.

The ratio of the smaller to larger area (and hence the ratio of data storage requirements) is given by:

$$F = \frac{\frac{\beta}{2 \sin \frac{\beta}{2}} - \cos \frac{\beta}{2}}{2 \operatorname{versin} \frac{\beta}{2}} \quad (1)$$

where  $\beta$  equals the active scan angle.

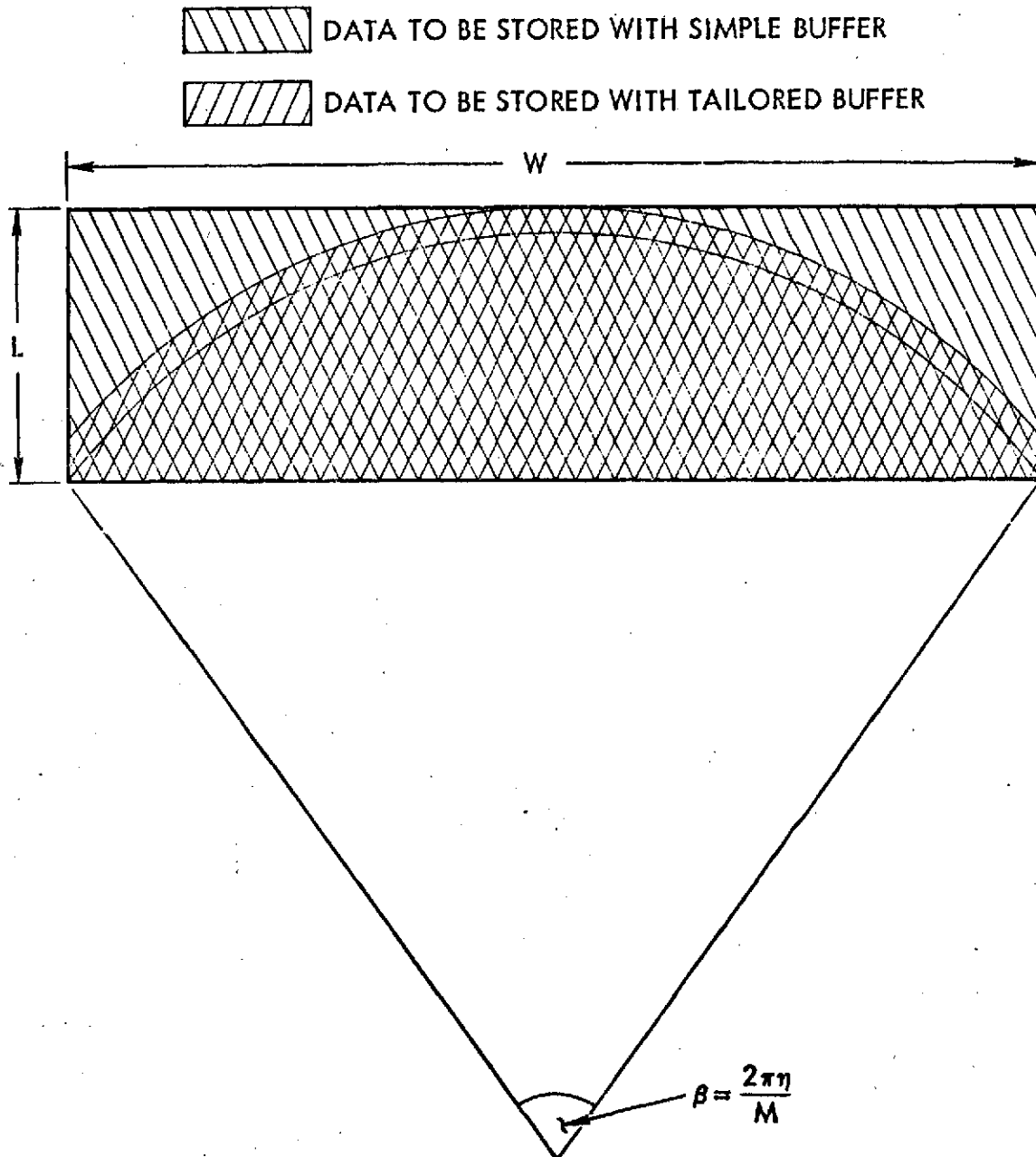


Figure 4-2. Data Storage Requirements Associated with Simple and Optimized Buffer

In Part 2 it is shown that

$$\beta = \frac{2\pi\eta}{M} \quad (2)$$

where:

$\eta$  is the scan efficiency

$M$  is the number of scan mirrors

Solving Equations 1 and 2 gives Table 4-1a, which shows the factor  $F$  for each of several scan mirror numbers, and indicates that the number of mirrors has very little effect on  $F$ .

Table 4-1a. Data Storage Factor for Optimum Buffering

Number of Mirrors (M)	$\beta$ (degrees)	Data Storage Factor (F)
3	96.0	0.692
4	72.0	0.680
5	57.6	0.675
6	48.0	0.672

If a rearward pointing scan is used, the data storage factor becomes  $1-F$ . The ratio of the buffer requirements of the Honeywell scanner to that of the other scanners is given by

$$\frac{S_h}{S_o} = \frac{W \operatorname{versin} \frac{\beta}{2}}{4N \sin \frac{\beta}{2}} + 1 \quad (3)$$

where:

$W$  is the swathwidth (in pixels)

$N$  is the number of detectors along track

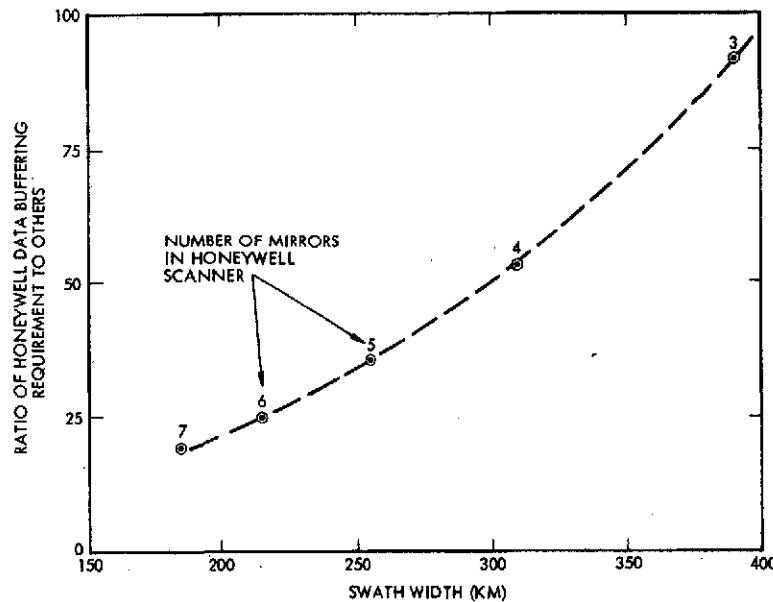


$S_h$  is the buffer requirement of the Honeywell scanner optimum buffering

$S_o$  is the buffer requirement of the Hughes or Te scanners.

Equation 3 assumes that each scanner uses the same number of detectors. For the case of 715 km altitude, 30 km resolution, and minimum data buffering in the Honeywell scanner,  $S_h/S_o$  can be calculated using Equation 3. The result is plotted below.

If extremely sophisticated real-time processing of Honeywell data can be used then data buffering needs may be reduced considerably providing linear imagery is not required. In this case the data might be improved in quality by comparison of adjacent pixels. To do this,



buffering requirements would be one complete swath plus the leading detector of the previous swath. The value of  $S_h/S_o$  could be reduced to:

$$\left(\frac{S_h}{S_o}\right)^1 = \frac{N+1}{N} \quad (4)$$

This is a 6.3 percent increase for a 16-detector instrument. It is emphasized that the processing hardware implied by this method is probably not economically feasible at this time.

## 4.2 HIGH RESOLUTION POINTABLE IMAGER

### 4.2.1 HRPI Status and Interface Review

There are presently four companies pursuing development of a high resolution pointable imager for the EOS satellite. Three are proposing to modify their mechanical scanning thematic mappers to meet the HRPI requirements (Honeywell, Hughes, and Te); the fourth company (Westinghouse) is proposing a solid-state electronically scanned camera. All four companies have performed HRPI point design studies for NASA.

Key differences between the four approaches are outlined in Table 4. The solid-state camera was selected as the baseline HRPI sensor. The photo-detector array design offers high geometric registration and mechanical reliability. Since image scanning requires no moving parts, vibrational impact upon other satellite subsystems is minimal. For a given size and weight, the solid-state camera signal-to-noise exceeds the capability of mechanical scanners because of its high detector dwell time (4800 detectors per spectral band). Estimated cost of the Westinghouse camera is \$16 million compared to \$22 to 27 million for mechanical scanners. The major problem with the solid state camera is detector-to-detector dark current and gain variation. Detector and/or calibration technique development is needed to meet performance requirements.

#### Optical Configurations

Te Company's version of the HRPI is shown conceptually in Figure 4-2a. A pointing mirror performs the cross-track field-of-view pointing. The scene image is developed by the spherical primary mirror. Image plane scanning is accomplished by 64 "roof mirrors" mounted on the rotating scan wheel. The wheel rotation rate is 0.21 rps (adjustable in 0.2 percent increments to account for changes in ground track velocity). The motion of the roof mirrors directs light from different areas of the image into the spectrometer portion of the instrument. As with the TM design, the cone of light leaving the second mirror surface is tilted as a function of scan angle. Oscillating mirror ICC compensates for this tilt such that the light distribution at the corrector mirror is constant with scan angle. The Aft-Schmidt corrector mirror achieves acceptable imagery over the total +1.9-degree scan field. In order to simplify the

Table 4-2. HRPI Instrument Comparison

Item	Te	Hughes	Honeywell	Westinghouse
Development status	Analysis - Scanner and optics fabrication to start soon	Modified ERTS MSS - Scanner and drive fabrication to start soon	Proposing modified Skylab S192 - In test.	Breadboard photodiode array optical bench and display
Image scan configuration	Image plane linear scan - rotating "water wheel" mirror assembly	Object plane linear scan oscillating flat mirror	Image plane conical scan - rotating conical mirror assembly	Image plane "push-broom" scan - electronically sampled linear photo detector array
Spectral separation method	Filters	Filters	Filters	Prism assembly
Pointing technique	Object plane pointing mirror	Instrument rotation	Instrument rotation	Object plane pointing mirror
Detectors and electronics	Silicon photodiodes cooled FET Post amplification 5-pole butterworth	CCD/TDI, Differential Video amplifier	Silicon photodiodes, FET pre-amplifier, 2-pole butterworth	Silicon photodiodes, preamplifier design to be determined
Image detection channels per color band	50	18	80	4800
Point design altitude	715 Km	717 Km	717 Km	914 Km
Collection aperture at point design altitude	803 cm <sup>2</sup>	1320 cm <sup>2</sup>	973 cm <sup>3</sup>	1650 cm <sup>2</sup> (1020 cm <sup>2</sup> at 717 Km)

Table 4-2. HRPI Instrument Comparison (continued)

Item	Te	Hughes	Honeywell	Westinghouse
Signal-to-noise:				
Band 1 (.5 - .6 $\mu$ ) (2.2 W/m <sup>2</sup> -ST Background radiance)	5.4	8	8.9	53
Band 2 (.6 - .7 $\mu$ ) (1.9 W/m <sup>2</sup> - ST )	5.4	9	9.8	47
Band 3 (.7 - .8 $\mu$ ) (1.6 W/m <sup>2</sup> - ST )	6.1	9	9.4	36
Band 4 (.8 - 1.1 $\mu$ ) (3.0 W/m <sup>2</sup> - ST )	6.9	10	9.5	38
Size (inches)	36 x 38 x 84	42 x 45 x 55	36 diameter x 72	25 x 30 x 72
Weight (lbs) (Beryllium components)	362	329	500	330
Power				
Electronics	80	69	198	100
Pointing	8	20	80	2
Heaters	<u>15</u>	<u>50</u>	<u>50</u>	<u>19</u>
Maximum con- tinuous	95	69	248	119
Cost (\$ Million)	22 - 27	22 - 27	22 - 27	16

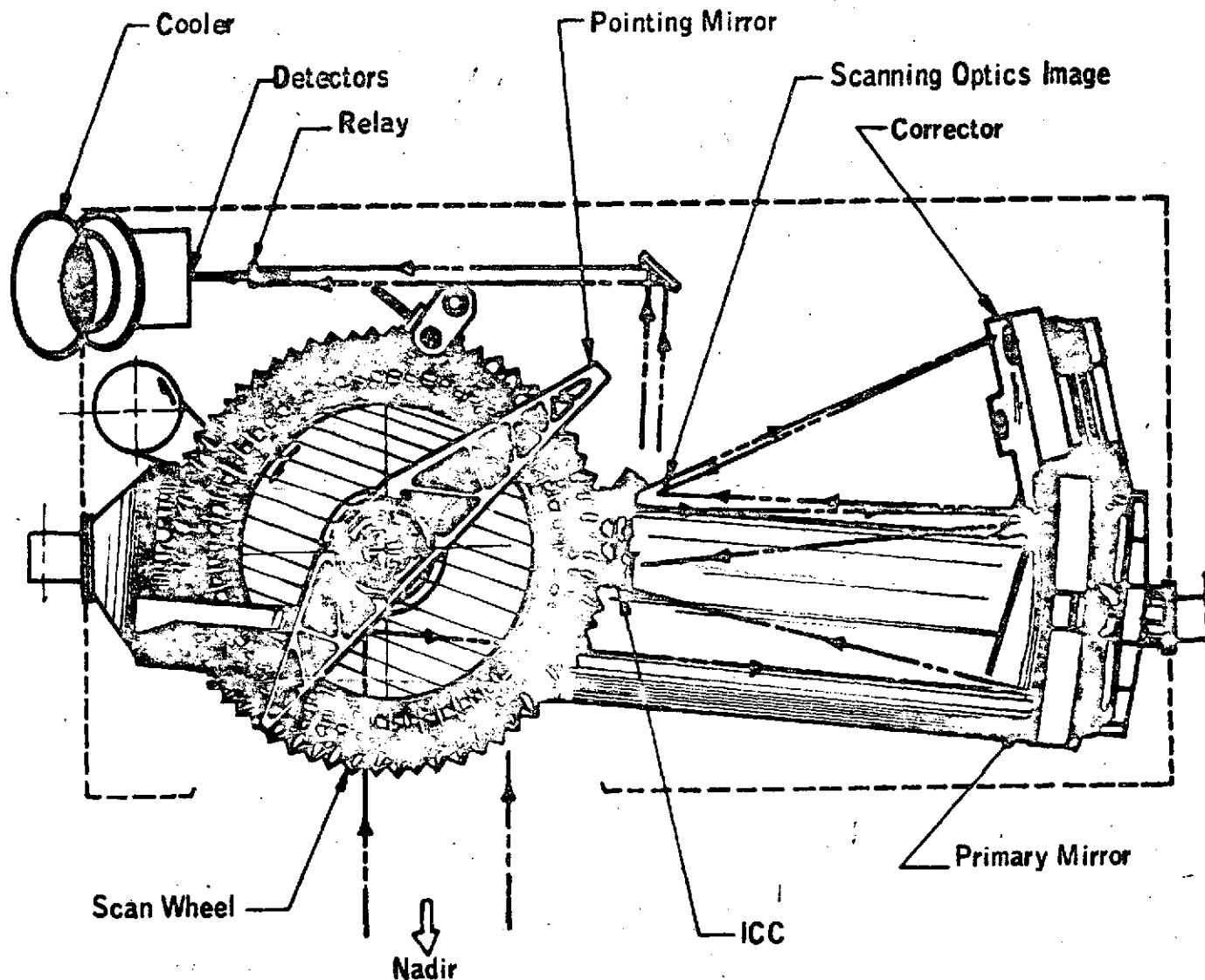


Figure 4-2a. HRPI Optical Configuration (Te Company Approach)

spectrometer optics and minimize the optics losses, the Te design requires spatial separation of the field-of-view for Bands 1 through 4 detectors.

Honeywell's optical configuration is shown in Figure 4-3. The primary mirror images the ground scene on to a small area at the periphery of the scan wheel. Six flat mirror segments are positioned on the periphery of the wheel. The scan wheel rotates at 1.4 rps. As it rotates, light from different points in the image plane are directed to the latter elements of the optical train. A conical scan of the image plane results from the mirror motion. Successive arcs are swept as each mirror segment passes through the image plane. Spherical relay mirror M2 and aspheric mirror M3 transfers the light to the spectrometer portion of the optics, and corrects the final imagery over the total scanned field. Contrary to the Honeywell Thematic Mapper approach (fiber optics/prism assembly) HRPI spectral separation is accomplished with filter assemblies. Cross-track field-of-view pointing is accomplished by rotating the entire instrument on ring bearings.

The Hughes HRPI is the only version that employs object plane scanning (Figure 4-4). The scan mirror, constructed of sandwiched lightweight beryllium, rotates through  $\pm 0.8$  degree of mechanical rotation to produce  $\pm 1.6$  degrees of optical deflection (40 Km swathwidth at 717 Km altitude). Light from the scan mirror is directed into a 16 inch, f/10, Richey-Chretien telescope. Similar to the thematic mapper, the rays entering the telescope are all essentially on-axis. This simplifies the telescope design and allows for near diffraction limited performance. The image plane detector system uses filters for spectral separation and charge coupled device (CCD) arrays with time delay integration for photodetectors. Each CCD element and each spectral band are spatially separated in the scan direction so image reconstruction requires appropriate time/space phasing. As with the Honeywell sensor, offset field-of-view pointing is performed by instrument rotation.

A modified version of the Westinghouse HRPI is shown in Figure 4-5. The Westinghouse point design pointing mirror and telescope, have been reoriented in the cross-track direction. This provides non-skewed off-nadir imagery. It also affords the most convenient packaging for the

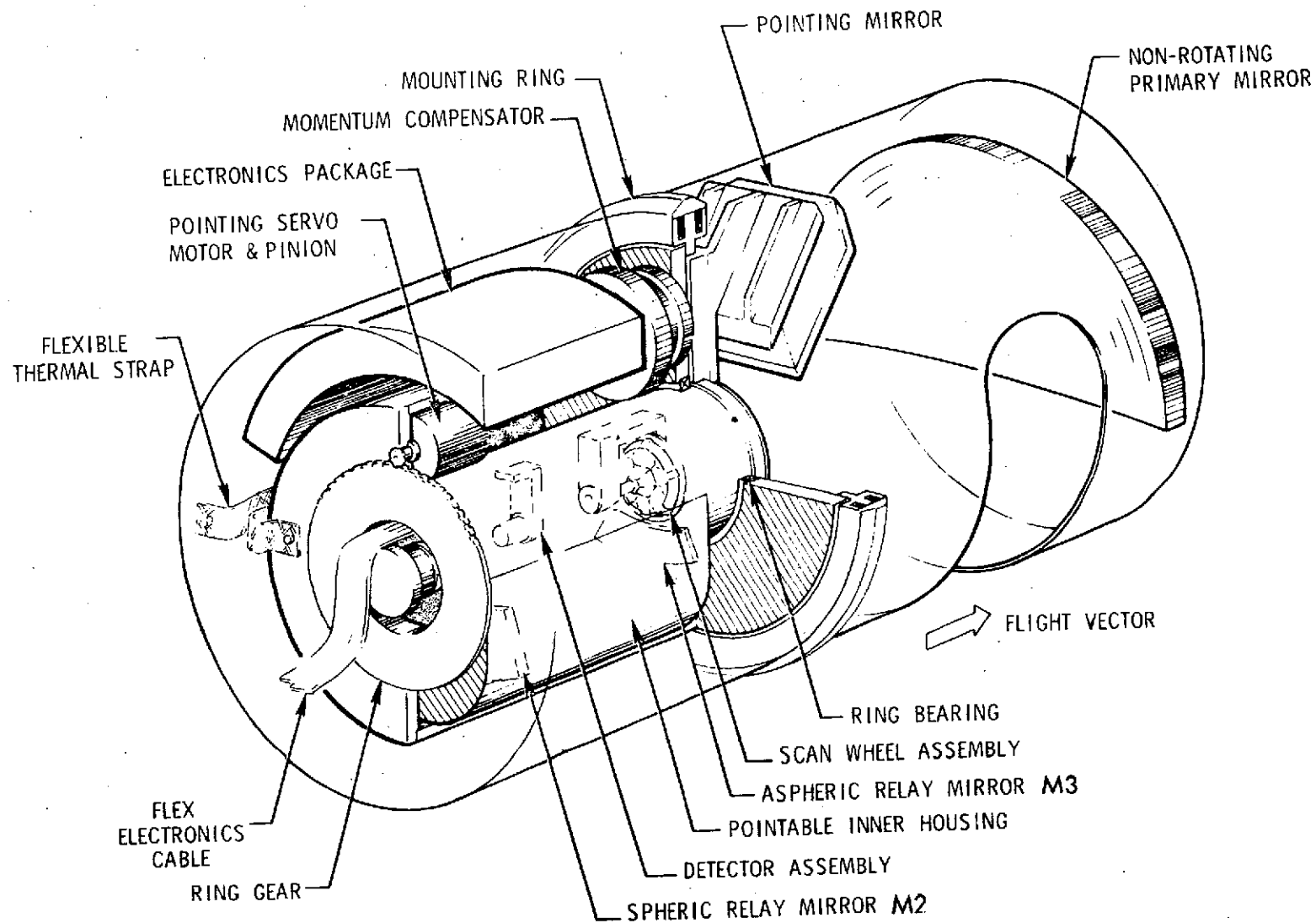


Figure 4-3. HRPI Optical Configuration (Honeywell Approach)

2

ORIGINAL PAGE IS  
OF POOR QUALITY

4-15

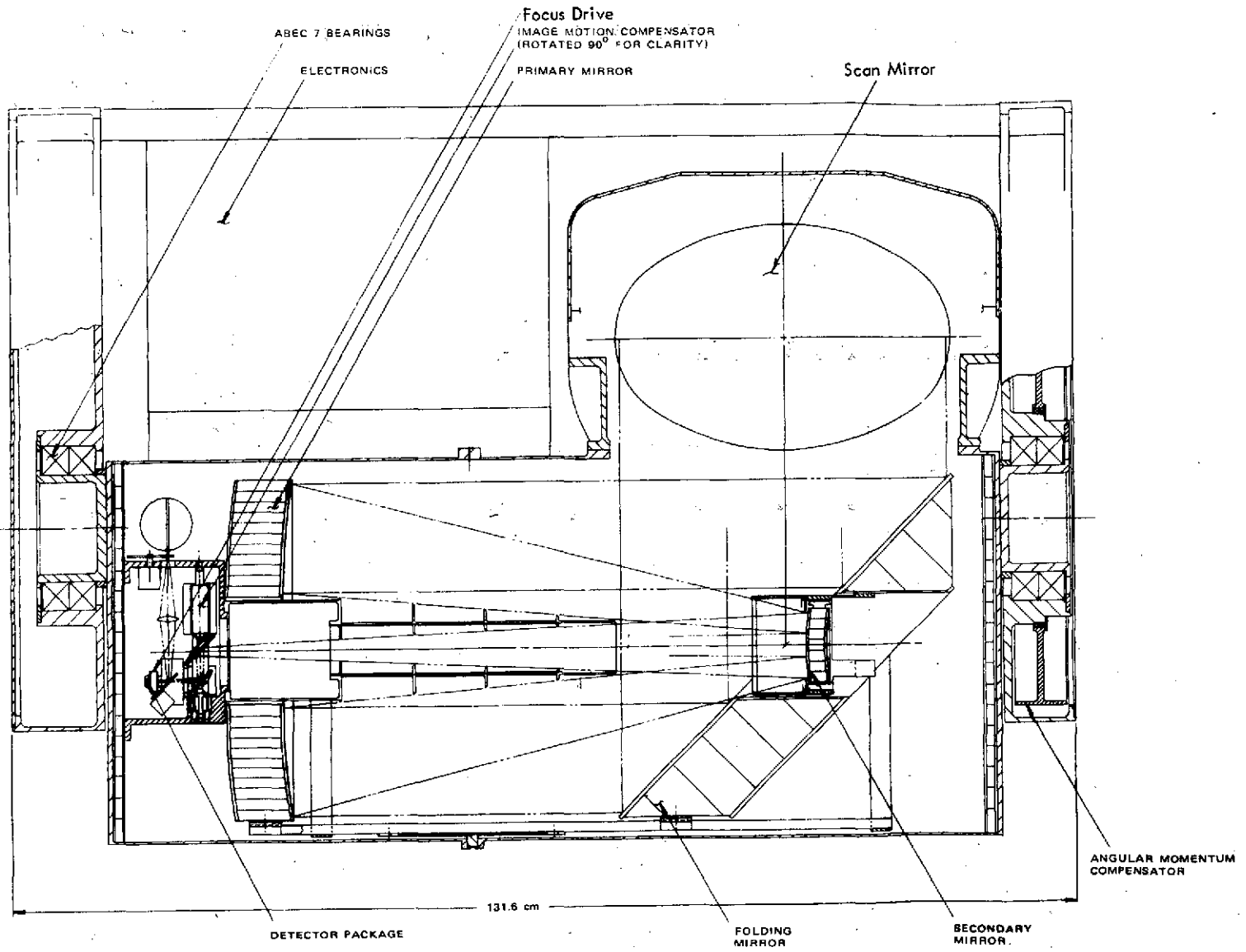


Figure 4-4. HRPI Optical Configuration (Hughes Approach)



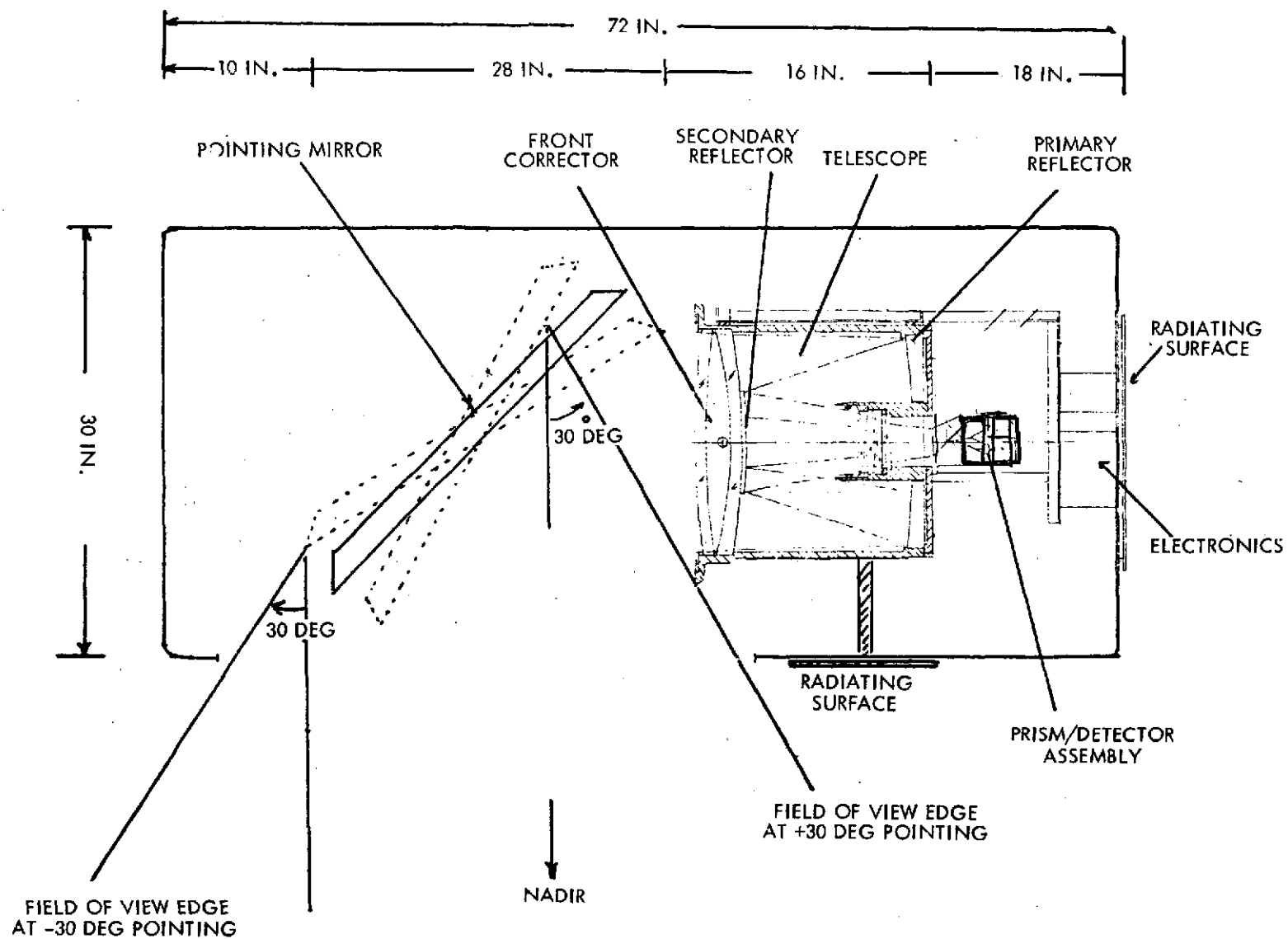


Figure 4-5. HRPI Optical Configuration (Westinghouse Approach)

TRW baseline spacecraft design. The 15 by 30 inch oval pointing mirror directs the scene energy into the 15-inch, f/3 catadioptric telescope. These dimensions represent appropriate changes in the Westinghouse point design to accommodate a 717 Km orbit (the point design study assumed a 914 Km altitude). The front corrector lens protects the telescope interior from contamination. After reflection by the primary and secondary telescope mirrors and distortion correction by the rear corrector assembly, the scene energy is spectrally separated by a six-prism assembly and imaged upon four linear photo-diode arrays (approximately 4800 photo-diodes per color band). Image scanning is performed by electronically sampling the light energy signal that is integrated by each photo-diode during each frame time (1.484 milliseconds per 10 meters ground track at 717 Km). The Westinghouse instrument is the only HRPI that uses prism-type spectral separation, providing simultaneous ground resolution element viewing by all four color bands. Offset field-of-view pointing is accomplished by  $\pm 15$  degrees rotation of the beryllium pointing mirror.

#### Development Status

Out of the above-mentioned four manufacturers, only Westinghouse is developing a breadboard system that is specifically designed to demonstrate HRPI performance. The other manufacturers are developing mechanical scanners that are mainly directed toward thematic mapper applications and are relying on conceptual extrapolations of their results to provide HRPI instrument credibility.

Honeywell is furthest along in development of the thematic mapper. Their Skylab S192 instrument demonstrated feasibility of conical scanner imagery. They have an operating thematic mapper breadboard. Breadboard measurements satisfy scanner stability and optical quality requirements.

The Hughes design is patterned after the ERTS MSS instrument. Their next development phase is to fabricate and test a larger scan mirror assembly to satisfy thematic mapper requirements.

The Te Company has performed extensive analysis to support their design concept. A breadboard scan wheel and optical assembly will be built in the near future. With respect to hardware development, the Te version is the least developed.

The Westinghouse hardware development is a breadboard system incorporating a line photodiode array, optical bench, and image display. Standard camera lens optics are used. The breadboard electronics presently contribute noise equal to the detector noise. Chip-type electronic packaging will hopefully reduce the electronic noise and afford a detector noise-limited system.

#### 4.2.2 HRPI Design Improvements

Recent improvements in detector performance offer a potential for reducing the size and weight of the baseline Westinghouse HRPI design (Figure 4-6). A sensor noise equivalent signal (NES) of 0.25 microjoule/m<sup>2</sup> appears attainable. The Westinghouse point design was based upon an NES of 1.5 microjoules/m<sup>2</sup> (1 mW/m<sup>2</sup> x 1.5 millisecond integration time).

The relationship between required aperture diameter and NES for constant signal-to-noise is derived from the background signal-to-noise (S/N) equation:

$$S/N = \frac{\pi N (1 - \emptyset) T}{4 (F/D)^2} \frac{\eta t}{NES} \quad (1)$$

where N = Background radiance (mW/m<sup>2</sup>-ster.)

$\emptyset$  = Obscuration of optics

T = Optical transmission

F = Focal length (inches)

D = Aperture diameter (inches)

$\eta$  = Quantum efficiency (photo electrons/photon)

t = Integration time (msec)

NES = Noise equivalent signal at the selected integration time ( $\mu$ joules/m<sup>2</sup>) (2)

It can be seen from Equation (1) that

$$D \sim \frac{1}{2} (NES)$$

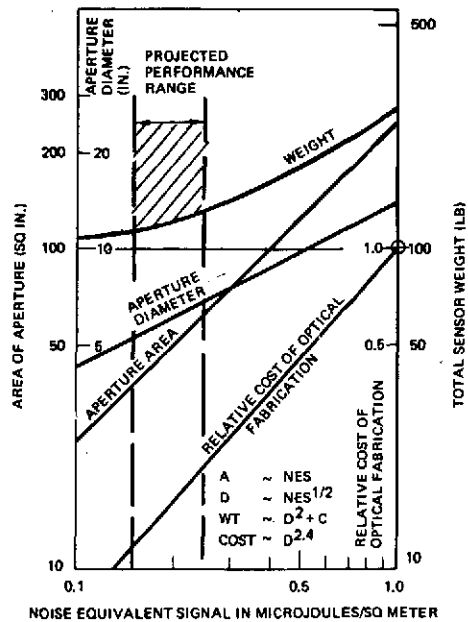


Figure 4-6. Projected Improvements in Detector Noise Can Reduce System Weight

A six-fold reduction in NES should therefore reduce the required baseline aperture diameter from 15 to 6 inches with unchanged signal-to-noise. However, the effect of diffraction on optical transfer function must be considered as aperture drops.

A corresponding reduction in fabrication costs should also be afforded. Westinghouse estimates a cost savings of 5 to 10 percent in reducing their HRPI aperture from the point design 18.3-inch system to the TRW baseline 15-inch system (due to baseline altitude change from 914 to 717 km). Another 5 to 10 per-

cent savings should result from the further aperture reduction due to reduced NES.

The sensor weight is largely dependent upon required aperture diameter. In the above discussion, the required aperture diameter was traded off against detector NES. There are also reasons for considering a tradeoff of aperture diameter against sensor signal-to-noise. These are as follows:

- The Westinghouse f/3 system ( $F/D = 3.0$ ) has a relatively high S/N. The background S/N = 36 in the worst case band (See Table 5.2-2, Section 5.2, Report 3).
- The NASA requirement is S/N = 6 in all bands against the specified background (Table 5.2-2).
- The competing mechanical scanner HRPI S/N ranges from 5.4 to 8.9 (worst case bands in Table 1).

Therefore it appears that additional weight savings might be possible by reducing the Westinghouse aperture size so that the S/N performance more nearly reflects the NASA requirement. In addition, the proposed 8-bit data handling system would degrade the sensor data quality if the dark current variations are not subtracted from the analog signal prior to analog-to-digital conversion. This subtraction is not presently proposed for the baseline system.

A two-dimensional matrix of weight components is given in Table 4-3 for two values of S/N and NES. The telescope weight was scaled down from the heaviest system by the second power of the aperture diameter (except at the lightest weight system a 3 pound telescope was not deemed to be adequate). The mirror and pointing assembly was scaled more conservatively because the pointing mechanism weight is not strictly size dependent. Angular momentum compensation was scaled according to the pointing mirror weight. Thermal control was scaled according to telescope size. Structure was scaled according to total sensor weight.

The resulting sensor total weight is plotted as a function of desired background S/N for three sensor NES values. The parameter assumptions used for the S/N calculation (Equation 1) are also given in the Figure 4-7. With a moderate improvement in sensor NES ( $NES = 0.75 \text{ microjoules/m}^2$ ), a 180 pound Westinghouse type HRPI could provide a background S/N of 20. Mechanical scanning HRPIs that weigh twice as much provide only half the S/N performance.

#### 4.2.3 HRPI Offset Pointing Options

Three possible options for optical field-of-view pointing were briefly examined in terms of required size, weight, and power. The three options are illustrated in Figure 4-8. Table 4-4 summarizes instrument dimensions, swept volume for  $\pm 30$  degree pointing, component weights and power requirements for each option. All three options assume that the telescope and detection electronics are configured after the selected baseline Westinghouse HRPI.

A fixed telescope with a rotating pointing mirror is the selected baseline pointing method (Option 1). It offers the lowest sensor weight

Table 4-3. Required HRPI Weight Estimates for Reduced S/N and Improved Detector Noise Equivalent Signal (NES)

Background S/N Against Specified Background (1.6 W/m <sup>2</sup> ST - Band 3)		9		36	
Sensor NES (Microjoules/m <sup>2</sup> )		0.25	1.5	0.25	1.5
Required Aperture Diameter (inches)		3	7.5	6	15
<u>Component Weights (pounds)</u>					
Telescope		5	18	12	70
Detectors and Beamsplitter		8	8	8	8
Mirror and Pointing Assembly		10	25	20	54
Angular Momentum Compensation		8	12	10	19
Electronics		28	28	28	28
Thermal Control		6	10	8	16
Miscellaneous		20	20	20	20
Structure		<u>35</u>	<u>50</u>	<u>45</u>	<u>85</u>
Net		120	171	151	300
Contingency (10 percent)		<u>12</u>	<u>17</u>	<u>16</u>	<u>30</u>
Total (pounds)		132	188	167	330

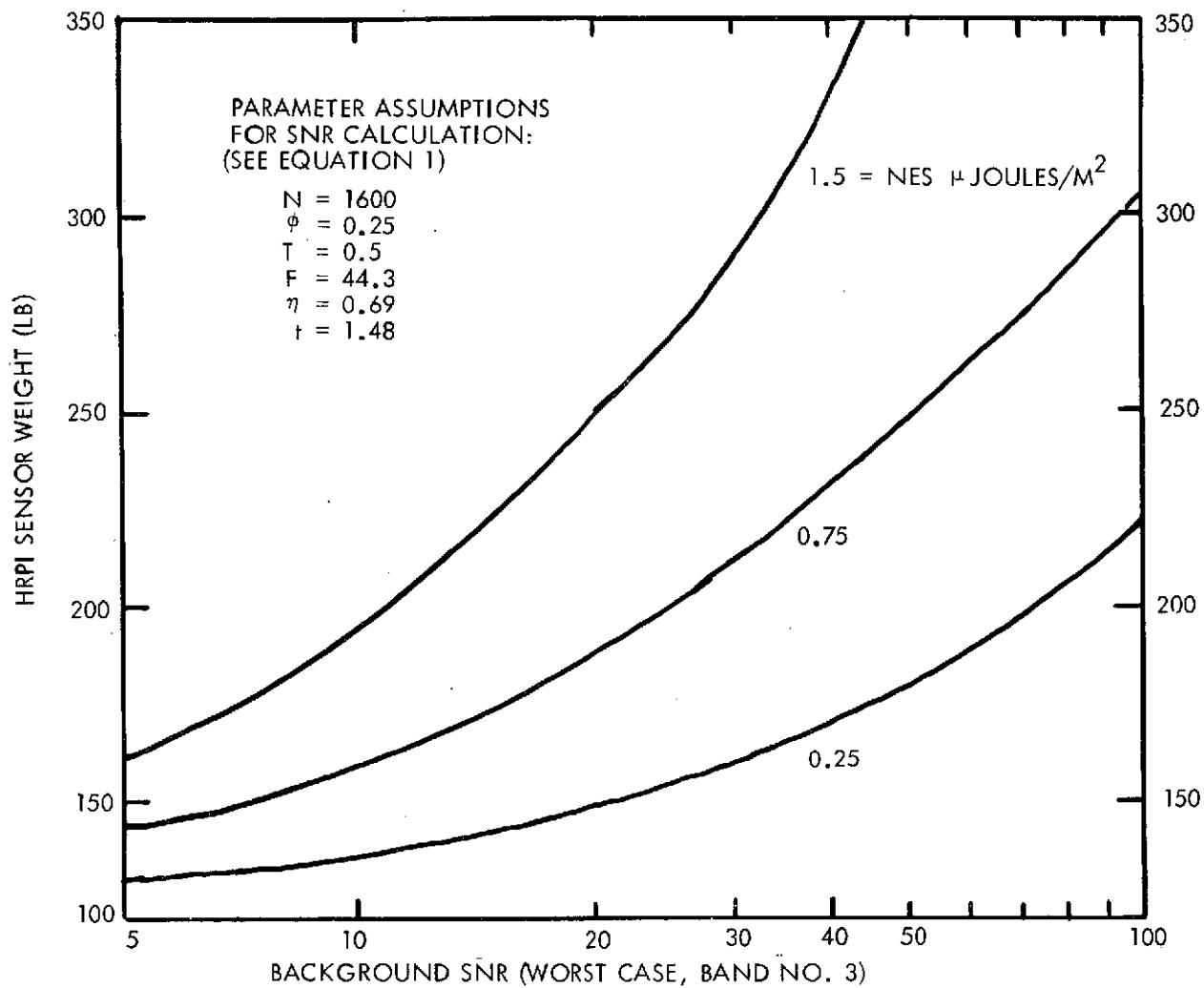
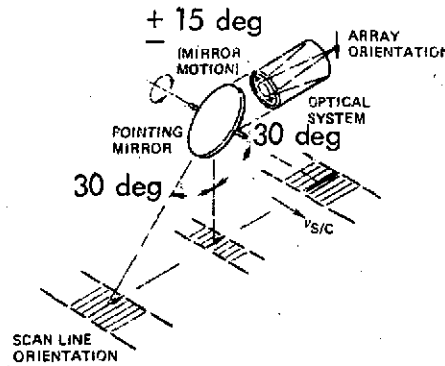
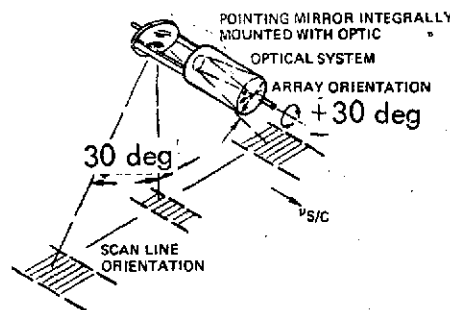


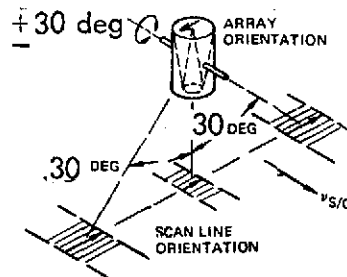
Figure 4-7. HRPI Sensor Weight as a Function of Worst-Case Background SNR and Sensor NES



OPTION 1: FIXED TELESCOPE WITH ROTATING POINTING MIRROR



OPTION 2: ROTATING TELESCOPE AND POINTING MIRROR



OPTION 3: GIMBALLED TELESCOPE - NO POINTING MIRROR

Figure 4-8. HRPI Offset Pointing Options

and requires the least pointing power of the three options. Since the offset pointing requirements were reduced from  $\pm 45$  degrees to  $\pm 30$  degrees, the size of the pointing mirror is no longer excessive. The fixed telescope and electronics provide design simplicity with respect to spacecraft electrical and thermal interface. By using a beryllium mirror (approximately 10 pounds), the power requirement for pointing is only a few watts and momentum compensation is simpler than the



Table 4-4. HRPI Pointing Option Tradeoffs

Item	Option 1	Option 2	Option 3
Pointing Method (See Figure 7)	Fixed telescope with rotating point mirror	Rotating Telescope and pointing mirror	Gimballed telescope - no pointing mirror
Scan line skew on terrain	None	None	None
Instrument Dimen- sions			
Cross track axis	72 inches	25 inches	25 inches
Along track axis	25 "	60 "	35 "
Nadir axis	30 "	25 "	40 "
Instrument Volume	3.1 ft <sup>3</sup>	2.2 ft <sup>3</sup>	2.0 ft <sup>3</sup>
Swept Volume for $\pm 30$ degrees pointing	Same as instrument volume	Same as instrument volume	4.1 ft <sup>3</sup>
Weight Estimates			
Telescope	70 lbs	70 lbs	70 lbs
Detectors/beam- splitter	8	8	8
Mirror/structure	20	20	20
Pointing assembly	34	110 <sup>(1)</sup>	70 <sup>(2)</sup>
Angular Momentum Compensation	19	19	19
Electronics	28	28	28
Thermal control	16	16	16
Miscellaneous	20	20	20
Structure	85	90	90
Net	<u>300</u>	<u>381</u>	<u>321</u>
10% contingency	30	38	32
Total	<u>330 lbs</u>	<u>419 lbs</u>	<u>353 lbs</u>

Table 4-4. HRPI Pointing Option Tradeoffs (continued)

Item	Option 1	Option 2	Option 3
Power Estimates			
Electronics	100 Watts	100 watts	100 watts
Pointing	2	56 <sup>(1)</sup>	22 <sup>(2)</sup>
Heaters	19	19	19

(1) Estimate based upon similar Honeywell pointing system, scaled down for lighter instrument. (Honeywell HRPI Point Design, May 1974)

(2) Estimate based upon similar Hughes pointing system, scaled up for slightly heavier system (Hughes HRPI Point Design, June 1974)

other options which require large mass motions. The cross-track telescope orientation is also the most suitable for packaging into the TRW baseline spacecraft configuration.

Options 2 and 3 both require telescope motion for pointing. This adds complication (and therefore cost) to the electrical and thermal design. Flexible cabling must be used for electrical connections between the detector electronics and the fixed sensor housing. Thermal radiation to space would require either flexible heat piping to a fixed radiator or large exit apertures to allow for motion of a radiator that is fixed to the telescope.

Both options 2 and 3 require the motion of large masses for field-of-view pointing. Pointing power and momentum compensation requirements are therefore more severe than the selected fixed telescope approach.

Option 2 (rotating telescope and pointing mirror) has the lowest swept volume requirement, but the estimated sensor weight is 90 pounds greater than the selected option. The swept volume is lower because the pointing mirror does not move relative to the telescope axes. The increased weight requirement is due to the need for an inner telescope housing and an outer thermal housing since the telescope rotates relative to the fixed sensor outer housing.

At first glance, one would conclude that Option 3 would require the least weight since that approach does not require a pointing mirror. The original Westinghouse HRPI point design had allotted 143.7 pounds for the mirror and pointing assembly. The mirror/pointing assembly weight is now reduced to 54 pounds due to reduced pointing requirements and the use of beryllium in the mirror structure. Based upon the Hughes estimate for instrument gimbaling and pointing control, the Option 3 (no pointing mirror) pointing assembly weight estimate is 70 pounds. Some additional structure weight is also anticipated so that the Option 3 weight estimate exceeds 350 pounds. This is 20 pounds more than the baseline Option 1 configuration.

In summary, the fixed telescope configuration (baseline Option 1) has been selected because of the following features:

- Lowest weight
- Least pointing power
- Simplest electrical and thermal spacecraft interface
- Minimum momentum compensation requirement
- Most suitable configuration for TRW baseline spacecraft design

### 4.3 DATA COLLECTION SYSTEM

The concept for the data collection system (DCS) associated with the Earth Observatory Satellite (EOS), illustrated in Figure 4-9, provides for a large number of simple, low-cost data collection platforms (DCPs). These widely dispersed platforms take data from as many as eight sensors and assemble short digital messages (~100 bits) for random-emission burst transmission approximately every two minutes. The orbiting EOS would then relay the DCP messages, either with or without processing, directly to a local user terminal (LUT) as well as to the NASA ground tracking stations via the spacecraft unified S-band downlink. In addition to the direct transmission to user, another desirable innovation is the addition of a "command link", from LUT to DCP via the Earth Observatory Satellite, which allows the user to vary the sensor measurement range, turn on a new sensor bank, open a flood control valve, etc. Finally, a DCS traffic capacity on the order of 20,000 data collection platforms is projected.

This section is a brief investigation of the above DCS concept for EOS. Section 4.3.1 discusses possible DCS configurations, degree of on-board processing, and frequency selection considerations. Section 4.3.2 presents link analyses and power budgets for configurations with and without satellite processing and detection of DCP messages. Finally, Section 4.3.3 reviews the implications of the preceding link analysis, presents a possible DCS configuration accommodating the above-mentioned command link and considers optimization of spacecraft UHF antenna for the constraint on power flux density on the earth's surface.

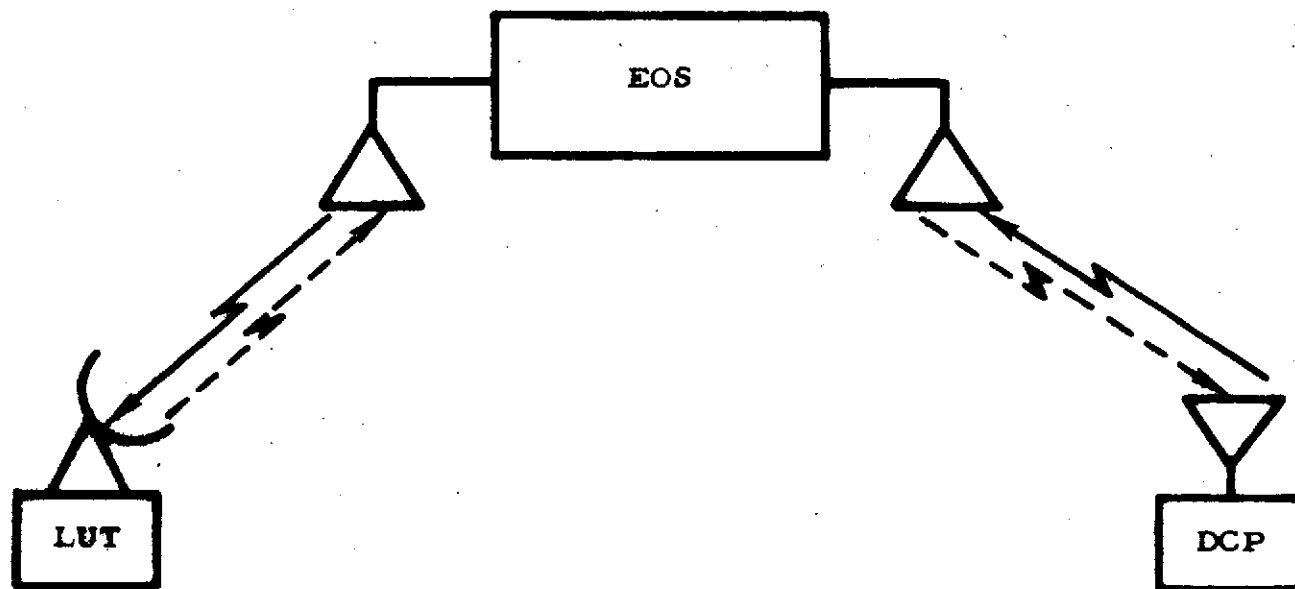


Figure 4-9. DCS Concept Illustrating Direct Transmission to User Concept Showing Platform Message and LUT Command Links (S-Band Transmission to STDN is Omitted)

#### 4.3.1 DCS Configuration

The degree of on-board processing (either on-board or ground processing is required to separate a desired signal from the background of signals intended for other users) and choice of frequencies are fundamental system considerations and directly influence the cost of the overall DCS network — to both the spacecraft and local user equipment. These topics are treated, respectively, in the remainder of this section.

##### 4.3.1.1 Frequency Selection Considerations

The choice of frequencies for the DCS uplink/ downlink is made consistent with the concept of simple, low-cost user equipment.

Transmitter efficiency will decrease sharply as the frequency increases (typically 35 percent at VHF and 16.5 percent at S-band). Generally, equipment expense increases with frequency. The higher frequencies exhibit a greater free space path loss which the uplink power budget cannot tolerate with the limited DCP transmitter power. The Doppler frequency uncertainty increases with transmitted frequency. The increased requisite bandwidth required, if a bentpipe repeater is used, reduces the SNR at the satellite and, hence, increases the downlink SNR degradation caused by uplink turnaround noise.

On the other hand, the higher frequencies have wider channel allocations and thus more bandwidth — an advantage for configurations including satellite processing. At higher frequencies, such as S-band, antenna size decreases with frequency and the antenna gain increases with frequency for a fixed antenna size, thereby offsetting the increased path loss at the higher frequencies. The low frequencies, particularly VHF, suffer under worst-case local RFI conditions, increased interference problems caused by a wide spectrum of commercial usages. This last disadvantage, which can in the future only grow worse, is considered sufficient to eliminate the VHF frequency region from consideration.

Atmospheric attenuation effects are neglected since they are negligible for the frequencies considered (below 3 GHz) and for antenna elevation angles of 5 degrees\* and above.

---

\*See Reference 3.

The utilization of UHF uplink and downlink frequencies appear as an attractive compromise. Local user cost can be kept low and DCP transmitter efficiency is reasonable (a consideration for battery operated units). The same antennas may be used with a diplexer for both receiving and transmitting on the spacecraft and on the DCP.

In the remainder of this memo, therefore, the DCS uplink and downlink frequencies (for both DCP messages and command messages) are fixed at 401.55 MHz and 465 MHz, respectively.

#### 4.3.1.2 On-Board Processing

The degree of satellite on-board processing of the uplink signal prior to downlink transmission and the cost and complexity of user ground equipment are, for a given level of system performance, inversely related. The present concept of a DCS network for EOS involves a massive amount of user equipment, perhaps on the order of 20,000 DCP's and 50 to 100 LUT's. Placing the burden of processing complexity with the user would result in a manifold duplication of facilities and cost at each user installation. In addition, it is clear that the problem of DCP mutual interference, or message collision, will increase with the number of platforms simultaneously in view and that this problem can be reduced by parallel processing and detection in the spacecraft. These arguments vie with the outright simplicity of the "bentpipe" approach — frequency translation only with no on-board processing.

The bentpipe approach (ERTS 1 concept) is illustrated in Figure 4-10. The block diagram (showing redundancy) indicates that the 401.55 MHz uplink signal is sent to a UHF receiver preamp through an antenna/diplexer arrangement. The signal is then frequency up-converted, without detection and sent to a UHF transmitter (power amplifier) and thereon to the diplexer/antenna for downlink transmission at 465 MHz. The link calculation for this approach is presented in Section 4.3.2.

The addition of an on-board DCS processor is shown in Figure 4-11. Such an arrangement would allow for parallel processing and detection in the spacecraft. The DCS processor could be implemented in several ways, of which Figure 4-12 is typical. This approach is similar to the Nimbus F



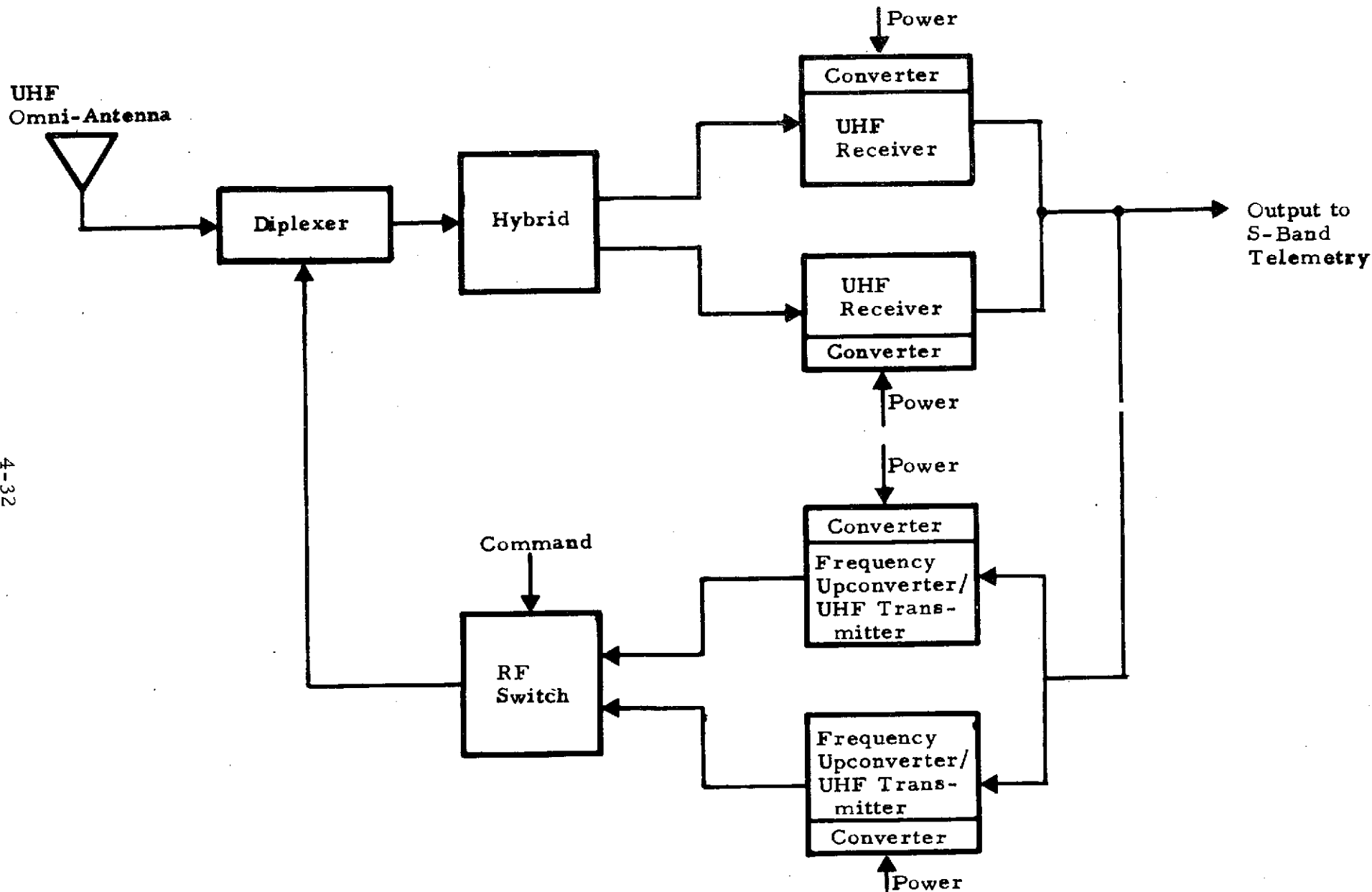


Figure 4-10. Spacecraft DCS Module Bentpipe Block Diagram Showing Redundancy

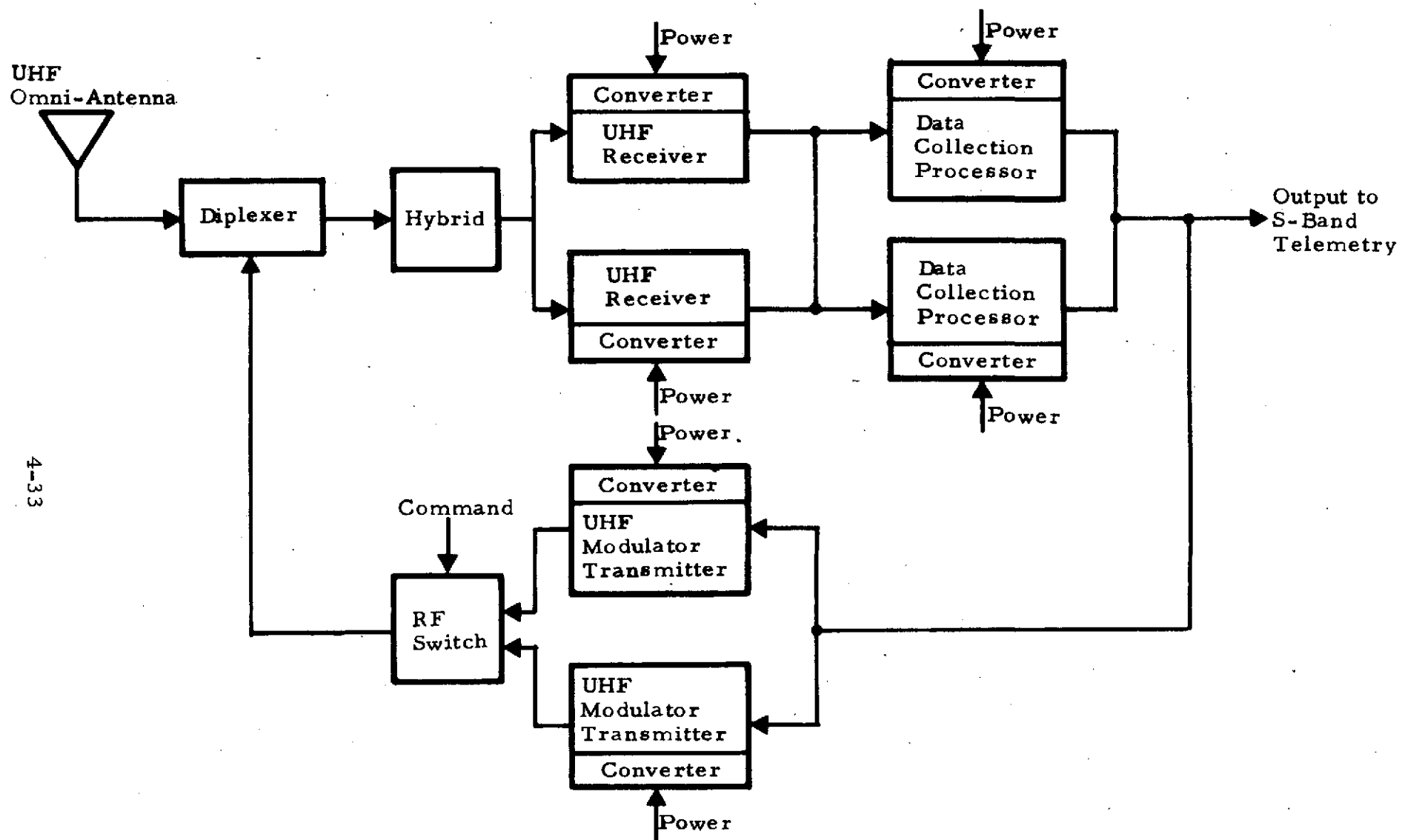


Figure 4-11. Spacecraft DCS Module Block Diagram Indicating On-Board Processing and Detection

RAMS\* without time compression. Assume the initial frequency uncertainty is 100 kHz. The region of frequency uncertainty is searched in 5 kHz steps by mixing with the stepping oscillator as shown. The signal presence detector consists of an envelope detector whose output is compared with an adaptive threshold. If a signal is located within a 5 kHz "cell", the control unit assigns one of three (or more) phase-locked loops to that signal. In this manner multiple simultaneous signals may be tracked if they are at least 5 kHz apart. The demodulated data are recovered, formatted, and stored serially with each message intact in an output buffer for a more constant bit-stream downlink transmission. The downlink bit rate (~1 kbps) is less than the uplink data (2.5 kbps for each message) to reduce the EIRP requirements and, hence, lower the power flux density on the earth's surface.

Tradeoffs of on-board processing complexity must await a firm definition of the scope of the data collection subsystem for EOS.

---

\*See Reference 4

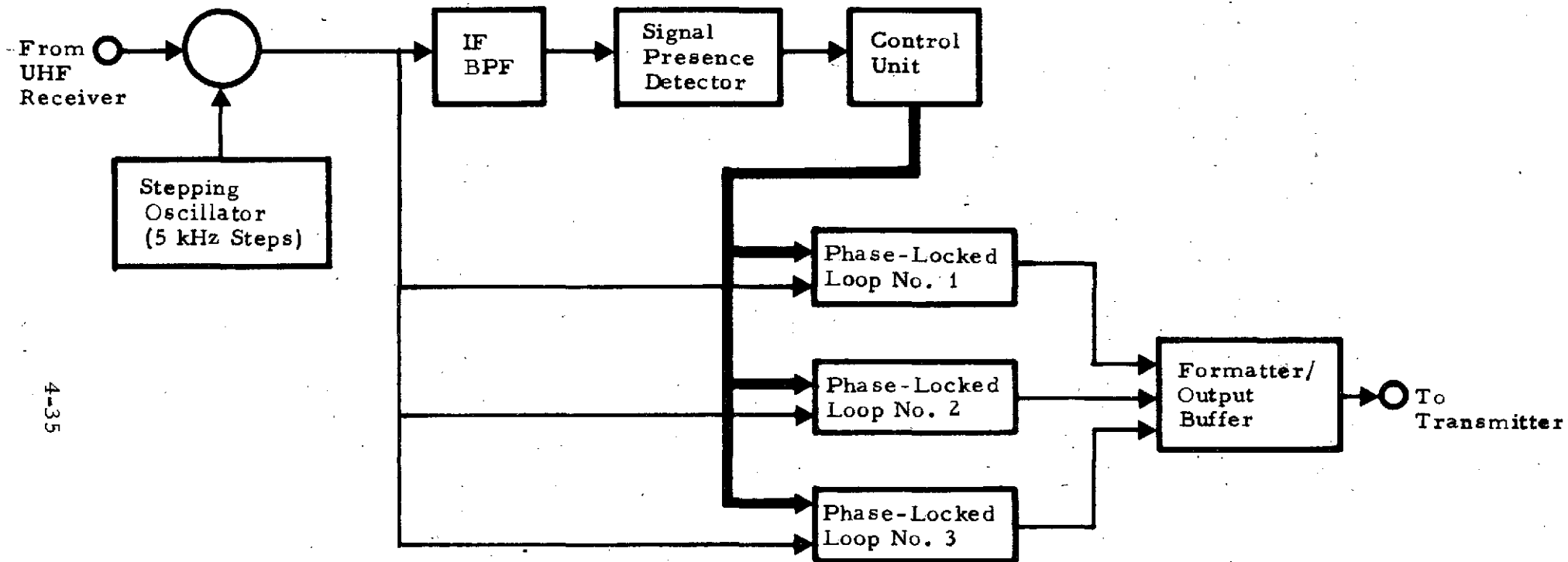


Figure 4-12. DCS Processor

#### 4.3.2 Link Analysis

This section presents the link analyses relating to the direct transmission of message data from the Data Collection Platforms (DCP's) to the Local User Terminal via the EOS satellite.

Two power budgets are included, one based on a degree of satellite on-board parallel processing with detection and the other based on a "bent-pipe" approach with no on-board processing.

The UHF transmitter in the platform will feed an omnidirectional antenna, and transmits a narrowband PSK signal to the satellite. PSK modulation was selected since it provides a low bit error rate for the order of SNR involved and its energy distribution optimizes the frequency domain random emission performance.

The power flux density of  $-152 \text{ dBw/m}^2/4 \text{ KHz}$ , as specified by NASA\*, for an orbit of 386 nmi, limits spacecraft transmitted EIRP to 6 dBm. The spacecraft UHF antenna is selected, as nearly as possible, to equalize the power flux density on the earth's surface, providing a -1 dB gain on-axis and a +2.5 dB gain  $\pm 60$  degrees off-axis.

The results of the link analyses, summarized in tabular form, follow the detailed supporting work of Sections 4.3.2.1 through 4.3.2.4.

##### 4.3.2.1 Uplink Parameters (Bent Pipe)

- Platform Transmitter Power -- The DCP transmitter power is assumed to be 5 watts RF.
- DCP Transmission Circuit Loss -- This factor combines the transmission line loss, VSWR loss and radiation efficiency. The combined total loss is estimated about 1 dB.
- DCP Transmitter Antenna Gain -- The proposed DCP antenna will provide an elliptically polarized beam with some 165 degree sky coverage and has a gain of 0 dB above an isotropic radiator.

---

\* See Reference 1

- **Free Space Transmission Loss** -- For a 386 nmi orbit spacecraft, the communication range limits vary from 386 nmi to 1402 nmi for a 5 degree limit elevation angle. The associated space losses for 401.55 MHz carrier frequency are then 141.6 dB and 152.8 dB, respectively.
- **Spacecraft Receiving Antenna Gain** -- The spacecraft antenna will incorporate a crossed dipole overground plane to provide an elliptically polarized earth coverage with half power beam width of 120 degrees. The antenna has an on-axis gain of -1 dB with respect to isotropic radiator, and off-axis gain of +2.5 dB (+60 degrees).
- **Polarization Loss** -- The Polarization Loss is obtained by a consideration of the axial ratio performance for both the transmitting and receiving antennas. The assumed value of axial ratio for the spacecraft receiving antenna is 1 dB on-axis and 6dB at +60 degrees off-axis and for DCP antenna is 5 dB and 5 dB, respectively. The combination of these two implies a loss of 0.5 dB on-axis and 1.6 dB off-axis.
- **Spacecraft Receiving Circuit Loss** -- The spacecraft circuit loss comprises the feedline and coupling losses. These are estimated to be ~1 dB.
- **Receiving System Noise Power Spectral Density** -- The noise power per unit bandwidth is  $KT_{(syst)}$ , where  $K$  = Boltzmann's constant and  $T_{(syst)}$  is the effective system noise temperature in  $^{\circ}K$ . The effective noise temperature  $T_{(syst)}$  is obtained from the following relationship:

$$T_{system} = (F - 1) T_o + \frac{T_s}{L_R} + T_o \left( 1 - \frac{1}{L_R} \right)$$

where

$T_o$  = thermal equilibrium noise temperature,  $290^{\circ}K$  with cold sky

$F$  = receiver noise figure, 2 dB

$T_s$  = source noise temperature,  $660^{\circ}K$  (see Reference 2)

$L_R$  = receiver feedline loss ratio, 1.26

The nominal  $T_{(syst)}$  is  $753.3^{\circ}K$  and noise power spectral density is 169.8 dBm/Hz.

- **Bandwidth** -- The 30 KHz bandwidth is required to allow for +10 KHz Doppler and +2.5 crystal frequency uncertainty of the DCP transmitter. The modulation bandwidth of 5 KHz for the 2500 bps information rate is also included.

- Hardware Degradation -- SNR degradation caused by filter band-limiting and imperfection of spacecraft hardware is assessed to be 1.5 dB.

On the basis of the parameter values enumerated above, the Uplink Power Budget for the bent pipe configuration is as tabulated below.

Table 4-5. Uplink Power Budget (Bent pipe)

Uplink frequency = 401.55 MHz

Assumed orbit = 386 nmi

	90° Elev.	5° Elev.
DCP Transmitter Power	+37 dBm	+37 dBm
DCP Transmission Circuit Loss	-1 dB	-1 dB
DCP Antenna Gain	0 dB	0 dB
Space Loss	-141.6 dB	-152.8 dB
Spacecraft Antenna Gain	-1.0 dB	+2.5 dB
Polarization Loss (worst-case)	-0.5 dB	-1.6 dB
Spacecraft Receiving Circuit Loss	-1.0 dB	-1.0 dB
Total Received Power	-108.1 dB	-116.9 dB
Spacecraft Receiver Noise Spectral Density, $N_v$ $T_{\text{system}} = 754^\circ\text{K}$	-169.8 dBm/Hz	-169.8 dBm/Hz
C/KT	61.7 dBm-Hz	52.9 dBm-Hz
Bandwidth (30 KHz)	44.8 dB	44.8 dB
Hardware Degradation	1.5 dB	1.5 dB
$S_v/N_v$ (SNR at space vehicle)	15.4 dB	6.6 dB

#### 4.3.2.2 Downlink Parameters (Bent Pipe)

- Spacecraft Transmitter Power -- The spacecraft transmitter power is limited to 7.95 milliwatts (9 dBm) in order that the power flux density limit of  $-152 \text{ dBW/m}^2 / 4 \text{ KHz}^*$ , as established by NASA, is not exceeded.
- Losses -- The spacecraft transmission circuit losses caused by transmission line, VSWR, and radiation efficiency is estimated at 2 dB.

\*See Reference 1 for 465 MHz downlink frequency.

- **Spacecraft Transmitting Antenna Gain** -- Utilizing the same antenna for receiving/transmitting results in an off axis gain of -1 dB and an off-axis (+60 degrees) gain of +2.5 dB.
- **EIRP** -- Maximum allowable EIRP imposed by power flux density requirements (for the 386 nmi (715 Km) spacecraft orbit) is:  

$$-122 + 10 \log (4\pi) + 10 \log [(7.15 \times 10^5)^2] = 6.08 \text{ dBm}$$
- **Free Space Transmission Loss** -- For a 386 nmi orbit spacecraft, the communication range limits vary from 386 nmi to 1402 nmi for a 5 degree limit elevation angle. The associated space losses for 465 MHz carrier frequency are then 142.9 dB and 154.1 dB, respectively.
- **Receiving Antenna Gain** -- Proposed receiving antenna gain of 23 dB would require an approximate 12 foot dish with a 13 degree beamwidth at 465 MHz.
- **Tracking Loss** -- Estimated at ~1 dB for the 13 degree beamwidth antenna.
- **Polarization Loss** -- The polarization loss is obtained by a consideration of the axial ratio performance for both the transmitting spacecraft antenna and the ground station receiving antenna. The assumed value of axial ratio is 1 dB on-axis and 6 dB at +60 degrees off-axis for the spacecraft antenna and 1.5 dB for the ground station dish antenna. The combination of these two implies a loss of 0.1 dB on-axis and 0.7 dB off-axis.
- **Receiving System Noise Power Spectral Density** -- The noise power per unit bandwidth is  $KT_{(syst)}$ , where  $K$  = Boltzmann's constant and  $T_{(syst)}$  is the effective system noise temperature in  $^{\circ}\text{K}$ . The effective noise temperature  $T_{(syst)}$  is obtained from the following relationship:

$$T_{\text{system}} = (F - 1) T_o + \frac{T_s}{L_R} + T_o \left( 1 - \frac{1}{L_R} \right)$$

where

$T_o$  = thermal equilibrium noise temperature,  $290^{\circ}\text{K}$  with cold sky

$F$  = receiver noise figure, 3 dB

$T_s$  = sky temperature,  $65^{\circ}\text{K}$

$L_R$  = receiver feedline loss ratio, 1.2

The nominal  $T_{(syst)}$  is  $393.5^{\circ}\text{K}$  and noise power spectral density is  $-172.7 \text{ dBm/Hz}$ .



- Detection Noise Bandwidth -- The bandwidth required to recover the data is taken as 1.2 times data rate, i.e., 3.0 kHz. The excess bandwidth, 20 percent over the theoretical minimum of 50 percent of the bit rate, is used to reduce the intersymbol interferences. It represents initial optimization of the carrier SNR, the intersymbol interference and the frequency domain spectral width.
- Degradation of Downlink SNR -- Caused by turnaround of uplink noise for the linear case (no spacecraft transmitter limiting) is given by

$$\text{Degradation} = 1 + \frac{S_g/N_g}{S_v/N_v}$$

where

$S_g/N_g$  = SNR at input to ground station in the absence of uplink noise ( $N_v = 0$ )

$S_v/N_v$  = SNR at space vehicle transmitter input

For a worst-case calculation we take the value of  $S_v/N_v$  to be a minimum (corresponding to the 5° elevation slant range uplink path. The resulting downlink SNR degradation for the 90 degree elevation and 5 degree elevation downlink is 16.4 dB and 8.2 dB, respectively.

On the basis of the parameter values enumerated above, the Downlink Power Budget for the bent pipe configuration is as tabulated in Table 4-6.

Table 4-6. Downlink Power Budget (Bent Pipe)

Downlink frequency = 465 MHz  
Assumed orbit = 386 nmi

	90° Elev.	5° Elev.
Spacecraft Transmission Power	+9 dBm	+9 dBm
Transmission Losses	-2 dB	-2 dB
Spacecraft Antenna Gain	-1 dB	+2.5 dB
EIRP	+6 dBm	+9.5 dBm
Space Loss	-142.9 dB	-154.1 dB
LUT Antenna Gain	+23 dB	+23 dB
Tracking Loss	-1 dB	-1 dB
Polarization Loss (worst-case)	-0.1 dB	-0.7 dB
Received Signal Power	-115.0 dB	-123.3 dB
LUT Receiver Noise Spectral Density, $N$ $T_{\text{system}} = 393.5^\circ\text{K}$	-172.7 dBm/Hz	-172.7 dBm/Hz
$C/KT$	57.7 dBm-Hz	49.4 dBm-Hz
Detection Noise Bandwidth (3 kHz)	34.8 dB	34.8 dB
$S/N_{\text{noise}}$ (SNR in absence of turnaround noise)	22.9 dB	14.6 dB
Degradation in Downlink SNR	16.4 dB	8.2 dB
$S/N$	6.5 dB	6.4 dB
$S/N \mid P_E = 5 \times 10^{-5}$	8.8 dB	8.8 dB
Margin	-2.3 dB	-2.4 dB

#### 4.3.2.3 Uplink Parameters (On-Board Processing)

Analysis of the uplink parameters is the same as in Section 4.3.2.1 except for the bandwidth processing improvement gained by on-board detection. The detection bandwidth required to recover the data is taken as 1.2 times data rate, or 3 kHz.

Table 4-7. Uplink Power Budget (w/Processing)

Uplink frequency = 401.55 MHz

Assumed orbit = 386 nmi

	90° Elev.	5° Elev.
DCP Transmitter Power	+37 dBm	+37 dBm
DCP Transmission Circuit Loss	-1 dB	-1 dB
DCP Antenna Gain	0 dB	0 dB
Space Loss	-141.6 dB	-152.8 dB
Spacecraft Antenna Gain	-1.0 dB	+2.5 dB
Polarization Loss (worst-case)	-0.5 dB	-1.6 dB
Spacecraft Receiving Circuit Loss	-1.0 dB	-1.0 dB
Total Received Power	-108.1 dB	-116.9 dB
Spacecraft Receiver Noise Spectral Density, $N_v$ $T_{\text{system}} = 754^\circ\text{K}$	-169.8 dBm/Hz	-169.8 dBm/Hz
C/KT	61.7 dBm-Hz	52.9 dBm-Hz
Detection Noise Bandwidth (3 kHz)	34.8 dB	34.8 dB
Hardware Degradation	1.5 dB	1.5 dB
$S_v/N_v$ (SNR at space vehicle)	25.4 dB	16.6 dB
$S_v/N_v \mid P_E = 5 \times 10^{-5}$	8.8 dB	8.8 dB
Margin	16.6 dB	7.8 dB

#### 4.3.2.4 Downlink Parameters (On-Board Processing)

Analysis of the downlink parameters is the same as in Section 4.3.2.2 except for the lessening of the downlink SNR degradation caused by the improvement in the uplink SNR as shown in Table 4-7. For the worst-case uplink  $S_v/N_v$  of 16.5 dB (corresponding to the 5 degree elevation uplink), the degradation in downlink SNR amounts to 10.8 dB for the 90 degree elevation downlink and 4.2 dB for the 5 degree elevation downlink. A 4 dB improvement is also gained by the narrowing of the detection noise bandwidth for a 1000 bps downlink data rate.

Table 4-8. Downlink Power Budget (w/ Processing)

Downlink frequency = 465 MHz

Assumed orbit = 386 nmi

	90° Elev.	5° Elev.
Spacecraft Transmission Power	+9 dBm	+9 dBm
Transmission Losses	-2 dB	-2 dB
Spacecraft Antenna Gain	-1 dB	+2.5 dB
EIRP	+6 dBm	+9.5 dBm
Space Loss	-142.9 dB	-154.1 dB
LUT Antenna Gain	+23 dB	+23 dB
Tracking Loss	-1 dB	-1 dB
Polarization Loss (worst-case)	-0.1 dB	-0.7 dB
Received Signal Power	-115.0 dB	-123.3 dB
LUT Receiver Noise Spectral Density, $N$ $T_{\text{system}} = 393.5^\circ\text{K}$	-172.7 dBm/Hz	-172.7 dBm/Hz
$C/KT$	57.7 dBm-Hz	49.4 dBm-Hz
Detection Noise Bandwidth (1.2 kHz)	30.8 dB	30.8 dB
$S_g/N_g$ (SNR in absence of turn-around noise)	26.9 dB	18.6 dB
Degradation in Downlink SNR	10.8 dB	4.2 dB
$S/N$	16.1 dB	14.4 dB
$S/N$ $P_E = 5 \times 10^{-5}$	8.8 dB	8.8 dB
Margin	+7.3 dB	+5.6 dB

#### 4.3.3 Concluding Remarks

The link analysis of Section 4.3.2 clearly favors a DCS configuration involving on-board processing. The addition of convolutional coding (as used in ERTS 1) would yield an approximate 4 dB increase in processing gain allowing the bentpipe to operate with  $\sim 1.6$  dB margin. This would, however, place added complexity and cost on the DCS user and would, therefore, seem contrary to the DCS goals for EOS, as stated in the introductory section.

The concept of a low-cost and straightforward addition of a command link from LUT to platform was considered. For simplicity and without the need of dedicated on-board processing, the command message can be identical in format and bit rate with the platform message. In light of the link calculations of Section 4.3.2, it would be essential for "commandable" platforms to be provided with a minimum of an 18 dB gain antenna (using on-board processing). If a separate on-board processor and a portion of the channel bandwidth is devoted to command messages, a 20 dB processing gain could be realized by lowering the downlink data rate to 10 bps, thereby eliminating the need for platform antenna gain.

Theoretical and experimental studies have been performed by TRW to determine the manner in which optimum earth coverage could be obtained from an S-band antenna.\* The desired radiation pattern of the antenna was one which would provide maximum gain at the earth's horizon and provide a gain elsewhere proportional to the decrease of path loss from the spacecraft to earth. The ideal realization would produce a uniform power flux density over the earth surface in view of the spacecraft.

The result of these efforts can be depicted in the curve of Figure 4-13, which shows the relative power flux density on the earth's surface versus the angle from antenna axis. Note that the power flux density is the same at  $0^\circ$  and  $60^\circ$  and has a pronounced maximum at  $\sim 50^\circ$ . The antenna, therefore, has an approximate 11 dB greater gain off axis ( $\pm 60^\circ$ ) additional slant-range path loss. The peak at  $50^\circ$  off-axis would, however, mean a reduction in EIRP of 6 dB. Overall, then, a 5 dB improvement in the worst-case link power budget ( $5^\circ$  elevation) could be realized.

---

\* See Reference 2.

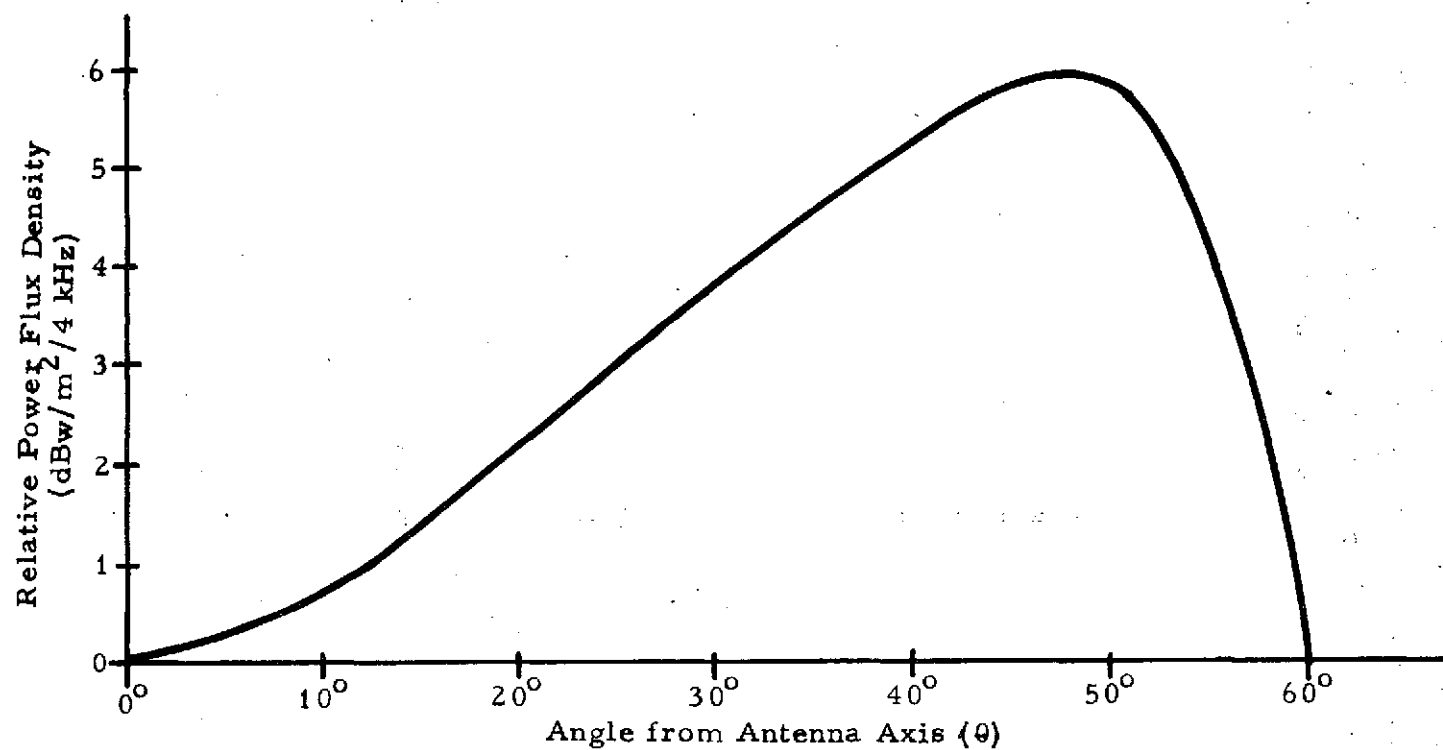


Figure 4-13. Effective Gain Versus Aspect Angle Over Earth Coverage. Free Space Path Losses are Included.

An outline sketch of the antenna (as designed for S-band operation) is shown in Figure 4-14. At UHF frequencies, the bandwidth of the antenna would be insufficient for both receiving and transmitting frequencies, therefore, two separate antennas would be required. Also at UHF, the antenna size would become large requiring an increase in dimensions by a factor of 5.61 for the receiving antenna and 4.84 for the transmitting antenna.

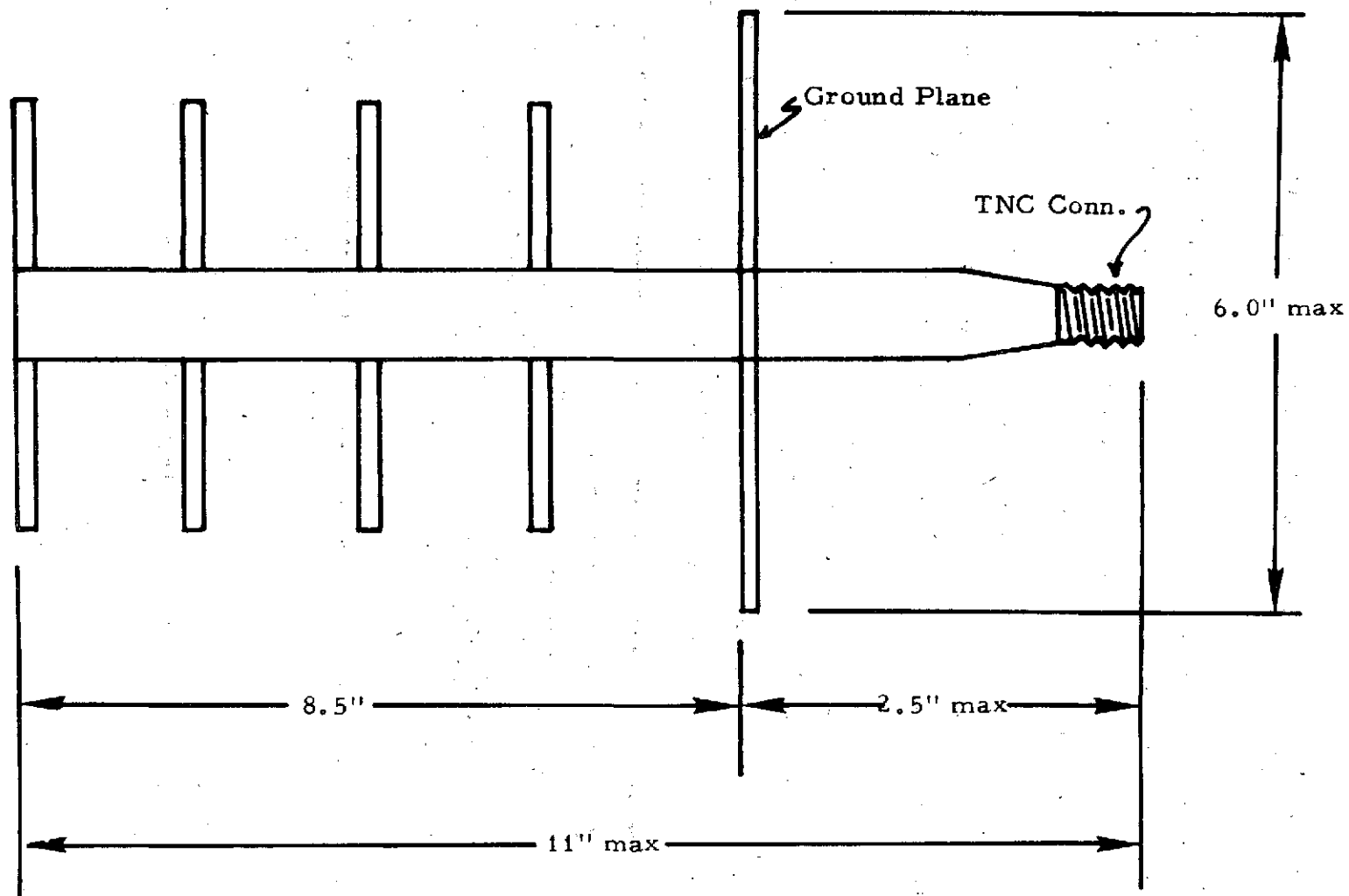


Figure 4-14. S-Band Shaped Beam Antenna  
(Outline Sketch)

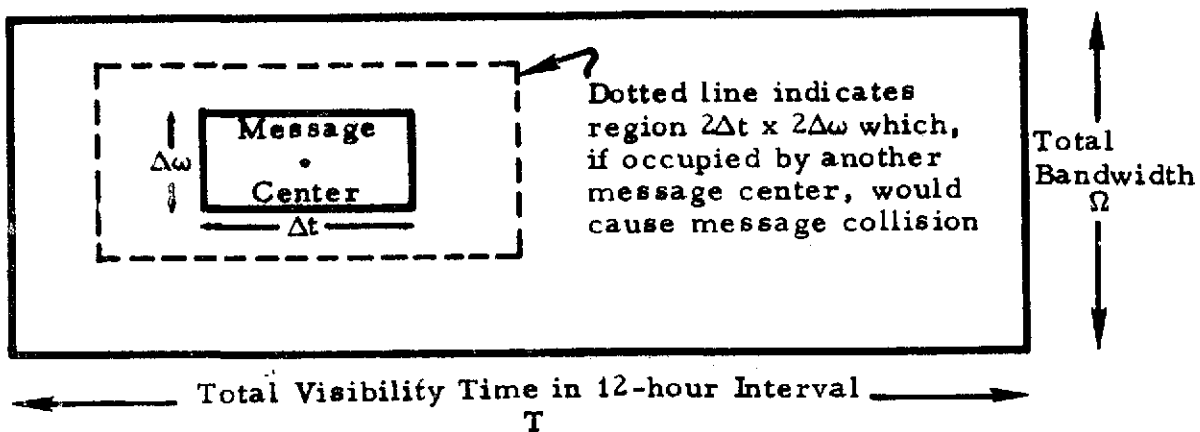


#### 4.3.4 Platform Capacity of the Data Collection Subsystem\*

The following discussion concerns the number of platforms which can be simultaneously visible from the satellite for a given time – bandwidth product,  $\Omega T$ , to provide a given probability of correctly receiving a 100-bit message from each platform.

Bit errors are assumed to be caused by message collision only since those randomly-occurring errors, occurring for a reasonable SNR, are at least an order of magnitude less frequent ( $BER = 5 \times 10^{-5}$  for  $E_b/N_o = 8.8$  dB).

Let the duration of the message be  $\Delta t$  and occupy a portion of the allocated spectral bandwidth,  $\Delta\omega$ . From the figure below, it is readily seen that mutual interference, or message collision, occurs if more than one message "center" occupies a subregion  $2\Delta t \times 2\Delta\omega$  of the total area,  $\Omega T$ .



Assume, on the average, that each of  $N+1$  platforms transmits  $k$  times in the interval  $T$ . The probability that any one message occupies the region  $2\Delta\omega \times 2\Delta t$  is

$$\frac{4\Delta\omega\Delta t k}{\Omega T}^\dagger$$

Assume that a desired message is centered in the  $2\Delta\omega \times 2\Delta t$  region. The probability that none of the other  $N$  platform messages interfere is

\* See Reference 5

† Simplifying assumption of uniformly distributed random frequency is used.

$$\left[ 1 - \frac{4\Delta\omega\Delta t k}{\Omega T} \right]^N$$

The probability that collisions occur in each of the  $k$  transmissions is

$$\left[ 1 - \left( 1 - \frac{4\Delta\omega\Delta t k}{\Omega T} \right)^N \right]^k$$

Hence, the probability of success (at least one message not interfered with) is one minus the above or

$$P_s = 1 - \left[ 1 - \left( 1 - \frac{4\Delta\omega\Delta t k}{\Omega T} \right)^N \right]^k$$

Now, since  $\Omega T / 4\Delta\omega\Delta t k$  must be greater than  $N$ , let

$$\frac{4\Delta\omega\Delta t k}{\Omega T} = \frac{X}{N}, \quad 0 \leq X < 1$$

Also let

$$\frac{4\Delta\omega\Delta t}{\Omega T} = \frac{1}{A}$$

then

$$\frac{k}{A} = \frac{X}{N}$$

and the probability of success may be written

$$P_s = 1 - [1 - (1 - X/N)^N]^{AX/N}$$

For  $N$  large, we use the approximation

$$1 - (1 - X/N)^N \approx 1 - e^{-X}$$

to obtain

$$P_s = 1 - (1 - e^{-X})^{AX/N}$$

Differentiating  $P_s$  with respect to  $X$ , and setting the result equal to zero, we obtain

$$X = \ln 2 = 0.693$$

as a maximum value of  $P_s$  for the parameter  $X$ . For this case, we have

$$\begin{aligned} P_s &= 1 - (1 - e^{-0.693})(0.693A/N) \\ &= 1 - (0.6185)^{A/N} \end{aligned}$$

which yields probability of message success as a function of the number of platforms,  $N$ , and the parameter,  $A = \Omega T / 4\Delta\omega\Delta t$ . For a .95 probability of success of a 100 bit message ( $\Delta\omega\Delta t = 100$ ), one obtains the relation for the required time-bandwidth product

$$\Omega T = 2494 \cdot N$$

Figure 4-15 shows the total visibility,  $T$ , of satellite/ground station links in 12-hour intervals as a function of latitude for the 386 nmi orbit. Using the implied value of  $T$  from this plot, Figure 4-16 yields the required channel bandwidth as a function of  $N$  for various latitudes.

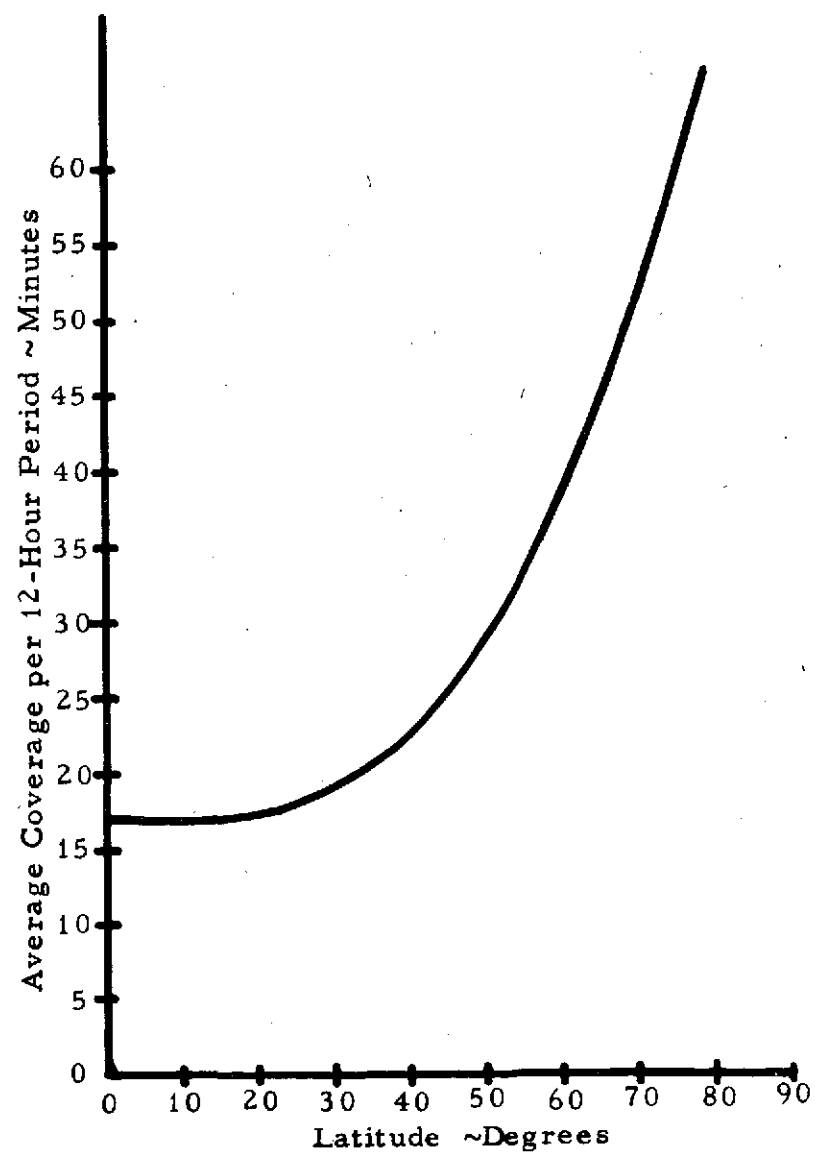


Figure 4-15. Total Visibility of Satellite/Ground Station Links

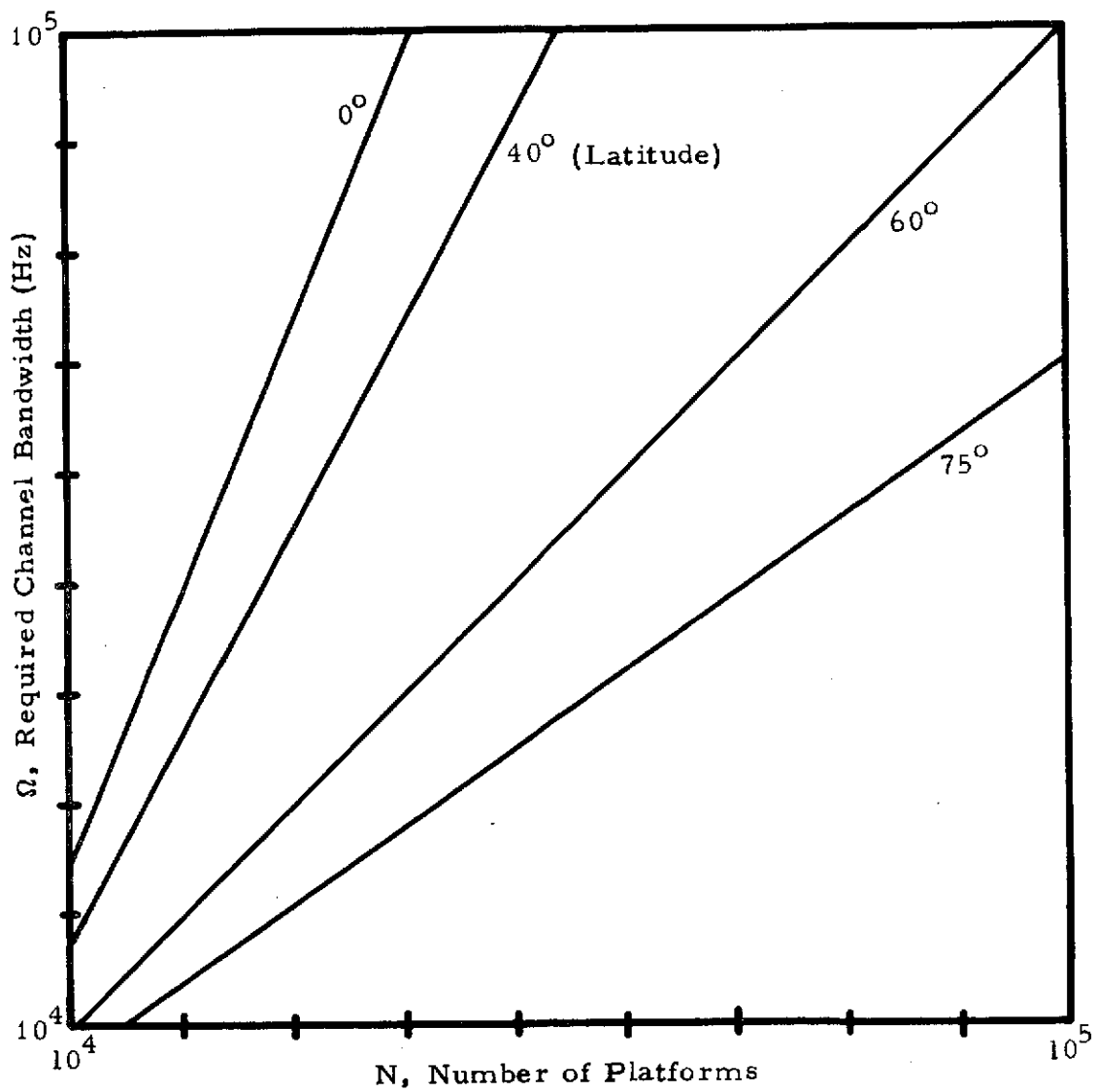


Figure 4-16. Channel Bandwidth for Various Latitudes

## REFERENCES

1. "Radio Frequency Allocations for Space and Satellite Requirements", Mission and Data Operations Directorate, Goddard Space Flight Center, June 15, 1973, p.7.
2. Tucker, R. F., "S-Band Shaped Beam Antenna for ERTS Satellite Proposal Study", TRW Interoffice Correspondence, March 13, 1969.
3. Final Report, DCS: "A Global Satellite Environmental Data Collection System Study", System Engineering Department, Radiation, Inc., January 1973, p. 30.
4. Cote, C. E., Dubose, J. F., and Coates, J. L., "The Nimbus F Random Access Measurement System", Fifth Annual Southeastern Symposium on System Theory, March 23, 1973.
5. Based on private communication with J. Taber, EOS Phase B Study, May 1974.

## 4.4 SYNTHETIC APERTURE RADAR

Synthetic aperture radar designs were reviewed to derive the characteristics for integration into the modular observatory.

The following documents were used as references:

Reference 1. Final Report, Spaceborne Synthetic Aperture Radar Pilot Study, April 11, 1974, Westinghouse Systems Development Div., Baltimore, Md.

Reference 2. Oral Progress Review, 22 August 1973, and Final Report, January 1974, Orbital Earth Resources Radar Program Definition Study, GERA-1985, Goodyear Aerospace Corp., Litchfield Park, Arizona.

### 4.4.1 Comparison of Westinghouse and Goodyear Designs

Table 4-9 lists the parameters of the Westinghouse and Goodyear designs extracted from References 1 and 2.

#### 2.1 X-Band-Dual Polarization

Examination of Table 4-9 reveals that the parameter values are quite similar for the X-band, dual polarization designs, differing significantly only in the length of the antenna, peak power, and data rates. The difference in data rates is accounted for by the fact that Goodyear included 2.5:1 azimuth pre-compression in the radar, while Westinghouse does not include any azimuth pre-compression. Westinghouse points out that such pre-compression could be included in order to reduce the data rate, but chose to omit it because it increases the complexity of the radar and is not necessary as the total data rate is within the capacity of the high speed data link.

Table 4-9. Parameters of the Westinghouse and Goodyear Designs (From References 1 and 2)

	X-Band Dual Polarization		X- and L-Band	
	Westinghouse	Goodyear	Westinghouse	Goodyear
Frequencies (GHz)	9.5	10	9.5 1.7	10 1.5
Average Transmitter Power (W)	150	161	150 25	161 30
Peak Power (KW)	4	18	4 .75	18 3
Pulse Length ( $\mu$ sec)	10-17	3	10-17	3
PRF (PPS)	3-4 k	2.99 k	3-4k	3k
Resolution (m)	30 (9 looks)	30	30	30
Depression Angle (deg.)	60-75	60	75	60
Polarization	Dual	Dual	Single*** Single	Dual Dual
Altitude (km)	914	914	914	914
Swath Width (km)	50	50	50	50
Antenna Size (LxHxD ft)	13.5 x 2.5 x 1	27 x 2.5 x 1	27 x 2.5 x 1	27 x 15 x 3 unfurled
Antenna Weight (lbs)	92	48*	174	130
Electronics Package Size (L x H x D in.)	31 x 22 x 9.5		38 x 24.5 x 19	
Electronics Volume ( $\text{ft}^3$ )	3.75	7.4	10.25	12.0
Electronics Weight (lbs)	170	220	387	365
Total Weight (lbs)	262	268	539	495
DC Power (W)	1143	1400	1262	1835
Thermal Power (W)	993	1240	1087	1644
Data Quantization (Bits)	4 + sign	4 + sign	4 + sign	4 + sign
Data Rate	2-79 MB/S channels	2-24 MB/S channels**	2-62.4 MB/S channels	4-24 MB/S channels*
Attitude Control	+0.02° Pitch & Yaw -0.06° Roll	+0.02° Pitch & Yaw -0.06° Roll	+0.02° Pitch & Yaw -0.06° Roll	+0.02° Pitch & Yaw -0.06° Roll
Attitude Rate	0.01°/sec. Pitch & Yaw Figs. 4-17 & -18 Roll	0.01°/sec. Pitch & Yaw Figs. 4-17 & -18 Roll	0.01°/sec. Pitch & Yaw Figs. 4-17 & -18 Roll	0.01°/sec. Pitch & Yaw Figs. 4-17 & -18 Roll

\* Not including spacecraft structure for antenna support.

\*\* Requires azimuth prefilter in radar for 2.5/1 pre-compression.

\*\*\* Dual polarization at X-band adds 138 pounds, 130 watts and one 62.4 MB/S channel.



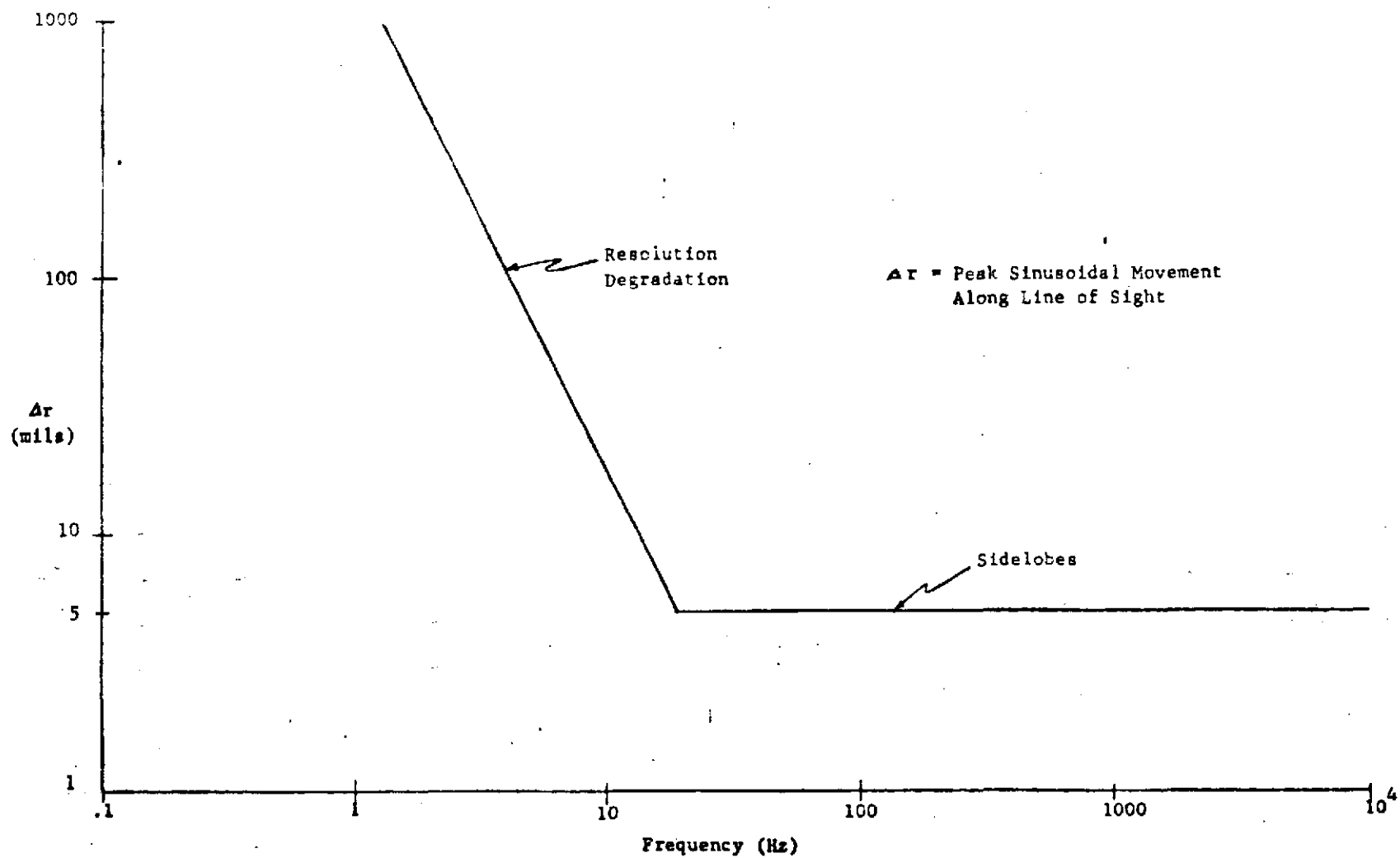


Figure 4-17. Deterministic Antenna Motion Requirement

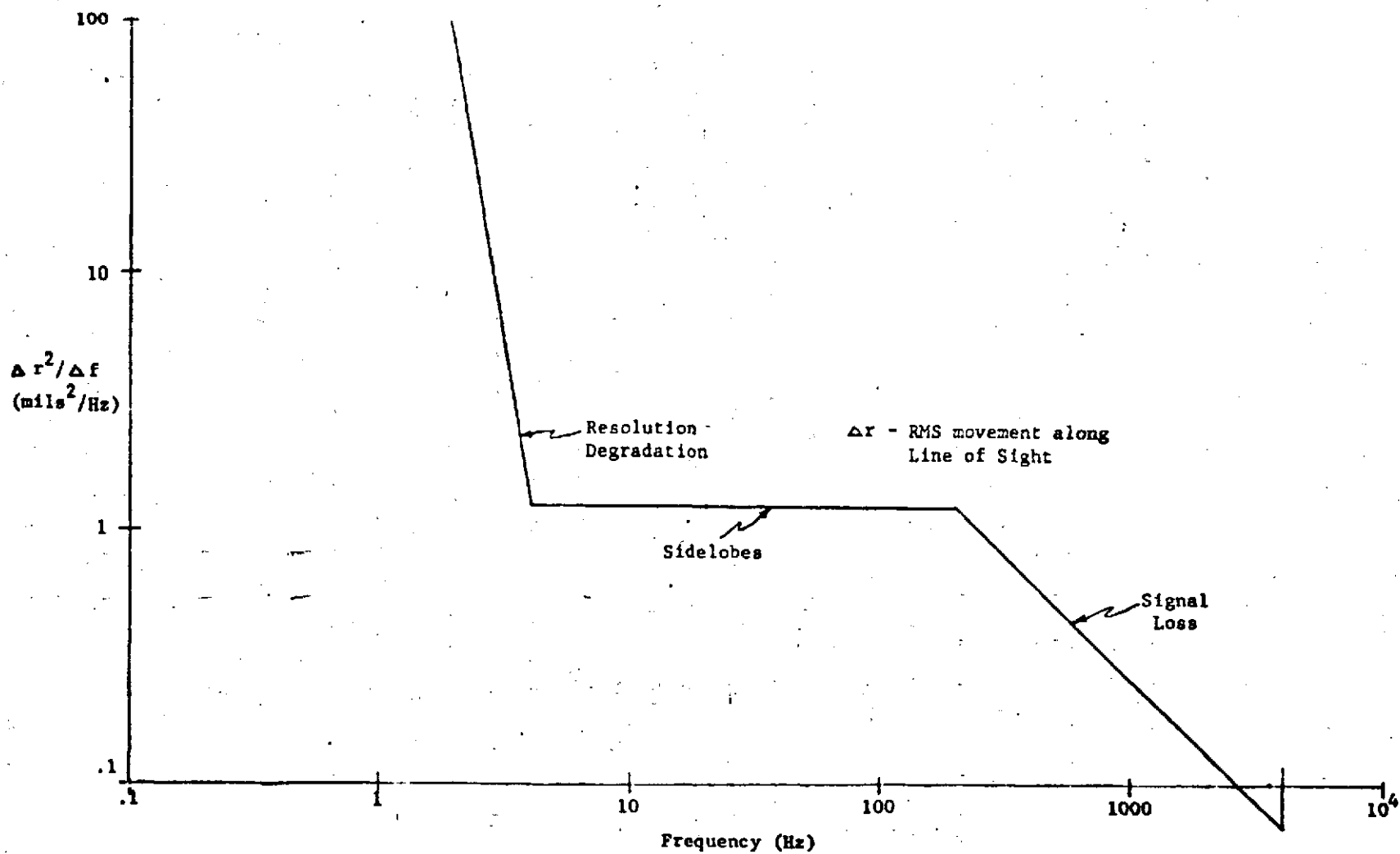


Figure 4-18. Nondeterministic Antenna Motion Requirement  
(Power Spectral Density)

The difference in peak power is accounted for by the pulse compression ratio assumed, as the average transmitter powers are very close. Westinghouse assumed a compression ration of 300:1 vs. 50:1 assumed by Goodyear. The 300:1 ratio is within the present state-of-the-art and is preferable because it results in an overall improvement in reliability, without any increase in complexity of the electronics.

The difference in antenna length has a significant impact on the spacecraft configuration. Whereas the 13.5 ft. antenna used by Westinghouse might be accommodated in a Delta configuration, the 27 ft. antenna used by Goodyear could only be accommodated on Delta by folding the antenna. Because of the line feed and the tight requirements for alignment, folding would be difficult to implement without impairing performance and reliability.

#### 4.4.1.2 X- and L-Band

As in the X-band dual polarization case, the major difference is in the antenna. The problem area is the suppression of range ambiguities at L-band. Generally, range ambiguities are suppressed by making the beam width narrow enough to have the ambiguous swaths fall in the sidelobe regions of the antenna pattern. That approach requires that the aperture increase in elevation from the X-band value by the ratio of the L-band to X-band wavelength, or about 5 to 1. Thus, the 2.5 ft. dimension would increase to about 13 feet. That approach, which Goodyear elected, requires the use of some form of unfurlable parabolic antenna, in order to achieve an aperture of 27 x 13 ft with a structure which can be stowed in compact form for launch. This type of antenna has the advantage of light weight since it uses a compact point feed, with a mesh reflector. It has the disadvantages of requiring a much more complex mechanical structure for unfurling and erecting the antenna, and substantially higher cost than the line-fed cylindrical parabolic antenna.

Westinghouse achieves the L-band range ambiguity suppression with a 2.5 x 27 ft. aperture. Although the L-band beam width is about five times as wide as the X-band beam width, the returns from the first ambiguous swaths, which fall within the main beam, are effectively suppressed by shifting the transmitter and receiver local oscillator

phase 180 degrees at every pulse. The video signals from the main swath is unaffected by the phase shifts, but those from the ambiguous swaths are shifted in frequency by one-half the PRF so that their Doppler frequencies fall outside the azimuth processor bandwidth. This technique results in a slight increase in the complexity of the electronics, but that is more than offset by the much simpler antenna structure and lower cost.

#### 4.4.2 Extended X- and L-Band Designs

Table 4-10 lists parameters for two SAR configurations, one for the Thor-Delta and another for the Titan launch. The Thor-Delta configuration is the same as Configuration 1 (X-band, dual-polarization) of Reference 1, which uses a cylindrical parabolic reflector antenna with a line feed. The antenna dimensions of 10 x 2.5 x 1 ft. are about the largest that can be accommodated without folding the antenna, which would present great difficulty because of the line feed and the limited space for stowage.

The Titan configuration is based on Configuration 2 (X-band and L-band, single polarization) of Reference 1, modified to permit a range of depression angles, and to include dual polarization at both X- and L-band. The main modifications are an increase in antenna size from 27 x 2.5 x 1 ft. to 27 x 5 x 2 ft., and provision of two more channels in the electronics. The basic data rate for the four channels is 250 MB/S which slightly exceeds the wide band data system capacity. However, since the SAR will be used with HRPI or other instruments, the data rate is reduced by 2/1 azimuth pre-processing in the radar to provide the capacity required by the other instruments.

#### 4.4.3 Spacecraft Attitude Requirements for SAR

Control of the yaw and roll angles by the on-board computer will permit the effects of altitude and earth rotation variations with latitude to be corrected while maintaining constant range gate timing and antenna depression angle (with respect to the spacecraft). The final image generated would have a latitude dependent skew if uncorrected. However, it can be easily rectified during ground data processing.

Table 4-10. Parameters for Two SAR Configurations  
(Thor-Delta and Titan Launch)

	Thor-Delta	Titan
Frequencies (GHz)	9.5	9.5 1.7
Average Transmitter Power (W)	160	150 25
Peak Power (KW)	4.3	4.5 .75
Pulse Length (μsec)	10-16	10-17
PRF (PPS)	3.2-4.3 k	3-4k
Resolution (m)	30 (9 looks)	30 (7 looks)
Depression Angle (deg.)	62.5 - 73	60 - 75
Polarization	HH, HV or VV, VH	HH, HV or VV, VH
Altitude	914 km	914 km
Swath Width (km)	40	50
Antenna Size (L x H x D ft)	10 x 2.3 x 1	27 x 5 x 2
Antenna Weight (lbs)	85	332
Electronics Package Size (L x H x D in.)	31 x 22 x 9.5	38 x 24.5 x 19
Electronics Volume (ft <sup>3</sup> )	3.75	10.25
Electronics Weight (lbs)	170	365
Total Weight (lbs)	257	697
DC Power (W)	1200	1522
Thermal Power (W)	1040	1347
Data Quantization (Bits)	4 + sign	4 + sign
Data Rate	2-68.8 MB/S channels	2-62.4 MB/S channels *
Attitude Control	±0.02° Pitch & Yaw 0.06°/sec. Roll	±0.02° Pitch & Yaw 0.06°/sec. Roll
Attitude Rate	0.01°/sec. Pitch & Yaw Figs. 4-17 & -18 Roll	0.01°/sec Pitch & Yaw Figs. 4-17 & -18 Roll

\* Data rate reduced by 2/1 azimuth pre-processing in spacecraft.

The yaw angle offset required varies from about 1.5 to 2.2 degrees during a pass over the United States, while the roll angle offset varies from 0 to 2.0 degrees for a 75 degree depression angle (0 to 1.0 degree for 60 degrees depression angle). The required yaw angle offset from the orthogonal to the orbit plane is given as a function of latitude and depression angle by

$$\Delta\theta = \tan^{-1} \left[ \frac{V_o \cos \lambda \cos \phi \left( 1 + \frac{R}{R_E} \sin \phi \right)}{V} \right] \quad (1)$$

where

$R$  = slant range

$R_E$  = radius of the earth

$V_o$  = surface velocity at the equator ( $1.521 \times 10^3$  ft/sec)

$V$  = orbital velocity

$\lambda$  = latitude

$\phi$  = depression angle.

The required roll angle offset is given as a function of altitude differential and depression angle by

$$\Delta \phi = \frac{\Delta h}{R} \left[ 1 + \tan^2 \left( \phi - \frac{R \cos \phi}{R_E} \right) \right]^{\frac{1}{2}} \quad (2)$$

where

$\Delta h$  = altitude differential from a constant altitude

and the other variables are as previously defined.

#### 4.4.4 Electromagnetic Interference

Both the SAR and the Wide Band Communications System (WBCS) will operate at X-band, so that interference is possible unless suitable precautions are taken in the designs of both systems and their integration into the payload configurations. To reduce the interference the frequencies and the physical location of the antennas should be separated as much as possible. Both the WBCS and the SAR designs should include EMI specs which insure that all possible interfering signals are attenuated below the SAR receiver noise level (after range and azimuth compressions).

#### 4.4.5 Cost

The following SAR cost estimates are based on a review and extension of cost estimates by Goodyear and Westinghouse, and comparison with SAR costs estimated for SEASAT.

	<u>Development (Millions)</u>	<u>Flight Unit</u>	<u>Ground Processing Equipment (Digital)</u>
X-Band-Dual Polarization (2 channels)	4.1	1.6	1.55
X- and L-Band Dual Polarization (4 channels)	5.8	2.6	2.85

#### 4.5 PASSIVE MULTICHANNEL MICROWAVE RADIOMETER

PMMR conceptual designs were reviewed to assess characteristics and compatibility with the modular observatory concept.

References: Earth Observatory Satellite (EOS) Definition Phase Report, Vol 1, August 1971, GSFC.

Passive Multichannel Microwave Radiometer (PMMR) Feasibility Study, 15 June 1973, Interim Report; Operations Research, Inc.

Advanced Microwave Radiometer Antenna System Study, RFP, GSFC, 29 April 1974.

##### 4.5.1 PMMR Conceptual Design – Phased Array Antenna

Table 4-11 shows the preliminary physical characteristics of the PMMR for EOS, as defined in Reference 1. It consists of a five-frequency (4.99, 10.69, 18.0, 21.5, 37 GHz) microwave radiometer, using separate electronically scanned planar array antennas for each frequency.

The weights and powers were scaled up from the Nimbus F ESMR system. Because conical scan is required, the aperture plane is mounted parallel to the nadir pointing axis of the spacecraft. This requires that the height of the aperture is about twice the width in order to produce a circular footprint with a  $45^\circ$  half cone angle. The antenna configuration is shown schematically in Figure 4-19.



Table 4-11. Preliminary Physical Characteristics  
of the PMMR for EOS

Frequency (GHz)	I FOV <sup>*</sup> (km)	Antenna Width (m)	Antenna Height (m)	Weight (lbs)	Power (watts)
37	22	0.86	2.12	128	95
21.5	88	0.37	0.92	55	40
18.0	88	0.44	1.10	68	50
10.69	88	0.75	1.84	107	80
4.99	183	0.77	2.02	155	90

\* 3 dB beamwidth footprint from 1000 km  
altitude, 45° half cone angle.

TOTALS: Power 355 watts  
Weight (513 lbs) 233 kg  
Data Rate 0.01 Mb/sec (10 channels)  
Antenna Area 5.5 m<sup>2</sup> (58 ft<sup>2</sup>)

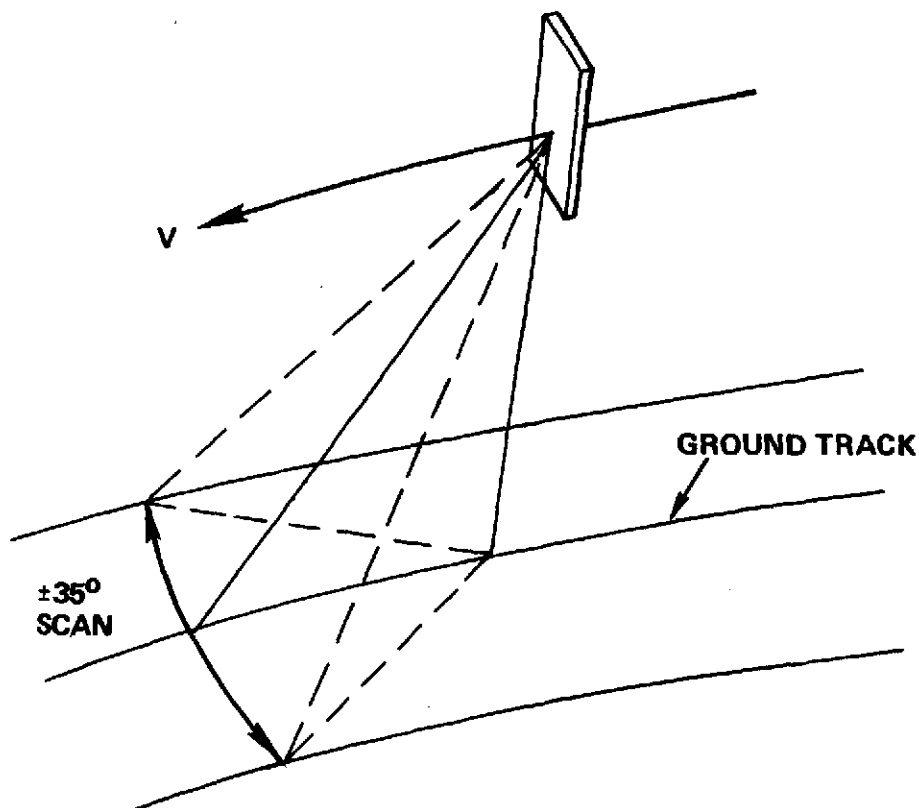


Figure 4-19. Planar Array Antenna Configuration

This type of antenna has the advantages of simple mechanical construction, no dynamic interaction with the spacecraft, linear scan with nearly 100 percent scan efficiency, beam efficiency over 85 percent at all frequencies, low side levels over  $\pm 35^\circ$  scan angle and coaxial IFOV at all frequencies.

Table 4-12 presents the results of a study (Reference 2) of a five-frequency PMMR using mechanically scanned, single reflector antennas with a multi-frequency feed. Five different designs were studied. The most favorable of these designs from the point of view of interaction with the spacecraft is the first one; that is, the rotating off-set parabolic reflector with a fixed array feed. The configuration is shown schematically in Figure 4-20. Although that configuration requires additional ground data processing to separate the cross-polarizations resulting from the rotation of the reflector with respect to the feed, it minimizes the oscillating mass and, therefore, the momentum compensation required to avoid excessive perturbation of the spacecraft. Weight, power and projected area compare very favorably with the planar array type of antenna as shown in Table 4-13.

The disadvantages of this off-set parabolic dish antenna are low beam efficiency (70 to 85% depending on frequency), high sidelobe levels, 60% scan efficiency due to sinusoidal motion, and extra ground data processing to correct the image for the sinusoidal scan and to unscramble the polarizations.

#### 4.5.2 Comparison of Conceptual Designs

Table 4-13 shows the physical characteristics of a five-frequency PMMR with the two types of antenna described.

Table 4-12. Summary of One Reflector Approaches

	Beam Efficiency	Maximum Sidelobes	Weight lbs Volume m <sup>3</sup> Power watts	Comments
OFFSET PARABOLIC REFLECTOR (Array Feed)	70-85%	20 dB	106 1.11 60	Excessive spill over
OFFSET PARABOLIC REFLECTOR (Multiple Horn Feed)	80-85%	20 dB	106 1.11 60	Angles vary with scan
TELESCOPE	70-75%	17 dB	121 10.4 65	Severe aperture blockage
PARABOLIC TORUS	80-85%	20 dB	143 12.0 47	Dimensions exceed Delta requires deployment
MECHANICAL SCANNED ANTENNAS (Offset Parabolic Reflector)	70-85%	20 dB	136 1.5 75	Excessive momentum - polar- ization does not vary with scan

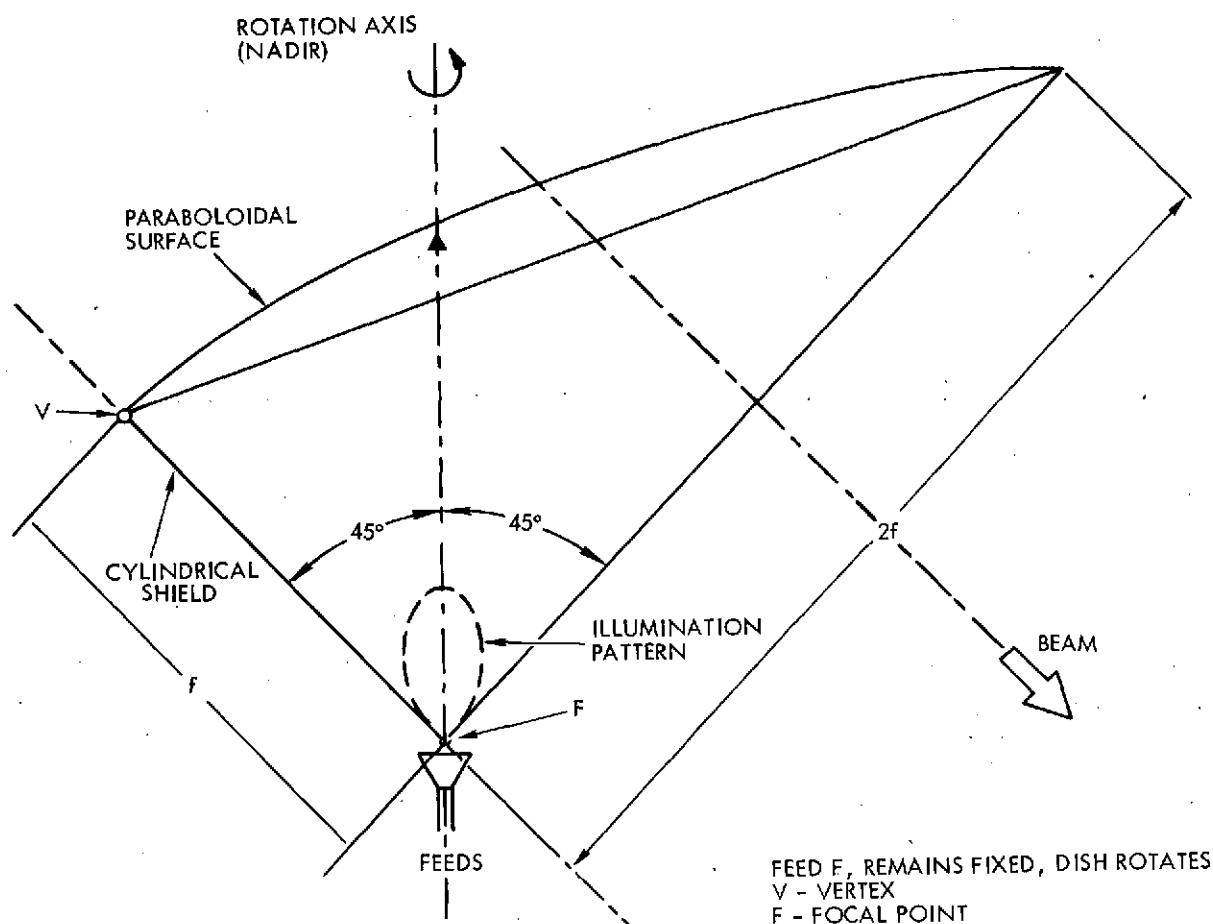


Figure 4-20. Offset Parabolic Reflector Antenna Feed Configuration

Table 4-13. 5 Frequency PMMR

Antenna Type	Weight (lbs)	Power a (w)	Volume (ft <sup>3</sup> )	Area (ft <sup>2</sup> )
PMMR - Planar Array	513	355	36 (1.1)	58
PMMR - Offset Parabola	106	60	38 (1.11)	10

At the present time no clear choice is possible as to the type of antenna to be used for the EOS PMMR. It should be noted that GSFC has recently proposed to fund a contract for a new study of antennas for use in spacecraft (Reference 3). The study work statement covers both planar arrays and mechanically scanned, multi-frequency antennas. The results of the study may indicate a clear choice for EOS.

#### 4.5.3 Compatibility with EOS Modularity Concept

Consideration of the volumes, areas and mounting requirements for the planar array and offset parabola antenna leads to the conclusion that either type can be considered to be compatible with the modularity concept for EOS, insofar as weight, power and data rate are concerned. Because of the large projected area of the five-frequency planar arrays, they will require stowing with their aperture planes parallel to the long dimension of the spacecraft, and deployment to an orthogonal orientation after launch as shown in Figure 4-21. These antennas are very thin compared to their length and width, thus lending themselves to stacking, if necessary, to fit within the available area.

The offset parabolic reflector type takes less projected area, but requires as much volume as the array type antennas. Sufficient rigidity is required in the reflector support and drive structure to maintain alignment of the reflector with the feed while scanning, and under the various thermal conditions which will exist during the mission. The drive for the reflector must include momentum compensation for the sinusoidal scan motion of the reflector.

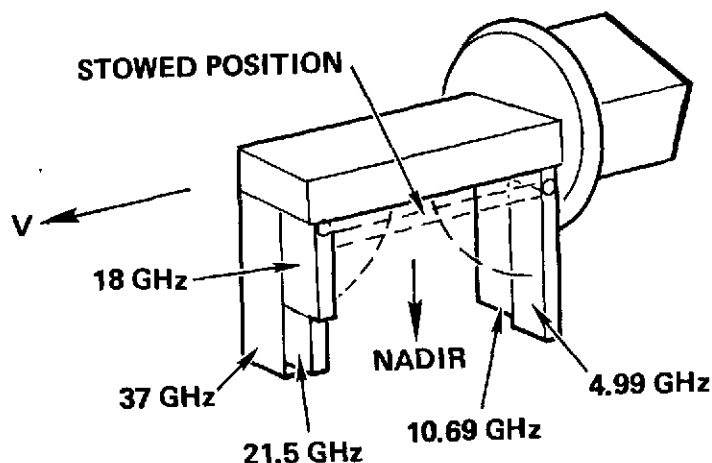


Figure 4-21. Accommodation of 5-Frequency Planar Array Antenna

#### 4.5.4 Cost

Estimated cost, based on available information at present for PMMR is dependent on the type of antennas as follows:

5-Frequency Phased Array -----	3.5M <sup>*</sup>
Offset Parabola -----	2.0M <sup>**</sup>

These costs include the antennas and electronics, protoflight and flight units.

---

\*Source of estimate -- verbal communication with Aerojet General.

\*\*Source of estimate -- SEASAT Study Task Team Report, October 1973  
Modified for 5 frequencies versus 4.

## 4.6 WIDEBAND COMMUNICATIONS AND DATA HANDLING

### 4.6.1 EOS-A Data Handling

Data handling requirements for EOS-A and future missions are determined by surveying the various sensors that may be used. Data rates, accuracy, channels, housekeeping are determined (or estimated) and compared with the projected capabilities of the recommended data handling system. Impact of future missions on the data handling equipment are determined as a part of this analysis.

Applicability of the Multi-megabit Operational Multiplexer System (MOMS) is determined by verifying the MOMS requirements/capabilities as contained in various documents including the final developmental report.<sup>(1)</sup> From the data handling requirements outlined in the above, a modularized data handling system (MODS)<sup>(2)</sup> is developed to reduce impact (cost) of post-EOS-A instruments.

Requirements for on-board data compression have also been analyzed. In summary, no data compression (or coding, speed buffering or editing) is necessary. Addition of these functions could only result in reduction in transmitter power or antenna diameter. These are presently 1/2 watt and 24 inches, respectively, so a slight reduction will be more than offset by additional component weight and power required for the data compression, coding, etc.

---

<sup>(1)</sup> For NASA contract numbers NAS5-21955 and NAS5-21690.

<sup>(2)</sup> Multi-megabit Operational Data System.

#### 4.6.1.1 Assumptions

Tradeoffs in other sections of this report have resulted in the following system definition and requirements:

- The sensor data must be oversampled by the digital data handling system by at least 1.3X
- No schemes will be used to reduce the data rate such as data compression data editing or line stretching for the standard ground station
- An error correcting code will not be used
- No on-board tape recorder will be used for the LCGS or the standard stations
- The on-board data handling requirements are listed in Table 4-14.

#### 4.6.1.2 Analysis and Tradeoffs

##### 4.6.1.2.1 On-Board Data Handling Requirements

The on-board handling requirements for EOS-A as well as future missions are listed in Table 4-14. As shown in this table the data rates vary from a low of 300 bits/sec for the SEASAT-A pulse compression radar altimeter, to a high of more than 300 Mbit/sec where picture imagers as well as synthetic aperture radar are used. In general, all of the sensor outputs are analog. The A/D conversion accuracy requirement varies from 4 to 10 bits per sample. Housekeeping requirements also vary over a wide range.

##### 4.6.1.2.2 Applicability of the MOMS System

The MOMS system includes the multiplexer and A/D converters (located in the instrument package), the controller and the speed buffer. This section includes the speed buffer in the block diagrams, but no design tradeoffs are made. Figure 4-22 illustrates the EOS-A configuration of this equipment.

A review of the MOMS system indicates that the multiplexer and A/D conversion speed is adequate. The 7-bit accuracy is low; 8 bits is desirable. Apparently modification to 8 bits is straightforward. The major disadvantage is the inflexible format; each mission would require major redesign or additional buffering components would have to be added.



Table 4-14. Wideband Data Handling - MODS Multiplexer Baseline and Advanced Missions -  
Requirements Versus Capabilities

Space-craft	Typical Payload Instruments	Requirements					Capabilities							
		Output Data Rate (Mbit/sec)	Encoder Word Accuracy (bits)	Science Data Analog Channels	House-keeping Data Analog Channels	Comment	Output Data Rate (Mbit/sec)	Encoder Word Accuracy (bits)	Science Data Analog Channels	House-keeping Data Analog Channels	Size (in. 3)	Weight (lb)	Power (w)	Comment
Baseline EOS	• Thematic mapper (Te)	124	8	100	50	Synchronize both data streams to 4φ	128	8	128	64	168	7	12	Altitude = 717 km includes overhead
	• MRPI (Westinghouse)	105	8	304	50		128	8	320	64	264	9	13	
	Totals	229	8	404	100	Plus overhead	256	8	448	128	432	16	25	Plus MODS controller, etc.
SEASAT	• SAR (1 freq., 1 pol.)	10	5	2	50	Needs 7:1 pre-summary	128	8	64	128	168	7	11	Capable of accommodating SAR without pre-summary
	• PMMR	0.01	8	10	50									
	• IRI	0.26	8	2	20	Separate system								
	• DCS	--	--	--	--									
	Totals	10.27	8	14	120									
SMM	• UV magnetograph		8	12	20	MODS technology not required	0.032	8	64	128	77	2	3	Use DIU of C and DH system
	• EUV spectrometer		8	12	20									
	• X-ray spectrometer	0.005	8	12	20									
	• Hard X-ray imager		8	12	20									
	• Low energy polarimeter		8	12	20									
Totals	0.005	8	60	100										
SEOS	• LAST	57	8	1900	100	Main frame	128	8	1920	128	936			Use 6 MODS multiplexers and 1 ADC LAST and framing camera on main frame. Sounders on sub-commutator
	• Microwave sounder	0.001	8	6	20	Subcommutator	128	8	64	128	936	24	24	
	• Framing camera	13	8	4	20		128							
	• Atmospheric sounder and radiometer	0.001	8	15	35		128							
	Totals	70	8	1925	175				1984	256	936	24	24	Plus MODS controller, etc.

Note: Physical characteristics are for MODS multiplexer portion only.

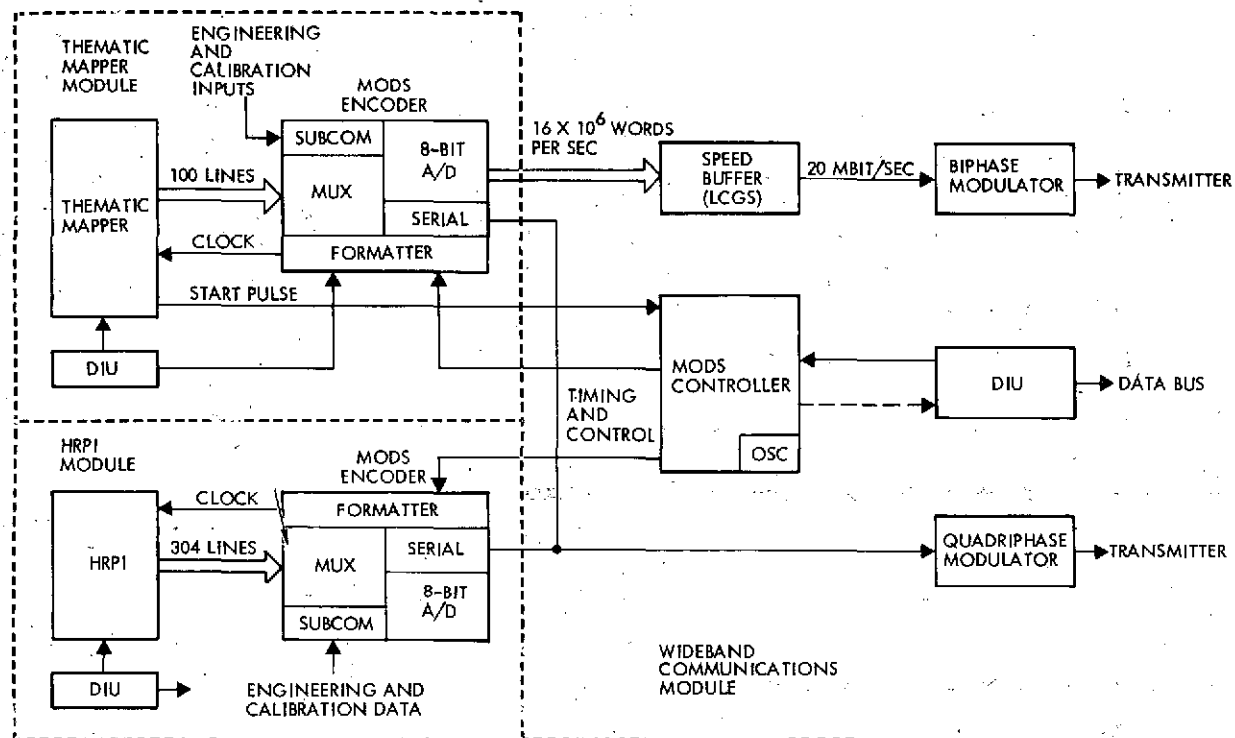


Figure 4-22. Wideband Data Handling Equipment

ORIGINAL PAGE IS  
OF POOR QUALITY

#### a. The Modular Data Handling System

The ideal PCM data handling system will operate over the entire range shown in Table 4-14 with no design changes. This can be accomplished by using read only memories (ROMS) or programmable ROMS (PROMS) for control of the major and minor frames. Word length can also be variable by simple hardwiring. Figure 4-23 shows how this might be accomplished with two ROM's: one for the minor frame organization and one for the major frame. The operation of this system is straightforward: the bit counter is hardwired for a predetermined word length. Word synchronization pulses are counted in the word counter. When the word count compares with a predetermined output from ROM-A, an "event" is recognized and the ROM-A 8-bit event counter is updated. This causes ROM-A to update and a new data word changes the multiplexed data. ROM-B and the minor frame counter operate similarly.

The major advantage of this formatting scheme is that virtually any mission can be handled with one basic system. In conjunction with the firmware formatting, the multiplexer should also be constructed in modules so that additional sections can be added or removed as the need arises. A high-speed multiplexer that incorporates most of these desirable features is described in this volume, Section 4.6.3. This multiplexer, called the modular multimegabit operational data system (MODS), is compared with the MOMS system in Table 4-15.

#### b. The EOS-A Data Formats

The data rates for the HRPI and the Te TM are identical. Two ROM formatters accommodate the data for these two instruments as shown in Figures 4-24 and 4-25. Detailed derivation of these numbers is given in Table 4-16.

The data formats for the two EOS-A instruments show that the major frame for the Te TM exactly synchronized with one swath. In order to minimize buffering, minor frame synchronization is inserted in place of band 7 data three out of four sampling sequences in each minor frame. The long header accommodates mirror "fly back" time without speed buffers for the Te TM and allows adequate recalibration time for the HRPI sensors.

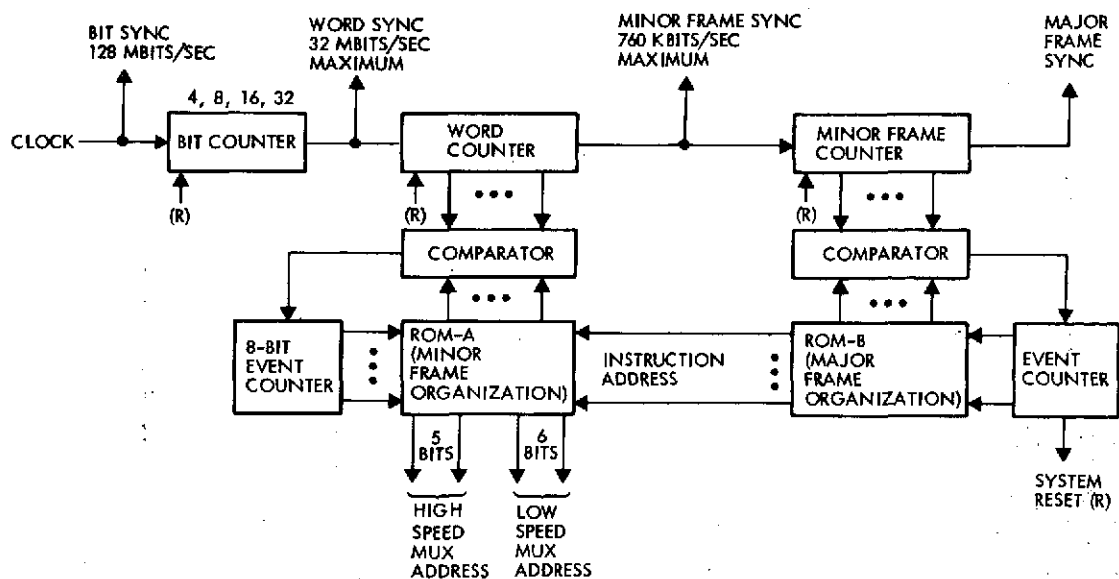


Figure 4-23. Micro-Controller for the High-Speed Multiplexer

Table 4-15. Comparison of MODS with MOMS System

Item	MODS		MOMS		Comment
	TM	HRPI	TM	HRPI	
<u>Multiplexer</u>					
Maximum speed	20 MHz	20 MHz	20 MHz	20 MHz	Science channels Housekeeping channels
Number of input channels	100	394	100	80	
Number of input channels	64	64	28	112	
Modularity	Yes - 64 channel	Yes - 64 channel	No	No	
Technology	C-MOS and bipolar	C-MOS and bipolar	Bipolar	Bipolar	
EOS-A power	0.4 w	0.4 w	4.54 w	5.38 w	
<u>Sample - Hold</u>					
Aperture time	20 pico-sec		390 pico-sec		EOS-A Power for both is 400 mw
Technique	Hot carrier diode bridge		Switching amplifier		
Technology	Thin film - bipolar		Discrete - bipolar		
<u>ADC</u>					
Technique	Series parallel feedback		Series parallel feed-forward		TRW uses 2-bit quantizer LSI ICs
Maximum sample speed	20 ms/sec		20 ms/sec		
Accuracy	8 bits		7 bits		
Technology	ECL LSI and TTL		Discrete ECL and TTL		
EOS-A power	7.2 w		12.0 w		
<u>Controller</u>					
Frame size	Variable (firmware)		Fixed		
Frame organization	Variable (firmware)		Fixed		
Synchronization	MAJOR AND MINOR FRAME		Minor frame		
EOS-A power	20.2 w		24.5 w		
Construction	Modular		N. A.		
Total EOS-A power	28.6 w		46.8 w		Power is for both instruments data acquisition

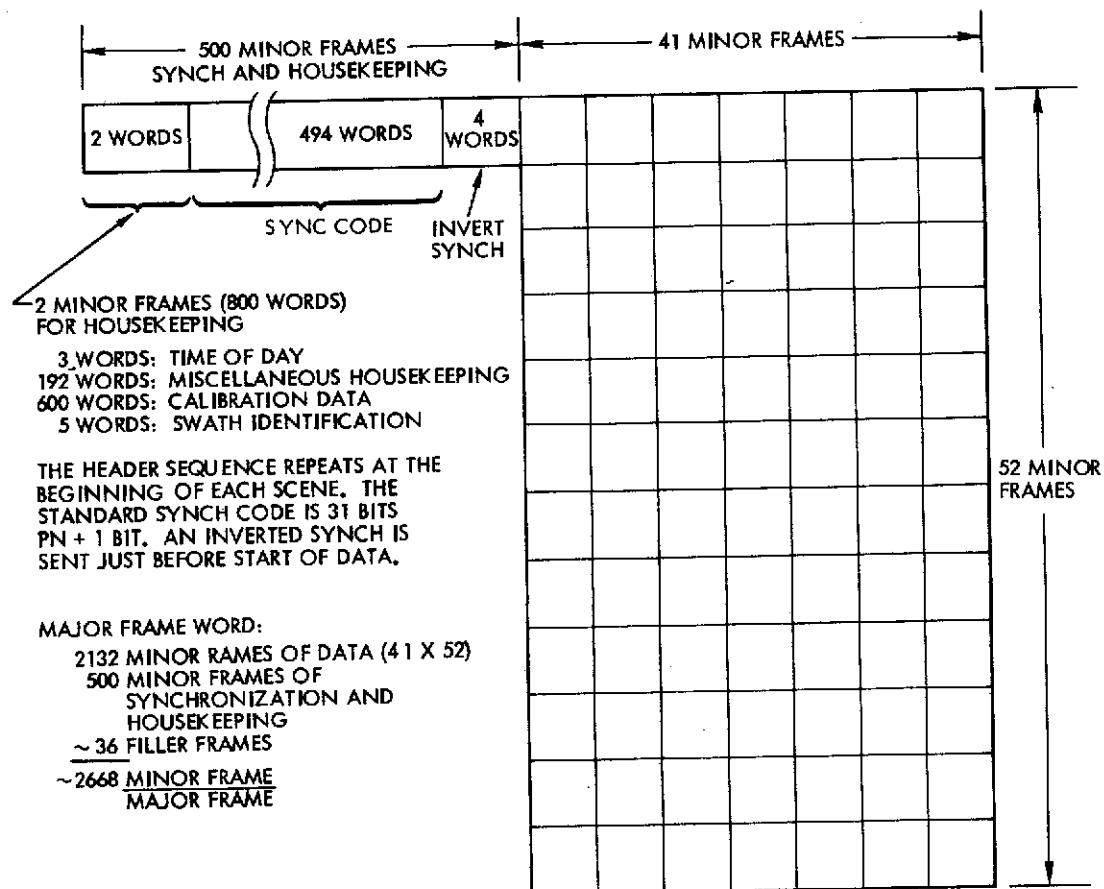
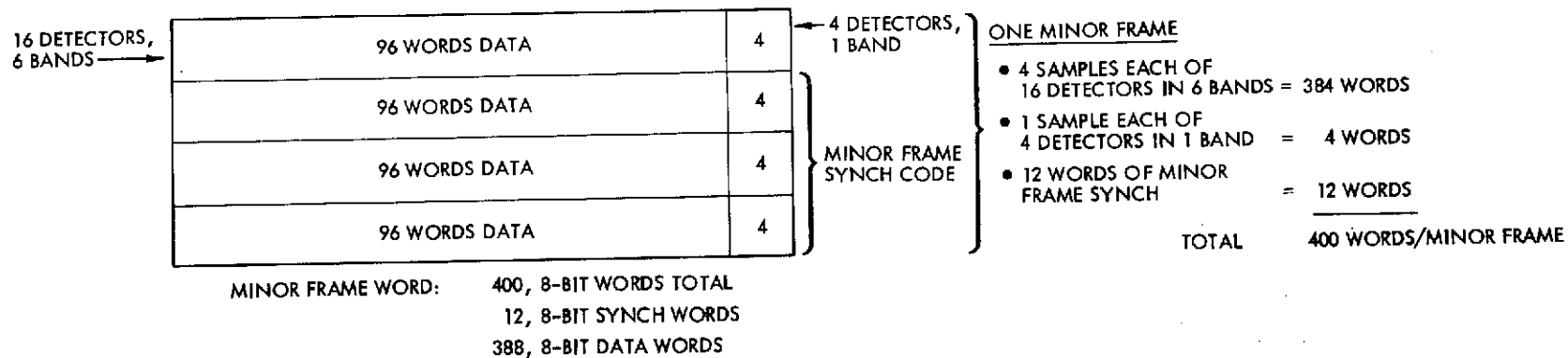


Figure 4-24. EOS-A Wideband Data System Thematic Mapper – CDPF Data Format

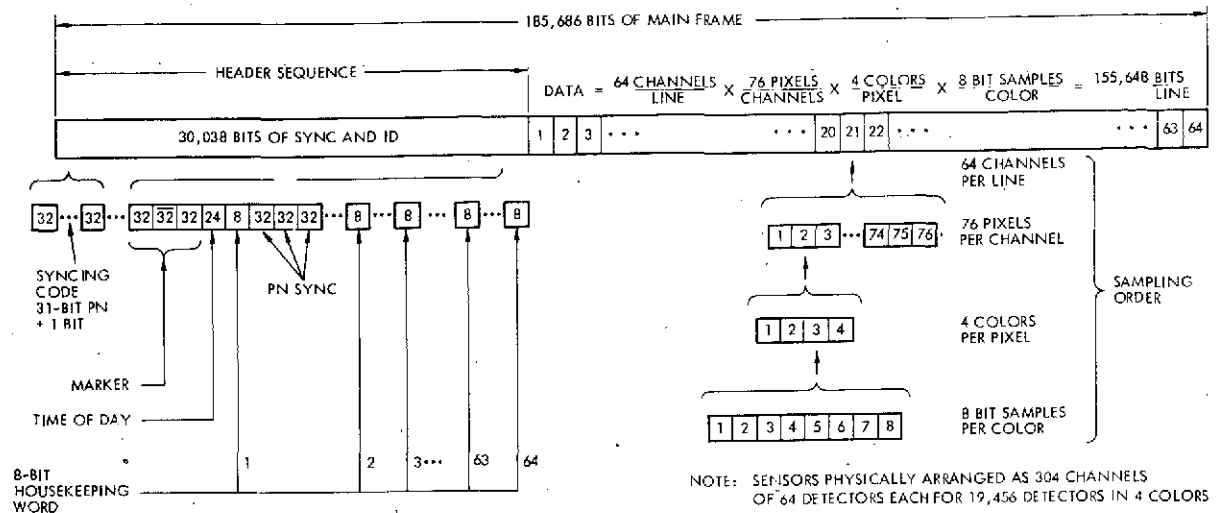


Figure 4-25. EOS-A Wideband Data System CDPF Format

Frequency synchronization between the sensors and multiplexer is achieved with a common clock\* (supplied by the multiplexer). Phase synchronization is achieved with a start pulse from the thematic mapper; the start pulse initiates insertion of a short synchronization code (16 bits) and the start of the multiplexer sequence. Phase accuracy for the swath time has no closed loop control.

#### 4.6.1.3 Conclusions

The MOMS system, while probably adequate for EOS-A or one specific mission, will not handle all projected missions without major modification. A firmware programmed modularized system is recommended. Further study of this problem is in order and will probably indicate that flexibility and modularity can be accomplished with little or no cost increase.

\* Stability requests for the clock are not severe. Preliminary analysis indicates the following:

- Long-term stability. Less than 1 percent frequency change for the life of the mission
- Medium-term stability. Less than  $1 \times 10^{-9}$  frequency change averaged over any 30-second period
- Short-term stability. Less than 6 nsec peak jitter at each sample. Samples occur every 62.5 nsec.

Table 4-16. EOS-A Wideband Data Requirements

Thematic Mapper

Data rate = 120 Mbit/sec =  $15 \times 10^6$  8-bit words/sec

Spacecraft advance per scan = 16 detectors/scan x 30 meters/detector = 480 meters

Scan period =  $\frac{480 \text{ meters/sec}}{6746.2 \text{ meters/sec}} = 71.15 \text{ msec}$

Where the ground velocity of the spacecraft at 714 km is 6746.2 m/s

Total words per scan =  $15 \times 10^6 \times 71.15 \times 10^{-3} = 1,067,300$

Each detector except band 7 repeats every 100 words

Total words/detector/scan = 10,673

Let the active portion of the scan use 8528 words

Scan efficiency =  $8528/10673 = 79.9$  percent

Ground separation of samples =  $\frac{185,000 \text{ m/swath}}{8528 \text{ words/swath}} = 21.693 \text{ m}$

Oversampling ratio =  $\frac{30 \text{ meters/resolution element}}{21.693 \text{ meter/sample}} = 1.383$

HRPI

Synchronize HRPI to the thematic mapper

Sample each HRPI detector 48 times for each TM scan

Ground advance/sample =  $\frac{480 \text{ meters/TM scan}}{48 \text{ HRPI samples/TM scan}} = 10 \text{ m/sample}$

HRPI total scan period =  $71.15/48 = 1.482 \text{ msec}$

Total samples available per scan =  $15 \times 10^6 \times 1.482 \times 10^{-3} = 22,234$

There are 4864 detectors/color x 4 colors = 19,456 samples/scan

Thus HRPI scan efficiency =  $\frac{19,456}{22,234} = 87.5$  percent

#### 4.6.2 Wideband Tape Recorder

Storage of high-data rate digital data from the sensors may be required for EOS type missions. A projection of storage devices (1975 to 1985) clearly shows the superiority of magnetic tape recordings for high-storage capacity serial memory systems (see Table 4-17).

##### 4.6.2.1 Assumptions

A projection of storage capacity is shown in Figure 4-26, and it can, in 1978, be anticipated that 4200 feet of 2" tape or two 4200 feet of 1" tape will be required for 10 minutes' recording.

##### 4.6.2.2 Analysis

It is at present known that two manufacturers will consider development of these recorders, RCA a 2" version (under a potential NASA contract) and Odetics, who has a transport designed for 1" tape. Specifications are shown in Tables 4-18 and 4-19.

##### 4.6.2.3 Conclusion

A recorder for on-board use can be developed. It would require 24 manmonths plus 12 months qualification, at a cost of 3-4 million dollars.

Table 4-17. Project Characteristics of Various Data Storage Devices (1975 to 1985)

Data Storage Technologies	Performance				Response to Environmental Conditions				Mean Time Between Hours	Max. Weight Lbs.	Volume In <sup>3</sup>
	Packing Density Bits/in <sup>2</sup>	Potential Capacity Bits	Write/Read Data Rate B/S (Serial Mode)	Energy/Bit J	Temp	Shock	Vibration	Radiation			
Tape Recorders	$5 \times 10^7$	$10^{10}$	$20 \times 10^6 / 20 \times 10^6$	$10^{-4}$	A	A	A	G	$10^4$	50	2,000
Bubble Memory	$10^6$	$10^8$	$3 \times 10^6 / 3 \times 10^6$	$5 \times 10^{-5}$	P	G	G	G	$2 \times 10^4$	200	3,000
Plated Wire	5,000	$10^7$	$8 \times 10^6 / 8 \times 10^6$	$10^{-3}$	A	A	A	G	Depends on electrical connection	300	2,000
Ferrite Core	2,000	$10^7$	$2 \times 10^6 / 2 \times 10^6$	$10^{-3}$	A	A	A	G	$5 \times 10^3$	400	10,000
Thin Film	$10^4$	$10^7$	$2 \times 10^7 / 2 \times 10^7$	Not available	G	A	A	G	Not available	-	-
Sonic BORAM	3,000	$10^8$	$10^7 / 10^7$	$2 \times 10^{-6}$	A	A	A	G	$10^4$	450	7,000
DTPL	2,500	$10^8$	$5 \times 10^5 / 5 \times 10^5$	$2 \times 10^{-5}$	A	G	G	P	$10^4$	100	2,000

A - adequate  
 G - good  
 P - poor



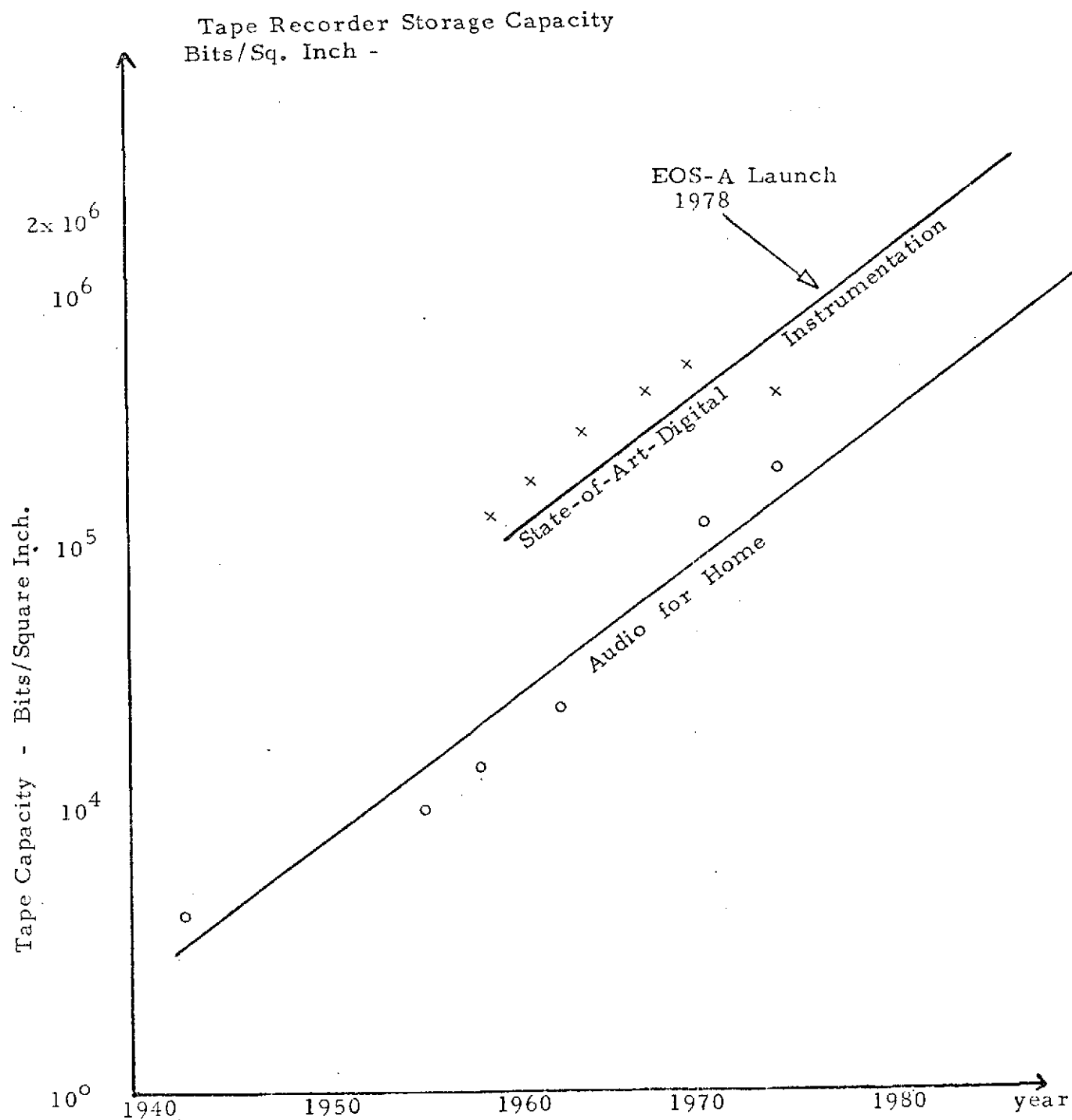


Figure 4-26. Historic and projected trend in storage capacity of tape recorders assuming a constant BER of  $10^{-6}$  (or identical listening quality of audio tapes, for comparison of trends).

Table 4-18. Tape Recorder Characteristics

	PROJECTED FEATURES	
	42 Tracks per 1" Tape	> 100 Track per 2" Tape
Tape Width	1"	2"
Tape Length	4200 ft	4200 ft
Tape Speed	~ 80 IPS	~ 60 IPS
Packing Density	38 KBPI	38 KBPI
Bits Per Square Inch	$1.4 \times 10^6$	$1.4 \times 10^6$
Record Encoding	Miller or Enhanced NRZ <sup>TM</sup>	Miller or Enhanced NRZ <sup>TM</sup>
Heads	Ferrite or Alfesil	Ferrite or Alfesil
Track Width	.018"	> .008"
Tape	Best Grade Instrumentation	Best Grade Instrumentation, selected for best tracking
COMMENTS:	It is conceivable that this unit could be designed with 90 tracks, bringing the packing density up to $3 \times 10^6$ Bits per square inch.	

Table 4-19. Projected Tape Recorder Specification

SPECIFICATION	CAPABILITY	
	42 Tracks per 1" Tape	>100 Tracks per 2" Tape
Record Time	10 Min	10 Min
Record Rate	2 x 120 MB/S	240 MB/S
Reproduce Rate	2 x 120 MB/S	240 MB/S
BER	$10^{-6}$	$10^{-6}$
MTBF, Transport	$10^4$	$10^4$
MTBF, Electronics	$10^5$	$10^5$
Record/Repro Cycles (Tape & Head)	4000	4000
Power, Standby	5 watts	5 watts
Power, Record	40 watts	70 watts
Power, RE	100 watts	200 watts
Weight	75 lbs	150 lbs
Volume	4000 cu. in.	6000 cu. in.

#### 4.6.3 Wideband Data Handling Design

Major design problems in the wideband data handling design are as follows:

- The system should handle EOS-A and all projected missions with minimum redesign. This implies a programmable format as well as modularized construction
- Choice of component parts is critical. At the time of fabrication and assembly, the component parts should be realistically deliverable as well as space qualified. On the other hand, judicious use of new and better components may result in substantial size, weight, power and reduction as well as cost savings.

##### 4.6.3.1 Analysis and Tradeoffs

The wideband data handling system design is based upon the flexible-format, modular system described in Section 4.6.1 of the Appendix. The principal advantage of this system, the MODS, is that no design change is required to handle any of the projected future missions listed in Table 4-14 of Section 4.6.1.

The EOS-A MODS system consists of three components: two encoders including analog multiplexers and high speed A/D converters each located with their respective instruments; the TM and HRPI; and the MODS controller which is located in the wideband communications module. The interface with the thematic mapper and the multiplexers requires 100 analog data lines and the HRPI/multiplexer interface requires 304 lines. With the multiplexers located next to the instruments, these lines can be made short, minimizing noise pickup, obviating AC coupling and reducing weight. The thematic mapper multiplexer requires an eight-line output interface to the speed buffer and each instrument requires a single line output to the quadriphase modulator in the wideband communications module.

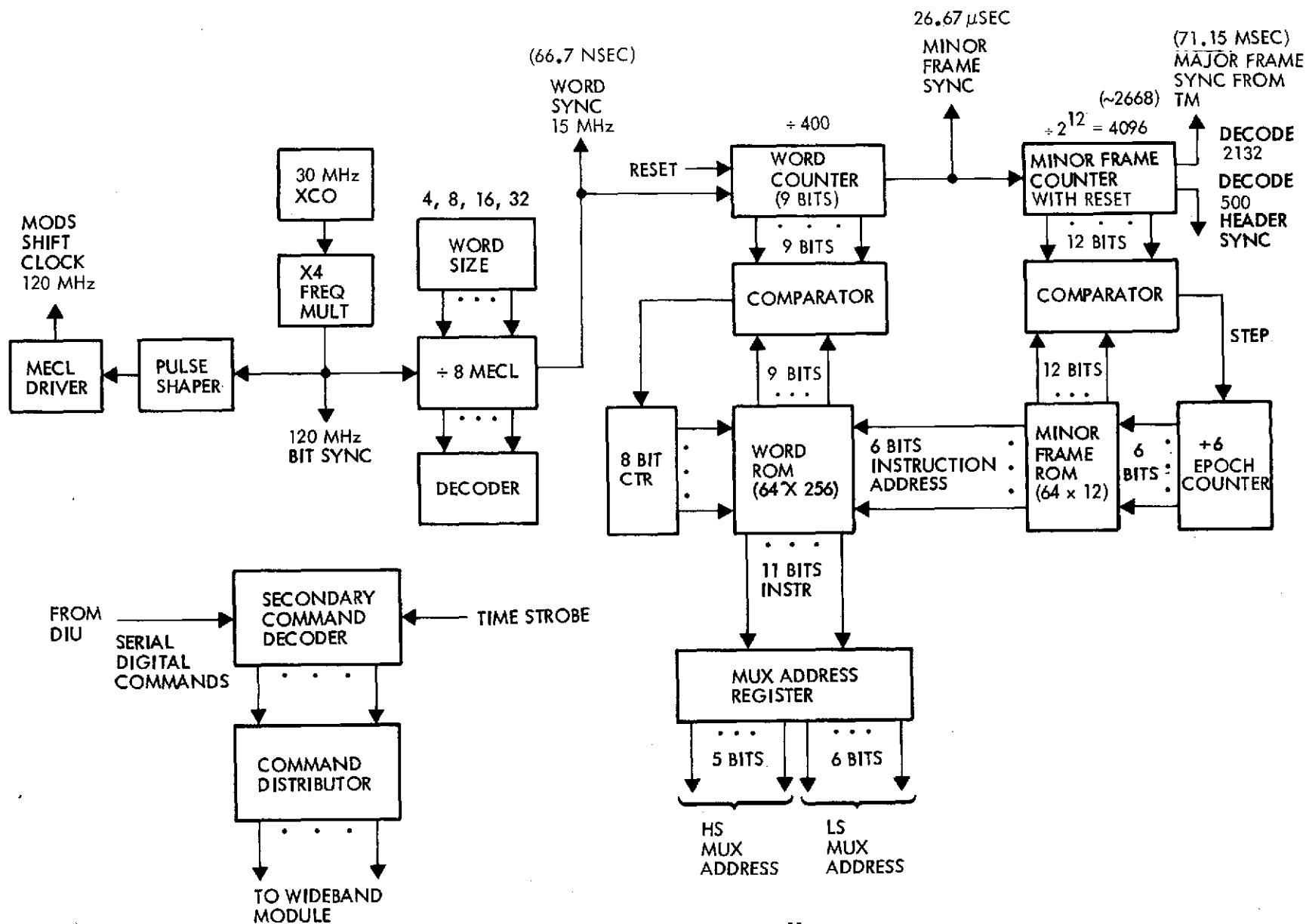


Figure 4-27. MODS Controller

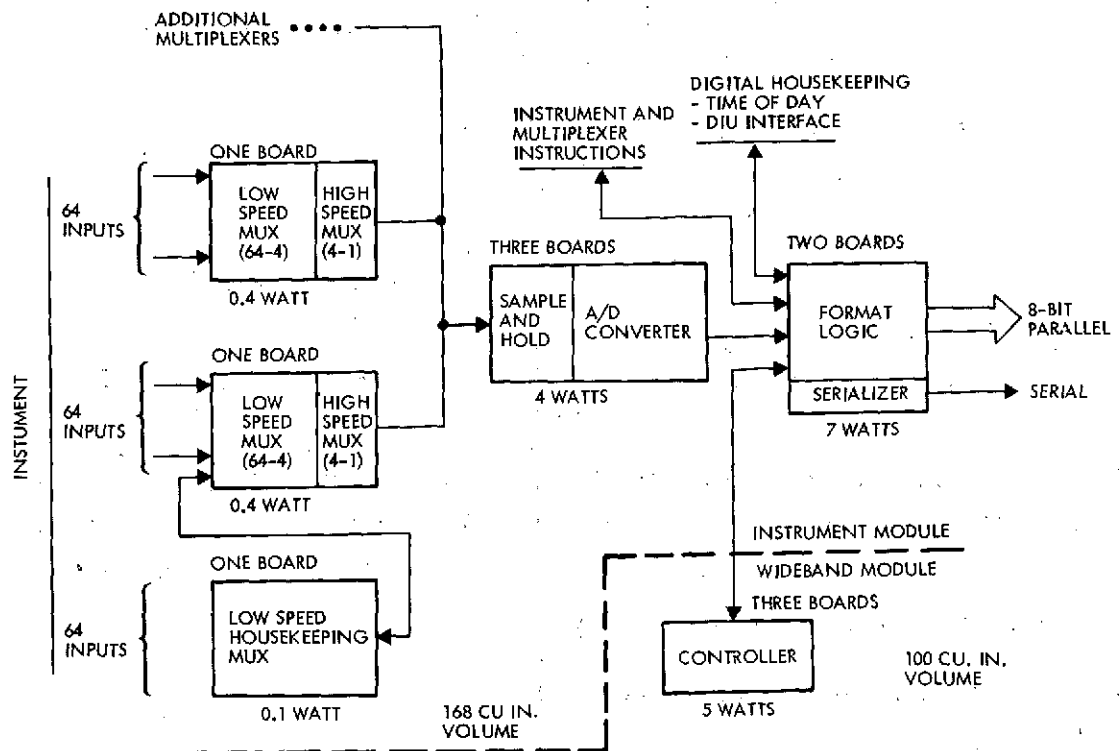


Figure 4-28. MODS Partitioning

#### 4.6.3.1.1 MODS Controller

##### Modular Design

Study of future EOS requirements indicated that the wideband data handling system could be designed with modular components so that one design will fit all missions as well as all instruments. Special-purpose signal conditioning boards/slices (a part of the component) will probably be necessary in many instances, but the major portion of the system will require only firmware changes in the controlling read only memories (ROMS) to be adapted to different instruments. This is the fundamental difference between the recommended baseline system (MODS) and the proposal baseline system (MOMS). A block diagram of this baseline, MODS controller is shown in Figure 4-27.

Modularization is achieved as follows:

- Standard boards/slices are designed. These sections are combined to perform the desired functions. Figure 4-28 shows how these boards/slices are combined for the baseline system (Te TM and HRPI).

- ROMS or PROMS are used to program minor and major frame events to the following quantization levels (refer to the block diagram, MODS controller, Figure 4-27).

Major Frame Timing: 12 bits (8192)  
The major frame may be quantized in as many as 8192 minor frame groups.

Minor Frame Timing: 9 bits (512)  
The minor frame may be quantized in as many as 512 word groups.

Word Timing: Word lengths of 4, 8, 16 and 32 are selectable.

The controller as described requires approximately 150 component parts. These are mounted on three boards which are contained in a 6 x 8 x 2 inch package weighing three pounds. The controller requires approximately 5 watts of secondary power.

#### 4.6.3.1.2 Hardware Description

##### Multiplexers

As discussed earlier, the MODS multiplexers and formatters are located within the TM and HRPI instrument modules, respectively. Data are acquired and converted to digital data streams under control and timing provided by the MODS controller located in the wideband communications module. The MODS are essentially identical, with their differences being in the number of input channels dictated by instrument requirements.

The system organization of the MODS multiplexer is shown in Figure 4-28. The MODS multiplexer is constructed of functionally modular and expandable building blocks as shown in Figure 4-29. The modular multiplexing scheme consists of expandable boards of 64 analog inputs each.

The analog multiplexer is a two-tier multiplexing system. It basically provides a high speed switching capability. The first tier consists of 100 thematic mapper channels or 304 HRPI channels. The second tier consists of eight high speed thematic mapper channels and 19 high speed HRPI channels that have typical switch open and close times of 66.7 nanoseconds.

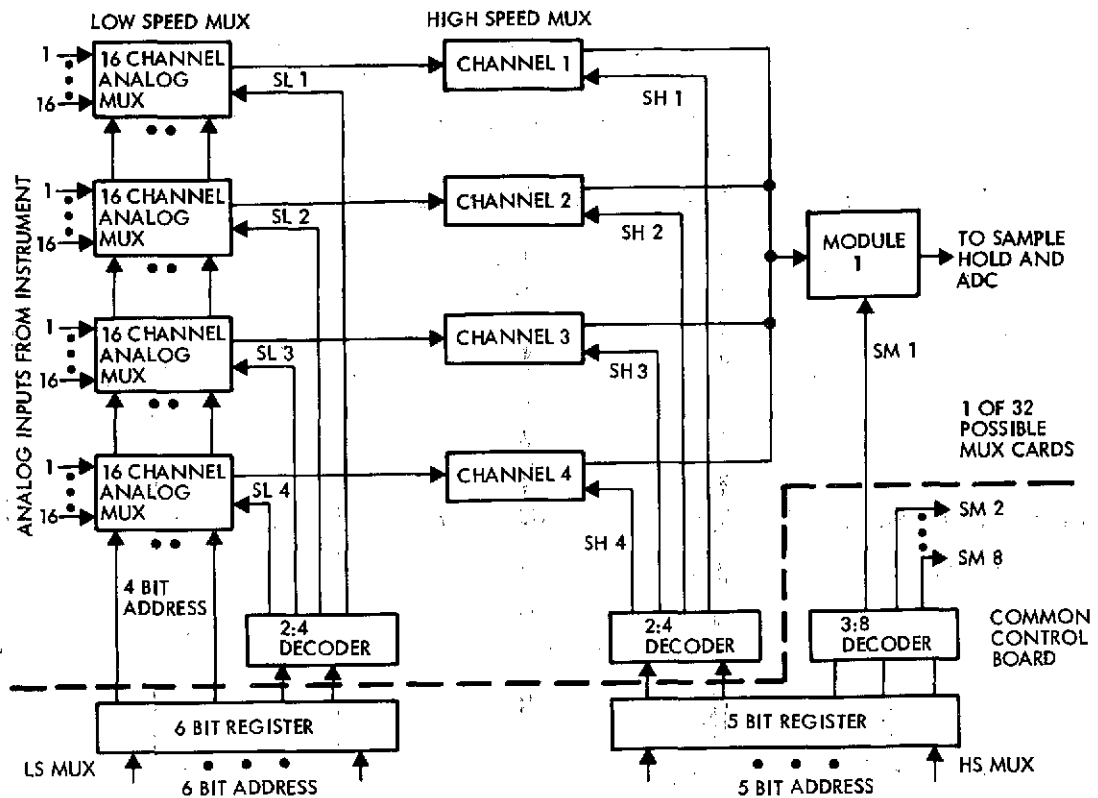


Figure 4-29. Modular Multiplexing Scheme

The use of a two-tier multiplexing system achieves the following:

- It effectively reduces the common output node capacitance of the system
- It reduces the amount of error voltage developed as a result of leakage current flow through the "off" switches into the common output node.

The low speed multiplexer level of the system has adequate time for settling to permit the use of CMOS analog switches because the thematic mapper and HRPI outputs are low impedance. The low charge transfer error will result from that low impedance. The charge transfer error equivalent circuit is shown in Figure 4-30.

$$V_E(t) = \frac{(E_i - V_{n-1})}{C_{ot} C_m} e^{-t/R_o(C_o + C_m)}$$



where

$R_o$  = TM or HRPI output impedance

$C_o$  = Stray cable capacitance between the TM or HRPI and multiplexer

$C_m$  = The multiplexer output capacitance

$V_{n-1}$  = The previous sample level

$$2 \text{ mv} = \frac{2 \times 30 \times 10^{-12}}{(20 + 30) \times 10^{-12}} e^{-t/100(20+30) \times 10^{-12}}$$

Allowing 400 nanoseconds for the multiplexer response time, the charge transfer error is less than 0.1 percent.

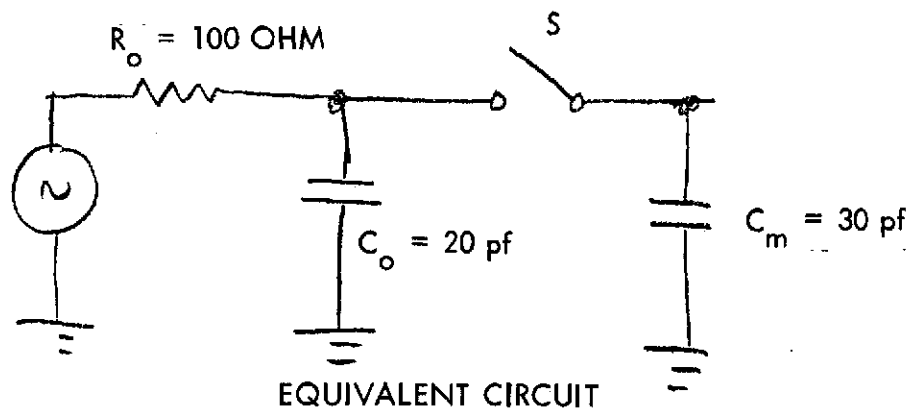


Figure 4-30. Circuit for Analyzing Charge Transfer Error

The high speed multiplexer, shown in Figure 4-31, consists of input amplifiers, differential current switches, and an output amplifier. The differential pair of current switches are used for fast switching response. In order to reduce power dissipation a common current sink is shared by all channels. The parts and power requirements for the multiplexer portion of the MODS are summarized in Table 4-20.

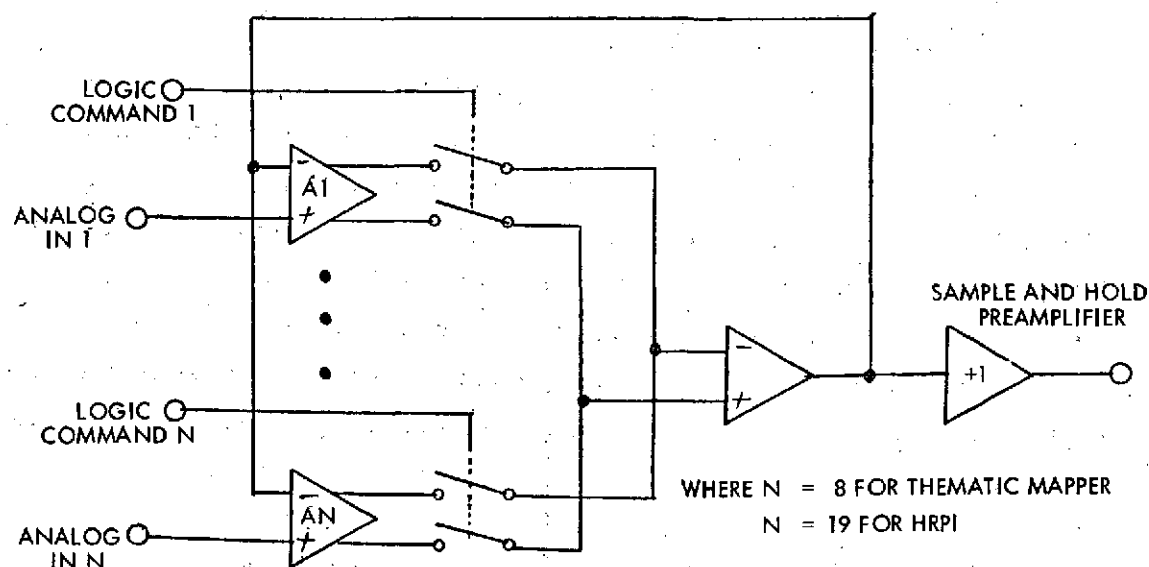


Figure 4-31. High-Speed Multiplexer Functional Block Diagram

Table 4-20. EOS-A Wideband Data Handling Subsystem Multiplexers

Part Name	Type	IC	Disc	Power (mw)
<u>TM Channels</u>				
Input amplifier	LM3026	8 (SSI)	16	31
Output stage			40	89
Swath current sink			34	48
Coder buffer amplifier	TRW-GEF	1 (MSI)		100
Gate driver			30	48
Low speed multiplexer	RCA	15 (SSI)	15	50
		24 IC	135 D	366
100 TM channels multiplexers = 159 parts at 366 mw				
<u>HRPI Channels</u>				
Input amplifier	LM3026	9 (SSI)	18	31
Output stage			40	89
Switch current sink			38	48
Coder buffer amplifier	TRW-GEF	1 (MSI)		100
Gate driver			33	48
Low speed multiplexer	RCA	38 (SSI)	36	60
	CD4051A	48 IC	165D	376
304 HRPI channels multiplexers = 211 parts at 376 mw				

### Sample and Hold Circuits

A simplified functional sample and hold block diagram is shown in Figure 4-32. The preamplifier and post-amplifier are wideband amplifiers. The analog switch is typically a hot carrier diode bridge for the high-speed sample and hold. A FET is usually used for the input stage of the post-amplifier to minimize the input bias current. A high bias current will change the voltage on the hold capacitor while the sample and hold is active. A high-speed monolithic sample and hold is not presently available principally because of the variety of device technologies required: bipolar transistors, field effect transistors, and hot carrier diodes.

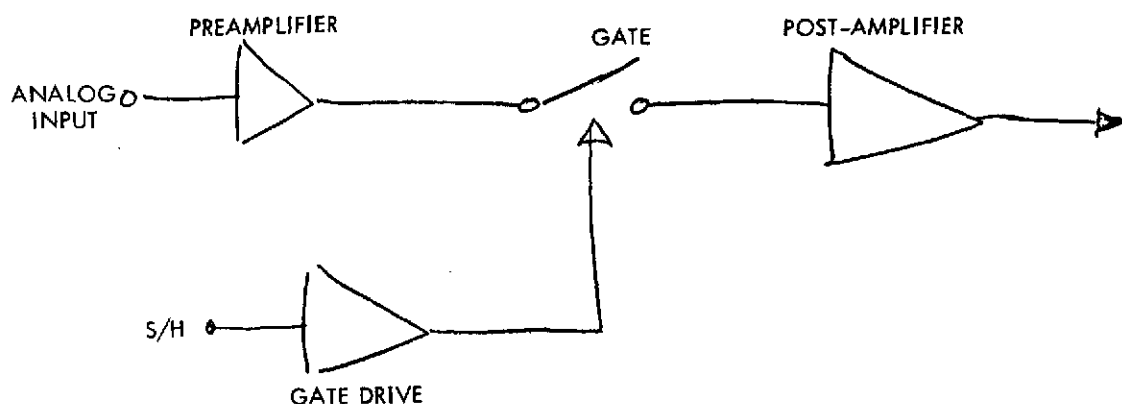


Figure 4-32. Sample and Hold Block Diagram

### Analog-to-Digital Converter

A number of analog-to-digital converter circuits were reviewed and analyzed to determine candidates for meeting the 15 Ms/s, 8-bit accuracy goals. Baseline A/D converter candidates:

- 1) Successive approximation (two 7.5 Ms/s, 10 bits)
- 2) Serial-parallel feed forward (15 Ms/s, 8 bits)
- 3) Serial-parallel feedback (15 Ms/s, 8 bits).

The successive approximation circuits employ two sample/hold circuits and two 10 Ms/s, 10-bit monolithic converters which have significant merit in terms of low complexity and comparatively high reliability. The serial-parallel feed forward circuits easily achieve 20 Ms/s

speed at 8-bits accuracy. The serial-parallel feedback circuits have lower power, fewer parts and better accuracy than the feed forward circuits and can also achieve 20 Ms/s speed.

### A/D Converter Organization

Successive Approximation Approach. The 10 bit successive approximation approach is illustrated in Figure 4-33. At the start of the conversion sequence, all the latches except the one for the most significant bit (MSB) are set false. The MSB is set true. The D/A converter thus provides a voltage equal to one half of full-scale. This voltage is compared with the analog input. If the analog input is larger, the latch for the MSB remains in the positive state. Otherwise it is set false, and the latch for the second most significant bit is set true. The process is repeated until all 10 bits have been determined. The data ready signal indicates the conversion process is completed.

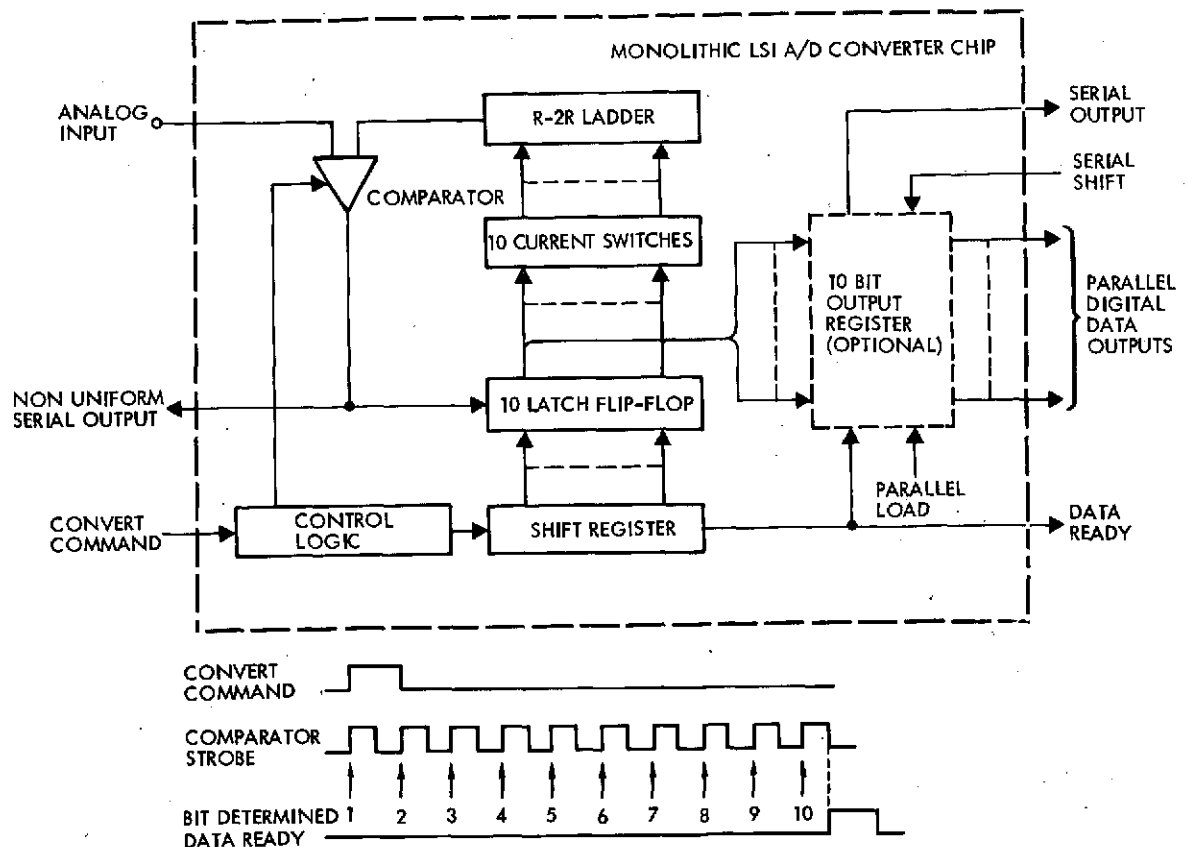


Figure 4-33. Timing Diagram and Monolithic LSI Successive Approximation A/D Converter

Serial-Parallel Feedforward Approach. This approach is illustrated in Figure 4-34. The converter first encodes the sampled signal to the most significant 4 bits in one timing step. The second 4 bits are determined in a second timing step. The feedforward signal is derived by subtracting the D/A converter output from the input signal and multiplying the remainder for the second stage to get the last 4-bit conversion.

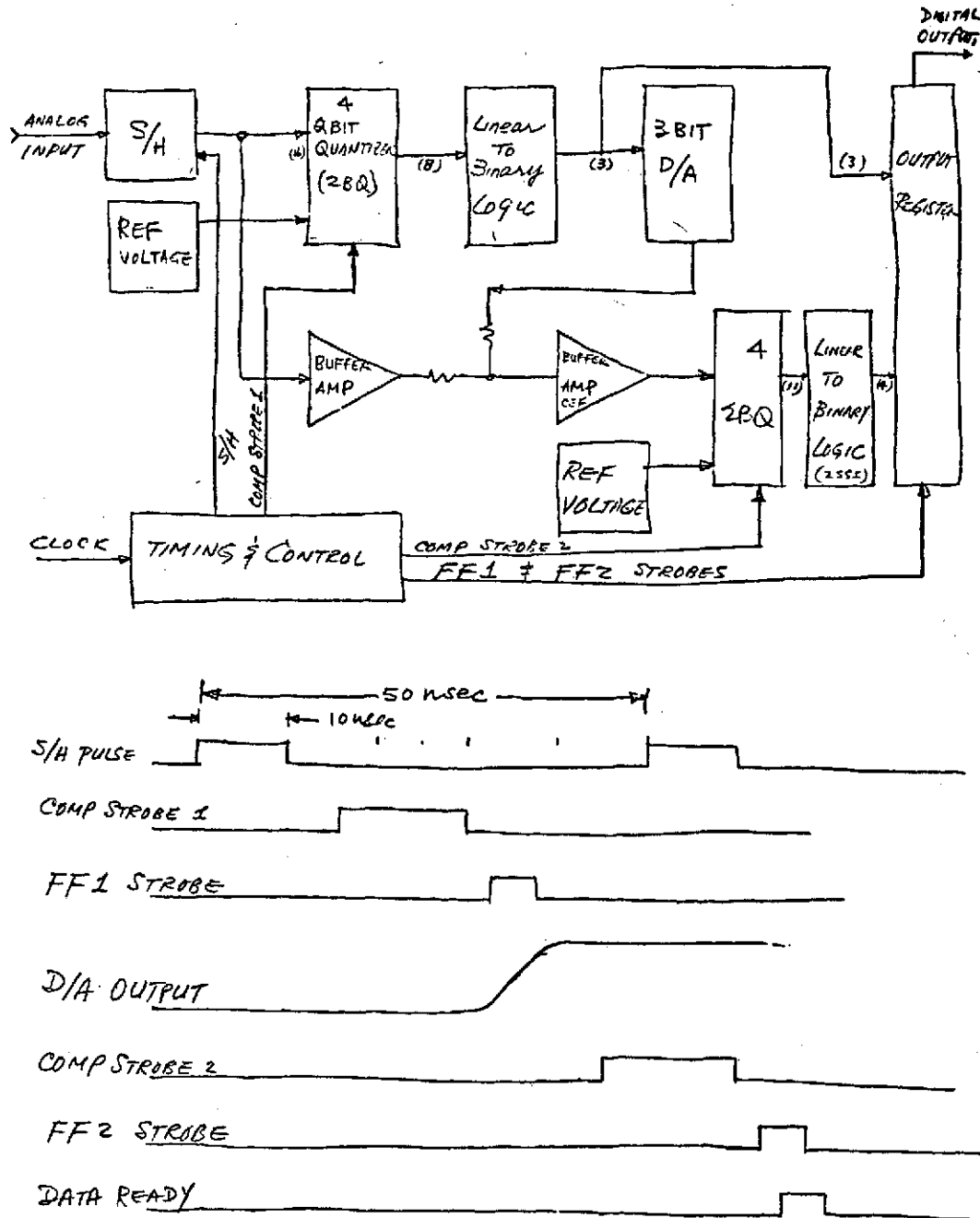


Figure 4-34. 20 MS/S Serial-Parallel Feed Forward A/D Conversion

Serial-Parallel Feedback Approach. This approach is illustrated in Figure 4-35.

The conversion period is divided into two cycles by the timing logic. The first cycle begins by sampling the analog input and holding this sampled value until the start of the next conversion period. Throughout the first cycle the A/D control logic inhibits the D/A output to zero and sets the step selector currents to  $k$  ma (where  $k$  and reference resistance  $R$  generates one step size). This results in a step size of 128 mv with the center threshold at zero volts. At the end of the first cycle, the four 2-bit quantizers (2 BQ) are strobed and its 4-bit digital output indicates the step which contained the analog input voltage. These four bits are MSB, 2, 3 and 4 of the 8-bit result and are fed back to the D/A to determine the four 2-BQ center threshold voltages for the second cycle of the conversion period.

During the second cycle, the step selector current is reduced to 16 ma, resulting in an 8 mv step size. The 15 thresholds of the 2 BQs are now equally spaced within the one 128 mv step determined by the four 2-BQs at the end of the first cycle. At the end of the second cycle, the four 2-BQs are strobed again, the four least significant bits of the 8-bit result are determined which completes the conversion period.

The ADC tradeoff summary is shown in Table 4-21 and a listing of the advantages and disadvantages are shown in Table 4-22. Table 4-23 shows the parts and power summary for the recommended baseline version 8-bit, 20 Ms/s SPFB ADC in both discrete and LSI configurations.

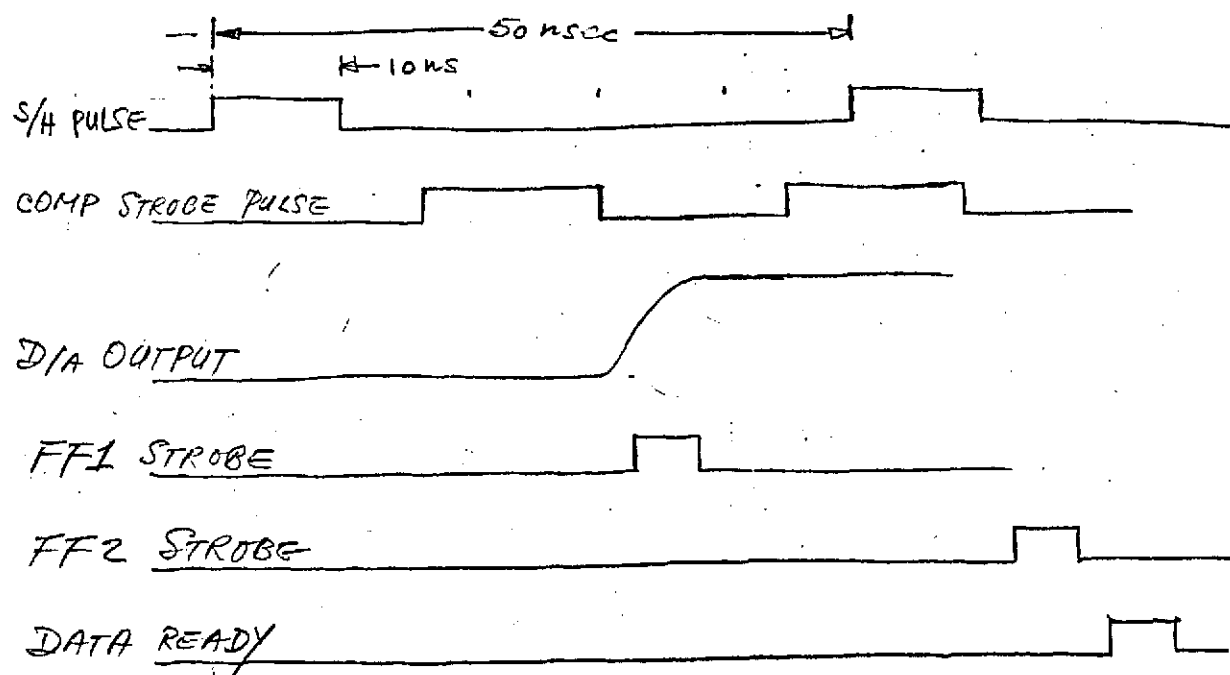
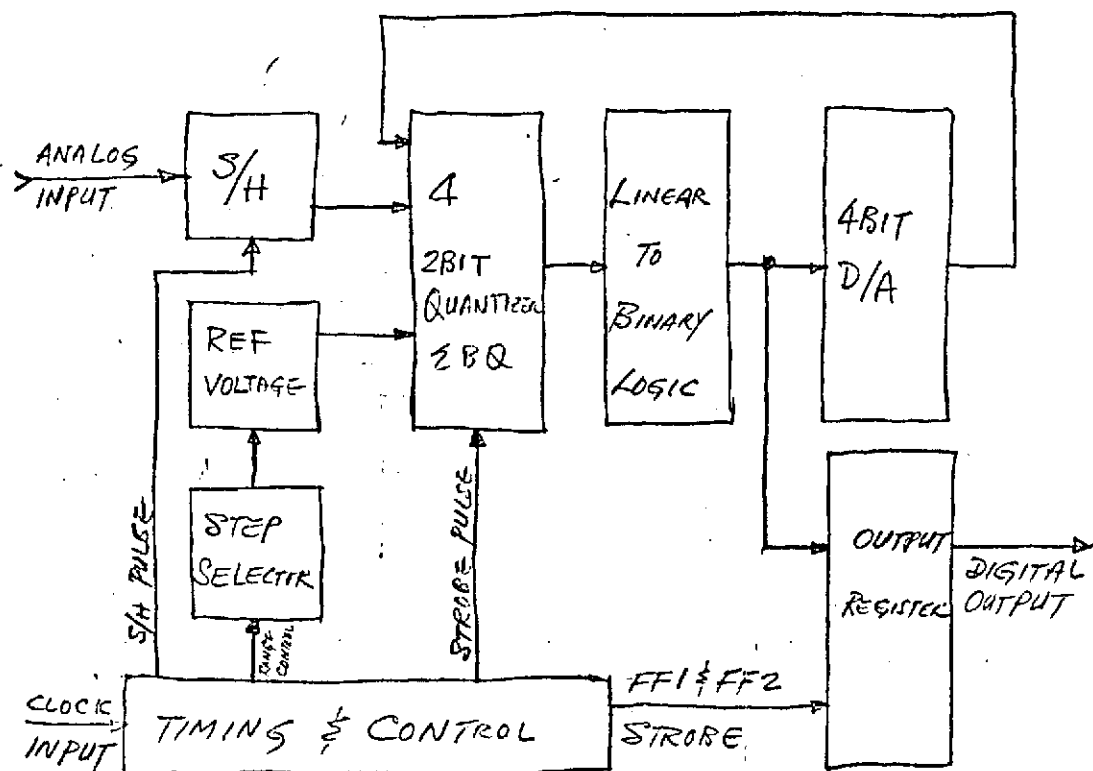


Figure 4-35. 20 MS/S Serial-Parallel Feedback A/D Converter

ORIGINAL PAGE IS  
OF POOR QUALITY

Table 4-21. ADC Tradeoff Summary

Sampling Rate	20 Ms/s			10 Ms/s
Approach	Subranging (MOMS)	Serial-parallel feedforward (SPFF)	Serial-parallel feedback (SPFB)	Successive approxima- tion
Converter	2	2	2	2
Fast time of analog channel	50 ns	50 ns	50 ns	50 ns
Total power	12 watts	8 watts	7 watts	6.60 watts
Resolution	7 bits	7 bits	8 bits	10 bits
Relative accuracy	Third	Third	Second	Highest
Size (each) — discrete, sample and hold, circuit	100 in <sup>2</sup>	75 in <sup>2</sup>	65 in <sup>2</sup>	26 in <sup>2</sup>
Size (each) — monolithic S/H circuit	100 in <sup>2</sup>	50 in <sup>2</sup>	45 in <sup>2</sup>	2 in <sup>2</sup>
Number of parts with mono- lithic S&H		181	173	60
Number of parts with discrete S&H CKT		614	598	564



Table 4-22. A/D Converter Advantages and Disadvantages

System	Speed Ms/s	Resolution (bits)	Power (watts)	Advantages	Disadvantages	Comments
MOMS	20	8	12	Requires slower speed S/H	<ul style="list-style-type: none"> <li>• Discrete compa- rator</li> <li>• Highest power</li> <li>• Large parts count</li> <li>• Large variation for reference voltage</li> </ul>	Parts count 5 to 7 times of other sys- tems
Serial/parallel feed- forward (SPFF)	20	8	9.74	Highest speed can be achieved with parts count tradeoff	Requires offset adjustment for comparators	2 BO offset can be laser trimmed ap- proximately .1 mv
Serial/parallel feed- back (SPFB)	20	8	7.32	<ul style="list-style-type: none"> <li>• Relatively simple timing</li> <li>• Speed is ready attainable</li> <li>• Relatively less parts</li> </ul>	Requires offset adjustment for comparators	<ul style="list-style-type: none"> <li>• 2 BO offset can be laser trimmed ap- proximately .1 mv</li> <li>• Second choice</li> </ul>
Monolithic successive approximation (1 bit at a time)	10	10	6.6	<ul style="list-style-type: none"> <li>• Lowest power</li> <li>• Converter design provides linearity and resolution without necessarily having correspond- ing absolute accur- acy D/A drives only 1 comp</li> <li>• Lowest part count</li> </ul>	<ul style="list-style-type: none"> <li>• Slowest speed</li> <li>• Requires 4 S/H</li> </ul>	Best choice from the standpoint of power, parts count and

Table 4-23. ADC - 8 Bit 20 Ms/s SPFB

Part Name	Type	IC	Disc	Power (mw)	Comment
Sample and hold			155	400	TRW monolithic version will be available at the end of 1974
2-Bit quantizer	TRW 2 BO	(MSI)		960	
Linear-to-binary logic		2 (SSI)	10	200	
4-Bit D/A converter	TRW CGS	6 (MSI)	28	400	
Output register		4 (MSI)	8	900	
Reference voltage and step selector	LM108	4 (MSI)	38	400	
Timing and control	LM108	6 (SSI)	38	400	
Delay line		4 (SSI)			
		30 IC	263D	3660	

Each A/D converter = 293 parts at 3.66 w

Both A/D converters = 586 parts at 7.32 w

Both A/D converter with monolithic S/H = 276 parts at 7.32 w

#### 4.6.4 High-Speed Buffer

The high-speed buffer accepts 120 Mbit/sec data from the thematic mapper, then edits and buffers the data for two purposes:

- 1) Reduce the data rate to the LCGS to 20 Mbit/sec through a factor of six reduction in sample rate or alternatively to 15 Mbit/sec by also reducing the 8-bit word to 6 bits.
- 2) Reformat the data to be line-sequential rather than column sequential, as is the data format when it is leaving the A/D converter (MODS).

##### 4.6.4.1 Problem Discussion

The LCGS speed buffer/reformatter is charged with the task of stripping a requested portion of data from the thematic mapper data stream and reformatting this data in accordance with the LCGS application. The data reformatting is provided to ensure line-sequential, rather than column-sequential data transmission. If this reformatting is accomplished in the satellite, then the LCGS is able to display the data via a filmwriter/display as the data is received directly from the demodulator, without further processing. An introduction to the reformatting problem is presented first, followed by a discussion of the line-stripping problem.

Figure 4-36 depicts the reformatting which is to be accomplished. The arrows in Figure 4-36 depict the order of data as it emerges from the MODS Encoder and enters the line-stripper section of the speed buffer. Minor frame 1 emerges first, followed by minor frame 1B, etc. When the second swath of data emerges, pixels 1 through 16 of minor frame 1A emerge first, so that, without satellite reformatting, this data must now be aligned with minor frame 1 of the first swath, requiring either considerable memory at the ground station for reformatting, or complex mechanization to realign the data at the beginning of every swath. For the data rate considered, present technology does not allow the latter approach. Furthermore, any buffering scheme must be limited to the capability of a minicomputer. If buffered reformatting is accomplished at the LCGS, then one-half of the minicomputer memory will be dedicated to reformatting, allowing only one-half of the memory for all other tasks. For these reasons, the baseline proposal includes reformatting by the data handling section of the satellite.

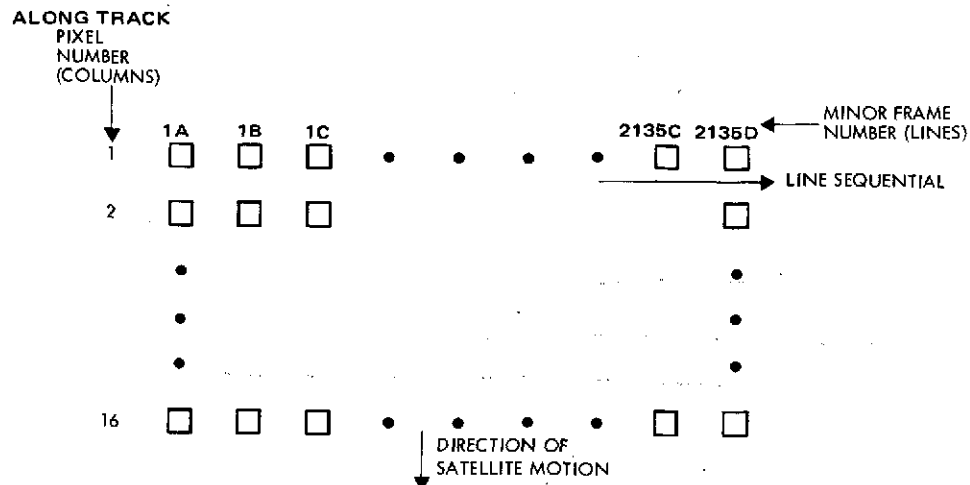


Figure 4-36. Order of One Swath of Data out of MODS

The speed buffer/reformatter ensures that the data transmitted to the LCGS is in the order depicted in Figure 4-37. As in Figure 4-36, the arrows in Figure 4-37 depict the order of data as it emerges from the speed buffer/reformatter. Pixel 1 of all minor frames emerge first, followed by pixel 2 of all minor frames, etc. With this reformatting scheme, a complete scene of data can be displayed or photographed without further data processing on the ground.

The LCGS is to receive thematic mapper (TM) data at a 20 Mbit/sec data rate, whereas the TM actually produces data at the rate of 120 Mbit/sec. Since only a portion of the TM data can be transmitted to the LCGS, considerations must be made for extraction of meaningful data. The following four options have been suggested.

- 1) All data from one band (out of seven bands possible), full swath
- 2) Two bands for 1/2 swath
- 3) Four bands for 1/4 swath
- 4) Seven bands, full swath, reduced resolution.

Although only these four major options exist, there are many further possibilities: Which band to select for option 1, which two bands for option 2 or four bands for option 3; where does a one-half or one-quarter swath begin? These suboptions are considered in further detail below.

The LCGS speed buffer is partitioned as depicted in Figure 4-38.

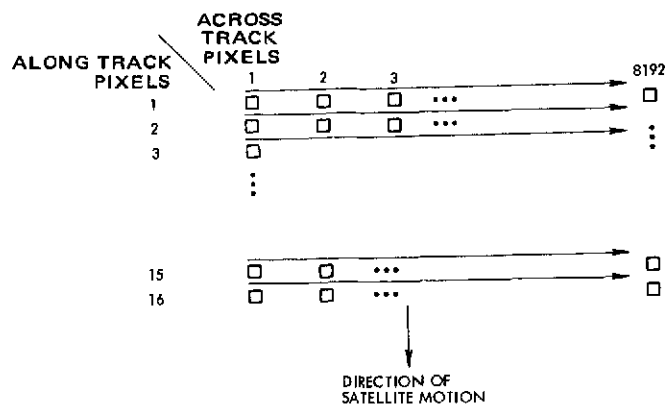


Figure 4-37. Order of One Swath of Data Emerging from the LCGS Speed Buffer/Reformatter

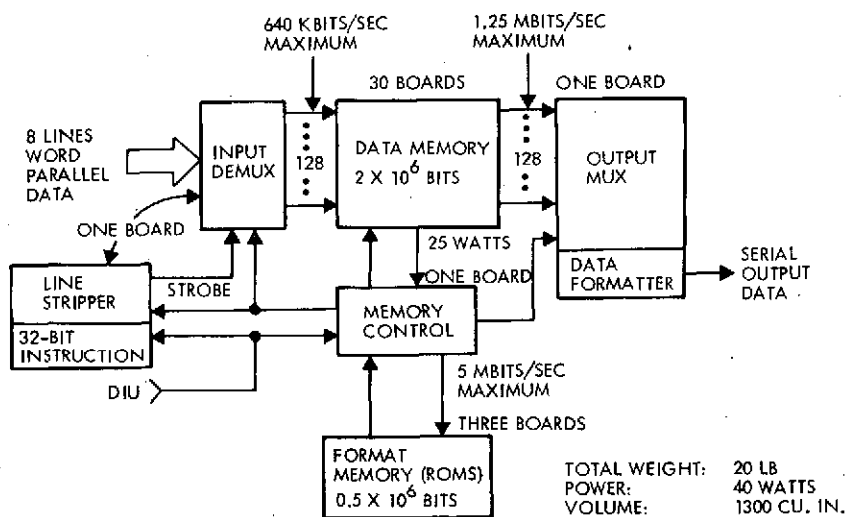


Figure 4-38. Speed Buffer (LCGS) Simplified Block Diagram and Partioning (Includes a Line Stripper and Formatter)

The line stripper section of the speed buffer (Figure 4-38) receives a 32-bit instruction (option select word) and a word clock as data and produces a strobe signal on the output line when the next word out of the MODS encoder is to be stripped from the data stream and stored in the speed buffer. The line stripper is used solely to determine whether or not the next word out of the MODS encoder is to be transmitted to the LCGS.

The reformatting scheme is performed in the speed buffer memory section. A double buffering technique is recommended which allows use of NMOS random access memories. Double buffering techniques allow simple addressing techniques for all four options.

A detailed description of the line stripper is presented, followed by the methods of programming the line stripper for each of the four major data options. Finally, the high-speed buffer addressing scheme is presented.

Although four major options are discussed, there exists many possible suboptions. For option 1 (one band, full swath) any one of six bands may be selected. For options 2 and 3, (two- and four-band options) any two out of six bands or any four out of six bands may be chosen, respectively. Since the seventh band is transmitted with one-quarter of the density of the other six bands, the full capability of the high-speed buffer is not realized if the seventh band is available as an option. However, the seventh band may be included. Many possible starting points exist for options 2 and 3. Dividing the complete swath into 16 segments allows the LCGS flexibility in determining the beginning of a partial swath, as well as allowing a simplified approach to the implementation of the starting point. The number of segments (16) is not fixed; its alteration affects only the sizes of a counter and a divider. The total number of suboptions are determined as follows:

$$\begin{array}{ccccccc}
 & & \text{color} & & \text{starting point} & & \\
 & & \text{select} & & \text{select} & & \\
 & & \swarrow & \searrow & \downarrow & & \\
 6 & + & \binom{6}{2} \times 8 & + & \binom{6}{4} \times 12 & + & 1 = 307 \text{ total option} \\
 \hline
 \text{option} & & \text{option} & & \text{option} & & \text{option} \\
 1 & & 2 & & 3 & & 4
 \end{array}$$

A 14-bit word is used for the option select.

#### 4.6.4.1.1 Line Stripper Organization

The line stripper may be segmented into three sections (Figure 4-39):

- 1) Minor frame select
- 2) Band select
- 3) Option 4 - reduced resolution

Options 1, 2, and 3 require selection of a portion of the swath; either full, 1/2, or 1/4. In the case of a full swath, information is

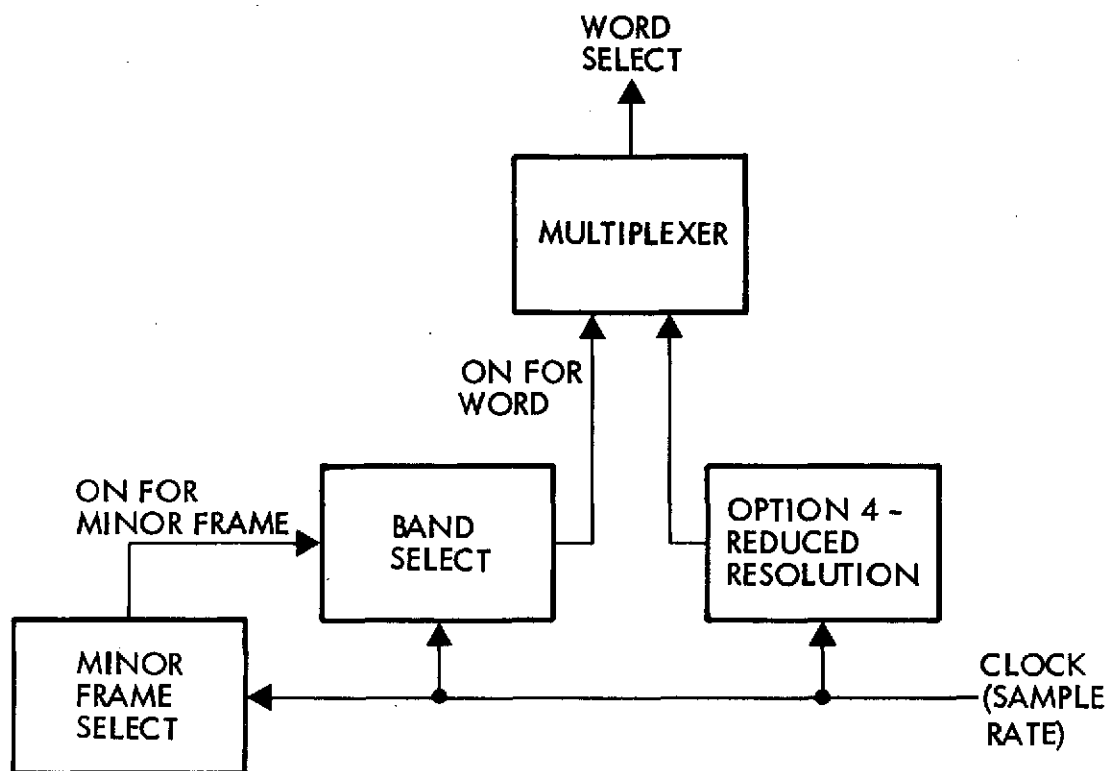


Figure 4-39. Line Stripper

extracted from every minor frame. In the case of a  $1/2$  or  $1/4$  swath, only a portion of the total 2132 minor frames are selected for data extraction.

a. Minor Frame Select

The minor frame select portion receives the 15 MHz word rate clock and, through a divider, pulses a resettable 4-bit counter every  $1/16$  swath (Figure 4-40). This counter sets the minor frame select latch, which, when active, signifies that the next minor frame is a frame from which data is to be extracted. This latch also resets a 3-bit counter, which pulses every  $1/16$  swath. This counter clears the latch at the end of  $1/4$  or  $1/2$  swath, depending on the option selected at the LCGS. The minor frame select latch is set and never cleared for the one band, full swath option. The value of this latch constitutes input data to the band select segment of the line stripper.

Figure 4-40. Line Stripper Detailed Block Diagram



#### b. Band Select

The band select segment maintains two 6-bit registers: the band select register and the word pulse register. The band select register is loadable upon request via command. Each bit in this register corresponds to one of the possible bands which can be selected for transmission. For the one band, full swath option, 1 bit of this register is active at the position corresponding to the desired band. For the two band, 1/2 swath option, 2 bits are active. Two bits are active for the 4-band, 1/4 swath option; in this case, the bits correspond to the two colors not chosen.

When the frame select latch is active, the high-order position of the word pulse register is set to 1. This register then cycles at the word rate such that the active bit shifts through all six positions and returns to its original position every six pulses. It is instructive here to consider the data format of the thematic mapper minor frame. The 400-word minor frame is organized in accordance with Table 4-24.

The position of the 1 bit in the band-select register corresponds to the band of the next word available for transmission. When the position of the 1 bit in the word pulse register matches a 1 position in the band select register, the next word out of the MODS is to be transmitted. The switching function,  $f$ , which determines this transmission is just the inner product function of the two registers. This function is active when the next word out of the MODS is to be placed into the high-speed buffer. For the 4-band option, the function  $f$  is complemented, such that when the 1 bit in the word pulse register is adjacent to one of the four positions not selected in the band select register, the next word out of the MODS is placed into the high-speed buffer.

#### c. Option 4 - Reduced Resolution

For option 4 (reduced resolution, full swath) a center pixel from each 6-pixel rectangle (in accordance with Figure 4-41) is stripped from the data stream. In the first swath transmitted, data is extracted from pixels 2, 5, 8, ..., 14. In the second swath, data is extracted from

Table 4-24. Thematic Mapper Minor Frame

<u>Word</u>	<u>Pixel, Band</u>	<u>Word</u>	<u>Pixel, Band</u>
1	1, 1	21	4, 3
2	1, 2	22	4, 4
3	1, 3	23	4, 5
4	1, 4	24	4, 6
5	1, 5	25	4, 7
6	1, 6	26	5, 1
7	2, 1	27	5, 2
8	2, 2	28	5, 3
9	2, 3	29	5, 4
10	2, 4	30	5, 5
11	2, 5	31	5, 6
12	2, 6	32	6, 1
13	3, 1	33	6, 2
14	3, 2	34	6, 3
15	3, 3	—	—
16	3, 4	—	—
17	3, 5		
18	3, 6		
19	4, 1		
20	4, 2		

All bands of pixel 1 are transmitted, then all bands of pixel 2 are transmitted, etc. Since band 7 consists of 1/16 of the number of pixels as the other six bands, band 7 is transmitted only once every four pixels, i.e., once every 25 words and thus only once in every four sequences (minor frame synchronization is sent to the other three sequences). When the line stripper extracts one or more colors from a minor frame, the colors from pixel 1 must be extracted first, then the color from pixel 2 must be extracted, etc. The band select register cycles once every pixel — during that cycle, the appropriate words are selected.

pixels 1, 4, 7, ..., 16. In the third swath, data is extracted from pixels 3, 6, 9, ..., 15. The process repeats for the fourth swath. In every case, the second and fourth rows in each minor frame are selected for data transmission. Figure 4-42 and Table 4-25 depict this concept. The rate reduction here is six to one as in the previous cases.

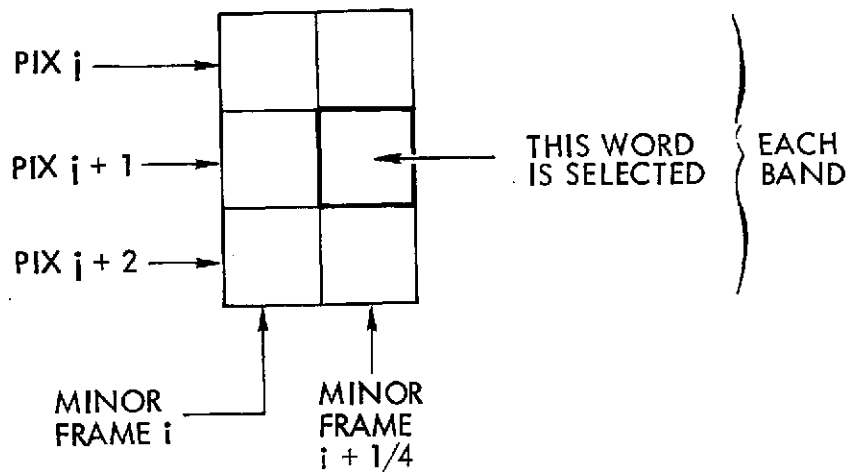


Figure 4-41. Data Selection for Option 4

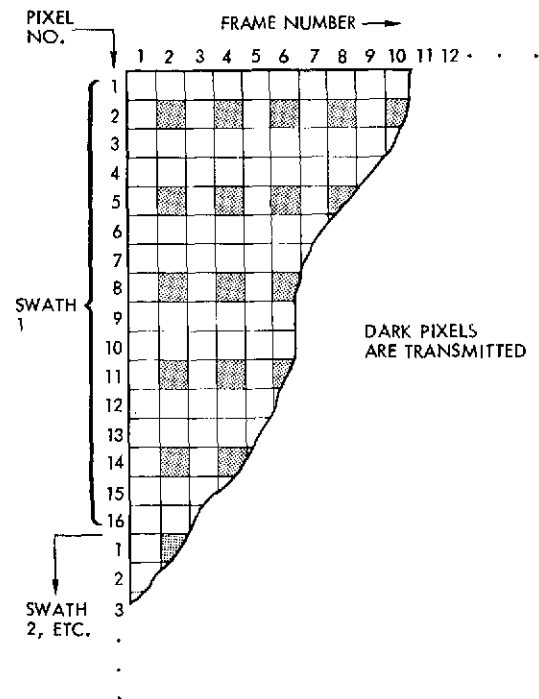


Figure 4-42. Option 4 Pixel Select

Table 4-25. Pixel Select for Option 4

Swaths 1, 4, 7, 10, ...		Swaths 2, 5, 8, 11, ...		Swaths 3, 6, 9, 12, ...	
<u>Pixel,</u>	<u>Band</u>	<u>Pixel,</u>	<u>Band</u>	<u>Pixel,</u>	<u>Band</u>
2	1-6	1	1-6	3	1-6
5	1-6	4	1-7	6	1-6
8	1-7	7	1-6	9	1-6
11	1-6	10	1-6	12	1-7
14	1-6	13	1-6	15	1-6
		16	1-7		

The option 4 portion of the line stripper selects words in accordance with Table 4-25 for transmission to the LCGS. A simple configuration of dividers and counters assures that the word select line is active when the desired word is present at the output of the MODS Encoder.

#### 4.6.4.1.2 Line Stripper Options

The methods of handling the four baseline options available to the LCGS are enumerated below.

##### a. Option 1 - One Band, Full Swath

Each major frame (full swath) consists of 2132 minor frames. Designating band A as the selected band, all band A words are extracted from each minor frame and transmitted to the LCGS. Table 4-26 shows which data is stripped from each minor frame and placed into the high-speed buffer for reformatting and transmission. For this option, every sixth word is stripped from the data stream and placed into the high-speed buffer, with the exception that when the seventh band is transmitted, an additional interval is passed up before stripping off the desired word. Figure 4-43 shows the selection procedure for this option. The line stripper now extracts all pixels of the desired band over the complete swath.

Table 4-26. Data Transmitted for Option 1

<u>Pixel,</u>	<u>Band</u>
1	A
2	A
:	
:	
:	
16	A

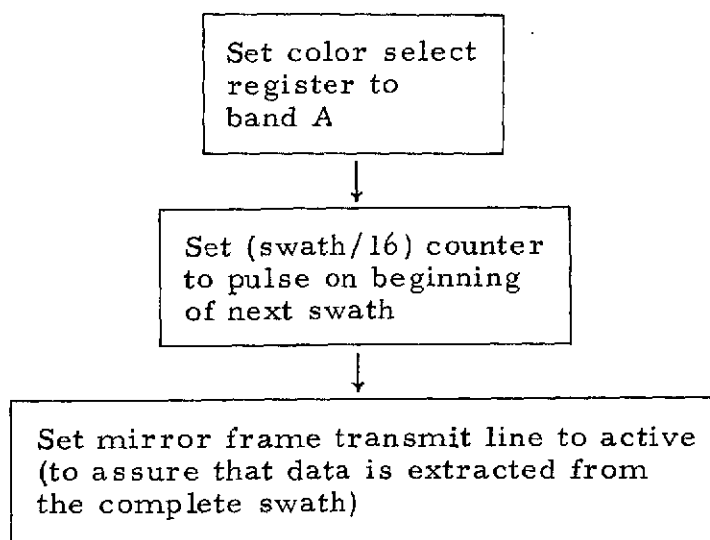


Figure 4-43. Selection Procedure for Option 1

b. Option 2 — Two Bands, 1/2 Swath

Designating bands A and B as the selected bands, all band A and B words are selected from 1066 contiguous minor frames of the complete swath. As the swath is partitioned into 16 equally spaced sections one of eight starting positions is possible with this option; we may start with any one of the eight sections which comprise the first half of the swath. Table 4-27 gives the words which are stripped from each minor frame and placed into the high-speed buffer. In this case, two out of every six words (two out of seven when the seventh band is transmitted) for 1/2 of the swath period are stripped from the data stream. The procedure for this option is depicted by Figure 4-44.

Table 4-27. Data Transmission for Option 2

<u>Pixel,</u>	<u>Band</u>
1	A
	B
2	A
	B
	:
	:
16	A
	B

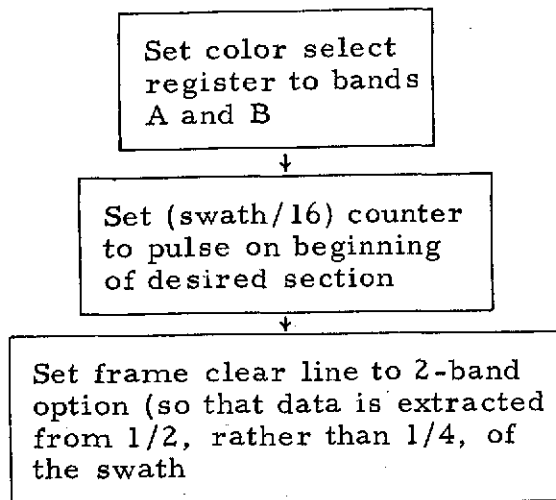


Figure 4-44. Selection Procedure for Option 2

c. Option 3 – Four Bands, 1/4 Swath

Designating bands A, B, C, and D as the selected bands, all band A, B, C, and D words are transmitted from 533 contiguous minor frames. Since only 1/4 swath is transmitted, there exists 12 possible starting locations – we may begin with any one of the 12 sections which comprise the first 3/4 of the swath. Table 4-28 shows which words are stripped from each minor frame.

Four out of every six words (four out of every seven when the seventh band is transmitted) for 1/4 of the swath period are stripped from the data stream and placed into the high-speed buffer, as depicted in Figure 4-45.

Table 4-28. Data Transmission for Option 3

<u>Pixel,</u>	<u>Band</u>
1	A
	B
	C
	D
2	A
	B
	C
	D
3	A
	B
	C
	D
:	
:	
etc.	

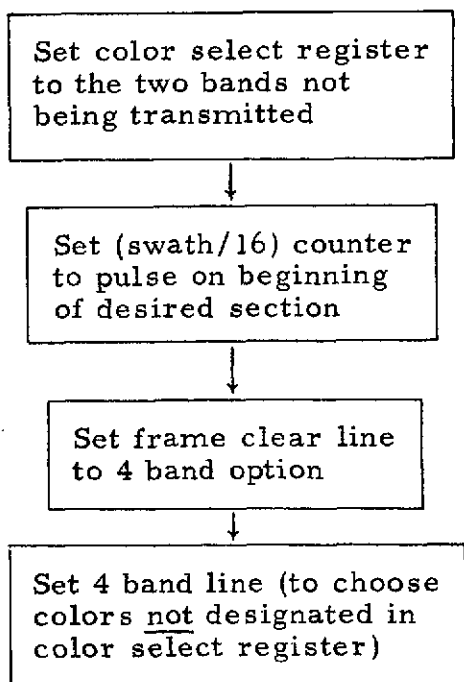


Figure 4-45. Selection Procedure for Option 3

d. Option 4 – Seven Bands, Reduced Resolution

Table 4-29 shows which words are stripped from minor frames (assuming swath 2, 5, 8, ...). The data stripping concept for this option was depicted in detail in Section 4.6.4.1.1

For this option, all bands are transmitted for every third pixel, twice each minor frame. The procedure here is simply to set the option 4 line active, which causes the stripping of one-sixth of the data for transmission to the LCGS.

Table 4-29. Data Transmitted for Option Four

<u>Pixel,</u>	<u>Band</u>
2	1
2	2
2	3
2	4
2	5
2	6
5	1
5	2
5	3
5	4
5	5
5	6
8	1
8	2
8	3
8	4
8	5
8	6
8	7
11	1
11	2
	:
	:



#### 4.6.4.1.3 High-Speed Buffer

A double buffering technique is used to perform the desired reformatting. Each one of the two memory sections is organized as shown in Figure 4-46. The addressing techniques for each of the four LCGS options follow.

##### a. Option 1 - One Band, Full Swath

Designating band A as the one selected, the most significant 6 bits of Band A for the complete swath are organized in the high-speed buffer in accordance with Table 4-30. The first word out of the MODS is word (1, 1). This word is loaded into RAM 1. The second word, (1, 2), is loaded into RAM 2; the third word into RAM 3, etc. RAM 1 is loaded again with the 17th word, RAM 2 with the 18th word, etc. In this manner, the data arriving at the word rate of 66.7 nsec can be multiplexed into NMOS memories with a 450 nsec write time.

In transmission, RAM 1 is completely unloaded, then RAM 2 is completely unloaded, ..., finally, RAM 16 is completely unloaded. With

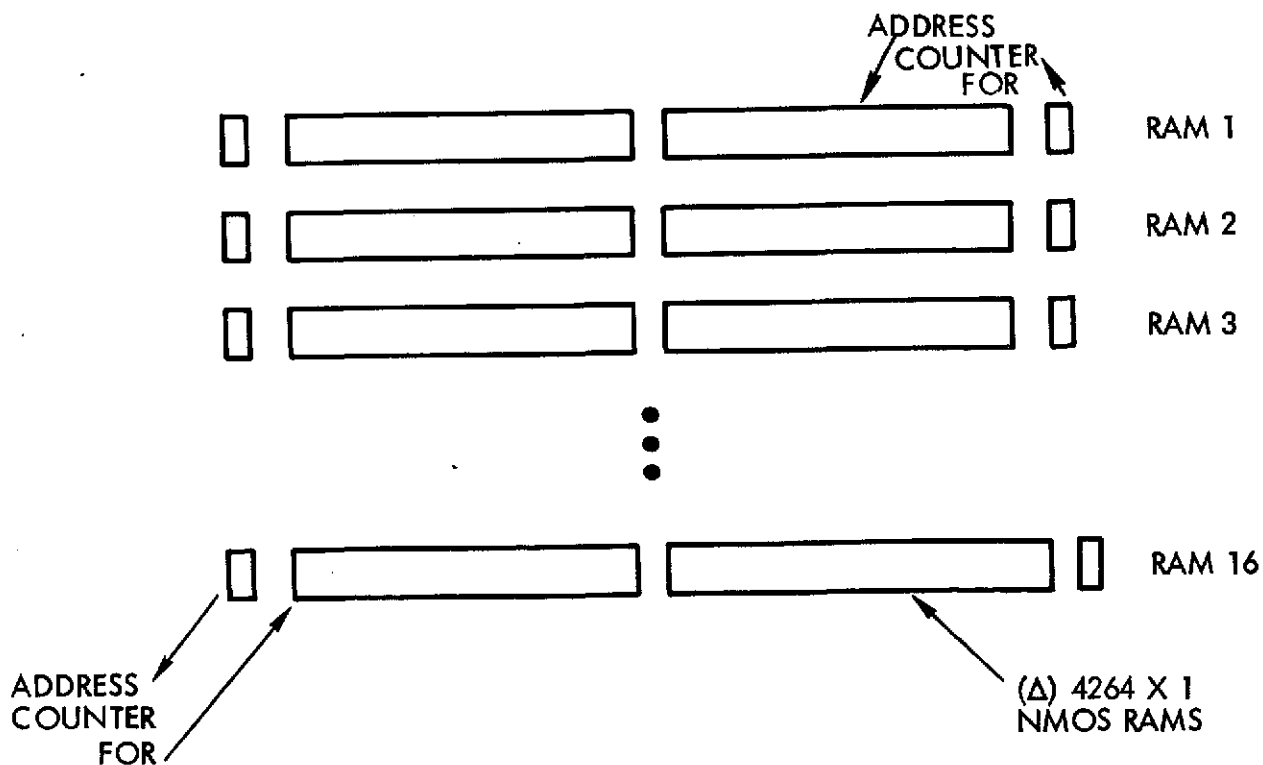


Figure 4-46. Block Diagram of the High-Speed Buffer

Table 4-30. Data Organization for Option 1

(1, 1)	(2, 1)	(3, 1)	...	(8528, 1)	RAM1
(1, 2)	(2, 2)	(3, 2)	...	(8528, 2)	RAM2
(1, 3)	(2, 3)	(3, 3)	...	(8528, 3)	RAM3
⋮					
(1, 16)	(2, 16)	(3, 16)	...	(8528, 16)	RAM16
(frame, pixel)					

this addressing scheme, the desired data transformation – column sequential to line sequential – is performed.

b. Option 2 – Two Bands, 1/2 Swath

Designating bands A and B as the one selected, the 8-bit quantizations for both bands A and B over 1/2 of the swath (pixels 1 through 4264) are organized in accordance with Table 4-31. The first word out of the MODS, word (1, 1, A), is loaded into the first half of Ram 1. The second word (1, 1, B), is loaded into the second half of RAM 1. The third word (1, 2, A), is loaded into the first half of RAM 2, etc.

As in the case for option 1, in transmission, all of RAM 1 is unloaded, then all of RAM 2, etc.

Table 4-31. Data Organization for Option 2

Position 4264			
(1, 1, A)	(2, 1, A)	(1, 1, B) (2, 1, B)	RAM1
(1, 2, A)	(2, 2, A)	(1, 2, B) (2, 2, B)	RAM2
(1, 3, A)	(2, 3, A)	... (1, 3, B) (2, 3, B)...	RAM3
⋮	⋮	⋮	
(1, 16, A)	(2, 16, A)	(1, 16, B) (2, 16, B)	RAM16
(frame, pixel, band)			

c. Option 3 – Four Bands, 1/4 Swath

Designating bands A, B, C, and D as the ones selected, the 8-bit quantizations for all four bands over 1/4 of the swath, pixels 1 through 2132 are organized in accordance with Table 4-32. For this option, the order of transmission to the LCGS is as follows:

(1, 1, A) (2, 1, A) ... (2048, 1, A) (1, 1, B) (2, 1, B) ...

In transmission, 1/2 of RAM 1 is unloaded (1/2 of the first 4264 word memory section, followed by 1/2 of the second 4264 word memory section). Identical sections of RAM's 2, 3 and 4 are then unloaded, followed by the remaining data from RAM's 1, 2, 3, and 4, respectively. The same procedure is then used on RAM's 5 through 8, then 9 through 12, and, finally, 13 through 16.

d. Option 4 – Full Swath, Reduced solution

For this option, as stated in Section 4.6.4.1.2, 1/6 of the available data is extracted for transmission to the LCGS. The data is organized in the memory in accordance with Table 4-33. As in options 1 and 2, RAM 1 is completely unloaded first, then RAM 2 is unloaded, followed by RAM 3, etc.

Table 4-32. Data Organization for Option 3

Position 4097		
(1, 1, A) (1, 3, A) (2, 1, A) ...	(1, 1, B) (1, 3, B) (2, 1, B)	RAM1
(1, 1, C) (1, 3, C) (2, 1, C)	(1, 1, D) (1, 3, D) (2, 1, D)	RAM2
(1, 2, A) (1, 4, A)	(1, 2, B) (1, 4, B)	RAM3
(1, 2, C) (1, 4, C)	(1, 2, D) (1, 4, D)	RAM4
(1, 5, A)	(1, 5, B)	
(1, 5, C)	(1, 5, D)	
(1, 6, A) :	(1, 6, B) :	
(1, 6, C)	(1, 6, D)	
(frame, pixel, band)		

Table 4-33. Data Organization for Option 4

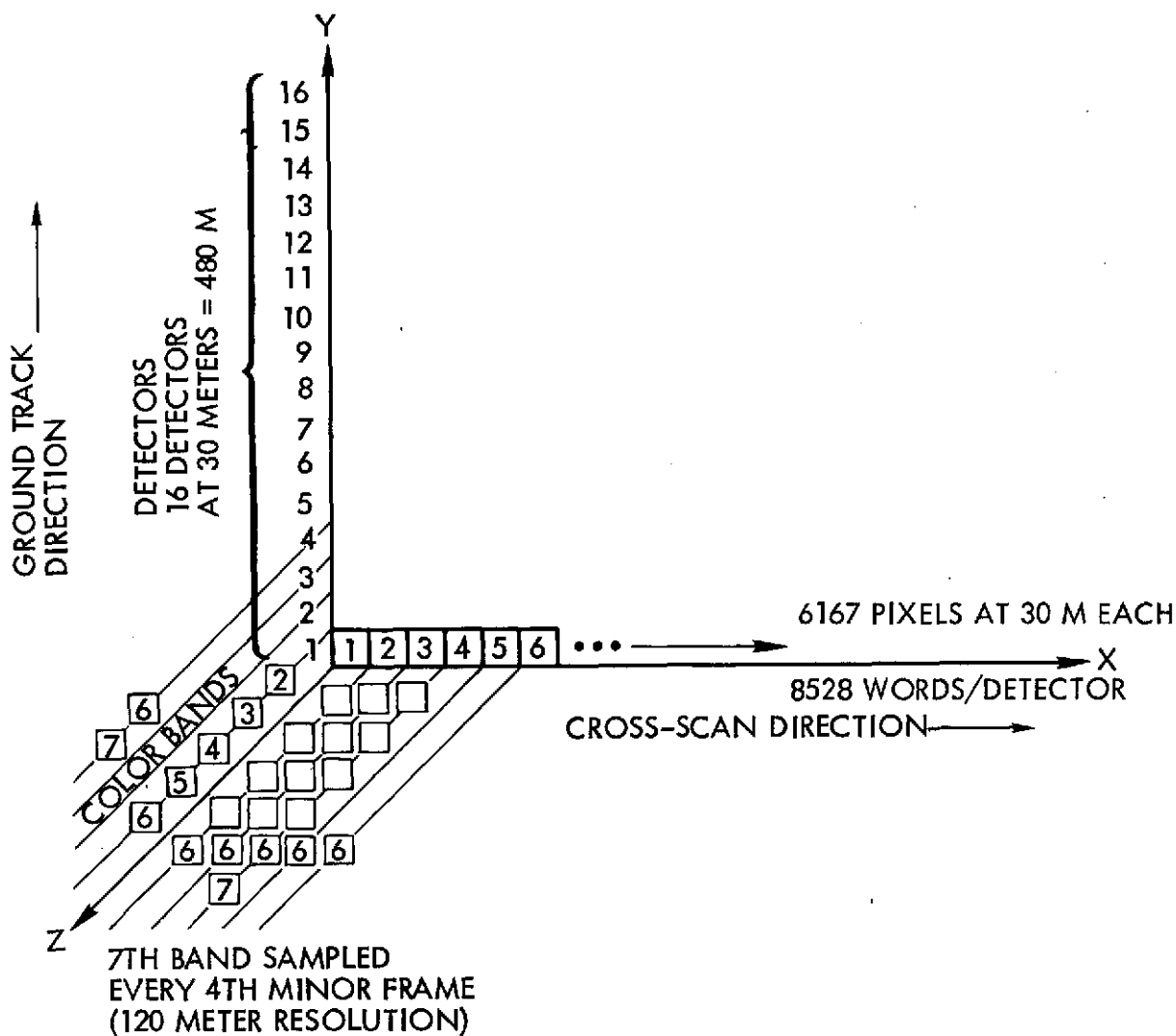
Position 4264			
↓			
(2,2,1)(5,2,1) ... (8528,2,1)	(2,2,2)(5,2,2) ... (8528,2,2)	RAM1	
(2,2,3)(5,2,3)	(2,2,4)(5,2,4)	RAM2	
(2,2,5)(5,2,5)	(2,2,6)(5,2,6)	RAM3	
(2,5,1)(5,5,1)	(2,5,2)(5,5,2)		
(2,5,3)(5,5,3)	(2,5,4)(5,5,4)		
(2,5,5)(5,5,5)	(2,5,6)(5,5,6)		
(2,8,1)(5,8,1)	(2,8,2)(5,8,2)		
(2,8,3)(5,8,3)	(2,8,4)(5,8,4)		
(2,8,5)(5,8,5)	(2,8,6)(5,8,6)		
(2,11,1) .	(2,11,2) .		
(2,11,3) .	(2,11,4) .		
(2,11,5) .	(2,11,6) .		
(2,14,1)	(2,14,2)		
(2,14,3)	(2,14,4)		
(2,14,5)	(2,14,6)		
(2,8,7)(5,8,7) ...			
(frame, pixel, band)			

The data rate out of the MODS allows 66.7 nsec between words. For all options, a minimum of 8 words are written into the high-speed buffer prior to rewriting into any one RAM, allowing  $8 \times 66.7 = 533.3$  nsec between write times into any one RAM, justifying the use of 450 nsec write time RAM's. The output rate of 20 Mbit/sec, equivalent to 400 nsec between transmitted words, allows the use of 350 nsec read-time NMOS memory.

#### 4.6.4.2 Analysis and Tradeoffs

##### 4.6.4.2.1 Description of Operation: Line Stripper (Input Data Editor)

The MODS output is a word parallel data stream from the thematic mapper at 15 M word rate (unedited). The front end of the LCGS speed buffer, shown in Figure 4-38, contains a line stripper that performs the data editing function (see Figure 4-47). The line stripper is functionally flexible to accommodate future missions. The data editing sequence is selected upon command via a data transfer from the on-board computer. The DIU sends a serial digital command to the LCGS speed buffer which receives the command in a register. The command instruction is decoded by



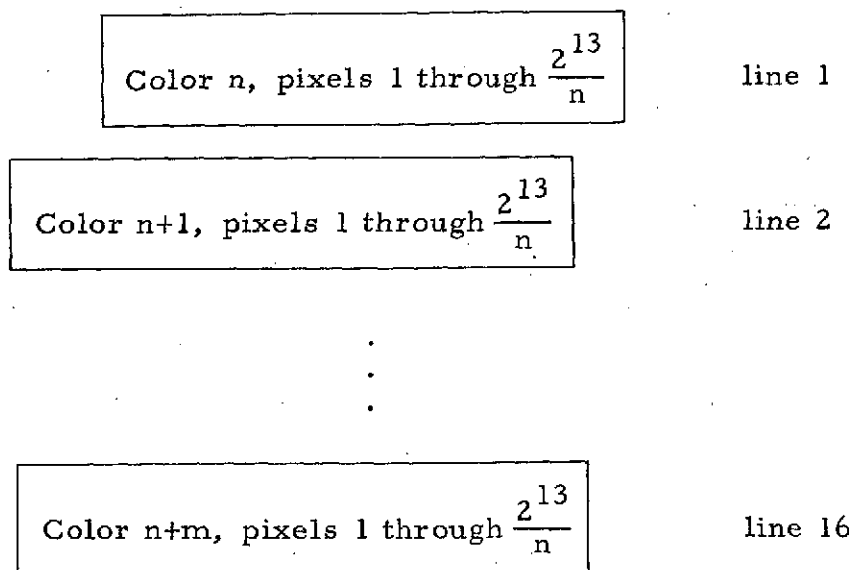
SAMPLING ORDER:

ALL COLOR BANDS 1ST PIXEL AND 1ST DETECTOR, THEN  
 ALL COLOR BANDS 1ST PIXEL AND 2ND DETECTOR, THEN  
 ALL COLOR BANDS 1ST PIXEL AND 16TH DETECTOR, THEN  
 ALL COLOR BANDS 2ND PIXEL AND 1ST DETECTOR, THEN  
 ALL COLOR BANDS 8192ND PIXEL AND 16TH DETECTOR

Figure 4-47. Thematic Mapper Data Acquisition Sequence  
 Speed Buffer Input Format (Unedited)

setting word lengths into the appropriate counters that may determine such parameters as output bit rate, frame length, and color options (Figure 4-48). This feature permits inflight reconfigurability of the above parameters. Future missions may be accommodated with this flexible approach by programming the generalized logic board of the line stripper both for input bit rate and editing sequence since the line stripping function is determined by programmable modulo-n counters. This programming may be accomplished in two ways.

The simplest method is to build generalized logic boards with modulo-n counters sized for the worst-case future mission requirements. The generalized line stripping board would accept a clock input from the central timing and control unit at a frequency high enough to be the least common denominator of all required future LCGS bit rates. The mission/instrument peculiar bit rate for a specific mission (e.g., EOS-A) could be accommodated by programming the length "n" of the modulo-n counter that divides down the input frequency to the desired bit rate via a logic card connector pin programming technique. Thus, the generalized logic card is specifically hardwired prior to launch for the specific mission.



Color and line sequential

where    n = number of colors of option  
           m = last color of option

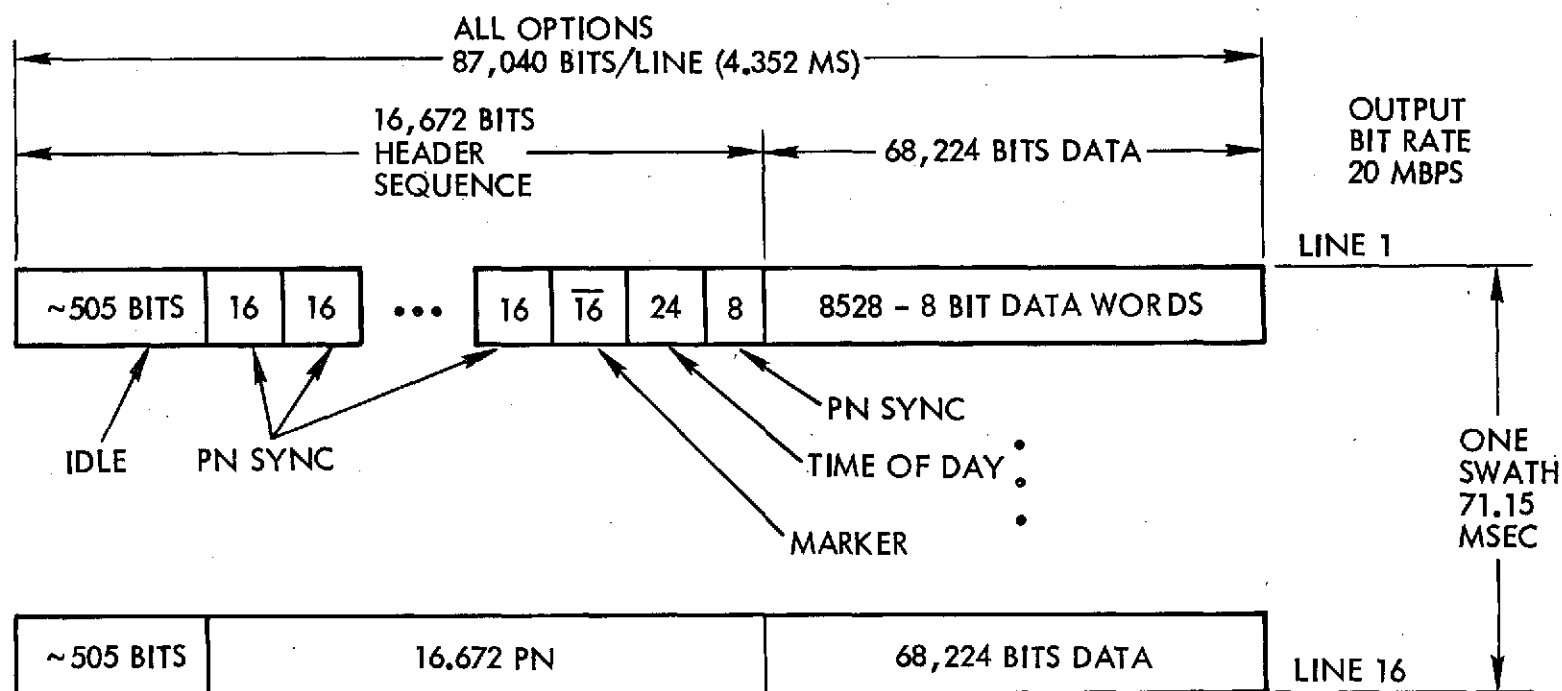
Figure 4-48. LCGS Speed Buffer Output (Edited and Formatted)

The other approach is to also build the generalized logic card as before, however, adding the feature of inflight software programmability via a computer word. The additional hardware required consists of a data register to hold the computer word that sets the length "n" of the modulo-n counter as above. In similar fashion the other parameters may also be determined via computer words. The hardware required to perform the line stripper function consists of TTL, MSI, and SSI logic with the exception of TTL Shottkey or ECL logic for the input frequency counter.

#### 4.6.4.2.2 Output Data Formatter

The selected thematic mapper input data, appropriately edited for the desired option (discussed in Section 4.6.4.1.2), is loaded into one of two alternating swath buffers in the required sequence for later unloading in the required format shown in Figure 4-49. The alternating buffer technique permits simultaneous loading of edited input data and unloading of formatted data for downlink transmission. The format sequencing is under firmware control. The firmware control function may be accomplished by two methods, specialized or generalized. The specialized method requires read only memories (ROM's) to store the addresses of the data located in the speed buffer random access memory (RAM). The RAM address of each data word requires a corresponding word in the ROM to access it. The size of the ROM is dictated by the number of data words to be addressed. The RAM stores two swaths of  $2^{20}$  bits each ( $\approx 10^6$  bits). Each word is  $2^3$  bits in length (8 bits), therefore the ROM size must be  $2^{20}/2^3 = 2^{17} \approx 131 \times 10^3$  bits. Both halves of the double swath speed buffer are identical thereby requiring only one ROM (for each color option) for both halves. The total RAM size is  $2 \times 2^{20} = 2^{21} \approx 2 \times 10^6$  bits. There are four color options, therefore four separate ROM's are required, each coded with the particular sequence of RAM addresses for each option.

The other method of accomplishing the format function is the generalized approach. The technique, usually referred to as indirect addressing, employs the computer memory. The (indirect) addresses of the data stored in the speed buffer RAM are stored in the computer memory (formerly ROM's). This method requires 8K of computer



$$\frac{400 \text{ WORDS}}{6 \text{ MINOR FRAME}} \times (36 + 500 + 2132) \frac{\text{MINOR FRAMES}}{\text{SCAN}} = 177872 \text{ WORDS/SCAN}$$

$$177,872 \frac{\text{WORDS}}{\text{SCAN}} \times 8 \frac{\text{BITS}}{\text{WORD}} \times 14.055 \frac{\text{SCAN}}{\text{SEC}} = 20 \text{ MBIT/SEC}$$

ALTERNATELY FOR A 6-BIT WORD

$$177,872 \frac{\text{WORDS}}{\text{SCAN}} \times 6 \frac{\text{BITS}}{\text{WORD}} \times 14.055 \frac{\text{SCAN}}{\text{SEC}} = 15 \text{ MBIT/SEC}$$

Figure 4-49. LCGS Format



memory for each option. To store all four options requires 32K of computer memory (16-bit computer words). The LCGS speed buffer would contain one 131 kbit RAM to store the indirect addresses of the 2 Mbit swath data, thus the four 131 kbit ROM's would be replaced by one 131 kbit RAM. The 131 kbit RAM (format memory) would store the indirect addresses for only one color option. To change color options would require a computer memory dump via direct memory access (DMA) of 8K words (131 kbits) to load the format memory in the speed buffer with the indirect addresses of the new color option. Requiring 32K of computer memory for LCGS alone appears to impose a severe requirement upon the computer system which would then double the size of the computer memory.

A more realistic approach would be to load the indirect address format RAM in the LCGS speed buffer via ground command. An entire load sequence would require 200 seconds of 40 uplink commands per second of 16-bit data words per command.

The hardware required for the firmware method (ROMs) is  $2^{17}$  bits /  $10 \times 2^{10}$  bits per package (bipolar 10K bit ROM's) = 12.8 packages per color option. The ROM's are organized 1024 x 10 and since 17 bit words are required in parallel for each indirect address, 16 packages are required (8 pairs) to obtain the required 131 kbits. The software method (RAM's) requires  $2^{17}$  bits /  $2^{12}$  bits per package =  $2^5 = 32$  packages. The NMOS 4K RAMs are organized 4096 x 1 therefore  $17 \times 2 \times 2^{12} = 139$  kbits are obtained with 34 packages. In summary, the firmware (ROM) approach requires  $16 \times 4 = 64$  packages for four options versus 34 packages of RAM's for the software approach. The firmware approach costs more in parts and power with no flexibility, while the software approach has less parts and power with complete programmable flexibility for any option, including those developed after launch.

#### 4.6.4.2.3 Key Features LCGS Speed Buffer, Editor and Formatter

- Buffers two thematic mapper swaths ( $2 \times 10^6$  bits)
- Alternating buffer technique – simultaneous load and unload
- Flexible data editing functions via command

- High speed data rate buffering function
  - Edits from 120 Mbit/sec input data stream
  - Outputs a 20 Mbit/sec data stream
- Flexible data reformatter (via command)
  - Inputs color-pixel sequential formatted data
  - Outputs color-line sequential formatted data
  - Performs data format transformation required by LCGS
  - Firmware controlled format (RAM loaded from computer)
- State-of-the-art technology
  - NMOS 4K bit RAM LSI components

Table 4-34 shows the semiconductor features traded off to select the baseline memory technology.

#### 4.6.4.3 Conclusions

Although designed to accommodate only the four major options available to the LCGS, the line stripper can be programmed to strip a combination of two or more options of data from the data stream, i.e., four bands, 1/2 swath. For a choice of this nature, the high-speed buffer cannot accommodate the total amount of data stripped from the data stream. However, the use of ROMs for high-speed buffer addressing allows complete flexibility in ordering the data for transmission to the LCGS. This flexibility is useful for some future special-purpose option.

Synchronization code is transmitted between each swath of data. This sync code constitutes the header of a swath. The header length (the number of sync sequences transmitted) can be altered by the modification of a counter or a ROM. A programmable sync counter can be incorporated into the design, giving a dynamic flexibility, useful in case of a change in data rate.

An alternate method of configuring option 4 — reduced resolution, full swath — is presented in Attachment A.

Table 4-34. Semiconductor Memory Features

Memory Technology	Access Time (ns)	Cycle Time (ns)	Power $\mu$ w/bit		Total Power (watts)/ 2 x 10 <sup>6</sup> bits		Bits/ Package	Estimated Size/Wt		Cost/Bit	Memory Organization	Availability (year)	Comments
			Active	Standby	Active	Standby		Size (in <sup>3</sup> )	Weight (lbs)				
Bipolar	60	90	500	500	1K	1K	1K	2200	20	-	1024 x 1	Now	Parts and power too high
PMOS	300	600	440	58	196	116	1K	2200	20	50¢	1024 x 1	Now	Too slow, parts and power too high
NMOS	200	400	88	1	22.6	2.0	4K	1100	10	12.5¢	4096 x 1	1975	Baseline (best trade-off)
CMOS	600	600	30	0.0003	0.8	0.6	1K	2200	20	10¢	1024 x 1	Now	Too slow, parts too high
CGD	-	50	-	0.1	0.2	-	32K	-	-	-	32K x 1	1976	Shift register configuration only (not applicable)
SOS C-MOS	100	100	30	0.0003	0.8	0.6	4K	900	20	-	4096 x 1	1977	Best choice when available

## ATTACHMENT A.

### PREPROCESSOR

In the thematic mapper, the sensor output voltage for each of 100 channels varies with time as well as illumination. This sensor output voltage is corrected by calibrating the thematic mapper every designated time interval, say once per orbit. This calibration is accomplished by sensing a dark spot and noting the sensor (channel) output voltage. The output voltage is subtracted from each subsequent data reading to compensate for dark current. Also, various known illuminations are tested during calibration and the corresponding output voltages are sensed. For each of the 100 sensors, this set of points at various illumination levels constitutes a curve (Figure A-1) which must be fitted to obtain an accurate correction during data transmission.

The present method of correction involves using a DC restoration circuit (Figure A-2) on each of the 100 sensor lines in the thematic mapper. With this restoration circuit, a gain mode command is required to set a variable gain control to restore the channel. This gain mode command is either computer generated and entered via the data bus, or received from the ground. An inherent assumption is that a linear correction is sufficient.

An alternative to this method of correction is a single digital preprocessor which performs a radiometric correction on each sense word prior to transmission. This preprocessor would receive data from the A/D converter and form radiometric correction prior to passing the data to the QPSK modulator. Since this device performs the correction serially, only one such item need be constructed.

With little additional hardware, further processing is possible for use in transmission to the LCGS. One of the options is 7 bands, reduced resolution. Here, rather than transmit 1 pixel for each 9 pixels, an average of the 9 pixels can be taken with some additional high-speed memory.

On additional option is now possible: linear transformations of the form  $d + \sum a_i p_i = c$ , where  $a_i$  are coefficients,  $p_i$  are sense words,  $d$  is

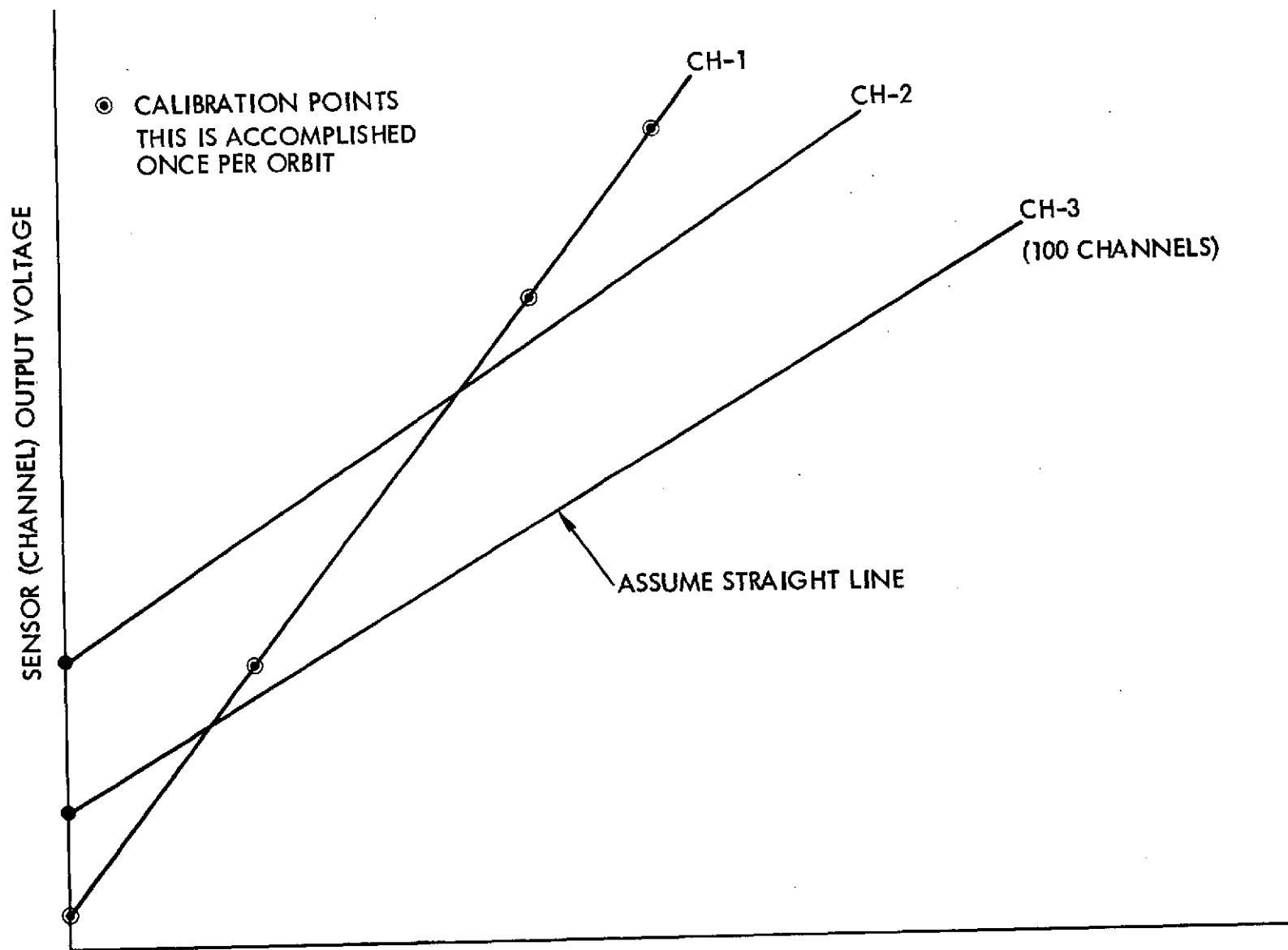


Figure A-1. Sensor Illumination

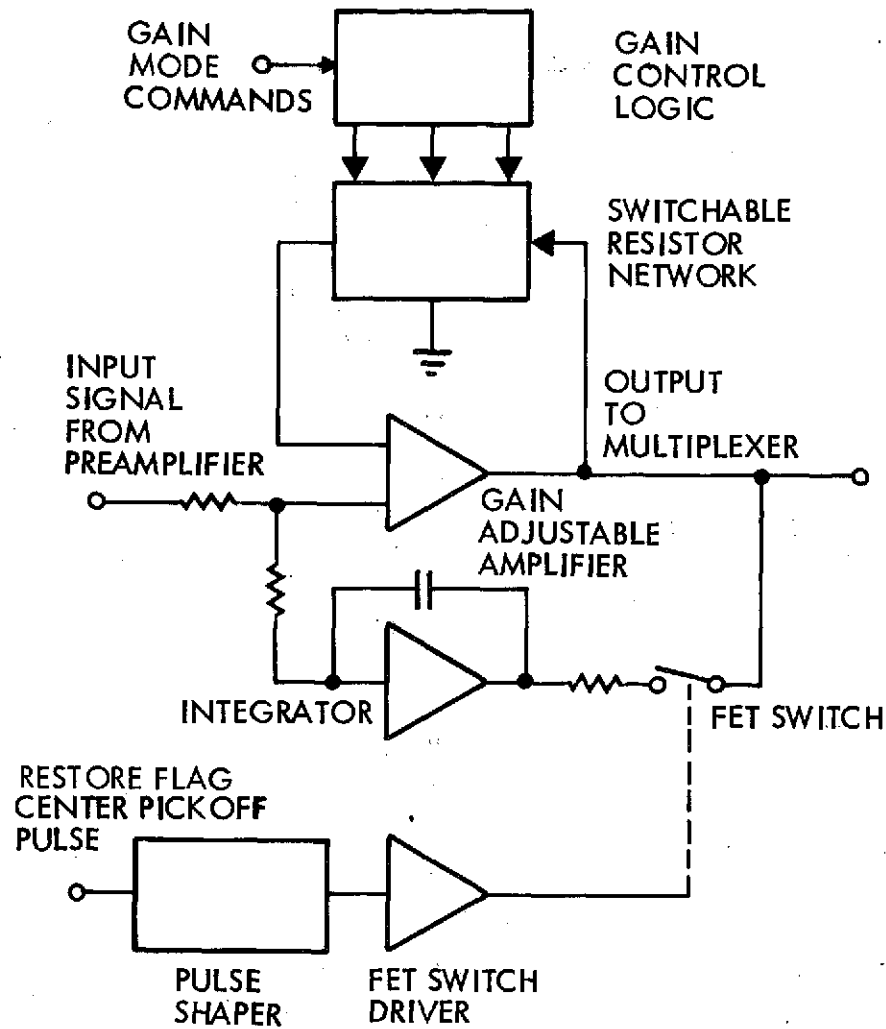


Figure A-2. DC Restored Channel Amplifier

a displacement, and  $c$  is transmitted. The sense words (pixel words) can be of various bands spread over three minor frames.

The radiometric correction can be performed in conjunction with each of these other options.

Figure A-3 is a block diagram of the preprocessor. Figures A-4 and A-5 are algorithms for radiometric correction and linear transformations, respectively. Table A-1 depicts the required computation on each 3 frames,  $\ell$ ,  $\ell + 1$ ,  $\ell + 2$ , for  $\ell = 1, 4, 7, 10, \dots$ , for option 4.

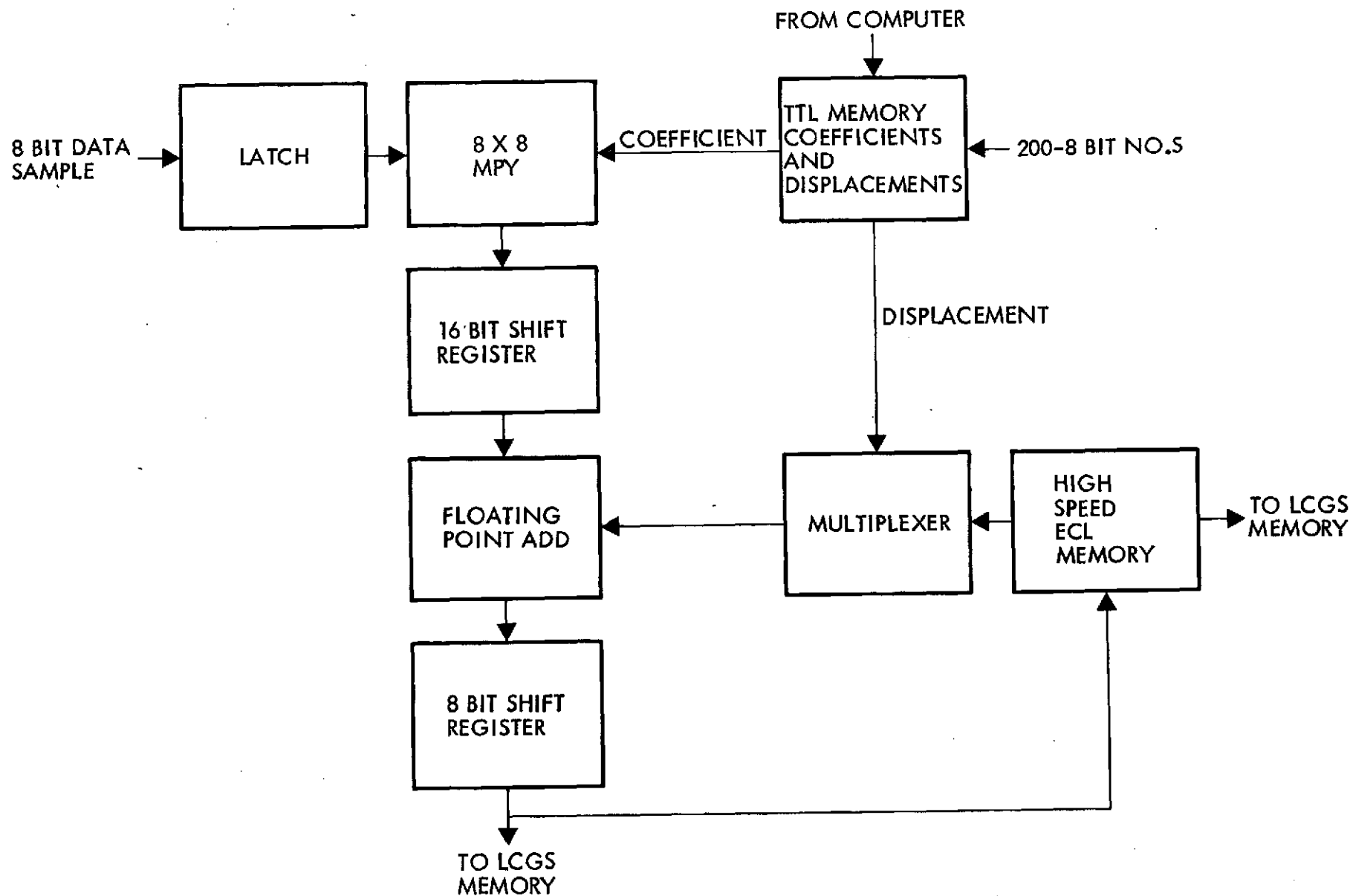


Figure A-3. Preprocessor Block Diagram

## 1. RADIOMETRIC CORRECTION

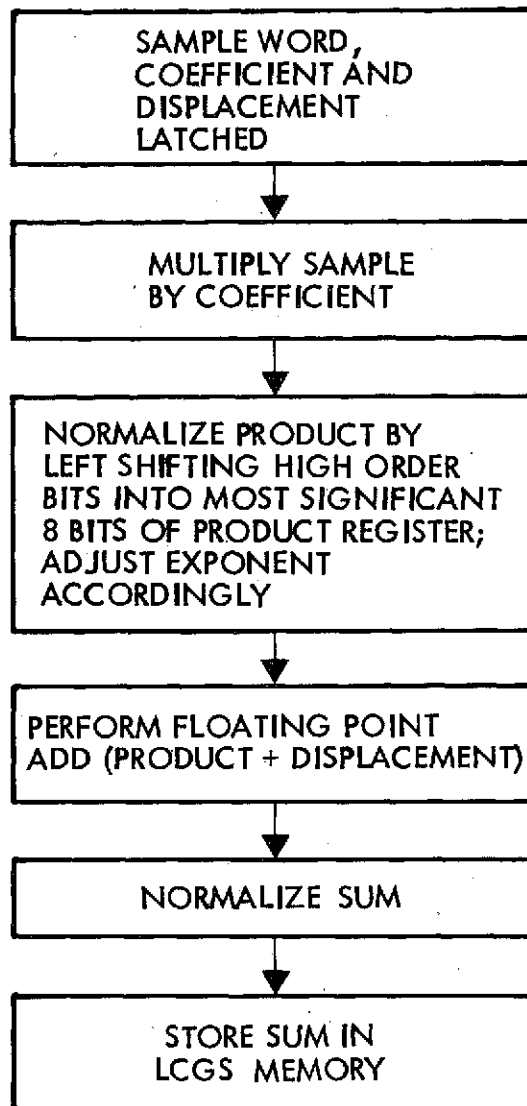


Figure A-4. Algorithms for Radiometric Correction



## 2. LINEAR TRANSFORMATION OF THE TYPE

$$d + \sum_{i=1}^7 a_i b_i = C, \text{ WHERE } C \text{ IS TRANSMITTED,}$$

$\{a_i\}$  ARE COEFFICIENTS AND  $\{b_i\}$  ARE SENSE WORDS

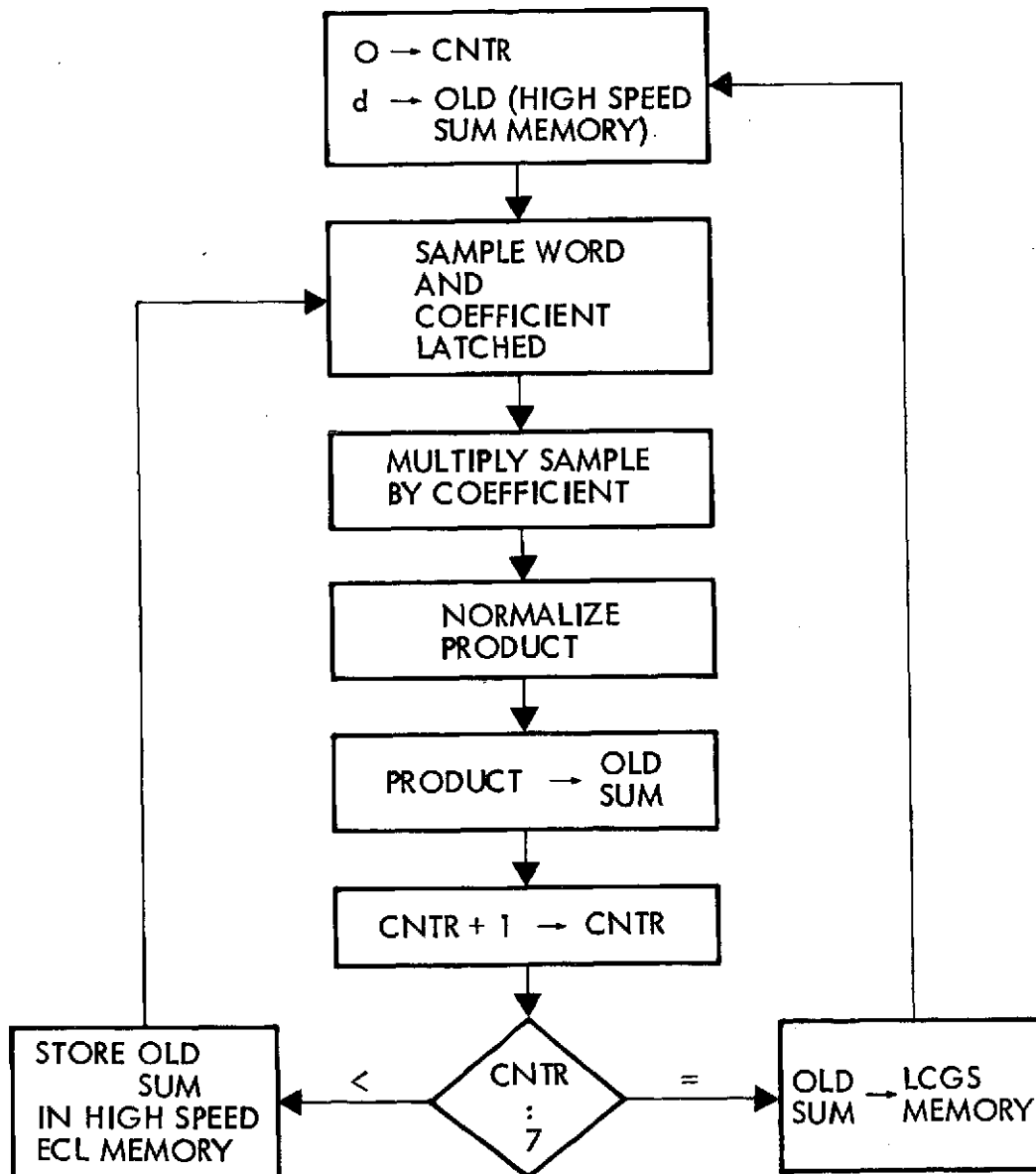


Figure A-5. Algorithms for Linear Transformations

Table A-1. Required Computation for Option 4

$$A \quad \frac{1}{9} \left\{ \sum_{i=\ell}^{\ell+3} \sum_{j=1}^3 [i, j, k] \right\}_{k=1, \dots, 6}$$

then

$$B \quad \frac{1}{9} \left\{ \sum_{i=\ell}^{\ell+3} \sum_{j=4}^6 [i, j, k] \right\}_{k=1, \dots, 6}$$

⋮

$$E \quad \frac{1}{9} \left\{ \sum_{i=\ell}^{\ell+3} \sum_{j=13}^{15} [i, j, k] \right\}_{k=1, \dots, 6}$$

also,

$$\frac{1}{9} \left\{ \sum_{i=\ell}^{\ell+3} \sum_{j=4, 4}^{12} [i, j, 7] \right\}$$

[frame, pixel, band]

#### 4.6.5 Wideband Communications System

##### 4.6.5.1 System Requirements

The wideband communications system (WBCS) is the major component of the wideband communications system. This system functions to modulate, amplify, and transmit the data received from the LCGS speed buffer and the HRPI and TM multiplexers. Two X-band links relay the sensor data to NASA STDN stations and to any selected one of a set of low-cost ground stations (LCGS). The band allotted to these links is 8.025 to 8.400 GHz (total 395 MHz bandwidth). For full-earth coverage the WBCS would require either a Ku-band relay link to TDRSS or a wideband video tape recorder for playback of data collected in remote areas.

The data rates of the TM processor and the HRPI multiplexer are 120 Mbits/sec. The LCGS speed buffer selects a subset of TM data which is fed into the LCGS modulator at 20 Mbits/sec. The combined TM and HRPI multiplexer outputs (each at 120 Mbits/sec) are converted to quadriphase modulation at 240 Mbits/sec. Minimum shift keying (MSK) was considered as an alternative for this channel but was not significantly better than QPSK. Binary PSK (BPSK) is preferred over FSK because power flux density (PFD) limits for the LCGS channel at 20 Mbits/sec. The modulation tradeoffs are discussed in Section 4.6.5.2.

A simplified block diagram of the EOS wideband communications module is shown in Figure 4-50. For reliable systems operation each power amplifier and each X-band antenna (high-rate and medium-rate) are able to support either channel by commandable RF transfer switches positioned between these units. This requires identical power amplifiers and antennas. The alternative to identical power amplifiers would be commandable power outputs, e.g., commandable drive levels, or commandable switching of the final stage in a two-stage power amplifier. Both alternative implementations are undesirable in terms of power efficiency and reliability.

With identical EIRP's the limiting output power level becomes that of the 20 Mbit/sec channel, as shown in Section 4.6.5.3. Since large ground station antennas (about 30-foot diameter) are available for the 240 Mbit/sec channel the reduction of EIRP to satisfy the PFD limit is offset by ground antenna gain and ground station system temperature. Thus, identical channel design can be achieved which satisfies the PFD limits and still has adequate link margin in each channel as shown in Section 4.6.5.4.

The allotted bandwidth at X-band is 375 MHz. MSK (minimum-shift-keying) modulation was considered for the 240 Mbit/sec data as a means of conserving bandwidth. It was found, however, that MSK does not have a substantial advantage in this regard over QPSK. The bandwidth required for QPSK has been a matter of much discussion in the literature (see Section 4.6.5.2). However, a bandwidth equal to the bit rate, i.e., 240 MHz, appears adequate, with only about 1 dB overall degradation due to bandwidth limiting effects. Therefore, the 375 MHz allotted channel appears adequate for the X-band communications.

Future missions which significantly affect the wideband communications link include the EOS-A'. The projected data rate for this mission

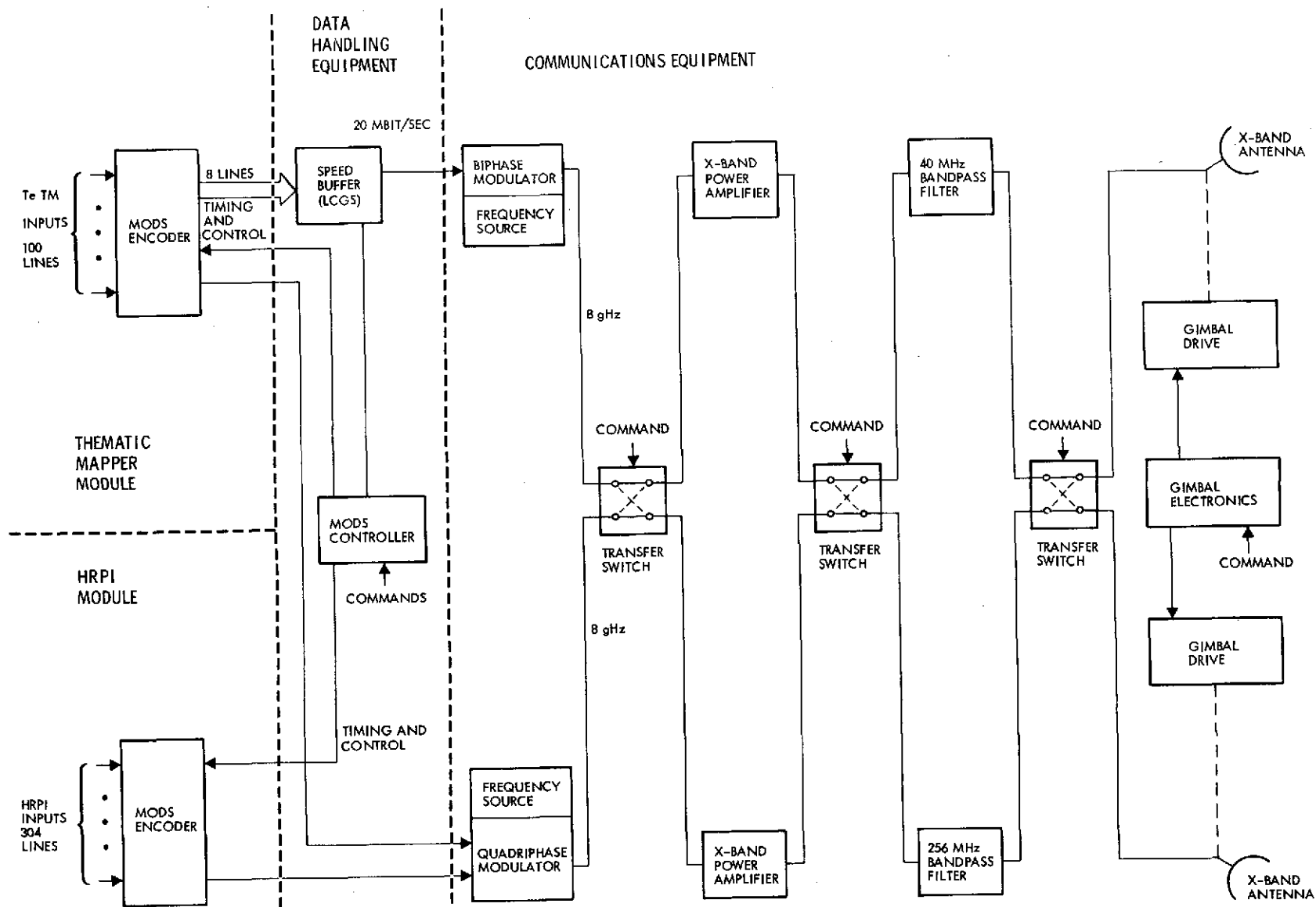


Figure 4-50. EOS-A Wideband Communications and Data Handling Module Block Diagram

is about 650 Mbit/sec. Assuming no increase in the allotted 375 MHz bandwidth at X-band a possible approach is to expand the current quadriphase modulation to octaphase modulation at about twice the information bit rate of EOS-A. The primary limitation would be the PFD limit on radiation impinging on the earth. The high-rate channel EIRP can be increased somewhat as noted above, without violating PFD limits, provided non-identical channel design is acceptable.

#### 4.6.5.2 Selection of Modulation Formats

Because of the limited spectral bandwidth available for high-rate data links from spacecraft to ground, the spectral occupancy of the modulation formats should be within prescribed limits. Four modulation formats were considered for the EOS wideband communication link: FSK (frequency-shift keying), MSK (minimum-shift keying), PSK (phase-shift keying), and QPSK (quadraphase shift keying).

##### 4.6.5.2.1 FSK

FSK with discontinuous phase is generated by switching between two oscillators at the "mark" and "space" frequencies  $f_1$  and  $f_2$ . Detection may be accomplished noncoherently with mark and space filters, or coherently with phase-locked loops (PLL's) tracking the discrete spectral components at  $f_1$  and  $f_2$ .

The spectral occupancy of discontinuous FSK is a function of the modulation index  $h$ , defined as

$$h = (f_2 - f_1)T$$

where

$f_1$  = mark frequency

$f_2$  = space frequency

$1/T$  = bit rate

The modulation spectral density consists of  $\sin^2 x/x^2$  functions centered at  $f_1$  and  $f_2$  containing  $1/2$  the total power, plus two discrete components containing the remaining power. Therefore, the spectral occupancy for reasonable values of  $h$  (say  $h = 1$ ) is much greater than comparable PSK

or QPSK systems. Because of the large required bandwidth FSK modulation can be eliminated from consideration.

#### 4.6.5.2.2 Continuous-Phase FSK

Some bandwidth reduction is obtained if the phase transitions are continuous from bit to bit. The continuous-phase FSK signal is:

$$s(t) = \sin \left[ 2\pi \frac{(f_1 + f_2)}{2} t + \phi(0) + \phi(t) \right]$$

where

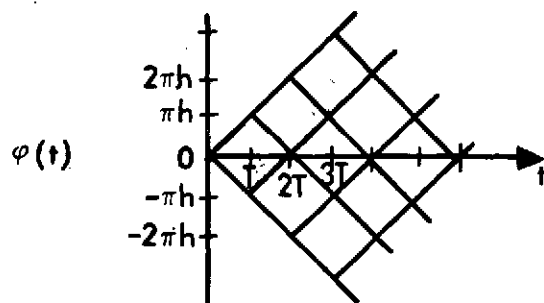
$\phi(0)$  = initial random phase

$$\phi(t) = \left( \sum_{i=1}^n a_i \pi h \right) + a_{n+1} \pi (f_2 - f_1)(t - nT),$$

$$nT \leq t < (n+1)T$$

$$a_i = \pm 1$$

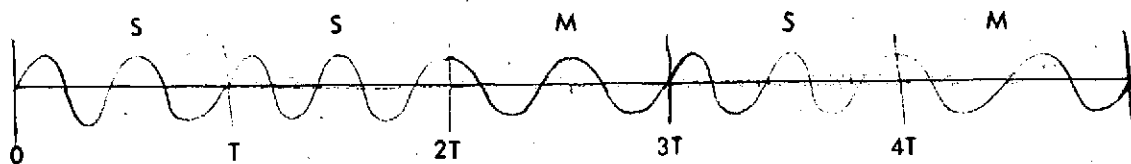
The phase function  $\phi(t)$  follows the continuously branching path sketched below, increasing by  $\pm \pi h$  during each bit interval



Allowed Paths of the Phase for Continuous Phase PSK

The value  $h = 1$  for continuous phase FSK was proposed by Sunde<sup>(1)</sup>. However, this modulation is inefficient because it contains discrete components at  $f_1$  and  $f_2$ .

Another special case of continuous-phase FSK is the so-called minimum shift keying. MSK modulation is a continuous-phase FSK with  $h = 1/2$ , so that a phase difference of  $\pi/2 - (-\pi/2) = \pi$  separates the mark and space frequencies. Hence a "space" (at frequency  $f_2$ ) is exactly  $1/2$  cycle longer than a "mark" (at frequency  $f_1$ ). A typical MSK waveform is sketched below (notice that  $f_1$  and  $f_2$  need not be half integer multiplies of the bit rate  $1/T$  although this may be a convenient implementation). The optimal detector for MSK consists of in-phase and quadrature channels at baseband. These each perform an integrate-and-dump operation on interleaved pairs of bits rather than on a single bit, since bit phases are interrelated by the continuous phase restricted modulation<sup>(2)</sup>.



Typical MSK Waveform

#### 4.6.5.2.3 PSK

The binary PSK modulation signal is

$$s(t) = a_i \sin \left[ \omega_c t + \phi(0) \right]$$

<sup>(1)</sup> E. D. Sunde, "Ideal Binary Pulse Transmission by AM and FM", Bell Syst. Tech. J., Vol. 38, pp 1357-1426, Nov. 1959.

<sup>(2)</sup> Rudi BeBuda, "Coherent Demodulation of FSK with Low Deviation Ratio", IEEE Trans. on Comm., pp 429-435, June 1972.



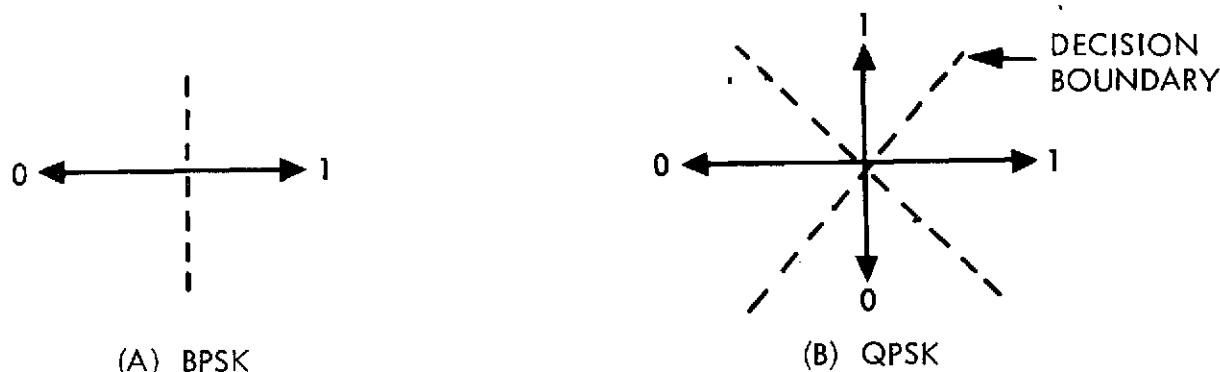
where

$$a_i = \pm 1$$

$$\omega_c = 2\pi f_c = \text{carrier frequency}$$

$$\phi(0) = \text{initial random phase}$$

Since this coding is antipodal, it uses both power and bandwidth very efficiently. The bit rate of PSK can be doubled in the same bandwidth by transmitting two 90 degree shifted biphasic carriers at a symbol rate equal to 1/2 the bit rate. The signal vectors for BPSK and QPSK are shown below. The QPSK spectrum is a  $\sin^2 x/x^2$  function with the frequency between the first nulls equal to the bit rate or twice the symbol or baud rate.



BPSK and QPSK Decision Regions

#### 4.6.5.2.4 Comparison of Formats

The spectral density of MSK, PSK, and QPSK is shown in Figure 4-51. For the MSK spectral density the bandwidth between first nulls is 1.5 times the bit rate. This bandwidth is exactly intermediate between the nulls of the BPSK and QPSK modulations.

The power excluded by an ideal rectangular filter should be as small as possible. The signal normally passes through a link whose overall bandwidth is about equal to the bit rate. The amount of power lost by bandpass filtering gives a lower bound to the link degradation (intersymbol interference and adjacent channel interference may also contribute degradation). The power loss for MSK, BPSK and QPSK is shown in Figure 4-52.

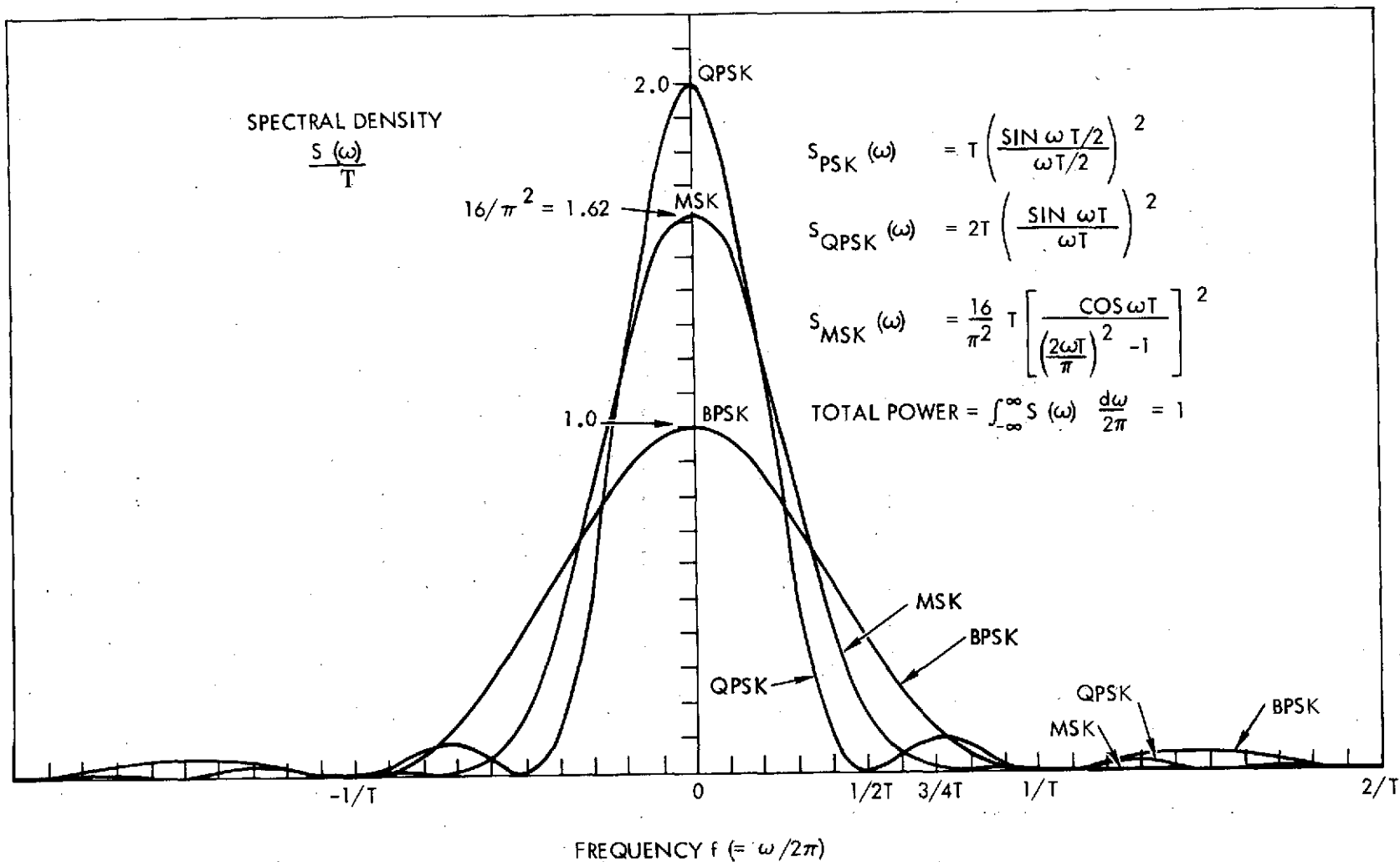


Figure 4-51. Spectral Density Functions

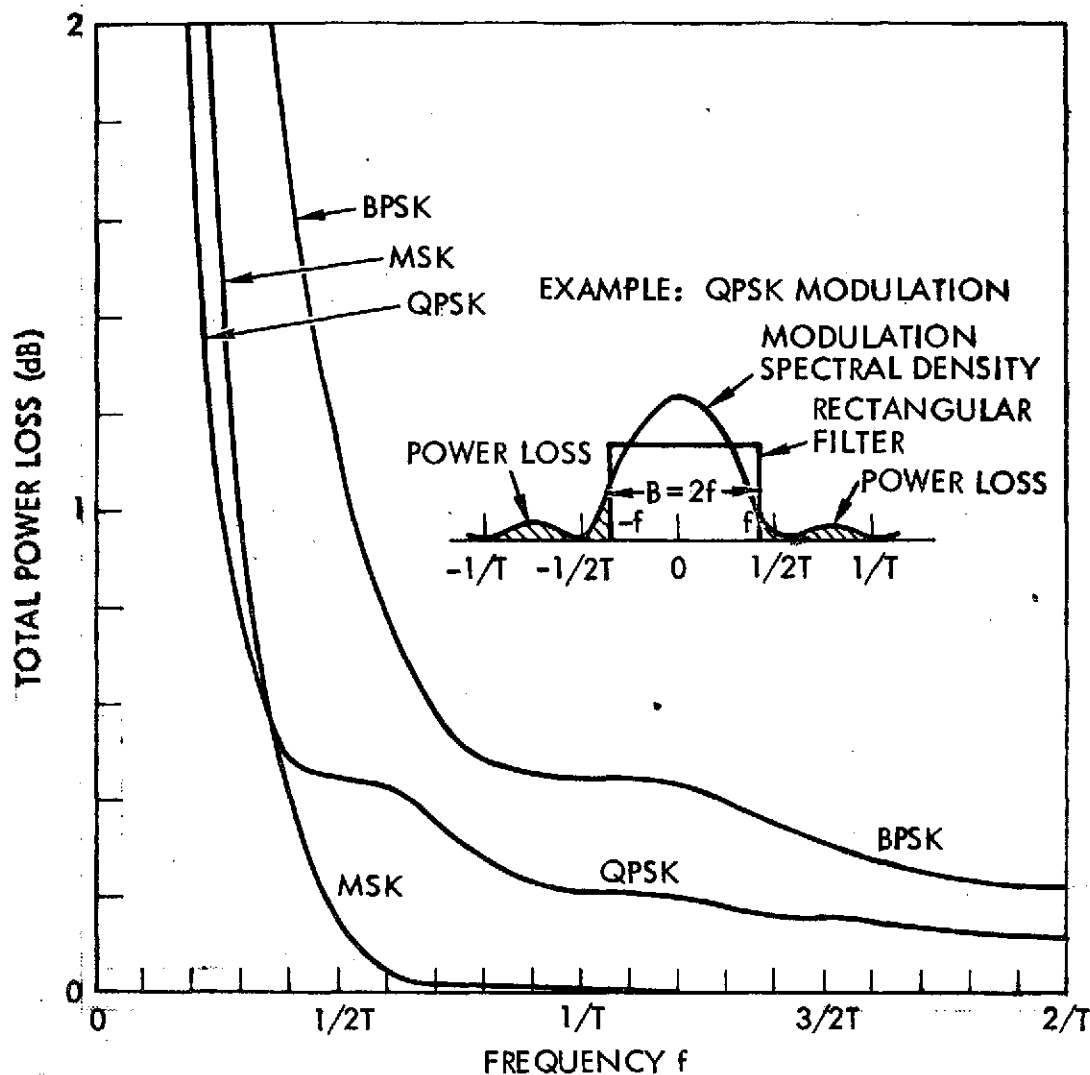
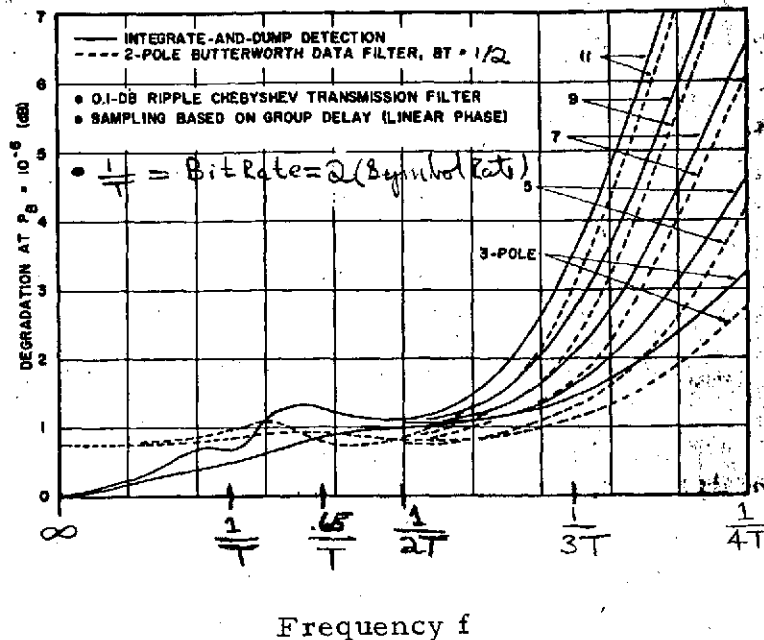


Figure 4-52. Power Loss Curves

For example, consider a filter with bandwidth equal to the bit rate. The power loss for MSK is negligible, but about 0.44 dB for QPSK and about 1.1 dB for BPSK. Notice that the QPSK loss curve is almost flat at this point and down to a bandwidth of about 0.8 times the bit rate. The QPSK power loss even at this narrow bandwidth is less than 0.5 dB.

The total degradation in  $E_b/N_0$  ratio for QPSK at bit error rate  $10^{-6}$  is shown in Figure 4-53.<sup>(3)</sup> A Chebyshev transmission filter with between 3 and 11 poles is assumed. This curve includes degradation due to power loss, degradation due to intersymbol interference, mismatched detection filter (integrate-and-dump is not necessarily optimum after filtering) and group delay of the signal.



(Transmission filter 3 dB RF bandwidth =  $2f$ )

Figure 4-53. Degradation due to Transmission Filtering Versus Filter Cut-off Frequency  $f$  for QPSK

For the bandwidth equal to the bit rate the degradation is about 1 dB for all the filters. This 1 dB includes the previously specified 0.44 dB due to power loss only, plus the additional degradation sources. Furthermore, the degradation is approximately 1 dB for all bandwidths between 0.9 and 1.4 times the bit rate. Hence, there is essentially no advantage in using a bandwidth of 1.3 times the bit rate rather than 1.0 times the bit rate.

#### 4.6.5.2.5 Selection of 240 Mbit/sec Modulation

As can be seen from Figure 4-53, the power loss for a bandwidth of  $1.3 \times$  the bit rate (332.8 MHz) is 0.38 dB for QPSK and 0.02 dB for MSK. Decreasing the bandwidth to 1.0 times the bit rate causes the power loss to increase to 0.44 dB and 0.04 dB for QPSK and MSK, respectively. Thus, MSK has a power advantage of about 0.3 to 0.4 dB over QPSK.

Filter distortion will cause additional degradation. Jones<sup>(3)</sup> has shown that for QPSK the total degradation due to symmetrical band-pass filtering (including power loss) is 1.0 dB for a bandwidth of two times the symbol rate ( $2 \times 120 \text{ Mbit/sec} \pm 240 \text{ MHz}$ ), and a bit error rate of  $10^{-6}$ . Increasing the bandwidth to 332.8 MHz does not improve performance at all for symmetrical filtering. However, Jones' analysis shows that degradation increases rapidly for bandwidth less than 2.0 times the symbol rate. For example, a bandwidth of 176.2 MHz (1.4 times symbol rate) causes a degradation of from 1.5 dB to almost 3 dB depending on the number of poles in the transmission filter.

Cuccia<sup>(4)</sup> indicates that the bandwidth used for a QPSK system should be 1.3 times the bit rate in order "to avoid undue degradation due to group delay distortion". However, Jones' analysis indicates that a QPSK signal which has been bandlimited to 1.0 times the bit rate is not sensitive to parabolic or cubic phase distortion. Cuccia does not elaborate on what is meant by "undue degradation"; however, the extra degradation caused by decreasing the bandwidth from 1.3 to 1.0 times the bit rate is probably less than about 0.7 dB in a real system.

No similar literature on bandwidth limiting of MSK signals could be found. Degradation of MSK signals due to simple power loss will be less than QPSK degradation, as shown earlier; however intersymbol interference and filter distortion degradation of MSK signals may not be any less than for QPSK. Qualitative discussions in References 2 and 5 indicate that somewhere between 0.75 and 1.0 times the bit rate (a bandwidth of 180 to 240 MHz) is required to keep intersymbol interference effects minimal. The overall impression is that MSK performs better in a given bandwidth than QPSK.

---

(3) J. Jones, "Filter Distortion and Intercymbol Interference Effects on PSK Signals", IEEE Trans. on Comm., April 1971, pp 120-132.

(4) C. L. Cuccia, "Phase Shift Keying: The Optimum Modulation Technique for DIGICOM", Microwave Systems News, Jan., 1973.

(5) W. A. Sullivan, "High-Capacity Microwave System for Digital Data Transmission", IEEE Trans. on Comm., June 1972, pp 466-470.

#### 4.6.5.2.6 Selection of 20 Mbit/sec Modulation

In order to compare the various modulation systems BPSK will be used as a baseline and the maximum PFD for each system relative to BPSK will be calculated. There are three components of this power comparison and Table 4-35 summarizes the results.

- 1) Power loss relative to BPSK due to 40 MHz bandlimiting
- 2) Peak PSD of system relative to BPSK
- 3)  $E_b/N_o$  required for a bit error rate of  $10^{-5}$  relative to BPSK

Table 4-35. Comparison of Three Power Components

Modulation Scheme*	Relative Power Loss (dB)	Relative Peak PSD (dB)	Relative $E_b/N_o$ Required (dB)	Relative PFD (dB)
BPSK	0	0	0	0
QPSK	-0.13	+3.0	0	+2.87
MSK	-0.43	+2.1	0	+1.67
FSK (dis-continuous phase)	(Depends on carrier sep.)	+67.0 (spikes)**	+3.0	≈+74.00

\* Assumes NRZ coding of data stream.

\*\* Relative to BPSK at 20 Mbits/sec.

As can be seen, BPSK is better suited for the Mbit/sec stream than either MSK or QPSK. The only other candidate is FSK. However, FSK requires 3.8 dB more power to achieve a bit error rate of  $10^{-5}$  than any of the other systems. Thus its combined peak PSD and power loss must be at least 4 dB better than BPSK just to break even. The PSD of FSK depends on the frequency shift between the two carriers used in the modulator, and whether it is continuous or discontinuous in phase. Discontinuous phase FSK contains spikes in its PSD at the carrier frequencies which waste half the power of the FSK signal. Thus, FSK does not appear to be a viable alternative to BPSK.

#### 4.6.5.2.7 Conclusions

In view of the tradeoffs presented above there is no significant advantage in using MSK for the 256 Mbit/sec data. QPSK appears to be the best choice for this channel (QPSK modulators in the 200 Mbit/sec range have been built in the past). For the 20 Mbit/sec channel BPSK appears to be the best choice. The degradation due to transmission filter bandlimiting is about 1 dB, which is acceptable in this system, and the PFD requirements can be met (see Section 4.6.5.3). A simulation run with a TRW computer program<sup>(6)</sup> gave 1.3 dB degradation for a 256 MHz filter and 1.0 dB degradation for a 332.8 MHz filter in the QPSK channel. Thus, the 256 MHz transmission filter is an adequate choice for the high-rate channel.

For the medium-rate channel (20 Mbit/sec), Table 4-35 shows that FSK has a large PFD compared to the other formats. Since FSK has a relatively large bandwidth and power requirement also, the disadvantages of FSK appear to outweigh the advantages (mainly simplicity of implementation). The next simplest modulation is BPSK. Since BPSK has relatively narrow bandwidth (40 MHz) and low PFD (see Table 4-35), BPSK seems to be the best choice for the LCGS (20 Mbit/sec) channel.

#### 4.6.5.3 Power Flux Density (PFD)

In order to prevent radiation from the EOS satellite from interfering with terrestrial radio relay stations, PFD limits are imposed by U. S. government and by the CCIR. These limits are expressed as the maximum power flux density in watts/meter<sup>2</sup> measured in a 4 kHz band. Since radiation arriving at a low angle  $\theta$  above the horizon is more likely to interfere with a terrestrial horn antenna, the limits are low for small  $\theta$  but less restrictive at  $\theta = 90$  degrees. The power flux density limits are plotted versus elevation angle in Figure 4-54. These limits apply to the

---

<sup>(6)</sup> "Transponder Computer Simulation", TRW 73-7131.45-31, December 1973.

frequencies from 8.025 to 11.7 GHz in the case of the U. S. Government limits<sup>(7)</sup> and 1-10 GHz in the case of the CCIR limits<sup>(8)</sup>. Hence, they are applicable to the X-band communications link at 8.025 to 8.4 GHz.

The spectral densities  $S(\omega)$  for MSK, PSK, and QPSK are shown in Figure 4-51. These curves show that the maximum spectral density is  $S(0)$ .

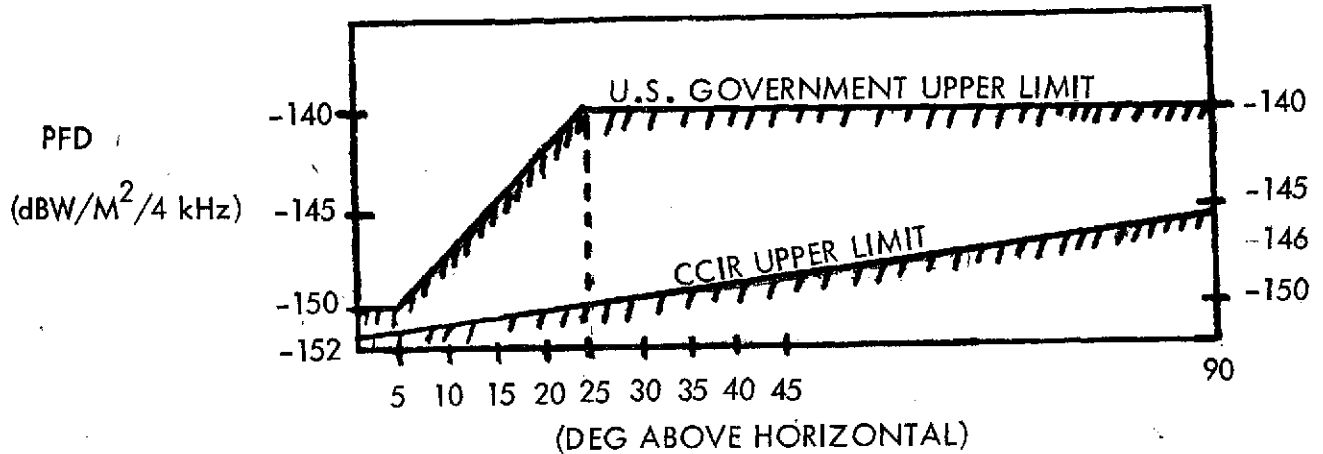


Figure 4-54. Power Flux Density Limitations

The relative values of  $S(0)$  for the three modulation formats are shown in the table below.

	<u>MSK</u>	<u>PSK</u>	<u>QPSK</u>
$S(0)$	$\frac{16/\pi^2}{\text{Bit Rate}}$	$\frac{1}{\text{Bit Rate}}$	$\frac{2}{\text{Bit Rate}}$

Notice that the spectral densities of QPSK and MSK are respectively 3 and 1.62 dB greater than BPSK at the same bit rate.

The PFD in watts/m<sup>2</sup> in a 4 kHz band is given by the following equation:

$$\text{PFD} = \frac{\text{EIRP}}{4\pi R^2} \times S(0) \times 4000$$

(7) "Radio Frequency Allocations for Space and Satellite Requirements", Goddard Space Flight Center, 15 June 1973.

(8) Recommendation 358-1, C. C. I. R. XII Planary Assembly, Vol. 4, p. 288, New Delhi, India, 1970.



where

EIRP = effective isotropically radiated power (watts)

R = satellite-to-ground range (meters)

S(0) = spectral maximum (see Table above)

The satellite-to-ground range is given by:

$$R = r_o \sqrt{\left(1 + \frac{A}{r_o}\right)^2 - \cos^2 \theta} - r_o \sin \theta$$

where

$r_o$  = radius of the earth (6,378.388 km)

A = satellite altitude

$\theta$  = angle above horizon

The term  $1/R^2$  which appears in the PFD equation is shown in Figure 4-55. Since PFD is directly proportional to  $1/R^2$ , the PFD upper limit is also shown in Figure 4-55. The PFD is greatest at  $\theta = 90$  degrees (satellite directly overhead). Notice that the shape of the curves shown in Figure 4-55 is such that if the PFD is less than the upper limit at  $\theta = 90$  degrees then it is also less than the upper limit at all other values of  $\theta$ .

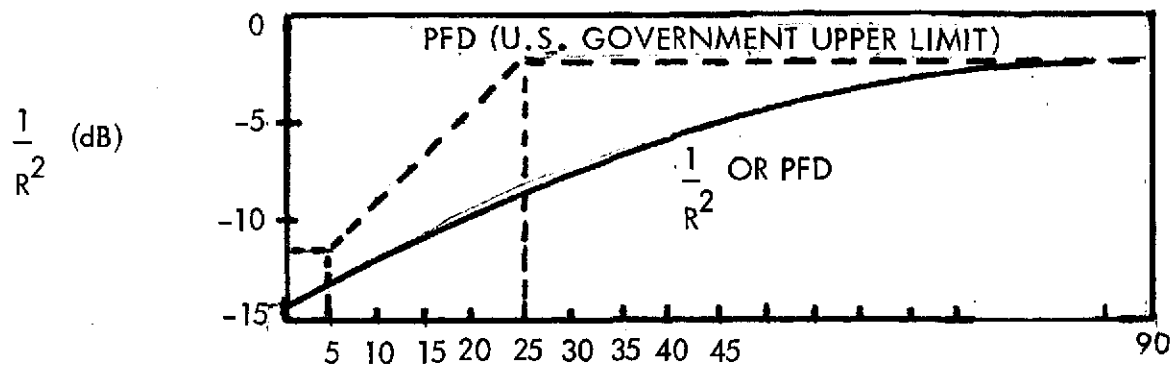


Figure 4-55.  $1/R^2$  Versus  $\theta$  for A = 715 km

The equations above for PFD and range allow the maximum allowable EIRP to be computed. The calculation is summarized in Table 4-36. The first entry is the maximum EIRP (dBW). Then the losses are entered

due to range  $(-10 \log 4\pi R^2)$  and to conversion of the spectrum to a 4 kHz band  $(10 \log S(0) + 10 \log 4000)$ . For example, for 240 Mbits/sec QPSK:

$$\begin{aligned} 10 \log S(0) + 10 \log 4000 &= 10 \log 2 - 10 \log 240 \text{ Mbit/sec} \\ &\quad + 10 \log 4000 \\ &= 3 - 84.1 + 36 \\ &= -45.1 \text{ dB} \end{aligned}$$

Thus the value -45.1 dB is entered under "Conversion to 4 kHz Band" in Table 4-36.

The EIRP minus the total loss gives the maximum PFD. The maximum PFD equals the upper limit (shown in Figure 4-54) when  $\theta = 90$  degrees. When  $\theta = 5$  degrees the maximum PFD is less than the upper limit. Notice that the "Maximum Allowable EIRP" shown in Table 4-36 is not the EIRP actually specified in the baseline design. Instead, it is the maximum value of EIRP that can be transmitted without violating the PFD upper limit at any elevation angle.

Thus, the maximum EIRP for domestic ground stations is 33.2 dBW and 25.1 dBW for the 240 and the 20 Mbit/sec channels, respectively. The international (CCIR) PFD limits are 6 dB low so that the maximum EIRP for international ground stations is 6 dB less than the figures given for domestic ground stations.

In case the same EIRP value is used for both channels, then the lower of the above two maximum values, viz. 25.1 dBW, is the maximum allowable EIRP. The design EIRP for both channels is 25.0 dBW.

#### 4.6.5.4 RF Link Analysis

##### 4.6.5.4.1 High-Rate X-Band Link (256 Mbit/sec)

As discussed in Section 4.6.5.3, the maximum EIRP at X-band which satisfies the U. S. government PFD limits is 25.0 dBW (PFD  $\leq -140$  dBW/ $\text{m}^2/4\text{kHz}$  at  $\theta \pm 90$  degrees).. Because of spectral spreading the 240 Mbit/sec EIRP could go about 8 dB higher than the 20 Mbit/sec channel without exceeding the PFD limit.

Table 4-36. PFD Calculation for the X-Band Downlinks  
(U. S. and International Limits)

Baseline Orbit = 715 km (386 nmi)

	$\theta = 90$ degrees R = 715 km (386 nmi)		$\theta = 5$ degrees R = 2597 km	
	240 Mbit/sec QPSK	20 Mbit/sec BPSK	240 Mbit/sec QPSK	20 Mbit/sec BPSK
<u>U. S. Limit</u>				
<u>Maximum Allowable EIRP</u> (U. S. limit)	33.2 dBw	25.1 dBw	33.2 dBw	25.1 dBw
<u>Losses</u>				
-10 log $4\pi R^2$	-128.1	-128.1	-139.3	-139.3
Conversion to 4kHz band	- 45.1	- 37.0	- 45.1	- 37.0
Total Loss	-173.2	-165.1	-184.4	-176.3
<u>PFD</u> (dBw/m <sup>2</sup> /4 kHz)	-140.0	-140.0	-151.2	-151.2
<u>U. S. Government Upper Limit</u>	-140.0	-140.0	-150.0	-150.0
Margin	0	0	+1.2 dB	+1.2 dB
<u>International Limit</u>				
<u>Maximum Allowable EIRP</u> (CCIR limit)	27.2 dBw	19.1 dBw	27.2 dBw	19.1 dBw
<u>PFD</u> (dBw/m <sup>2</sup> /4 kHz)	-146.0	-146.0	-145.2	-145.2
<u>CCIR Upper Limit</u>	-146.0	-146.0	-151.7	-151.7
Margin	0	0	+6.5 dB	+6.5 dB

In order to have switchable power amplifiers, the high-rate and medium-rate EIRPs should be identical (i. e., both should be 25 dBw). This simplifies the design as well as provides redundant reliability. The link analysis based on this design is summarized in Tables 4-37 and -38.

The transmitter TWT power amplifier output is assumed to be 0.5 watts. The transmitter losses of 2 dB include transfer switches, filters, circuit feedline, and antenna coupling losses. A 30 dB antenna gain is assumed. (The WBCS module includes two computer-pointed

Table 4-37. 256 X-Band Link Analysis (5 Degree Elevation)  
Altitude = 386 n mi = 715 km)

Spacecraft Transmitter Power (0.5 watt)	-3 dBw
Spacecraft Transmitter Losses	-2 dB
Spacecraft Antenna Gain (1.7 foot dish)	<u>30 dB</u>
EIRP	25 dBw
Space Loss (2597 km)	-178.8 dB
Atmospheric Loss	- 3 dB
STDN Receive Antenna Gain (Net) (30 foot dish)	<u>53.7 dB</u>
Received Signal Power	-103.1 dBw
Bit Rate (256 Mbit/sec)	- 84.1 dB-Hz
Received Energy per Bit ( $E_b$ )	-187.2 dBw/Hz
Receiver Noise Spectral Density ( $N_o$ )	206.2 dBw/Hz
$N_o = k T_{sys}$	
$T_{sys} = 166.5^\circ K$ (parametric amplifier)	
$E_b/N_o$	<u>19 dB</u>
$E_b/N_o$ required at $P(E) = 10^{-5}$	9.5 dB
Demodulator Losses	2.0 dB
Spectral Truncation Losses	<u>1.0 dB</u>
Margin	6.5 dB

Table 4-38. 20 Mbit/sec X-Band Link Analysis (5 Degree Elevation)  
(Altitude = 386 n mi = 715 km)

Spacecraft Transmitter Power (0.5 watt)	-3 dBw
Spacecraft Transmitter Losses	-2 dB
Spacecraft Antenna Gain (1.7 foot dish)	<u>30 dB</u>
EIRP	25 dBw
Space Loss (2597 km)	-178.8 dB
Atmospheric Loss	- 3 dB
LCGS Receive Antenna Gain (Net)	<u>43.7 dB</u>
Received Signal Power	-113.1 dBw
Bit Rate (20 Mbit/sec)	- 73 dB-Hz
Received Energy per Bit ( $E_b$ )	-186.1 dBw/Hz
Receiver Noise Spectral Density ( $N_o$ )	-205.2 dBw/Hz
$N_o = k T_{sys}, T_{sys} = 184^\circ K$	
$E_b/N_o$	<u>19.1 dB</u>
$E_b/N_o$ required at $P(E) = 10^{-5}$	9.5 dB
Demodulator Losses	-2.0 dB
Spectral Truncation Losses	<u>-1.0 dB</u>
Margin	6.6 dB

1.7 foot dishes with 30 dB gain and 3 dB beamwidth of 5.2 degrees). This gives the required 25 dBW for EIRP.

The path loss is computed for 5 degrees above horizontal elevation. The atmospheric losses of 3 dB include attenuation due to oxygen and water-vapor absorption, rain and clouds, for the atmospheric path at  $0 \pm 5$  degrees.

The ground station antenna gain including pointing losses and polarization losses is 53.7 dB for the addition of X-band feeds to existing 30 foot S-band dishes. The receiver system temperature is assumed to be 166.5°K.

Truncation due to the transmitter filter gives about 1 dB degradation (as shown in Section 4.6.5.2) and demodulator-bit synchronizer degradation is about 2 dB. Thus, the required energy to noise ratio  $E_b/N_o$  including these losses is 12.5 dB for QPSK at  $10^{-5}$  error probability. Since the received energy to noise ratio is 19 dB, the system margin is +6.5 dB. For the zenith path ( $\theta = 90$  degrees, range = 715 km) the system margin is  $6.5 + 11.2 = 17.7$  dB.

#### 4.6.5.4.2 Medium-Rate X-Band Link (20 Mbit/sec)

A principal requirement here is to keep the LCGS as simple and economical as possible. Biphase PSK modulation was chosen as adequate for this reason instead of QPSK. The transmitter filter bandwidth of 40 MHz degrades the signal only about 1 dB, as shown in Section 4.6.5.2.

The LCGS antenna pointing system uses computer-pointing rather than auto-tracking. For the X-band system, antennas up to about 8 feet in diameter can easily be program-pointed. The gain of this antenna is about 43 dB. In order to achieve adequate  $E_b/N_o$  level a parametric amplifier preamp was selected for the LCGS instead of a TDA. The paramp is available with a noise figure of about 1.5 to 4 dB whereas a TDA typically has noise figure of about 5 dB.

The system temperature of the receiver is given by

$$T_{\text{sys}} = T_a + (NF - 1)T_{\text{REF}}$$

where

$T_a$  = antenna temperature

NF = noise figure

$T_{REF} = 290^{\circ}\text{K}$  = reference temperature.

This equation assumes no losses, i. e.,  $L = 1$ . The antenna temperature is assumed to be about  $65^{\circ}\text{K}$  in the worst case when earth noise enters the antenna at lower elevations. For a 1.5 dB noise figure the system temperature is  $T_{sys} = 184^{\circ}\text{K}$ . With this system temperature the system margin on the 20 Mbit/sec link is 6.6 dB at  $\theta = 5$  degrees and  $6.6 + 11.2 = 17.8$  dB at zenith.

#### 4.6.5.4.3 Transmitter Filter Calculations

Two transmitter filters are required: a 40 MHz filter for the low-rate biphase data, and a 240 MHz filter for the high-rate quadriphase data. Since the total bandwidth is 375 MHz for the WBCS, the available guard band is  $275 - 40 - 256 = 79$  MHz. Guard bands of proportionate widths  $(1/8) \times 40$  and  $(1/8) \times 240$ , were allotted to the outer edge of the 40 and 240 MHz filters, respectively. Thus, equal guard bands of 30 MHz are obtained on either side of the 240 MHz filter. The resulting center frequencies are  $f_1 = 8.050$  GHz (40 MHz filter) and  $f_2 = 8.235$  Hz (240 MHz filter) which implies the modulation spectral densities, as shown in Figure 4-56.

Consider the 40 MHz filter rejection requirements. The spectral density of the biphase 20 Mbit/sec data is

$$S(\omega) = P_1 T_1 \left( \frac{\sin \omega T_1 / 2}{\omega T_1 / 2} \right)$$

where

$P_1$  = received power from 20 Mbit/sec data

$T_1 = 1/20$  MHz

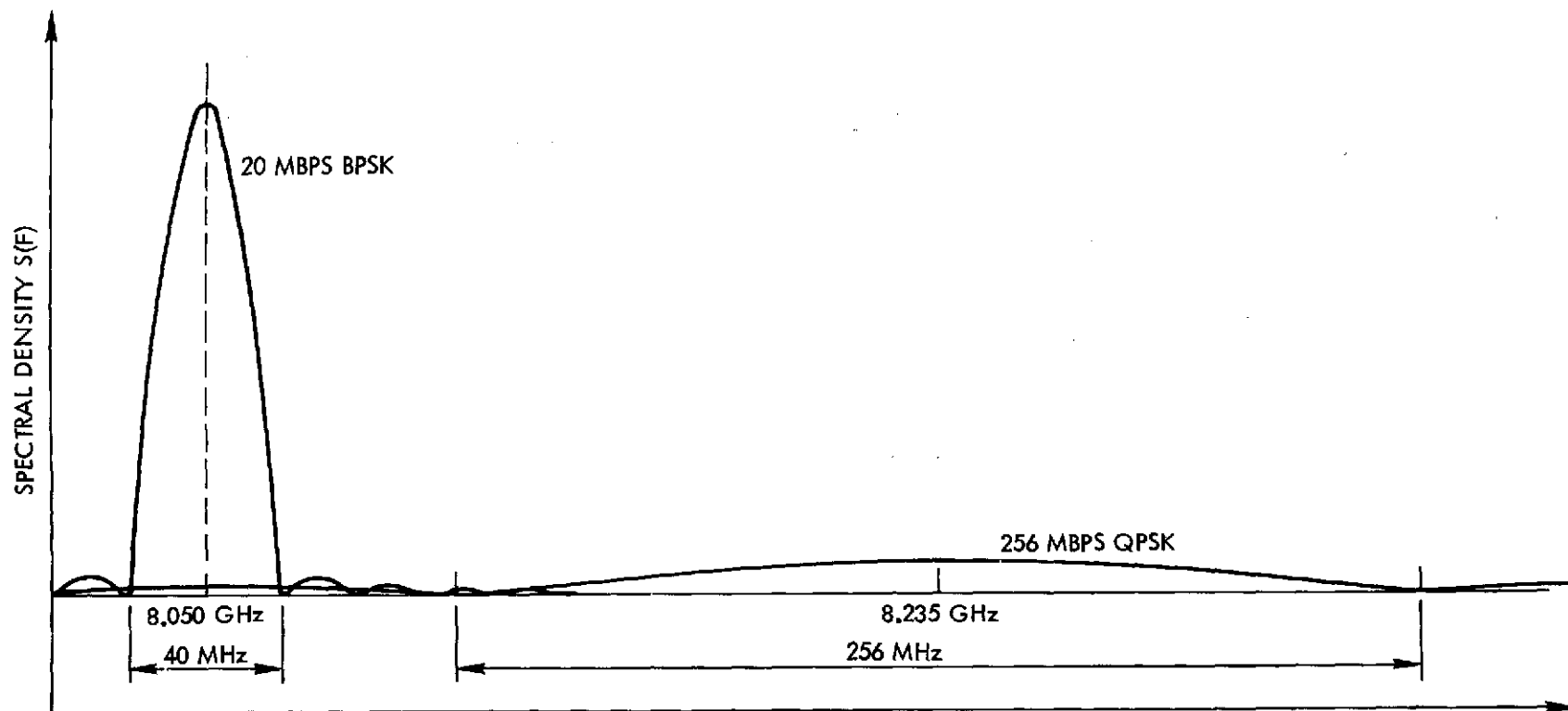


Figure 4-56. Modulation Spectral Densities (WBCS)

The interference power received in the 240 Mbit/sec channel is

$$P_1 = \text{EIRP}_1 - \text{Losses}_2$$

where

$\text{EIRP}_1$  = EIRP of 20 Mbit/sec channel

$\text{Losses}_2$  = total net losses of 256 Mbit/sec channel (including antenna gain)

Thus, for  $\theta = 5$  degree and  $\theta = 90$  degree elevations (see Tables 4-37 and -38)

$$P_1 = \begin{array}{ll} 25 \text{ dBW} - 128.1 \text{ dB} = -103.1 \text{ dBW} & (5 \text{ degrees}) \\ 25 \text{ dBW} - 116.9 \text{ dB} = -91.9 \text{ dBW} & (90 \text{ degrees}) \end{array}$$

Since the 240 Mbit/sec spectrum reaches the band edge (BE) of the 240 MHz filter at about the second sidelobe ( $\omega T_1 = 5\pi$ ) of the  $\sin^2 x/x^2$  function, the BE interference is

$$\begin{aligned} S(\omega)_{\text{BE}} & \leq P_1 T_1 \frac{1}{(5\pi/2)^2} \\ & \leq -103.1 \text{ dBW} - 73 \text{ dB-Hz} - 17.9 \text{ dB} = -194.0 \text{ dBw/Hz} \quad (5 \text{ deg}) \\ & \quad - 91.9 \text{ dBW} - 73 \text{ dB-Hz} - 17.9 \text{ dB} = -182.8 \text{ dBw/Hz} \quad (90 \text{ deg}) \end{aligned}$$

The noise level in the 256 MHz channel is  $N_0 = -206.2 \text{ dBw/Hz}$ .

Therefore, the 40 MHz filter rejection should be  $-182.8 - (-206.2) = 23.4 \text{ dB}$  so that the interference at band edge is equal to the noise level at zenith (90 degrees), and 11.2 dB less at  $\theta = 5$  degrees. Therefore the co-channel interference does not degrade the signal. Notice that interference at band edge was calculated and thus interference at band center will be much smaller than the noise level.



A similar calculation for the interference by the 240 Mbit/sec channel into the 20 Mbit/sec channel was carried out. For the interference level to be equal to the band edge noise level the filter rejection requirement is set at 5.7 dB. The filter rejection calculations are summarized in Table 4-39 and the resulting filter requirements are given in Table 4-40.

Table 4-39. Filter Rejection Calculation (Maximum Rejection  $\theta = 90$  degrees)

	40 MHz Filter	240 MHz Filter
EIRP	+25 dBw	+25 dBw
Loss ( $\theta = 90$ degrees)	-116.9 dB	-126.9 dB
Bit Rate	-73 dB-Hz	-84.1 dB-Hz
Sidelobe Maximum Level at Edge of Other Channel	-17.9 dB	-13.5 dB
Interference Level	-182.8 dBw/Hz	-199.5 dBw/Hz
Noise Level	-206.2 dBw/Hz	-205.2 dBw/Hz
Filter Rejection Required	23.4 dB	5.7 dB

Table 4-40. WBCS Transmission Filter Requirements

Medium Rate Channel	High Rate Channel
$f_1 = 8.050$ GHz	$f_2 = 8.235$ GHz
1 dB bandwidth = $\pm 20$ MHz	1 dB bandwidth = $\pm 128$ MHz
Rejection at $\pm 57$ MHz = 23.4 dB	Rejection at $\pm 165$ MHz = 5.7 dB

#### 4.6.5.5 Equipment Description

The wideband communications module contains the RF equipment necessary to generate and transmit the biphasic and quadriphase modulated X-band signals. A block diagram of this equipment is shown in Figure 4-57. As shown, the modulation is performed directly at X-band with two frequency sources providing the X-band carriers. A pair of half watt solid state power amplifiers are used to drive the steerable antennas. Cross strapping is used throughout to provide redundancy. A tradeoff study of the power amplifiers, modulators, filters, and antenna designs is presented below. As will be shown, direct modulation at X-band using a double balanced mixer implementation and solid state X-band impact amplifier is the recommended design.

##### 4.6.5.5.1 Modulator Design

Of the various techniques available for achieving biphasic and quadriphase modulation, TRW has chosen to study four basic designs. These are the indirect modulation technique where low modulation index PM is multiplied to increase the modulation index, two methods of direct modulation, and an S-band to X-band upconversion technique.

The indirect method of biphasic modulation is shown in Figure 4-58. In this technique the data linearly modulates a phase modulator with a modulation index of  $\pi/2N$  radians. The modulator is followed by a  $XN$  multiplier which simultaneously upconverts the IF to the desired frequency (e.g., 8 GHz) while increasing the modulation index. For biphasic modulation the binary data stream is converted into two voltage levels that drive the modulator whereas for quadriphase modulation the data stream produces four voltage levels. These voltage levels and the modulator phase versus voltage characteristics must be precise in order to produce suppressed carrier modulation. For this reason the indirect modulation equipment is difficult to align and is sensitive to temperature variations.

One technique for direct modulation is shown in Figure 4-59. This technique employs double balanced mixers and a quadrature X-band carrier reference. Each mixer is biphasic modulated with data and quadriphase modulation is achieved by summing the (quadrature suppressed carrier) mixer outputs. Double balanced mixers are currently available

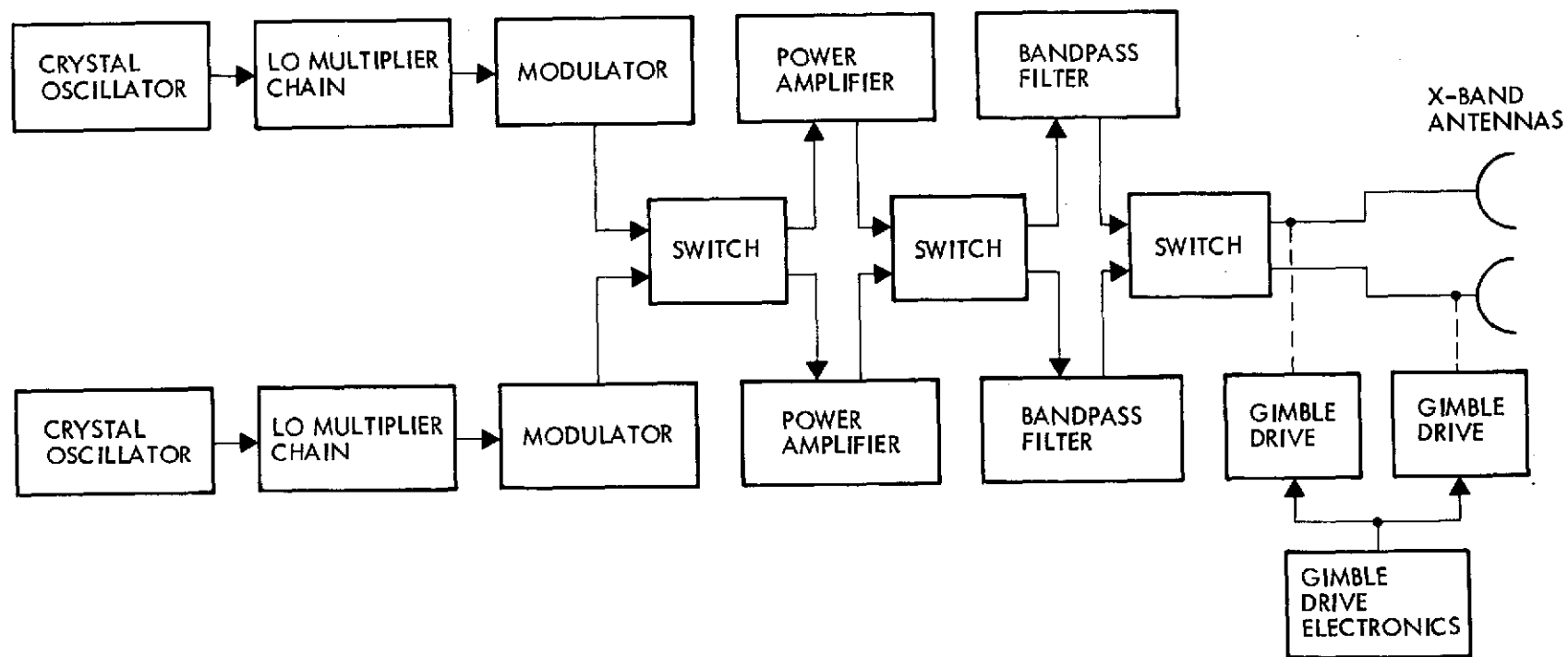


Figure 4-57. Wideband Communications Equipment

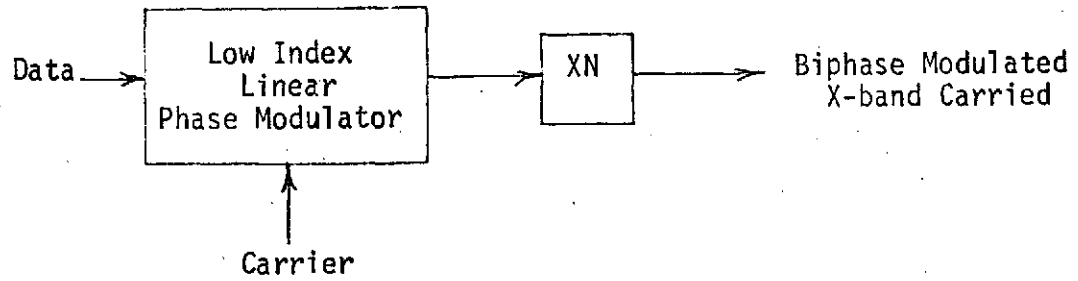


Figure 4-58. Indirect Biphase Modulator

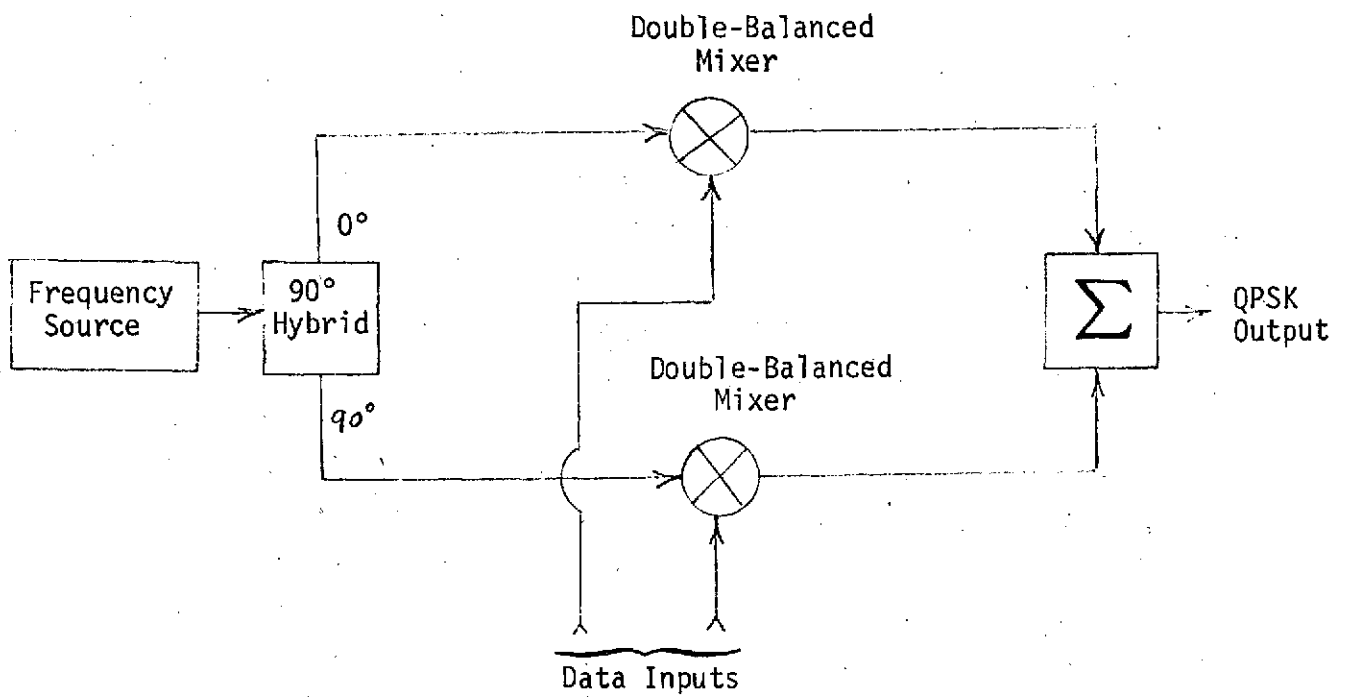


Figure 4-59. Direct Modulator Design Using Balanced Mixers

with LO and RF ports which operate from 6 to 14 GHz and DC coupled IF ports which are flat to 3 GHz. Broadband quadrature hybrids and summers are also available.

256 Mbit/sec quadriphase modulation is produced by applying independent 128 Mbit/sec data streams to each mixer. To produce 20 Mbit/sec biphasic modulation a single 20 Mbit/sec data stream is applied to both mixers. In the event of failure of one double balanced mixer in the open mode, biphasic modulation would still be transmitted. If the mixer failed in the short mode the biphasic would degrade to a  $\pm 45$  degree modulation index residual carrier signal but would still be operable.

Another technique for achieving direct modulation at X-band employs a path length modulator. As shown in Figure 4-60, the modulator is similar to the double balanced mixer design described above except that each mixer is replaced with a circulator, transmission line, and diode. Quadrature X-band references are generated as above and applied to one port of each circulator.

The phase modulation of the RF carrier is generated at the second port of the circulator by opening or closing a pin diode switch. The switch position is based on the input data level. As shown in Figure 4-60, when the switch is closed (diode shorted) the RF power is reflected a half wavelength or 180 degrees earlier in phase than it is when the diode switch is open and the RF power is reflected from the fixed short located a quarter wavelength from the diode. Consequently, the phase of the RF carrier changes by 180 degrees as the diode is switched from "open" to "short". If the diode presents a near perfect open or short, very little RF power is lost in the diode. Typically, the modulator insertion loss due to the diode switch is approximately 0.6 dB. Adding a second similarly modulated data stream in carrier quadrature then provides the QPSK signal. Biphasic modulation is produced by applying the 20 Mbit/sec data to both modulators.

An alternative configuration using the path length technique is the four-level modulator shown in Figure 4-61. A 90-degree modulator is placed in series with a 180 degree modulator. The first modulator reflects the phase of the RF a quarter wavelength (or 90 degrees) earlier when the

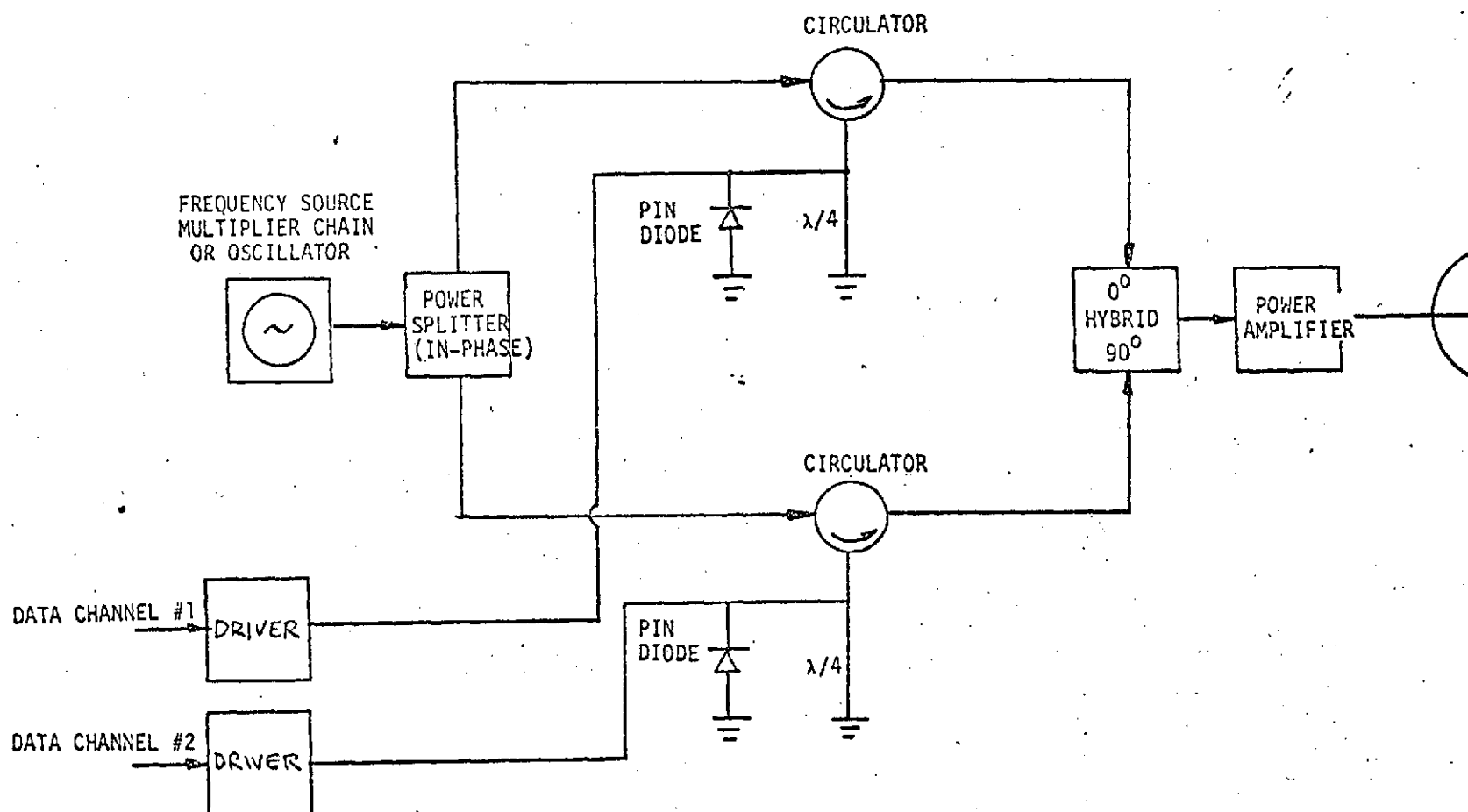


Figure 4-60. Quadriphase Path Length Modulator

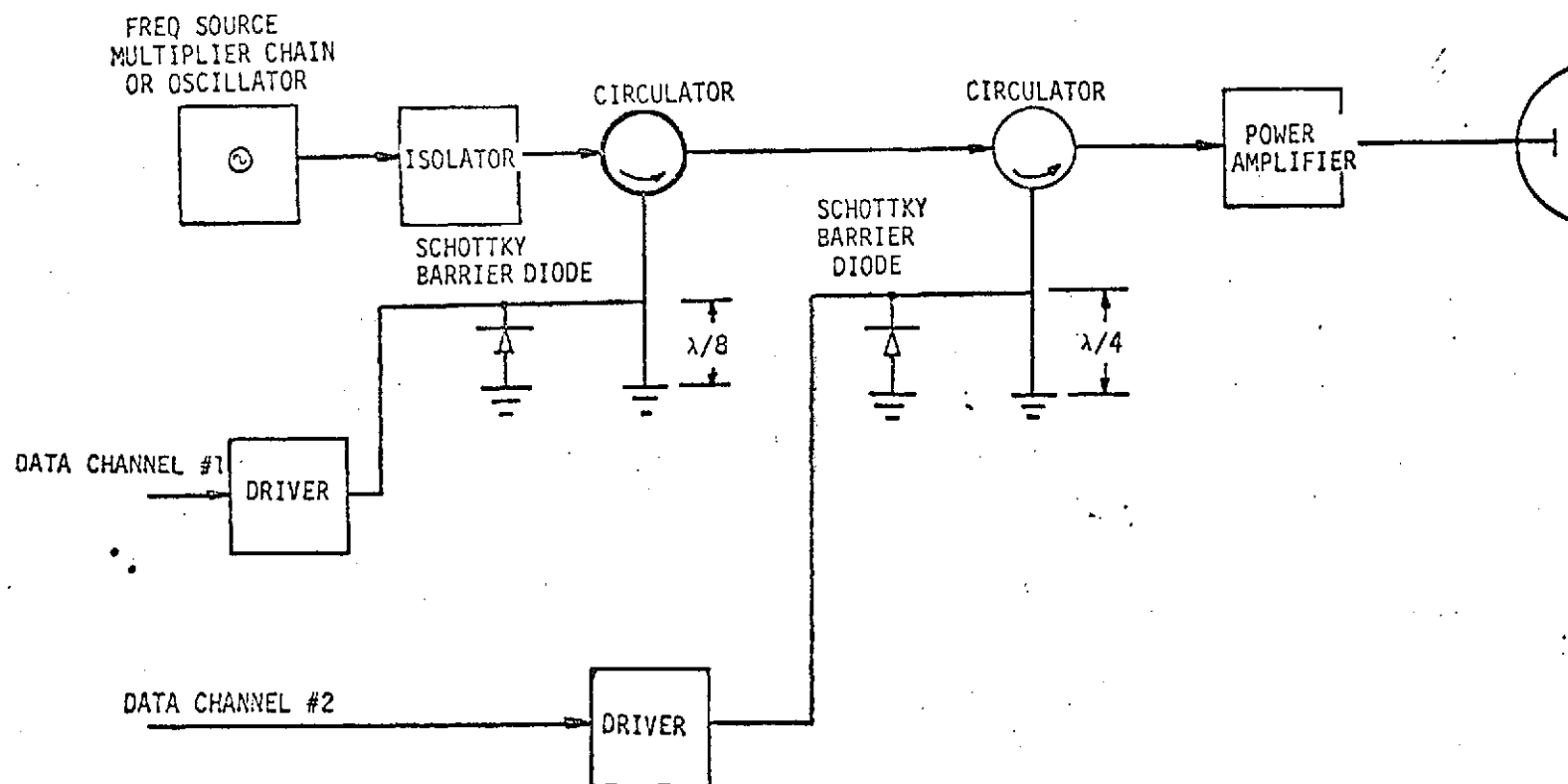


Figure 4-61. Four-Level Path Length Modulator

diode is closed. This is followed by a second modulator identical to the biphase modulator described above. Quadriphase modulation is accomplished by shorting the  $\lambda/4$  and  $\lambda/8$  wavelength line sections in and out of the circuit. Biphase modulation is produced by driving the  $\lambda/4$  section only.

The power loss for the path length modulator between the 90-degree hybrid input and summer output terminals is about 2 dB. The advantages of the direct path length modulator is its simplicity and the high power levels available at the output. However, low loss circulators are needed and the design is very sensitive to temperature drift due to the diode and ferrite sensitivity and the mechanical expansion of the line lengths. A failure of one diode in the path length modulator configurations of Figures 4-60 and -61 will allow biphase modulation to be generated as in the case of the double balanced mixer design.

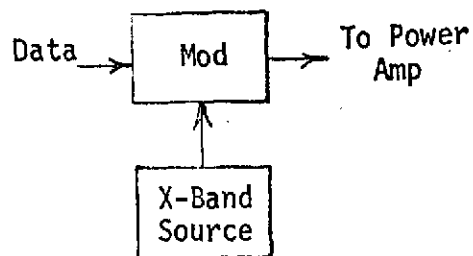
The S-band to X-band upconversion modulation technique is shown in Figure 4-62. The modulator design is identical to the X-band double balanced mixer implementation described above except that the unit operates at S-band. The modulator output is then upconverted to form the X-band QPSK or biphase signal. Until recently, this was the method used to generate X-band modulation since X-band modulator components were not available. The upconverter equipment presently exists and has been space-qualified on several TRW programs.

#### a. Modulator Design Tradeoffs

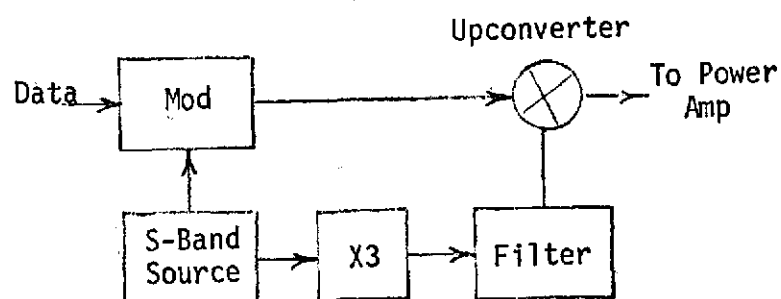
In considering which design is best suited for the modulator requirements, cost, size, weight, and power become the key concerns. Three cost categories are included due to the future applications of this study: 1) the development cost to breadboard and develop new hardware, 2) nonrecurring engineering (NRE) costs involved in minor redesign of existing hardware, and 3) recurring costs to duplicate existing designs. Three techniques are considered as candidates for the X-band modulator: 1) direct modulation at X-band using double balanced ring modulators, 2) S- to X-band upconversion, and 3) indirect modulation with multiplication of a low index signal. The direct path length modulation was not considered because of the availability of X-band double balanced mixers.



1. Direct X-Band Mod (8 GHz)



2. Upconverter S-Band Modulated Signal



3. S-Band Linear Modulator w/Multiplier

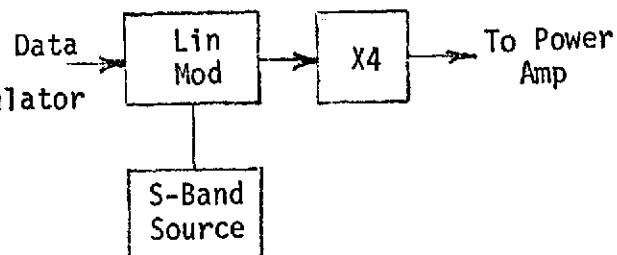


Figure 4-62. Candidate Modulator Block Diagrams

Figure 4-62 shows the three candidate designs and Table 4-41 lists their advantages and disadvantages. As can be seen from Table 4-41, the direct approach is clearly undesirable due to the alignment difficulties and temperature sensitivity. Therefore, this approach will not be considered any further. The two remaining candidates are direct X-band modulation and S- to X-band upconversion. These two are considered next on the basis of size, weight, power, and cost. As can be seen from Table 4-42, the direct X-band modulator is less than half the weight and volume of the upconverter approach and costs less to design and manufacture, even though the S-band modulator and S- to X- upconverter requires no development cost. Based on these considerations, the direct X-band modulator is clearly the preferred design.

#### b. Frequency Source Design

The direct X-band modulator requires a reference frequency input to drive the balanced mixers. Two different frequencies must be provided for the RF carriers to accommodate the 20 and 240 Mbit/sec data rates. The available techniques of generating an X-band reference are limited to the conventional multiplier chain approach and a few newly developed methods. These include low frequency stability microwave oscillators which must be phase locked to a stable reference and highly stable acoustic surface wave oscillators. TRW currently has several in-house programs to develop direct X-band sources. The sources will have the advantages of smaller size, higher efficiency, lower power consumption, and lower cost than the conventional multiplier chain. However, the availability of a fully developed, space-qualified source of this sort for the EOS program would be difficult to predict. Therefore, a multiplier chain design is recommended. Figure 4-63 is a block diagram of an X-band source that has been qualified and used on several space programs at TRW.

Table 4-41. X-Band Modulator Candidate Designs

<u>Advantages</u>		<u>Disadvantages</u>	
<u>Direct X-Band Modulator</u>			
<ul style="list-style-type: none"> <li>• Straightforward</li> <li>• Simple, requires less hardware</li> <li>• Lower power and less weight</li> <li>• Higher reliability</li> <li>• Less component bandwidth restrictions</li> </ul>		<ul style="list-style-type: none"> <li>• Some technical risk</li> <li>• Space qualification of modulator required</li> </ul>	
<u>S- to X-Band Upconverter Modulator</u>			
<ul style="list-style-type: none"> <li>• High credibility</li> <li>• Minimum development</li> <li>• Proven hardware parts</li> </ul>		<ul style="list-style-type: none"> <li>• Requires more hardware</li> <li>• Added complexity</li> <li>• Decreased reliability</li> </ul>	
<u>Indirect Modulator</u>			
<ul style="list-style-type: none"> <li>• Provides linear analog modulation with minimum change</li> <li>• Proven technique at lower frequencies</li> </ul>		<ul style="list-style-type: none"> <li>• Difficult to align</li> <li>• Temperature sensitive</li> <li>• Added complexity</li> <li>• Decreased reliability</li> </ul>	

Table 4-42. EOS Modulator Tradeoff

Module	Per Module			Cost Per Module		
	Size/Vol (in x in x in)	Weight (lb)	DC Power (Watt)	DEV	NRE	RE
				*	**	***
X-Band QPSK Modulator	6 x 6 x 1.5/54	1.6	4.7	150K	35K	30K
S-Band Modulator	10.5 x 6 x 2/126	2.4	4.7	—	35K	30K
S X Upconverter Unit	12.5 x 6 x 2.5/188	3.7	0	120K	40K	40K
S X Multiplexer	2 x 2 x 0.5/2	0.12	0	—	30K	15K

\* Development

\*\* Nonrecurring Engineering

\*\*\* Recurring Engineering

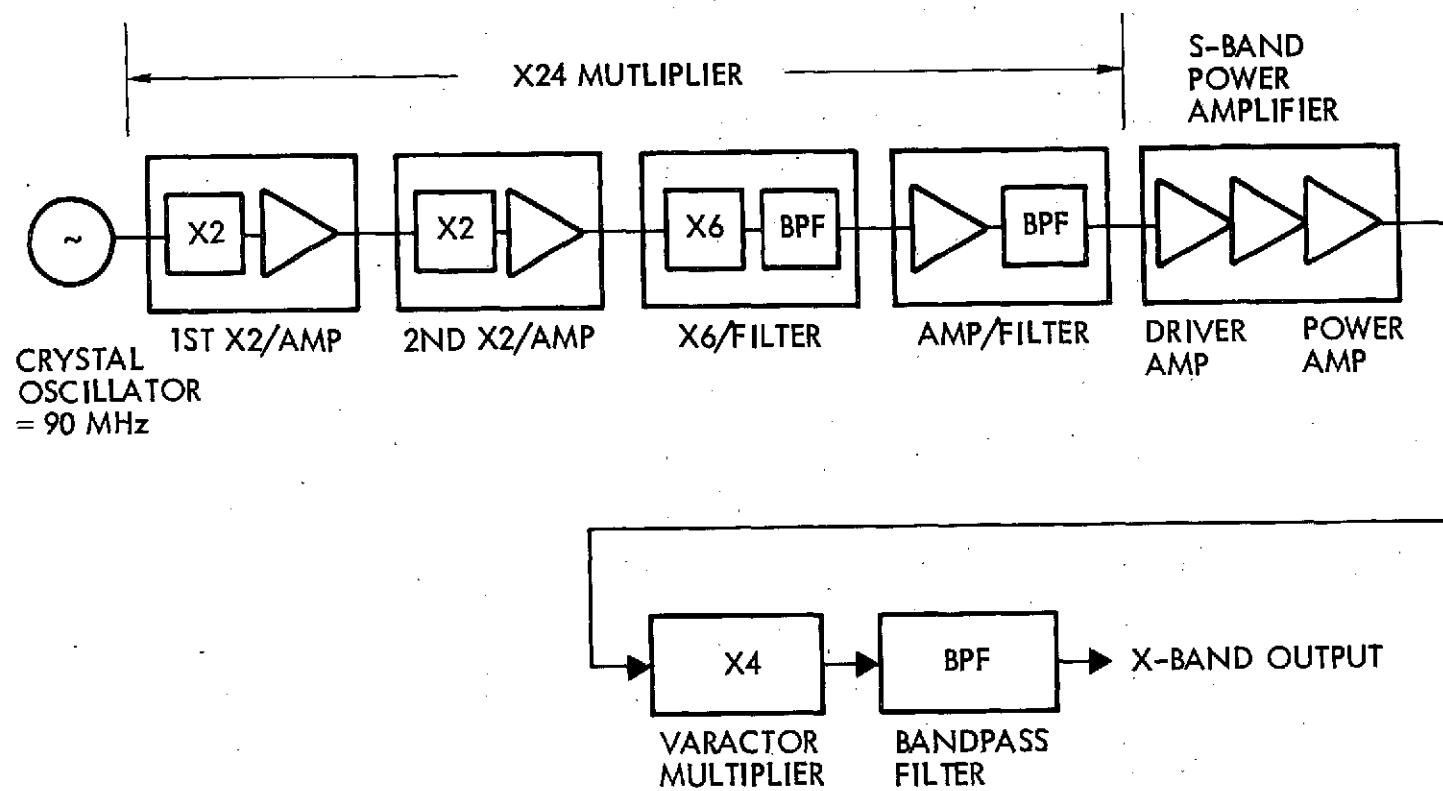


Figure 4-63. X-Band Frequency Source

As shown, a stable crystal oscillator operating at approximately 90 MHz is used to drive a series of cascaded multipliers/amplifiers. Transistor stages operating in a class C mode are used as the multipliers up to S-band. The final X4 stage is implemented with a varactor multiplier followed by a bandpass filter. Two identical multiplier chains are used to provide the 20 and 256 Mbit/sec X-band references. The multipliers are driven by two crystal oscillators which differ slightly in frequencies.

#### 4.6.5.5.2 X-Band Power Amplifiers

The requirements for the X-band downlink power amplifiers are shown in Table 4-43. As shown, both data rates require half-watt amplifiers.

Because of the very close frequency spacing between the wideband QPSK channel and narrowband biphase channel at X-band, it would be desirable to design a common amplifier with sufficient bandwidth to accommodate either carrier. In the event of failure in one amplifier, the remaining amplifier could be used to broadcast the more crucial data.

Two candidate devices exist for providing a half-watt output power level at X-band: 1) a travelling wave tube amplifier, and 2) a solid state Impatt diode amplifier.

Table 4-43. Transmitter Power Amplifier Requirements

Application	Center Frequency (GHz)	Minimum Bandwidth (MHz)	Output Power (dBm)	Nominal Gain (dB)
X-band - 20 Mbit/sec	8.050	40	+27	27
X-band - 240 Mbit/sec	8.235	240	+27	27

Table 4-44 presents a performance summary of a TWTA and solid state X-band amplifier. The outstanding features of the solid state approach are the increased reliability and lower recurring costs. Note that based on existing high-reliability silicon impatt diodes (such as the NEC 1ST15UR) 12 watts DC power is required to produce a half-watt output, while space-qualified TWTA's (such as Hughes' Model 1202H) need only 4 watts. However, it is highly likely that within the next 2 years, space-qualified GaAs impatt diodes will also become available. The improved efficiency of these devices plus their lower weight, smaller size, higher reliability, and lower cost would certainly make the solid-state design preferable to a tube and is the recommended design. Also, it is likely that the solid state amplifiers development costs will be absorbed or shared by other programs.

Table 4-44. X-Band Power Amplifier Tradeoff

Parameter	Performance		
	TWTA	Solid-State (Impatt)	
		Silicon	GaAs
DC power	4 watts	12 watts	6 watts
Weight	4.5 lbs	2 lbs	2 lbs
Size (in)	12 x 5 x 3	7 x 6 x 2	7 x 6 x 2
Reliability MTBF (hrs)	50,000	500,000	Projected MTBF 500,000
Risk	Low	Low	Medium
Development and NRE cost	—	\$100K	\$150K
Recurring cost	\$80 to 100K	\$10K	\$12 to 15K

The amplifier design uses the negative impedance of the impatt diode to provide amplification. A three-stage amplifier is envisioned integrated with a multi-port circulator to provide directivity between the input and output RF. Selection of the proper load impedances is critical to maintaining stable operation. However, the detailed design theory and realization are well proven in practice and, therefore, will not be discussed here.

#### 4.6.5.5.3 Bandpass Filter Design and Fabrication

The requirements for the X-band pretransmission filters as dictated by the systems link budget analysis are shown in Table 4-45. Also shown in the table is a comparison of the capabilities of the waveguide bandpass filters that can be fabricated to meet or exceed all the system specifications. The design and fabrication techniques for filters of this type have been shown to be exceptionally accurate. Refined computer-aided design techniques make it possible to predict a filter response in detail. A computer aided design has been used here to predict the filter performance that meets the requirements of Table 4-45.

Table 4-45. X-Band Bandpass Filter Requirements Versus Capability

Specification	20 Mbit/sec Link		240 Mbit/sec Link	
	Requirement	Capability	Requirement	Capability
Center frequency ( $f_o$ )	8.045 GHz	8.045 GHz	8.245 GHz	8.245 GHz
Ripple	<1 dB	0.1 dB	<1 dB	0.1 dB
Ripple bandwidth	$\geq 40$ MHz	50 MHz	$\geq 240$ MHz	240 MHz
Insertion loss	<1.5 dB	1.3 dB	<1.5 dB	0.3 dB
Number of poles	Minimal	5-pole	Minimal	5-pole
Rejection at $f_o + 45$ MHz	>17.6 dB	29 dB	—	—
Rejection at $f_o - 180$ MHz	—	—	>13.2 dB	21 dB
Phase linearity in passband	< $\pm 10$ deg	4 deg	< $\pm 10$ deg	9 deg

Using this design technique the insertion loss, rejection requirements, bandwidth, and number of sections were used as design inputs. As a compromise between phase linearity requirements and minimizing the number of sections, a 0.1 dB ripple Chebyshev design was considered. These quantities were traded off to obtain the optimum combination of bandwidth and number of sections to achieve the desired results. These results are displayed in Figures 4-64 through 4-69. The basis for the curves displayed in these figures, which show the amplitude, phase, and time delay response for the 20 and 256 Mbit/sec filters, are computer calculations which were specifically derived for waveguide bandpass filters. Note that although the 4-pole filter had sufficient rejection to meet the 20 Mbit/sec system specifications, a 5-pole filter with a 50 MHz ripple bandwidth was nevertheless the selected design. This was done for several reasons. With such narrow ( $\sim 1/2$  percent) filters, the temperature drifts are sufficient to move the passband and attenuate some of the desired modulation. Furthermore, even order filters have poorer VSWR and consequently, the total insertion loss is higher at band center. Also, widening the filters will decrease the insertion loss even though the number of poles is increased and provides a more linear phase response in the passband. A standard WR(112) waveguide operating in the  $TE_{10}$  mode is assumed in the design. Based on past filter experience, an unloaded  $Q$  of 3850 (70 percent of the theoretical value of 5500) is found to be readily realizable in practice and was used in the calculations. Some filter designs at TRW have exhibited  $Q$ 's in excess of 80 percent of theoretical. The 5-pole filter is also recommended for the 256 Mbit/sec link.

Based on the number of sections and the bandwidth required, the physical dimensions of the filter were also determined. Again, a computer-aided design was employed. Computer programs have been written to determine to a high degree of accuracy the dimensions necessary to construct the filter with the specified response. This capability has been realized by generating a set of correction factors which are folded into the standard iterative parameter determination such that the computer print-out yields the final precise dimensions required for a fixed tuned design. The correction factors are known to be valid at different bandwidths and frequencies. A fixed tuned design results in significant cost savings in



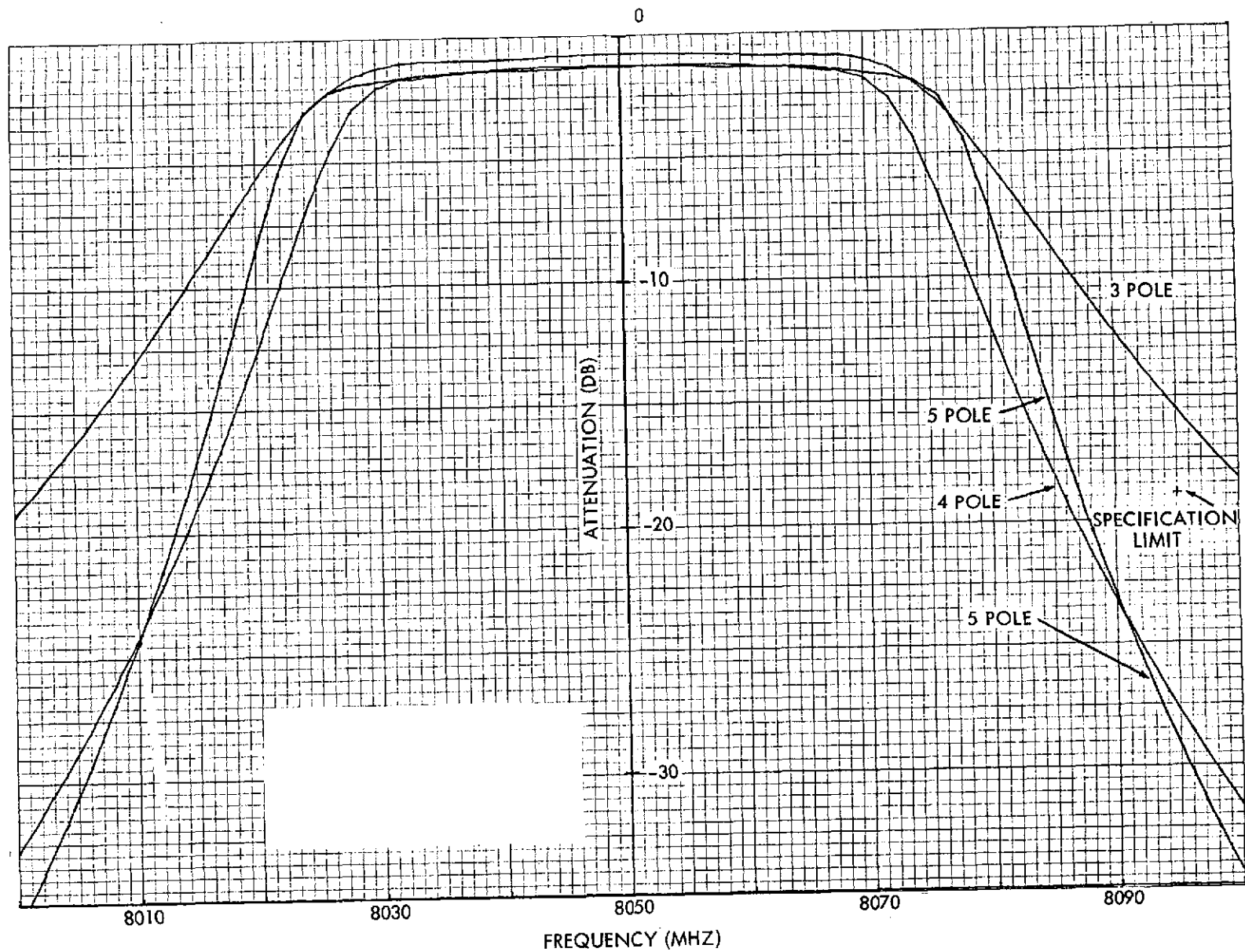


Figure 4-64. X-Band 0.1 dB Ripple Chebyshev Filter  
Amplitude Response  $Q = 3850$ ,  $BW = 40$  MHz

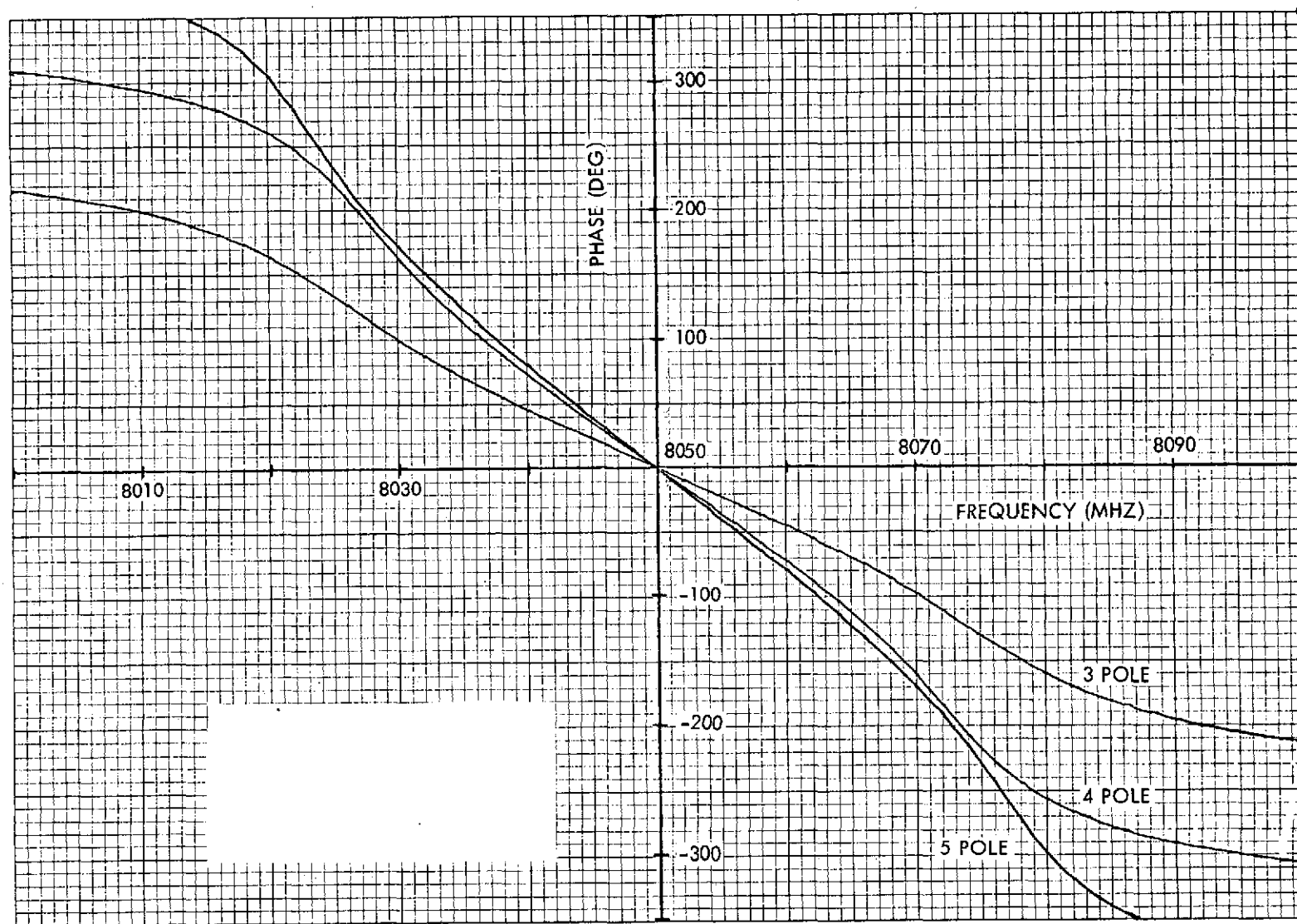


Figure 4-65. X-Band 0.1 dB Ripple Chebyshev Filter  
Phase Response  $Q = 3850$ ,  $BW = 40$  MHz

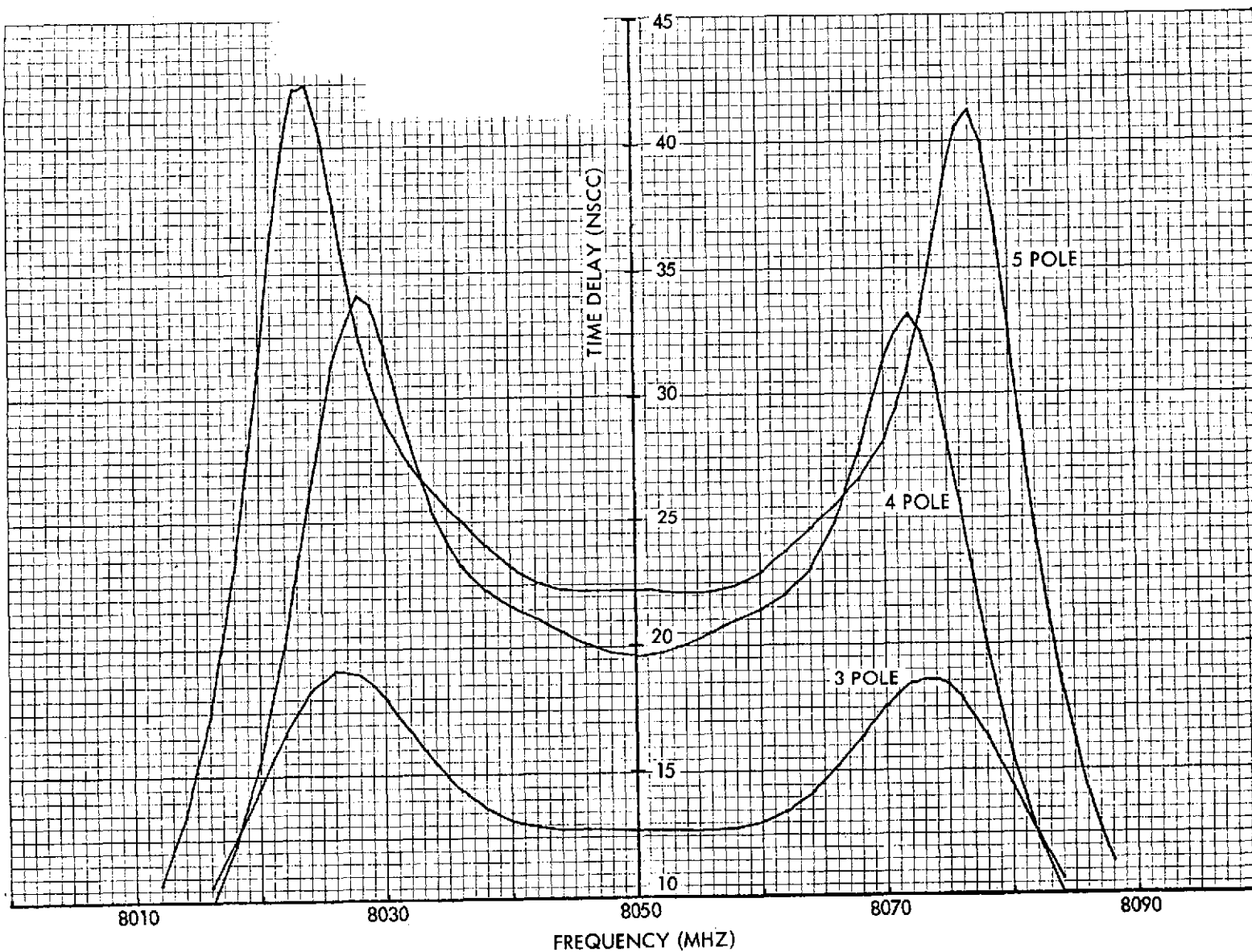


Figure 4-66. X-Band 0.1 dB Ripple Chebyshev Filter  
Time Delay Response  $Q = 3850$ ,  $BW = 40$  MHz

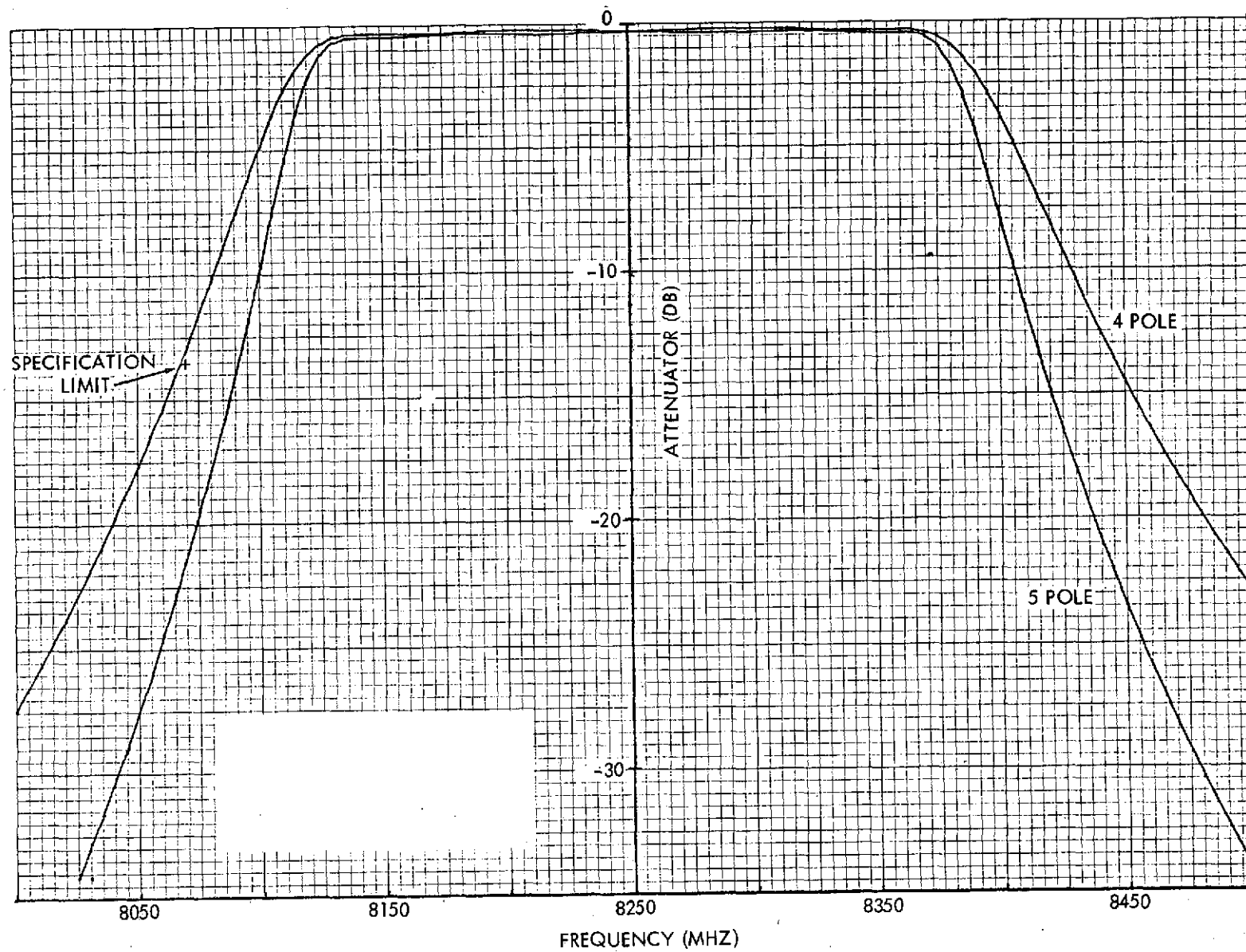


Figure 4-67. X-Band 0.1 dB Ripple Chebyshev Filter  
Amplitude Response  $Q = 3850$ ,  $BW = 240$  MHz

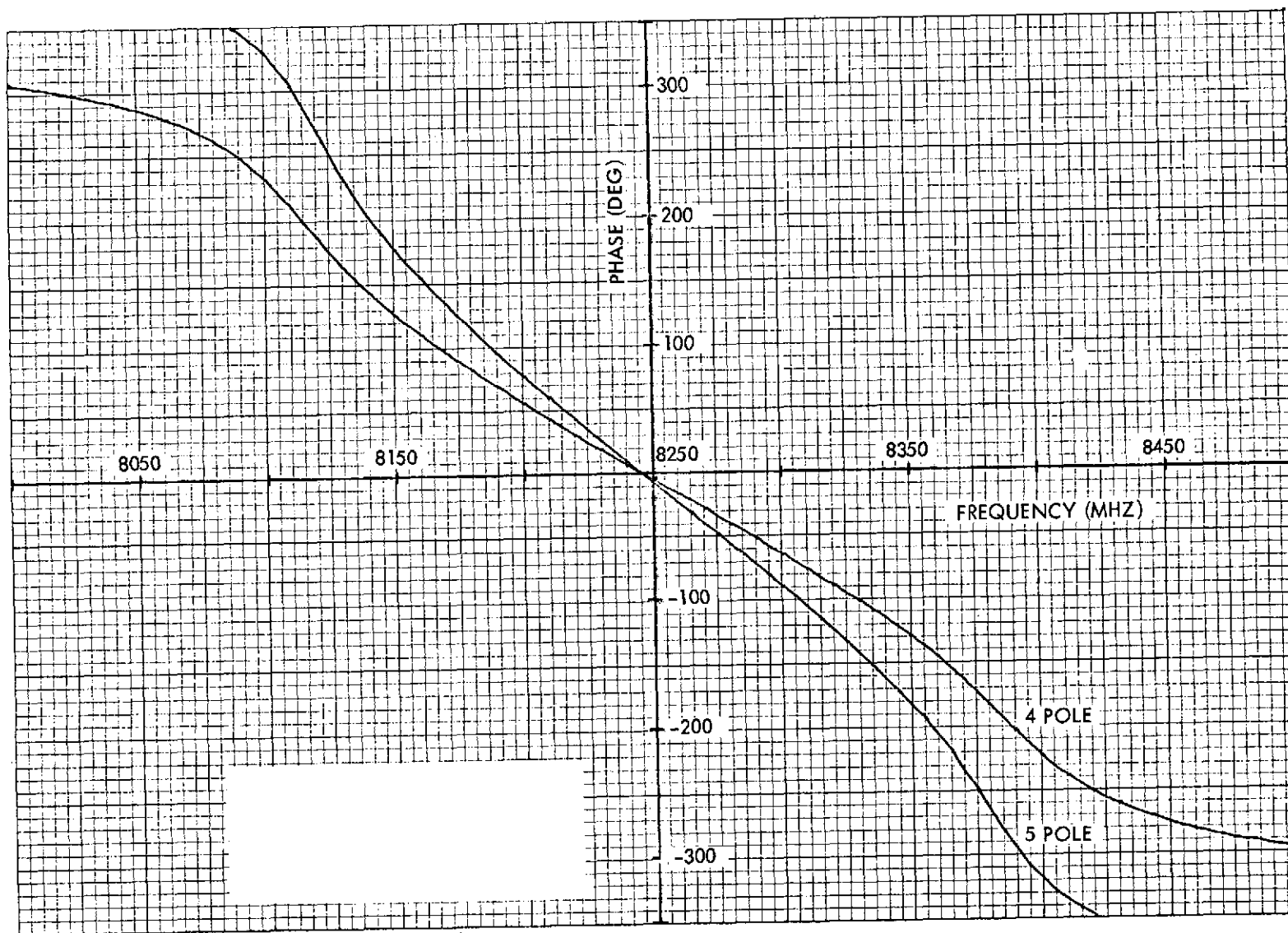


Figure 4-68. X-Band 0.1 dB Ripple Chebyshev Filter  
Phase Response  $Q = 3850$ ,  $BW = 240$  MHz

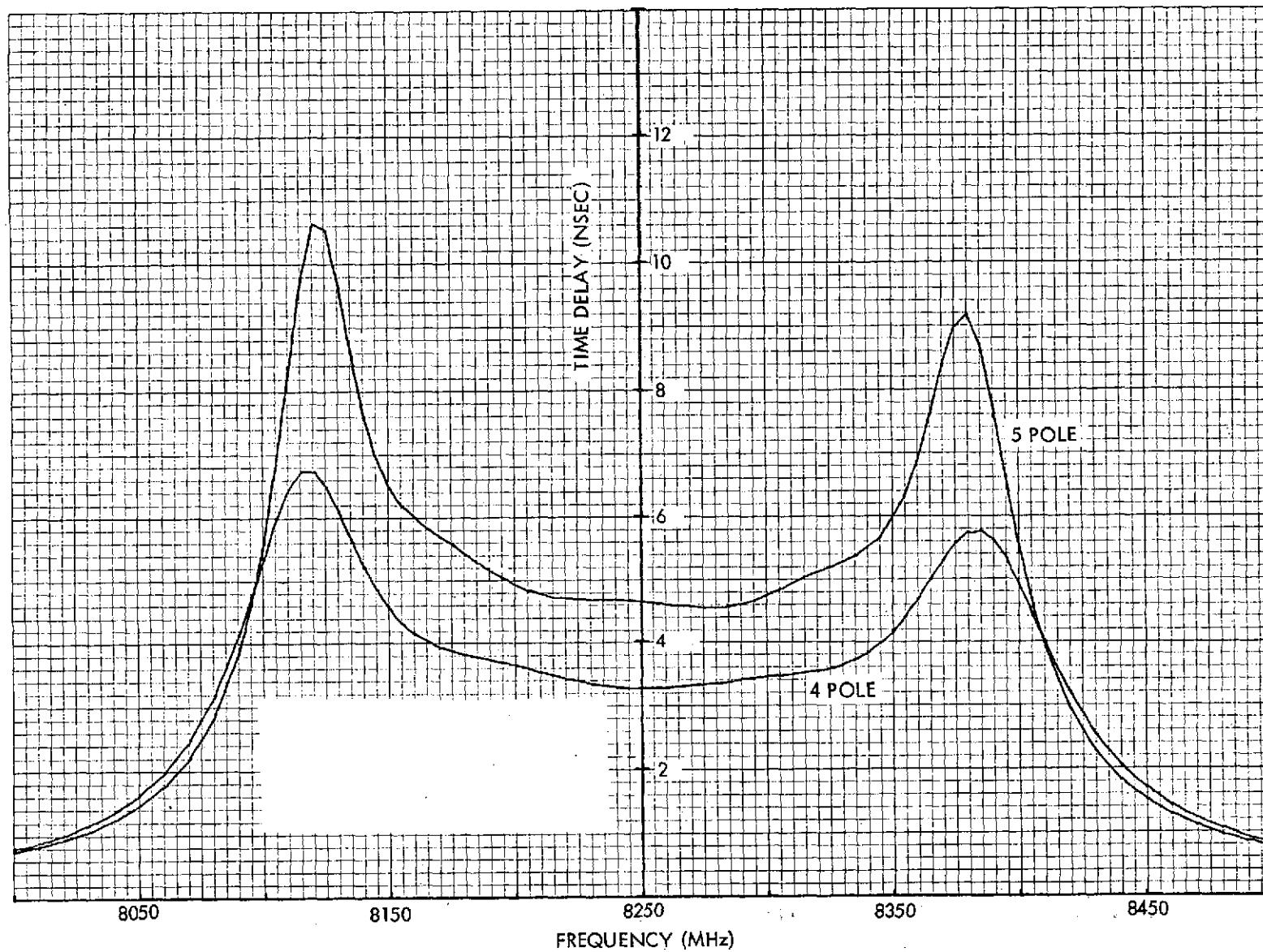


Figure 4-69. X-Band 0.1 dB Ripple Chebyshev Filter  
Time Delay Response  $Q = 3850$ ,  $BW = 240$  MHz

terms of recurring engineering and manufacturing costs of reproducing the filters since no adjustments of the filters will be necessary.

The size of both filters was determined to be approximately 5 inches long using a WR(112) waveguide (1.250 x 0.625 inches). In the construction of the filters single posts can be used for coupling at the input and output of the waveguide while triple posts can be used within the waveguide to form the resonant cavities and couple the signal. This post configuration was selected to provide post diameters of the order of 50 to 150 mils, which is a very convenient dimension in terms of hole size and structural strength.

The construction of the waveguide filters is described as follows. The initial and key fabrication step consists basically of carefully jig boring the hole pattern into an aluminum mandrel blank. The mandrel is then machined and polished, and this high quality external surface is later translated to the internal waveguide surface as a result of the electroform process. In jig boring the holes, the sizes are usually nonstandard and drills are carefully selected. This high degree of accuracy is necessary for precise frequency and bandwidth control.

After machining of the mandrel, inspection is performed to ensure proper hole positioning. Following this inspection, electroforming is initiated. Highest quality materials and fabrication techniques are used in the electroforming process to ensure maximum performance. High quality, high strength copper is formed on all exposed mandrel surfaces, including the jigbored holes. In this way, the reactance posts are formed as an integral part of the waveguide structure. Upon completion of the electroforming cycle, the aluminum mandrel is etched from the electroformed component. This is followed by final external clean-up machining as well as the attachment of the flanges. In the final processing step, electroless gold is deposited, usually over the entire structure. This construction and basic filter design yields a component which is virtually impervious to the environment under which it must operate. The proposed filters are mechanically rigid and light weight, with 270 grams being a typical figure.

The proposed waveguide filters will not present any difficulty in terms of the environmental requirements. Sufficient bandwidth margins have been included in the specifications to minimize any center frequency drift. Shock and vibration are of minimum concern since the structure is small in size and mechanically sound. A reduced pressure environment is not considered to be a problem, again due to the rigidity of the structure. Vacuum tests have been performed on filters of comparable construction. Filters with post diameters as small as 0.031 inch exhibited no failures at levels as low as  $10^{-7}$  torr.

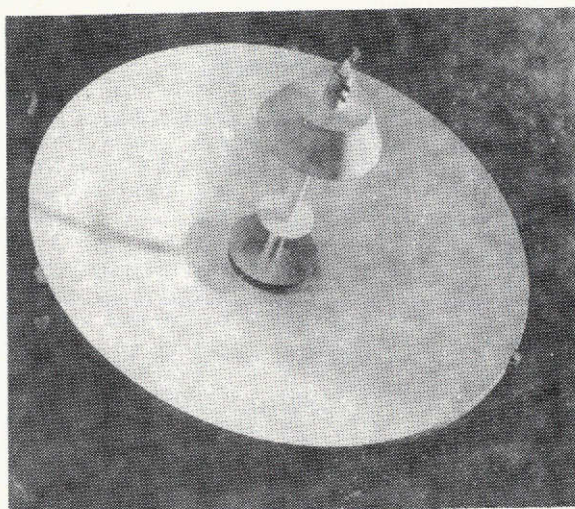
#### 4.6.5.5.4 X-Band High Gain Antenna

The X-band high gain antenna is a 2-foot diameter parabolic antenna similar to the S-band high gain antenna used on the Defense Satellite Program (DSP). The feed system consists of unequal length crossed dipoles fed from a split tube balun. A cupped-shaped splashplate directs the RF energy into the reflector. Circular polarization is obtained by adjusting the crossed dipoles to the proper length. The antenna will provide a gain of 31.5 dBi and a half power beamwidth of 4.3 degrees. The axial ratio of the right-hand circularly polarized radiation will be less than 1.0 dB over the HPBW.

The reflector is constructed from aluminum honeycomb sandwiched between two fiberglass facesheets. The RF reflecting surface is obtained by vacuum depositing aluminum (VDA) to the fiberglass facesheet. Thermal distortion is minimized by painting the reflector and feed with a white thermal paint. A thermal analysis which computed distortion to both the reflector and feed was performed on the antenna as part of the DSP development program. This information was verified during qualification test of the antenna. The antenna pattern and gain were calculated at X-Band from this analysis. These calculations showed that the degradation to electrical boresight was less than 0.1 degree. Gain degradation was negligible. Figure 4-70 presents the antenna configuration and pertinent characteristics.



ANTENNA CHARACTERISTICS	
PEAK GAIN	31.5 DB
HP BW	4.3 DEG
POLARIZATION	RHCP
AXIAL RATIO	1.0 DB (MAX)
VSWR	1.3:1 (MAX)
SIZE	24 IN. DIA
WEIGHT	2 LB



DSP 2-ft antenna

Figure 4-70. X-Band High-Gain Antenna

#### 4.6.5.5.5 X-Band Waveguide

A coaxial to WR-112 waveguide transition is attached to the back of the reflector. WR-112 rectangular waveguide is used as the transmission line between the transition and transfer switch. The waveguide is fabricated from aluminum and internally gold flashed to minimize losses. The external surface is iridited. Flexible waveguide, similar to that used on the DSCS-II spacecraft program (Figure 4-71) is used on each axis of the two-axis pedestal to eliminate the need for RF rotary joints. This method was successfully used on the spot beam pointable antennas which were mounted on the previously mentioned spacecraft. The flexible waveguide is fabricated from seamless, non-twistable, beryllium copper flexible waveguide and has a minimum length of 12 inches. Sections of this waveguide have been subjected to repeated bending of  $\pm 90$  degrees with no physical or electrical degradation.

#### 4.6.5.5.6 X-Band Transfer Switch

The X-band transfer switch is the conventional four-port rotor type using curved waveguide to opposite ports. This switch, which is the latching type, uses the same opposing linear solenoid actuator used in the DSCS-II three-port switch. This type actuator is also being used for the NATO III spacecraft. The insertion loss of this switch is less than 0.1 dB.



#### 4.6.5.5.7 X-Band Antenna Gimbal Drive Mechanism and Electronics

The antenna gimbal drive and electronics is shown in Figure 4-72, along with the physical characteristics of these units.

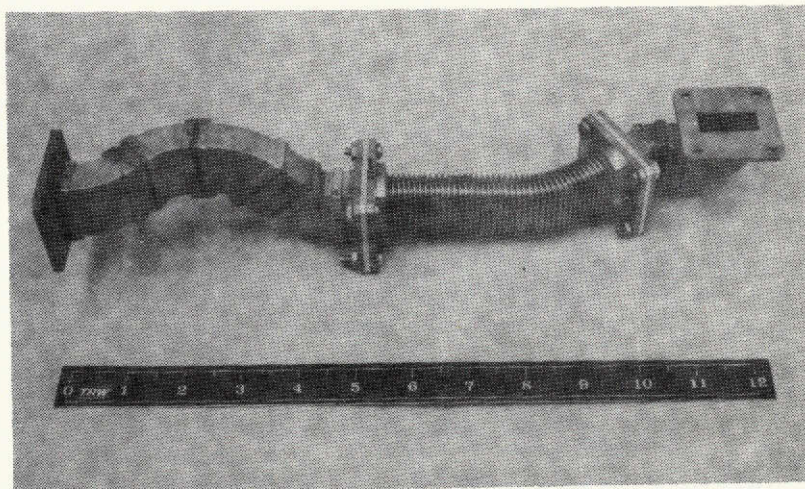
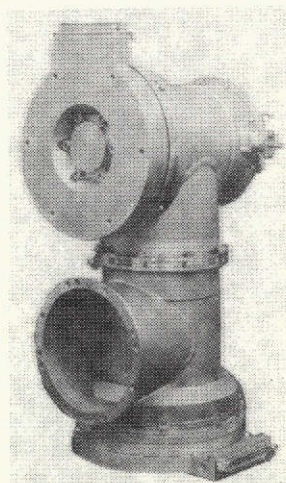
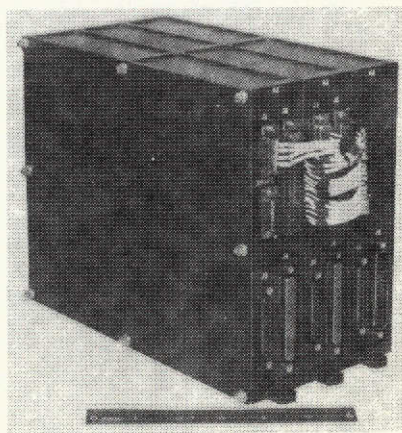


Figure 4-71. Flexible Waveguide



- STEP SIZE: 0.0315 DEG
- POWER: 5.6 WATTS AT SLEW
- SLEW SPEED: 1.5 DEG/SEC
- DRIVE TORQUE: 13.0 FT-LB
- SIZE: 6.4 x 7.1 x 13.6 IN.
- WEIGHT: 14.2 LB



- SIZE: 5.5 x 7.7 x 11.5 IN.
- WEIGHT: 6.3 LB
- POWER: 3.5 WATTS AT SLEW
- GIMBAL READOUT ACCURACY: 0.03 DEG

Figure 4-72. Antenna Gimbal Drive and Electronics

### a. Requirements

The gimbal drive requirements have been determined based on orbital altitudes ranging from 315 to 493 nmi and considering communication time from horizon to horizon. The relationship of gimbal angle and orbital altitude can be seen on Figure 4-73. Expressions are derived, based on this geometry, that give gimbal angle and gimbal angle rate for the parameters of orbital altitude, orbit range of spacecraft, gimbal angle, and the angle locating the position of the spacecraft with respect to the ground station. In the following equation, the small effect of earth's rate has been omitted to simplify the analysis and the ground station is assumed to be in the plane of the spacecraft's orbit so that the maximum gimbal angle and gimbal angle rate will be found. using the two equations shown on Figure 4-73 and using a gear ratio of 2860/1, the result is the data shown in Table 4-46. The stepping rate for each orbit altitude is calculated based on a 90 degree stepper motor. It may be noted that the stepping rate in each case starts from zero and varies to the maximum rate shown which occurs directly over the ground station.

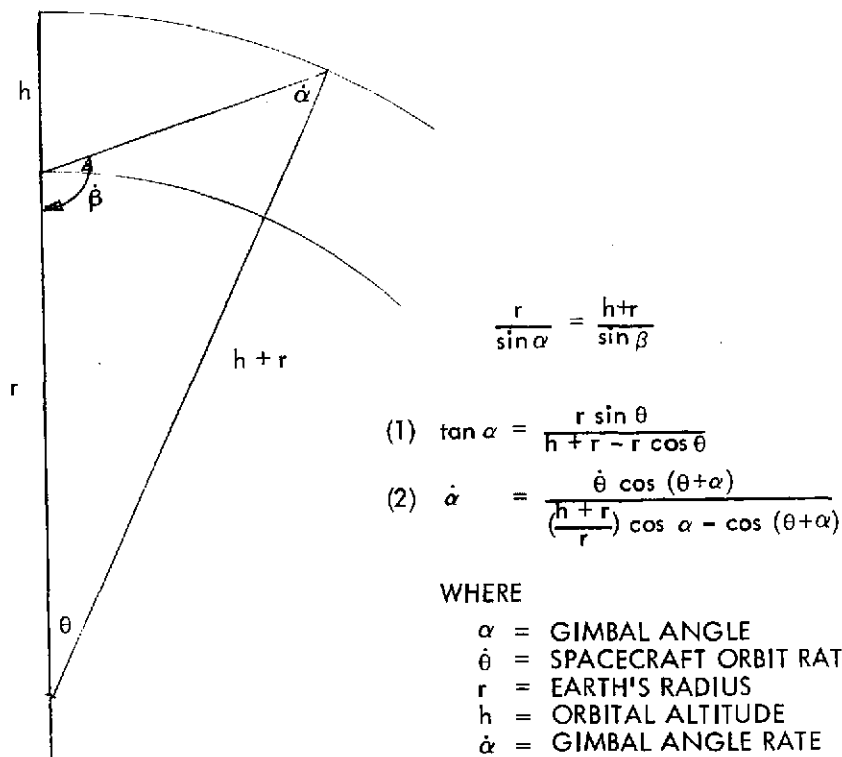


Figure 4-73. Relationship of Gimbal Angle and Orbital Altitude

Table 4-46. Gimbal Drive Requirements

	Orbit Altitude (nmi)		
	315	386	493
Gimbal Angle (degrees)	$\pm 66.2$	$\pm 64.2$	$\pm 61.0$
Gimbal Angle Rate (deg/sec) Maximum	0.685	0.547	0.415
Time for Communication (minutes) (horizon to horizon)	12.5	14	16
Motor Stepping Rate (steps/sec) Maximum	21.8	17.4	13.2
Spacecraft Time per Orbit (minutes)	96	98	101
Spacecraft Orbit Rate (deg/sec)	0.0625	0.0612	0.0594

b. Description of Baseline Design

Each X-band antenna is gimballed in two orthogonal axes by a geared mechanism using a stepper motor drive for each axis. The mechanism is the flight-proven two-axis antenna positioner on DSCS-II. This unit employs a permanent magnet stepper motor driving through two stages of gearing: 1) a spur gear type head integral with the stepper motor, and 2) a harmonic type gear reducer. A multi-speed resolver on the output shaft which drives the antenna provides an indication of the output shaft position. Lubrication of the gears is accomplished by using a fluid lubricant stored in sintered nylon reservoirs. A detailed discussion of this feature is treated in the latter part of this section. Each axis of the antenna positioner is limited in angular travel. A cable wrapup carries the electrical signals of shaft position directly from the rotor to the output connector, thereby eliminating the use of brushes.

Precision ball bearings are used to support the output shaft. A preloaded duplex bearing prevents the axial displacement of the shaft during the launch environment and provides the axial and transverse stiffness required to provide the pointing accuracy needed during the time when the antenna is in use. A radial ball bearing provides the increased transverse stiffness during the launch environment. The exterior surface of the shaft between the ball bearings is coated with a high emissivity paint to promote heat transfer from the shaft to the housing, thereby reducing temperature gradients across the ball bearing. The ball cages of the bearings are impregnated with the fluid lubricant to provide an additional source of the lubricating medium in close proximity to the balls and bearing races.

Each axis of the two-axis antenna positioner is identical to the other resulting in economies during the manufacture of the unit and in its operation. Since the two axes are identical the assembly and test of each can progress without dependence upon the other until the time of final integration of the two axes. At that time the two axes are joined in a "T" manner by effecting a simple mating of flanges of each axis.

#### c. Materials

Since the stiffness to weight ratios of the various aluminum, steel, and titanium alloys are essentially the same, selection of the metal for structural purposes such as the housing and shaft was based on matching the coefficient of thermal expansion of the stainless steel used in the ball bearings. Strength-to-weight ratio was not a limiting factor because the basic diameters of the design provided a section modulus more than adequate to result in working stresses with ample factors of safety. Titanium 6Al-4V was used for those structural parts. In actuality the minimum wall thickness of the housings and shafts was dictated primarily by the manufacturing methods of machining. The spur gears are made of heat treatable corrosion resistant stainless steel. The pinion gears are made of a different alloy of corrosion

resistant stainless steel, gold-plated and lubricated with a fluid lubricant. The harmonic drive uses a gold-plated flexspline gear made of type 32] corrosion resistant steel meshing with its circular spine gear made of ]7-4 ph corrosion resistant stainless steel.

d. Lubrication Mechanism

The low vapor pressure BRAY NPT-4 fluid lubricant is applied in a thin film on all bearing and gear surfaces, and on the inner walls of the drive.

The flexspline and pinion gears are gold plated as an additional lubrication mechanism. Bearing retainers and oldham coupling insert are made of cotton base phenolic which is impregnated with the fluid. Sintered nylon reservoirs (Nylasint) impregnated with the fluid are placed near the bearings and gears.

Lubricant replenishment is accomplished primarily as follows:

- 1) Oil in the reservoirs outgasses slowly until equilibrium is reached between the oil coated surfaces and the oil vapor above them in the enclosed drive. At equilibrium there is a continuous interchange of oil molecules between the liquid and vapor phases. As an oil molecule is lost from any surface by evaporation, it is replaced by one condensing on that surface.
- 2) Oil molecules lost permanently by effusion through the resolver gap are replaced by ones from the reservoirs. A safety factor of 50 minimum has been used in sizing the reservoir capacity to replace the lubricant lost by effusion. The reservoirs are placed so that the vapor flow path of oil molecules from the reservoirs to the exterior of the drive is across the bearings and gears.
- 3) Local replenishment is provided by surface mobility of the fluid, as follows:
  - As the bearings rotate, oil is wiped from the surface of the phenolic retainers. Oil in the interior of the retainer moves through the pores to again wet the retainer surface.

- Sintered nylon reservoirs are placed close to the bearings and gears so that the oil that may creep along the surfaces will find their way to these components. Coating all interior surfaces with oil precludes dry walls which may act as sinks to condensing oil and oil that may creep off of bearings and gears. The coating is very thin so that excess lubricant and flooding of bearings will not occur.

Evaporation rate characteristics of Bray Oil NPT-4 neopentyl triester fluid were used in sizing the reservoirs. This fluid has superior boundary lubrication properties and is therefore suited to this application in which lubrication must be provided by a very thin fluid film. Both the low atmospheric pressure and the slow speeds of the harmonic drive and outboard bearings do not allow for maintenance of a hydrodynamic film.

The reservoirs were sized by calculating lubricant evaporation loss through the resolver gap. A design goal life of 7 years, and NPT-4 evaporation rate at 130°F after 2 percent higher volatiles have vaporized were used (also conservative). The Knudsen equation for effusion through an orifice was employed, and the Clausing's correction factor for wall thickness was applied:

$$G_t = KAG_A t$$

where  $G_t$  = quantity effused in time  $t$   
 $K$  = Clausing's correction factor for flow path configuration  
 $A$  = Orifice area,  $\text{cm}^2$   
 $G_A$  = evaporation rate,  $\text{gm}/\text{cm}^2/\text{unit time}$

Area of orifice:

$$A = (3.14)(4)(.010)(2.54)^2 = 0.810 \text{ cm}^2$$

Clausing's correction factor (K), for a rectangular slit where  $a \gg b$  and  $l \gg b$  was applied:

$$K = \frac{b}{l} \ln \frac{l}{b}$$

where  $a$  = long dimension of cross section =  $d$

$b$  = short dimension = 0.010 in. (.0254 cm)

$l$  = wall thickness = 1.35 cm

$K = .0744$  ( $K$  for other values of  $l/b$  is plotted in Figure 4-51)

At evaporation rate of NPT-4 of  $2 \times 10^{-5} \text{ gm/cm}^2/\text{hr}$ ,

$$G_t = 0.0744 \times 0.810 \times 2 \times 10^{-5} \times 61320 = 0.0737 \text{ gm}$$

Density of NPT-4 = 0.95.

Volume lost = 0.0776 ml

The Nylasint reservoir material has a minimum porosity of 23.2 percent. Therefore, 0.335 cc would be needed to hold the volume of NPT-4 needed to replenish that lost by effusion. Applying a safety factor of 50, a total volume of 16.8 cc minimum of Nylasint has been specified. A 2.5 cc plug is placed in the motor and in the gearhead. Reservoirs are also placed on the harmonic drive spline and between the outboard bearings. By this distribution, critical areas are constantly bathed by fluid molecules vaporizing from the reservoirs, and the path of movement of vapors from the reservoirs, through each compartment, and finally to the exterior of the drive, is across the bearing and gear surfaces.

An examination of the interior configuration of the drive shows that actual lubricant loss will be quite a bit less than that calculated



using the resolver gap only as the leak path. The drive consists of a series of compartments containing reservoirs and having finite openings.

e. Performance

Step Rate

The ability of the gimbal drive to accelerate and position the antenna load is shown as follows.

Assuming an antenna inertia of  $20 \text{ in.-lb-sec}^2$ , the reflected antenna inertia to the motor rotor is:

$$I_R = \frac{20}{(2860)^2} = 2.45 \times 10^{-6} \text{ in.-lb-sec}^2$$

The combined motor rotor and wave generator moment of inertia is:

$$I_M = 2.92 \times 10^{-6} \text{ in.-lb-sec}^2$$

The total moment of inertia is:

$$I_T = I_R + I_M = 5.37 \times 10^{-6} \text{ in.-lb-sec}^2$$

The running torque of the motor is:

$$T_M = 3.5 \text{ in.-oz or } 0.22 \text{ in.-lb}$$

The breakout friction of the motor is:

$$T_F = 0.015 \text{ in.-lb}$$

The useful torque output is:

$$T = T_M - T_F = 0.205 \text{ in.-lb}$$

The angular acceleration of the motor rotor is:

$$\alpha_M = \frac{T}{I_T} = \frac{0.205 \text{ in. -lb}}{5.37 \times 10^{-6} \text{ in. -lb-sec}^2} = 3.92 \times 10^4 \text{ rad/sec}^2$$

The antenna acceleration is:

$$\alpha_A = \frac{3.92 \times 10^4}{2860 \text{ (gear ratio)}} = 13.7 \text{ rad/sec}^2$$

The angle through which the antenna moves during the acceleration half of the motor step is:

$$\theta = 1/2 \alpha_A t^2$$

The resultant travel time is:

$$\therefore t = \sqrt{\frac{2\theta}{\alpha_A}} \text{ where } \theta = \frac{0.03146 \text{ deg}}{2}$$

$$t = \sqrt{\frac{0.03146 \text{ deg } (1.74 \times 10^{-2} \text{ rad/sec})}{13.7 \text{ rad/sec}^2}}$$

$$t = 6.3 \text{ milliseconds}$$

Therefore the total step time is:

$$t_{\text{step}} = 2 \times t = 12.6 \text{ milliseconds}$$

This means in effect that the gimbal drive could move the antenna at a step rate of 1/12.6 ms or 79.5 steps/sec. But the maximum step rate required is only 21.8 steps/sec.

### Power Requirements

The motor utilizes 28 VDC nominally with each winding drawing approximately 0.28 amps. Since two windings are energized at a time, the power required at 100 percent duty cycle would be:

$$P = 2(28) (0.28) = 15.68 \text{ watts}$$

However, the actual duty cycle during the time of antenna use varies from zero up to a maximum power and back to zero. At a stepping rate of 21.8 steps/sec, the time per pulse is  $1/21.8$  or 0.0459 seconds, and the step time required to drive the antenna is 0.0216 seconds. Using a step time of  $2 \times (0.0126) = 0.0252$  seconds which is a safety factor, the peak power is:

$$P_{\text{peak}} = 15.68 \frac{.0252}{.0459} = 8.62 \text{ watts}$$

### Gimbal Angle

The two-axis antenna positioner has the capability of moving each axis over a gimbal angle of  $\pm 100$  degrees. The only limitation to this angular travel is the cable wrapup from the resolver and this could be extended if the need arises.

#### 4.6.5.5.8 Gimbal Electronics Assembly

The gimbal electronics assembly contains two identical gimbal control subassemblies and a resolver electronics subassembly which provide redundant control of two antenna biax drive assemblies. Each gimbal control subassembly (GCS) is capable of stepwise driving four antenna gimbal stepper motors, one at a time, in response to input commands from the on-board computer.

The signal inputs are in the form of a digital code and include a:

- Motor address, selecting the gimbal motor to be stepped
- Sign bit, identifying the direction of motor rotation
- Step pulse for each step of the addressed motor.

After the address is received the GCS executes one motor step command for each gimbal step pulse received. The quiescent state of the step pulse is a logical "0". A logical "1", 31.2 milliseconds in duration is generated for each desired gimbal increment.

The command inputs from the on-board computer result in outputs which control four bifilar wound DC step motors. GCS Channels 1 or 2 are operable upon the application of switched secondary power from the power control unit.

The resolver electronics subassembly contains three synchronous demodulators which process the X36 speed sine, X36 speed cosine, and X1 speed sine outputs of each of four identical resolvers. The resolvers are processed one at a time through an input multiplex network. Resolver processing selection is controlled through ground commands and identification of the resolver being processed is provided with two bilevel telemetry outputs. The demodulators convert the suppressed carrier resolver outputs into DC voltages for telemetry. The excitation for all four resolvers is also provided by the subassembly. A precision 1.027 kHz clock signal is used to chop a 2.56 VDC level reference into a squarewave. This squarewave is filtered and power amplified to provide a sinusoidal excitation for the resolvers. An internal 20 degree phase shifter and zero detector provides a phase shifted square wave to drive the demodulators. This phase shift is designed to match the nominal phase shift of the resolver output signals.

## 5. SPACECRAFT STUDIES

### 5.1 COMMUNICATIONS AND DATA HANDLING

#### 5.1.1 Communication System Definition

This section is concerned with the definition of the systems requirements and configuration for the communications equipment contained within the spacecraft Communications and Data Handling Module.

##### 5.1.1.1 Problem Discussion

The communications equipment contained within the communications and data handling module provides the spacecraft with the capability for receiving information from, and transmitting information to, NASA ground-based stations. As such, it should be flexible enough to accommodate the requirements of EOS-A while providing sufficient modularity of design to accommodate the requirements of future missions. This should take into account future mission requirements for increased antenna gain and coverage; EIRP; data rate; and system reliability. Further, the present and future capabilities of the NASA ground network should also be taken into account. With the advent of TDRSS, an alternate communications path to EOS will be established. Again, the modularity of design concept should be sufficiently flexible to accommodate TDRSS with a minimum of impact.

##### 5.1.1.2 Assumptions

The assumptions made in configuring the communications system were reasonably general. It was assumed that communications with the NASA Spaceflight Tracking and Data Network (STDN) represented the primary method of communications for EOS-A and that communications with TDRSS, if required for later missions, would be accommodated by adding equipment as necessary, to the wideband communications module and not the communications and data handling module. This approach essentially treats TDRSS as an advanced mission with minimal effect to the EOS-A baseline design.

Spacecraft communications with the STDN requires that all communications parameters be compatible with the provisions of the "Spaceflight Tracking and Data Network Users Guide Baseline Document", STDN 101.1, April 1972, Revision 1. An exception to this occurred when it was assumed that the uplink command data rate was 2 kbit/sec instead of the NASA Unified S-band (USB) rate of 1 bit/sec. This resulted from the requirements of the "Communications and Data Handling Performance Specification for EOS", EOS-L-129, revised Section II, dated 30 January, and is presumably for Shuttle command compatibility.

Finally, it was assumed that the provisions of the "Aerospace Data Systems Standards", GSFC X-560-63-2 were generally not applicable for the case of S-band communications to the STDN.

#### 5.1.1.3 Analysis and Tradeoffs

The communications equipment contained within the communications and data handling module provides the spacecraft with the capability for uplink and downlink communications with the STDN. The uplink information will consist of command data, spacecraft computer memory fill data, and tracking data. The tracking data will in turn, consist of uplink range and range-rate information obtained by coherently transponding the uplink range information onto the downlink. The downlink data will consist of real-time engineering data time-division multiplexed with computer memory dump information. Further, medium rate user data such as that provided from onboard tape recorders or other users (selectable by ground command) will also be provided on the downlink.

The baseline and alternate system designs presented in subsequent paragraphs provide a spacecraft communications system which is capable of meeting not only the immediate objectives of EOS-A but also the objectives of future missions with little or no modification to the baseline design.

##### 5.1.1.3.1 EOS-A System Requirements

The requirements imposed upon the communications system are presented largely in the "Communications and Data Handling Performance Specification for EOS," (EOS-L-129, revised Section II) dated 30 January 1974. Other requirements are imposed as a result of operating within

the framework of the NASA Unified S-band system as presented in the "Spaceflight Tracking and Data Network Users' Guide Baseline Document", STDN 101.1, dated April 1972.

Other requirements must be self-imposed. A reliable communications system implies the use of reliable components suitably configured to meet all mission objectives over the duration of the mission period. System flexibility and design modularity must also be of concern to allow for expansion to meet the objectives of later missions. The interface between the communications and data handling systems may also impose requirements. Finally, it is important that the system be configured with proven components to ensure a cost effective design. Table 5-1 lists the requirements which were used to configure the communications system as well as the capabilities of the baseline communications system design.

#### 5.1.1.3.2 EOS-A Baseline Design Description

##### a. System Description

Figure 5-1 presents the baseline communications system contained within the spacecraft communications and data handling module. This design, making use of flight-proven components, provides for command reception and telemetry transmission via two, opposite, circularly-polarized omni-directional antennas which, in turn, provide over 97 percent spherical coverage measured relative to the -1.0 dBi point. The outputs from each of the antennas are coupled to a hybrid combining network by means of two diplexers. The hybrid combines the two signals from the diplexers to provide a signal output to an S-band receiver tuned to a frequency located within the 2050 to 2150 MHz range. One output of the hybrid network is terminated. Since one of the antennas is right-hand circularly-polarized and located on the earth-pointing or forward side of the spacecraft, and the other is left-hand circularly-polarized and located on the opposite or aft side, an antenna polarization address scheme is implemented, which allows the STDN to command the spacecraft via one of the two antennas, regardless of how the spacecraft is orientated.

The input to the S-band receiver contains command and ranging information in Unified S-Band (USB), STDN compatible form. The receiver detects

Table 5-1. Requirements and Constraints Versus Capabilities

Requirement or Constraint	Source/Specification Paragraph	Capability
<u>RF Group</u> All communications fully compatible with GSFC Aerospace Data Systems Standards X-560-63-2	EOS-L-129-Section II, 2.2.1	Command and telemetry formats compatible with Aerospace Data Systems Standards USFC X-560-63-2
<u>Antenna Polarization</u> Output to C and DH receivers may be single linearly polarized or dual left and right circularly polarized signals	EOS-L-129-Section II, 2.2.1	Dual right and left hand circularly polarized omnidirectional antennas are provided
<u>Transmit Frequency</u> Transmit carrier shall be in 2200 to 2300 MHz range	EOS-L-129-Section II, 2.2.1	USDS compatible transmitters are provided which operate in 2200-2300 MHz range
<u>Receive Frequency</u> Receive carrier shall be in 2050 to 2150 MHz range	EOS-L-129-Section II, 2.2.1	USDS compatible receivers are provided which operate in 2050-2150 MHz range
<u>RF Characteristics</u> Transmit frequency: TBD MHz $\pm 0.001\%$	EOS-L-129-Section II, 2.2.1	Transmit carrier lies in 2200-2300 MHz range with stability of one part in $10^5$
Receive frequency: TBD MHz	EOS-L-129-Section II, 2.2.1	Receive carrier lies in 2050-2150 MHz range
Transponder ratio: 221/240	EOS-L-129-Section II, 2.2.1	Ratio of uplink carrier frequency to downlink carrier frequency is 221/240
Transponder sidetone frequency: 500 kHz	EOS-L-129-Section II, 2.2.1	Transponder bandwidth compatible with 500 kHz sidetone frequency
Command bit rate: 2000 bps	EOS-L-129-Section II, 2.2.1	2 kbps command bit rate provided
Command modulation: PCM/PSK/FM/PM	EOS-L-129-Section II, 2.2.1	PCM, split-phase-M command data frequency modulates a 70 kHz subcarrier which, in turn phase modulates carrier
Telemetry narrow band data rate: Selectable: 32, 16, 8, 4, 2, and 1 kbps	EOS-L-129-Section II, 2.2.1	Selectable: 32, 16, 8, 4, 2, and 1 kbps
Telemetry narrow band modulation: Splitphase PCM/PM on subcarrier	EOS-L-129-Section II, 2.2.1	PCM-split-phase/PSK/PM. 1.024 MHz telemetry subcarrier
Telemetry medium data rate: 500 kbps maximum	EOS-L-129-Section II, 2.2.1	512 kbps maximum
Telemetry medium rate modulation: split-phase PCM/PM	EOS-L-129-Section II, 2.2.1	PCM-split-phase/PM (direct carrier modulation)
Transmitter power: 2 or 0.2 watts	EOS-L-129-Section II, 2.2.1	2 watt transmitter - single mode
Telemetry data coding: manchester (split-phase)	EOS-L-129-Section II, 2.2.1.1	Gain antenna mode - manchester (split-phase)
<u>Receiver/Demodulator Options</u> 1) Single receiver/demodulator (baseline configuration) 2) Dual receiver/demodulators with right and left CP diversity combining	EOS-L-129-Section II, 2.2.1.2	1) Baseline design: single receiver/demodulator with right and left CP antenna diversity combining 2) Alternate design: dual receiver/demodulators with right and left CP antenna diversity combining
<u>Command Performance</u> 1) Probability of a false command execution shall be less than $1 \times 10^{-10}$ for any input signal condition 2) Probability of good command rejection shall be less than $1 \times 10^{-3}$ over a signal range of -105 to -40 dBm	EOS-L-129-Section II, 2.2.1.2	1) Probability of false command execution is less than $1 \times 10^{-10}$ for input levels of -112 dBm and above 2) Probability of good command rejection is less than $1 \times 10^{-5}$ for input signal levels of -112 dBm and above

ORIGINAL PAGE IS  
OF POOR QUALITY



ORIGINAL PAGE IS  
OF POOR QUALITY

Table 5-1. Requirements and Constraints Versus Capabilities (Continued)

Requirement or Constraint	Source/Specification Paragraph	Capability
<u>Receiver Combining</u> Receiver combining such that highest quality signal will be used for each bit decision for dual receiver option. Single point failure protection.	EOS-L-129-Section II, 2.2.1.2	Diversity combining plus receiver squelching ensures highest output signal level into demodulator for dual receiver option. Dual receivers provide single point failure protection
<u>Transmitter</u> S-band transmitter shall be capable of simultaneously transmitting up to 32 kbps of real-time low-rate housekeeping/sensor data and up to 640 kbps of medium rate data	EOS-L-129-Section II, 2.2.1.3	S-band transmitter capable of transmitting simultaneously 32 kbps of real-time/sensor data and up to 512 kbps of medium rate data
<u>Transmitter Data Selection</u> Four possible medium rate sources selectable by command 1) Ranging tones (500 kHz) 2) Memory dump (128 kbps) 3) Tape recorder dump (640 kbps)* 4) Special instrument data	EOS-L-129-Section II, 2.2.1.3	Selectable medium rate modes: 1) Ranging tones (500 kHz) 2) Tape recorder dump (512 kbps)* 3) Special instrument data (up to 512 kbps) Computer memory dump does not require a high data rate and is therefore multiplexed into 32 kbps (maximum) housekeeping data
<u>RF Group - Receiver/Demodulator</u> Active redundancy for dual receivers/demodulators	EOS-L-129-Section II, 2.3.1.1	Active redundancy provided
<u>RF Switch</u> Transponder transmitter output switched by command to an antenna other than that used by a receiver	EOS-L-129-Section II, 2.3.1.2	RF transfer switch provided to switch transmitter to either antenna
<u>Spherical Antenna Coverage</u>	TRW self-imposed	97% spherical antenna coverage provided at -1.0 dBi
<u>Reliable Command Performance</u>	TRW self-imposed	Worst case link margins: Carrier - 49.2 dB Command - 47.3 dB ( $10^{-6}$ BER)
<u>Reliable Telemetry Performance</u>	TRW self-imposed	Worst case link margins: Mode 1 - 32 kbps/housekeeping + 512 kbps medium rate data Carrier - 33.8 dB 32 kbps - 7.3 dB ( $10^{-6}$ BER) 512 kbps - 8.4 dB ( $10^{-6}$ BER) Mode 2 - 32 kbps housekeeping + 500 kHz tone ranging: Carrier - 38.5 dB 32 kbps - 20.0 dB ( $10^{-6}$ BER) Ranging - 18.3 dB (5 m rms l)

\* If present. Not part of baseline design.

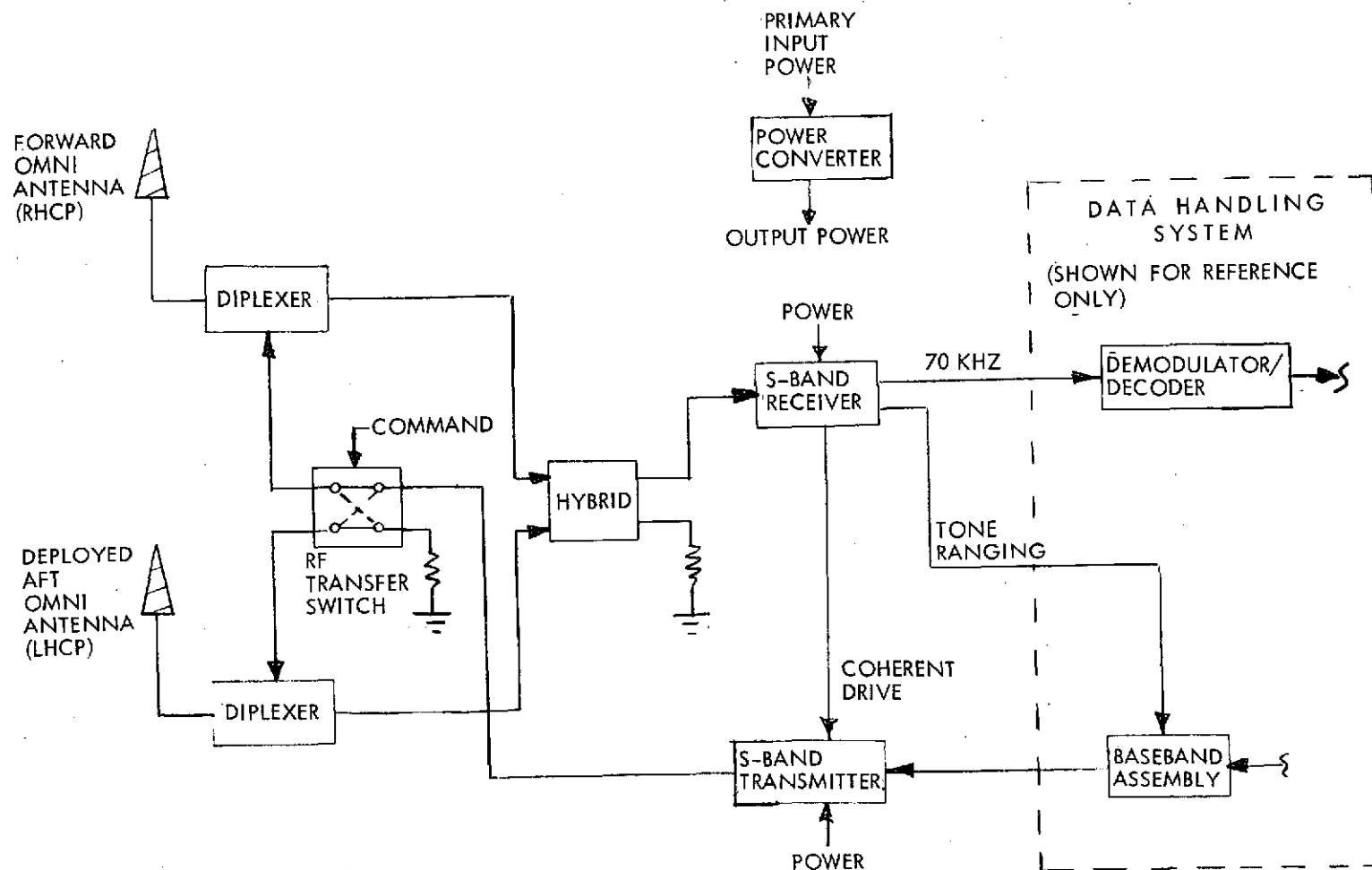


Figure 5-1. EOS-A Baseline Communications System  
(Communications and Data Handling Module)

this information and provides the command data as an output to a demodulator/decoder unit contained within the data handling system portion of the module. The demodulation/decoder input from the receiver consists of a 70 kHz sub-carrier containing 2 kbits/sec command data. The detected ranging data is provided as an output from the receiver to a baseband assembly unit also contained within the data handling subsystem. The baseband assembly unit sums the range data with a 32 kbits/sec, biphasic modulated, 1.024 MHz telemetry sub-carrier and a 512 kbits/sec (medium rate data) direct digital data stream to form the baseband signal which phase modulates the downlink RF carrier.

A frequency reference, coherent with the uplink carrier, is provided as an output from the receiver to the S-band transmitter. This reference, suitably multiplied in frequency, is phase modulated by the composite baseband signal from the baseband assembly unit to form the modulated downlink carrier. Furthermore, since the downlink carrier is phase coherent with the uplink (with a frequency ratio of 240/221), two-way range rate or Doppler information is provided. The S-band transmitter provides a two-watt RF output which is coupled to the two omni antennas by means of an RF transfer switch. The switch allows the transmitter to couple its output to either antenna.

#### b. Diversity Tradeoffs

Important to the configuration of the communications system is a consideration of the technique by which spherical antenna coverage is achieved. Spherical antenna coverage is an implied requirement from a spacecraft command reception and telemetry transmission standpoint and is especially important during the orbital insertion and spacecraft recovery phases.

Spherical antenna coverage can be achieved by several candidate techniques. In general, all of the techniques are concerned with communications diversity and may be categorized into the general areas of frequency, switching, and polarization diversity.

Figure 5-2a illustrates a system which employs frequency addressing on the uplink and frequency diversity on the downlink to achieve spherical antenna coverage. In this system, the forward omni-antenna is coupled to an S-band receiver tuned to an uplink frequency  $f_1$  while the aft antenna is coupled to a second antenna tuned to  $f_2$ . The ground station then commands the spacecraft on either of the two frequencies (frequency addressing) and is assured that the uplink carrier will be received by either of the two antennas, regardless of the spacecraft orientation relative to the ground station. Further, since transmission can take place on either or both of two downlink carriers ( $f_1$ ,  $f_2$ ) spherical coverage is provided by means of frequency diversity. The advantage of frequency diversity over other techniques is that it requires no signal combining hardware onboard the spacecraft for its implementation and can, therefore, be configured with readily available spacecraft equipment. The disadvantages are that each antenna requires a dedicated receiver — even for a non-redundant system; two transmitters are required in order to obtain two-way range-rate information on each of the two frequencies; and, finally, an RF frequency allocation equal to twice that of other approaches is required.

Figure 5-2b illustrates a system employing switching diversity. In this system, a diversity selection unit samples the received signal strength of each receiver as indicated by receiver AGC voltage, and selects for processing, the receiver output having the strongest signal level. Simultaneously, the transmitter is switched to the antenna coupled to the receiver having the strongest signal. The advantages of this technique are that both receivers can operate at the same frequency, and only a single transmitter is required for the non-redundant configuration. The main disadvantage of this technique is that it requires a diversity selection unit as well as redundant receivers for its implementation.

Finally, Figure 5-3 shows a polarization diversity system. In this approach, the signals from opposite-sense circularly-polarized antennas are combined by means of a diversity combining network. This network combines the outputs from each diplexer in such a way that a maximum signal is always provided as an input to the receiver. Further, the transmitter output power is split, by means of a hybrid, into each of the two antennas

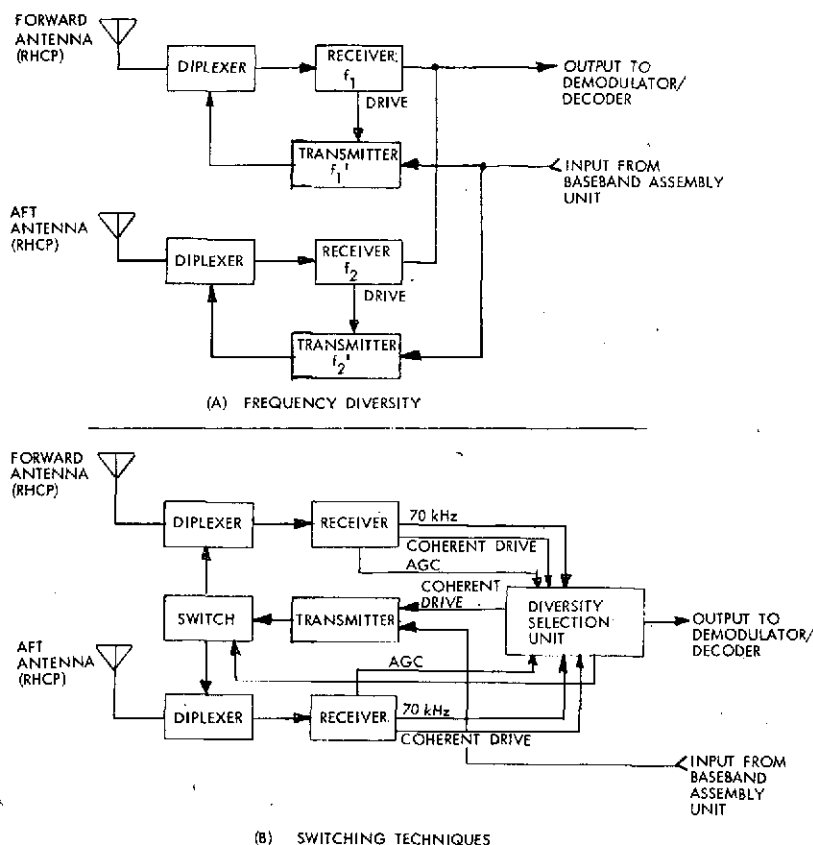


Figure 5-2. Diversity Techniques

achieving polarization diversity on the downlink. If the spacecraft orientation is fixed, the hybrid can be replaced by a simple RF switch which couples the transmitter to the antenna which is pointing towards earth.

The exact form that the diversity combining network assumes is dependent upon the method of transmission chosen by the ground station. If both right-hand and left-hand polarized signals are transmitted simultaneously, the spacecraft diversity combining network must be an active network which measures and weighs the outputs from each of the two antennas according to received signal level. If the ground station transmits only one polarized signal at a time, i.e., polarization selection, the combining network can be a passive combining network, implemented by a simple hybrid. This latter approach has been selected as the EOS-A baseline as presented in Figure 5-1.

A detailed study of diversity combining techniques for EOS was conducted by TRW and is presented in Section 5.1.2. In general, the results of this study

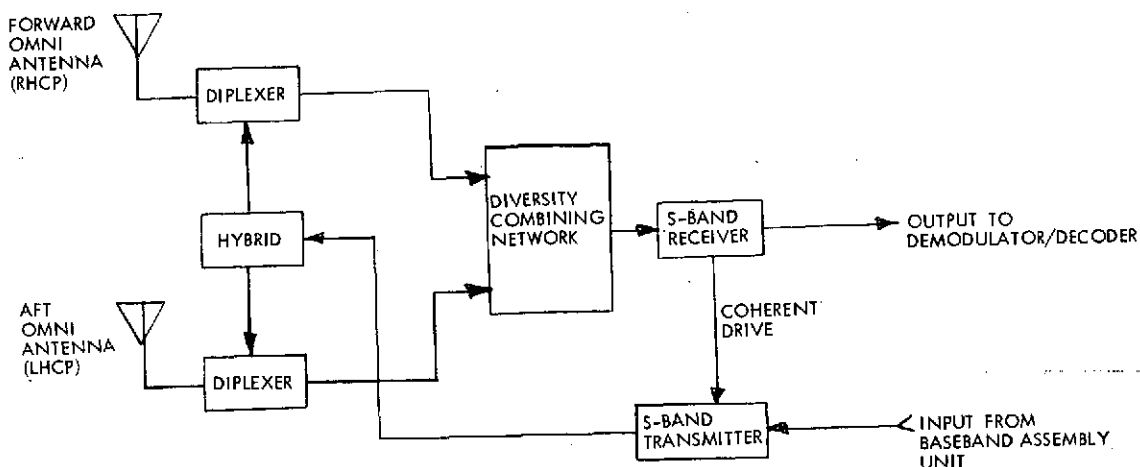


Figure 5-3. Polarization Diversity Combining

have shown that except for the passive combining technique selected for the EOS-A baseline, spacecraft combiners can assume a very complicated and costly form. Further, the improvement in performance obtained by the more involved combining networks hardly warrants their use. This is especially true when they are considered with respect to the large command performance margins present on the uplink.

### c. Omni-Antenna Selection

There are several techniques by which one or more transmission and reception antennas can be used to provide omni-directional coverage. A single antenna mounted at the end of a long boom yields only partial spherical coverage due to interference and blockage resulting from the spacecraft structure. Switching between two hemispherical coverage antennas mounted on opposite sides of the spacecraft for reception creates not only a potential spacecraft "lockout" situation, but also a design complication.

Two or more omni-antennas connected to feed the same receiver results in narrow peaks and deep nulls in the overlap region unless antenna spacing can be maintained at less than one wavelength. An interference-free pattern requires that individual antenna patterns not overlap. Pattern tailoring can minimize, but not completely eliminate this region. Figure 5-4 shows the interference resulting from pattern overlap from two antennas

having different coverage patterns and like senses of circular polarization. This system consists of a cavity-backed Archimedeian spiral antenna mounted to the surface of the spacecraft, and a conical log spiral antenna mounted on the end of a boom opposite the Archimedeian spiral. A 5 dB directional coupler is used to couple the two antennas and balance the individual antenna gain difference. Test results have shown that a composite antenna gain of -5.0 dBi can be maintained over 87 percent of the coverage sphere.

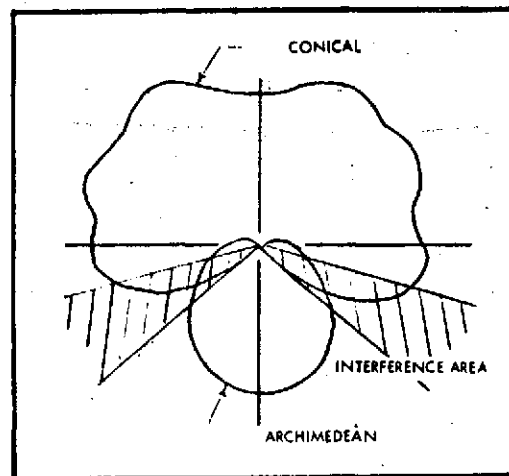


Figure 5-4. Antenna Patterns and Interference Region – Same Sense Circular Polarization

An alternate approach couples two omni-antennas by means of a hybrid ring to the receiver. In this manner, a signal from either of the two antennas is provided as an input to the receiver for any spacecraft orientation. In the pattern overlap and interferometer region, signal cancellation will result. However, since this region lies on an axis which is nearly perpendicular to the spacecraft to earth-viewing axis, it will be encountered only during a loss of spacecraft attitude control. Furthermore, if the spacecraft does encounter this condition, it will generally persist for only a short period of time. If redundant receivers are provided, the hybrid combining network will provide an output to at least one of the receivers at any particular time. In the pattern overlap region, the signals to each receiver will fade in and out, but at opposite times. Cross-strapping the redundant receiver outputs ensures that a signal will always be received. Since both antennas in this

configuration will have the same sense of circular polarization, if only one antenna is excited, a signal will appear at each receiver's input with a 3-dB coupling loss. Figure 5-5 illustrates the output signal levels from each of the hybrid's output ports as a function of wavefront incident angle. Figure 5-6 shows the pattern resulting from an Archimedean spiral and a conical log spiral antenna developed respectively, for the NASA Pioneer 10 and 11 spacecraft and the Air Force DSP program.

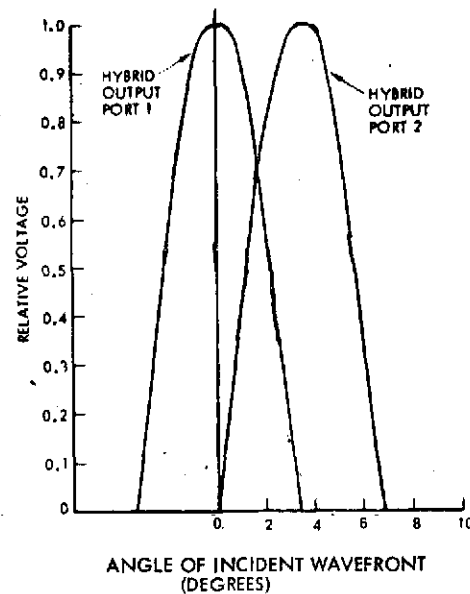


Figure 5-5. Hybrid Combiner Signal Outputs

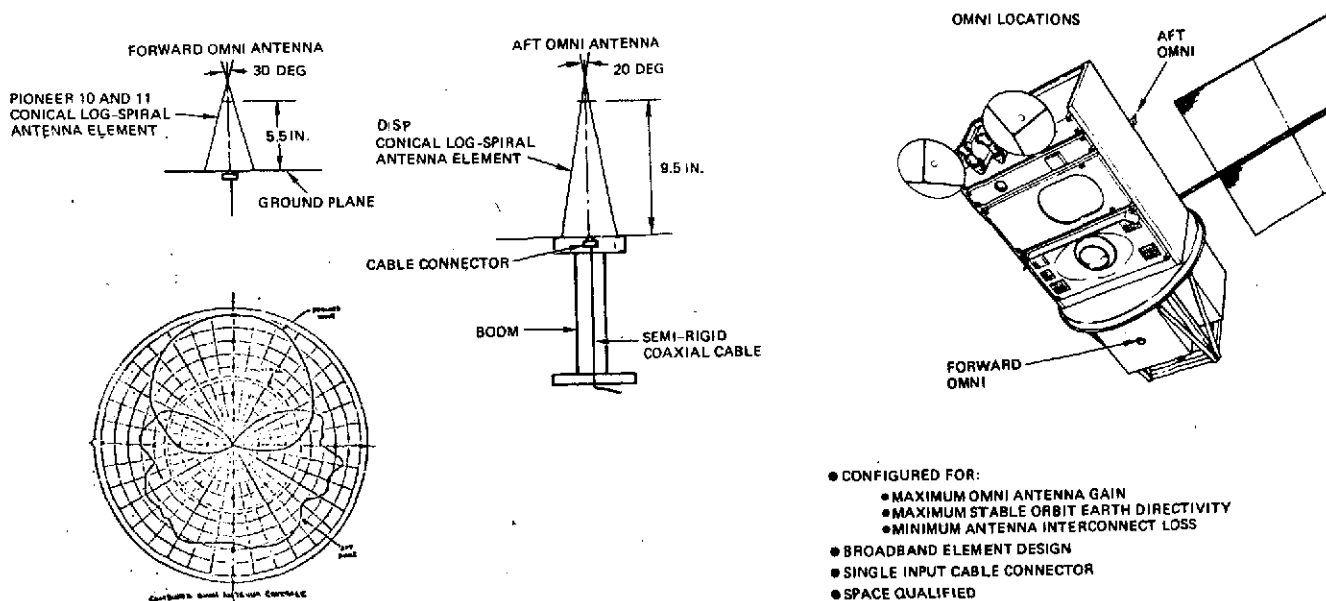


Figure 5-6. S-Band Omni Antennas



As was pointed out, an interference region results when two antennas having the same sense of polarization and overlapping coverage patterns are combined. For the baseline omni-antenna system, this problem has been eliminated by providing two opposite sense circular polarized antennas and operating them in a polarization diversity as shown earlier in Figure 5-1. Since each of the opposite sense polarized antennas have cross-polarization components which are at least 12 dB below the principal polarization, the interference region is effectively eliminated and the resulting patterns will be similar to those shown in Figure 5-6. The resulting combined antennas will have a gain of -1.0 dBi over 97 percent of the coverage sphere.

d. Impact of Redundancy on EOS-A Baseline Configuration –  
An Alternate System Design

The previous discussion was concerned primarily with the EOS-A baseline configuration which contained no equipment redundancy. The addition of redundant equipment to the communications and data handling module communication system to achieve higher reliability is readily accomplished by adding a second S-band receiver to the previously terminated output port of the antenna hybrid combiner network in Figure 5-7 and adding a second transmitter to the previously terminated input port of the RF transfer switch. Figure 5-7 illustrates a fully redundant communications system. Since room has been provided within the communications and data handling module to accommodate equipment additions over that required by the baseline configuration, the addition of a redundant transmitter and receiver will present very little, if any, impact to the module design.

5.1.1.4 System Performance

5.1.1.4.1 Frequency Plan and Modulation Format

The uplink and downlink frequency plan and modulation formats will be compatible with the NASA STDN/USB system. Uplink command data at 2 kbps will be split-phase, mark encoded and frequency modulated onto the USB, 70 kHz command subcarrier. The subcarrier will be summed with tone ranging data and the composite baseband will phase modulate an uplink S-band carrier lying in the 2050 to 2150 MHz range. Figure 5-8a shows the downlink command modulation spectra and Table 5-2 lists some of the command uplink communications parameters as well as the downlink parameters.

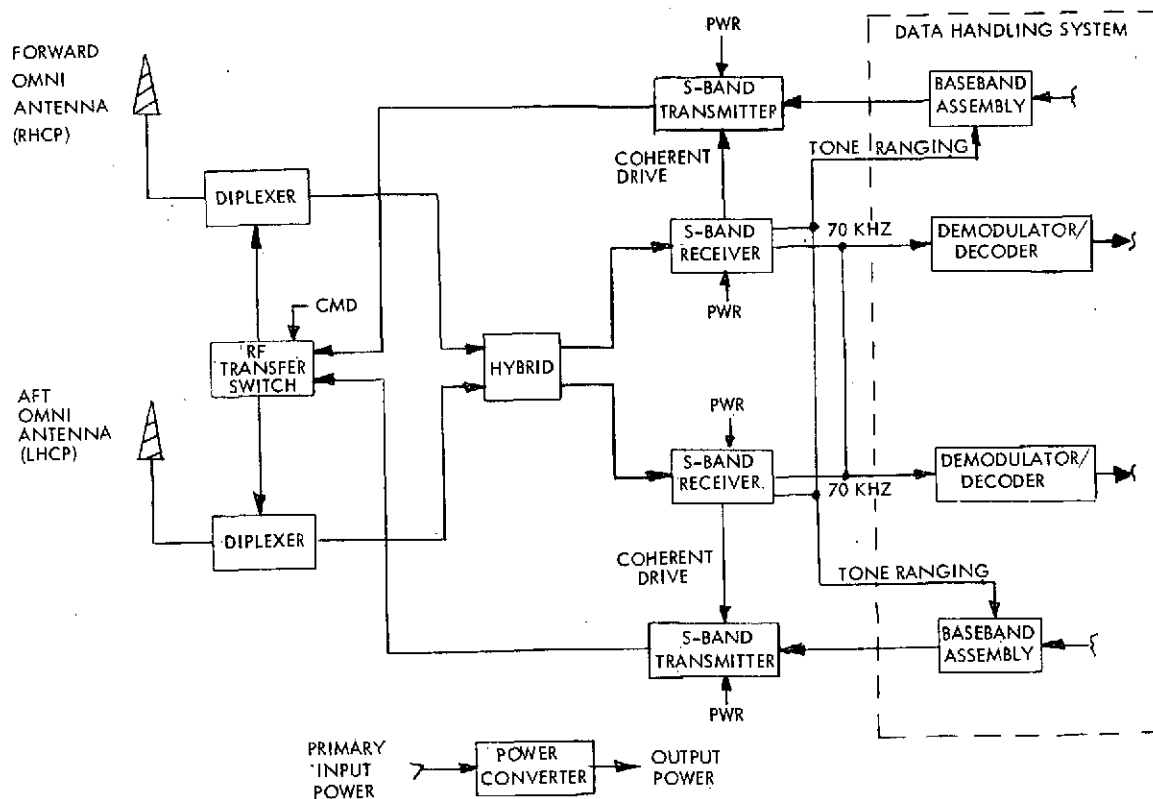
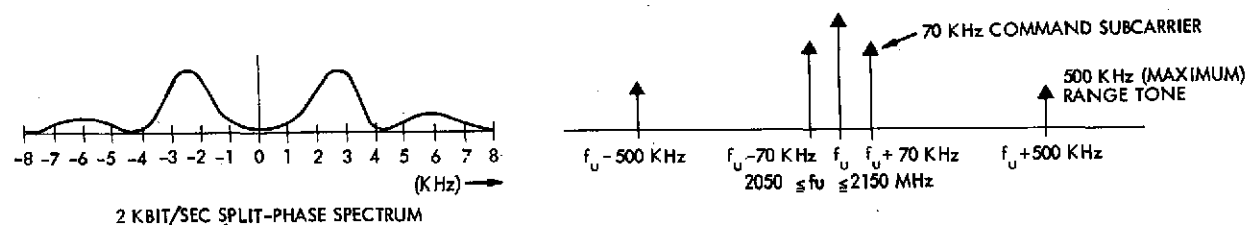


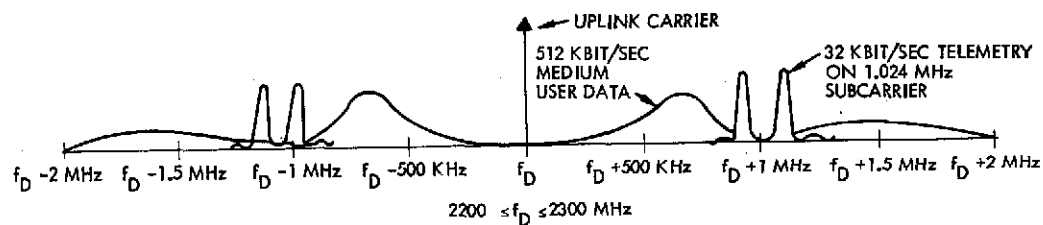
Figure 5-7. EOS-A Alternate Communications System  
Communications and Data Handling Module

Information to be telemetered on the downlink will be transmitted in two modes. In Mode 1, real-time data consisting of housekeeping telemetry and on-board computer memory dump information is time-division multiplexed and transmitted at a 32 kbps, maximum rate. In addition, command selectable, medium rate user data at 512 kbps maximum will also be transmitted. The 32 kbps data will split phase modulate the standard, USB 1.024 MHz subcarrier which will, in turn, phase modulate a downlink S-band carrier lying in the 2200-2300 MHz region. The 512 kbps medium rate user data will be split-phase encoded and directly phase modulate the downlink carrier. Figure 5-8b depicts the downlink modulation spectra for Mode 1.

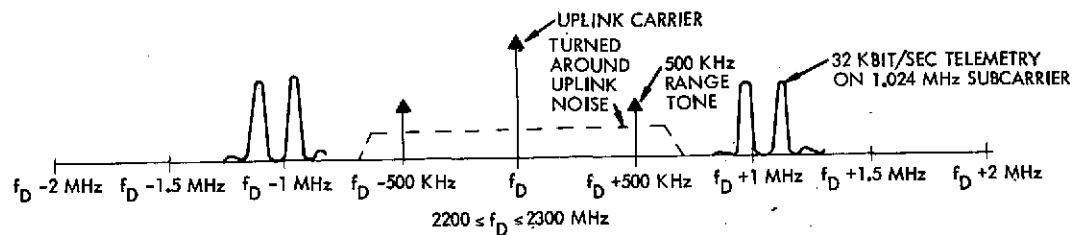
In telemetry Mode 2, the real-time, 32 kbps telemetry will again split-phase modulate the 1.024 MHz subcarrier which will, in turn, phase modulate the downlink carrier. In place of the 512 kbps, medium rate user data of Mode 1, transponded uplink tone ranging data with a 500 kHz maximum, tone frequency will directly phase modulate the carrier. Figure 5-8c shows the modulation spectra for Mode 2.



A) UPLINK MODULATION SPECTRUM



B) MODE 1 DOWNLINK MODULATION SPECTRA



C) MODE 2 DOWNLINK MODULATION SPECTRA

Figure 5-8. Communications Modulation Spectra

Table 5-2. S-Band TT and C Parameters

---

Command Uplink

- Carrier frequency: 2050.0 MHz (assumption)
- Modulation: PCM/PSK/FM/PM
- Modulation indices: command =  $1.2 \pm 10\%$  radian  
ranging =  $0.6 \pm 10\%$  radian
- Bit rate: 2 kbps
- Command modulation: PCM split-phase (mark)
- Command bit error rate:  $10^{-6}$

Telemetry Downlink

- Carrier frequency: 2226.2 MHz (assumption)
- Modulation: Mode 1 — real time telemetry — PCM/PSK/PM  
512 kbps medium telemetry — PCM/PM  
Mode 2 — real time telemetry — PCM/PSK/PM  
ranging — 500 kHz maximum
- Modulation indices: Mode 1 — real time telemetry —  $0.8 \pm 10\%$  radian  
512 kbps medium telemetry —  $1.1 \pm 10\%$  radian  
Mode 2 — real time telemetry —  $1.4 \pm 10\%$  radian  
ranging —  $0.1 \pm 10\%$  radian
- Data rates: Modes 1 and 2 real time telemetry — 32 kbps  
Mode 1 medium rate data — 512 kbps
- Bit error rate:  $10^{-6}$

Tracking

- Ranging: tone ranging with 500 kHz maximum frequency
  - Range rate: two-way range rate; uplink/downlink carrier ratio  
221/240
- 

Finally, two-way range rate or Doppler information will be provided by coherently heterodyning and phase tracking the uplink carrier by means of a phase lock loop receiver and providing a coherent reference to the transmitter which, when suitably multiplied in frequency, will provide the downlink S-band carrier. The uplink carrier frequency will be related to the downlink carrier frequency by the ratio 221/240.

#### 5.1.1.4.2 S-Band TT and C Link Calculations

This section presents the S-band link calculations for command, ranging and telemetry. The spacecraft communications and data handling systems are fully compatible with the NASA USB system. As is evident from Tables 5-3 and 5-4, a more than adequate performance margin exists for the three functions.

##### a. S-Band Uplink

Table 5-3 presents the link calculations which were performed for the S-band uplink. The calculation was performed at 2050 MHz with an assumed ground station transmitter power level of 1 kw. This level is a typical value for the NASA STDN. The ground station antenna gain was taken as 43.0 dB, which is a typical value for the NASA 9 meter dish having a 50 percent efficiency. Assuming a spacecraft altitude of 716 km, the slant range to the spacecraft was found to be 2590 km for a 5 degree ground antenna elevation angle.

The spacecraft omni antenna gain was taken as -3.0 dBi over 95 percent of the sphere which is in effect, conservative since the combined patterns for the two omni antennas which will be used for EOS, typically provide -1.0 dBi coverage over 97 percent of the sphere. The spacecraft system equivalent noise temperature referred to the input to the receiver was calculated at  $2900^{\circ}\text{K}$  for a 10 dB noise figure receiver and a  $290^{\circ}\text{K}$  reference temperature. The resulting worst-case performance margins were found to be 49.2 dB for the carrier and 47.3 dB for command. The command performance margin was calculated for a command bit error rate of  $10^{-6}$ .

##### b. S-Band Downlink

Table 5-4 presents the link calculations which were performed for the S-band telemetry link. The calculation was performed at 2226.2 MHz for two telemetry modes. In Mode 1, 32 kbps real-time housekeeping and computer memory dump data is transmitted along with 512 kbps medium rate user data. In Mode 2, the 32 kbps real-time data is transmitted with tone ranging data.

Table 5-3. Command Uplink Power Budget

Parameter	Nominal Value	Adverse Tolerance	Notes
1) Modulation format	PCM/PSK/ FM/PM	---	---
2) Frequency (MHz)	2050.0	0.0	---
3) Ground station transmitter power (dBm)	60.0	0.0	1 kw; "Spaceflight Tracking and Data Network User's Guide," STDN 101.1, p. 3-4
4) Ground station transmission losses (dB)	0.0	0.0	Assumed included in antenna gain
5) Ground station antenna gain (dB)	43.0	0.0	9 meter dish; RCP/LCP STDN User's Guide, STDN 101.1, p. 3-9
6) Polarization loss (dB)	0.0	0.0	Assumed included in antenna gain
7) Atmospheric attenuation at 5° elevation angle (dB)	0.3	0.1	Hogg and Mumford, "The Effective Noise Temperature of the Sky," The Microwave Journal, March 1960, p. 80
8) Space loss at 5° antenna elevation angle and 2590 km slant range (dB)	166.9	0.0	716 km circular orbit
9) Spacecraft antenna gain (dBi)	-3.0	0.0	95% spherical coverage
10) Spacecraft reception losses (dB)	5.1	0.2	Cabling = 0.3 dB Diplexer = 1.5 dB Hybrid combiner = 3.2 dB
11) Total received power at input to receiver (dBm)	-65.1	0.3	---
12) Spacecraft equivalent noise temperature referred to receiver input (°K)	2900.0	0.0	Assumes a spacecraft antenna temperature of 290°K with a noise figure of 10 dB referred to receiver input

Table 5-3. Command Uplink Power Budget (Continued)

Parameter		Nominal Value	Adverse Tolerance	Notes
13)	Spacecraft reception system noise power spectral density (dBm/Hz)	-164.0	0.0	---
14)	Received power to noise spectral density ratio (dB-Hz)	91.7	0.3	---
<u>CARRIER PERFORMANCE</u>				
15)	Carrier modulation loss (dB)	4.3	1.0	Assumes 70 kHz command and subcarrier is phase-modulated onto the carrier at $1.2 \pm 10\%$ radian simultaneously with tone ranging data at $0.6 \pm 10\%$ radian.
16)	Received carrier to noise spectral density ratio (dB-Hz)	87.4	1.3	---
17)	Carrier loop noise bandwidth (dB-Hz)	29.0	0.0	$2 B_{LO} = 800 \text{ Hz}$
18)	Carrier to noise ratio (dB)	58.4	1.2	---
19)	Carrier loop threshold (dB)	6.0	2.0	---
20)	Carrier performance margin (dB)	52.4	3.2	---
21)	Carrier performance margin less adverse tolerance (dB)	49.2	---	---
<u>COMMAND PERFORMANCE (70 kHz SUBCARRIER)</u>				
22)	Command subcarrier modulation loss (dB)	3.8	0.5	See note under Item 15
23)	Received subcarrier power to noise spectral density ratio (dB-Hz)	87.9	0.8	---

Table 5-3. Command Uplink Power Budget (Continued)

Parameter		Nominal Value	Adverse Tolerance	Notes
24)	Discriminator FM improvement factor (dB)	6.7	0.0	$3\beta^2$ . Assumes that command PSK data frequency modulates 70 kHz subcarrier with a modulation index of 1.25
25)	Post-detection signal to noise spectral density ratio (dB-Hz)	94.6	0.0	---
26)	Detection noise bandwidth (dB-Hz)	33.0	0.0	2 kHz for 2 kbps data
27)	Command data energy to noise spectral density ratio (dB)	61.6	0.8	---
28)	Theoretical energy to noise spectral density ratio required for BER = $10^{-6}$ (dB)	10.5	0.0	Coherent PSK detection
29)	Degradation due to non-optimum detection (dB)	2.0	1.0	Assumed value
30)	Command performance margin (dB)	49.1	1.8	---
31)	Command performance margin less adverse tolerance (dB)	47.3	---	---



Table 5-4. Telemetry Downlink Power Budget

Parameter	Nominal Value	Adverse Tolerance	Notes
1) Modulation format	PCM/PSK, SPLIT-PHASE/PM	---	---
2) Frequency (MHz)	2226.2	0.0	---
3) Spacecraft Transmitter power (dBm)	33.0	0.0	2.0 watts
4) Spacecraft transmission losses (dB)	1.8	0.2	Cabling = 0.3 dB RF transfer switch = 0.3 dB Diplexer = 1.2 dB
5) Spacecraft antenna gain (dBi)	-3.0	0.0	95% spherical coverage
6) Space loss at 5° elevation angle and 2590 km slant range (dB)	167.6	0.0	716 km circular orbit
7) Atmospheric attenuation at 5° elevation angle (dB)	0.3	0.1	Hogg and Mumford, "The Effective Noise Temperature of the Sky," The Microwave Journal, March 1960, p. 80
8) Polarization loss (dB)	0.0	0.0	Assumed included in antenna gain
9) Ground station antenna gain (dB)	44.0	0.0	9 m dish. "Spaceflight Tracking and Data Network User's Guide," STDN-101.1, p. 3-9
10) Total received power (dBm)	-95.7	0.3	---
11) Ground station system noise temperature (°K)	166.0	0.0	Assumes a 150°K parametric amplifier noise temperature at zenith plus 16°K antenna temperature contribution at 5° elevation
12) Ground station system noise spectral density (dBm/Hz)	-176.4	0.0	---

Table 5-4. Telemetry Downlink Power Budget (Continued)

Parameter	Nominal Value	Adverse Tolerance	Notes
13) Received power to noise spectral density ratio (dB-Hz)	80.7	0.3	---
Mode 1: 32 kbps Housekeeping and Computer Dump Data Plus 512 kbps Medium Data Rate User Telemetry			
<u>CARRIER PERFORMANCE</u>			
14) Carrier modulation loss (dB)	8.3	2.5	Assumes 32 kbps housekeeping and computer dump data split-phase modulates the 1.024 MHz subcarrier which in turn, phase modulates the carrier at $0.8 \pm 10\%$ radian. The 512 kbps data directly phase modulates the carrier at $1.1 \pm 10\%$ radian.
15) Received carrier power to noise spectral density ratio (dB-Hz)	72.4	2.8	---
16) Carrier loop noise bandwidth (dB-Hz)	27.8	0.0	$2 B_{LO} = 600 \text{ Hz}$
17) Carrier to noise ratio (dB)	44.6	2.8	---
18) Carrier loop threshold (dB)	6.0	2.0	Assumed tolerance
19) Carrier performance margin (dB)	38.6	4.8	---
20) Carrier performance margin less adverse tolerance (dB)	33.8	---	---
<u>32 kbps HOUSEKEEPING PLUS COMPUTER DUMP TELEMETRY PERFORMANCE</u>			
21) 1.024 MHz subcarrier modulation loss (dB)	12.5	3.0	See note under Item 14
22) Received data power to noise spectral density ratio (dB-Hz)	68.2	3.3	---

C-4

Table 5-4. Telemetry Downlink Power Budget (Continued)

	Parameter	Nominal Value	Adverse Tolerance	Notes
23)	Detection bandwidth equivalent to bit rate (dB-Hz)	45.1	0.0	32 kHz for 32 kbps
24)	Received data energy to noise spectral density ratio (dB)	23.1	3.3	---
25)	Theoretical energy to noise spectral density ratio required for $10^{-6}$ BER (dB)	10.5	0.0	Optimum detection of PSK
26)	Degradation due to non-optimum detection (dB)	1.0	1.0	"Specification for a Manned Spaceflight MSTFP-3 PCM Decommutator System," NASA/GSFC, June 16, 1970, GSFC-S-8121P135, p. 6. Assumed tolerance
27)	32 kbps telemetry performance margin (dB)	11.6	4.3	---
28)	32 kbps telemetry performance margin less adverse tolerance (dB)	7.3	---	---

512 kbps MEDIUM RATE USER TELEMETRY PERFORMANCE

29)	512 kbps data modulation loss (dB)	2.5	0.9	See note under Item 14
30)	Received data power to noise spectral density ratio (dB-Hz)	77.2	1.2	---
31)	Detection bandwidth equivalent to bit rate (dB-Hz)	57.1	0.0	512 kHz for 512 kbps
32)	Received data energy to noise spectral density ratio (dB)	22.1	1.2	---

Table 5-4. Telemetry Downlink Power Budget (Continued)

Parameter	Nominal Value	Adverse Tolerance	Notes
33) Theoretical energy to noise spectral density ratio required for $10^{-6}$ BER (dB)	10.5	0.0	Optimum detection of PSK
34) Degradation due to non-optimum detection (dB)	1.0	1.0	See note under Item 26
35) 512 kbps telemetry performance margin (dB)	10.6	2.2	---
36) 512 kbps telemetry performance margin less adverse tolerance (dB)	8.4	---	---

Mode 2. 32 kbps Housekeeping and Computer  
Dump Data Plus 500 kHz Tone Turn-  
Around Ranging

#### CARRIER PERFORMANCE

37) Carrier modulation loss (dB)	5.0	1.1	Assumes 32 kbps telemetry data split-phase modulates the 1.024 MHz subcarrier which in turn, phase modulates the carrier at $1.3 \pm 10\%$ radian. The 500 kHz range tone phase modulates the carrier at $0.9 \pm 10\%$ radians
38) Received carrier power to noise spectral density ratio (dB-Hz)	75.7	1.4	---
39) Carrier loop noise bandwidth (dB-Hz)	27.8	0.0	$2 B_{LO} = 600 \text{ Hz}$
40) Carrier to noise ratio (dB)	47.9	1.4	---
41) Carrier loop threshold (dB)	6.0	2.0	Assumed
42) Carrier performance margin (dB)	41.9	-3.4	---

Table 5-4. Telemetry Downlink Power Budget (Continued)

Parameter	Nominal Value	Adverse Tolerance	Notes
43) Carrier performance margin less adverse tolerance (dB)	38.5	---	---
<u>32 kbps HOUSEKEEPING PLUS COMPUTER DUMP TELEMETRY DATA</u>			
44) 1.024 MHz subcarrier modulation loss (dB)	2.3	0.5	See note under Item 37
45) Received data power to noise spectral density ratio (dB-Hz)	78.4	0.8	---
46) Detection bandwidth equivalent to bit rate (dB-Hz)	45.1	0.0	32 kHz for 32 kbps
47) Received data energy to noise spectral density ratio (dB)	33.3	0.8	---
48) Theoretical energy to noise spectral density ratio required for $10^{-6}$ BER (dB)	10.5	0.0	Optimum detection of PSK
49) Degradation due to non-optimum detection (dB)	1.0	1.0	See note under Item 26
50) 32 kbps telemetry performance margin (dB)	21.8	1.8	---
51) 32 kbps telemetry performance margin less adverse tolerance (dB)	20.0	---	---
<u>500 kHz (GRARR) RANGING PERFORMANCE</u>			
52) 500 kHz tone modulation loss (dB)	28.0	2.2	See note under Item 26
53) Received 500 kHz tone signal to noise spectral density ratio (dB)	52.7	2.4	---

Table 5-4. Telemetry Downlink Power Budget (Continued)

	Parameter	Nominal Value	Adverse Tolerance	Notes
54)	Signal to noise ratio required for 5 meter RMS error due to thermal noise (dB)	32.0	0.0	1 Hz bandwidth
55)	500 kHz tone ranging performance (dB)	20.7	-2.4	---
56)	500 kHz tone ranging performance less adverse tolerance (dB)	18.3	---	---

As seen from the table, a 2-watt transmitter is sufficient to telemeter the information in both modes to the ground station. In the calculation, the transmitter omni antenna minimum gain was taken as -3.0 dBi over 95 percent of the coverage sphere.

For Mode 1, the performance margin for the 32 kbps real-time telemetry was found to be 7.3 dB under adverse conditions. The 512 kbps medium rate user performance is 8.4 dB and the carrier performance is 33.8 dB.

For Mode 2, the performance margin for the 32 kbps real-time telemetry is 20.0 dB, and the carrier performance is 38.5 dB. The ranging performance as indicated in Table 5-4 was found to be 20.7 dB under nominal conditions and 18.3 dB under adverse conditions. The performance margin was calculated for a ranging signal having a maximum frequency of 500 kHz. The performance threshold signal-to-noise ratio was taken as 32 dB, which corresponds to an error due to thermal noise of 5 meters, rms.

In Table 5-4, the calculations were performed using optimized carrier phase modulation indices.

c. Probability of False Command Execution and Valid Command Rejection

This section is concerned with the calculation of the probability of false command execution and valid command rejection.

The command word format for EOS is shown in Figure 5-9. The initial bit of the command word is a logical "1." Following this is a 7-bit spacecraft address. The next 13 bits are used within the data handling system to route the command data represented by the next 16 bits. Finally, the last 7 bits of the command word contains a polynomial check code which is a check on the previous 29 bits.

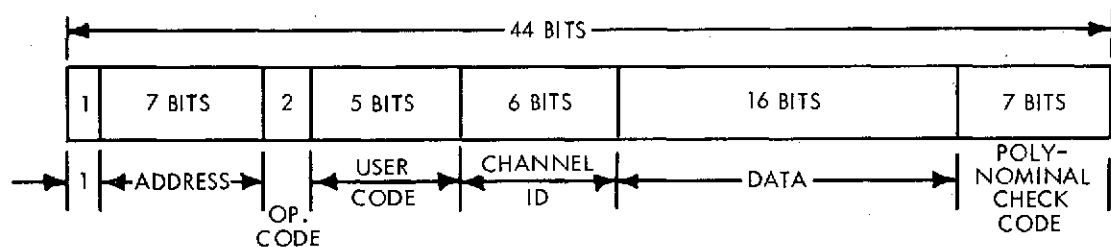


Figure 5-9. EOS Command Word Format

The command demodulator/decoder unit checks the incoming command word for an initial logical "1." Following this, it checks for a valid spacecraft address. Finally, it checks the next 29 bits with respect to the 7-bit polynomial check code. An erroneously received command will be executed and cause an undetected error if, and only if, all verifications have been performed successfully and an error in the next 29 bits goes undetected with respect to the polynomial check code.

A code word of length  $n$  containing  $k$  information bits has a rate  $R$  given by

$$R = \frac{k}{n} \quad (1)$$

Furthermore, if the Hamming distance between code words is  $d + 1$ , an error detecting code can detect  $d$  or less errors, since no pattern of  $d$  errors can alter one code word into another.

The Hamming or sphere-packing code bound provides a relationship which bounds the minimum distance for the best code as a function of the code rate  $R$ . If the assumption is made that the check code is only on the 29 bits following the address portion, the code rate is then

$$R = \frac{29}{36} = 0.81 \quad (2)$$

From Peterson,\* for a code rate of 0.81, the Hamming upper bound gives the minimum distance between code words as

$$d = 0.12 n = 4.3 \text{ bits} \quad (3)$$

Therefore, accepting the Hamming bound as a means for determining the minimum distance between code words, the minimum distance between any two command words is then 4 bits, and the polynomial check code will detect three errors or less. That is, all code words having three errors or less will be rejected.

The probability that a command error will go undetected and executed is then the probability that the first 8 bits of the command are correct and no more than three errors exist in the succeeding 29 bits, given that the polynomial check bits are also correct. That is,

$$P\left(\begin{array}{c} \text{false command} \\ \text{execution} \end{array}\right) = (1 - p)^{15} \sum_{i=4}^{29} \binom{29}{i} p^i (1 - p)^{29-i} \quad (4)$$

where  $p$  is the probability of a bit error.

From the command uplink power budget, Table 5-3,  $p = 10^{-6}$  with a 47.3 dB margin for a receiver input of -65.1 dBm. For small values of  $p$ , the following approximation can be used:

$$(1 - p)^n \approx 1 - np, \quad p \ll 1 \quad (5)$$

Then,

---

\* W. Wesley Peterson, "Error Correcting Codes," The M. I. T. Press, p. 50, 1961.



P (false command execution)

$$\begin{aligned}
 &\cong (1 - 15p) \left[ \binom{29}{4} p^4 (1 - 25p) + \binom{29}{5} p^5 (1 - 24p) + \dots \right] \quad (6) \\
 &\cong (1 - 15P) \left[ 2.38 \times 10^4 (10^{-24}) + 1.19 \times 10^5 (10^{-30}) + \dots \right] \\
 &\cong 2.4 \times 10^{-20}
 \end{aligned}$$

The probability of rejecting a good command is equal to the probability that all command bits are received correctly and the 7-bit polynomial check code is in error. That is,

P (good command rejection)

$$\begin{aligned}
 &= (1 - p)^{37} \left[ \sum_{i=1}^7 \binom{7}{i} p^i (1 - p)^{7-i} \right] \quad (7) \\
 &\cong (1 - 37p) \left[ \binom{7}{1} p (1 - p)^6 + \binom{7}{2} p^2 (1 - p)^5 + \dots \right] \\
 &\cong 7p = 7 \times 10^{-6}
 \end{aligned}$$

Since the uplink margin of 47.3 dB ( $10^{-6}$  BER) for an input signal level into the receiver of -65.1 dBm, the probability of a false command execution is then  $2.4 \times 10^{-20}$  and the probability of a good command being rejected is  $7 \times 10^{-6}$  for input levels of -112.4 dBm and above.

#### 5.1.1.5 EOS-A Baseline Systems Requirements Summary

Based upon the previous discussion, minimum systems requirements can be established for the EOS-A baseline communications design.

##### Antenna Coverage and Gain

Antenna Coverage:	95 percent spherical
Antenna Gain:	-3.0 dBi minimum
Antenna Polarization:	RHCP and LHCP operated in polarization diversity

##### S-Band Receiver

Carrier Frequency:	2050 to 2150 MHz range
Noise Figure:	10 dB, maximum
Carrier Modulation:	PCM/PSK/FM/PM
Carrier Data:	2 kbps split phase command data plus 500 kHz maximum tone ranging
Coherency Ratio:	221/240
Baseband Outputs:	70 kHz FM subcarrier output to data handling demodulator/decoder unit; 500 kHz maximum tone ranging output to data handling baseband assembly unit
RF Outputs:	Coherent reference output to transmitter

##### S-Band Transmitter

Carrier Frequency:	2200 to 2300 MHz range
RF Output Power:	2 watts, minimum
Carrier Modulation:	PCM/PSK/PM
Carrier Data:	Mode 1: 32 kbps real-time telemetry on 1.024 MHz subcarrier plus 512 kbps direct medium rate data Mode 2: 32 kbps real-time telemetry on 1.024 MHz subcarrier plus 500 kHz tone ranging data
RF Input:	Coherent reference input from S-band receiver

##### S-Band Diplexer

Reception Frequency:	2050 to 2150 MHz
Transmission Frequency:	2200 to 2300 MHz
Insertion Loss:	
Reception:	1.5 dB maximum
Transmission:	1.2 dB maximum

#### 5.1.1.6 Impact of Future Missions

The EOS-A baseline communications system was established for a maximum, real-time telemetry data rate of 32 kbps; a maximum medium data rate of 512 kbps; and a maximum uplink data rate of 2 kbps. Since these rates represent the maximum requirements for the spacecraft, the communications system design is essentially independent of post-EOS-A mission requirements for those programs which have nearly the same altitude as EOS-A. Table 5-5 shows the impact of altitude on the communications system. In general, the EOS-A baseline design can provide more than adequate performance for those missions having an orbit altitude of 1810 km (975 nmi) or less. Synchronous missions such as SEOS, requires that an earth coverage, fixed mounted, 2-foot antenna be mounted on the module for operation with the EOS-A baseline 2-watt S-band transmitter. Table 5-6 lists post-EOS-A missions as well as required design modifications to the baseline design. Figure 5-10 shows the system block diagram for synchronous operation. The weight impact of the 2-foot antenna and associated RF switch is 2.5 pounds. Presumably, the spacecraft would be operated at a low data rate capable of being supported by an omni-antenna until the spacecraft is properly positioned in synchronous orbit. After this, telemetry would be transmitted via the 2-foot antenna.

Table 5-5. Impact of Orbit Altitude on Communication System

Orbit altitude (km)	716	1810	3796	36,041
5-deg slant range (km)	2590	4602	7276	41,384
Downlink (2226.2 MHz)				
RF path loss (dB)	167.6	171.9	176.6	191.7
Transmitter power (w)	2.0	2.0	2.0	2.0
Antenna type	omni	omni	omni	omni
Antenna diameter (ft)	--	--	--	--
Antenna gain (dB)	-3.0	-3.0	+1.7	20.5
Antenna beamwidth (deg)	220	220	80.0	17.0
<u>Mode 1 performance</u>				
• Carrier (dB)	33.8	29.5	29.5	32.2
• 32 kbit/sec telemetry (dB)	7.3	3.0	3.0	5.7
• 512 kbit/sec telemetry (dB)	8.4	4.1	4.1	6.8
<u>Mode 2 performance</u>				
• Carrier (dB)	41.9	37.6	37.6	40.3
• 32 kbit/sec telemetry (dB)	20.0	15.7	15.7	18.4
• 500 KHz ranging (dB)	18.3	14.0	14.0	16.7
Uplink (2050.0 MHz)				
RF path loss (dB)	166.9	171.2	175.9	189.8
Antenna type	omni	omni	omni	omni
Antenna gain (dBi)	-3.0	-3.0	-3.0	-3.0
<u>Performance</u>				
Carrier (dB)	49.2	47.1	42.4	28.5
Command (dB)	47.3	45.2	40.5	26.6

Table 5-6. Post EOS-A Missions and Design Impacts  
Using 2-Watt Transmitter and Omni  
Uplink Antenna

Mission	Orbit Altitude (km)	Downlink Antenna	Weight Impact	Power Impact
EOS-B	556	Omni	None	None
EOS-C	1300 - 1850	↑	↑	↑
EOS-A'	890 - 925	↓	↓	↓
EOS-B'	556	↓	↓	↓
EOS-C'	1300 - 1850	Omni	None	↓
SEOS	36,041	2-ft dish	2.5 lbs	↓
SEASAT-A	725	Omni	None	↓
Solar Max Mission	556	↑	↑	↓
Gap Filler (5-Band MSS)	861	↓	↓	↓
SEASAT B	723	↓	↓	↓
Advanced SMM	556	Omni	None	None

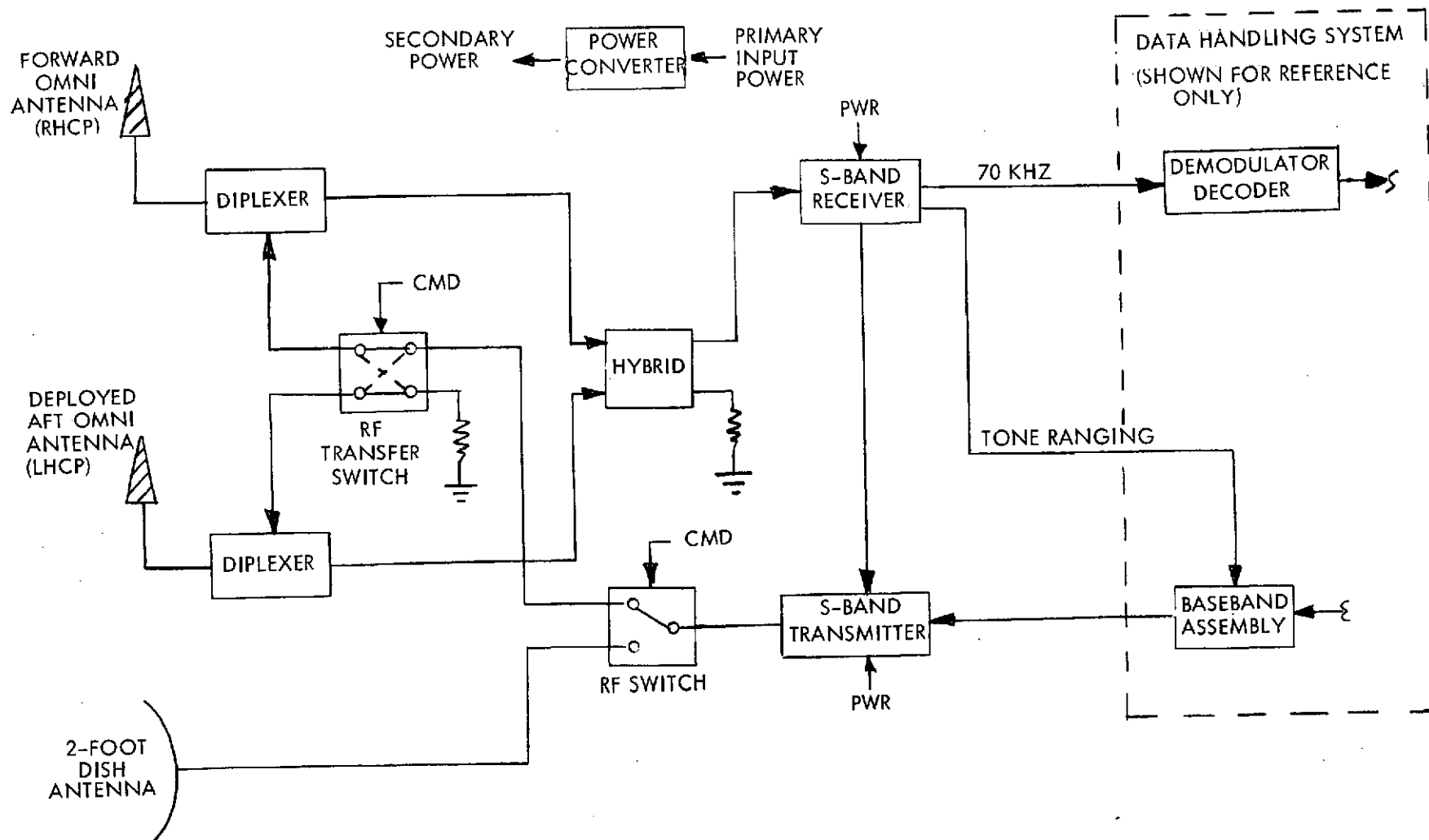


Figure 5-10. Modification of EOS-A Baseline Design for Synchronous Operation

#### 5.1.1.7 Conclusions

The EOS-A baseline design presented herein offers sufficient flexibility and performance capability to accommodate a wide range of EOS missions with no modification to the basic design. The use of omni-directional antennas operated in polarization diversity (or address) with a 2-watt S-band transmitter provides more than adequate uplink performance and adequate downlink performance. Furthermore, the design is sufficiently flexible to allow the installation of redundant equipment for higher reliability and synchronous orbit operation with little or no impact to the baseline design.

## 1.2 Polarization Diversity Systems for EOS

Increased antenna coverage can be obtained with the EOS spacecraft by using diversity receiving and transmitting system. Also, the active redundancy used in diversity systems increases the reliability since no single point failure can jeopardize the mission. Simple antennas can be used on the spacecraft and their outputs can be electronically combined for reception. The antennas are arrayed for transmission, but their emissions do not interfere since the diversity states are orthogonal. No mechanically moving parts are required and antenna blockage of the spacecraft is reduced by using diversity. Transponders can be arrayed similarly in redundant configurations.

The principles of diversity combining are well known.<sup>1</sup> Diversity systems have been in common use in radio communication since 1927<sup>2</sup> and have proven advantages for communication when the channel states are either uncorrelated or anticorrelated.<sup>3</sup> If the designer can be reasonably sure that the channel states selected for the diversity system do not simultaneously fade on a regular basis, then an overall improvement in reliability results from combining the channel outputs after suitable signal processing.<sup>4,5</sup>

Two diversity types are appropriate to the EOS spacecraft. These are frequency diversity and polarization diversity. Simple arraying of identical antennas at the same frequency is unsatisfactory because the antennas must be located on opposite sides of the spacecraft to avoid blockage. This separation of (typically) many wavelengths causes an interferometer pattern with a large number of nulls in the region of mutual visibility. (The number of interferometer nulls in one angular quadrant is equal to the number of wavelengths between a pair of antennas). Frequency diversity assigns nonoverlapping frequency channels to each antenna. This eliminates the interferometer effect since electromagnetic waves of different frequencies are uncorrelated. The main disadvantage of this method is the additional bandwidth required for the second channel. This is hard to justify if the spacecraft has primarily an earth-pointing mission and the additional antenna coverage is a contingency requirement. Polarization diversity has the advantage that all missions occur in a single frequency channel. Careful antenna design and placement



on the spacecraft is required to assure orthogonal polarization states, but if this is accomplished, the antennas can be addressed individually by the appropriate polarization state and their emissions will not produce interferometer nulls when received by a matched aperture. A matched aperture is achieved by diversity combining the outputs of co-located orthogonally polarized antennas; i.e., right circular and left circular, or horizontal and vertical polarization. This is commonly done in STDN by amplitude weighting based on signal strengths and phasing of the outputs of each receiving antenna before predetection summing.<sup>6</sup> Post detection summing and selection of the stronger signal are two other methods which are also used.

Because of the advantage of a 2:1 saving in bandwidth the polarization diversity system is strongly favored over frequency diversity, and will be discussed further, below. A brief review of polarization diversity theory is followed by a discussion of some relevant STDN system requirements and capabilities. Some of the problems in conforming to these requirements are discussed and possible solutions are offered in several levels of complexity. Qualitative tradeoffs are discussed.

#### 5.1.2.1 Polarization Diversity Theory

A propagating TEM wave is a time-varying vector process. Since the magnetic field is uniquely determined by a knowledge of the electric field, only the properties of the electric field are described. The horizontal and vertical electric field components are not usually independent, but have a definite time-phase relationship, or coherence, which can be interpreted by describing the orientation and length of the electric vector as the wave propagates. The locus of points described by the tip of the electric field vector, projected onto a plane normal to the direction of propagation is an ellipse, as shown in Figure 5-11. The axes of the polarization ellipse do not, in general, coincide with the x and y axes. Several descriptive parameters are used to define the polarization ellipse. The line segment OA is the semimajor axis, and the line segment OB is the semiminor axis.

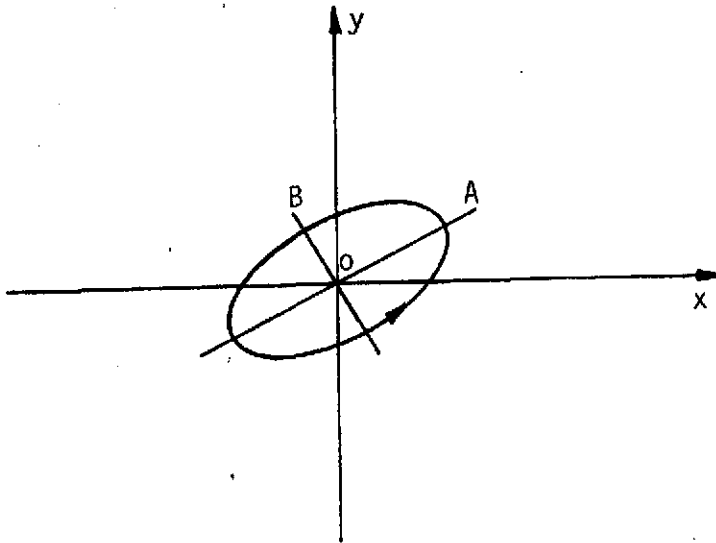


Figure 5-11. Polarization Ellipse

The ratio  $OA/OB$  is the axial ratio (AR). The tilt angle  $\tau$  describes the major axis orientation relative to the reference axis. Linear polarization occurs when the semiminor axis has length, zero. Circular polarization occurs when the axial ratio is unity ( $AR=1$ ). The chirality, or "handedness" describes the sense of rotation of the electric field vector in time sequence as the wave propagates through a plane normal to the direction of propagation. Right-hand circular polarization is conveniently remembered by the right hand rule: with the right-hand closed in a fist with thumb extended, the thumb points in the direction of propagation and the fingers points in the sense of rotation of the electric field vector.

Elliptically polarized waves can be decomposed into the sum of two circularly polarized waves. If the amplitudes are equal, linear polarization results. The orientation is determined by the relative phasing. The chirality of an elliptically polarized wave is that of the dominant circular component. Another decomposition makes use of vertically and horizontally polarized waves.

The polarization coherency matrix is a simple  $2 \times 2$  matrix whose elements are the covariances of the linear components of a polarized wave, defined as shown in Equations (1).

$$\begin{aligned}
[J] &= \left\langle \begin{bmatrix} E_h \\ E_v \end{bmatrix} \begin{bmatrix} E_h^* & E_v^* \end{bmatrix} \right\rangle \\
&= \begin{bmatrix} \langle E_h E_h^* \rangle & \langle E_h E_v^* \rangle \\ \langle E_v E_h^* \rangle & \langle E_v E_v^* \rangle \end{bmatrix} \\
&= \begin{bmatrix} J_{11} & J_{12} \\ J_{21} & J_{22} \end{bmatrix}
\end{aligned} \tag{1}$$

The symbol  $\langle \dots \rangle$  implies a time-average. The polarization properties of an aperture can similarly be described by a coherency matrix

$$[A] = A_e \begin{bmatrix} a_{11} & a_{12} \\ a_{21} & a_{22} \end{bmatrix} \tag{2}$$

where  $A_e$  is the effective aperture in the given direction. The elements of the coherency matrix are determined from power measurements using three pairs of antennas. Two dipoles at right angles yield power measurements  $W_x$  and  $W_y$ ; two more measurements  $W'_x$  and  $W'_y$  are obtained by rotating the dipoles  $45^\circ$ ; and two helical beam (circularly-polarized) antennas of left and right-hand sense produce power measurements  $W_L$  and  $W_R$ . The normalized coherency matrix  $[a_{ij}]$  is given by

$$[a_{ij}] = \frac{1}{W_x + W_y} \begin{bmatrix} W_x & \frac{1}{2} (W'_x - W'_y + jW_L - jW_R) \\ \frac{1}{2} (W'_x - W'_y - jW_L + jW_R) & W_y \end{bmatrix} \tag{3}$$

The power available to an antenna from a wave of arbitrary polarization is given by

$$W = \text{Tr} \{ [A] [J] \} \quad (4)$$

where  $\text{Tr}\{\dots\}$  denotes the trace; i.e., the sum of the diagonal elements for a square matrix, or

$$W = A_e (a_{11} J_{11} + a_{12} J_{12} + a_{21} J_{21} + a_{22} J_{22}) \quad (5)$$

The aperture coherency matrix can be factored as follows.

$$[A] = [E] [E]^*{}^T \quad (6)$$

where

$$[E] = \begin{bmatrix} E_h \\ E_v \end{bmatrix} \quad (7)$$

Then the output power can be written as a Hermitian form

$$W = (E, JE) \quad (8)$$

or

$$W = [E]^*{}^T [J] [E] \quad (9)$$

This form is called a Hermitian form because the matrix  $[J]$  satisfies the condition of Hermiticity; i.e.

$$[J]^*{}^T = [J]. \quad (10)$$

Define the effective aperture  $A_e$  as the output power when receiving an unpolarized wave of total power, 2; i.e.,

$$A_e = [E]^*{}^T [E] \quad (11)$$

The efficiency with which a receiving aperture processes a given polarized wave is measured by the ratio of the output power to the effective aperture; i.e.,

$$\frac{W}{A_e} = \frac{[E]^*{}^T [J] [E]}{[E]^*{}^T [E]} \quad (12)$$

The method of Lagrange multipliers can be used to optimize this ratio, by maximizing the output power subject to a fixed effective aperture. Form the function

$$H([E]) = [E]^*{}^T [J] [E] + \lambda (1 - [E]^*{}^T [E]) \quad (13)$$

A necessary condition for the extremum values of  $H$  is that  $[E]$  satisfy the eigenvalue problem

$$([J] - \lambda[I]) [E] = 0, \quad (14)$$

where  $I$  is the identity matrix and  $\lambda$  is the eigenvalue parameter. Only certain values of  $\lambda$  will satisfy this equation. These values satisfy the determinantal equation

$$\det ([J] - \lambda[I]) = 0. \quad (15)$$

Since  $[J]$  is a  $2 \times 2$  matrix, there are only two eigenvalue solutions. The eigenvalues are real and, in general, unequal. The two eigenvalues are the maximum and minimum values of the ratio in Equation (12). The  $[E]$  vectors which satisfy equation (14) for each value of  $\lambda$  are called the eigenfunctions. The eigenfunctions

corresponding to different eigenvalues are orthogonal to each other. This means that there exist pairs of polarized waves such that an aperture, synthesized to maximize the ratio  $W/A_e$  in Equation (12) for one member of the pair, gives zero response to the other. This is illustrated by the following example.

It is convenient to choose LCP and RCP waves as a basis. Then, the general elliptically polarized wave is synthesized as the sum of a left circularly polarized wave of rms complex amplitude A and a right circularly polarized wave of rms complex amplitude B. The  $[E]$  matrix of this wave is

$$[E] = \begin{bmatrix} E_{LCP} \\ E_{RCP} \end{bmatrix} = \begin{bmatrix} A \\ B \end{bmatrix} = \frac{1}{\sqrt{2}} \begin{bmatrix} E_h + j E_v \\ E_h - j E_v \end{bmatrix} \quad (16)$$

and the polarization coherency matrix is

$$[J] = [E] [E]^*{}^T = \begin{bmatrix} AA^* & AB^* \\ BA^* & BB^* \end{bmatrix} \quad (17)$$

The eigenvalues are

$$\lambda_{\max} = |A|^2 + |B|^2 \quad (18)$$

and

$$\lambda_{\min} = 0$$

as stated above,

corresponding to the eigenfunctions

$$[E]_{\max} = \frac{1}{\sqrt{|A|^2 + |B|^2}} \begin{bmatrix} A \\ B \end{bmatrix}, \quad (20)$$

and

$$[E]_{\min} = \frac{1}{\sqrt{|A|^2 + |B|^2}} \begin{bmatrix} B \\ A \end{bmatrix}. \quad (21)$$

Thus,  $[E]_{\max}$  and  $[E]_{\min}$  are orthogonal for the general elliptically polarized wave.

The "matched" aperture can be realized as shown in Figure 5-12, using LCP and RCP antennas, weighted by the conjugates of the complex gains in Equation (20), above.

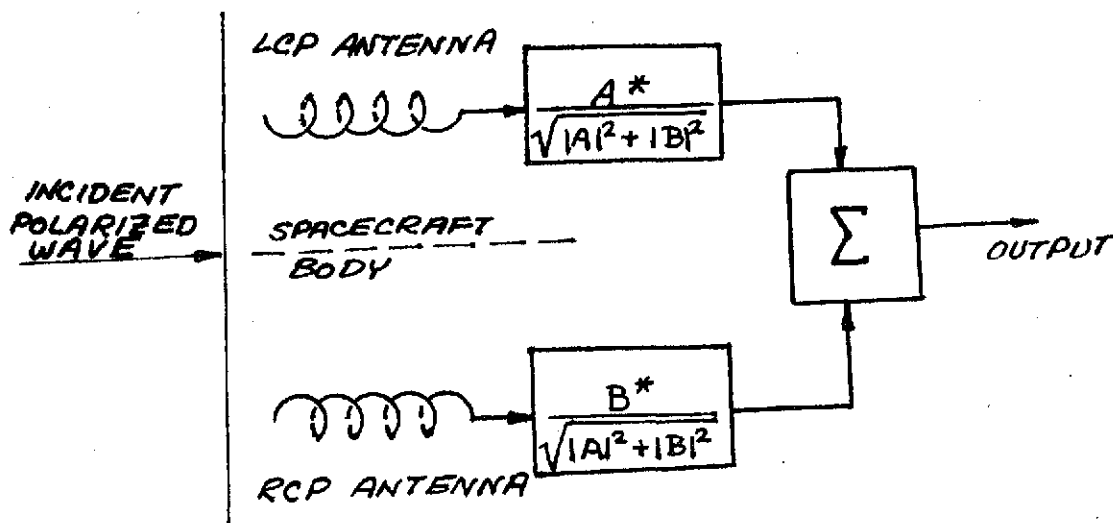


Figure 5-12. Polarized Receiving Aperture Synthesis.

The maximal ratio combining rule is based on the above results. Optimum use of the available antenna effective aperture is achieved by weighting the basis antenna outputs with complex gains having phase angles conjugate to, and amplitudes proportional to the amplitudes of, the respective components in the received wave. This requires that the respective components be estimated and used to control the complex gains before summing.

The implementation complexity of the combiner also means that reliability of the amplitude weighting and phasing units will be expensive to obtain. Also, in the spacecraft application, if one antenna is earth-pointing and the other is occulted by the spacecraft, the reliability of the receiver connected to the earth-pointing antenna becomes critical, since it represents a single-point failure threat. It is necessary to consider optional designs which incorporate redundancy.

The eigenvalues of the polarization coherency matrix are invariant under a unitary transformation. This means that we can perform a transformation on the basis antenna outputs which increases the reliability without losing the diversity advantage under normal conditions. A unitary matrix  $U$  has the property that

$$U^*{}^T U = I . \quad (22)$$

This property is shared by both of the transformations below, which describe the  $180^\circ$  hybrid and the  $90^\circ$  hybrid, respectively.

$$\frac{1}{\sqrt{2}} \begin{bmatrix} 1 & 1 \\ 1 & -1 \end{bmatrix} , \quad (23)$$

and

$$\frac{1}{\sqrt{2}} \begin{bmatrix} 1 & 1 \\ j & -j \end{bmatrix} . \quad (24)$$



The maximal ratio combining rule can be applied to the outputs of a hybrid whose inputs are the responses of the basis antennas. The resulting polarization coherency matrix is illustrated in Equation (25) for the case of a 180° hybrid.

$$[\underline{J}'] = \begin{bmatrix} \frac{|A+B|^2}{2} & \frac{|A|^2 - |B|^2 + A^*B - B^*A}{2} \\ \frac{|A|^2 - |B|^2 + AB^* - A^*B}{2} & \frac{|A-B|^2}{2} \end{bmatrix} \quad (25)$$

This still represents a general elliptically polarized wave, and the eigenvalues are given by Equations (18) and (19), corresponding to the eigenfunctions,

$$\begin{aligned} [\underline{E}]_{\max} &= \frac{1}{\sqrt{2} \sqrt{|A|^2 + |B|^2}} \begin{bmatrix} 1 & 1 \\ 1 & -1 \end{bmatrix} \begin{bmatrix} A \\ B \end{bmatrix} \\ &= \frac{1}{\sqrt{2} \sqrt{|A|^2 + |B|^2}} \begin{bmatrix} A + B \\ A - B \end{bmatrix} \end{aligned} \quad (26)$$

and

$$\begin{aligned} [\underline{E}]_{\min} &= \frac{1}{\sqrt{2} \sqrt{|A|^2 + |B|^2}} \begin{bmatrix} 1 & 1 \\ 1 & -1 \end{bmatrix} \begin{bmatrix} B \\ A \end{bmatrix} \\ &= \frac{1}{\sqrt{2} \sqrt{|A|^2 + |B|^2}} \begin{bmatrix} A + B \\ B - A \end{bmatrix} \end{aligned} \quad (27)$$

The implementation of this scheme is shown in Figure 5-13, below. The improved reliability of this arrangement can be seen by noting that if the

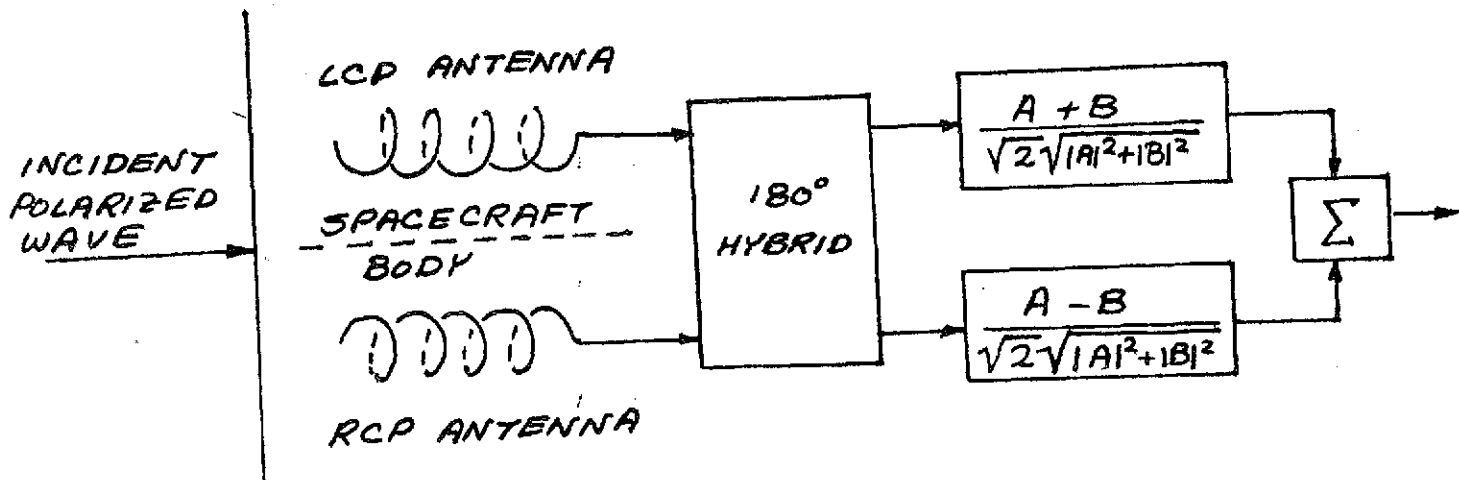


Figure 5-13. Improved Polarized Receiving Aperture Synthesis.

spacecraft is addressed by an LCP wave, half of the power appears at each output of the hybrid. If either receiver is functioning, commands can be received. If the LCP antenna is not visible, the RCP antenna can be addressed by an RCP wave from the ground and power is again divided between the two receivers. Assuming that the spacecraft can not be reoriented without receiving a command, and letting the receiver reliabilities be equal to  $p$ , the reliability of the system in Figure 5-12 is just  $R=p$  while the system of Figure 5-13 has a reliability of

$$R' = 2p - p^2. \quad (25)$$

For example, if  $p = 0.9$ ,  $R' = 0.99$ .

Arrays of circularly polarized antennas have properties which are important to polarization diversity systems for spacecraft. Transmission on the downlink will likely use both antennas. A suboptimum implementation is simple arraying of the RCP and LCP antennas. Multipath effects due to skin reflections are treated by considering arrays of the antennas and their images. As shown above, the general elliptically polarized wave can be decomposed into the sum of two circularly polarized waves of opposite chirality. Arrays of circularly polarized antennas with the same chirality emit a circularly polarized resultant field. A linear array of sources with alternating chirality, however, produces an elliptically polarized field, with the axis of orientation a function of the angle. This observation has implications for circularly polarized antennas used above a reflecting surface.

A circularly polarized antenna in the vicinity of a perfectly conducting ground plane produces a distant field which is equivalent to an array of two orthogonally polarized antennas: the original antenna and its mirror image. The image antenna has the opposite sense of polarization. If the original antenna is an isotropic source, the sum of the direct and reflected fields is linearly polarized with angle dependent direction of polarization. This means that it is likely to be very difficult to produce broad coverage fields from antennas operated near a ground plane. Thus, it should be expected that the LCP and RCP antennas in Figures 5-12 and 5-13 are actually elliptically polarized, in practice. This being the case, the  $180^\circ$  hybrid used to array the antennas and receivers for redundancy will cause some fringing due to interference of wave components having the same chirality. If the antennas are addressed by circularly polarized waves the amount of fringing depends only on the axial ratio achievable in the region of mutual visibility. This is a function of antenna design and is not subject to analysis at this point. If the antennas are addressed by a linearly polarized wave, there will likely be deep interferometer fringing, visible as the line of sight angle to the spacecraft changes in the region of mutual visibility. However, the hybrid arrangement shown in Figure 5-13 prevents both outputs from fading simultaneously.

This fringing may cause some problems with phase-lock loop receivers. A receiver which loses lock may drift off-frequency and not relock when the signal returns. Thus, careful attention to the design and placement of the spacecraft antennas is necessary and the use of circular polarization RCP or LCP addressing is desirable. The degree of multipath effects should be investigated by model tests.

#### 5.1.2.2 System Requirements and Procedures

The EOS interface with the STDN imposes certain requirements on the polarization diversity system design. These requirements and operating procedures constrain the choices in combining techniques and help to narrow the choices in the design.

##### 5.1.2.2.1 Two-Way Coherent Doppler Tracking

By using phase lock loop receivers a two-way coherent lock is established for doppler tracking and coherent demodulation. The frequency standard at the ground station establishes the frequency and phase reference. This is a straightforward problem with a single spacecraft transponder. However, a polarization diversity system, using two receivers on the same frequency must either establish a phase synchronism between the two receivers or allow for coherent turn-around of both uplink carriers. The first approach could be used with the conventional ratio-type transponders if a coherent oscillator combiner is used to establish the downlink carrier by diversity combining the oscillators of two spacecraft receivers (if both are in lock). The second approach uses a crystal-type transponder in the spacecraft as described in the STDN Users Guide, paragraph 3.3.2.1.

"The GRARR System, in S-band operation, may operate with either a crystal as ratio type transponder. When a crystal transponder is used, the phase-modulated uplink carrier is received by the transponder and heterodyned down to a pre-assigned subcarrier frequency. This subcarrier is, in turn, phase-modulated on the downlink carrier. The downlink carrier frequency is derived from the same reference oscillator that was used to heterodyne

the uplink carrier to a subcarrier frequency. This permits the downlink signal to be useable for two-way doppler extraction for range-rate measurements free of the effects of transponder reference instabilities. The measurements can be made from as many of three different GRARR systems simultaneously, provided that different uplink frequencies are utilized. This results in up to three subcarrier frequencies 1.4 MHz, 2.4 MHz, and 3.2 MHz being generated in three transponder subchannels. The three subcarriers are summed prior to phase modulating the downlink carrier. When using a crystal type transponder, a frequency (uplink 1750 to 1850 MHz) is utilized. The planned Rosman modification (uplink 2025 to 2120 MHz) will provide a frequency ratio of 60/55 when crystal transponders are used. When using a ratio or phase-locked transponder the coherence ratio is 240/22."

#### 5.1.2.2.2 Range and Command Modulation Turnaround

Ranging information is obtained by direct modulation of the uplink and downlink carriers. Command data modulates a subcarrier, which phase-modulates the uplink carrier. Coherent demodulation of the ranging and command subcarrier occur in the spacecraft. Means must be provided for turnaround of this modulation on the downlink. Since the uplink polarization diversity systems uses two transponders the demodulated outputs must somehow be combined for transmission on the downlink.

#### 5.1.2.2.3 Uplink Polarization Diversity Capability

The STDN User's Guide describes the capabilities of ground station equipment and facilities to meet the requirements of a polarization diversity system. The uplink polarization capability of several representative antenna systems is illustrated in Table 5-7. As shown in this table, extracted from the STDN User's Guide, the uplink polarization capability is switch-selectable RCP or LCP. This means that circularly polarized spacecraft antennas are individually addressable by switch selection at the ground station. The GRARR stations have optimal diversity combining capability, which permits both spacecraft antennas to be excited simultaneously.

Table 5-7. Polarization Capability of STDN Stations\*

S-Band System	Antenna	Location	Receive Gain (dB)	Polarization	
				Receive	Transmit
GRARR	30'	Fairbanks, Alaska Santiago, Chile	42	Orthogonal Linear - Optimally combined in receiver	Switch selectable RCP or LCP
	14'	Rosman, N. C.	35	Orthogonal linear - Optimally combined in receiver	Switch selectable RCP or LCP
USB	30' x-y	Guam Hawaii	44	Remotely selectable RCP/LCP	Remotely selectable RCP/LCP
	85' x-y	Goldstone, Ca.	53.5	Remotely selectable RCP/LCP	Remotely selectable RCP/LCP

\*Reference: STDN User's Guide

The resulting elliptically polarized wave is tracked by the combiner as its orientation changes during the satellite pass over the station. The USB stations apparently do not have optimal combining capability, but can use selection diversity, based on a monitored AGC, with remotely selectable RCP/LCP feed. For primarily earth-pointing missions, this is not a serious handicap when both spacecraft antennas are excited simultaneously. It causes some data loss during the switch over in a rapidly tumbling spacecraft. The USB stations may be updated to optimal diversity combining before the EOS mission. Excitation of both spacecraft antennas simultaneously simplifies the spacecraft design.

The types of diversity combining receivers and demodulators available in the STDN are summarized in Table 5-8, as reported in the STDN User's Guide and a typical time line supporting ground station coverage is shown in Figure 5-14.

#### 5.1.2.2.4 Reacquisition Procedure

The reacquisition procedure is an important consideration in polarization diversity combining systems employing phase lock receivers. The following procedure is assumed to be compatible with the STDN and is offered as a guide to the choice of the spacecraft combiner design.

##### a. Assumptions

1. During acquisition, no up-link modulation is present. This is to insure that the transponder does not acquire one of the sidebands.
2. Spacecraft transponder, if not in lock, is excited by an auxiliary oscillator or by the oscillator of another transponder which is in lock.
3. Doppler is known by monitoring downlink excited by auxiliary oscillator, by monitoring turnaround when one receiver is in lock, or by estimate based on last known doppler.

##### b. Reacquisition Steps (Auxiliary Oscillator Control)

1. Two-way RF lock.
  - a. Remove uplink modulation.

Table 5-8. Diversity Combining Telemetry Receivers and Demodulators in STDN.\*

Receiver	Tuning Range	IF Bandwidths	Type of Combining	Demodulation	Autotrack Capability
General Dynamics Diversity Receiver	130-140 MHz Extendable by heterodyning	10 KHz-3 MHz	Postdetection	FM,AM External	No
Vitro Model R-2074A Dual-channel Receiver	55-2300 MHz	4 MHz	Vitro DCA-5100A Diversity Combiner	---	TEL TRAC antennas
DE I Model TR-109 Dual-channel Receiver	VHF-S-band	10-3300 KHz	Post detection TDC-1B Diversity Combiner	IRIG	?
Microdyne 2200R Receiver	105-420 MHz Plug-in Heads Extendable by heterodyning	?	Used with matched diversity combiner provides combined predetection and postdetection outputs for recording and real-time processing.	FM, PM Plug-in	?

\*Reference: STDN User's Guide.



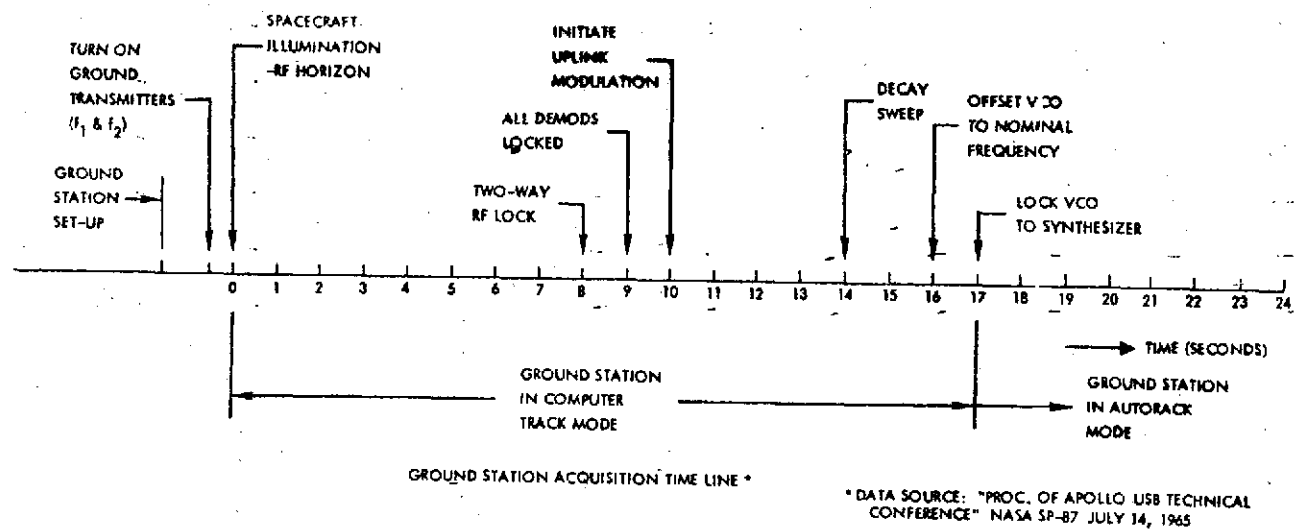


Figure 5-14. Time Line Diagram

- b. Tune ground receiver carrier tracking loop and acquire downlink signal.
- c. Offset transmitter frequency an amount equal to the doppler frequency.
- d. Sweep the transmitter VCO over the frequency uncertainty.
- e. When the phase error in the ground receiver begins to follow the triangular sweep of the ground transmitter, slowly decay the sweep voltage to zero.
- f. Retune the transmitter VCO to nominal frequency.
- g. Retune the receiver VCO control potentiometer to the nominal frequency dial setting.
- h. Lock the transmitter VCO to the frequency synthesizer.

## 2. Data Acquisition

- a. When the downlink receiver locks to the auxiliary oscillator, downlink data is being received and the data demodulator and PCM decommutator can be synchronized. Data can be received during acquisition, but the ground receiver may not be able to remain locked when the spacecraft receiver acquires the uplink and switches from the auxiliary oscillator to turnaround.
- b. When two-way RF lock is obtained, uplink modulation is initiated.
- c. If ground receiver temporarily loses lock during switchover, it may be necessary to reinitiate data demodulator and PCM decommutator acquisition.

## 3. Range Acquisition

- a. After two-way RF lock is obtained, initiate uplink range modulation.
- b. Initiate range receiver acquisition.
- c. Initiate range code acquisition.
- d. Range readout.

c. Reacquisition Steps (Spacecraft Transponder Control)

1. Two-way RF lock

- a. Remove uplink modulation.
- b. Sweep the transmitter VCO over the frequency uncertainty.
- c. Uplink lock indication must be obtained on downlink sub-carrier. When this occurs, slowly decay the sweep voltage to zero.
- d. Retune the VCO to nominal frequency.
- e. Lock the transmitter to the frequency synthesizer.

2. Data Acquisition

- a. When two-way RF lock is obtained on both receivers, uplink modulation is initiated.
- b. Data demodulator should remain locked during reacquisition if one transponder is in lock and downlink frequency is determined by carrier turnaround.

3. Range Acquisition.

- a. When two-way RF lock is obtained both receivers, initiate uplink ranging modulation.
- b. Initiate ranging receiver acquisition.
- c. Initiate range code acquisition.
- d. Range readout.

d. Discussion of Reacquisition Procedures

Several conclusions are drawn from the above outline of the reacquisition procedure.

1. Since both transponders operate on the same frequency, some means of providing individual downlink lock indication must be provided so that the operator will know if one or both transponders are in lock.

2. To provide for coherent turn-around, some means of diversity combining of the spacecraft oscillators must be provided, or an independent means of deriving downlink frequency control.
3. If the two spacecraft transponders are not mutually synchronized, some loss of command and ranging opportunity is lost during the pass due to acquisition procedures. Mutual synchronization allows a receiver to pull in after loss of lock if the other receiver remains locked, since the L.O. for the initial frequency conversion stages is derived from a transponder which is locked.

#### 5.1.2.3 Diversity Combining Techniques

Only two types of diversity combining are appropriate to the EOS requirements. These are selection diversity and maximal ratio combining. In selection diversity, at any given time, the system picks the best of  $N$  noisy signals, and uses that one alone. The term, maximal ratio combining, was coined by Brennan to denote a choice of weighting coefficients which maximizes the signal-to-noise ratio resulting from the most general linear combination of a number of available noisy channels. Under the assumption of independent noises in each diversity channel, the maximal ratio rule weights each signal proportional to the signal amplitude and inversely proportional to the noise variance in each channel.

In this section, examples of polarization diversity combining systems incorporating each of these techniques are given and some of the design problems and possible solutions associated with each approach are discussed.

Two subcategories of classification should be defined. These are 1) pre-demodulation combining and 2) post-demodulation combining. Pre-demodulation combining requires RF phasing of the diversity signals so that they can be weighted and summed before demodulation. The advantage over post demodulation combining is that the fading below the demodulator threshold is less likely to occur. Post-demodulation combining allows the individual RF signals to be coherently demodulated, then added (provided that the absolute time delays between the diversity channels are small in comparison with the reciprocal of the bandwidth of the modulation signals. Post-demodulation combining is inherently simpler, but is not as effective at low signal/noise ratios because of threshold effects.

#### 5.1.2.3.1 Selection Diversity

Figure 5-15 shows a block diagram of a selection diversity polarization diversity system. The circularly polarized antenna outputs are combined in a hybrid which produces two elliptically polarized outputs, but increases the redundancy, as discussed previously. The two S-band phase locked loop receivers are existing hardware items similar to the Apollo block II and ERTS receivers. They contain wide-band phase demodulators and provide coherent drive for the downlink as well as turn-around of the ranging and the command subcarrier. Coherent AGC is used to control the gain. The AGC voltage is a measure of the signal amplitude. If the noise figures of the receivers are equal, a comparison of the AGC voltages gives a relative measure of the signal/noise ratios and, therefore, data quality in the two channels. Since coherent drive and range and command subcarrier turn-around must be provided, AGC selection combiners are used. The implementation of a selection diversity combiner is relatively simple, as illustrated in Figure 5-16. An AGC comparator drives a flip/flop whose complementary outputs operate analog selection gates to allow either input #1 or input #2 to appear in the output, but not both. Independent command subcarrier demodulators and subbit detectors are used to increase the redundancy and avoid problems from switching transients at the command demodulator input.

The outputs of the sub-bit detectors are selected for each sub-bit decision, using a clocked selection diversity combiner, for input to the command decoder. The clock is derived from the independent clock loops in the sub-bit detectors, provided they are both in-sync, or from one if either loses sync, as illustrated in Figure 5-17. A VCO tracking loop compensates for small differences in phase shift by averaging the phase angles of the two clocks. The remaining selection logic is based on AGC comparisons with selected thresholds and with each other, satisfaction of the "in-sync" condition and clock timing.

The major disadvantage of the selection diversity system shown in Figure 5-15 is that the independent S-band PLL receivers will lose lock frequently under some operating conditions, since they are arrayed by the hybrid combiner to form

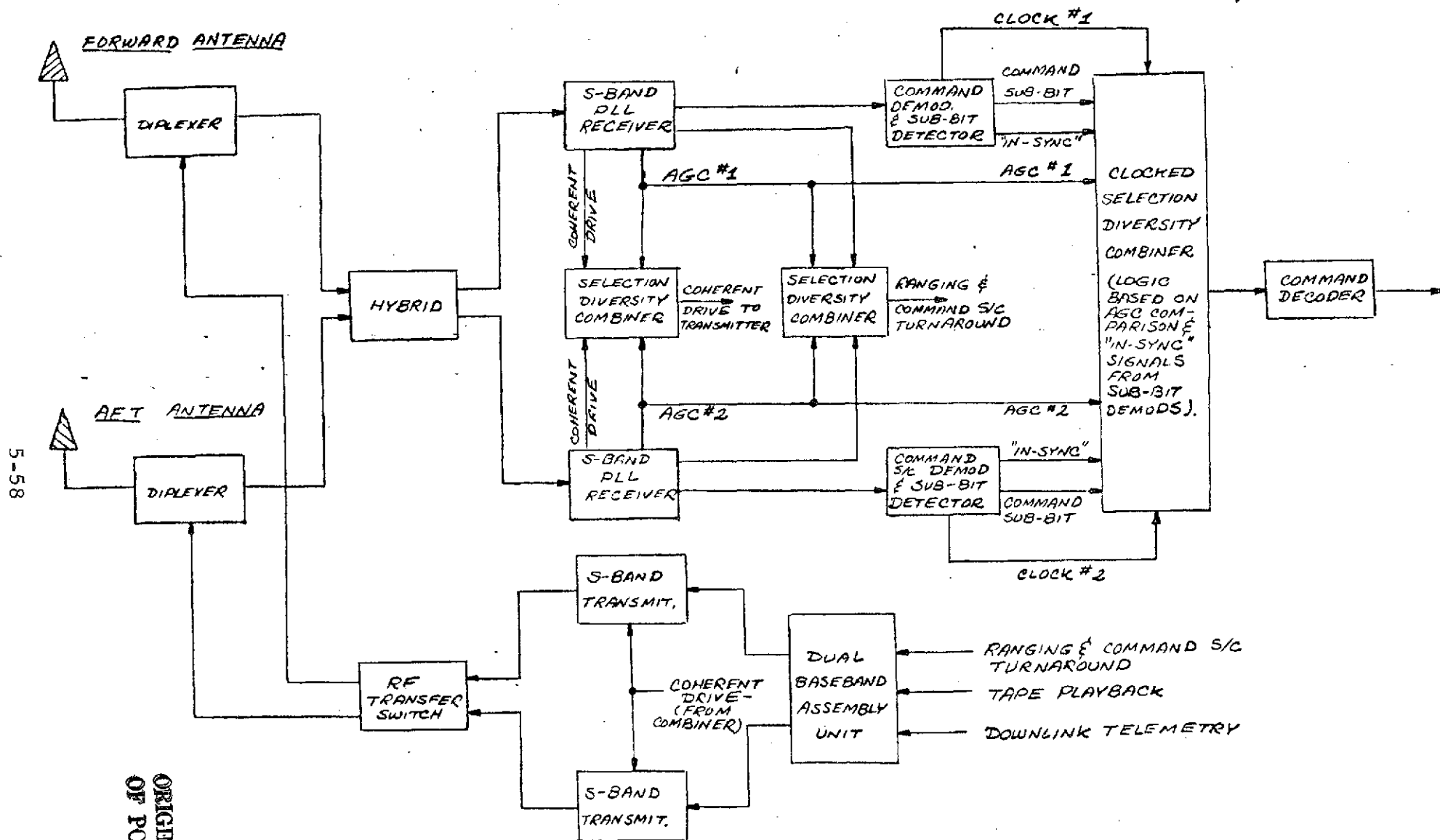


Figure 5-15. Selection Polarization Diversity System

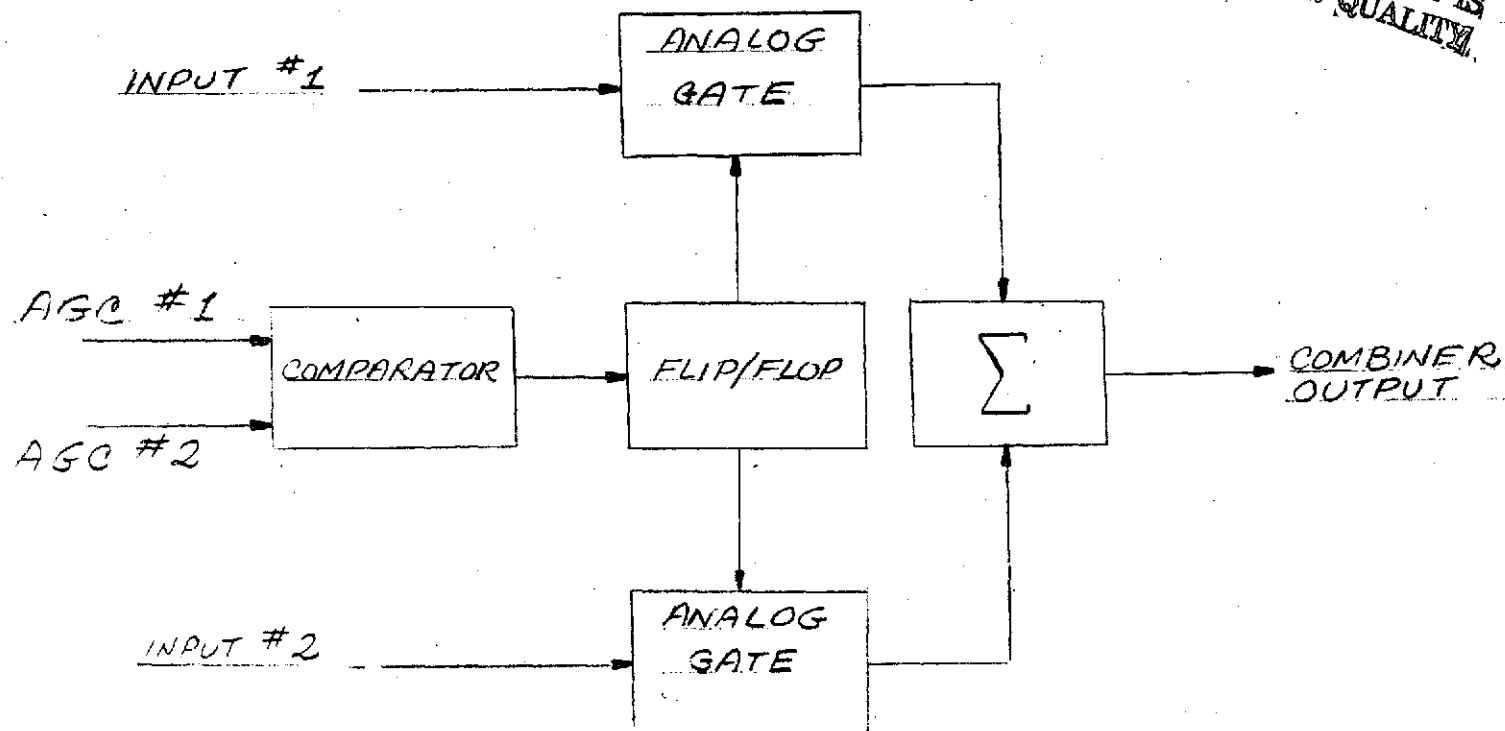


Figure 5-16. Selection Diversity Combiner

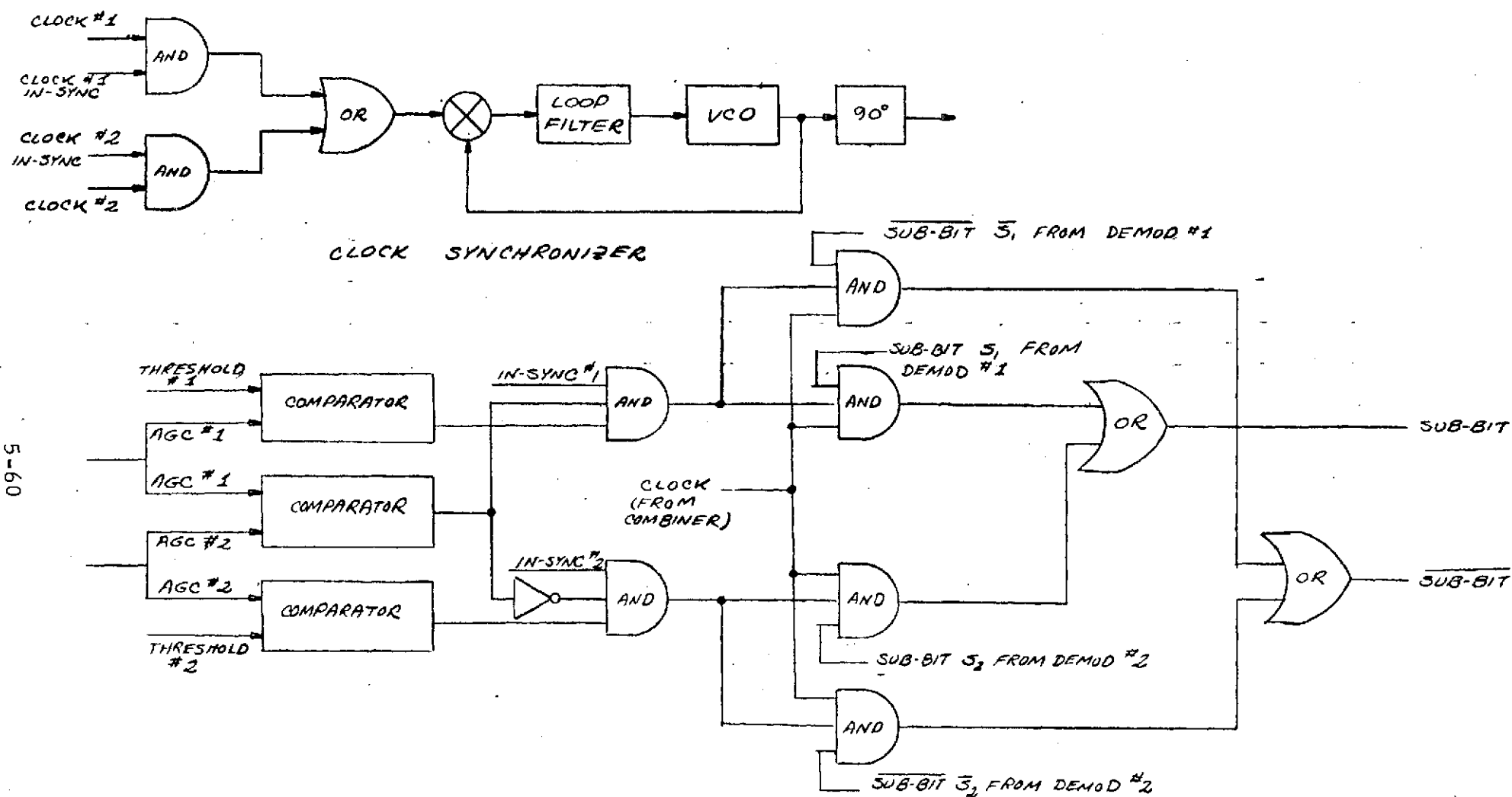


Figure 5-17. Clocked Sub-Bit Selection Diversity Logic



elliptically polarized arrays. Multipath from the spacecraft may result in poor axial ratios in the zone of mutual antenna visibility, producing interferometer fringing in the array pattern and rapid fluctuations in signal strength in the two receiver inputs. After loss of lock, a receiver may drift off frequency and not automatically reacquire when the signal returns, necessitating a reacquisition procedure. The degree to which this condition occurs in practice is a function of antenna design and operational orientation of the spacecraft.

#### 5.1.2.3.2 Optimal Diversity Combining

Switching transients are eliminated and improved performance is obtained with a slight increase in complexity, by using optimal combining for the command sub-carriers prior to demodulation. Also, with minor modifications to existing hardware items and development of a simple coherent diversity combiner, the phase-lock reliability of the S-band receivers can be improved and the reacquisition procedure simplified. With this system, if one receiver of a pair loses lock it remains on frequency because the local oscillator is derived by diversity combining the two receiver VCO's. The phase angle of the combined coherent drive corresponds to the phase center of the array and the rms phase jitter is lower than the best of the two channels by a factor of up to 50 percent.

In this section, the optimal combining rule is derived for the case of phase-locked loop receivers with coherent AGC. Realizations of this rule are demonstrated together with applications to the EOS polarization diversity system.

The block diagram of Figure 5-18 shows a polarization diversity combining system using two S-band PLL receivers. The coherent drive for the transmitters and for the receiver local oscillator is derived by diversity combining the VCO outputs of the two receiver phase lock loops. The diversity combining is controlled by the individual coherent AGC voltages which indicate data quality as well as receiver lock condition. The turn-around ranging signal and the command sub-bit carrier are combined to produce the highest possible signal/noise ratio at the input to the command subcarrier demodulator and sub-bit detector.

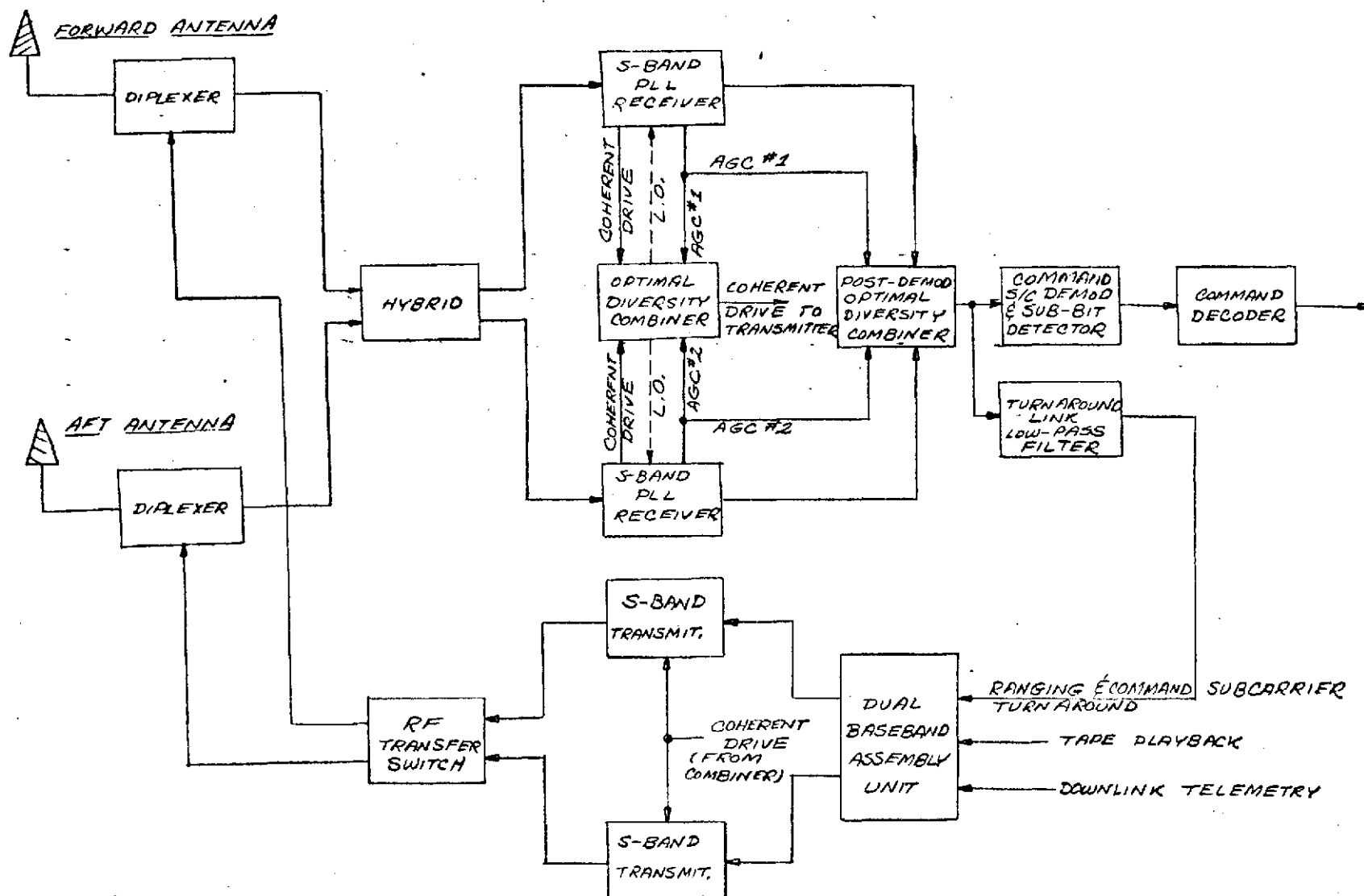


Figure 5-18. Optimal Polarization Diversity System

Now, the design of the optimal combiners is considered in more detail. The block diagram of Figure 5-19 shows a basic model for diversity combining with AGC controlled phase-locked loop receivers. The notations on the coherent AGC loops are those of the Victor-Brockman<sup>10</sup> model for an AGC loop. It can be shown that the AGC voltage is linearly proportional to the signal power, in dB, and that the output signal power is essentially constant over a wide dynamic range in a well designed AGC system. The output noise power is inversely proportional to the input signal/noise ratio.

Since the noise sources are receiver noise, and sky noise over largely non-lapping sectors of the celestial sphere, the noises are assumed to be equal power and independent. The AGC controlled amplifier outputs have equal signal powers and unequal noise powers. We write the outputs in the form

$$u_1(t) = \left(1 + \frac{n_{c1}(t)}{a_1^*(t)}\right) \cos(\omega_c t + \theta_1) - \frac{n_{s1}(t)}{a_1^*(t)} \sin(\omega_c t + \theta_1) \quad (1)$$

and

$$u_2(t) = \left(1 + \frac{n_{c2}(t)}{a_2^*(t)}\right) \cos(\omega_c t + \theta_2) - \frac{n_{s2}(t)}{a_2^*(t)} \sin(\omega_c t + \theta_2). \quad (2)$$

If there are no modulation components in the tracking loop bandwidth, and the signal/noise ratio is large in the loop bandwidth, the phase-locked loops track the signal phase with an rms phase jitter of

$$\sqrt{\frac{2}{\epsilon_i}} = \sqrt{\frac{N_i B_L}{S_i B_{IF}}} \quad \text{radians, rms} \quad (3)$$

where  $\frac{S_i}{N_i}$  is the input carrier to noise ratio in the IF bandwidth and  $2B_L$  is the loop noise bandwidth, corresponding to the  $i^{\text{th}}$  channel.

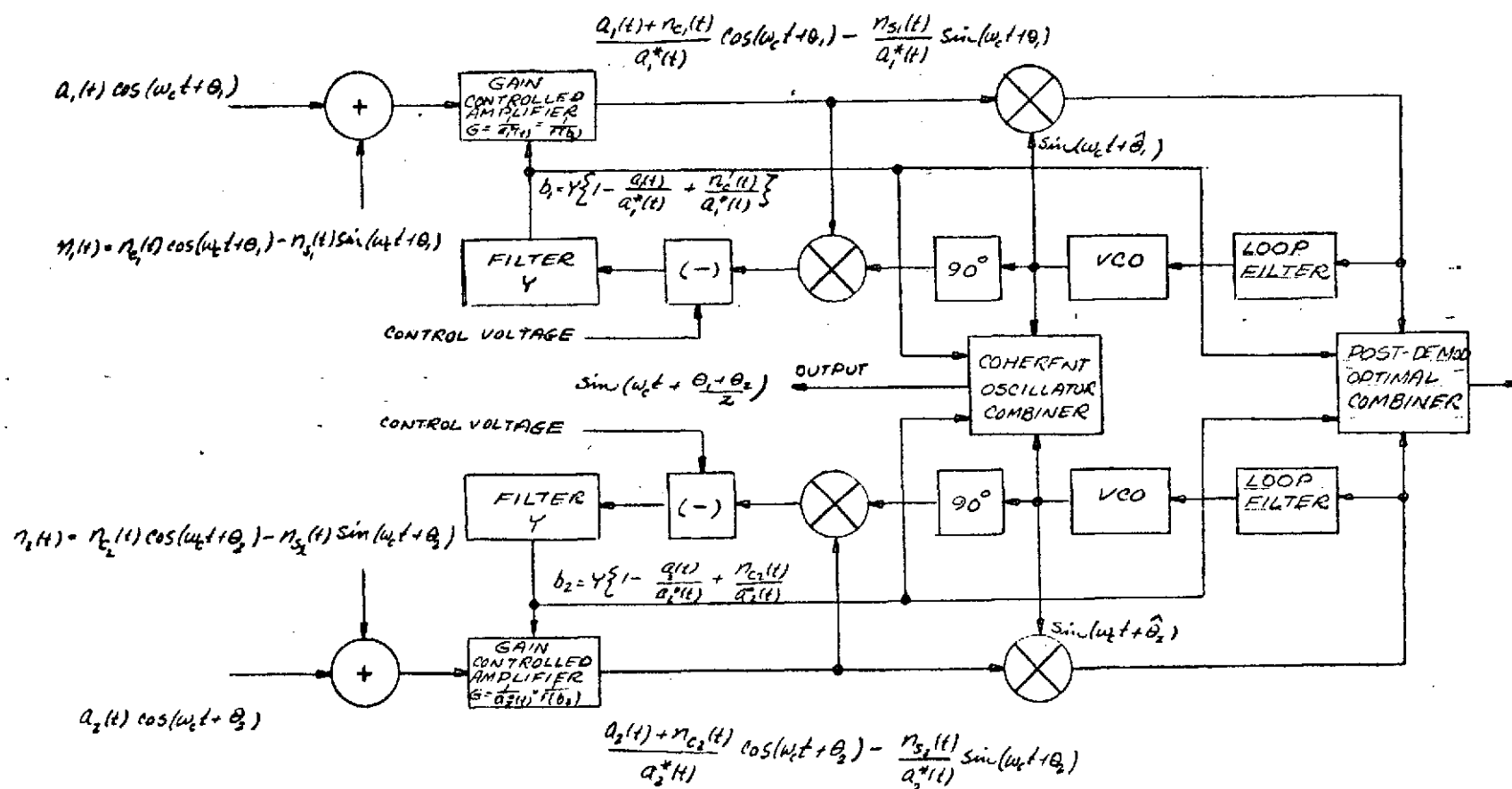


Figure 5-19. Model for Diversity Combining with AGC Controlled Phase-Locked Loop Receivers

ORIGINAL PAGE IS  
OF POOR QUALITY

The optimum combining rule seeks to choose real coefficients  $\{X_i: i=1,2,3,4\}$  to maximize the signal-to-noise ratio of the sum

$$V(t) = [X_1, X_2, X_3, X_4] \begin{bmatrix} \sin(\omega_c t + \psi) + \epsilon_1(t) \cos(\omega_c t + \psi) \\ \sin(\omega_c t - \psi) + \epsilon_2(t) \cos(\omega_c t - \psi) \\ \cos(\omega_c t + \psi) - \epsilon_1(t) \sin(\omega_c t + \psi) \\ \cos(\omega_c t - \psi) - \epsilon_2(t) \sin(\omega_c t - \psi) \end{bmatrix} \quad (4)$$

where  $\epsilon_i(t)$  is the (normalized) noise voltage in the  $i^{\text{th}}$  channel, with rms value given by (4-3). The angle  $\psi$  is  $\psi = \frac{\theta_1 + \theta_2}{2}$ . The signal covariance matrix is

$$\Phi_{SS} = \frac{1}{2} \begin{bmatrix} 1 & \cos 2\psi & 0 & \sin 2\psi \\ \cos 2\psi & 1 & -\sin 2\psi & 0 \\ 0 & -\sin 2\psi & 1 & \cos 2\psi \\ \sin 2\psi & 0 & \cos 2\psi & 1 \end{bmatrix} \quad (5)$$

and the noise covariance matrix is

$$\Phi_{NN} = \frac{1}{2} \begin{bmatrix} \overline{\epsilon_1^2} & 0 & 0 & 0 \\ 0 & \overline{\epsilon_2^2} & 0 & 0 \\ 0 & 0 & \overline{\epsilon_1^2} & 0 \\ 0 & 0 & 0 & \overline{\epsilon_2^2} \end{bmatrix} \quad (6)$$

The approach taken to obtain the solution is to minimize the output noise power subject to a constant output power. This constraint is one which can easily be realized with bandpass limiters or with incoherent AGC controlled amplifiers. Using the method of Lagrange multipliers,<sup>11</sup> form the quadratic function

$$H(\underline{X}) = \underline{X}^T \Phi_{NN} \underline{X} + \lambda [1 - \underline{X}^T \Phi_{ZZ} \underline{X}] \quad (7)$$

which is just the output noise power, when the output power is equal to unity, and  $\Phi_{ZZ} = \Phi_{SS} + \Phi_{NN}$ . The Lagrange function  $H$  is minimized by a choice of  $\underline{X}$ . Thus

$$\nabla_{\underline{X}} H = \Phi_{NN} \underline{X} - \lambda \Phi_{ZZ} \underline{X} = \underline{0} \quad (8)$$

implies that  $\underline{X}$  must be a solution of the eigenvalue problem

$$\mu \Phi_{NN} \underline{X} = \Phi_{ZZ} \underline{X}. \quad (9)$$

where  $\mu$  is a root of the polynomial

$$\det(\mu \Phi_{NN} - \Phi_{ZZ}) = 0. \quad (10)$$

For the present problem, there are four eigenvalues:

$$\mu_1 = \mu_2 = 1 + \left( \frac{S_1}{N_1} + \frac{S_2}{N_2} \right) \frac{B_{1F}}{B_L} > \mu_3 = \mu_4 = 1. \quad (11)$$

These eigenvalues are the maximum and minimum attainable ratios of total output power to noise power. Thus, the best output signal-to-noise ratio is

$$\frac{S_o}{N_o} = \left( \frac{S_1}{N_1} + \frac{S_2}{N_2} \right) \frac{B_{1F}}{B_L}. \quad (12)$$

The eigenfunctions  $X_i$  which satisfy equation (4-10) for the dominant eigenvalues in Equation (4-11) are

$$x_{11} = K \frac{S_1}{N_1} \cos \psi \quad (13)$$

$$x_{21} = K \frac{S_2}{N_2} \cos \psi \quad (14)$$

$$x_{31} = K \frac{S_1}{N_1} \sin \psi \quad (15)$$

$$x_{41} = K \frac{S_2}{N_2} \sin \psi \quad (16)$$

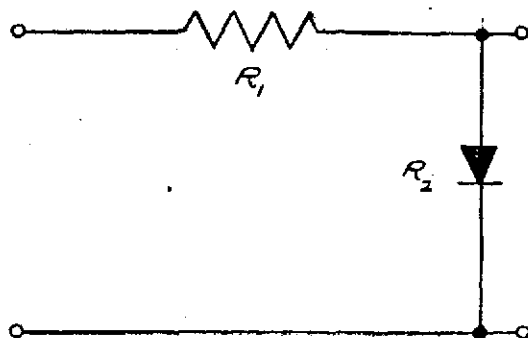
where

$$K = \frac{\sqrt{2}}{\left( \frac{S_1}{N_1} + \frac{S_2}{N_2} \right) \sqrt{1 + \frac{1}{\left( \frac{S_1}{N_1} + \frac{S_2}{N_2} \right) \frac{B_{1F}}{B_L}}}} \quad (17)$$

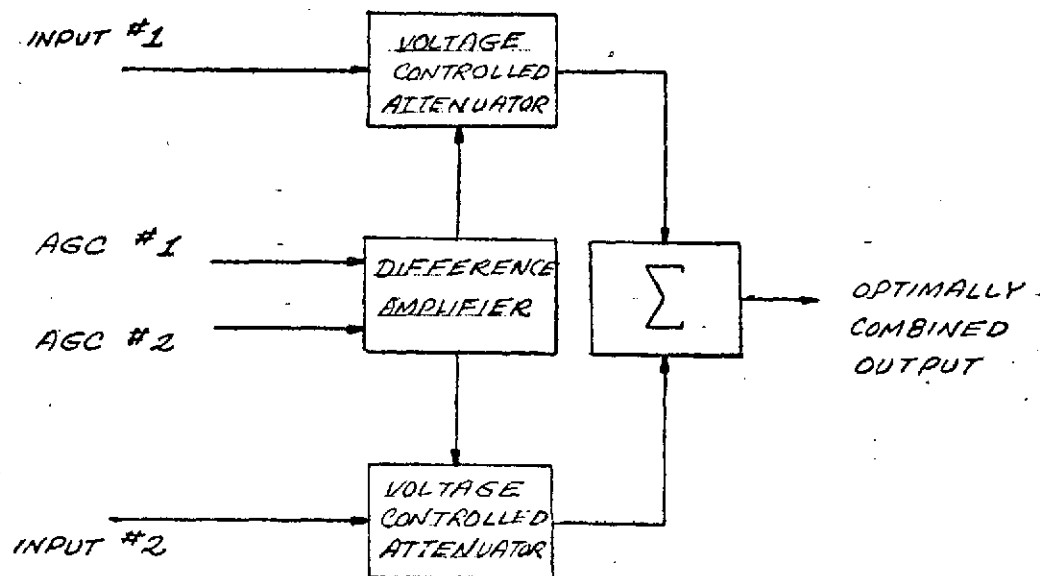
is a normalization factor which assures unity total output power, as required by the constraint.

The optimum weighting functions are proportional to the product of the channel signal/noise ratio and a trigonometric function of the phase difference between the combiner inputs and the desired output signal. This weighting can be accomplished in two parts: (1) amplitude weighting and (2) phasing.

Weighting by factors proportional to the signal/noise ratio is a straightforward problem in combining which has been solved in many existing systems. For example, Figure 5-20 illustrates a system used by DiLosa.<sup>7</sup> The volt-ampere characteristic of the diode gives it an exponentially varying a-c resistance which can be controlled by an applied d-c bias, or control voltage, from the receiver AGC system to give the desired weighting law, as illustrated below.



(a) BASIC VOLTAGE-CONTROLLED ATTENUATOR



(b) OPTIMAL DIVERSITY COMBINER

Figure 5-20. Optimal Weighting System



The attenuation of the network in (a) is

$$a = \frac{e_0}{e_1} = \frac{1}{1 + \frac{R_2}{R_1}} \quad (18)$$

The a-c resistance of the diode can be written in the form

$$R_2 = R_0 10^{-K_1 E} \quad (19)$$

Let E be the output of a difference amplifier whose inputs are AGC voltages, which are a measure of the signal/noise ratios in the respective channels (linear in dB).

$$E = 10 K_2 \left( \log_{10} \left( \frac{S_2}{N_2} \right) - \log_{10} \left( \frac{S_1}{N_1} \right) \right) \quad (20)$$

If

$$K_1 = \frac{1}{10 K_2}, \text{ and } R_1 = R_0, \quad (21)$$

the attenuation of the channel 1 VCA is

$$a_1 = \frac{S_1/N_1}{\frac{S_1}{N_1} + \frac{S_2}{N_2}}, \quad (22)$$

and with a reversal in sign of the control voltage, the attenuator in channel 2 realizes

$$a_2 = \frac{S_2/N_2}{\frac{S_1}{N_1} + \frac{S_2}{N_2}} \quad (23)$$

For reasons that will become apparent, some applications will require that  $K_1 = 1/20K_2$ . Then, the attenuations are proportional to the square root of the channel signal/noise ratios.

Practical realizations<sup>8</sup> of the system illustrated in Figure 5-20 use emitter-follower transistor amplifiers with a common load impedance for summing and with d-c biases derived from a difference amplifier driven by the AGC voltages. In some devices, provision is made for cancellation of the control current in the output.<sup>9</sup> This design problem is straightforward and numerous solutions are available.

Phasing, or multiplication by trigonometric functions of the phase error is easily accomplished. In the system illustrated in Figure 5-21, each of the input signals and noise are correlated, in-phase and quadrature with the combined output signal. From these correlation products, weighting coefficients proportional to the sine and cosine of the phase error are derived. These coefficients weight the quadrature and in-phase components of the inputs, respectively. The voltage controlled attenuators at the combiner inputs apply the previously discussed weighting factors, which in this case must be proportional to the square roots of the respective input signal/noise ratios, to equalize the noise variances in the two inputs. With this weighting, it is easily shown that the mean output of the summer in Figure 5-21 is proportional to  $\sin \omega_c t$  and the output signal/noise ratio is given by Equation (4-12). Thus, the system shown in Figure 5-21 is an optimal diversity combiner.

The above heuristic discussion is intended to show that the system proposed is plausible. It can be shown, more rigorously, that the system of Figure 5-21 solves the eigenvalue problem in Equation (4-9) corresponding to the dominant eigenvalue by the method of successive approximations.<sup>12</sup> That is, the system uses the recursion rule

$$\underline{X}(k+1) = \lambda(k) \Phi_{NN}^{-1} \Phi_{ZZ} \underline{X}(k) \quad (24)$$

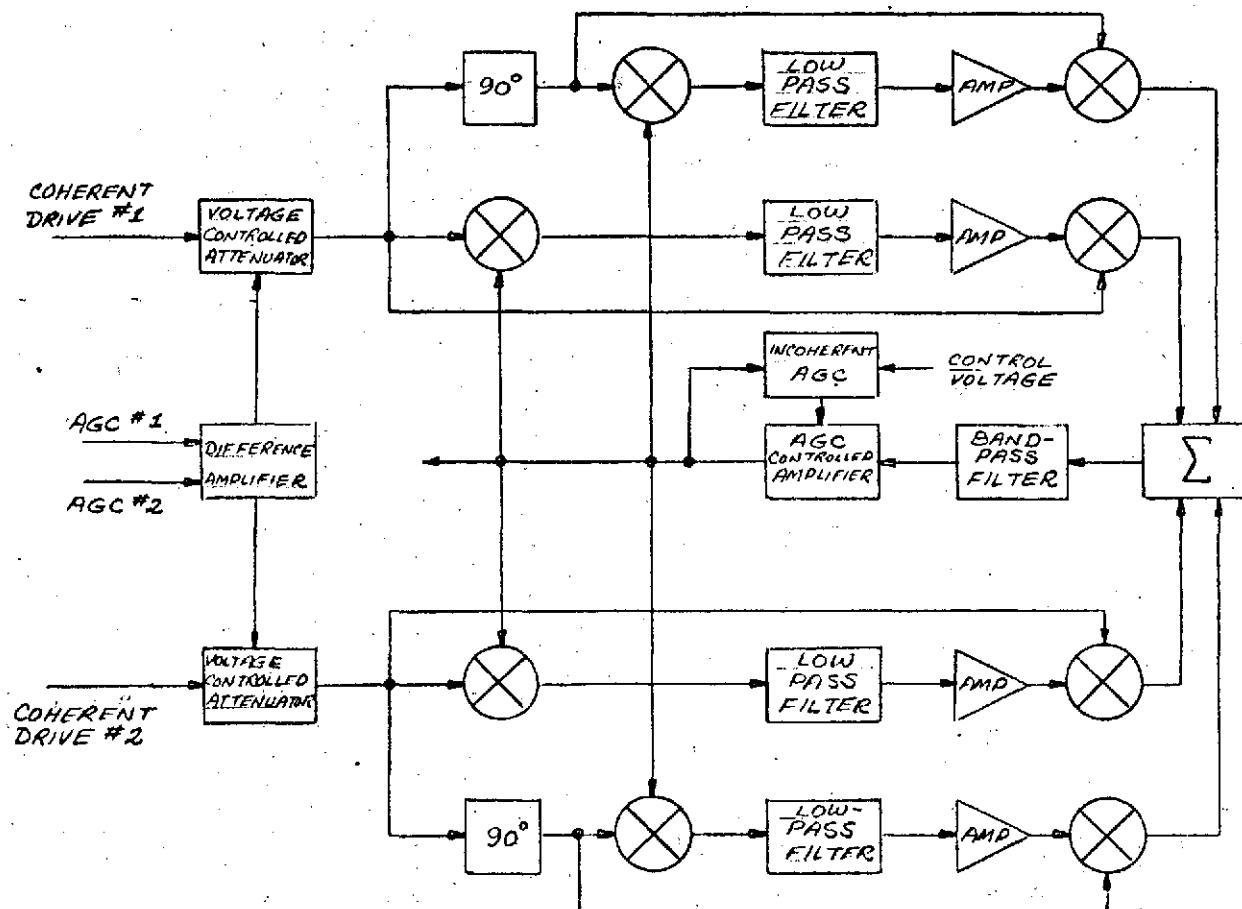


Figure 5-21. Optimal Coherent Drive Combiner

Note that an arbitrary starting value,  $\lambda(0)$ , can be expressed as a linear combination of the eigenfunctions of the problem. The constant output power, achieved by the AGC controlled amplifier, assures that after  $k$  iterations, the gain,  $\lambda(k)$ , is expressed as the ratio of sums of powers of the eigenvalues. Since all the eigenvalues are greater than unity, the largest eigenvalues will clearly dominate the sums. Thus,  $\lambda(k)$  converges to the reciprocal of largest eigenvalue, which is the desired result. As the gain converges to this value, the weighting coefficients converge to their optimum values. The attenuator preceding the phase correction system realizes the square root of the inverse noise covariance matrix. The square root is used with the attenuator in this configuration since the signal amplitudes are subsequently squared. Other possible configurations place the attenuators 1) following the phasing system and 2) in the weighting coefficient branches.

Practical applications of a similar type of diversity combiner have been reported by Bickford, *et. al.*<sup>13</sup> and by Tsao *et. al.*<sup>14</sup>. Their device is a regenerative combiner using bandpass correlation for amplitude weighting and phase shifting. The phase of the output is independent of the inputs and therefore the device is not useful as a coherent drive combiner.

The coherent diversity combiner discussed here was described and analyzed by DuPree<sup>15</sup> of TRW in a HEAO polarization diversity study report.

Detailed design applications of optimal polarization diversity combining are shown in Figures 5-22 and 5-23. Figure 5-22 shows two S-band phase-lock receivers, together with a coherent drive combiner (Figure 5-21) and post-demodulation combiner (Figure 5-20). The only modification made to the receivers involves breaking the local oscillator multiplier chain to bring out the VCO signals for combining, then reintroducing the combiner output in the multiplier chain.

Deriving the coherent drive from a coherent combiner improves the reliability of receiver lock, reduces the phase jitter of the downlink coherent drive, and simplifies the problem of providing redundant coherent drive to the downlink transmitters. The minor modifications required by the combining system easily

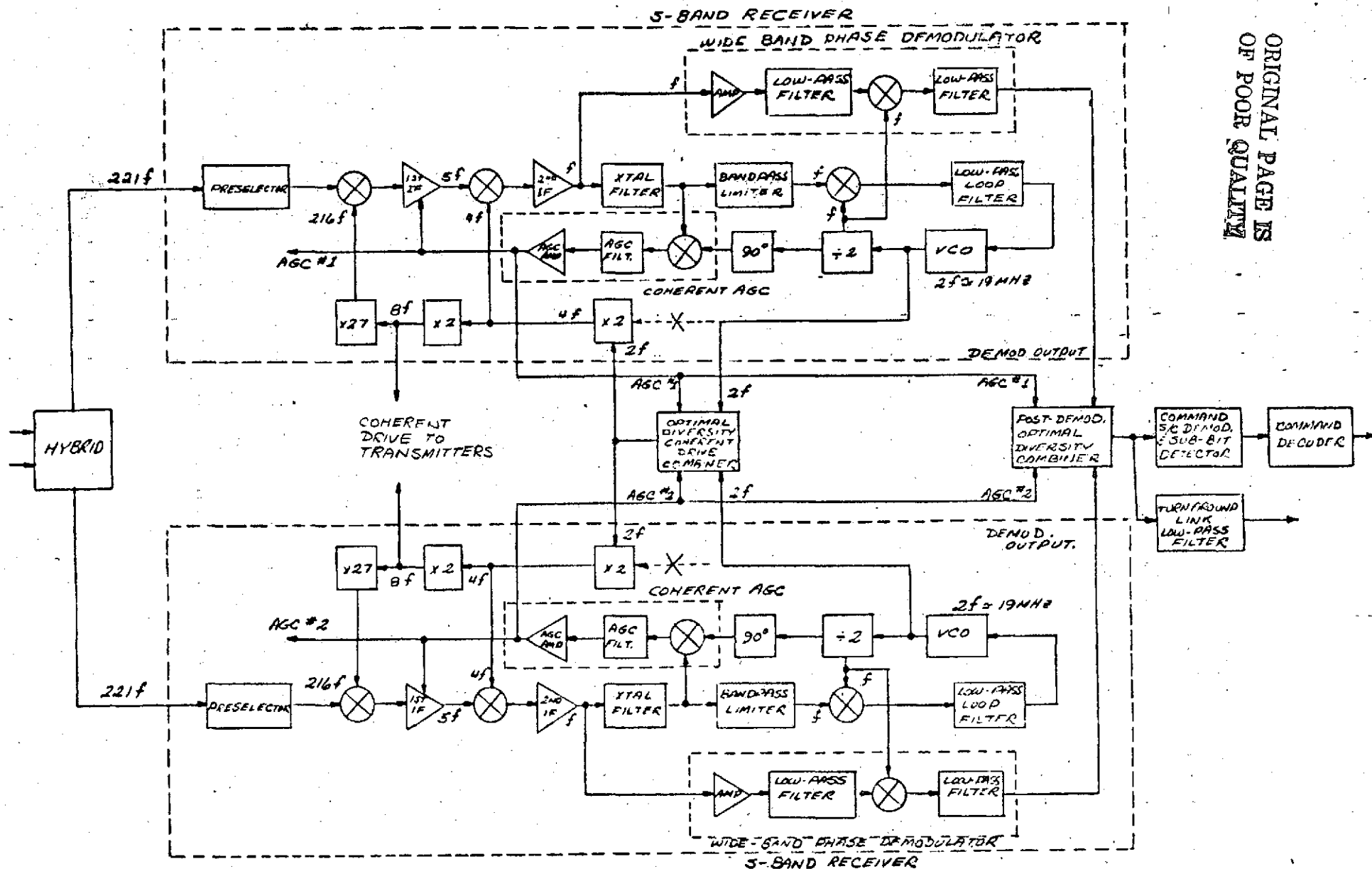


Figure 5-22. Optimal Polarization Diversity Combining System Using Apollo/ERTS Type Transponders

ORIGINAL PAGE IS  
OF POOR QUALITY

permits the coherent combiner to be by-passed in case of failure, to reconfigure the system for independent receiver operation.

The post-demodulation combiner is simple in concept and offers a fail-safe mode for command subcarrier demodulation. If one of the attenuators fails, the command subcarrier can be provided from the other receiver. If the attenuator bias fails and a receiver loses lock, a hard limiter limits the receiver output noise power and sufficient bandwidth reduction is available at the command demodulator to permit safe demodulation and command decoding.

The system of Figure 5-23 shows the application of optimal coherent combining with receivers which use an offset oscillator technique. The offset oscillator technique has the following advantages in receiver design.

- Non-coherent IF frequencies
- Choice of 2<sup>nd</sup> IF frequency permits minimization of 2<sup>nd</sup> mixer spurious response problems
- Eliminates multiplier isolation problem
- Compatible with small size, high efficiency design
- Eliminates transmitter feedback path.

Examples of programs using coherent receivers with an offset oscillator are:

- Pioneer V
- Able Star Second Stage Guidance Receiver
- VELA
- IQSY Pioneer
- SNAP 10A.

In the polarization diversity application, using the offset oscillator technique allows predetection coherent combining, since the IF outputs are phase-locked to the reference oscillators which are, in turn, mutually synchronized. The coherent drive

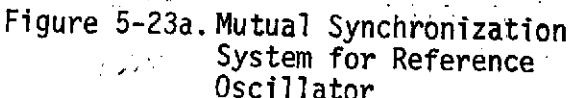


Figure 5-23b. Dual Polarization Diversity System Using S-Band PLL Receivers with Crystal Oscillator Offset, Permitting Choice of Pre-Demodulation or Post-Demodulation Combining

combiner allows coherent turnaround of the uplink frequencies for coherent doppler tracking. Frequency and phase errors introduced by the offset oscillator are eliminated by a double mixing technique. Furthermore, the receiver phase detector outputs are still available for redundant back-up or for post demodulation combining, so that two or three, subcarrier demodulator outputs are available depending upon the configuration desired.

Redundant reference oscillators with mutual synchronization<sup>16</sup> provide a high reliability reference signal. In the system illustrated in Figure 5-23a, both oscillators exercise a measure of control over the frequency at which the loop synchronizes. Frequency averaging is achieved by proper choice of the gain constants of the synchronization loop. Once mutual synchronization has been obtained, the outputs of the oscillators are combined to provide a single output signal which is free of phase jumps or amplitude fluctuations upon failure of one of the oscillators. If one oscillator fails, the frequency of the remaining oscillator gradually returns to its natural frequency. The length of time required for this return depends on the time constants of the loop filter. In the polarization diversity application with offset oscillators, the receivers could be modified to permit both receivers to be driven from the mutual synchronization combiner so that in the event of oscillator failure, both receivers would continue to operate.

#### 5.1.2.4 Conclusions

The advantage of polarization diversity over frequency diversity for increased antenna coverage is a 2:1 saving in bandwidth. Interferometer fringing with extended coverage is prevented by addressing oppositely (circularly) polarized RCP and LCP antennas positioned on opposite sides of the spacecraft. Dual receiver/demods and a hybrid combiner allow the receivers to be arrayed in a redundant configuration.

Either selection diversity or maximal ratio diversity appears to be appropriate to the EOS spacecraft. Both techniques can be implemented based on an AGC comparison. Post demodulation maximal ratio combining is not significantly more complex



to implement than post-demodulation selection combining, and it offers the advantages of up to 3 dB improvement over the best signal/noise ratio performance of a selection combiner. There is a history of reliable combiner designs for use in long range radio communications.

A summary of the features of three basic polarization diversity systems is given in Table 5-9.

The requirements of doppler tracking and the choice of a ratio type transponder with redundant transmitter/receiver configurations demands some type of coherent drive combiner. A selection diversity combiner is simplest but introduces some switching transient and reacquisition problems. A simple optimal diversity combiner design is derived and presented in this report. This device allows mutual frequency synchronization of the two S-band receivers so that the receivers can pull in automatically after a loss of lock if the other receiver remains locked. This eliminates the need to initiate a reacquisition procedure and contributes to the reliability and smooth operation of the system. Only minor modifications to existing hardware items are required.

Table 5-9. Summary of Polarization Diversity Designs

REQUIREMENTS	CAPABILITY		
	SELECTION DIVERSITY	OPTIMAL DIVERSITY WITH APOLLO/ERTS RATIO TRANSPONDER	OPTIMAL DIVERSITY WITH OFFSET OSC TYPE TRANSPONDER
RCP/LCP SIGNALS	TWO ANTENNAS WITH OPPOSITE CIRCULAR POLARIZATION	TWO ANTENNAS WITH OPPOSITE CIRCULAR POLARIZATION	TWO ANTENNAS WITH OPPOSITE CIRCULAR POLARIZATION
MAXIMUM ANTENNA COVERAGE	LOCATE ANTENNAS ON OPPOSITE SIDES OF S/C	LOCATE ANTENNAS ON OPPOSITE SIDES OF S/C	LOCATE ANTENNAS ON OPPOSITE SIDES OF S/C
DUAL RECEIVER/DEMOS	TWO S-BAND RECEIVERS, DUAL WIDEBAND PHASE DEMODULATORS, DUAL COMMAND S/C DEMODS & SUB-BIT DETECTORS	TWO S-BAND RECEIVERS, DUAL WIDEBAND PHASE DEMODULATORS, SINGLE COMMAND S/C DEMOD & SUB-BIT DETECTOR	TWO S-BAND RECEIVERS, OPTIONAL 1/2/3 WIDEBAND PHASE DEMODS, OPTIONAL 1/2/3 COMMAND S/C DEMOD & SUB-BIT DETECTOR
RECEIVER COMBINING SUCH THAT HIGHEST QUALITY SIGNAL IS USED FOR EACH BIT DECISION	SELECTION DIVERSITY BASED ON LARGEST AGC ALWAYS SELECTS BEST SIGNAL/NOISE CHANNEL	POST-DEMODULATION OPTIMAL COMBINING BASED ON AGC COMPARISON. UP TO 3 DB SNR IMPROVEMENT OVER BEST CHANNEL.	CHOICE OF PRE- OR POST-DEMODULATION COMBINING BASED ON AGC COMPARISON. UP TO 3 DB SNR IMPROVEMENT OVER BEST SNR CHANNEL & EXTENDED THRESHOLD
RECEIVERS CONNECTED AS REDUNDANT UNITS & TOLERANT OF ANY SINGLE POINT FAILURE	HYBRID COMBINER, BOTH RECEIVERS ACTIVE, BACK-UP AUX. OSC.	HYBRID COMBINER, BOTH RECEIVERS ACTIVE, BACK-UP AUX. OSC.	HYBRID COMBINER, BOTH RECEIVERS ACTIVE, REDUNDANT REF. OSC., BACK-UP AUX. OSC.
COHERENT DOPPLER TRACKING	SELECTION DIVERSITY COHERENT DRIVE COMBINER FOR RATIO/TRANSPONDER	OPTIMAL DIVERSITY COHERENT DRIVE COMBINER FOR RATIO/TRANSPONDER	OPTIMAL DIVERSITY COHERENT DRIVE COMBINER FOR RATIO/TRANSPONDER
REACQUISITION OF SINGLE RECEIVER AFTER LOSS OF LOCK	OBSERVE LOCK STATUS ON DOWN-LINK, SWEEP UPLINK	MUTUAL SYNCHRONIZATION REDUCES NEED FOR REACQUISITION	MUTUAL SYNCHRONIZATION REDUCES NEED FOR REACQUISITION
TRANSMITTER COVERAGE	ONE TRANSMITTER DRIVES BOTH ANTENNAS, POLARIZATION DIVERSITY RECEIVER TRACKS POLARIZATION	ONE TRANSMITTER DRIVES BOTH ANTENNAS, POLARIZATION DIVERSITY RECEIVER TRACKS POLARIZATION	ONE TRANSMITTER DRIVES BOTH ANTENNAS, POLARIZATION DIVERSITY RECEIVER TRACKS POLARIZATION
TRANSMITTER REDUNDANCY	HYBRID OR RF TRANSFER SWITCH	HYBRID OR RF TRANSFER SWITCH	HYBRID OR RF TRANSFER SWITCH

## References

1. D. G. Brennan, "Linear Diversity Combining Techniques," Proceedings of the IRE, June 1959. pp. 1075-1102.
2. B. B. Barrow, "Translation of a Historic Paper on Diversity Reception," Proc. IRE, Jan. 1961 Vol. 49, No. 1 pp. 367-369.
3. G. L. Turin, "Communication Through Noisy, Random Multipath Channels," 1956 IRE Convention Record, pt. 4, pp. 154-166.
4. G. L. Turin, "On Optimal Diversity Reception," IRE Transactions on Information Theory, July 1961. pp. 154-166.
5. S. Stein, Communication Systems and Techniques, Part III, by Schwartz, Bennett and Stein, New York, McGraw-Hill Book Co., Inc. 1966.
6. C. R. Laughlin, "The Diversity-Locked Loop - a Coherent Combiner," IEEE Transactions on Space Electronics and Telemetry, September 1968. pp. 84-92.
7. V. T. DiLosa, Diversity-Lock Phase Demodulator, NASA Tech. Note NASA TN D-3342, GSFC, July 1965.
8. C. L. Mack, "Diversity Reception in UHF Long Range Communications," Proc. IRE October 1965. pp. 1281-1289.
9. Paul E. Treynor, "Design of a Transistorized Optimum Ratio Combining Circuit," Microwave Journal/Telecommunication Systems, July 1966. pp. 36-42.
10. W. K. Victor and M. H. Brockman, "The Application of Linear Servo Theory to the Design of AGC Loops," Proceedings of the IRE, February, 1960. pp. 234-238.
11. J. W. Dettman, Mathematical Methods in Physics and Engineering, McGraw-Hill Book Co., Inc., 1962. pp. 68-75.
12. R. W. Hamming, Numerical Methods for Scientists and Engineers, McGraw-Hill Book Co., Inc., 1962. pp. 366-369.
13. W. T. Bickford et. al., Study of a Signal Processor Employing a Synthetic Phase Isolator, NASA Contractor Report NASA CR-728, Raytheon Company for NASA-ERC Washington D.C., May 1967.
14. C. K. H. Tsao et. al., "Analysis of a Signal Processor for an Antenna Array," IEEE Transactions on Aerospace and Electronic Systems. Vol. AES-6 No. 1, Jan. 1970. pp. 79-86.
15. J. E. DuPree, Polarization Diversity Study, HEAO S-73-570, TRW Systems, for NASA MSFC, 31 August 1973.
16. W. B. Warren, "A Two Oscillator Combiner Using Mutual Synchronization," Frequency Technology, April 1969. pp. 13-14.

#### 5.1.2.5 Polarization Diversity Theory

Omnidirectional communications coverage with the EOS spacecraft can be obtained by using polarization-diversity. Two broad coverage antennas, with opposite senses of circular polarization can be located on opposite sides of the spacecraft, to permit the radiation of two non-interfering waves on the same frequency. With good antenna design, the interference nulls usually associated with an array of antennas do not occur, and the locations are chosen to eliminate blockage by the spacecraft. Since the superposition of two plane waves (far field) with opposite senses of circular polarization produces an elliptically polarized wave, the polarization-diversity receiver must track the state of the received wave in order to provide the best performance.

This section is intended to provide a fundamental discussion of the polarization diversity approach. A discussion of the fundamental concepts and language of polarization is followed by examples in the calculation of patterns of arrays of polarized sources. The principles behind the design of polarization tracking receivers are presented.

#### Polarization Properties of Electromagnetic Waves

The vector description of electromagnetic fields is essential in a discussion of their polarization properties. The vector description is referenced to the electric field vector, since the magnetic field vector is uniquely determined by the electric field vector and the direction of propagation in free-space. The vector directions are referenced to a coordinate system as shown in Figure 5-24. A set of orthogonal coordinate axes is shown, together with a set of spherical coordinates.

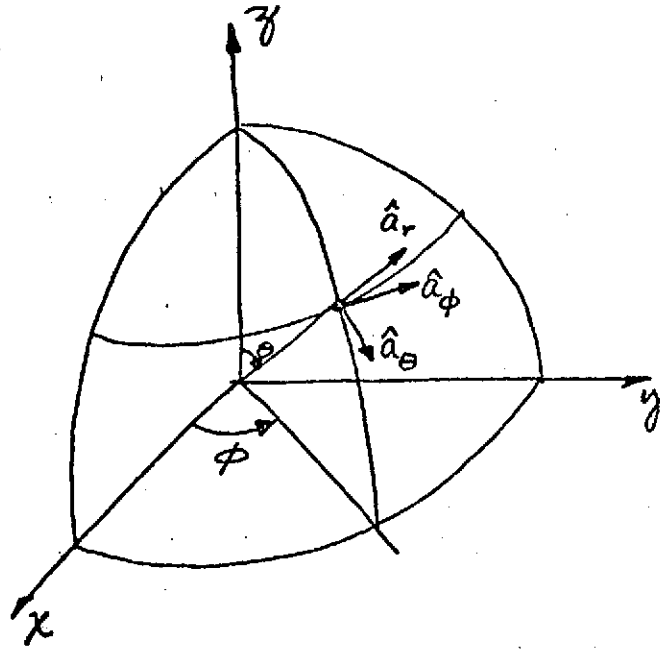


Figure 5-24. Coordinate System Convention

The two coordinate systems are related by the equation.

$$\begin{bmatrix} x \\ y \\ z \end{bmatrix} = r \begin{bmatrix} \sin \theta \cos \phi \\ \sin \theta \sin \phi \\ \cos \theta \end{bmatrix} \quad (1)$$

Both sets of coordinates are useful in our discussion.

The vector properties of fields at a given point  $(x, y, z)$  are expressed in terms of the unit vectors  $(\hat{a}_x, \hat{a}_y, \hat{a}_z)$  which are orthonormal. That is,

$$\hat{a}_i \cdot \hat{a}_j = \delta_{ij}, \quad (2)$$

where  $\delta_{ij}$  is the Kronecker delta:

$$\delta_{ij} = \begin{cases} 1, & i = j \\ 0, & i \neq j \end{cases} \quad (3)$$

The waves radiated from an aperture can be described in terms the electric field distribution in the aperture. This discussion refers to Figure 5-25 which shows an aperture in the  $(x,y,0)$  plane. The electric field is a vector function  $\vec{E}(x,y,0)$  of the  $(x,y)$  coordinates. The electric field produced at a distant field point  $(x_0, y_0, z_0)$  can be expressed easily in terms of the angular spectrum,  $\vec{F}(w_x, w_y)$ ,

$$\vec{F}(w_x, w_y) = \iint_{\text{Aperture}} \vec{E}(x,y,0) \exp [j(w_x x + w_y y)] dx dy, \quad (4)$$

where the angular frequencies,  $w_x$  and  $w_y$  are proportional to the direction cosines of the position vector,  $\vec{R}$ , from  $(x,y,0)$  to  $(x_0, y_0, z_0)$ .

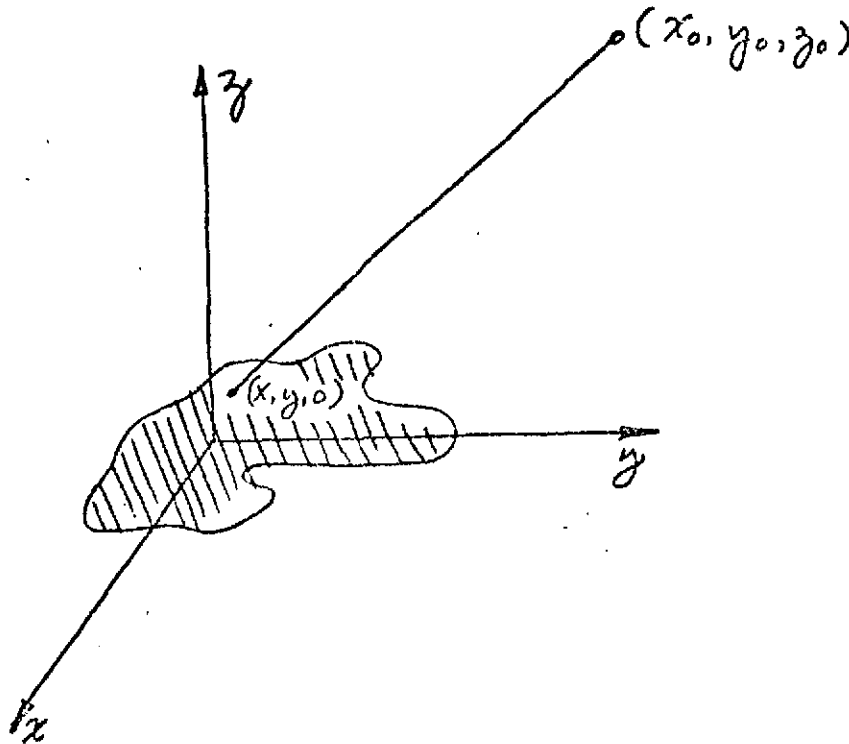


Figure 5-25. Geometry for Spatial Properties

$$\begin{bmatrix} w_x \\ w_y \end{bmatrix} = \frac{2\pi}{\lambda R} \begin{bmatrix} x_0 - x \\ y_0 - y \end{bmatrix} \quad (5)$$

$$R = \sqrt{z_0^2 + (x_0 - x)^2 + (y_0 - y)^2} \quad (6)$$

$$\lambda = \text{Wavelength} \quad (7)$$

Equation (4) is seen to be the inner product of the electric field distribution with the plane waves at angular frequencies  $w_x, w_y$ ; i.e. a double Fourier transform. The inverse transform relation therefore expresses the electric field distribution in the aperture as a superposition of plane waves propagating in the directions corresponding to the angular frequencies  $(w_x, w_y)$  over the range  $(-\infty, \infty)$  in each frequency.

A simple example illustrates the above ideas as follows. Let the electric field distribution in the aperture be confined to two point sources lying a distance,  $d$ , apart centered on the  $x$  axis as shown in Figure 5-26.

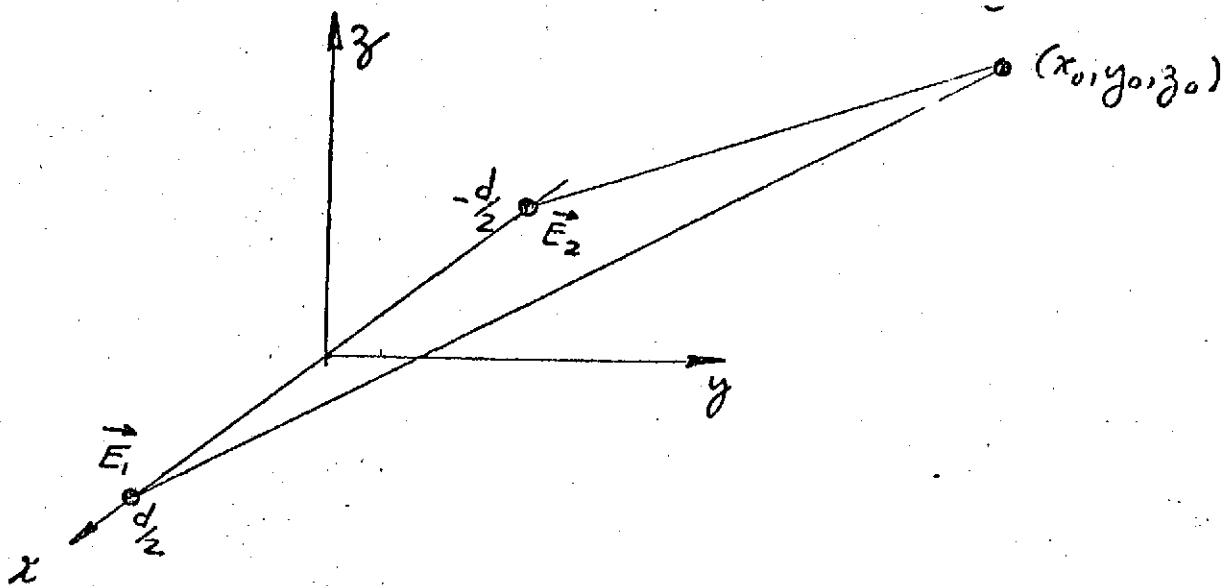


Figure 5-26. Array of Two-Point Sources

The electric field in the aperture can be described by the function

$$\vec{E}(x,y,0) = \vec{E}_1 \delta(x - d/2, y) + \vec{E}_2 \delta(x + d/2, y) \quad (8)$$

where  $\vec{E}_1$  and  $\vec{E}_2$  are the (complex) vector amplitude of the electric field at the two point sources. Use equation (8) in equation (4) to find the angular spectrum:

$$\vec{F}(w_x, w_y) = \vec{E}_1 \exp \left[ j w_x \frac{d}{2} \right] + \vec{E}_2 \exp \left[ -j w_x \frac{d}{2} \right] \quad (9)$$

where

$$w_x = \frac{2\pi}{\lambda} \cos \phi. \quad (10)$$

Two special cases of equation (9) are evaluated for illustration. In the first case, let  $\vec{E}_1 = \vec{E}_2$ . The angular spectrum for this case is

$$\vec{F}(w_x, w_y) = 2\vec{E}_1 \cos \left( \frac{w_x d}{2} \right) \quad (11)$$

The antenna pattern for this case is (except for an amplitude factor):

$$\vec{F}(\phi) = 2\vec{E}_1 \cos \left( \frac{2\pi}{\lambda} \frac{d}{2} \cos \phi \right) \quad (12)$$

The pattern described by equation (12) has nulls at the angles

$$\phi = \cos^{-1} \left[ (k + 1/2) \frac{\lambda}{d} \right] \quad (13)$$



where  $k$  is any integer. In the second case, let  $E_1$  be orthogonal to  $E_2$ . A linearly polarized antenna which is aligned with either  $E_1$  or  $E_2$  will respond to one of the waves and not the other. Thus, omni-directional patterns can be obtained for either of the two sources, and there is no interference shown in the pattern.

Since the electric field in the aperture has been described as a vector, the angular spectrum has polarization properties. The horizontal and vertical components are not usually independent, but have a definite time-phase relationship, or coherence, which can be interpreted by describing the orientation and length of the electric vector as the wave propagates. The locus of points described by the tip of the electric field vector, when projected onto a plane normal to the direction of propagation of the wave, is an ellipse, as shown in Figure 5-27. The axes of the polarization ellipse

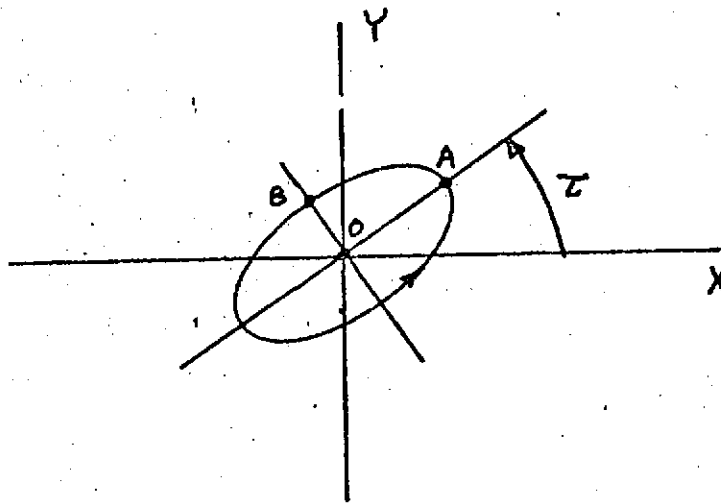


Figure 5-27. Polarization Ellipse

do not, in general, coincide with the  $x$  and  $y$  axes. Several descriptive parameters are necessary to define the polarization ellipse. The line segment  $OA$  is the semimajor axis, and the line segment  $OB$  is the semiminor axis of the ellipse. The ratio  $OA$  to  $OB$  is called the axial ratio (AR) of the polarization ellipse. The orientation of the polarization ellipse is defined by the tilt angle  $\tau$  of the major axis of the polarization ellipse with respect to the reference axis.

Two special cases of elliptical polarization are linear polarization and circular polarization. Linear polarization occurs when the semiminor axis is zero length. The tip of the electric field vector describes a straight line and the orientation of the

straight line is given by the tilt angle  $\tau$ . Circular polarization occurs when the semimajor axis is equal in length to the semiminor axis.

Circular polarization is considered in more detail now. The chirality, or "handedness", is an important descriptive parameter which describes the sense of rotation of the electric field vector in time sequence as the wave propagates through a plane normal to the direction of propagation. To avoid the confusion in sense of rotation between viewing the plane with the "wave-approaching" and with the "wave-receding", we will use the IRE definition, "clockwise circular polarization wave-receding is called right circular polarization." This definition is easier to remember because of a convenient relation for the hands. If the fingers of the right hand are closed into the palm with the thumb extended and pointing in the direction of propagation, the fingers point in the direction of the sense of rotation for right-circular polarization. Thus, a right-handed helical beam antenna transmits or receives right-circular polarization.

The general case of elliptical polarization can be decomposed into the sum of two circularly polarized waves with opposite chiralities. If the amplitudes are equal, linear polarization results. If one amplitude is zero, circular polarization in the remaining sense is obtained. Elliptical polarization can also be assigned a chirality which is that of the dominant circularly polarized component. The chirality is conveniently indicated graphically by an arrowhead drawn on the polarization ellipse if the direction of wave propagation is noted. This is indicated by symbols:  $\oplus$ , for "wave receding" and  $\ominus$ , for "wave approaching."

The best description of polarized waves for purposes of analysis is the polarization coherency matrix. This is a simple  $2 \times 2$  matrix whose elements are the covariances of the linear components of the polarized wave. The advantage of this description is that the type of polarization and sense of rotation are easily determined and matrix algebra describes the effect of coordinate transformations, reflection, and polarization filtering on the polarization of the wave. The polarization coherency matrix is developed as follows. A plane, quasi-monochromatic (narrowband) wave, of average frequency  $\bar{f}$ , propagating in the  $\hat{n}$  direction is resolved into vertical and horizontal components as

$$\vec{E}(x,y,z,t) = \hat{v} \hat{v} \cdot \vec{E} + \hat{h} \hat{h} \cdot \vec{E} = \hat{v} E_v + \hat{h} E_h \quad (14)$$

where

$$E_v = a_v(t) \exp \left[ j \left( \theta_v(t) + k(w) \hat{n} \cdot \vec{R} - 2\pi \bar{f} t \right) \right] \quad (15)$$

$$E_h = a_h(t) \exp \left[ j \left( \theta_h(t) + k(w) \hat{n} \cdot \vec{R} - 2\pi \bar{f} t \right) \right] \quad (16)$$

and

$a_v(t)$  = the amplitude of the vertical component

$a_h(t)$  = the amplitude of the horizontal component

$\theta_v(t)$  = the phase of the vertical component

$\theta_h(t)$  = the phase of the horizontal component

$k(w) = \frac{2\pi}{\lambda}$  = phase-shift constant

$\hat{n}$  = unit vector in the direction of propagation

$\vec{R} = \hat{x}x + \hat{y}y + \hat{z}z$

$\bar{f}$  = mean frequency of wave

$t$  = time variable

The polarization coherency matrix is defined as shown in Equation (17).

$$\left[ \underline{J} \right] = \left\langle \begin{bmatrix} E_h \\ E_v \end{bmatrix} \begin{bmatrix} E_h^* & E_v^* \end{bmatrix} \right\rangle = \begin{bmatrix} \langle E_h E_h^* \rangle & \langle E_h E_v^* \rangle \\ \langle E_v E_h^* \rangle & \langle E_v E_v^* \rangle \end{bmatrix} = \begin{bmatrix} J_{11} & J_{12} \\ J_{21} & J_{22} \end{bmatrix} \quad (17)$$

The symbol  $\langle \dots \rangle$  implies a time average. The polarization properties of an aperture can similarly be described by the coherency matrix

$$\begin{bmatrix} \underline{A} \\ \underline{A} \end{bmatrix} = A_e \begin{bmatrix} a_{11} & a_{12} \\ a_{21} & a_{22} \end{bmatrix} \quad (18)$$

where  $A_e$  is the effective aperture of the antenna in a given direction, the look-angle of the propagating wave launched by or received by the aperture. The elements of the coherency matrix can be determined from power measurements using three pairs of antennas. Two dipoles (linearly polarized) at right angles yield power measurements  $w_x$  and  $w_y$ ; two more dipoles at right angles, but turned  $45^\circ$  with respect to the first set, give power responses  $w'_x$  and  $w'_y$ ; and two helical-beam (circularly-polarized) antennas of left and right-hand sense produce power responses  $w_L$  and  $w_R$ . The elements of the coherency matrix  $[a_{ij}]$  are related to the power measurements by the relations

$$\begin{bmatrix} a_{11} & a_{12} \\ a_{21} & a_{22} \end{bmatrix} = \frac{1}{w_x + w_y} \begin{bmatrix} w_x & \frac{1}{2} (w'_x - w'_y + jw_L - jw_R) \\ \frac{1}{2} (w'_x - w'_y - jw_L + jw_R) & w_y \end{bmatrix} \quad (19)$$

Two factorizations of the polarization coherency matrix are useful. The first factorization, into a product of a column vector and its conjugate transpose, is useful for displaying the time-phase relationship between components. Let  $[E]$  be the column vector

$$[E] = \begin{bmatrix} E_h \\ E_v \end{bmatrix} \quad (20)$$

and represent the polarization coherency matrix as

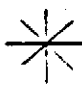







$$[J] = [E]^* [E]^T \quad (21)$$

The second factorization is useful in describing partially polarized waves. Let  $[W]$  be a triangular matrix with zeros above the main diagonal, and represent

$$[J] = [W]^* [W]^T \quad (22)$$

Some polarization examples are presented in Table 5-10, with the polarization coherency matrices and factorizations.

Table 5-10. Polarization Examples

POLARIZATION	[E]	[H]	[J]
 UNPOLARIZED	$\frac{1}{\sqrt{2}} \begin{bmatrix} 1 & -j \\ 1 & +j \end{bmatrix}$	$\begin{bmatrix} 1 & 0 \\ 0 & 1 \end{bmatrix}$	$\begin{bmatrix} 1 & 0 \\ 0 & 1 \end{bmatrix}$
 LINEAR HORIZONTAL	$\begin{bmatrix} 1 \\ 0 \end{bmatrix}$	$\begin{bmatrix} 1 & 0 \\ 0 & 0 \end{bmatrix}$	$\begin{bmatrix} 1 & 0 \\ 0 & 0 \end{bmatrix}$
 LINEAR VERTICAL	$\begin{bmatrix} 0 \\ 1 \end{bmatrix}$	$\begin{bmatrix} 0 & 0 \\ 0 & 1 \end{bmatrix}$	$\begin{bmatrix} 0 & 0 \\ 0 & 1 \end{bmatrix}$
 LINEAR 45°	$\frac{1}{\sqrt{2}} \begin{bmatrix} 1 \\ 1 \end{bmatrix}$	$\frac{1}{\sqrt{2}} \begin{bmatrix} 0 & 0 \\ 1 & 1 \end{bmatrix}$	$\frac{1}{2} \begin{bmatrix} 1 & 1 \\ 1 & 1 \end{bmatrix}$
 LINEAR 135°	$\frac{1}{\sqrt{2}} \begin{bmatrix} 1 \\ -1 \end{bmatrix}$	$\frac{1}{\sqrt{2}} \begin{bmatrix} 0 & 0 \\ -1 & 1 \end{bmatrix}$	$\frac{1}{2} \begin{bmatrix} 1 & -1 \\ -1 & 1 \end{bmatrix}$
 LEFT CIRCULAR	$\frac{1}{\sqrt{2}} \begin{bmatrix} 1 \\ -j \end{bmatrix}$	$\frac{1}{\sqrt{2}} \begin{bmatrix} 0 & 0 \\ 1 & 1 \end{bmatrix}$	$\frac{1}{2} \begin{bmatrix} 1 & j \\ -j & 1 \end{bmatrix}$
 RIGHT CIRCULAR	$\frac{1}{\sqrt{2}} \begin{bmatrix} 1 \\ j \end{bmatrix}$	$\frac{1}{\sqrt{2}} \begin{bmatrix} 0 & 0 \\ j & 1 \end{bmatrix}$	$\frac{1}{2} \begin{bmatrix} 1 & -j \\ j & 1 \end{bmatrix}$
 GENERAL ELLIPTICAL	$\frac{1}{\sqrt{ m ^2 +  n ^2}} \begin{bmatrix} m \\ n^* \end{bmatrix}$	$\frac{1}{\sqrt{ m ^2 +  n ^2}} \begin{bmatrix} 0 & 0 \\ m & n^* \end{bmatrix}$	$\frac{1}{\sqrt{ m ^2 +  n ^2}} \begin{bmatrix}  m ^2 & m^* n^* \\ mn &  n ^2 \end{bmatrix}$
PARTIALLY POLARIZED	---	$\begin{bmatrix} \sqrt{1-p^2} & 0 \\ p & 1 \end{bmatrix}$	$\frac{1}{2} \begin{bmatrix} 1 & p \\ p & 1 \end{bmatrix}$

If one chooses  $\hat{h}$  and  $\hat{v}$  in the x and y directions, respectively, it can be shown that the power available to an antenna from a wave of arbitrary polarization is given by

$$W = \text{Tr} \left[ \underline{A} \right] \left[ \underline{J} \right], \quad (23)$$

where Tr denotes the trace; i.e. the sum of the diagonal elements for a square matrix, or

$$W = A_e (a_{11}J_{11} + a_{12}J_{12} + a_{21}J_{21} + a_{22}J_{22}) \quad (24)$$

also, using the factorization with the matrix  $\underline{E}$ , the output power can be written as

$$W = \left[ \underline{E} \right]^T \left[ \underline{J} \right] \left[ \underline{E} \right]^* \quad (25)$$

Now, we consider some examples in calculation of the output power for polarized apertures receiving polarized waves. The purpose of these examples is illustrative and to demonstrate the orthogonality of polarized apertures.

Example 1. Left circular aperture. Receiving left circular wave: From Table 5-10,

$$W = \frac{1}{4} \begin{bmatrix} 1 & j \\ 1 & j \end{bmatrix} \begin{bmatrix} 1 & j \\ -j & 1 \end{bmatrix} \begin{bmatrix} 1 \\ -j \end{bmatrix} = 1 \quad (26)$$

Example 2. Left circular aperture receiving right circular wave: From Table 5-10,

$$W = \frac{1}{4} \begin{bmatrix} 1 & j \\ 1 & j \end{bmatrix} \begin{bmatrix} 1 & -j \\ -j & 1 \end{bmatrix} \begin{bmatrix} 1 \\ -j \end{bmatrix} = 0 \quad (27)$$

By comparing Examples 1 and 2, we see that the opposite senses of circular polarization are orthogonal, since the matrix product of the polarization coherency matrices has a trace of zero for opposite senses. Also, the standard forms of the polarization coherency matrices are orthonormal, as illustrated by Example 1.

The two senses of circular polarization can be used as the basis for the other types of polarization, as illustrated in the following examples.



Example 3. General Elliptical polarization. By summing two circularly polarized waves with the opposite senses of polarization, the general elliptically polarized wave can be synthesized, as shown by its polarization coherency matrix. From Table 5-10, sum the  $[E]$  matrices of a left circularly polarized wave of rms amplitude A and a right circularly polarized wave of rms amplitude B.


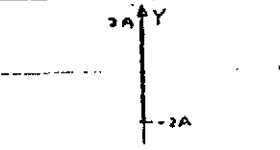
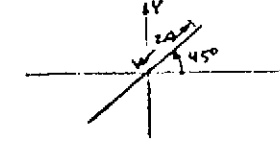
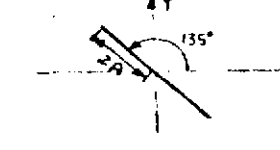
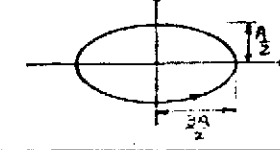
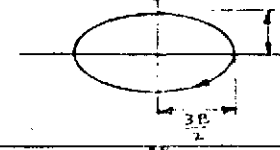
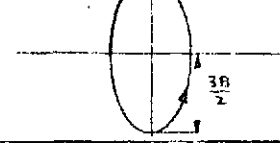
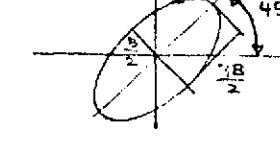
$$A \begin{bmatrix} E \\ \end{bmatrix} + B \begin{bmatrix} E \\ \end{bmatrix} = \frac{A}{\sqrt{2}} \begin{bmatrix} 1 \\ j \end{bmatrix} + \frac{B}{\sqrt{2}} \begin{bmatrix} 1 \\ -j \end{bmatrix} = \frac{1}{\sqrt{2}} \begin{bmatrix} A+B \\ j(A-B) \end{bmatrix} \quad (28)$$

From Equation (21), one calculates the polarization coherency matrix.

$$\begin{bmatrix} J \\ \end{bmatrix} = \frac{1}{2} \begin{bmatrix} |A+B|^2 & j(|A|^2 - |B|^2 + B^*A - A^*B) \\ -j(|A|^2 - |B|^2 + A^*B - B^*A) & |A-B|^2 \end{bmatrix} \quad (29)$$

which is the polarization coherency matrix for the general case of elliptical polarization. Some special cases are evaluated in the examples shown in Table 5-11

Table 5-11. Elliptical Polarization Examples

POLARIZATION	$A = F(B)$	$[J]$	ELLIPSE
LINEAR HORIZONTAL	$A = B$	$4 A ^2 \begin{bmatrix} 1 & 0 \\ 0 & 0 \end{bmatrix}$	
LINEAR VERTICAL	$A = -B$	$4 A ^2 \begin{bmatrix} 0 & 0 \\ 0 & 1 \end{bmatrix}$	
LINEAR 45°	$A = -jB$	$2 A ^2 \begin{bmatrix} 1 & 1 \\ 1 & 1 \end{bmatrix}$	
LINEAR 135°	$A = jB$	$2 A ^2 \begin{bmatrix} 1 & -1 \\ -1 & 1 \end{bmatrix}$	
LEFT ELLIPTICAL AR = 3 HORIZONTAL ORIENTATION	$A = 2B$	$\frac{ A ^2}{4} \begin{bmatrix} 9 & j3 \\ -j3 & 1 \end{bmatrix}$	
RIGHT ELLIPTICAL AR = 3 HORIZONTAL ORIENTATION	$A = \frac{1}{2}B$	$\frac{ B ^2}{4} \begin{bmatrix} 9 & -j3 \\ j3 & 1 \end{bmatrix}$	
LEFT ELLIPTICAL AR = 3 VERTICAL ORIENTATION	$A = -2B$	$\frac{ A ^2}{4} \begin{bmatrix} 1 & j3 \\ -j3 & 9 \end{bmatrix}$	
LEFT ELLIPTICAL AR = 3 45° ORIENTATION	$A = -2jB$	$\frac{ B ^2}{4} \begin{bmatrix} 5 & 4+j3 \\ 4-j3 & 5 \end{bmatrix}$	

A complete description of the polarization ellipse is readily obtained from the polarization coherency matrix. The descriptive parameters are expressed in terms of the elements of the coherency matrix. The amplitudes of the left and right circularly polarized components are, respectively,

$$|A| = \frac{1}{2} \sqrt{J_{11} + J_{22} + 2 \operatorname{Im} \{J_{12}\}} \quad (30)$$

$$|B| = \frac{1}{2} \sqrt{J_{11} + J_{22} - 2 \operatorname{Im} \{J_{12}\}} \quad (31)$$

The lengths of the semi-axes are

$$\text{semi-major axis} = |A| + |B|, \quad (32)$$

$$\text{semi-minor axis} = ||A| - |B||, \quad (33)$$

and the axial ratio is

$$AR = \frac{|A| + |B|}{||A| - |B||} \quad (34)$$

The tilt angle  $\tau$  of the semi-major axis from the horizontal axis is

$$\tau = \frac{1}{2} \tan^{-1} \left[ 2 \frac{J_{12} + J_{21}}{J_{11} - J_{22}} \right], \quad 0 \leq \tau \leq \pi \quad (35)$$

and the chirality is that of the dominant circular component: i.e., left elliptical if  $|A| > |B|$ .

In spacecraft communications problems, one frequently encounters the rotational coordinate transformation. The effect of a rotational transformation on the polarization coherency matrix is described as follows. If the  $\hat{h}$  and  $\hat{v}$  unit vectors are rotated  $\alpha$  radians with respect to the  $x$  axis of the receiving antenna coordinate system, the coherency matrix for the rotated system  $[\underline{J}]_R$  is

$$[\underline{J}]_R = [R(d)] [\underline{J}] [R(\alpha)]^T \quad (36)$$

where  $[R(\alpha)]$  is the rotation matrix

$$[R(\alpha)] = \begin{bmatrix} \cos \alpha & \sin \alpha \\ -\sin \alpha & \cos \alpha \end{bmatrix} \quad (37)$$

and the power available to an antenna whose aperture matrix is  $[\underline{A}]$  is

$$W = \text{Tr} \left\{ [\underline{A}] [\underline{J}]_R \right\} = \text{Tr} \left\{ [\underline{A}] [R(\alpha)] [\underline{J}] [R(\alpha)]^T \right\} \quad (38)$$

Equations (36) and (37) are used in the proof of Equation (35).

## Arrays of Polarized Sources

Antenna theory is usually presented in terms of the antenna patterns for a single component of the electric field. Here, we must consider the total effect of arrays of polarized sources. The discussion in the previous section will be applied to several examples to illustrate the effect of summing fields from an array of sources with a variety of polarizations. Since we have shown that the circularly polarized source is a basis for other polarizations, the discussion is begun with circularly polarized sources.

Consider an array of circularly polarized sources as shown in Figure 5-28. Each of the sources emits a circularly polarized wave which can be described in  $(\theta, \phi)$  coordinates as

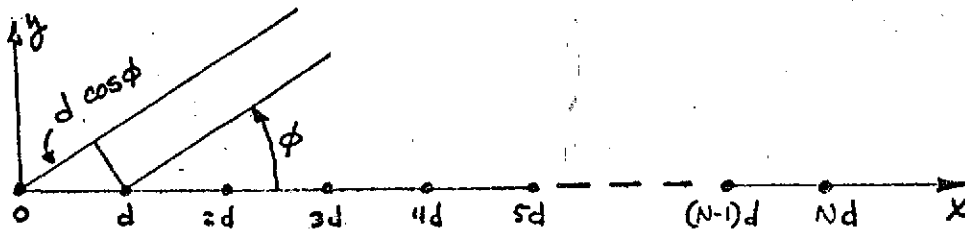


Figure 5 Linear Array of Polarized Sources

$$\vec{E}^i = \hat{a}_\phi E_\phi^i + \hat{a}_\theta E_\theta^i \quad (39)$$

for the  $i^{\text{th}}$  source, where the vector coefficients are complex amplitudes. The electric field distribution in the aperture is

$$\vec{E}(x,y,0) = \sum_{n=1}^N \vec{E}^n \delta(x-(n-1)d, y) \quad (40)$$

and the angular spectrum is

$$\vec{F}(w_x) = \sum_{n=1}^N \vec{E}^n \exp \left[ j(n-1)w_x d \right] \quad (41)$$

$$\text{where } w_x = \frac{2\pi}{\lambda} \cos \phi \quad (42)$$

For the case of circular polarization, one requires that

$$E_{\phi}^n = E_{\theta}^n \exp \left[ j \gamma_i \right] \quad (43)$$

where  $\gamma_i = \pm \pi/2$ . The "+" sign is used for right-hand polarization and the "-" sign is used for left-hand polarization. Because of the relationship in Equation (43) one can write Equation (41) in the form

$$[\underline{E}] = \sum_{n=1}^N E_{\theta}^n \begin{bmatrix} 1 \\ \exp(j \gamma_n) \end{bmatrix} \exp \{ j(n-1) \psi \} \quad (44)$$

$$\text{where } \psi = d_r \cos \phi + \delta \quad (45)$$

$d_r = \frac{2\pi}{\lambda} d$ , distance, in radians, between sources

$\delta$  = phase advance between  $i^{\text{th}}$  and  $(i+1)^{\text{th}}$  sources.

In the following examples, each of the components of the resultant field can be expressed in a form which permits the use of universal pattern charts such as those presented in Kraus (Reference 2). The polarization properties of the resultant field are conveniently represented by the polarization coherency matrices.

Example 4. Sources with the Same Polarization Sense. For this example,  $\gamma_n = \gamma$  for all  $n$ . Then,

$$[E] = E_0 \begin{bmatrix} 1 \\ e^{j\gamma} \end{bmatrix} \begin{bmatrix} \sin(n\psi/2) / \sin(\psi/2) \\ \exp[j(n-1)\psi/2] \end{bmatrix} \quad (45)$$

and where  $\psi$  is given by Equation (45). Thus, the resulting field is circularly polarized with an amplitude pattern given by the well-known expression for the field of an  $n$ -element linear array. Each of the field components is multiplied by the same array factor.

The polarization properties of the wave are conveniently displayed by the polarization coherency matrix, which is defined, for  $(\theta, \phi)$  coordinates as

$$J = \begin{bmatrix} E_\theta \\ E_\phi \end{bmatrix} \begin{bmatrix} E_\theta^* & E_\phi^* \end{bmatrix} = \begin{bmatrix} \langle E_\theta E_\theta^* \rangle & \langle E_\theta E_\phi^* \rangle \\ \langle E_\phi E_\theta^* \rangle & \langle E_\phi E_\phi^* \rangle \end{bmatrix} \quad (47)$$

The polarization coherency matrix for the field in Example 4 is

$$J = \frac{|E_0|^2}{2} \frac{\sin^2(n\psi/2)}{\sin^2(\psi/2)} \begin{bmatrix} 1 & \pm j \\ \mp j & 1 \end{bmatrix} \quad (48)$$

The fact that the resultant wave is circularly polarized can be seen by comparing the matrix in Equation (48) with Table 5-10.

The power received by an aperture  $[A]$  is related to the polarization coherency matrix  $J$  by the equation

$$W = T_r \{ [A] [J] \} \quad (49)$$

If  $[A]$  is the matrix of a right-hand circular aperture with a right-circular incident wave, the available power from a unit effective aperture is

$$W = |E_\theta|^2 \left( \frac{\sin(n\psi/2)}{\sin(\psi/2)} \right)^2 \quad (50)$$

on the other hand, if the receiving antenna is vertically polarized, then

$$W = T_r \begin{bmatrix} 0 & 0 \\ 0 & 1 \end{bmatrix} [J] = \frac{|E_\theta|^2}{2} \frac{\sin(n\psi/2)}{\sin(\psi/2)} \quad (51)$$

and only half of the power in the previous case is now available (3dB polarization loss). In both cases, interference nulls occur, due to the array factor.

The case,  $N = 2$ , is particularly interesting here. For this case, Equation (50) becomes

$$W = 4 |E_\theta|^2 \cos^2 \psi/2 \quad (52)$$

Several illustrative examples are evaluated below.



Example 5. Cardioid antenna pattern. An array of two right-hand (or two left-hand) circularly polarized isotropic point sources is formed with a spacing  $d = \lambda/4$  and a phase difference  $\delta = -90^\circ$ . The resulting pattern is shown in Figure 5-29. The null in the direction,  $\varphi = 0^\circ$ , occurs because of a  $180^\circ$  phase difference in the fields from the two sources in this direction:  $90^\circ$  due to the spacing and  $90^\circ$  due to the phase lag between the excitations. In the opposite direction, the phase differences compensate to produce constructive interference. Although the pattern was formed by an array of point sources, it was chosen to be a reasonable approximation to a log conical spiral antenna pattern such as that proposed for the HEAO spacecraft. Since isotropic sources were assumed, the antenna pattern has radial symmetry about the line  $\varphi = 0^\circ$ .

Example 6. Interferometer pattern. Consider an array of two isotropic point sources with identical phase, amplitude, and polarization. At large spacings many nulls occur in the pattern. The number of nulls in the quadrant  $0^\circ \leq \varphi < 90^\circ$  is equal to the spacing, in wavelengths. For example, the case  $d_\lambda = 20$  is illustrated in Figure 5-30.

Example 7. Cardioid array. The effect of non-identical antenna patterns is illustrated in Figure 5-31, by two cardioids placed 20 wavelengths apart with their nulls facing in opposite directions, along  $\varphi = 0^\circ$  and  $\varphi = 180^\circ$ , respectively. Incomplete cancellation occurs at the minima due to differences in amplitude of the individual fields. The envelope of the minima is given by the difference of the field amplitudes. The envelope of the maxima is given by the sum of the field amplitudes. The minima occur at the angles of the interferometer nulls, which is determined by the spacing of the two cardioid arrays from one another.

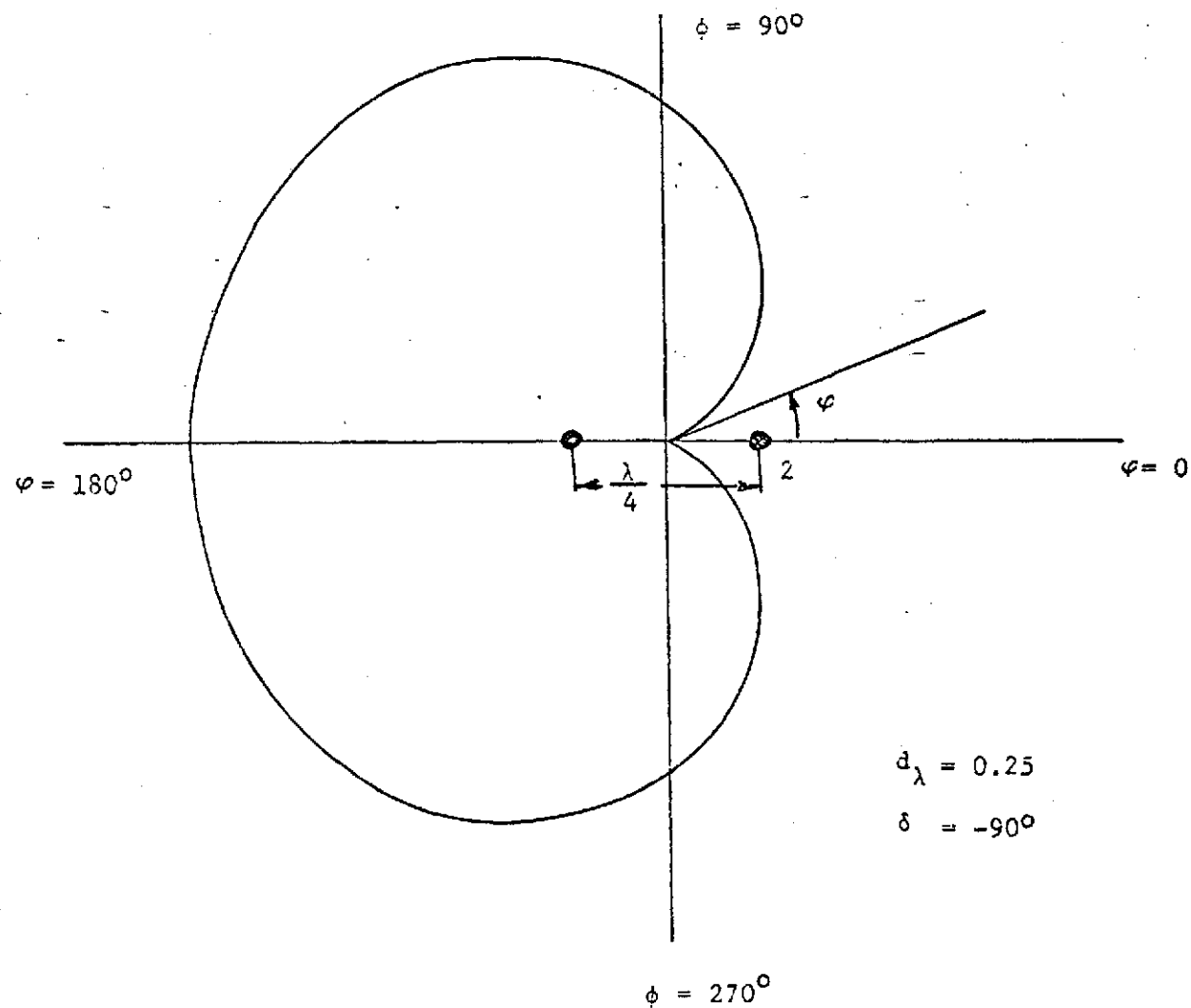


Figure 5-29. Cardioids Antenna Pattern (Similar to HEAO Individual Log Conical Spiral Patterns)

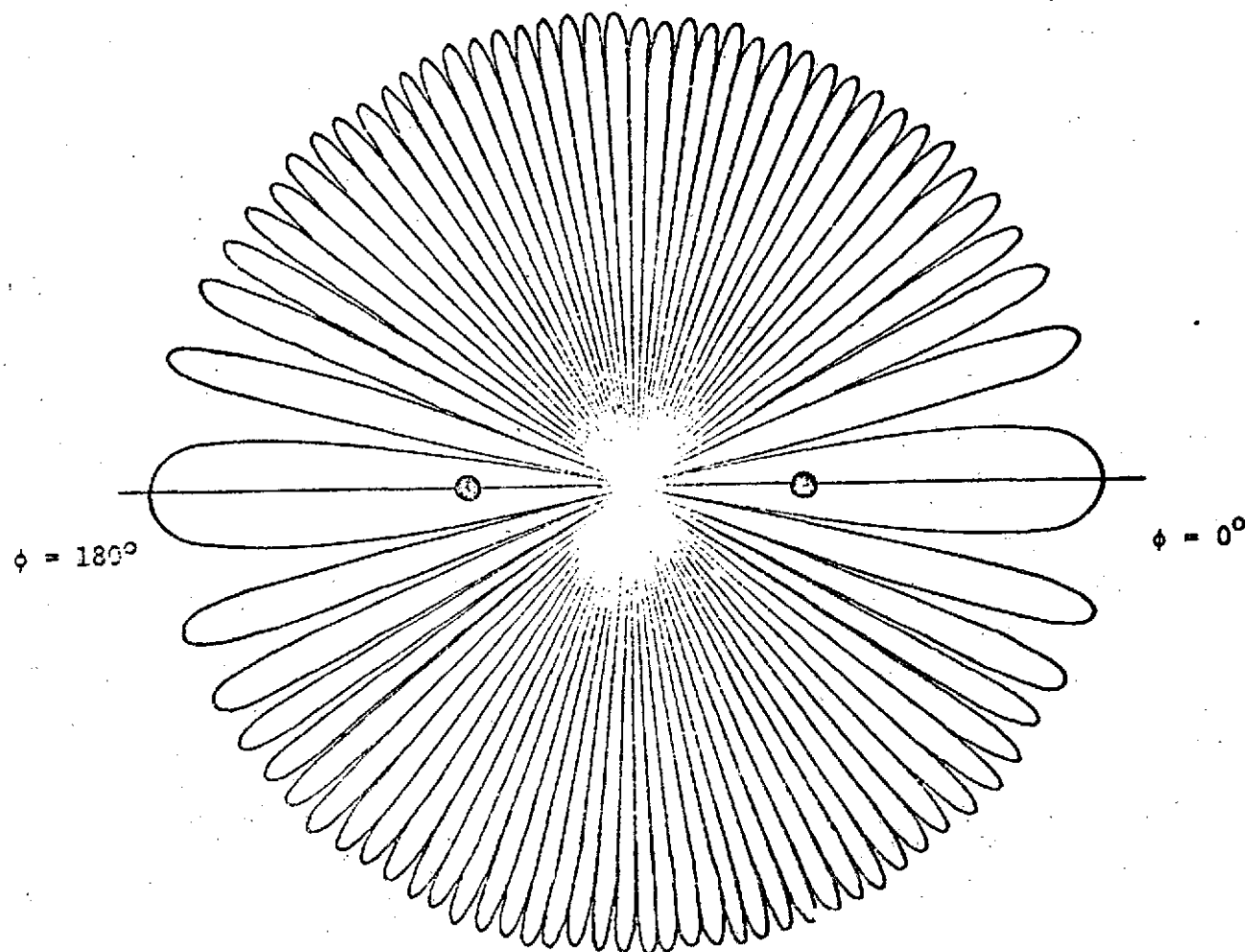


Figure 5-30. Interferometer Pattern for Two Isotropic Sources with a Spacing of 20 Wavelengths

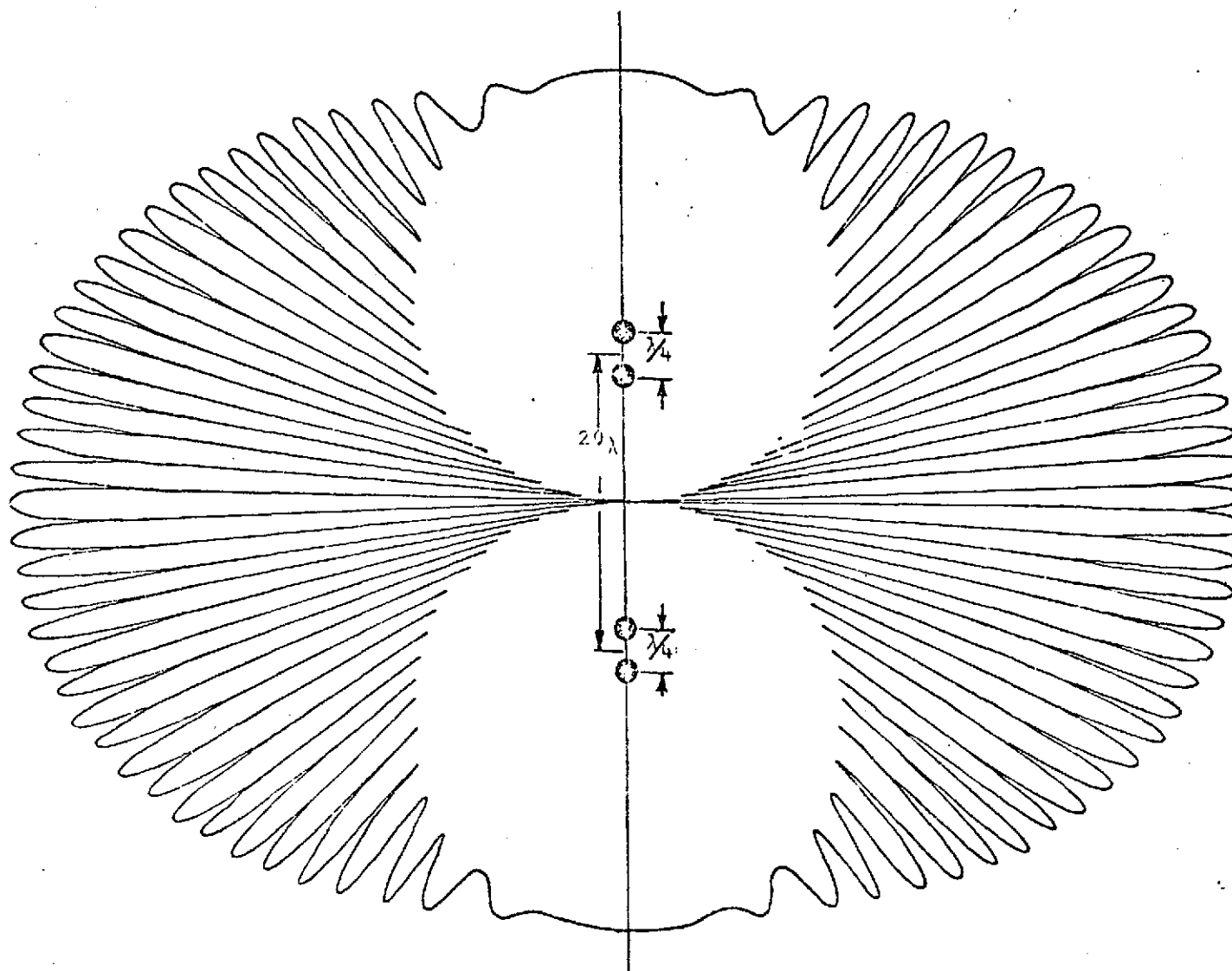


Figure 5-31. Antenna Pattern for Array of Two Cardioids,  $d_\lambda = 20$

Example 8. Sources with alternate polarization sense. The above examples have considered arrays of antennas with the same polarization sense. Now, we will consider arrays with sources having alternating senses of circular polarization.

Assume an even number of elements and sets

$$\gamma_n = \begin{cases} -\gamma, & \text{for } n \text{ even} \\ +\gamma, & \text{for } n \text{ odd} \end{cases} \quad (53)$$

then,

$$\begin{aligned} \hat{a}_\phi \cdot \vec{E} &= E_\phi \sum_{n=1}^N \exp \left[ j(n-1) \psi \right] \\ &= E_\phi \left( \frac{\sin \left( \frac{N\psi}{2} \right)}{\sin(\psi/2)} \right) \exp \left[ j(N-1) \frac{\psi}{2} \right] \end{aligned} \quad (54)$$

$$\hat{a}_\theta \cdot \vec{E} = E_\phi \left[ 1 + \exp \left[ -j(\psi + 2\gamma) \right] \right] \sum_{n=1}^{N/2} \exp \left[ j \left[ (2n-1)\psi - \gamma \right] \right]$$

$$= E_\phi \left( \frac{\sin \left( \frac{N\psi}{2} \right)}{\sin \psi} \right) \cos \left( \frac{\psi}{2} + \gamma \right) \exp \left[ j \frac{N-1}{2} \psi \right] \quad (55)$$

If  $\gamma = \pm \frac{\pi}{2}$ , then Equation (55) gives the result

$$\hat{a}_\theta \cdot \vec{E} = \mp E_\phi \left( \frac{\sin \frac{N\psi}{2}}{2 \cos \frac{\psi}{2}} \right) \exp \left[ j(N-1) \psi/2 \right] \quad (56)$$

A special case of interest occurs when  $N = 2$ .

Then

$$\hat{a}_\theta \cdot \vec{E} = \mp E_\theta \sin \psi/2 \exp \left[ j \frac{\psi}{2} \right] \quad (57)$$

and

$$\hat{a}_\phi \cdot \vec{E} = E_\phi \cos \frac{\psi}{2} \exp \left[ j \frac{\psi}{2} \right] \quad (58)$$

where

$$\psi = 2\pi \left[ d_\lambda \cos \phi + \delta \right] \quad (59)$$

The polarization coherency matrix for this wave is

$$|E_\phi|^2 \begin{bmatrix} \sin^2 \psi/2 & \mp \sin \psi/2 \cos \psi/2 \\ \mp \sin \psi/2 \cos \psi/2 & \cos^2 \frac{\psi}{2} \end{bmatrix} \quad (60)$$

A comparison of this result with those of Tables 5-10 and 5-11 show that the wave radiated by an array of two equal amplitude sources, of opposite polarization sense, is linearly polarized, with the direction of polarization depending upon  $\psi$ , hence upon  $\phi$ . A more detailed analysis of the polarization coherency matrix can be made using the Equations (30) - (35). From these relations, we find that

$$|A| = |B| = \frac{|E_\phi|}{2} \quad (61)$$

and the tilt angle is

$$\tau = \pm \psi/2 \quad (62)$$

A linearly polarized antenna oriented in the  $\hat{a}_\theta$  direction will receive the power

$$W = |E_\phi|^2 \sin^2 \psi/2 \quad (63)$$

while a linearly polarized antenna oriented in the  $\hat{a}_\phi$  direction will receive the power

$$W = |E_\phi|^2 \cos^2 \psi/2 \quad (64)$$

However, since there is no interference between waves of opposite polarization, circularly polarized antennas of either sense will receive half of the power, independent of direction.

## Effects of Multipath.

The polarization coherency matrix of a wave which is reflected from a plane interface can be expressed in terms of the Fresnel reflection coefficients.

$$r_h = \frac{\sin \zeta - \left[ (\epsilon_r - jX) - \cos^2 \zeta \right]^{1/2}}{\sin \zeta + \left[ (\epsilon_r + jX) - \cos^2 \zeta \right]^{1/2}} \quad (65)$$

$$r_v = \frac{(\epsilon_r - jX) \sin \zeta - \left[ (\epsilon_r - jX) - \cos^2 \zeta \right]^{1/2}}{(\epsilon_r - jX) \sin \zeta + \left[ (\epsilon_r - jX) - \cos^2 \zeta \right]^{1/2}} \quad (66)$$

$$X = \frac{\sigma}{\omega \epsilon_0}$$

$\sigma$  = conductivity of the reflecting surface

$\omega$  = angular frequency of the incident wave

$\epsilon_r$  = relative permittivity of the reflecting surface

$\zeta$  = elevation angle of the incident wave

The Fresnel reflection coefficients can be written in polar form

$$r_h = |r_h| e^{j\beta_h} \quad (67)$$

$$r_v = |r_v| e^{j\beta_v} \quad (68)$$



The reflected wave is written in the form

$$\vec{E}_r = \left[ \hat{h}_r E_{h_2} |r_h| e^{j\beta h} + \hat{v}_r E_{v_2} |r_v| e^{j\beta h} \right] e^{j\frac{2\pi}{\lambda} \delta} \quad (69)$$

where

$$\delta = \frac{h}{\sin \zeta} (1 - \cos 2\zeta) \quad (70)$$

and

$h$  = transmitting antenna height

$\zeta$  = elevation angle of receiver

The polarization coherency matrix of the reflected waves is written as

$$[J_r] = \begin{bmatrix} \langle |E_{h_2} r_h|^2 \rangle & \langle |E_h r_h E_{v_2} r_v|^2 \rangle e^{j\beta d} \\ \langle |E_h r_h E_v r_v|^2 \rangle e^{-j\beta d} & \langle |E_v r_v|^2 \rangle \end{bmatrix} \quad (71)$$

where

$$\beta_d = \theta_2 - \theta_1 + \beta_h - \beta_v \quad (72)$$

As a special case, let the plane interface be perfectly conducting and let the incident wave be circularly polarized. When

$$|E_h| = |E_v| \text{ and } \theta_2 - \theta_1 = \pm \pi/2 \quad (73)$$

also,

$$\lim_{x \rightarrow \infty} r_h = -1 = e^{j\pi} \quad (74)$$

and

$$\lim_{x \rightarrow \infty} r_v = +1 = e^{j0} \quad (75)$$

The polarization coherency matrix is

$$[J_r] = |E_h|^2 \begin{bmatrix} 1 & e^{j(\theta_2 - \theta_1 + \pi)} \\ e^{-j(\theta_2 - \theta_1 + \pi)} & 1 \end{bmatrix} \quad (76)$$

analysis of this matrix shows that the reflected wave is circularly polarized with the opposite sense to the incident wave. Thus, a circularly polarized antenna above a perfectly conducting ground plane is equivalent to an array of two oppositely polarized antennas: the original antenna and its mirror image. We have also established that the image antenna has the opposite sense of circular polarization. If the original antenna is an isotropic source, the sum of the direct and reflected fields will be linearly polarized.

Since the general case of elliptical polarization can be decomposed into a superposition of two opposite sense circularly polarized waves, the above discussion of the effect of reflections on circularly polarized waves applies to each of the components in the general case.

## Linear Combining for Polarized Aperture Synthesis.

We have shown in the previous sections that the polarization properties of waves and apertures can be represented by either an  $\underline{E}$  vector or by the polarization coherency matrix,  $\underline{J}_p$ . We have also shown, by examples, that simple summing of antenna outputs produces undesirable interference nulls in some cases. In this section, we extend the vector representation to derive the optimum linear combining rule for polarized aperture synthesis. We also show that RCP and LCP apertures can be considered the basis vectors in a linear vector space. For this purpose, we review the basic definitions of linear vector spaces and the complex form of the Schwarz inequality which is needed for the above development.

A vector space over a field is a set of vectors together with two operations, addition and multiplication by a scalar from the field, satisfying the following postulates:

1. closure under addition: for every pair of vectors  $U$  and  $V$  there is a unique sum  $U+V$ , which is a vector.
2. associative addition:  $(U+V) + W = U + (V+W)$
3. commutative addition:  $U+V = V+U$ .
4. additive identity:  $U+0 = U$
5. additive inverse:  $U+(-U) = 0$
6. closure under multiplication by a scalar: For every scalar  $a$  from the field and every vector  $U$  there is a unique vector  $aU$ .
7. associative scalar multiplication:  $a(U+V) = aU + aV$ .
8. distribute scalar multiplication:  $(a+b)U = aU + b.U$ .
9. commutative scalar multiplication:  $(ab)U = a(bu)$ .
10. multiplicative identity:  $1U = U$ .

A set of vectors  $x_1, x_2, \dots, x_n$  is said to be linearly independent if for a set of scalars  $c_1, c_2, \dots, c_n$

$$\sum_{i=1}^n c_i x_i = 0 \quad (\text{sum on } i) \quad (77)$$

implies that  $c_i = 0$  for all  $i$ . A set of vectors  $x_1, x_2, \dots, x_n$  in a vector space is said to span the space if every vector in the space can be written as a linear combination of the set, i.e., for every  $U$  in the space there exists a set of scalars  $c_1, c_2, \dots, c_n$ , such that

$$U = c_i x_i \quad (\text{sum on } i) \quad (78)$$

A set of vectors may span the space and still not be linearly independent. However, if they are also linearly independent, they are said to form a basis of the vector space. We define the dimension of a vector space as the minimum number of nonzero vectors which span the space.

In this analysis, we are interested in the vectors which are formed as sets of  $n$ -tuples of complex numbers. They form a vector space over the field of complex numbers, if we define addition and multiplication as follows. If  $U = (u_1, u_2, \dots, u_n)$  and  $V = (v_1, v_2, \dots, v_n)$ , then

$$U+V = (u_1 + v_1, u_2 + v_2, \dots, u_n + v_n) \quad (79)$$

If  $\underline{a}$  is a complex scalar, then

$$\underline{a} U = (au_1, au_2, \dots, au_n) \quad (80)$$

It can easily be shown that all of the postulates are satisfied.

We define the inner product  $(U,V)$  which has a complex value and satisfies the following postulates:

1.  $(U, V) = (V, U)^*$
2.  $(U, V + W) = (U, V) + (U, W)$
3.  $(aU, V) = a^*(U, V)$
4.  $(U, U) \geq 0$
5.  $(U, U) = 0$  if and only if  $U=0$ .

The norm of a vector is defined as

$$||U|| = \sqrt{(U, U)} \quad (81)$$

A very important property is the Schwarz's inequality.

$$|(U, V)|^2 \leq ||U||^2 ||V||^2 \quad (82)$$

This can be proved as follows:

For any complex scalar,  $\underline{a}$ , it is true that

$$\begin{aligned} ||U + \underline{a}V||^2 &= (U + \underline{a}V, U + \underline{a}V) \\ &= (U, U) + \underline{a}^*(V, U) + \underline{a}(U, V) + |\underline{a}|^2 ||V||^2 \end{aligned} \quad (83)$$

Since this inequality is true for any  $\underline{a}$ , let

$$\underline{a} = \lambda(U, V)^* / |(U, V)|, \lambda \text{ real} \quad (84)$$

Then, the relation in Equation (83) becomes

$$||U||^2 + 2\lambda|U,V| + \lambda^2 ||V||^2. \quad (85)$$

If the quadratic equation in  $\lambda$  has real distinct roots, then the inequality is violated. This discriminant in the quadratic formula must therefore be negative or zero. Thus, Schwarz's inequality is proved.

$$|(U,V)|^2 \leq ||U||^2 ||V||^2 \quad (86)$$

The equality holds if  $U=V$ . For sets of  $n$ -tuples of complex numbers, the Schwarz's inequality is written in the form

$$\left[ \sum_{j=1}^N u_j^* v_j \right] \leq \left[ \sum_{j=1}^N |u_j|^2 \right] \left[ \sum_{j=1}^N |v_j|^2 \right] \quad (87)$$

Now, we consider the applications of linear vector space theory in a diversity communication system.

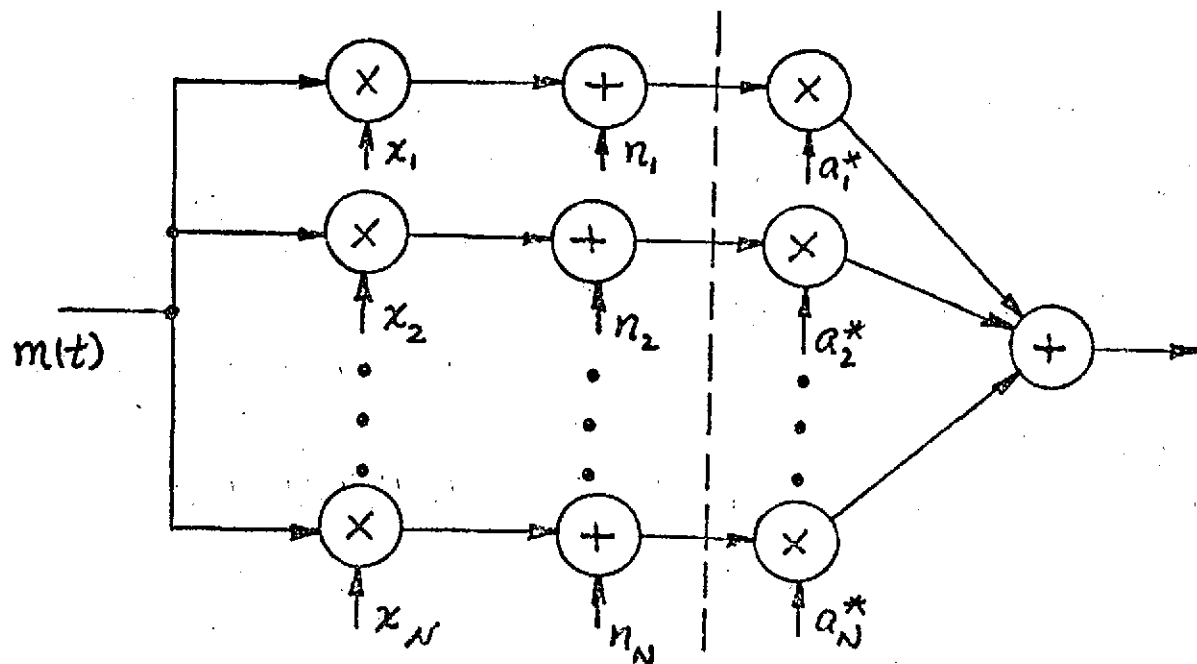


Figure 5-32. Diversity Communication

The diagram in Figure 5-32 shows a diversity communication system in which a common message,  $M(t)$  is multiplied by  $N$  channel gains,  $x_1, x_2, \dots, x_N$ . Also,  $N$  independent channel noises,  $n_1, n_2, \dots, n_N$  are added. The sums are multiplied by the receiver gains and summed. The result is expressed in terms of vector operations as

$$Y = mX + N \quad (88)$$

The diversity receiver performs an inner product operation on the received signal

$$\begin{aligned}(A,Y) &= (A,m(t)X) + (A,N,) \\ &= m(t) (A,X) + (A,N)\end{aligned}\tag{89}$$

The output signal power is the square of the norm of the output signal

$$S_{out} = \overline{|(A,m(t)X)|^2} = \overline{|m(t)|^2} \quad |(A,X)|^2 = \left| \sum a_j^* x_j \right|^2 \tag{90}$$

where the overbar implies a time average and the modulation has been assumed to have unit norm. The output noise power is the square of the norm of the output noise.

$$N_{out} = \overline{|(A,N)|^2} = \sum |a_j|^2 \quad \overline{|n_j|^2}.\tag{91}$$

Now, if we let

$$u_j = a_j ||n_j||\tag{92}$$

and

$$v_j = x_j / ||n_j||\tag{93}$$



the Schwarz's inequality gives the relation

$$\left| \sum_j a_j^* x_j \right|^2 \leq \left[ \sum_j |a_j|^2 \overline{|n_j|^2} \right] \left[ \sum_j |x_j|^2 / \overline{|n_j|^2} \right] \quad (94)$$

and

$$P \triangleq \frac{S_{out}}{N_{out}} \leq \sum_j p_j \quad (95)$$

where we have defined the output signal-to-noise ratio  $P$  and found from the inequality that it is bounded by the sum of the individual signal-to-noise ratios,  $p_j$ , in each of the  $N$  input channels. Since the equality holds in the Schwarz's inequality when  $u_j = v_j$ , it follows that the maximum output signal-to-noise ratio occurs when the weights,  $a_j$ , satisfy the relation

$$a_j = \frac{x_j}{\overline{|n_j|^2}} \quad (96)$$

Thus, the maximal ratio combining rule weights the receiver inputs proportionally to the amplitude of the input signal and inversely proportional to the power of the input noise. The phase of the weighting is conjugate to phase of the complex channel gains, since the scalar product, by definition, uses the conjugates  $a_j^*$ . This rule is optimum under the sufficient assumption of zero-mean independent white Gaussian noise sources in each receiver input. If the input noise is correlated between inputs or if it is non-white, the combining rule is more complicated. Then, there must be filtering for de-correlation and pre-whitening. It is assumed here that the channel noises in the systems we are considering satisfy the assumptions for maximal-ratio combining.

Now, we will be more specific in applying the theory of linear vector spaces to the polarization diversity combining problem. First, we note that in the  $[E]$  vector

notation developed previously, the polarized wave is represented in terms of its  $E_\theta$  and  $E_\phi$  components. The polarization vector space is two-dimensional and thus any polarization vector  $\underline{E}$  can be represented as a linear combination of any two linearly independent polarization vectors. A sufficient condition for linear independence of two polarization vectors, they must satisfy the relation

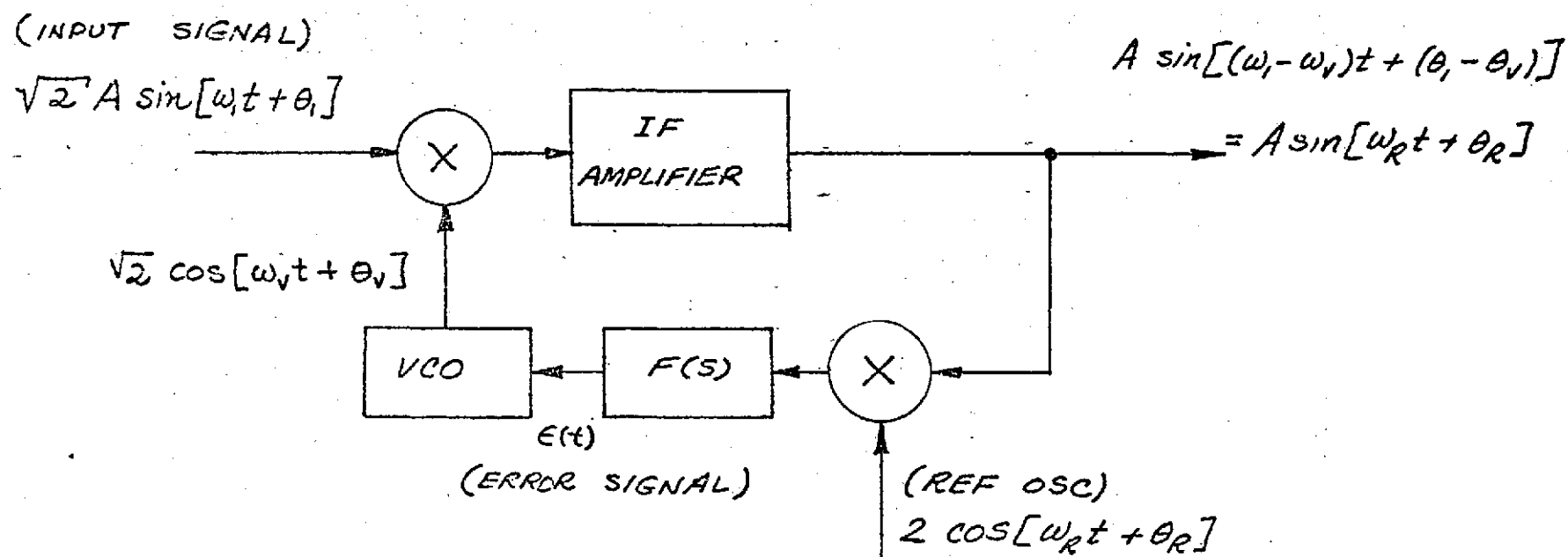
$$(U,V) = 0. \quad (97)$$

It is easy to verify, from the polarization examples presented in Table 5-10, that linear horizontal and linear vertical polarizations are orthogonal, as are linear  $45^\circ$  and linear  $135^\circ$ , as well as the pair, left circular and right circular polarization. Thus, we have shown that the left and right circular polarizations form a basis in a two-dimensional linear vector space by showing that the  $\underline{E}$  vectors satisfy the postulates of a linear vector space. The polarization diversity receiver forms an inner product of the polarization vectors of the wave and the aperture. In the presence of independent white Gaussian channel noises, the optimum weights  $a_j$  in the aperture vector,  $A$ , satisfy the maximal ratio combining rule (96).

Practical implementations of the optimum diversity receiver can be achieved by the use of differential phase shifts and attenuations prior to summing. Techniques for accomplishing this are discussed in the following paragraphs. The inner product requires multiplication by the complex conjugates of the channel gain. In effect what this accomplishes is a cancellation of the phase shift introduced by the channel to bring the diversity receiver inputs into phase. This can be accomplished by mixing with a local reference oscillator in a frequency -offset phase-locked loops as shown in Figure 5-33. The VCO, in lock, operates at a frequency

$$\omega_v = \omega_1 + \omega_R \quad (98)$$

where  $\omega_1$  = frequency of input carrier  
and  $\omega_R$  = frequency of the reference, oscillator



$$E(t) = \sin[(\omega_i - \omega_v - \omega_r)t + \theta_i - \theta_v - \theta_r]$$

$$\text{AT PHASELOCK, } \begin{cases} \theta_i - \theta_v = \theta_r \\ \omega_i - \omega_v = \omega_r \end{cases}$$

Figure 5-33. Frequency-Offset Phase-Locked Loop  
 Phase Shifter

with a phase angle of

$$\theta_V = \theta_1 + \theta_R \quad (99)$$

where  $\theta_1$  = phase of input carrier

$\theta_R$  = phase of reference oscillator

The output carrier is shifted in frequency and phase so that it has the same frequency as, and is in phase-quadrature with, the local reference oscillator. Phase modulation on the carrier is undistorted by the frequency offset loop because of the narrow bandwidth of the loop filter  $F(s)$ . The amplitude of the output signal is the same as the amplitude of the input signal except for a constant scale factor. Thus, the frequency offset PLL phase shifter when applied to each of the receiver inputs, brings them into phase without introducing a differential attenuation.

Since the carriers at the outputs of the PLL phase shifter have known frequency and phase, the amplitudes can be determined by means of a coherent amplitude detector (CAD). The amplitude weighting is obtained by multiplying each of the signals by a gain which is proportioned to its respective amplitudes before summing. The weighting is proportional to the total rms amplitudes, with a constant scale factor as long as the modulation index is constant. Such an amplitude weighting system is shown in Figure 5-34.

A maximal-ratio combiner which incorporates the above elements is shown in Figure 5-35. The signals from the two orthogonal polarizations are phase-shifted, amplitude-weighted and summed. An additional feature of this system is that the reference oscillator can be used as a phase reference for coherent phase detection.

A disadvantage of the maximal-ratio combiner shown in Figure 5-35 is that the individual loops may lose lock as a result of changes in the polarization of the received wave due to changes in the line-of-sight look angle or rotations of the spacecraft. This occurs if the received carrier level falls below the loop threshold or if accelerations exceed the loop tracking capability. If this occurs in the system of Figure 5-35, it may be difficult to re-lock the loop since the

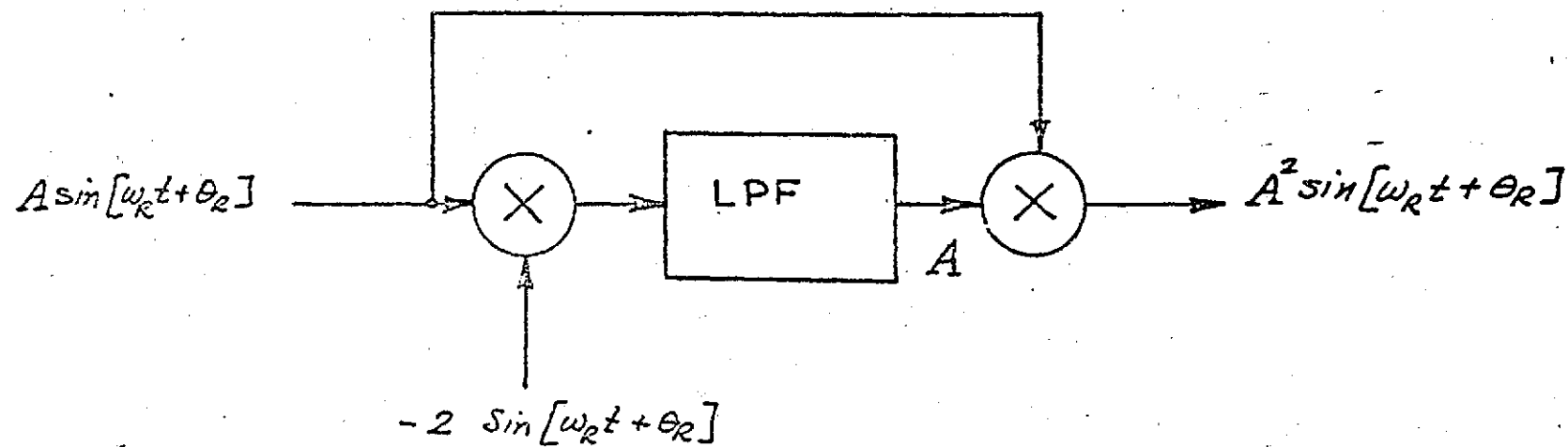


Figure 5-34. Maximal Ratio Weighting Network

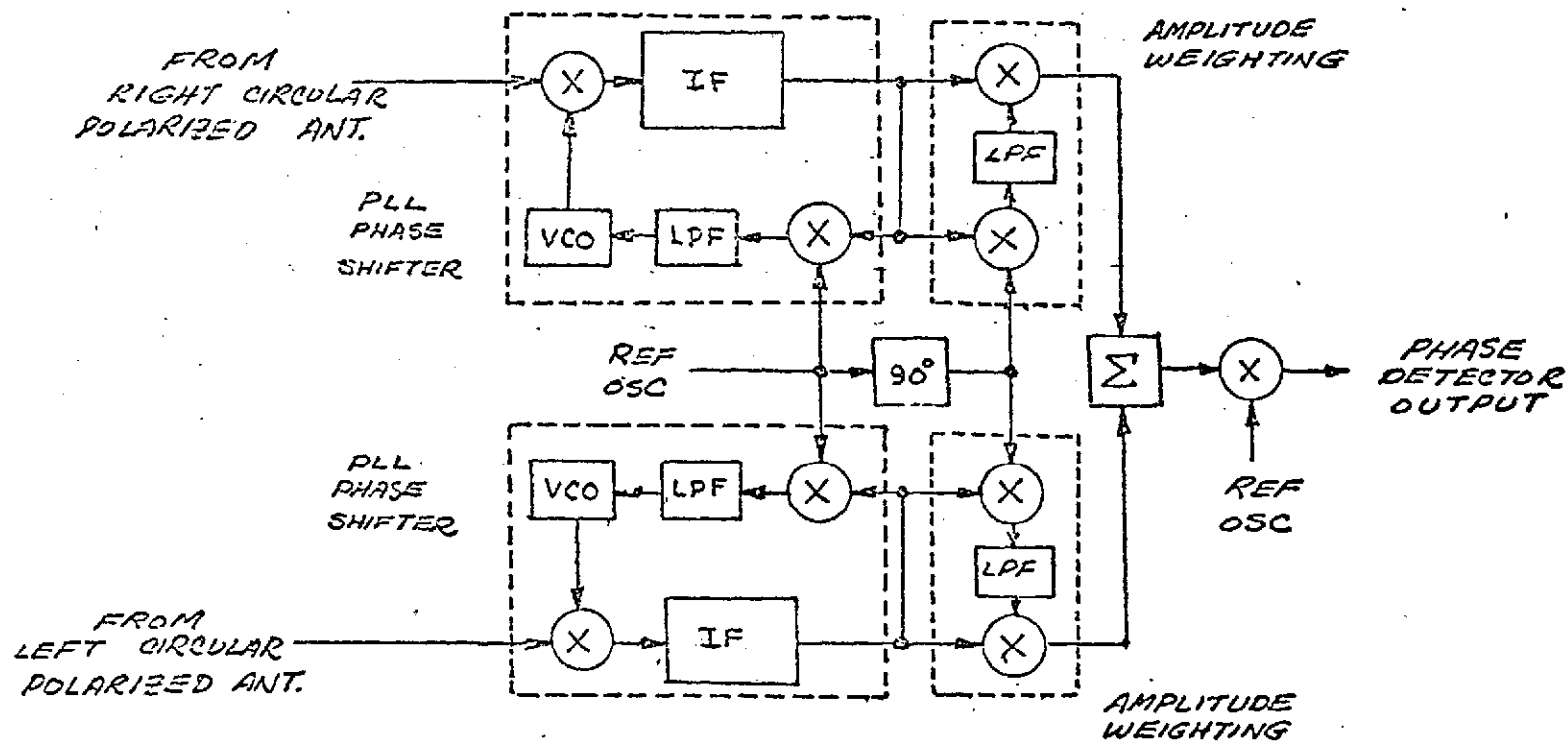


Figure 5-35. Maximal Ratio Combiner\*

\* Assumes equal noise power and independent noise in the two inputs.

doppler shift may place the received carrier beyond the pull-in range of the loop. This disadvantage is largely overcome in the modified system shown in Figure 5-35, known as the diversity-locked loop. This system uses an outer, primary, tracking loop to track out common doppler shifts. The auxiliary loops must track out only the differential doppler. Since this tends to be much smaller than the common doppler shift, the required pull-in range of the loops can be reduced, together with the threshold levels. Also, since the error signal for the primary loop is derived from the diversity combiner output, the signal-to-noise ratio is equal to the sum of the signal-to-noise ratios in the two channels. The error signal for the primary loop is thus more reliable than that of either input channel, and the primary loop has a greater probability of remaining in lock than both of the individual loops. The advantages of the maximal ratio combiner shown in Figure 5-35 are retained in the diversity-locked loop of Figure 5-36.

An alternative arrangement is shown in functional block diagram form in Figure 5-37. This system is discussed in detail in Appendix A of this report. The operation of this maximal ratio combiner is described briefly as follows:

Input signals and noise are divided into in-phase and quadrature channels. The resulting channels are correlated with the receiver output to determine the weighting. Those components that are highly correlated with the output are emphasized in the sum according to the maximal ratio rule. An AGC amplifier in the feedback path maintains constant output power, while the effect of the maximal ratio combining is to minimize the output noise power. Thus, the output signal-to-noise ratio is maximized.

A microwave implementation of the "bootstrap" linear diversity combiner is shown in Figure 5-38. Here, hybrids are used as power splitters and summers to avoid VSWR problems. An arrangement of this sort could be used as a predetection diversity combiner in HEAO to allow full spherical coverage on the uplink with one receiver, and to allow 100 percent redundancy over the entire sphere if two receivers are used.

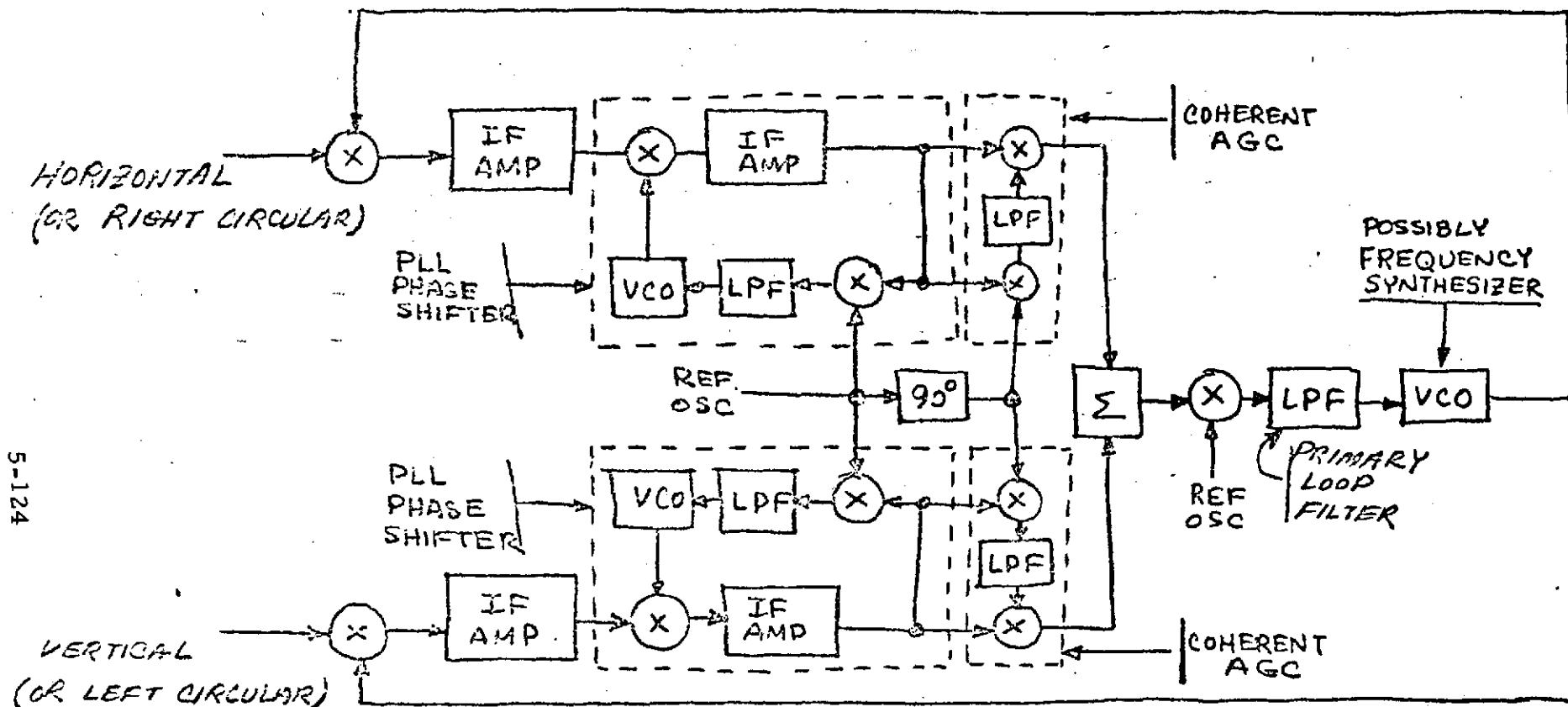


Figure 5-36. Polarization Diversity Phase-Locked Loop



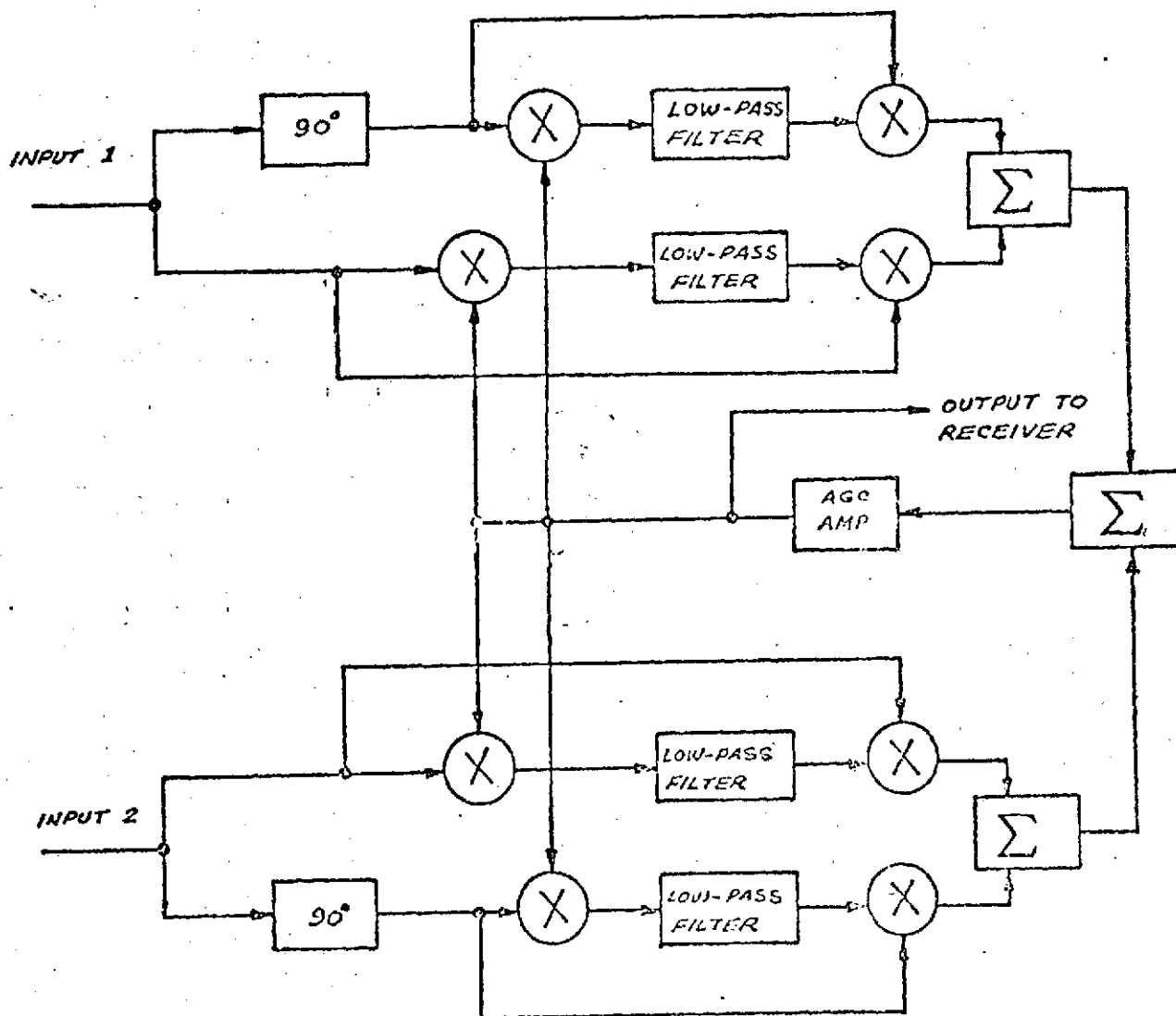


Figure 5-37. Maximal Ratio Combiner - Functional Block Diagram

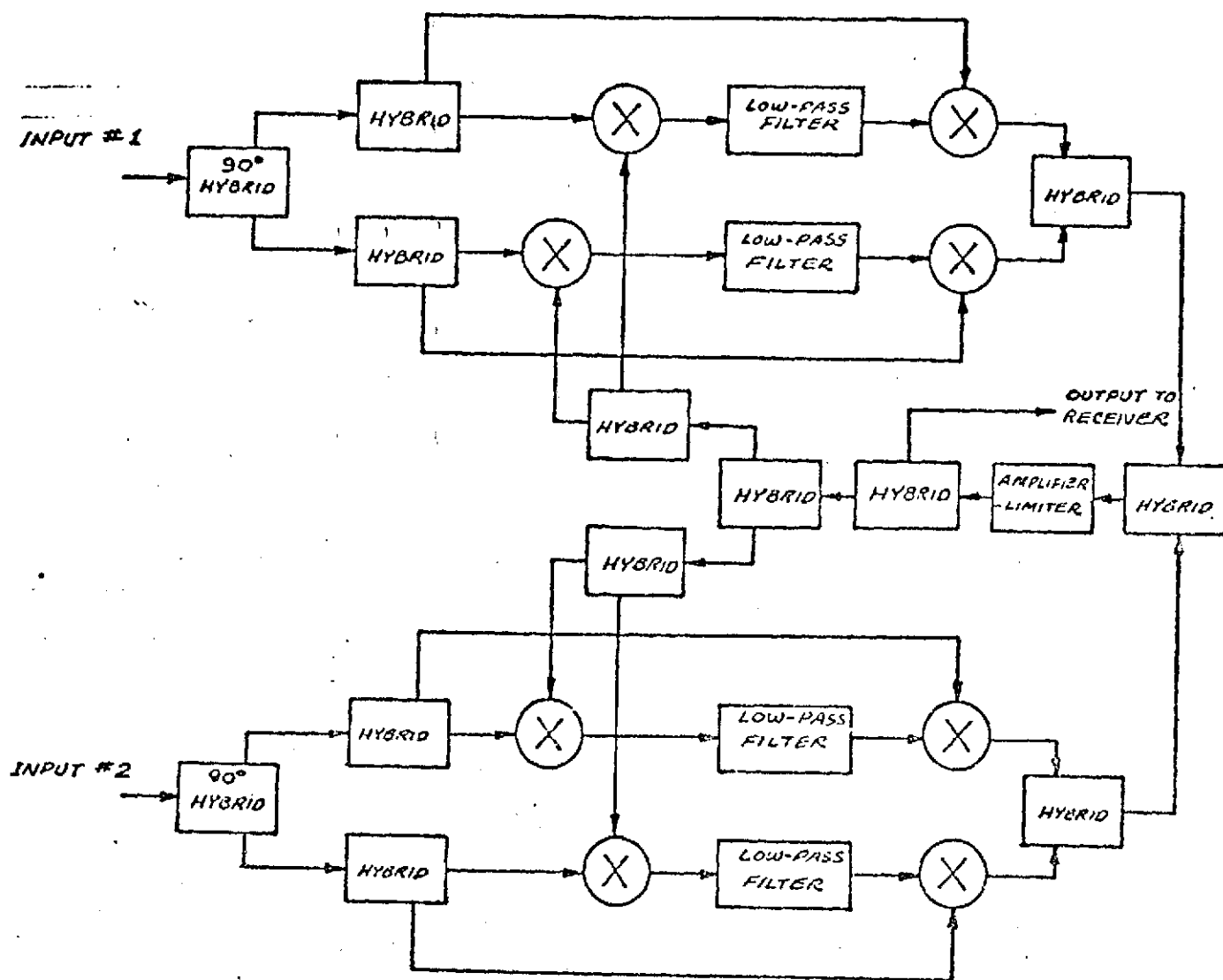


Figure 5-38. Predetection Maximal Ratio Combiner

### 5.1.3 Communication Equipment Design

This section describes the design of the communication equipment contained within the spacecraft communications and data handling module. The design is in response to the EOS Phase B Study Work Statement.

The communication system requirements and configuration for the communication and data handling module was described in Section 5.1.1. As stated there, the baseline configuration consists of a receiver and transmitter, forward and aft omni antenna and associated diplexers, combiner, and switch. The baseline system provides no redundancy.

A block diagram of the baseline communication system is shown in Figure 5-39. A functional description of the system was presented in Section 5.1.1. All the equipment required to implement the system has been developed on previous programs at TRW, as well as many other companies, and existing equipment will be used here in describing the baseline.

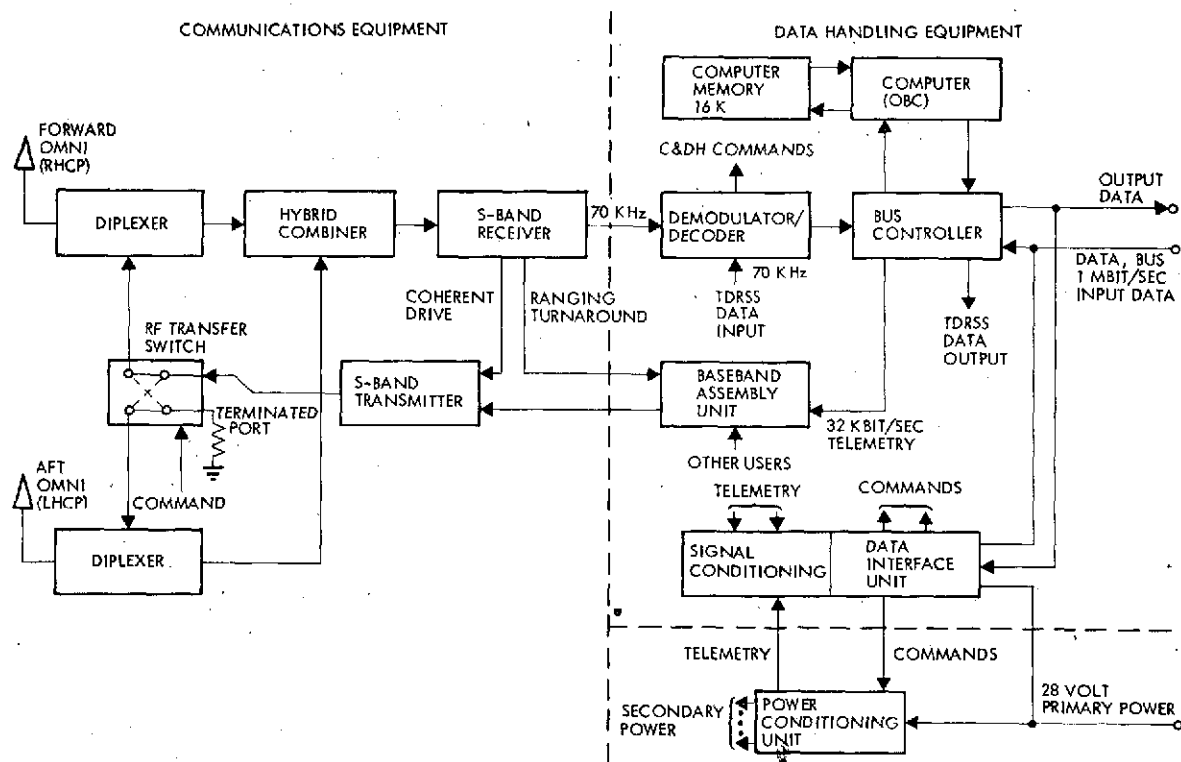


Figure 5-39. EOS-A Baseline Communications System for Communications and Data Handling Module

The antennas and diplexer designs presented here are from the Pioneer 10 and 11 and Defense Satellite Programs. The transponder (receiver and transmitter) required to meet the TT&C specifications can be configured in a variety of ways. Many manufacturers supply TT&C equipment that generally differs in the construction techniques and block diagram configuration employed. However, they all offer comparable performance, reliability, and cost.

Recently, TRW has developed a microelectronic TT&C transponder that offers reduced complexity, size, weight, and power consumption, resulting in a highly reliable low-cost unit. This transponder will be used in describing the baseline equipment.

#### 5.1.3.1 Equipment Description

##### 5.1.3.1.1 S-Band Omni Antenna (Forward and Aft)

The boom-mounted aft antenna is the Defense Satellite Program conical log spiral antenna having a peak gain of approximately 3 dBi and is circularly polarized. An infinite line balun is used to feed the antenna with a quarter-wave transformer at the feed trip. With this feed, a VSWR of less than 1.5 to 1 is provided. The axial ratio of the left hand circularly polarized radiated signal is not greater than 3 dB over  $\pm 90$  degrees. The antenna is 25.4 cm high by 8.89 cm in diameter at the antenna base and weighs 0.36 kg. A picture of the antenna and a typical measured radiation pattern is shown in Figure 5-40.

The forward looking antenna is the Pioneer 10 and 11 conical log spiral antenna having a half-power beamwidth of approximately 120 degrees. The antenna has a peak gain of 4.5 dBi and is circularly polarized. A Robert's type balun is used to excite the antenna and also provides an impedance match of less than 1.5 to 1. The axial ratio of the right hand circularly polarized radiated signal is less than 2 dB over  $\pm 60$  degrees. The antenna is 13.1 cm high by 5.2 cm in diameter at the antenna base and weighs 0.15 kg. A picture of the antenna and a typical measured radiation pattern is shown in Figure 5-41.

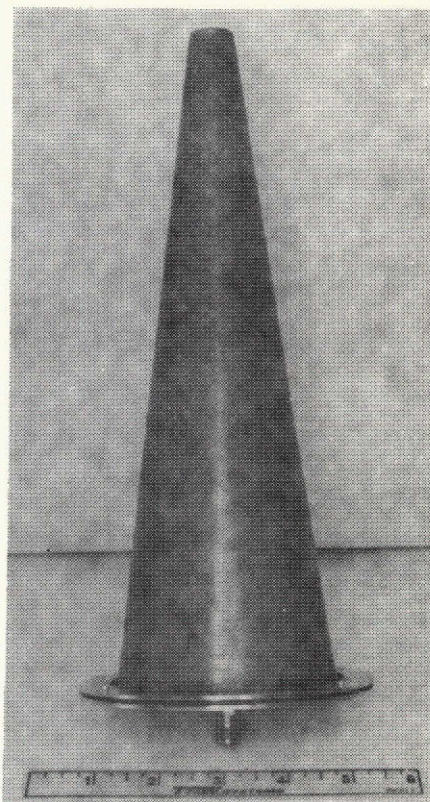
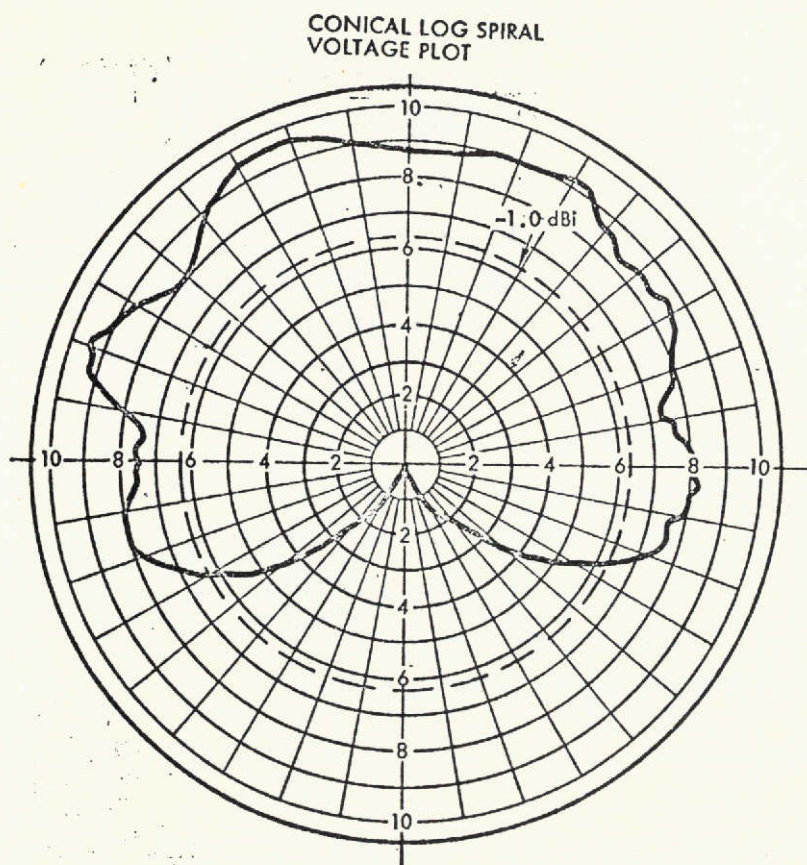


Figure 5-40. Defense Satellite Program S-Band Omni Antenna

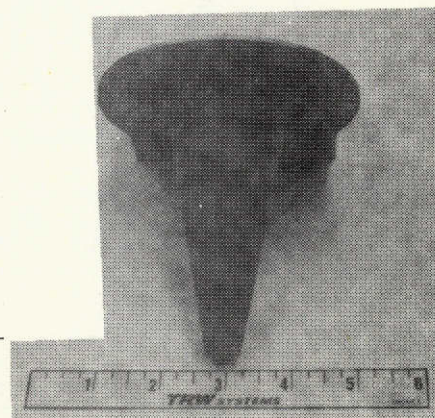
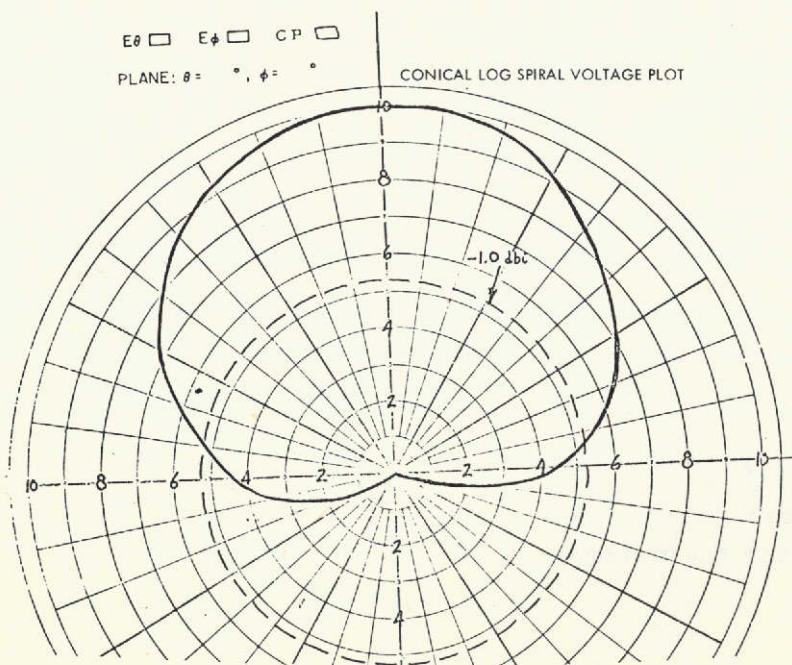


Figure 5-41. Pioneer 10 and 11-S-Band Omni Antenna

#### 5.1.3.1.2 S-Band Diplexer

The diplexer has been used on the Pioneer 10 and 11 spacecraft program and is flight qualified. This diplexer uses a 6-resonator bandpass filter in the receiver channel and an 11-resonator bandpass filter in the transmitter channel. Additional rejection is obtained in the transmitter channel with the use of three band-reject resonators mounted within the low-pass filter. The low-pass filter provides rejection at the second through fourth harmonics.

The bandpass filters are connected together at a common junction to form a diplexer. The stop-band impedance of each filter must not react within the pass-band of the adjacent filter. Therefore, the stop-band of each filter is designed to be essentially an open circuit at the pass-band frequencies of the other filters. Once this is attained, the two channels are connected together with little or no interaction.

Typical specifications of the diplexer are:

- Insertion loss: Receiver 0.75 dB  
Transmitter 0.30 dB
- Stop-band rejection 85 dB
- VSWR 1.3:1
- Power handling 20 watts
- Weight 1.36 kg

Actual response characteristics are shown in Figure 5-42.

#### 5.1.3.1.3 RF Cables

The RF cabling can be implemented with low-loss Teflon spline dielectric semirigid coaxial type cable having a loss of approximately 4.4 dB per 100 feet. The outer conductor diameter is 0.390 inch. This cable has been used on past spacecraft programs and is flight qualified. Where flexible cable is necessary, Type RG-142 is recommended. This cable uses solid Teflon dielectric and has a loss of approximately 22 dB per 100 feet. Its outer conductor diameter is 0.142 inch. This cable has also been space qualified.



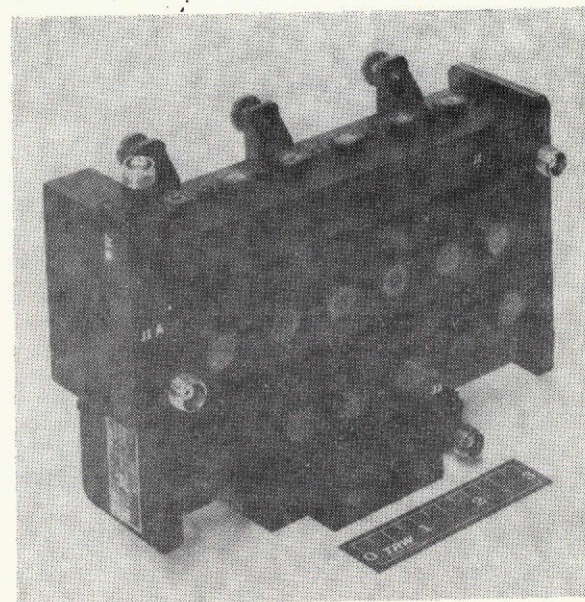
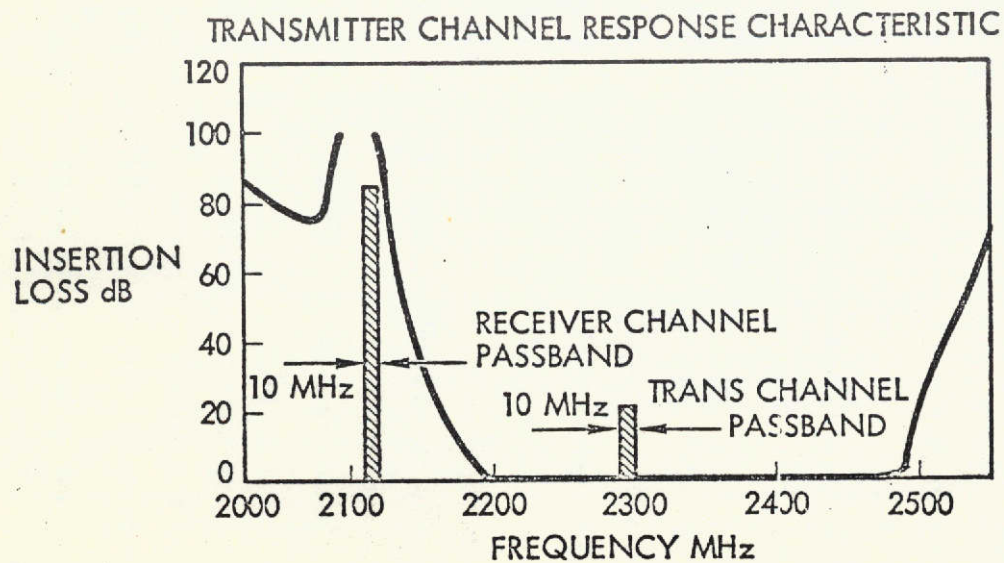
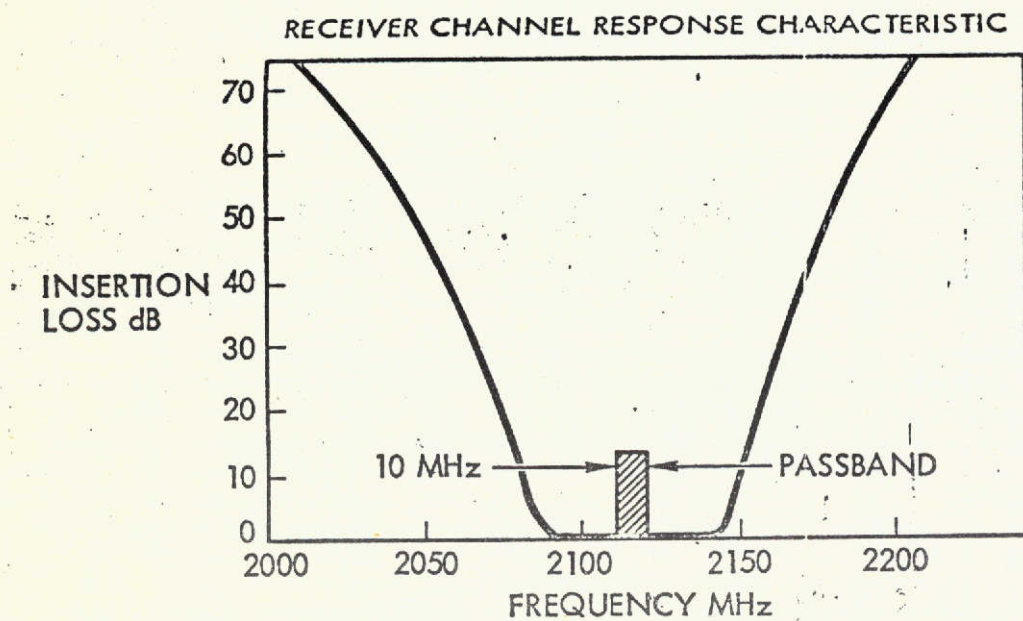


Figure 5-42. S-Band Diplexer





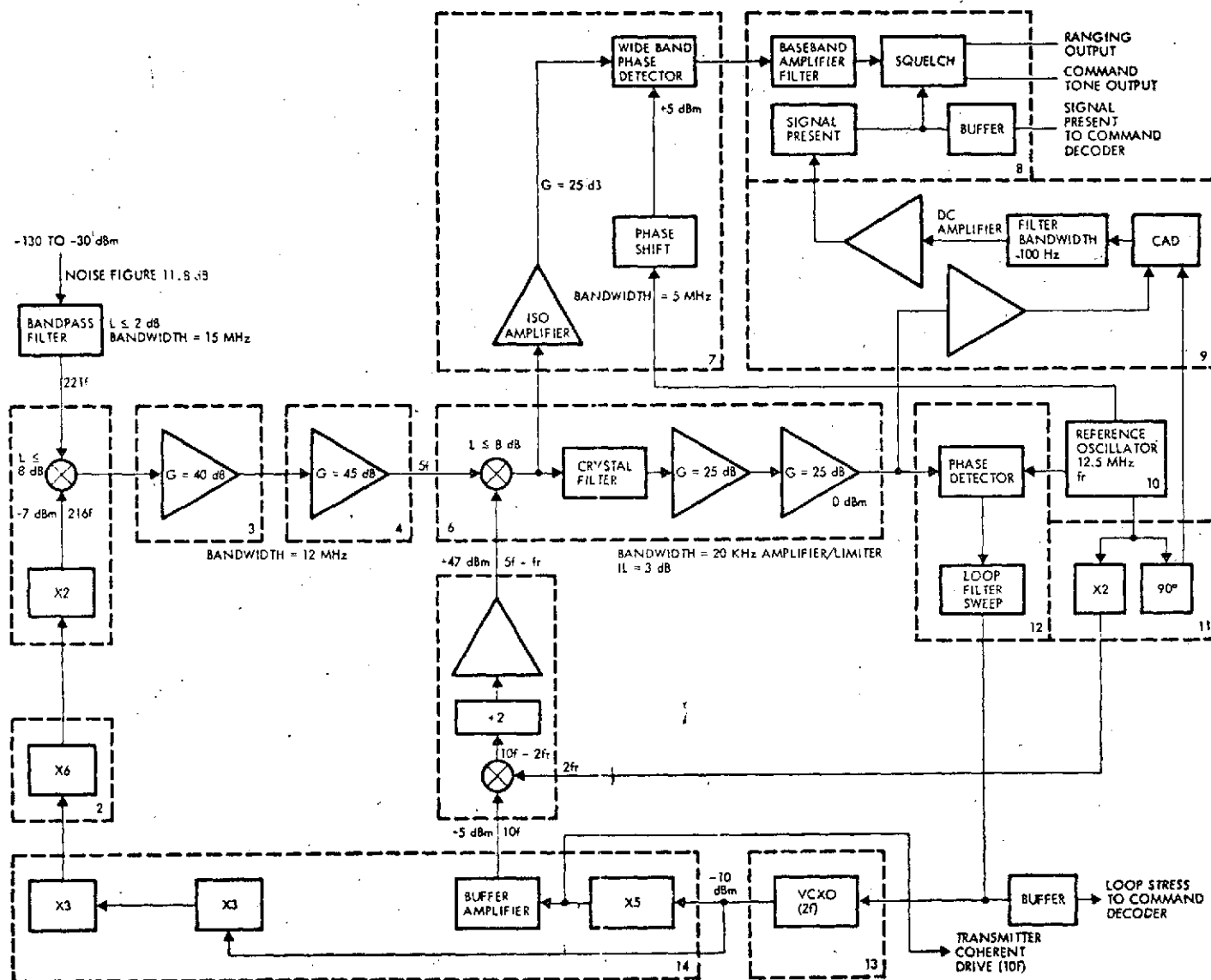


Figure 5-43. S-Band Command Receiver Block Diagram

mixer. The reference oscillator signal provides a reference signal for the phase detectors. As a result, the VCXO frequency and phase are controlled such that the frequency of each mixer injection signal is maintained in precisely the correct relationship.

Table 5-12. S-Band Command Receiver Specifications

Receiving frequency range (select channel)	2025-2120 MHz
Noise figure, maximum (including 2-dB preselector loss)	11.8 dB
Input VSWR, maximum	1.5 to 1
Input signal range	Threshold to -30 dBm
Maximum RF input level (no damage)	-10 dBm
Acquisition threshold (loop SNR = +6 dB)	126 dBm
Loop noise bandwidth at threshold	1000 Hz
Frequency acquisition range	$\pm 180$ kHz
Acquisition sweep period	10 sec
Static phase error	6 deg, maximum
Ranging channel bandwidth	1.5 MHz
Absolute range delay	600 nsec
Ranging time delay variation	50 nsec, maximum
Transmitter coherent drive level	0 dBm
Regulated power requirement, maximum	2.2 watts

### X2 and First Mixer

The X2 and first mixer circuit consist of a transistorized X2 frequency multiplier and a double balanced passive mixer. All tuning is accomplished by MIC transmission lines that are tuned by sliding a RF short between the line and ground. The X2 frequency multiplier drives the LO port of the mixer at +5 dBm.

### LO X6

The circuit consists of a transistorized X6 frequency multiplier. The desired harmonic is filtered out by a capacitive coupled double-tuned

circuit. All tuning is accomplished by MIC transmission, which is tuned by sliding a RF short between the line and ground. The circuit delivers 5 dBm with a drive of 9 dBm.

### First IF

First Stage. The first stage consists of cascading two transistor stages followed by a MC1550 (an IC RF amplifier operating as a limiter). Collector tanks on the transistor are low Q single-tuned circuits and required no variable elements. Input impedance matching is accomplished with an L-C L-section. When tuned, a noise figure of 5 dB is achieved. The overall gain of the first stage is 40 dB.

Second Stage. The second stage consists of cascading three MC1550. Each stage is driven in a differential configuration to provide symmetrical limiting. Bandwidth is achieved by using double-tuned tanks on the output of each stage. Input impedance matching is accomplished by an L-section consisting of C and L. The overall gain of the stage is 45 dB with a bandwidth of 15 MHz centered at 45 MHz.

### Third Mixer and Divide-by-Two

The function of the third mixer and divide-by-two circuit is to difference mix the 10f signal with twice the reference oscillator ( $2f_r$ ) and divide this signal by two. An Anzac double balance mixer mixes the 10f signal with  $2f_r$  and the difference frequency is filtered out with a lowpass filter. A MC1550 provides amplification to drive a Schottky-clamped TTL flip-flop (selected for its low DC power consumption), which divides the frequency by two. A buffer amplifier on the output provides +7 dBm of drive to the second mixer.

### Second Mixer/Second IF

The circuit consists of a mixer, crystal filter, and two stages of amplification. The mixer is a double-balanced diode mixer (Anzac type MD-113) selected to minimize undesired modulation products. The crystal filter has two poles and a bandwidth of 20 kHz, which allows the phase detector to operate at a S/N of -7 dB at acquisition threshold. Two stages of amplification following the crystal filter provide 50 dB of gain, which is adequate to bring the noise 15 dB into limiting. The output of the two-stage amplifier drives the phase detector at a level of 0 dBm.

### Wideband Phase Detector

The wideband phase detector circuit consists of a buffer amplifier driving the L and R ports of an Anzac mixer (type MD113). To ensure that the reference oscillator signal will not leak back into the second IF and cause a false lock, isolation between the reference oscillator and IF signal input is required. This is accomplished by using a MC1550 to amplify the IF signal, which has a reverse admittance of less than 0.001 milliohms, hence providing the necessary isolation.

### Baseband Amplifier and Filter

The baseband amplifier and filter circuitry consist of a five-section lowpass filter, an amplifier, and squelch circuit. Bandwidth of the filter is 1.5 MHz. The amplifier consists of a MC1550 followed by an emitter follower. Squelch control is accomplished by an LH201, used as a comparator, and a FET switch which controls the DC power to the MC1550.

### Coherent Amplitude Detector (CAD)

The CAD circuit consists of a buffer amplifier driving the L and R ports of an Anzac mixer (type MD-113) followed by a lowpass filter and DC amplifier. Isolation between the reference oscillator input and the IF input is achieved by using a MC1550 to amplify the IF signal. The low-pass is a single-section R-C filter with a bandwidth of 100 radians/sec. DC amplification is accomplished with an LH201 operational amplifier.

### Reference Oscillator

The reference oscillator circuit consists of a crystal oscillator followed by a buffer amplifier. The crystal oscillator oscillates at 12.515 MHz, which is the second IF center frequency. The output of the reference oscillator circuit has three outputs that drive the carrier-loop phase detector, the CAD, and the reference oscillator X2 and 90-deg phase shift circuits.

### X2 and 90-deg Phase Shift

The X2 and 90-deg phase shift substrate consists of two separate circuits, each performing a different function. One circuit is a 90-deg

phase shifter, which shifts the phase of the reference oscillator signal 90 deg to drive the coherent amplitude detector (CAD). The 90-deg phase shift is accomplished by an L-C section, which drives an amplifier to provide +7 dBm drive to the CAD.

A second circuit is the X2 frequency multiplier, which doubles the reference oscillator frequency to drive the third mixer. Frequency multiplication is accomplished by a transistor and a capacitive-coupled double-tuned circuit to filter out the second harmonic. The drive level to the third mixer is set at -10 dBm to reduce the level of spurious mixer products.

### VCXO

The VCXO is designed to operate on any USBS uplink channel. Channel changing is accomplished by replacing the crystal and tuning  $L_1$  and  $L_3$ .

The circuit consists of a common base crystal oscillator, with varicaps to control the frequency, and a buffer amplifier. Frequency pulling of the crystal is accomplished by applying a control voltage to two varicaps in series. A constant current diode in series with a fixed resistor generates the bias voltage for the varicaps. The bias capacitance of the varicaps is tuned out with  $L_3$  such that the VCXO frequency will oscillate at the crystal frequency. A resistive L-attenuator at the control voltage input allows the gain constant of the VCXO to be adjusted up to a maximum of 3 kHz/volt.

### X5 and LO X9

The X5 and LO X9 circuits consist of a X5 frequency multiplier and two X3 frequency multipliers. The frequency multipliers use transistors as the nonlinear element and a capacitive-coupled double-tuned tank to select the desired harmonic. The first transistor stage multiplies the VCXO frequency by five and drives the buffer amplifier to provide a +7 dBm output to the third mixer and also drives to the X2. The output of the two X3 drives the LO X6 circuit at 0 dBm.

### Mechanical Description

The TT&C receiver is packaged in three machined aluminum housing subunits. Each subunit is designed in a stand-alone configuration for assembly and testing purposes but mates with the adjoining subunit by means of recessed shoulders and screws (see Figure 5-44). The complete receiver assembly, including the preselector subunits, has a volume of 511.12 cu cm and a total (estimated) weight of 680.5 gms. The receiver envelope drawing is shown in Figure 5-45.

The receiver subunit (Figure 5-46) is housed in a shallow, 3.81 cm high, open-top machined chassis. The floor or bottom of the chassis is recessed inside of the platform mounting ribs to accept a flush-mounted RF gasket and sheet metal cover. The top of the chassis, on the edges adjacent to the platform mounting ribs, is machined to provide a shoulder to prevent line-of-sight penetration of the flush-mounted RF gasket and cover.

The receiver subunit has four modules with each module containing four alumina microstrip circuitry substrates, shown in Figure 5-47. This design gives a packaging capacity of 16 substrates and represents a 15 percent growth potential in the presently configured receiver. The modules are bottom mounted to the receiver chassis and secured by screws located in close proximity to circuit input/output pins.

The machined recess in the bottom of the receiver chassis accepts a stripline interconnect board. The module circuitry pins, both ground and signal, penetrate a clearance hole in the receiver chassis and the stripline interconnect board. The regulated DC voltages are carried on a secondary printed circuit plane and isolated from the stripline by the lower ground plane. A separable single-sided copper clad board provides insulation and isolation for the interconnect pin terminations. The insulation board is shielded by a sheet RF gasket and the RF gasket is compressed and retained by a light sheet aluminum cover that is mounted flush or slightly recessed to the mounting surface of the receiver chassis.

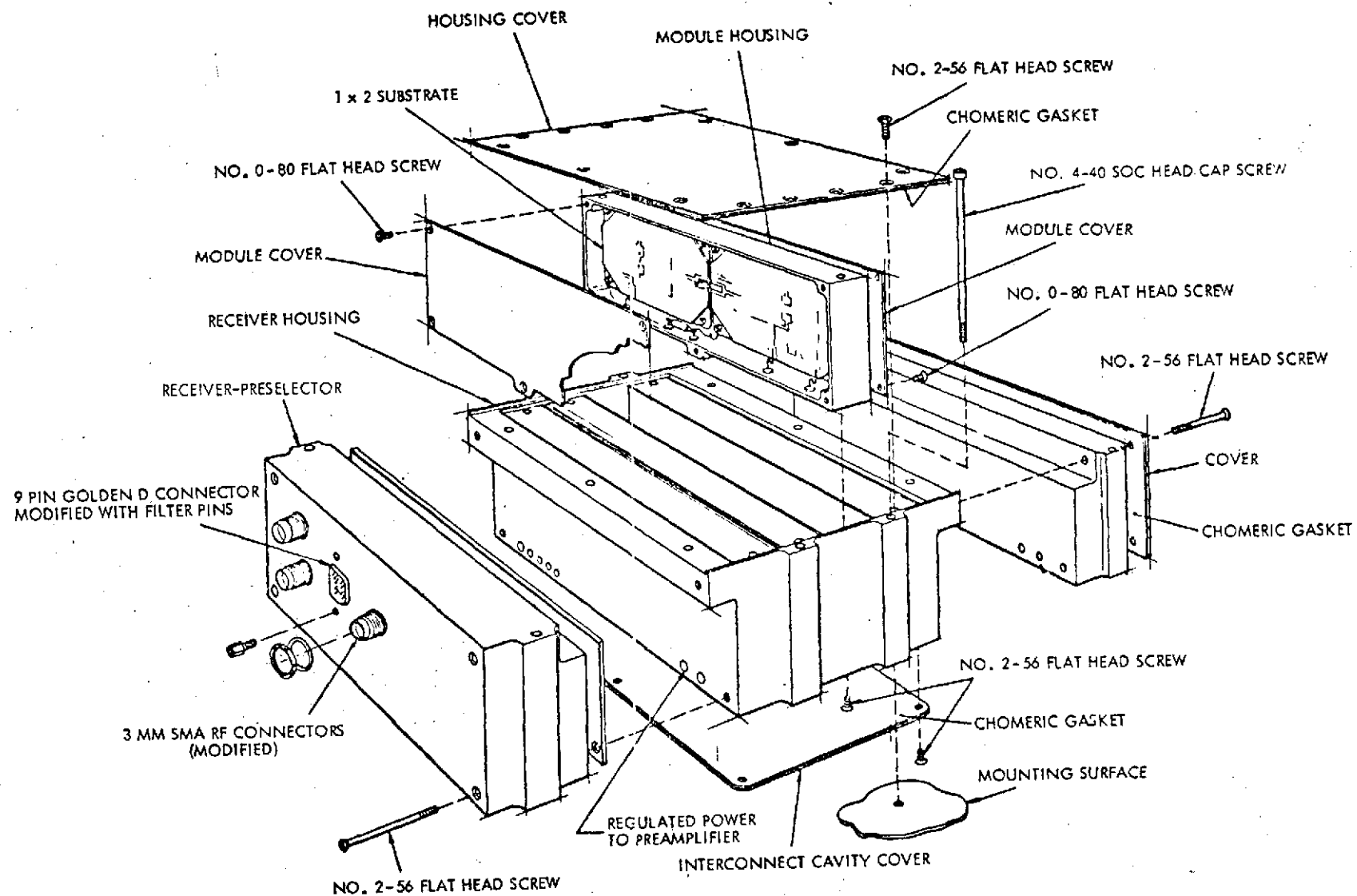


Figure 5-44. TT&C Transponder Subassembly

The total interconnect and shield assembly, from the module mounting surface to the receiver chassis mounting surface, including the gasket retention cover, is designed in 0.508 cm.

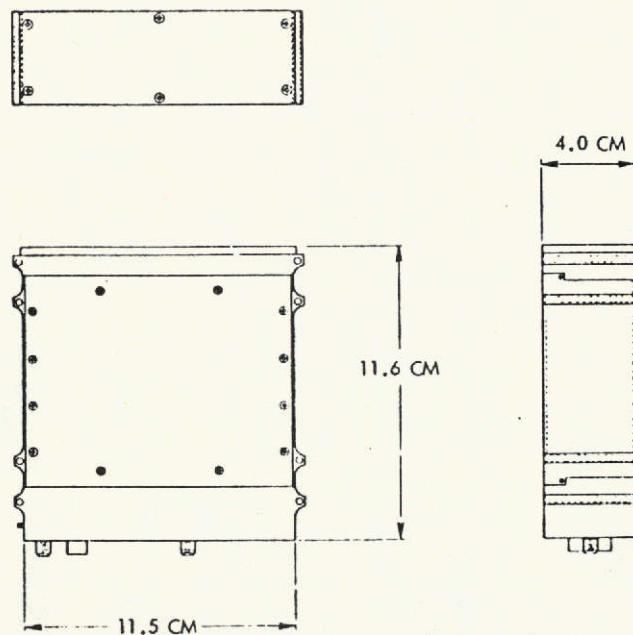


Figure 5-45. TT&C Receiver Envelope Drawing

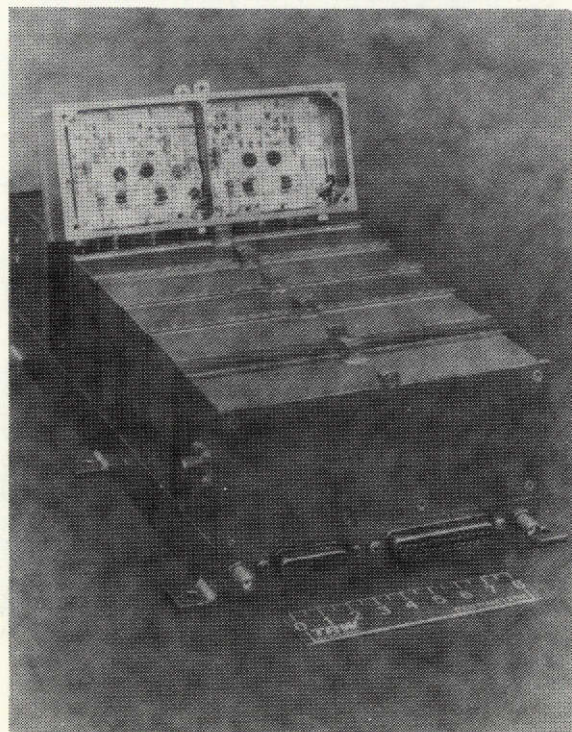


Figure 5-46. Receiver Housing



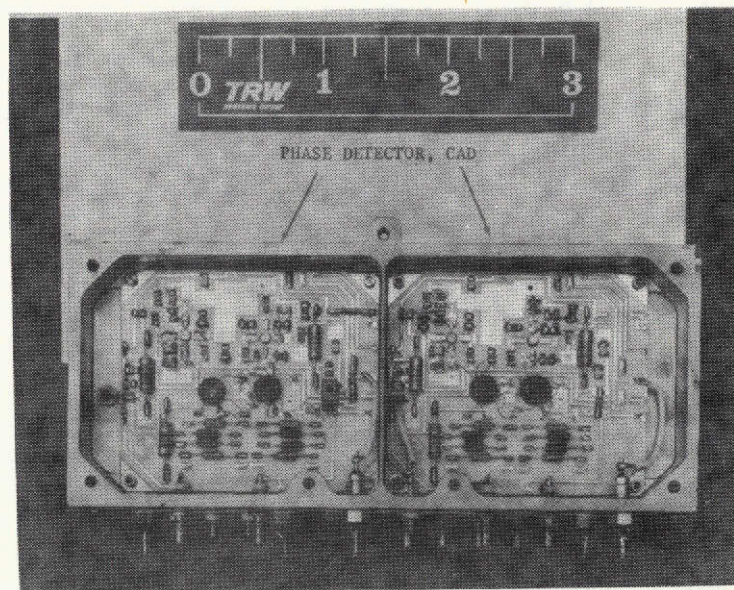


Figure 5-47. Typical Receiver Module

The top of the receiver subunit is shielded by a sheet RF gasket. The RF gasket is compressed and retained by a light sheet aluminum cover. The chassis is designed to provide a constraining vertical surface for the gasket and allows flush mounting of the retention cover. The cover is attached (in two places) to each module to assure positive closure of module entryway. The receiver chassis is designed with a minimum, but positive, tolerance with respect to the module to assure gasket compression at the chassis to cover entry.

The receiver module, as previously stated, is designed for four alumina microstrip circuit substrates. The substrates, in a 2.54 cm by 5.08 cm configuration, are mounted in pairs on each side of a central web. The substrate is mounted with the 5.08-cm dimension parallel to the module mounting surface. The module is closed, over the substrates, by lightweight aluminum covers. The covers are not designed to be RF tight in themselves, but full shielding is provided by the upper RF gasket. The cover is mounted on the module by five flathead screws, with three screws along the bottom or interconnect side. The module, with covers installed, is a testable and storable assembly in a configuration identical to its end item usage.

The module-to-module interconnect pins are located in the mounting surface or bottom of the module. This surface wall is also used to mount the DC voltage feed through capacitors. The DC voltage is filtered for each substrate by RF filters located inside the module. The filter is mounted to standoff insulated terminals. The input/output circuit intra-connects are made by thin tinned-nickel ribbons.

The alumina substrate is solder mounted to a tinplated Kovar frame. The Kovar frame serves a dual purpose of providing a dynamic isolator and a metal surface to use in securing the substrate to the module center web. The substrate and Kovar frame is attached to the module with spacers at the corners to assure double amplitude motion with dynamic inputs. This motion, with respect to the interconnect pins in the wall, is absorbed by flexure of nickel ribbon and complete decoupling is achieved.

The receiver preselector subunit is attached to the receiver subunit by four recessed screws. Alignment to the receiver chassis is minimally attained, but machine tolerances are held sufficient to assure a RF gasket constraint. The receiver preselector is attached to the mounting platform by means of two screws through the structural mounting ribs.

The receiver preselector chassis is divided into three machined cavities. One cavity is reserved for mounting the preselector alumina substrate. This substrate, like those substrates of the receiver subunit, is mounted with the 5.08-cm dimension parallel to the mounting surface with the 5.08-cm dimension parallel to the mounting surface and the interconnects along the lower edge. The second cavity is reserved for interconnecting the receiver preselector to the receiver subunit. The third cavity is used for mounting the interface connectors and interconnecting to the second cavity. The second or lower cavity is shielded by a RF gasket and lightweight aluminum cover in a manner similar to the receiver subunit. The first and third cavities are closed by a single machined cover flush mounted to the side open to the receiver subunit. The machined cover is designed to accept a woven metal RF gasket.

The first cavity of the receiver is designed to mount the preselector. The method of input interconnect is made by a modified SMA coaxial connector and a thin nickel ribbon that matches the 50-ohm characteristic impedance of the alumina microstrip circuitry.

The converter subunit is a single cavity machined housing with a machined cover. The open side of the housing is opposite the receiver subunit and is shielded by a RF gasket mounted on the cover. The power conditioning and rectifier-filter circuitry is mounted on the cover. The feedback control circuitry and regulated power interconnect terminations are located in the housing. The machined planer cover is used to mount the power circuitry for ease of assembly and test. This method also minimizes the unregulated power loop within the converter enclosure.

#### 5.1.3.1.6 S-Band TT&C Transmitter

Downlink telemetry is provided by a 2-watt S-band transmitter coupled into the S-band omni by a diplexer. The S-band transmitter generates a crystal-controlled carrier signal (noncoherent mode) or accepts a carrier signal from the receiver (coherent mode), phase modulates the carrier with video information from the telemetry encoder, and multiplies and amplifies the modulated carrier to produce an S-band output signal. Regulated DC power is provided from a central power converter mounted in the communications and data handling module. The key electrical characteristics are presented in Table 5-13.

The transmitter mechanical design is similar to the receiver design in that microelectronic alumina substrate construction is used. The transmitted block diagram is shown in Figure 5-48. The circuit and mechanical description is as follows.

Table 5-13. S-Band Transmitter Key Characteristics

<u>RF Output</u>	
Frequency	2.21 GHz
RF power	2 watt, minimum (end-of-life)
Load VSWR	2:1 maximum, any phase
<u>Modulation Characteristics</u>	
Modulation type:	Linear
Symmetry of sidebands:	10% maximum
Modulation input:	Composite PRN plus telemetry from dual telemetry encoder
<u>DC Power Required from Central Power</u>	
+15 volts $\pm 2\%$	1.5 watts, maximum
-15 volts $\pm 2\%$	0.5 watts, maximum
+23 volts $\pm 2\%$	5 watts, maximum

#### A1 Oscillator/Multiplier

In the non-coherent mode, the transmitter excitation is an internally mounted high stability oscillator in the oscillator-buffer assembly. The output of the oscillator is buffered and amplified by a high gain stage at the oscillator output.

#### Oscillator-Buffer (Figure 5-49)

Function. The oscillator-buffer supplies a basic frequency for subsequent multiplication and amplification for the transmitter S-band output.

Description. Two transistor stages are used. The first one is a crystal oscillator that uses a high Q series resonant quartz crystal to

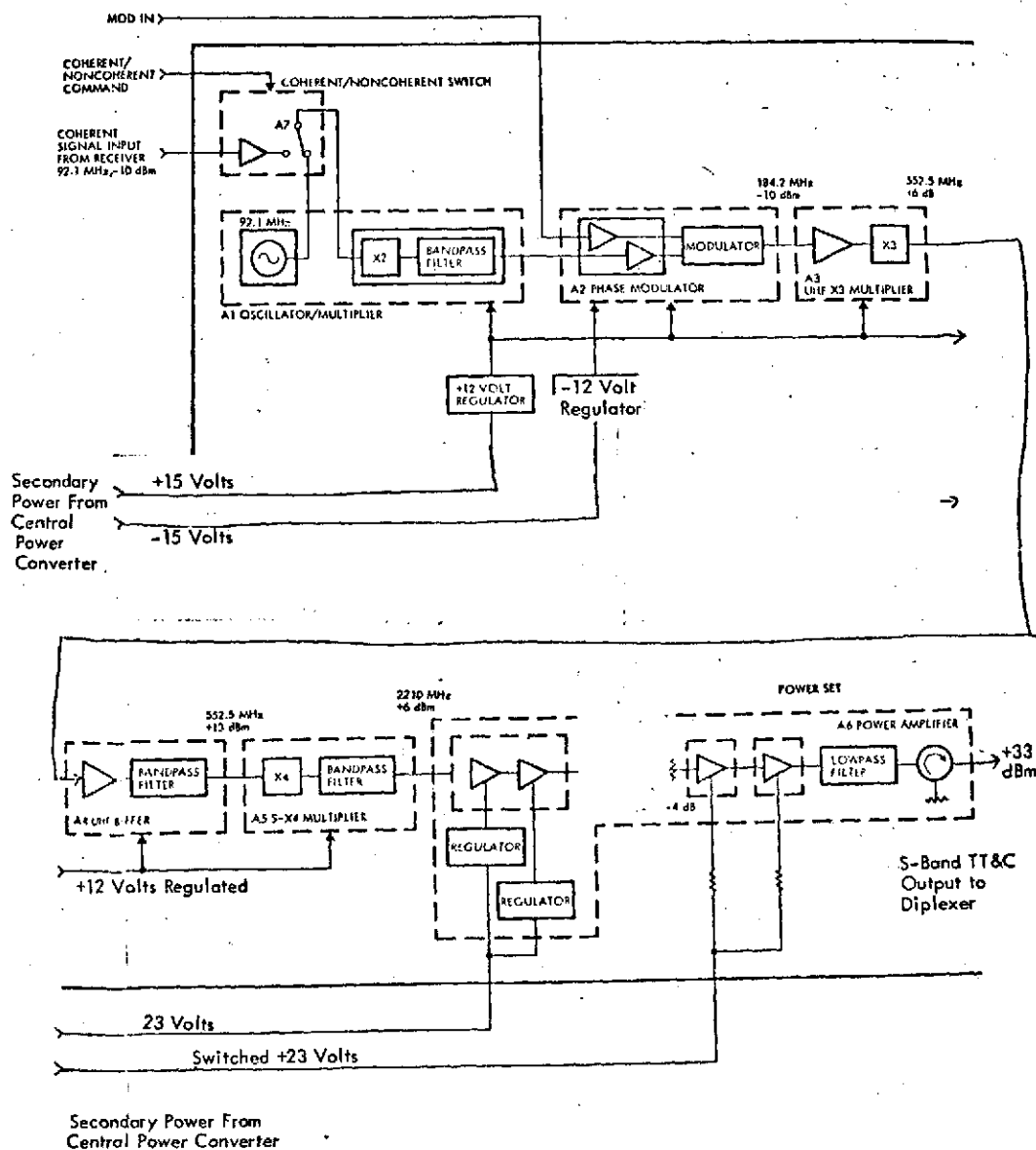


Figure 5-48. S-Band TT&C Transmitter Block Diagram

ORIGINAL PAGE IS  
OF POOR QUALITY

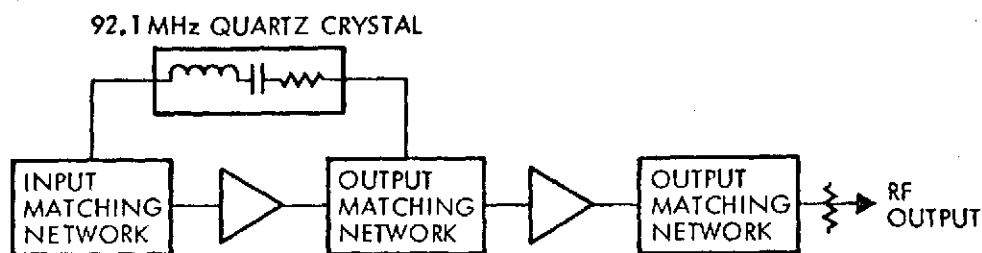


Figure 5-49. Oscillator Buffer

determine the basic output frequency. The second stage operates as a buffer amplifier to isolate the oscillator from external loading that otherwise might pull the oscillator center frequency. The second stage also amplifies the oscillator frequency to the desired level. Included in the output of the second stage is a resistive attenuator to permit setting the output level.

Principle of Operation. Oscillation is produced in a basic Colpitts circuit using a high Q series resonant quartz crystal in the feedback path. Stable operation over a wide temperature range is achieved by compensation of the inherent temperature coefficient characteristics of the AT cut quartz crystal. The output of the oscillator is buffered and amplified by an additional high gain stage at the output of the oscillator.

Physical Construction. All parts are reflow soldered onto a 2.54 x 5.08 x 0.0635 cm (1 x 2 x 0.025 inch) alumina etched circuit substrate. The transistors are housed in the TI line hermetic seal packages. The resistors and capacitors are chip-type components. The inductors are hand-wound toroids and plastic-molded variables. The quartz crystal is a TO-5 case cold weld-type unit.

#### Electrical Characteristics.

Frequency	92.1 MHz
RF power level	-10 dBm, adjustable
Frequency stability	<±0.001% (-15°F to 135°F) <±0.002% (-30°F to 168°F) <±2.5 ppm due to 2:1 VSWR, any phase <±5.0 ppm due to voltage (12.0 volts ±2%)
Frequency settability,	±0.5 ppm (by variable inductor)

Frequency spurious and harmonics products	> 40 dB below main carrier
Phase deviation due to 250-mV ripple	3 milliradians
DC power	+12.0 $\pm$ 0.15 volts, 250 mV

#### UHF X2-Multiplier (Figure 5-50)

The UHF-X2 multiplier provides one of the three multiplier functions to increase the oscillator frequency to the downlink frequency.

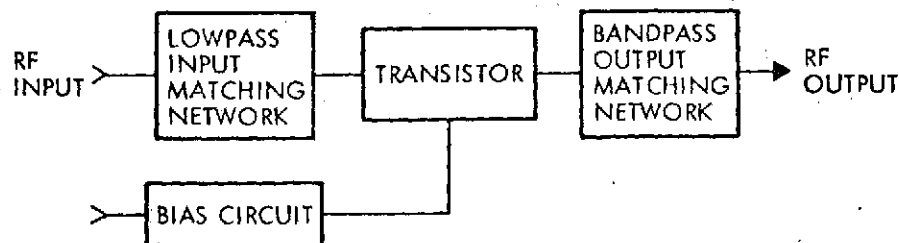


Figure 5-50. UHF X2 Multiplier

Description. The UHF-X2 multiplier circuit consists of a low pass input matching circuit, a transistor amplifier, and a bandpass output matching circuit.

Principle of Operation. Multiplication of input frequency is achieved by the selective amplification of the second harmonic and the suppression of the fundamental and third and fourth harmonics. The circuit is temperature compensated by two diodes: one constant current, one high speed switching.

Physical Construction. Chip components and flat pack transistor reflow soldered to 0.0635 x 2.54 x 5.08 cm (0.025 x 1 x 2 inches) alumina substrate. Substrate is soldered to a kovar carrier frame, which is mounted by screws into an aluminum housing.

#### Electrical Characteristics.

Input frequency	92.1 MHz
Output frequency	184.2 MHz
Input power level	-10.0 $\pm$ 1.0 dB
Output power level	6.0 $\pm$ 1.0 dB
DC power	12.0 $\pm$ 0.5 volts, 8.7 mA, nominal; 9 mA, maximum

Harmonic level

$1 f_{in}$ : -35 dB, maximum

$3 f_{in}$ : -30 dB, maximum

$4 f_{in}$ : -40 dB, maximum

$5 f_{in}$ : -40 dB, maximum

$6 f_{in}$ : -40 dB, maximum

### A2 Phase Modulator (Figure 5-51)

In the phase modulator, the RF input is amplified. The output of this amplifier drives the RF input of the linear phase modulator. External modulation is applied to a modulation input amplifier. This output provides the modulation input to the phase modulator. The phase modulator modulates the composite data onto the RF carrier.

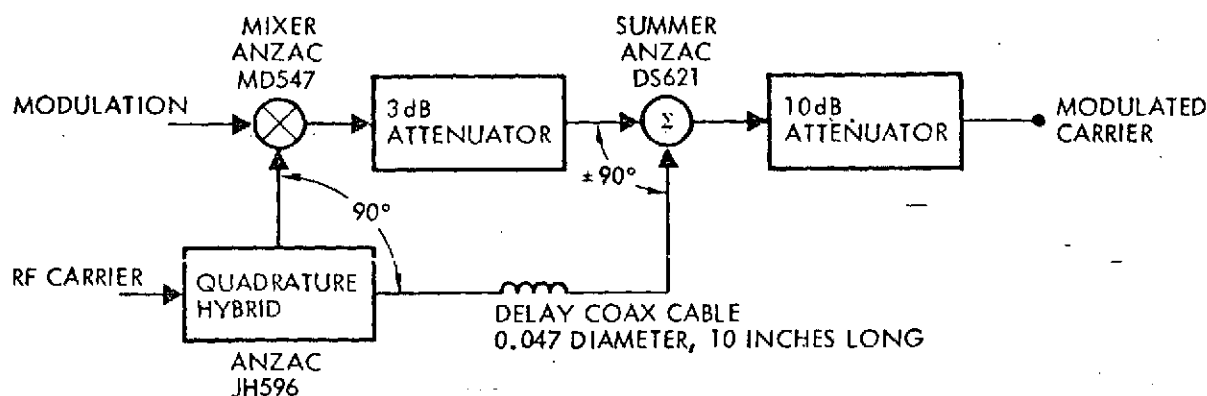


Figure 5-51. Phase Modulator

Description. The Phase Modulator consists of a quadrature hybrid, doubly balanced mixer, hybrid summer, delay line and attenuators.

Principle of Operation. The linear phase modulator is achieved by summing the carrier in quadrature with the double sideband suppressed carrier modulated signal. The modulation index is a function of the relative amplitudes of carrier and DSB signal, and consequently, for a linear multiplier, a direct function of the modulation signal. The fixed 3 dB attenuator further controls the modulator scale factor and desensitizes the multiplier to temperature variations. The delay line equalizes the delay through the multiplier and the output attenuator assures the summer of low VSWR and provides isolation between the phase modulator and multiplier circuitry.



Physical Construction. The quadrature hybrid, doubly balanced mixer, and the hybrid summer are 1.27 x 0.9525 x 0.3175 cm (0.5 x 0.375 x 0.125 inch) flat packs with four leads along both long dimensions. These will be reflow soldered together with the resistive  $\pi$ -pad attenuators to a 2.54 x 5.08 x 0.0635 cm (1 x 2 x 0.025 inch) alumina substrate that has the interconnections etched on its surface. The delay line will then be mounted above the flat packs and held in place with Lefko weld.

Electrical Characteristics (Breadboard Unit).

Input RF frequency	184.2 MHz
Input RF power	+6 dBm $\pm$ 1 dB
Modulation input	Adjustable about nominal of 160 mV, peak-to-peak
Temperature compensation of modulation input	See Figure 9.3-6
Linearity	$<\pm 1$ percent
Output power	-11 dBm $\pm$ dB

A3 X3 Multiplier (Figure 5-52)

The phase modulator output drives the X3 multiplier, which consists of a limiting amplifier and UHF X3 frequency multiplier.

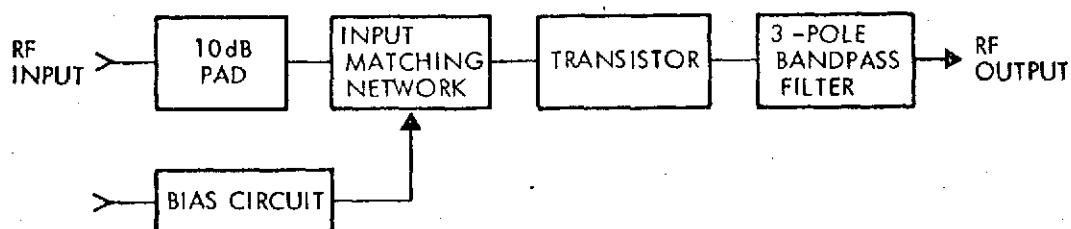


Figure 5-52. X3 Multiplier

RF Limiter

The RF limiter provides isolation between the phase modulator and the UHF X3 and supplies the drive for the UHF X3.

Description. The RF limiter consists of a 10-dB pad, an input highpass matching network, the transistor, and a bandpass filter.

Principle of Operation. The pad provides isolation and reduces the power from the phase modulator. The reverse gain of the transistor

increases the isolation. This phase modulator and the transistor supplies the power required by the UHF X3. The bandpass filter attenuates undesired frequency products.

Physical Construction. Chip components and transistors in a TI package are reflow soldered to a 0.0635 x 2.54 x 5.08 cm (0.025 x 1 x 2 inches) alumina substrate. The substrate is soldered to a kovar carrier frame, which is mounted by screws into a machined I beam housing.

Electrical Characteristics.

Frequency:	184.2 MHz
3 dB bandwidth:	20 MHz
Input power level:	-10 $\pm$ 0.5 dBm
Output power level:	+3 $\pm$ 1.0 dBm
DC power	12.0 $\pm$ 0.25 volts; 8 mA, nominal; 10 mA, maximum
Input VSWR:	1.2:1

UHF X3 Multiplier (Figure 5-53)

The UHF-X3 multiplier provides one of the three multiplier functions to increase the oscillator frequency to the down link frequency.

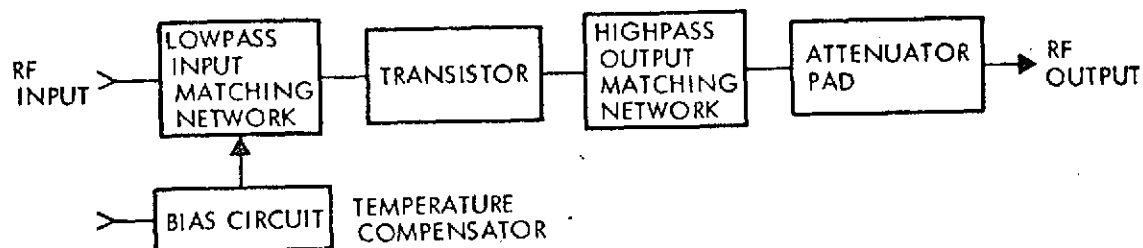


Figure 5-53. UHF X3 Multiplier

Description. The UHF-X3 multiplier circuit consists of a lowpass input matching circuit, a transistor amplifier, and a highpass output matching circuit.

Principle of Operation. Multiplication of input frequency is achieved by the selective amplification of the third harmonic and the suppression of the second and fourth harmonics. The circuit is temperature compensated by a high-speed switching diode and a resistive bias network. The output is isolated by a 3-dB attenuator, which also sets the output level.

Physical Construction. Chip components and flat pack transistor are reflow soldered to 0.0635 x 2.54 x 5.08 cm (0.025 x 1 x 2 inches) alumina substrate. Substrate is soldered to a kovar carrier frame, which is mounted by screws into an aluminum housing.

Electrical Characteristics.

Input frequency	184.2 MHz
Output frequency	552.5
Input power level	+3 dBm $\pm$ 0.5 dB
Output power level (available)	+6 dBm $\pm$ 1 dB
DC power	12 volts $\pm$ 2%; 13 ma, nominal; 16.0 ma; maximum
Return loss	>11 dB, minimum
Harmonic level (harmonic)	1 $f_{in}$ : -50 dB 2 $f_{in}$ : < -50 dB 4 $f_{in}$ : < -46 dB 5 $f_{in}$ : < -25 dB 6 $f_{in}$ : < -35 dB

A4 Buffer Amplifier (Figure 5-54)

The buffer amplifier provides amplification, limiting, and isolation between the two X3 and X4 multipliers.

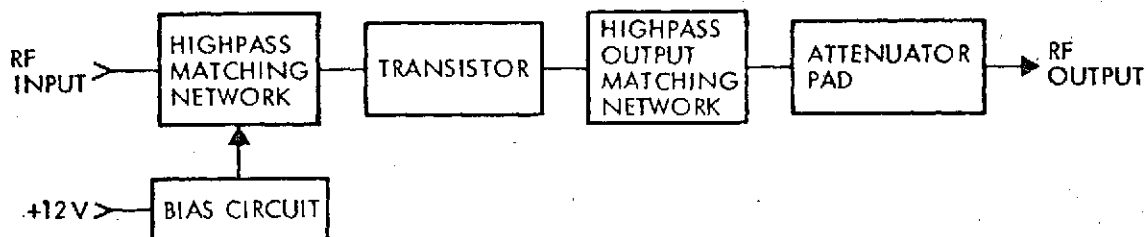


Figure 5-54. A4 Buffer Amplifier

Description. The buffer amplifier circuit consists of a highpass matching network, a transistor amplifier, and a highpass output matching circuit.

Principle of Operation. The input power level drives the amplifier into saturation. The amplifier operates at about the 3-dB compression

point. The circuit is temperature compensated by two diodes: one constant current, one high-speed switching.

Physical Construction. Chip components and flat pack transistor are reflow soldered to 0.0635 x 2.54 x 5.08 cm (0.025 x 1 x 2 inches) alumina substrate. Substrate is soldered to a kovar carrier frame, which is mounted by screws into an aluminum housing.

Electrical Characteristics.

Input frequency	552.5 MHz
Input power level	+6 dBm $\pm$ 1.5 dB
Output power level (available)	+13 dBm $\pm$ 0.5 dB
DC power	12.0 $\pm$ 0.5 volts; 17 ma, nominal; 20 ma, maximum
Return loss	13 dB, minimum

A5 X4 Multiplier, S-Band (Figure 5-55)

The S-X4 multiplier provides one of the three multiplier functions to increase the oscillator frequency to the downlink frequency.

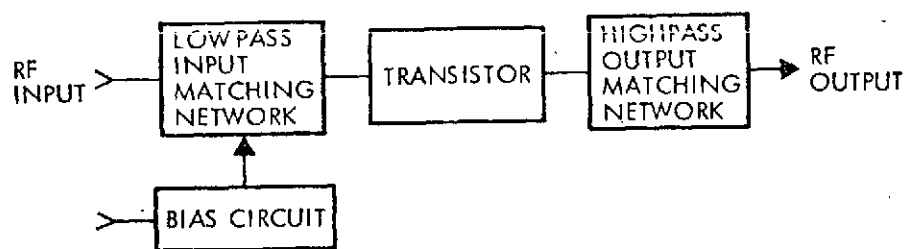


Figure 5-55. A5 X4 Multiplier

Description. The S-X4 multiplier circuit consists of a lowpass input matching circuit, a transistor amplifier, and a highpass output matching circuit.

Principle of Operation. Multiplication of input frequency is achieved by the selective amplification of the fourth harmonic and the suppression of the second and third harmonics. The circuit is biased by a high-speed switching diode and a resistor network. The transistor is operated at about the 1-dB compression point.

Physical Construction. Chip components and flat pack transistor reflow soldered to 0.0635 x 2.54 x 5.08 cm (0.025 x 1 x 2 inches) alumina

substrate. Substrate is soldered to a kovar carrier frame, which is mounted by screws into an aluminum housing.

#### Electrical Characteristics.

Input frequency	552.5 MHz
Output frequency	2210 MHz
Input power level	+13 dBm $\pm$ 1.0 dB
Output power level	+6 dBm $\pm$ 1.0 dB
DC power	12.0 volts; 20 mA, nominal; 22 mA, maximum
Return loss	10 dB Min
Harmonic level	$f_{in}$ : -40 dB
	$2 f_{in}$ : -30 dB
	$3 f_{in}$ : -30 dB
	$5 f_{in}$ : -20 dB
	$6 f_{in}$ : -20 dB

#### A6 Power Amplifier (Figure 5-56)

The S-band power amplifier increases the power output received from the S-band X4 multiplier from 5 to 35.1 dBm.

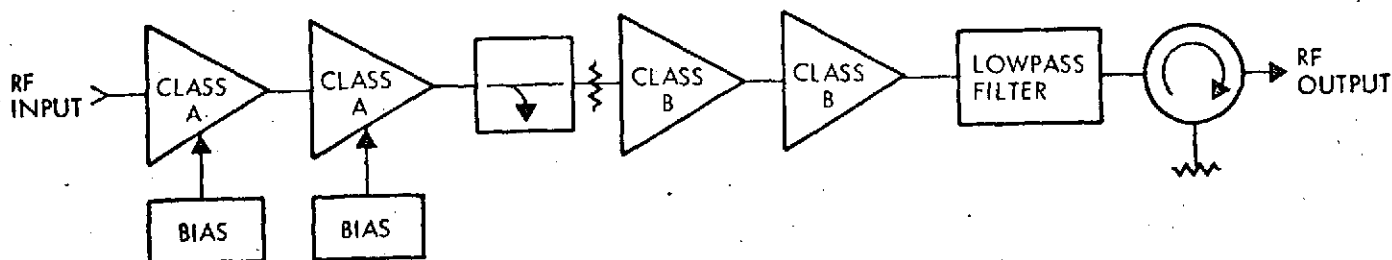


Figure 5-56. A6 Power Amplifier

Description. The S-band power amplifier consists of four stages of amplification. The first two stages are operated class A with the remaining two operated class C. L-sections are used for input and output matching. The output stage is followed by a lowpass filter for harmonic rejection. A ferrite isolator reduces the effect of load mismatch.

Principle of Operation. To achieve the required gain, the first stage is required to have a gain of 8 dB. This gain may be obtained from the HP 35821E transistor in class A operation. The predriver stage also is operated class A. Operation in class A requires a current regulator that maintains constant current over the operating temperatures encountered. A temperature-compensated zener diode and a second transistor are used in a feedback loop to maintain this current. The loop gain will also make up for a loss of beta due to radiation of other environmental effects.

A 10-dB coupler follows the two class A stages to provide a low level output for the 2/12 GHz upconverter. A 4-dB pad follows the coupler to adjust the power level into the driver stage. An external selectable pad is used as a power level set in the upconverter output path.

The driver is operated with a gain of approximately 7 dB across the band. The output stage at this input level is not saturated and both the efficiency and output power continue to increase with drive.

A lowpass 6-section filter follows the output stage and is effective up to the third harmonic. Measured insertion loss is  $\leq 0.25$  dB.

A isolator with a load capable of dissipating 2 watts follows the filter to protect against any load mismatch.

Physical Construction. Alumina substrate is reflow soldered to a kovar frame. Transistors are bar type mounted in slot in aluminum block between input and output substrates. Tuning screws are soldered to a kovar frame.

#### Electrical Characteristics.

Input frequency	2210 MHz
Input power level	+6 dBm
Output power level	+30 dBm

#### A8, A9 Regulators

The regulators operate from the central power converter +15 and -15 volts inputs to provide a stable power source for the oscillator and low-level stages of the transmitter. The requirements for the +12 volt regulator are greater than those of the -12 volt regulator and so a monolithic silicon integrated circuit is employed.

Requirements for the +12 Volt Regulator are:

Line regulation ( $V_{in}$ +14.7 to +15.3)	0.5% $V_{out}$
Load regulation ( $I_L$ - 3.5 mA to $I_L$ = 150 mA)	1.0% $V_{out}$
Ripple rejection (50 Hz to 10 kHz)	50 dB
Idling current	3.5 mA
Output voltage	12.0 VDC
Output current	150 mA, max.

The -12 volt regulator requirements are well within the capabilities of an ordinary zener diode regulator circuit. The diode is by-passed to eliminate noise from the -12 volt line.

#### 5.1.3.2 RF Switch

A single-pole, double-throw coaxial switch is required for the baseline TT&C system to connect the transmitter to either the forward or aft antennas. A low-loss, high-reliability unit, manufactured by Teledyne Microwave, is recommended for this function. The switch, shown in Figure 5-57, was used on the Pioneer 10 and 11 spacecraft. As shown, the switch is a double-pole, double-throw device and one port will be terminated for this application.

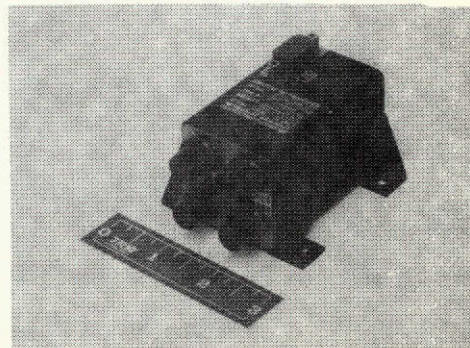
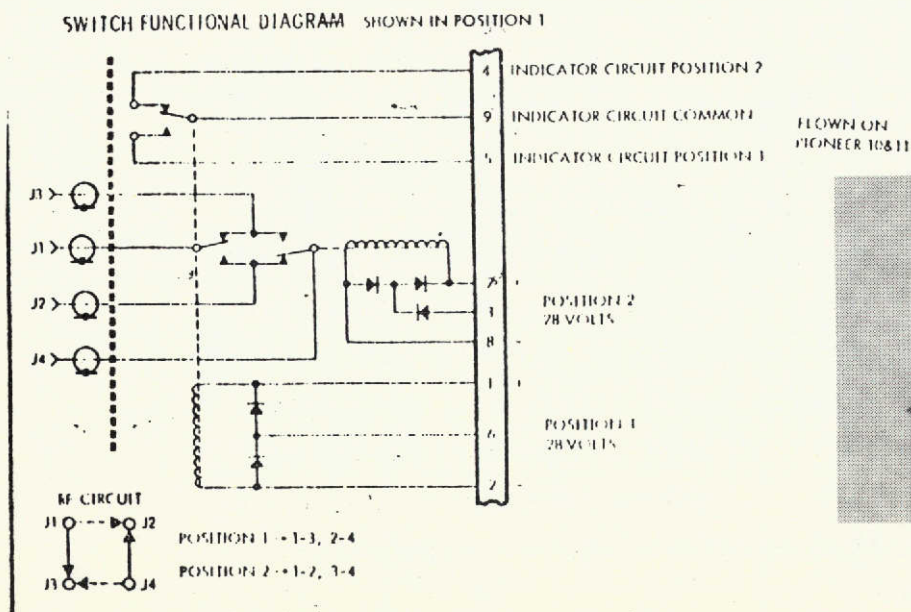


Figure 5-57. S-Band RF Switch

For the alternate (redundant) system configuration, the switch must connect one of two transmitters to either the forward or aft antennas. For this case, all four switch ports will be used (no termination).

The switch characteristics are as follows:

Frequency	2.0 to 2.3 GHz
Insertion loss	0.2 dB
Isolation	60 dB
VSWR	1.2:1
Power handling capability	15 watts
Weight	0.65 pounds

#### 5.1.3.3 Alternate Communication Equipment Design

An alternate design that provides redundant communication equipment is shown in Figure 5-58. The alternate design differs from the baseline design only in the addition of a (redundant) transceiver. The terminated port of the hybrid in the nonredundant configuration is used here to drive the additional receiver. Direct cross-strapping of the receiver outputs is used to avoid an additional switch.

#### 5.1.3.4 Impact of Future Missions

The communication equipment described above has been configured to meet the requirements of a low-orbit, high-data rate mission. The system power budget for this mission allows the use of omni antennas and a 2-watt transmitter. Modification of this equipment for use on future missions would be required only if a higher orbit was used. For example, synchronous altitude orbits would require a ERP increase of 24 dB. This could be achieved by the employment of a 20 dB gain, 2-foot S-band dish, and a 5-watt transmitter. The 5-watt transmitter power is easily achieved by replacing the 2-watt power amplifier output stage with a 5-watt stage. No change in the equipment complement is foreseen due to a change in the data rate since the maximum rate expected is employed in the EOS-A system.



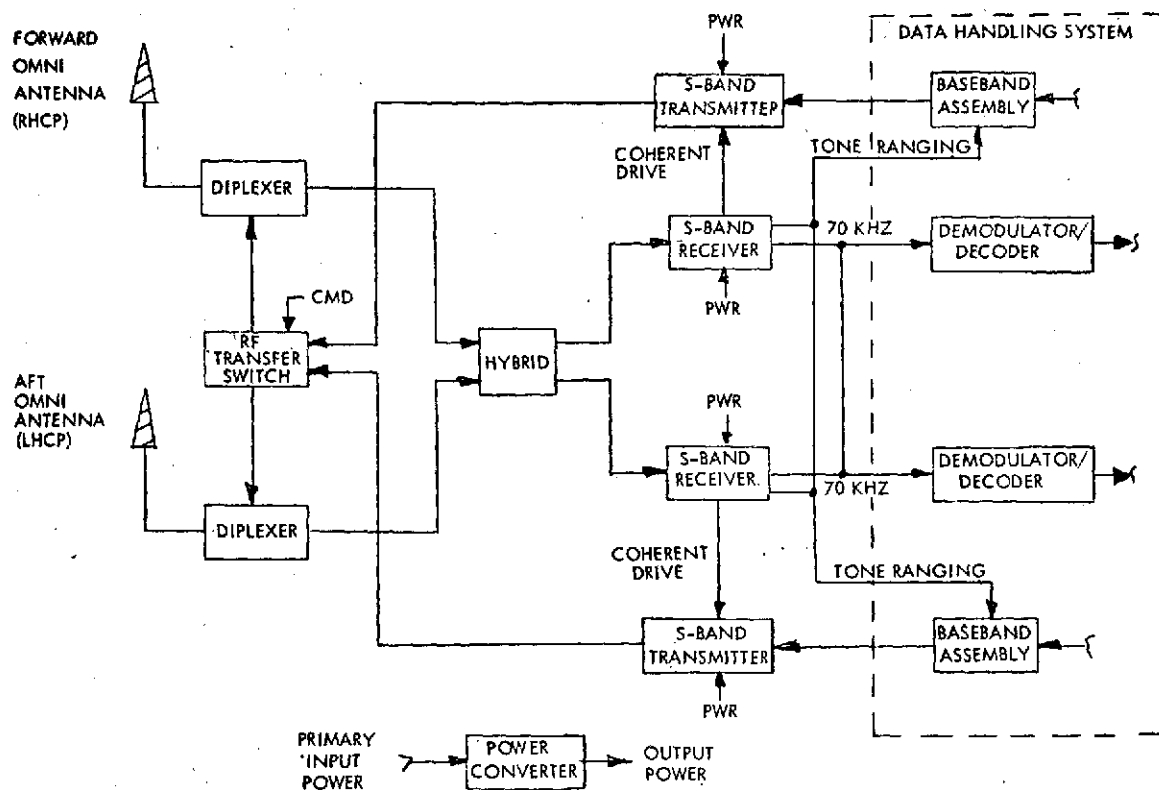


Figure 5-58. EOS-A Alternate Communications System - Communications and Data Handling Module

### 5.1.3.5 Equipment Summary

A summary of the communication equipment size, weight, power and cost is presented below in Table 5-14.

Table 5-14. Equipment Summary

Equipment	No. Required	Size	Weight (lbs)	Power (watts)	Cost
Forward omni antenna	1	5.1"hx2.0"d	.33	0	10K
Aft omni antenna	1	10"hx3.5"d	.79	0	10K
RF transfer switch	1	4"x6"x3"	.65	0.1 transient	5.5K
Diplexer	2	3"x5"x6" (ea)	3.0 (ea)	0	16K
Hybrid combiner	1	1"x1"x1"	0.1	0	1K
S-band receiver	1	2"x6"x8"	2.5	3.0	65K
S-band transmitter	1	1.7"x5"x8.3"	2.5	20.0	43K

#### 5.1.4 Computer Tradeoffs

The baseline On-Board Processor is selected by trading off key features of four candidate computers: the Goddard AOP, Autonetics D216, CDC469 and Bendix BD-910. Memory size is determined by the total software memory requirements for instruction storage as well as data storage. System cost impact of a full memory includes the net memory cost as well as the spacecraft cost for additional weight and power.

##### 5.1.4.1 Methodology

Important factors which influence the design and performance of the OBP and its associated memory include:

- System architecture
- Computational capability (precision, speed, throughput, memory capacity, input/output capability, instruction repertoire, etc.)
- Adaptability (expandability, flexibility, computability, etc.)
- Provision for interface with other components of the system
- Software (support and applications programs, ease of programming, etc.)
- Cost (money, weight, power, volume, time)
- Reliability (fault tolerance, failure rate, redundancy, ease of checkout, etc.)
- Environment (temperature, shock and vibration, electromagnetic and nuclear radiation, noise, power fluctuations, etc.)

All of these factors were examined in detail by: in-house discussions, survey of manufacturer, and a literature search. Therefore the tradeoffs reflect the expanding nature of the requirements, potential advances in the technological state of the art and the entire spectrum of environmental requirements. These tradeoffs were necessary to strike a balance between hardware complexity and software simplicity, and facilitate simulation, testing and checkout.

#### 5.1.4.2 Results

##### 5.1.4.2.1 Adequacy of the AOP

The selection of the computer organization and configuration depends upon the mission requirements; the choice must be carefully and thoroughly planned in light of available technology.

Table 5-15 is a summary of the computer requirements and the characteristics of 4 typical computers: Goddard AOP, Autonetics D216, CDC 469 and Bendix BD-910. In all cases the information is based on the 'standard' computer. We did not issue a Specification which spelled out the desired features. However, we did informally discuss the possibility of upgrading some of these computers to meet the requirements and were advised that the upgrading was possible without any large cost increase.

- Straightforward computer architecture
- Word length 16 bits minimum
- Hardware multiply and divide
- Capability of implement double length arithmetic (32 bits min); double length add in 40  $\mu$ sec, multiply in 200  $\mu$ sec
- Good logical and conditional branch instructions
- Fast add time; 5  $\mu$ sec minimum
- Direct memory access channels; expandable to 16
- Hardware protection against illegal write to memory; region selectable via software
- 16 interrupts; individually maskable
- Cycle by cycle power switching of memory modules

Table 5-16 clearly indicates that the AOP meets all of the EOS mission requirements. It is the only computer which has selectable write protect, cycle by cycle power switching, and 16 interrupt levels as standard items.

We shall not go into great detail about the other computers since they are just samples of what is available. The CDC-469 lacks DMA, is expandable only to 32 M (one-level of addressing), and does not have a straightforward architecture.

Table 5-15. Computer Requirements

Computer	Add Time μsec	Multiply Time μsec	Word Length	Memory Capacity	DMA	Micro-Programming	Selectable Write Protect	Number of Instructions	Interrupt Levels	Cycle by Cycle Power Switching	Double Length Add (hardware)	Double Length Multiply (hardware)
Goddard AOP	4.0	30	18	64K	Yes	No	Yes	55	16	Yes	No	No
Autonetics D216	2.0	11	16	64K	Yes	Yes	No	100	7	No	Yes	Yes
CDC 469	2.4	13	16	32K	No	No	No	42	3	No	Yes	No
Bendix BD-910	2.0	21	16	32K	Yes	Yes	No	72	12	No	No	No

Table 5-16. Characteristics of Standard Model of Candidate Computers

	Power watts	Weight pounds	Size In <sup>3</sup>	Relative Costs
Goddard AOP	10	9	175	4
Autonetics D216	65	10	164	1
CDC 469	23	8	200	1
Bendix BD-910	22	7.5	190	.8

\*Not including memory-processor and power converter only-  
assumes cycle by cycle power switching

The Autonetics DI216 has extensive arithmetic capability (double precision add and multiply) and is fast. Its power requirements are excessive but a slower model which requires less power is available.

The Goddard AOP is selected for the baseline computer. This selection is based on three major criteria: 1) the AOP meets all of the requirements listed above (none of the other candidates include two important features: "selectable write protect" and "cycle by cycle power switching"), 2) use of the AOP is planned for several future Goddard programs with similar applications; and 3) previous OAO-OBP flight experience has been satisfactory. The OBP is, in essence, the prototype AOP.

The selection of the AOP as the baseline is made independent of costs: the interfacing component, the bus controller will operate with any of the candidate computers, so the final selection can be made at any time. Also, normalized AOP costs as shown in Table 5-16, are not final. Present estimates for the AOP central processor LSI chips indicate that substantial reductions from the Table 5-16 costs are possible. In production, AOP costs should be competitive with alternate OBC selections.

#### 5.1.4.2.2 Memory Tradeoffs

Read-write memories are classified as volatile or nonvolatile depending on whether or not their contents remain intact when power is removed. Read-write memories may also be either destructive readout (DRD) or nondestructive readout (NDRD). In general, NDRD memories enjoy two advantages over DRD memories. They are less vulnerable to power fluctuations or other interruptions of the read process, since at no time during the reading operation is the information cleared from the memory. Secondly, they can operate at higher speeds since it is not necessary to restore the contents following each read cycle.

When nonvolatility is a requirement, plated wire (refs. 4, 7, 8, 9) is generally considered a good candidate for the present generation main-frame and mass memories. Speed, low power, moderate density, and

automated production give this device the potential advantage of use in all spaceborne computers. NDRD plated wire is being used for the memory of the Honeywell HDC-701 computer for Minuteman 3.

Most early spaceborne computers (e. g. Centaur, Titan II and III, Minuteman 1 and 2, Saturn 1) used electromechanical drums or discs as memory devices. However, these are disappearing from space application for several reasons/ref. 6): A substantial increase in packaging density of core, plated wire, and semiconductor memories, the serial access nature of drums and discs, and the limited time that discs and drums can operate without maintenance. Consequently, in recent years, the ferrite coincident-current core memory has been the cornerstone of computer technology, providing fast random access at a few cents per bit in the megabit range. DRD cores used for program memory suffer the disadvantage of requiring a write cycle following each read to restore the information.

Recent developments in LSI have made the semiconductor memory extremely attractive and practical, particularly for scratchpad or high-speed control applications (refs. 1 and 3). These memories are generally constructed of MOS or bipolar devices and provide NDRD operation, but they are volatile. However, several manufacturers are presently developing nonvolatile semiconductor memories (ref. 2). There is currently a definite trend toward the use of semiconductor memories, particularly MNOS (ref. 5), and they may become the major memory technology by the next decade.

#### 5.1.4.2.3 Flying Full Computer Memory

The advantages to flying full memory (64K) are

- Increased reliability; the extra memory is available as spare memory
- The Telemetry Data Compression algorithm operates more efficiently with more memory.
- The tendency is for computer programs to grow. During an extended mission it is certain that new tasks will be given to the computer. Flying full memory permits greater growth.
- The provision for full memory capability does not mean that full memory must be flown. If weight, volume or power becomes critical memory could be scrubbed.

## REFERENCES

1. Altman, Lawrence: Semiconductor Random-Access Memories, Electronics, pp. 108-110, June 13, 1974.
2. Appelt, Daren: Get Standby LSI Memory Power, Electronic Design, pp. 116-120, June 7, 1974.
3. Riley, W. B.: Special Report: Semiconductor Memories are Taking Over Data-Storage Application, Electronics, pp. 75-90.
4. Englund, W. A.: Plated Wire Memory for Military and Space Applications, Computer Design, pp. 83-88, March 1972.
5. Gilder, J. H.: MNOS Memory Upstaging MOS and Fixed Heads in Some Areas, Electronic Design, pp. 28-29, Sept. 1, 1973.
6. Hopkins, A. L., Jr.: Guidance Computer Design. Part 6 of Space Navigation, Guidance, and Control, J. E. Miller, ed., AGARDograph 105, Technivision Ltd., Maidenhead, England, 1966.
7. Ricci, R. C.: Present and Future State of the Art in Guidance Computer Memories. NASA TN D-4224, Electronics Research Center, Nov. 1967.
8. Kim, B. W.: The Plated Wire Memory and Its Potential for Aerospace Applications - Case 105-8. B70 05046, Bellcomm, Inc., May 20, 1970.
7. Lamson, R.: A Plated Wire Memory System. R-551, MIT Instrumentation Laboratory, June 1966.



### 5.1.5 Downlink Telemetry Carrier Phase Modulation Index Optimization

The downlink telemetry subcarrier modulation loss for multiple sinusoidal subcarriers in the presence of multiple square-wave subcarriers is given by

$$\frac{P_{Sm}}{P_T} = 2 J_1^2(\beta_m) \prod_{\substack{k=1 \\ k \neq m}}^M J_0^2(\beta_k) \prod_{j=1}^N \cos^2 \gamma_j \quad (1)$$

where  $P_{Sm}$  = power contained within the  $m^{th}$  subcarrier  
 $P_T$  = total power contained within the unmodulated carrier  
 $\beta_m$  = carrier phase modulation index for the  $m^{th}$  sinusoidal subcarrier  
 $\beta_k$  = carrier phase modulation index for the  $k^{th}$  sinusoidal subcarrier  
 $\gamma_j$  = carrier phase modulation index for the  $j^{th}$  square-wave subcarrier

Further, the subcarrier modulation loss for multiple square-wave subcarriers in the presence of multiple sinusoidal subcarriers is given by

$$\frac{P_{Rn}}{P_T} = \sin^2 \gamma_n \prod_{\substack{j=1 \\ j \neq n}}^N \cos^2 \gamma_j \prod_{k=1}^M J_0^2(\beta_k) \quad (2)$$

where  $P_{Rn}$  = power contained within the  $n^{th}$  square-wave subcarrier  
and  $\gamma_n$ ,  $\gamma_j$ , and  $\beta_k$  are defined as above for the  $n^{th}$  and  $j^{th}$  square-wave subcarrier and the  $k^{th}$  sinusoidal subcarrier.

Finally, the carrier modulation loss is given by

$$\frac{P_c}{P_T} = \prod_{k=1}^M J_0^2(\beta_k) \prod_{j=1}^N \cos^2 \gamma_j \quad (3)$$

where  $P_c$  is the power resident in the residual carrier component.

In addition to the above, the following performance threshold equations can be defined

$$T_{Sm} = \frac{P_{Sm}}{\Phi B_{Sm}} \quad (4)$$

$$T_{Rn} = \frac{P_{Rn}}{\Phi B_{Rn}} \quad (5)$$

where:  $T_{Tm}$  = signal to noise ratio required for some level of telemetry performance for the data contained on the  $m^{th}$  sinusoidal subcarrier

$T_{Sn}$  = signal to noise ratio required for some level of telemetry performance for the data contained on the  $n^{th}$  square-wave subcarrier

$P_{Sm}, P_{Rn}$  are as defined above

$\Phi$  = one-sided noise power spectral density

$B_{Sm}$  = detection noise bandwidth for the data contained on the  $m^{th}$  sinusoidal subcarrier

$B_{Rn}$  = detection noise bandwidth for the data contained on the  $n^{th}$  square-wave subcarrier.

Two downlink telemetry modes can be defined for the S-band telemetry to the STDN. In Mode 1, housekeeping telemetry and computer dump data, at 32 kbps, biphasic modulates a 1.024 MHz sinusoidal subcarrier which, in turn, phase modulates the carrier along with digital medium rate user data at 512 kbps. In Mode 2, the biphasic modulated 1.024 MHz subcarrier phase modulates the downlink carrier along with "turned-around" tone ranging data.

A) Mode 1. 32 kbps Housekeeping Plus 512 kbps Medium Rate User Telemetry

For this case, equations 1 through 4 can be written as follows:

$$\frac{P_S}{P_T} = 2J_1^2(\beta) \cos^2 \gamma \quad (5)$$

$$\frac{P_R}{P_T} = \sin^2 \gamma J_0^2(\beta) \quad (6)$$

$$\frac{P_c}{P_T} = \cos^2 \gamma J_0^2(\beta) \quad (7)$$

$$T_S = \frac{P_S}{\Phi B_S} \quad (8)$$

$$T_R = \frac{P_R}{\Phi B_R} \quad (9)$$

Solving equation (8) for  $P_S$  and substitution into (5) gives

$$\Phi B_S T_S = P_T \cdot 2J_1^2(\beta) \cos^2 \gamma \quad (10)$$

Similarly, solving for  $P_R$  in (9) and substitution into (6) gives

$$\Phi B_R T_R = P_T \cdot \sin^2 \gamma J_0^2(\beta) \quad (11)$$

Dividing (10) by (11),

$$\frac{B_S T_S}{B_R T_R} = \frac{2J_1^2(\beta) \cos^2 \gamma}{J_0^2(\beta) \sin^2 \gamma} \quad (12)$$

or,

$$\left( \frac{\sin \gamma}{\cos \gamma} \right)^2 = \frac{2J_1^2(\beta)}{J_0^2(\beta)} \cdot \frac{B_R T_R}{B_S T_S} \quad (13)$$

and,

$$\tan \gamma = \left[ \frac{B_R T_R}{B_S T_S} \cdot \frac{2J_1^2(\beta)}{J_0^2(\beta)} \right]^{1/2} \quad (14)$$

$$\text{Finally, } \gamma = \tan^{-1} \left[ \frac{B_R T_R}{B_S T_S} \cdot \frac{2J_1^2(\beta)}{J_0^2(\beta)} \right]^{1/2} \quad (15)$$

Equation (15) relates  $\beta$  and  $\gamma$  functionally to one another. Finally, the optimum values for  $\beta$  and  $\gamma$  which allow both the 32 kbps and 512 kbps services to threshold at the same point can be found by maximizing equation (5) over all  $\beta$  and  $\gamma$  determined by equation (15). That is, we want to maximize the following:

$$\max_{\beta, \gamma} \frac{P_S}{P_T} = \max_{\beta, \gamma} 2J_1^2(\beta) \cos^2 \gamma \quad (16)$$

An additional constraint in choosing  $\beta$  and  $\gamma$  is that they must be chosen such that there is sufficient residual carrier power to allow for carrier acquisition and tracking. Normally, a carrier residual of ten to fifteen percent of the total unmodulated carrier power is adequate to perform carrier tracking. Under this assumption, equation (7) becomes

$$\frac{P_c}{P_T} = \cos^2 \gamma J_0^2(\beta) \geq 0.1 \quad (17)$$

For optimum detection of binary phase-shift key data with a bit error rate of  $10^{-6}$ ,  $T_S$  and  $T_R$  must be equal to 10.5 dB. To this must be added any degradation due to non-optimum detection by the data bit synchronizer. Assuming a degradation of 2 dB,  $T_S$  and  $T_R$  must be equal to 12.5 dB or a factor of 17.7. Also,  $B_S$  and  $B_R$  are equal to 32 kHz and 512 kHz for the 32 kbps and the 512 kbps data, respectively. Substitution of  $B_R$ ,  $B_S$ ,  $T_R$  and  $T_S$  into (15) gives

$$\gamma = \tan^{-1} \left[ 32 \frac{J_1^2(\beta)}{J_0^2(\beta)} \right]^{1/2} = \tan^{-1} \left[ 5.65 \frac{J_1(\beta)}{J_0(\beta)} \right] \quad (18)$$

Solving (16) and (18) subject to (17), iteratively, yields the following optimum set of modulation indices:

$$\beta = 0.8 \text{ radian} \quad (19)$$

$$\gamma = 1.1 \text{ radian} \quad (20)$$

B) Mode 2. 32 kbps Housekeeping Plus 500 kHz  
Clock Sinusoidal Tone Ranging

For this case, since only the 500 kHz ranging and 1.024 MHz biphase modulated sinusoidal subcarriers are present, equation (10) may be written as follows:

$$\frac{P_{S_1}}{P_T} = 2J_1^2(\beta_1) J_0^2(\beta_2) \quad (21)$$

$$\frac{P_{S_2}}{P_T} = 2J_1^2(\beta_2) J_0^2(\beta_1) \quad (22)$$

where  $P_{S_1}$  = power contained within the 1.024 MHz biphase modulated telemetry subcarrier  
 $P_{S_2}$  = power contained within the 500 kHz sinusoidal range tone

- $\beta_1$  = 1.024 MHz telemetry subcarrier carrier phase modulation index  
 $\beta_2$  = 500 kHz range tone carrier phase modulation index  
 $P_T$  = total power contained within the unmodulated carrier

The carrier modulation loss is given by

$$\frac{P_c}{P_T} = J_o^2(\beta_1) J_o^2(\beta_2) \geq 0.1 \quad (23)$$

The following performance threshold equations can also be written:

$$T_{S_1} = \frac{P_{S_1}}{\Phi B_{S_1}} \quad (24)$$

$$T_{S_2} = \frac{P_{S_2}}{\Phi B_{S_2}} \quad (25)$$

Solving equations (19) for  $P_{S_1}$  and substitution into (21) gives

$$\Phi B_{S_1} T_{S_1} = P_T \cdot 2J_1^2(\beta_1) J_o^2(\beta_2) \quad (26)$$

$$\Phi B_{S_2} T_{S_2} = P_T \cdot 2J_1^2(\beta_2) J_o^2(\beta_1) \quad (27)$$

Dividing (26) by (27),

$$\frac{B_{S_1} T_{S_1}}{B_{S_2} T_{S_2}} = \frac{2J_1^2(\beta_1)}{J_o^2(\beta_1)} \cdot \frac{J_o^2(\beta_2)}{2J_1^2(\beta_2)} \quad (28)$$

or,

$$\frac{J_1(\beta_2)}{J_o(\beta_2)} = \left( \frac{B_{S_1} T_{S_1}}{B_{S_2} T_{S_2}} \right)^{1/2} \cdot \frac{J_1(\beta_1)}{J_o(\beta_1)} \quad (29)$$

Equation (29) relates  $\beta_1$  and  $\beta_2$ . Optimum values of  $\beta_1$  and  $\beta_2$  which allow both the 32 kbps and the 500 kHz tone ranging services to threshold at the same point can be found by maximizing equation (21) over  $\beta_1$  and  $\beta_2$  as determined by equation (29); and subject the constraint of equation (23):

$$\max_{\beta_1, \beta_2} \frac{P_{S_1}}{P_T} = \max_{\beta_1, \beta_2} 2J_1^2(\beta_1) J_0^2(\beta_2) \quad (30)$$

For optimum detection of binary phase-shift key data with a bit error rate of  $10^{-6}$ ,  $T_{S_1}$  must be equal to 10.5 dB. Adding to this 2.0 dB to include any degradation due to non-optimum detection by the bit synchronizer gives a total signal to noise requirement of 12.5 dB or a factor of 17.7.  $T_S$  is generally specified in terms of the signal to noise ratio required within the ground range subcarrier tracking loop noise bandwidth to achieve a certain RMS range error due to thermal noise. Typically, for the Goddard Range and Range-Rate (GRARR) system, a signal to noise ratio of 32.0 dB defined in a 1 Hz noise bandwidth produces an error due to thermal noise of 5 meters, RMS. Substitution of these values into (29) yields

$$\frac{J_1(\beta_2)}{J_2(\beta_2)} = \left[ \frac{32(17.5)}{(1)(1.585)} \right]^{1/2} \frac{J_1(\beta_1)}{J_0(\beta_1)} = 18.8 \frac{J_1(\beta_1)}{J_0(\beta_1)} \quad (31)$$

Solving (30) and (31) subject to (23) gives the following, optimum set of modulation indices:

$$\beta_1 = 1.4 \text{ radian} \quad (32)$$

$$\beta_2 = 0.1 \text{ radian} \quad (33)$$

#### 5.1.6 Command and Telemetry Autonomy

The presence of an on-board computer in the EOS Communications and Data Handling Module gives rise to questions regarding its most effective utilization, both in supporting subsystems (see subsystem/module design tasks) and in system-level support. Possible OBC use in command/telemetry functions is of particular interest, considering: elimination of telemetry tape recorder; reduction of ground operation requirements; and, on-board initiation of SAFE mode.

##### 5.1.6.1 Methodology

These topics were discussed by personnel responsible for: communications and data handling; attitude control; ground operations; spacecraft design; and, system design. The results below are based on those meetings as well as conversations with GSFC.

##### 5.1.6.2 Results

###### 5.1.6.2.1 On-Board Command Processing

The approach of letting a single command trigger an on-board generated sequence of commands appears undesirable.\* Implementation of this capability for the various possible sequences would impose a significant on-board computation requirement, without an increase in spacecraft autonomy. Generation of command patterns or sequences should have an insignificant effect on ground operations cost and will require a miniscule amount of communications time.

---

\* As distinguished from stored command sequencing for operations which must be conducted when the spacecraft is out-of-sight of a ground station.

#### 5.1.6.2.2 On-Board Telemetry Processing

A design objective is elimination of an on-board tape recorder for housekeeping telemetry storage. The alternative is reliance on real-time data when available and computer-stored measures of the telemetry for out-of-night periods. This housekeeping information will be used for:

- Routine engineering assessment of spacecraft and subsystem status.
- Diagnosis of equipment failures for redundancy utilization and resupply/retrieval planning.

Computer storage and subsequent transmission of the total housekeeping telemetry data base would be desirable; but at a typical sample rate of 1000 bits/sec, this would amount to 6 megabits (375,000 - 16 bit words) per orbit. An alternative is the use of "limit check" storage for each of the housekeeping telemetry points. One such scheme is to store, for each monitored variable, its maximum and minimum value since the previous real-time data pass and (perhaps) the time at which those extrema occurred. If 250 telemetry points are so monitored, a total computer memory allocation of 1000 words will be required. Another scheme, requiring less memory (but giving less flexibility), is to store data only when the monitored parameter exceeds some prescribed limits bounding its normal operating range. The min-max storage approach seems more desirable and quite feasible for the OBC.

The min-max data indicated above can be used by ground computers for a direct assessment of spacecraft health, in conjunction with real-time data. It's doubtful that any real simplification of spacecraft operation will result for on-board telemetry processing.

#### 5.1.6.2.3 On-Board Fault Detection and Reconfiguration

As a minimum, gross failures (those which would endanger the spacecraft) must be detected on-board and this knowledge used to put the spacecraft in a SAFE mode. However, unless the OBC is capable of self-diagnosis and autonomous reconfiguration, this failure detection and SAFE mode entry must be implemented external to the OBC (as must be all SAFE mode functions). Subsequent failure diagnosis and spacecraft reconfiguration can then be accomplished on the ground in a non-time-critical fashion.



Implementation of an all-up failure detection, identification, and re-configuration capability on-board the spacecraft is not recommended for reasons of: lack of development status (unproven, but probably feasible); lack of an urgent need to maintain continuous spacecraft operation without outage; increase in on-board complexity.

As indicated above, initiation of the SAFE mode must be an autonomous spacecraft function, implemented external to the computer. In the SAFE mode the observatory will be sun-pointed and other modules (and the payload) may also be reconfigured.

#### 5.1.7 Data Handling Subsystem

The conventional spacecraft command and data handling subsystem consists of a command decoder, electrical integration assembly, stored command processor, telemetry unit with signal conditioning, baseband assembly unit, and possibly a tape recorder. This conventional system has disadvantages in the modularized EOS satellite because:

- Spacecraft subsystem modules and experiments are electrically insulated, requiring AC coupling among their signal interfaces
- Centralized command telemetry functions require many long interface lines. AC coupling would tend to double the number of lines.
- Centralized system allows for very little flexibility and growth.
- To replace I/O for the centralized system module would be a higher cost and have more significant interface impact.

The design of the command and data interface is standardized to accommodate the data interface unit (DIU):

- User interface circuits may have to undergo signal conditioning
- A common design of the interface is necessary to meet the simplicity, cost, and reliability goals
- Coordination and combination of command and data types can minimize additional expanders needed.

The system should be responsive to uplink commands for diagnostic and emergency purposes such that lock-out due to failures in spacecraft equipment is minimized.

The data handling system should be designed to handle all EOS missions for the foreseeable future. This implies:

- An adequate length command (now 43 bits) to select users that may be added
- Flexible and expandable features at using modules to accommodate varieties of requirements
- Downlink diagnostics to enable fault isolation to the replaceable module level.

- Flexible computer interface to function with different computers and formats
- High enough bus rate and compact bus format to handle high-data/command volume.

The design of the system, with multiple use of the same functions, will be simple and efficient in order to minimize cost, complexity, and component type while providing high reliability.

- Remote module data interface units (DIU) of identical design will minimize engineering drawings, qualification and documentation
- DIU design use of LSI can minimize parts count and manufacturing costs
- Expanders at DIU, which can be stacked to provide greater capacity per user, can be of one design per expander.

#### 5.1.7.1 Assumptions

- Because of the modularized spacecraft, cabling must be minimized and AC coupling is a requirement. Therefore, a data bus system is required.
- A computer will be used for controlling the AD&C system and will be located in the data handling module. The computer is available for telemetry formatting, stored command processing, and computer data requests.
- The uplink command rate must be compatible with Space Shuttle: 2 kbit/sec.
- Downlink telemetry rates must be compatible with EOS-A selectable requirements of 1, 2, 4, 8, 16, 32 kbit/sec and a foreseeable requirement of 64 kbit/sec.
- The on-board computer receives all telemetry data, stores in memory as required, and dumps for downlink transmission.
- The remote DIU and computer receive power from A and B power bus and contain individual converters per unit.
- The design of the system assumed is 1974 and 1975 technology.
- The baseline system is nonredundant.
- All foreseeable requirements will be handled by 32 DIU's.

### 5.1.7.2 Analysis and Tradeoffs

This section considers the command decoder and data bus system. The computer functions and interfaces are discussed in relation to the data bus system. Computer design, software, tradeoffs, and desirability of a tape recorder are covered under Tasks HD-3, -4, and -5.

#### 5.1.7.2.1 Command Decoder

The command decoder simplified block diagram is shown in Figure 5-59. The decoder is a modified version of the Particle and Fields Satellite and HEAO decoders; many features are changed, however, requiring redesign of the data detector and digital processor. Table 5-17 compares the operational characteristics of these three decoders.

Not considering redundancy and cross-strapping, the EOS decoder has one input from the command receiver, one serial output, and several pulse outputs to the bus controller. Command priority (direct data bus

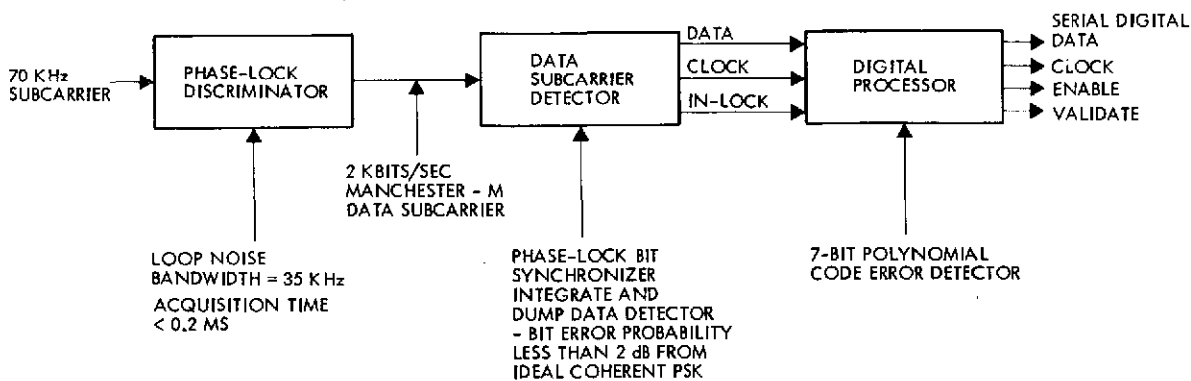


Figure 5-59. Baseline Command Decoder – Simplified Block Diagram

or computer stored) is established in the bus controller. At the end of the command word, a validate pulse indicates recognition of a valid sync code, decoder address, and the 7-bias polynomial check (see Figure 5-60).

Two special commands are decoded directly in the decoder giving discrete pulse outputs. The first command turns off computer power and the second puts the bus controller in the backup mode using the internal ROM to generate the telemetry format. In the nonredundant system, these special commands would no doubt be combined with the backup telemetry format being turned on with the computer power turn-off.

Table 5-17. Primary Command Decoder

	P&F	HEAO	EOS
70 kHz subcarrier discriminator	Yes	Yes	Yes
Sub-bit code (5)	Yes	Yes	No
A to M sync (1 kHz)	Yes	Yes	No
Data rate	1 kbit/sec	1 kbit/sec	2 kbit/sec
Data modulator	Biphase 2 kHz subcarrier	Biphase 2 kHz subcarrier	Manchester
7-bit error code	No	No	Yes
In-lock detector	No	No	Yes
Uplink word length	60 bits	60 bits	43 bits
Command outputs			
Pulse/discrete	24		10
Serial	0		1
Computer load	0		1
Total parts	225	324*	300*

\* Estimated.

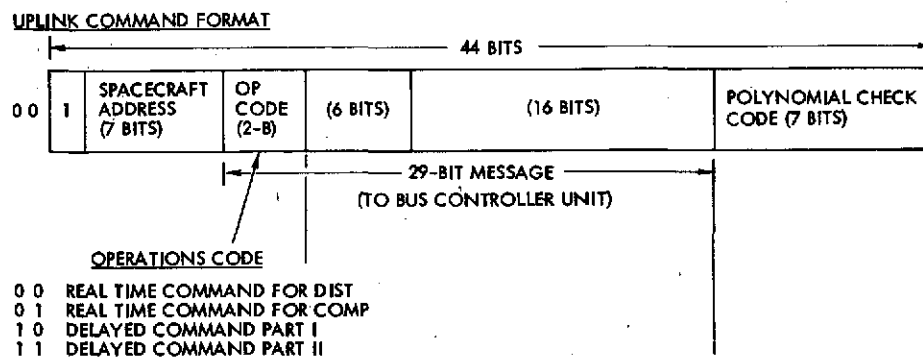


Figure 5-60. Data Format — Commands/Data Requests

#### 5.1.7.2.2 Data Bus System

The data bus system is discussed and described in the following paragraphs.

a. Tradeoffs

1. Serial Versus Spoke-Wheel Bus

Serial Bus

● Advantages

- Single output driver from central controller to all DIU and less complex output circuit, BCU logic coupling
- Less wire bulk per system
- One bus driver out and one receiver in for all foreseeable systems.

● Disadvantages

- Single open-failure on line or short-failure on the line at the output driver or at the input of a DIU disables the system
- Diagnosis of bus failure from ground virtually impossible
- Long runs to some boxes may make receiver design more critical to recapture waveform at high bus bit rate

Spokewheel Bus

● Advantages

- Each user can be fault isolated from others
- DIU's could be used for failure diagnosis of each bus line
- Shorter runs to most users may simplify design of buffers and receivers.

● Disadvantages

- More complex bus controller — each bus line has its own driver
- Bus controller needs to accommodate full number of bus lines — different from system to system
- Many more parts for the bus controller.

### Hybrid Bus. (Creating several groupings of serial buses.)

- Advantages

- Reduce number of bus input/output buffers in bus controller to reduce complexity, parts count, and wire bulk
- Critical users can be on different circuits and single failure could be diagnosed by downlink telemetry so fault isolation for a single failure could be achieved
- Shorter runs to users.

- Disadvantages

- Each system and bus assignments separately configured for specific user complement
- More complex parts and bus wire than serial scheme.

### Conclusion

The serial bus system does the best job of meeting the baseline goals of flexibility, simplicity, and complexity with fewer parts and lower costs and is selected for the baseline configuration.

## 2. Bus Signal System

### Full Duplex Versus Half Duplex Versus Simplex

Full Duplex. Simultaneous communication in both directions between called and calling unit.

- Advantages

- Messages between units can overlap
- Efficient use of time slots
- Flexible operation between units
- Can be operated at lower bus rate to format telemetry data
- Less complex system timing and mechanization.

- Disadvantages

Requires more complex bus modulation/demodulation, receiver/transmitter or separate buses for command/address and data.

Half-Duplex. Operated in one direction at a time.

- Advantages

- Easily be implemented on one line
- BCU can control by being able to override.

- Disadvantages

- Return message must wait until request is ended
- Requires more complex controls, sensing transmitted message, counting the length and providing DIU override
- One-way transmission is inefficient use of bus time
- May require higher bus bit rate to format at highest telemetry sample rates
- Failed DIU may continue to output, take over the bus and block out BCU control
- Less flexible operation between units as it requires one message to end, signal the other. New commands and data requests are delayed.

Simplex. Alternate transmission of signals in either direction.

- Advantage

Implemented on one line.

- Disadvantages

- Requires each message signal completion, hence more complexity
- Bus controller cannot override
- One-way transmission is inefficient use of bus time
- May require higher bus bit rate to accommodate highest telemetry sample rate
- Less flexible operation between units.

The full duplex system flexibility and time slot efficiency overrides possible disadvantages of circuit complexity or two bus lines in accomplishing the EOS goal of flexibility, system complexity, and reliability.



## Bus Bit Rate Selection

512 kbit/sec versus 1.024 Mbit/sec

### 512 kbit/sec

- Advantages

Use existing proven Pioneer P-MOS multiplexer

- Disadvantages

- Formatting 32 kbit/sec telemetry rate (4000 kw/sec) with up to 32-bit format and return data becomes crowded
- Growth to 64 kbit/sec telemetry rate would be difficult with 32-bit bus format.

### 1.024 Mbit/sec

- Advantage

Can accommodate the higher telemetry rates of 32 and 64 kbit/sec with 32-bit formats.

- Disadvantage

- A faster multiplexer with shorter settling time may have to be developed.
- Puts higher restrictions on source impedance of data inputs.

## Single-Bus Versus Dual-Bus System

Single Bus. Commands, requests for data to DIU, and return data from DIU to BCU are sent on a single bus (1 bus is a twisted shield pair of wires).

- Advantage

Less wire in the system.

- Disadvantage

More complexity of circuits. Each end of the bus must be a receiver/transmitter, which complicates the design and decreases reliability.

## Dual Bus

Commands and addresses are sent on CMD/ADD bus from BCU to DIU and data returned on DATA bus from DIU to BCU.

- Advantage

Less complexity of design. Each end of the bus is simply a transmitter/modulator or a receiver/demodulator resulting in less complexity and better reliability.

- Disadvantage

More wire in the system.

## Conclusions

With the goals of EOS being flexible, simplicity, lower costs, and higher reliability the following bus signal system is recommended to achieve system flexibility, message/data time slot efficiency, circuit simplicity, and foreseeable bit rates (64K bit/sec):

- Full duplex signaling
- Two-bus lines (two pairs of twisted shielded wire)
- Bit rate of 1.024 Mbit/sec.

### 3. DIU Clock – Single-Line Versus Separate-Line

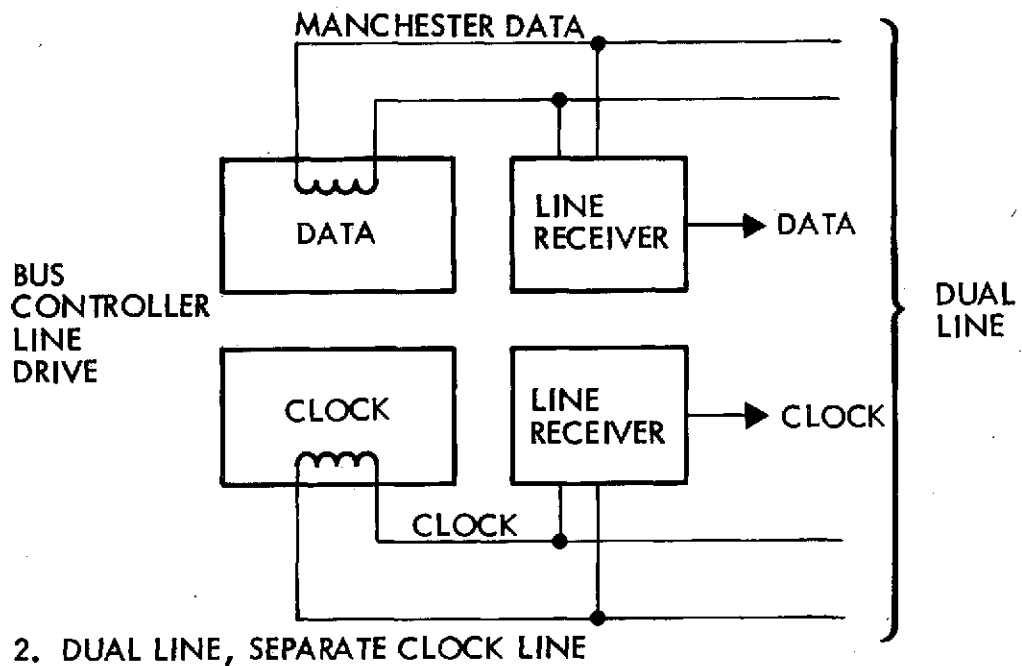
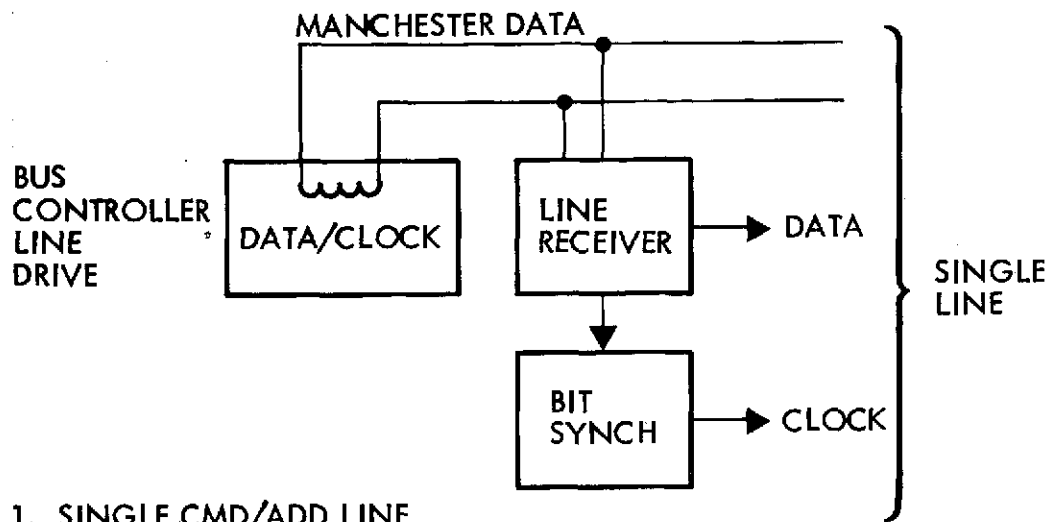
Figure 5-61 depicts the following configurations.

- Single CMD/ADD line, where the clock is obtained from the Manchester coded signal
- Dual line, where the clock is provided on a separate line.

Noted in the figure is the complement of drivers, receivers, bit synchronization, and bus wire for each configuration.

## Conclusions

Table 5-18 presents a tradeoff of the characteristics of the two approaches in which the single line configuration meets the EOS requirements of simplicity, flexibility, and lower parts count for all considerations.



	<u>LINE RECEIVER</u>	<u>LINE DRIVER</u>	<u>BIT SYNCH</u>	<u>WIRE</u>
SINGLE LINE	2 X RTU	2	0	20 FT
DUAL LINE	1 X RTU	1	1 X RTU	40 FT

Figure 5-61. Bus Clock Configurations

Table 5-18. Tradeoff - Dual Line Versus Separate Line

Wire weight: No. 28 twisted pair = 0.0047 lb-ft x 20 ft ( ) = 0.1 lb  
 Connector weight: 0.01 lb/RTV x 20 = 0.2 lb  
 Line receiver, components: 14  
 Bit sync, components: 16  
 Line driver, components: 27  
 Assume number of DIU: N

	<u>Line Receiver</u>	<u>Line Driver</u>	<u>Bit Sync</u>	<u>Total</u>	8	10	$\frac{N}{12}$	15	20
Single line	N x 14	27	N x 16	27 + 30N	267	327	387	477	627
Dual line	2 x N x 14 = N x 28	2 x 27 = 54	0	54 + 28N		334	390	474	614

- For 14 DIU's or less there is a parts advantage for the single line.
- Weight savings advantage of 0.3 lb for the single line.

#### 4.. DIU Power Input – Primary DC Bus Voltage Versus AC System

The DIU power must be on at all times. It is not desirable to derive its secondary power from the using module because of the inefficiency and unreliability of requiring the module converter be continually on. Also it is desirable from power switching and failure standpoints to have the DIU powered separate from the using module.

Power may be supplied to the DIU converter either from the communication and data handling subsystem (CDHS), module power converter, or from the primary DC power bus.

If power is supplied from the CDHS converter, it must be on an AC voltage because of the required ground isolation between modules. Such a voltage could be derived from the secondary of the CDHS converter power transformer and would be in the 1.6 to 6.4 kHz range of the DC to DC converter oscillator. The advantage to this approach is not apparent while the disadvantages appear to be:

- Routing of a moderate current AC voltage all over the spacecraft may offer EMI problems considering the frequency content of the rise and fall of the secondary voltage
- Such a concept would result in an additional pair of lines to each DIU and is in apparent conflict with the data bus and isolated module concept with a minimized number of interconnections.

To obtain the power from the primary bus, the power bus appears to be more desirable:

- The power bus is already available to the using modules thus additional long run wires for power to the DIU's are not necessary
- The converter circuits would be about the same complexity.
- The DIU power would not require additional winding and outputs from the module converter.

b. Requirements vs Capabilities

Table 5-19 compares the requirements for the data bus system with the mechanization described in paragraph c. The sources for the requirements are:

- A. EOS-L-129 Section III - Communication and Data Handling Performance Specification, revised 30 January 1974.
- B. NASA "Fleetlyer" Multiplex Data Bus Characteristics (Preliminary as of 4 June 1974).

Table 5-19. Requirements Versus Capabilities - Data Bus

Parameter	Definition	Source *	Capability
<b>1. Simultaneous Command Distribution</b>			
1.1 Bus command rate	16,000 commands/sec	Source B, page 3, item 4	All commands can be processed in any combination at the following rates: • Up to 24,000 cmd/sec (TLM BR=64 kbps) • Up to 31,875 cmd/sec (TLM BR= 1 kbps) 46.5 commands/sec $2000 \frac{\text{bits}}{\text{sec}} / 43 \frac{\text{bits}}{\text{cmd}} = 46.5 \text{ cmd/sec}$
1.2 Computer commands	62.5 commands/sec	Source A, paragraph 2.2.2	
1.2.1 Computer pulse commands	62.5 commands/sec	Source B, page 3, item 6	
1.3 Uplink commands	50 commands/sec $2000 \frac{\text{bits}}{\text{sec}} / 40 \frac{\text{bits}}{\text{cmd}} = 50 \text{ cmd/sec}$ 62.5 commands/sec (1 cmd/16 msec = 62.5 cmd/sec)	Source A, paragraph 2.2.2  Source B, page 3, item 5	
<b>2. Data Acquisition</b>			
2.1 Telemetry Data Bit Rate	Selectable: 1, 2, 4, 8, 16, 32 kbps up to 64 kbps Telemetry data fed to computer	Source A, para. 2.2.2 and 2.2.2.1.3 Source B, page 3, item 2 Source A, paragraph 2.2.2	Selectable bit rate: 1, 2, 4, 8, 16, 32, 64 kbps Telemetry data fed to computer  TLM BR=64 kbps Analog/bilevel up to 192 kbps Serial digital up to 384 kbps TLM BR=1 kbps Analog/bilevel up to 255 kbps Serial digital up to 510 kbps
2.2 Computer data bit rate	32 kbps 64 kbps	Source A, para. 2.2.2 Source B, page 3, item 3	
<b>3. Input Command Message</b>		Source A, para. 2.2.2.1.1	
Message length	40 bits		43 bits
Bit rate	2 kbps		2 kbps
Format definition	See Figure 5-62a		See Figure 5-62b
<b>4. Bus Configuration</b>			
• AC-coupled	Source B, page 1	Transformer coupled	
• Bus mode	Source A, para. 2.2.2.1.2, 2.2.2.1.4 and 2.2.2.1.5		
• Number of party lines	3 separate buses	Source A, para. 2.2.2.1	Each bus is a twisted shielded pair with capacitive coupling at the transmitter and transformer coupling at the receiver
• Rates and formats	• command party line 16 kbps, 125 cmd/sec, 24 bit format • TLM address party line 128 kbps, 8000 add/sec, 16 bit format • TLM data party line 64 kbps, 8 bit words	See Figure 5-63	Full duplex, 2 separate buses
• Data coding and phasing	Full duplex, 2 separate buses 1.024 MPBS, 32 KWPS • Supervisory (cmd/add) 32 bit format continuous Manchester code • Reply (Data) 12 to 29 bit format clocked by supervisory clock delayed 64 to 66 $\mu$ sec	Source B, page 1 See Figure 5-64	1.024 mbps, flexible slot assignments (See Figure 5-65) • cmd/add bus - cmd format - 32 bits - data request format-24 bits • Data bus - TLM data - 8 bit words - computer data AN/DL - 8 bit words SD - 16 bit words Data clock derived from CMD/ADD Manchester code
<b>5. Remote Units</b>			
5.1 Number of units	32 (decode of 5 bits user ID) 64	Source A, para. 2.2.2.1.2, 2.2.2.1.4 Source B, page 1	32 data interface units
5.2 Input Power	Two wire - 16 kHz square wave from C&DH module	Source A, para. 2.2.2.2	+28 volts from primary power buses A and B
5.3 Remote Multiplexer	64 data channels Any input for analog or bilevel (groups of 8) Any of 16 inputs for serial digital. 191 data channels 65 analog 64 bilevels 16 serial digital	Source A, para. 2.2.2.2.1	64 data channels/DIU Any input for analog or bilevel (groups of 8) Any of up to 16 inputs for serial digital. Can be expanded up to 512 data channels/DIU by addition of up to 7 expanders.
5.4 Remote Decoder	Command outputs 64 pulse 4 serial digital  121 commands 107 pulse 14 serial digital	Source A, para. 2.2.2.2.2  EOS-A Attitude Determination Module (largest user)	Command outputs 32 pulse 7 serial digital Can be expanded up to 256 pulse/DIU 56 serial digital/DIU by addition of up to 7 expanders.

Source A: EOS-L-129, Section II, Revised 30 January 1974  
 Source B: NASA "Freefixer" Multiplexer Data Bus Characteristics, 4 June 1974.

ORIGINAL PAGE IS  
 OF POOR QUALITY

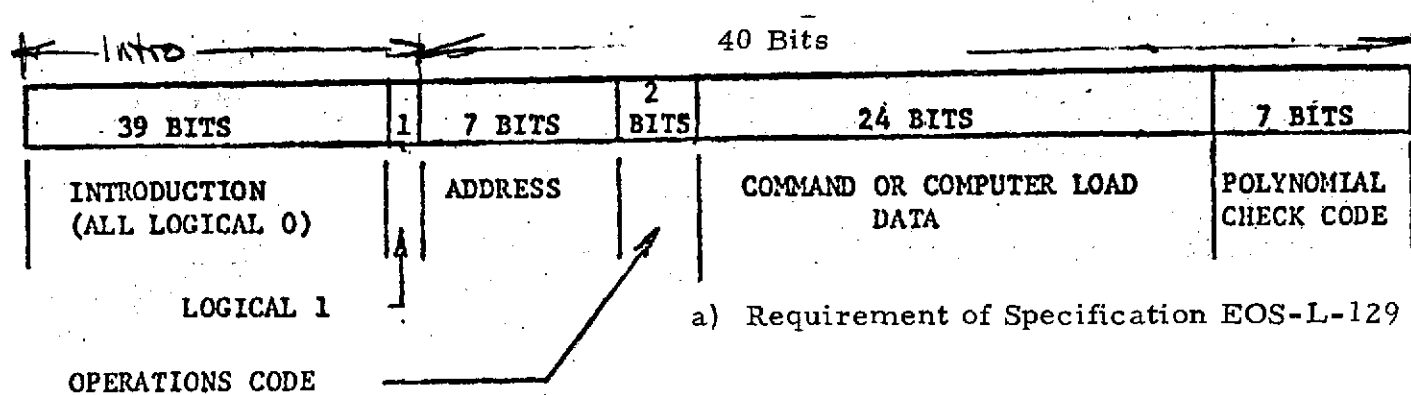
Table 5-19. Requirements Versus Capabilities - Data Bus (Continued)

Parameter	Definition	Source <sup>a</sup>	Capability
<b>6. Computer Interface</b>			
<b>6.1 Uplink Computer Commands</b>	Op code plus 24 bits real time-immediate execution delayed. Part I-time of execution Part II-command itself	Source A, para. 2.2.2.1.1	Op code plus 27 bits or more real time-immediate execution delayed. Part I-time of execution Part II-command itself Data input to computer by 18 bit register as long as enable is done.
<b>6.2 Telemetry</b>			
• Data requests	Computer program variable format to identify telemetry channel to be sampled. 16 bit message 8000 requests/sec Identify format, give synchronization code, identify and mechanize 128 eight bit word minor frames with 4 subcommutators, identify spacecraft time, return command verification data.	Source A, para. 2.2.2.1.3, 2.2.2.1.4	Computer program variable format selects telemetry channel to be sampled. • 17 bit message • Up to 8000 requests/sec • Format identification • Synchronization code (32 bits) • Input to BCU on 17 bit register • 128 word minor frame • 4x128 8-bit subcommutators • SCID • S/C time
• Data replies	20 bit message 8000 requests/sec 8 bit words 64 Kbps (bus rate) 8 kHz clock supplied to line by format generator. 12 bits, 4 bits synchronous 1.024 MBPS (bus rate)	Source B, page 2, Function III, page 3, Item 2 Source A, para. 2.2.2.1.5	8 bit words 1.024 Mbps (bus rate) Input to computer by DMA channel using same 17 bit register as data request.
<b>6.3 Computer Commands and Data Request</b>			
<b>Commands</b>			
Message size	24 bits 27 bits	Source A, para. 2.2.2.1.2 Source B, page 2, Type I&II	• 27 bits • Up to 24,000/sec (TLM BR=64 Kbps) • Up to 31,875/sec (TLM BR=1 Kbps)
Command rate	125 commands/sec pulse commands-62.5 CMDS/sec serial digital-up to 16,000 CMDS/sec	Source A, para. 2.2.2.1.2 Source B, page 3, Item 6 Source B, page 3, Item 4	• 16 bit register handles commands by parallel transfer from DMA output.
<b>Data Requests</b>			
Message size	16 bits	Source A, para. 2.2.2.1.4	• 16 bits • Up to 24,000/sec (TLM BR=64 Kbps) • Up to 31,875/sec (TLM BR=1 Kbps)
Message rate	Up to 8000 messages/sec	Source A, para. 2.2.2.1.4	• 16 bit register handles data requests by parallel transfer from DMA output
<b>Data</b>			
Word size	8 bits 12 to 29 bits, 4 bits synchronous	Source A, para. 2.2.2.1.5 Source B, page 1; page 2, Item 8	• Analog/bilevel - 8 bits • Serial digital - 16 bits • 16 bit register handles data for parallel transfer to DMA input
<b>6.4 Computer Memory Dump</b>	Dump by DMA Any set of memory locations including address and contents	Source A, para. 2.2.3.2	DMA channel is interrogated by DIU serial data channel
<b>7. Onboard Computer (OBC)</b>			
• Type	General purpose, digital, binary Full parallel organization One index register (minimum)	Source A, para. 2.2.3	One double length accumulator, one index register
• Arithmetic	Binary, fixed point 16 bit data word (minimum) Add instruction (<5 $\mu$ sec) Multiply instruction Divide instruction Double precision add (<40 $\mu$ sec) Double precision multiply (<200 $\mu$ sec) Four basic logical instructions (AND, OR, EX OR, and COM- PLEMENT) Conditional/unconditional transfers	Source A, para. 2.2.3.3	18-bit word 4 $\mu$ sec 30 $\mu$ sec 60 $\mu$ sec <30 $\mu$ sec <150 $\mu$ sec
• Memory	Non-volatile, expandable to 64K words in 8K word modules (16K minimum) Cycle-by-cycle power switching at 8K memory modules (100 mw maximum increase in standby power per 8K module) Protection against illegal write to memory	Source A, para. 2.2.3.1 Source A, para. 2.2.3.1 Source A, para. 2.2.3.3	<100 mw (2-mil plated wire memory)
• Input/Output	16 maskable interrupts (minimum) All I/O channels must be able to operate in both a DMA mode and program control mode	Source A, para. 2.2.3.2	16 independent cycle steal operations time share one DMA channel

<sup>a</sup>Source A: EOS-L-129, Section II, Revised 30 January 1974

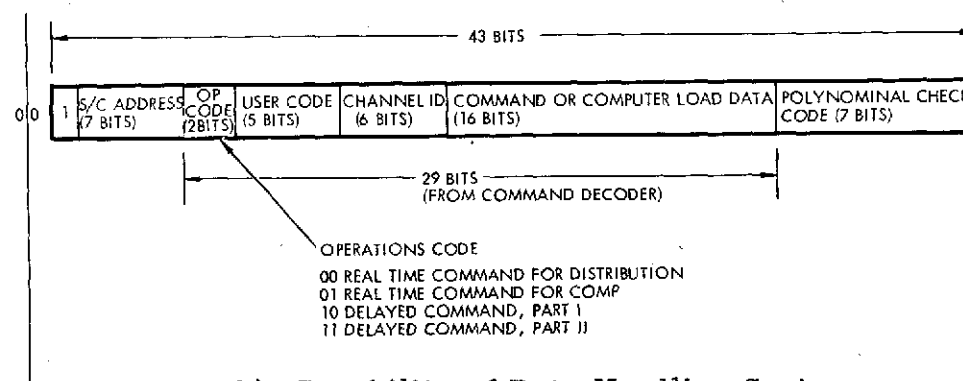
Source B: NASA "Freefixer" Multiplexer Data Bus Characteristics, 4 June 1974.





a) Requirement of Specification EOS-L-129

- 0 0 REAL TIME COMMAND FOR DISTRIBUTION
- 0 1 REAL TIME COMMAND FOR COMPUTER
- 1 0 DELAYED COMMAND, PART 1
- 1 1 DELAYED COMMAND, PART 2



b) Capability of Data Handling System

Figure 5-62. Uplink Command Format

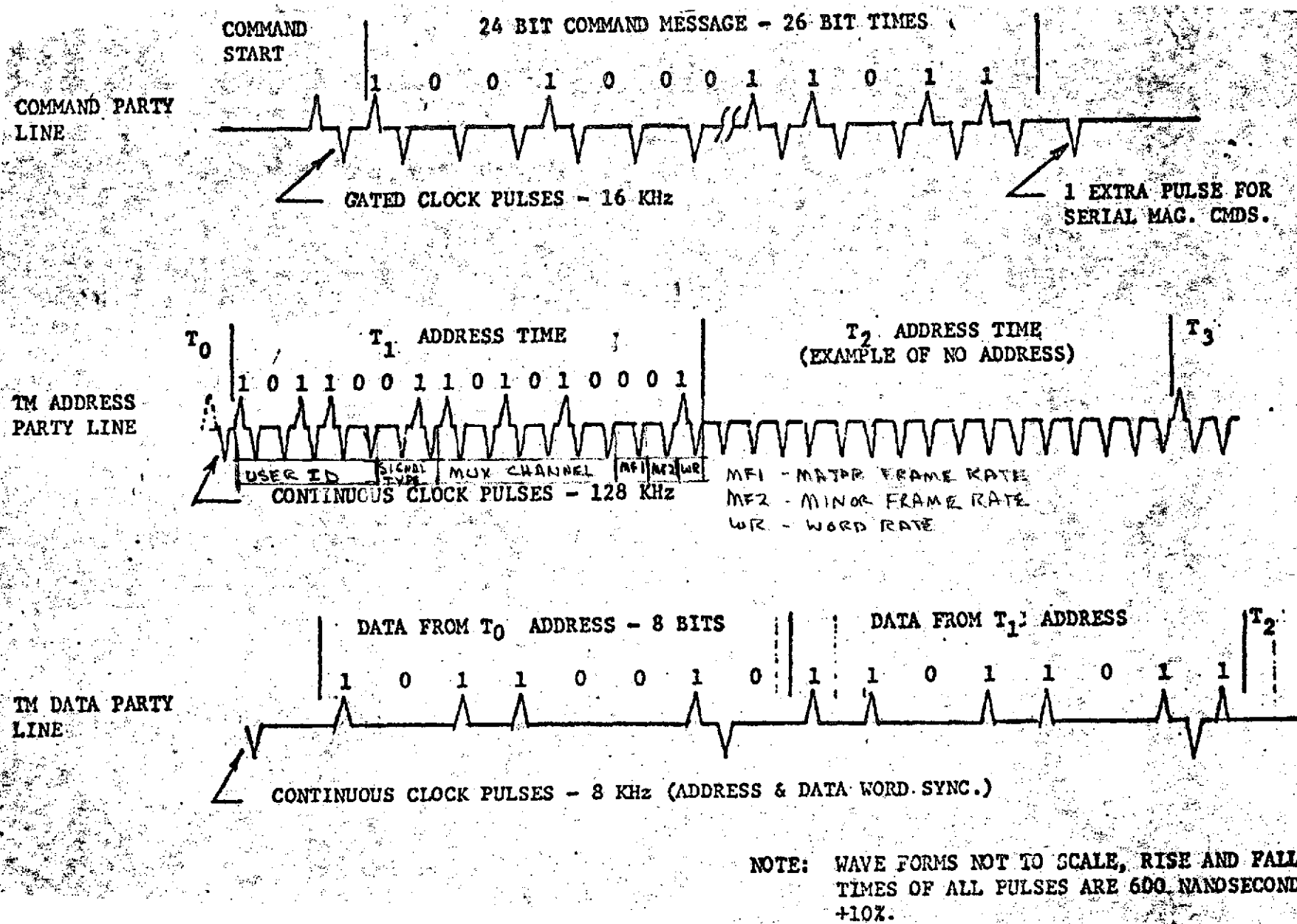
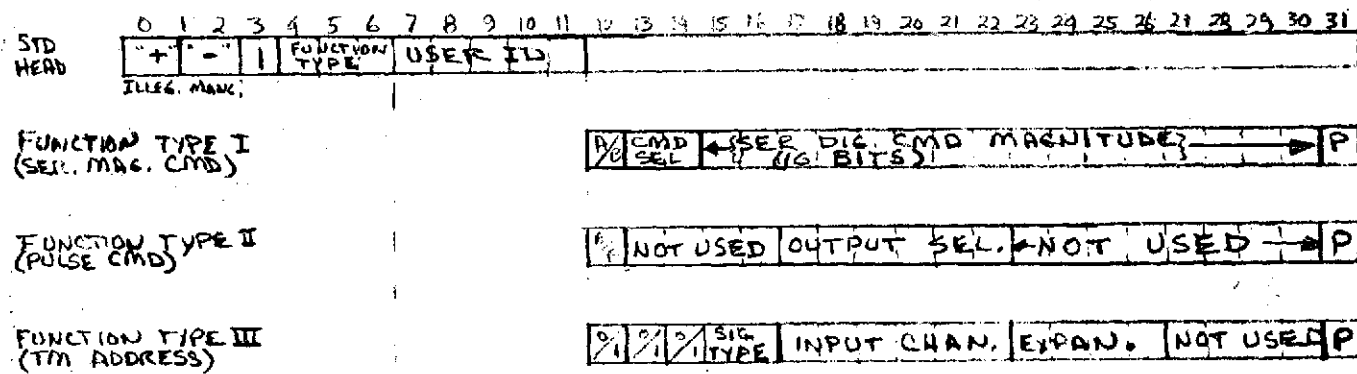
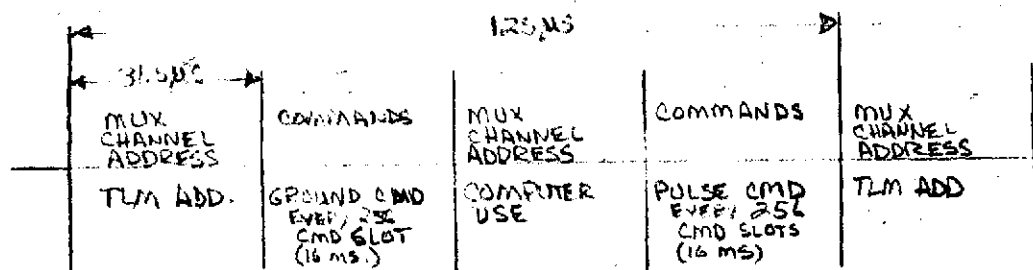


Figure 5-63. Party Line Waveforms

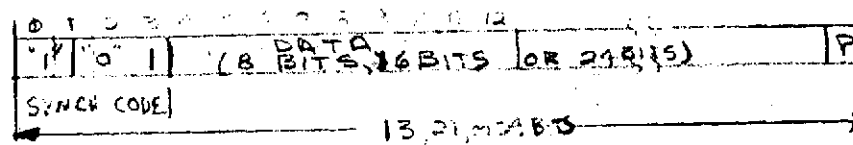


Function Types IV - VIII TBD

### A. Supervisory BUS FORMAT FOR DIFFERENT FUNCTION TYPES



### B. Supervisory Bus Time Slot Allocations (per bit to each)

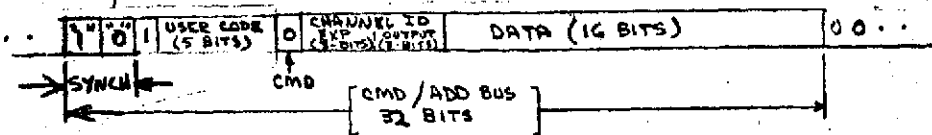


### C. Reply Bus Format

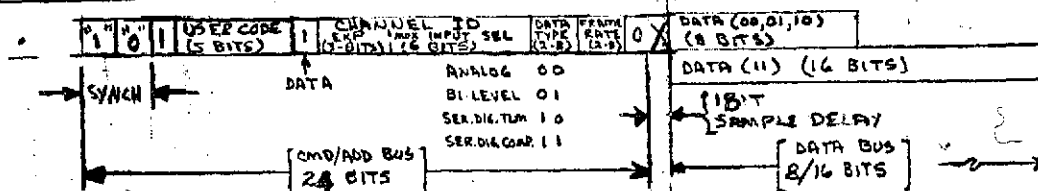
Figure 5-64. Source B Bus Format Requirement

## DATA FORMAT - COMMANDS/DATA REQUESTS

### BUS COMMAND FORMAT



### DATA REQUEST FORMAT



### BUS TIME SLOTS

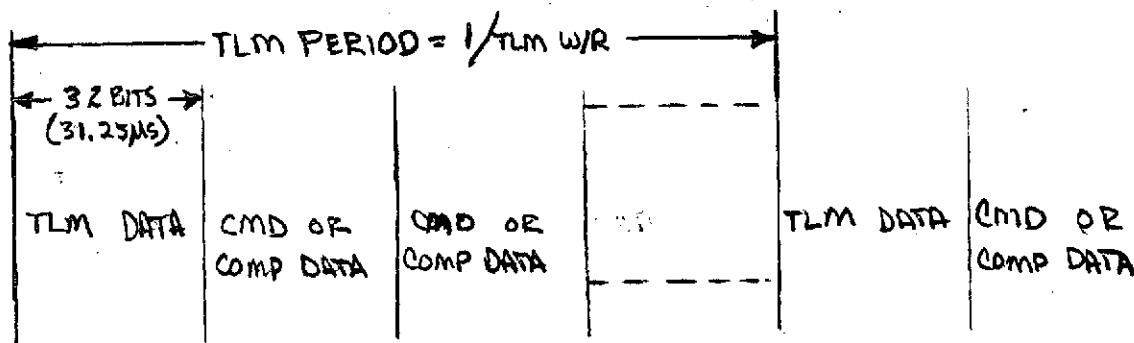


Figure 5-65. Bus Format Capability

### c. Baseline Configuration

#### 1. General Design

The nonredundant baseline data bus system configuration is presented in Figure 5-66 showing its interface with the demodulator decoder, on-board computer (OBC) and the baseband assembly. The data bus system comprises the bus controller unit (BCU), command/address bus, data bus, and the remotely located data interface units (DIU's).

The commands and data transmitted to and from bus users are controlled either by uplink commands, computer generated instructions, or by a fixed-backup telemetry format generated in the BCU.

Figure 5-66 presents the 29-bit message format for the uplink commands received from the demodulator decoder. The message has two parts:



## Op code

Two bits identifying command type

- 00, 01 – Real-time commands for bus users (00) or computer (01) to be executed directly
- 10, 11 – Delay commands for the computer to be implemented subsequently in normal computer operations.

## Command Message – 27 bits

- Computer inputs will have computer designated format
- Real-time commands have the following components.

The bus command format is the same for uplink real-time commands and computer commands. To identify the message as a command, a sync code and bit are added to the 27-bit uplink command format to form the 32-bit command message. The message has five parts:

- 1) 4-bit Sync Code. Illegal Manchester, 1-1/2 bits of "1" and 1-1/2 bits of "0" followed by a "1" to establish proper logic reference.
- 2) 5-bit User Code. Selects one of up to 32 DIU users.
  - User ID – 5 bits identifying up to 32 different remote users
  - Channel ID – 6 bits identifying up to 56 serial digital commands and 8-pulse command channels per user
  - Command data – 16 bits of data giving serial digital magnitude or identifying one of 64-pulse commands within a channel.

In addition, special commands to control critical functions are decoded within the demodulator/decoder and separately provided to the BCU.

The computer interface provides for transfer of uplink computer commands, computer generated telemetry formatting, computer request for data, stored computer commands, and data for the computer. Provision for dumping computer memory is made through a normal DIU telemetry channel whose dump rate is under computer format control.

There are two user AC-coupled buses; one bus for the address of commands and data requests designated the command/address (CMD/ADD) bus; one bus for the return data designated the data bus (DATA). Each bus operates at 1.024 Mbit/sec and is unidirectional, either transmitting data from the BCU to the DIU's (CMD/ADD) or from the DIU's to the BCU (DATA).

Each of the up to 32 DIU's provides command distribution and data acquisition as required by the using module. Figure 5-66 shows the expandable features of the DIU where the command and telemetry capability can be augmented by the addition of up to seven expanders per DIU. The using modules can interface directly with the DIU or unique signal conditioning slices which may be required for command pulse stretching, register buffering, or telemetry conditioning.

The telemetry data to be transmitted downlink is routed to the base-band assembly as NRZ-L data at the bit rate selected between 1 and 64 kbit/sec.

#### Bus Formats

The format for the CMD/ADD bus is derived from the uplink command format and Figure 5-67 shows their relationship. Data bus messages are shown following the end of the data request.

- 3) 1-bit Message type identifier. "0" is a command.
- 4) 6-bit Channel ID. Three bits select one of eight expanders and eight serial channels; seven of these channels are serial digital outputs; one of these channels is internally decoded into 32 pulse outputs.
- 5) 16-bits of Data. 16 bits for serial digital command magnitude or 5 bits decoded to select a pulse output.

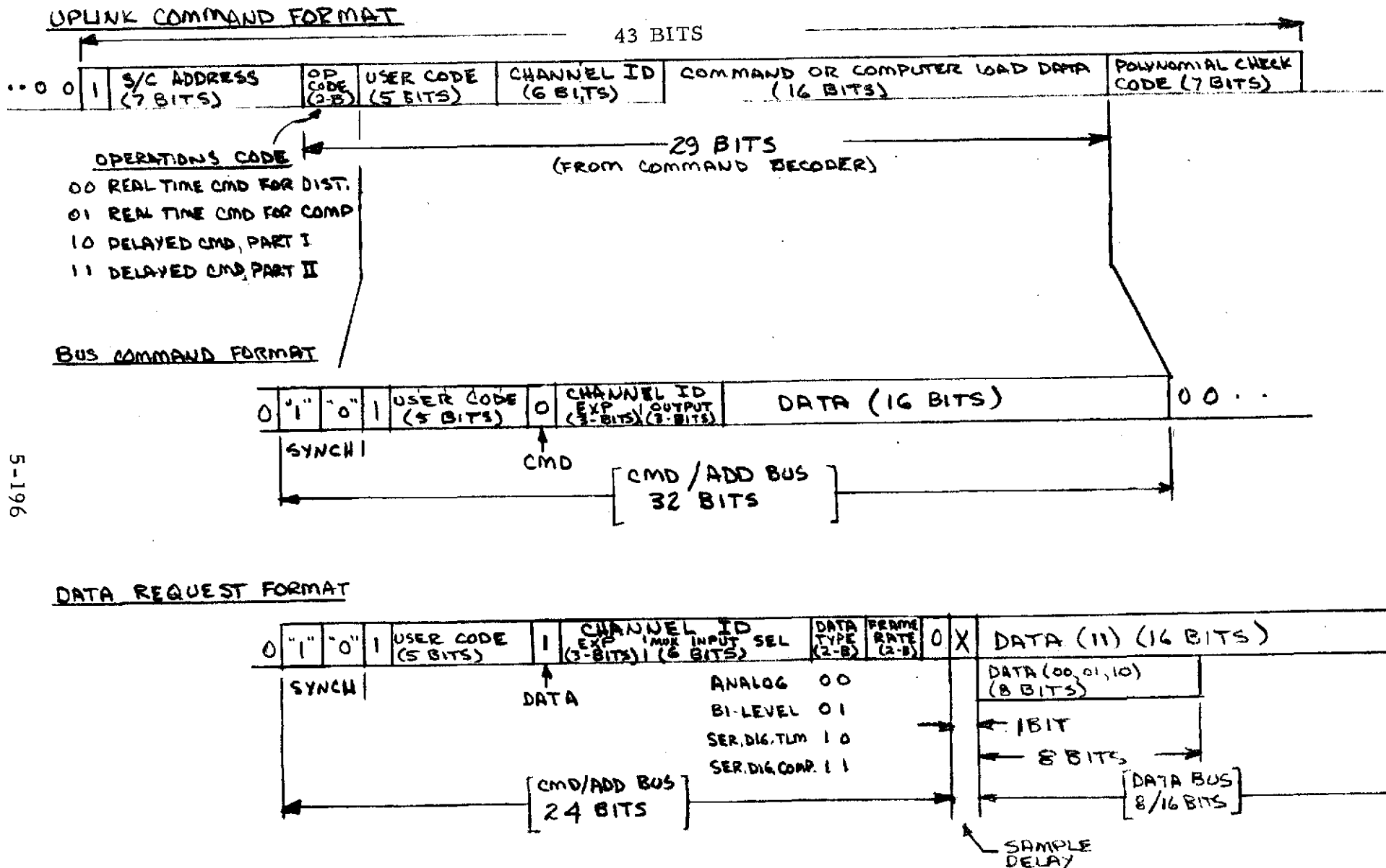


Figure 5-67. Data Format — Commands/Data Requests



This format provides an efficient usage of command bits to enable a synchronized message with seven 16-bit serial digital command magnitude outputs and 32 pulse command outputs. This format is designed to be flexible enough to allow continuous or intermittent bus message for either commands or data requests without losing synchronization.

The data request format presented in Figure 5-67 is the same as the command format, up through the expander identification, with the exception that the CMD/DATA bit is a one. The message has seven parts:

- 1) 4-Bit Sync Code. Same as for CMD message.
- 2) 5-Bit User Code. Same as for CMD message.
- 3) 1-Bit Message Type Identifier. "1" is a data request.
- 4) 9-Bits Channel ID. Three bits select one of eight expanders and six bits select one of 64-data input channels.
- 5) 2-Bits Data Type. Indicated AN/BL/DIG for TLM or computer.
- 6) 2-Bits Frame Rate. First to indicate minor TLM frame rate - MF1 and second to indicate major TLM frame rate - MF2.
- 7) 1-Bit "O." Lengthen time for multiplexer to settle.

#### Bus Characteristics

The CMD/ADD bus and DATA bus operational characteristics are listed in Figure 5-66 and discussed below.

AC Coupling. A single-twisted shielded pair, shielded line is used between the units in a balanced configuration using transformer coupling at the receivers and capacitor coupling at the transmitters. The bus transmitters and receivers in the BCU and DIU's are the same. Transformer coupling at the receiver provides common mode rejection while maintaining transmission line balance. Isolation resistors in the transformer lines preclude transformer shorts from disabling the bus. Capacitive coupling at the transmitters provide low impedance coupling to the transmission line maintaining DC isolation.

Manchester Coding (M). M coding is used to maintain zero DC component on the line. Encoding is 1 cycle/bit. The message on the CMD/ADD line begins with the 4-bit sync code followed by the specific command or data request (see Figure 5-68).

Bit Rate. 1.024 Mbit/sec rate enables handling the commands and data requests at a sufficient rate to handle anticipated maximum telemetry and command rate requirements.

Bus Time Slots. The time slots for the CMD/ADD bus related to the telemetry period is shown in Figure 5-66. The slot assignments are determined by the telemetry bit rate selected and the computer controlled format, command list, and data requests. In addition, but not shown is an uplink real-time bus command that would override any command currently being processed and be processed in the bus command format.

A time slot is assigned to telemetry at the telemetry word rate with the remaining slots available for commands or computer data requests under computer control. Figure 5-66 shows the relationships of telemetry word rate and command or computer data rates to telemetry bit rate.

#### Output Commands

Table 5-20 presents a summary of command requirements for EOS-A and expected growth missions and the mechanization showing DIU and expander requirements. Spares for each type of command/DIU are also indicated.

#### Telemetry

Table 5-21 presents the requirements for telemetry by module showing numbers of channels and expanders required. The data is grouped by signal types and priority levels. The mainframe and subcommutator data is grouped by priority levels as indicated. Figure 5-69 shows a suggested fixed-format including the fixed words (synchronization, format ID, S/C ID, SCID, S/C time) and the four subcommutators. By software, the computer will be able to reprogram or rearrange the format as required.

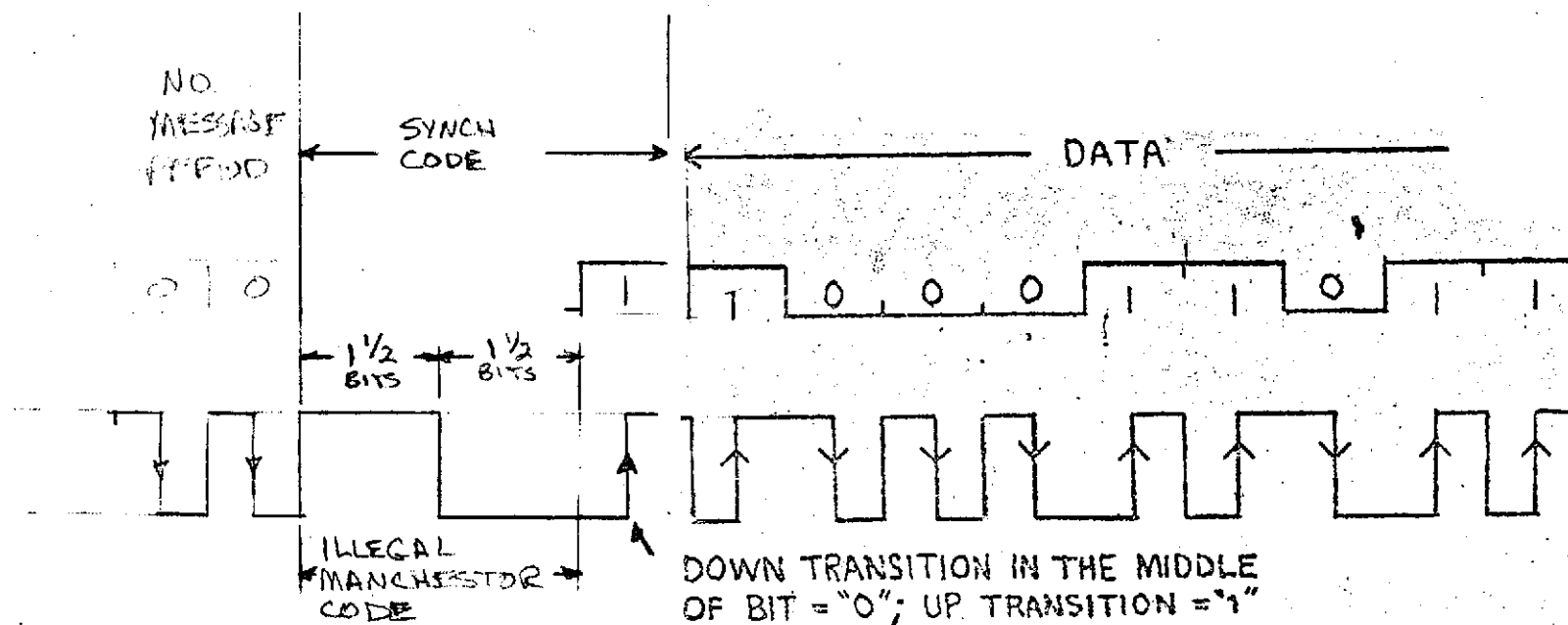


Figure 5-68. Typical Modulation Waveform

Table 5-20. Command Summary

Module	Pulse	SD	Total	Required No. of Expanders	DIU Capability		Spares	
					Pulse	SD	Pulse	SD
Electrical power	36	1	37	1	64	14	28	13
Solar array and drive	11	0	11	0	32	7	21	7
Attitude determination	107 <sup>(1)</sup>	14	121	2	96	21	5 <sup>(1)</sup>	6 <sup>(1)</sup>
Actuation	46	0	46	1	64	14	18	14
Comm and data handling	18	1	19	0	32	7	14	6
Wideband communication	16	1	17	0	32	7	16	6
Thematic mapper	18	3	21	0	32	7	14	4
HRPI	<u>7</u>	<u>3</u>	<u>10</u>	<u>0</u>	<u>32</u>	<u>7</u>	<u>25</u>	<u>4</u>
Total	259	23	282	4	384	84	141	60
SAR	12	3	15	0	32	7	20	4
SAR (SEASAT)	30	6	36	0	32	7	2	1
PMMR	18	0	18	0	32	7	14	7

<sup>(1)</sup>User will receive additional SD to decode for 16-pulse commands.

Table 5-21. Telemetry Signal Requirements

Module Name	Signal Priorities											
	1			2			3			4		
	A	B	SD	A	B	SD	A	B	SD	A	B	SD
Electrical power	-	-	-	-	-	-	16	20	-	-	-	-
Solar array	-	-	-	8	-	-	11	1	-	-	-	-
Attitude determination	-	-	6	-	-	-	65	64	10	-	-	-
Actuation	-	-	-	-	-	-	48	20	4	-	-	-
Communication and data	-	-	-	-	-	-	3	15	1	-	-	-
Wideband communication	-	-	-	-	-	-	7	11	0	-	-	-
Subtotal	6			8			150	131	15			
Thematic mapper	-	-	-	-	1	-	51	11	4	-	-	-
HRPI	-	-	-	2	1	2	35	3	-	-	-	-
Subtotal	0 0			2 2 2			86	14	4			
Total	0 6			10 2 2			236	145	19			
SAR	-	1	-	-	-	5	13	5	-	-	-	-
SAR (SEASAT)	-	1	-	-	-	5	17	14	-	-	-	-
PMMR	-	-	-	1	-	-	4	7	-	-	-	-
Subtotal	2 0			1 0 10			34	26	0			
Total	2 6			11 2 12			270	171	19			
Mainframe							3 AN 1 DIG Sub- Subcom com					

Notes:

Priority 1 Mission critical

Priority 2 Performance demonstration

Priority 3 State of health

Priority 4 Engineering data

Mainframe data  
(128-word mainframe)

Subcommutator data  
(128-word subcommutator)

- 2 science analog subcoms
- 1 engineering analog subcom
- 1 bilevel/serial digital subcom

128 WORDS - 8 WORDS X 16 LINES

4 SUBCOMS - 128 WORDS EACH

MAIN FRAME SYNCH - 32 BITS, 4 WORDS

SUBCOM IDENT - 8 BITS

S/C - TIME - 8 BITS

FORMAT MODE (SELECTABLE, NON-STD, BACK-UP) 8 BITS

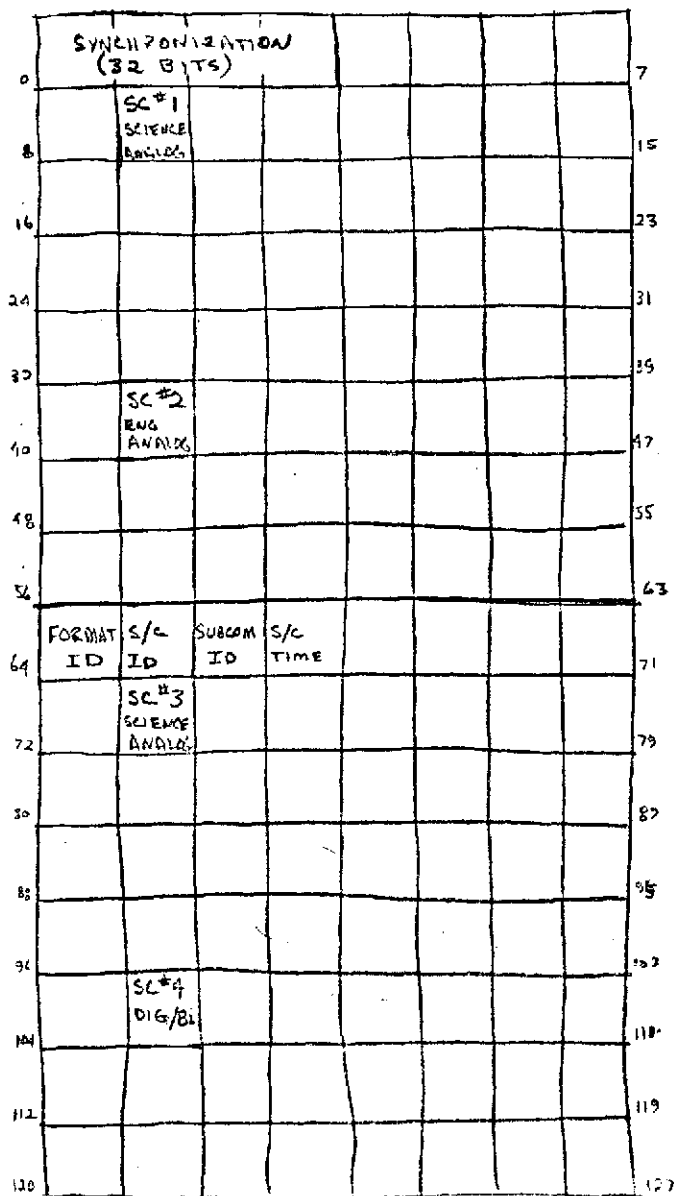


Figure 5-69. Format - Mainframe

## 2. Bus Controller Design

The functional block diagram for the BCU is presented in Figure 5-70, along with a list of the functions of the BCU to receive, process, and synchronize messages and data.

### Countdown Logic

Figure 5-70 shows the 29-bit countdown from the 4.096 MHz crystal oscillator. This chain provides all the timing signals necessary to synchronize the data bus system from the bus clocks to the major frame rate (MF2). Bit rates from 64K to 1 kbit/sec are available for selection by command. The selected bit rate is counted down to provide word rate, minor frame rate (MR1), and major frame rate (MF2). The subcommutator identification (SCID) is a 128-state countdown to identify the subcommutator pointer telemetered for ground data retrieval purposes.

### Uplink Command Routing

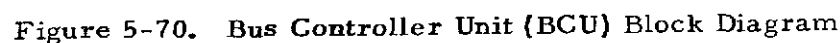
The OP code of the uplink command message received from the demodulator/decoder is decoded and the message is routed to either the assembler for CMD/BUS formatting or computer. If a real-time bus command is decoded it overrides other command message processing as shown in Figure 5-66.

The message is received at a 2 kbit/sec rate on three lines: clock, data, and enable. The data message format will be as shown in Figure 5-67. It is possible to handle longer messages for computer loading as the data will be continuously loaded into the computer as long as the enable is true.

### Computer Interface

The computer interface can be handled with three registers, shown in Figure 5-70 with their control logic. The additional slice is shown to indicate each computer may need a unique interface.

Uplink Commands. The uplink command register is to receive one 27-bit serial uplink message at 2 kbit/sec to be transferred into the computer in 18-bit parallel words. The logic will notify the computer when the register is loaded and the computer will transfer the 27 bits of





data in two cycles in less than 50  $\mu$ sec (computer cycle time is less than 16  $\mu$ sec).

Telemetry. The same 17-bit register is used for the telemetry format read-out and data read-in. Each word rate in the computer telemetry format is interrogated for the next instruction. When transferred to the telemetry register a "1" in the first bit indicates that the instruction is a request for data according to the format of Figure 5-67 and it is shifted serially through the bus message assembler onto the CMD/ADD bus. A "0" in the first bit of the telemetry instruction indicates that it is a format data/instruction according to the code allocation shown.

The return telemetry data (8 bit words) is input into the computer telemetry data DMA channel by the same telemetry register according to the bus timing of Figure 5-70. The data is serially shifted from the bus data routing block into the telemetry I/O register at the bus bit rate (1.024 Mbit/sec). The computer is notified when the register contains the eight bits of data. At the next available computer cycle time the data is parallel transferred into the computer memory through the DMA channel.

Computer CMD/Data Requests. A 16-bit register provides the interface for computer commands, requests for data, and transfer of computer data into the computer. When the computer has a command for execution or a request for data, the control logic is notified and the message is parallel transferred into the 16-bit register. At the beginning of the next command or computer data slot, the message is serially shifted into the bus message assembler and onto the CMD/ADD bus.

The return data is input into the computer data DMA channel by the same register according to the bus timing of Figure 5-70. The data words are 8 bits for analog and bilevel, and 16 bits for the serial digital data.

Bus Message Assembler. The command/data request messages to be transmitted onto the CMD/ADD bus in the bus message assembler are interleaved with information bits for synchronization, message identification, data type, frame timing, and DIU turn-on delay. The format for bus messages constructed for commands and requests for data are presented in Figure 5-70.

The uplink real-time commands are shifted in at 2 kbit/sec and shifted out at 1.024 Mbit/sec and all other messages are shifted in, assembled, and shifted out at 1.024 Mbit/sec.

Telemetry Formatting. Telemetry formatting for normal operation is provided by the computer flexible format scheme. However, for backup, a read-only-memory fixed-format generator is provided in the BCU. The format source is selected in the format select logic by a special uplink backup/ normal command received from the demodulator/decoder.

The backup format generator is addressed by a counter incremented by the word rate and uses the SCID to select the subcommutator. The format content is the same as the basic computer format: 128-word MF and five 128-word subcommutators. The required capacity of 11,880 bits ( $5 \times 128 \times 8$ ) is met by  $2 \times 10,240$  bit chips (20,480 bits) with expansion capability if future missions require more than four subcommutators.

Bus Interface Circuits. The bus modulator transmitter and receiver demodulators have been discussed earlier. The data is converted from NRZ-L to Manchester-M to remove the DC component in an unambiguous coding method. The bus clock rate is derived from the countdown logic and modulated by the data to be transmitted. The receiver/demodulator extracts the NRZ data and the clock rate used to synchronize the incoming data into the designated using registers.

Bus Data Processing. Incoming bus data is labeled TLM or COMP data according to whether the request came from the telemetry format select or the computer data interface. The bus routing block routes all data to the appropriate computer channels and only telemetry to the combiner register for downlink transmission.

The combiner interleaves downlink telemetry data with format data. Data is shifted into the combiner at the bus rate (1.024 Mbit/sec) and to the downlink data modulator at the selected bit rate. The data modulator transmits the formatted downlink telemetry data to the baseband assembly for carrier modulation.

### 3. Data Interface Unit (DIU)

Each DIU is connected to the CMD/ADD bus, data bus, and the A and B power buses. The timing for each unit is derived from the bus bit rate synchronizing the operation of each DIU with the BCU. This simplifies the overall data bus timing and minimizes design complexity.

The DIU is made up of seven functions which are implemented in Figure 5-71: 1) power converter, 2) bus interface circuits, 3) input register and decoding, 4) timing logic, 5) command decoding logic, 6) multiplexer decoding logic, and 7) data conditioning. The expandable command and data interface is also shown in Figure 5-71. Figure 5-72 presents the command distribution and data multiplexer mechanization.

#### Power Converter

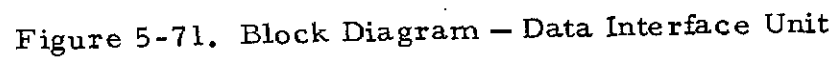
The power converter for each DIU is identical, receiving +28 A, B and supplying unswitched +5 volts to the receiver/demodulator, input decoding logic, and DIU timing logic. The converter will switch +5,  $\pm 15$  volts to the remainder of the unit if the user address is detected. This effects a power savings of approximately 80 percent of each DIU in the standby mode or about 2 watts per unit. This power gating improves reliability as well. In addition, the power converter supplies a precision +5 volts to the signal conditioner for analog signal conditioning.

#### Bus Interface Circuits

The receiver/demodulator detects the bus clock for DIU timing and demodulates the ADD/CMD bus message for processing by input decoding logic. The receiver/demodulator and modulator/transmitter are the same interface Manchester-M circuits used in the BCU.

#### Input Register and Decoding

This section of logic continually evaluates the CMD/ADD messages to recognize the DIU user address, determined by the patch plug unique for each using module and detects the occurrence of minor frame rate (MF1) or major frame rate (MF2). When the user ID is detected the power is switched on to the rest of the DIU, and the CMD/DATA bit is



ORIGINAL PAGE IS  
OF POOR QUALITY

5-209

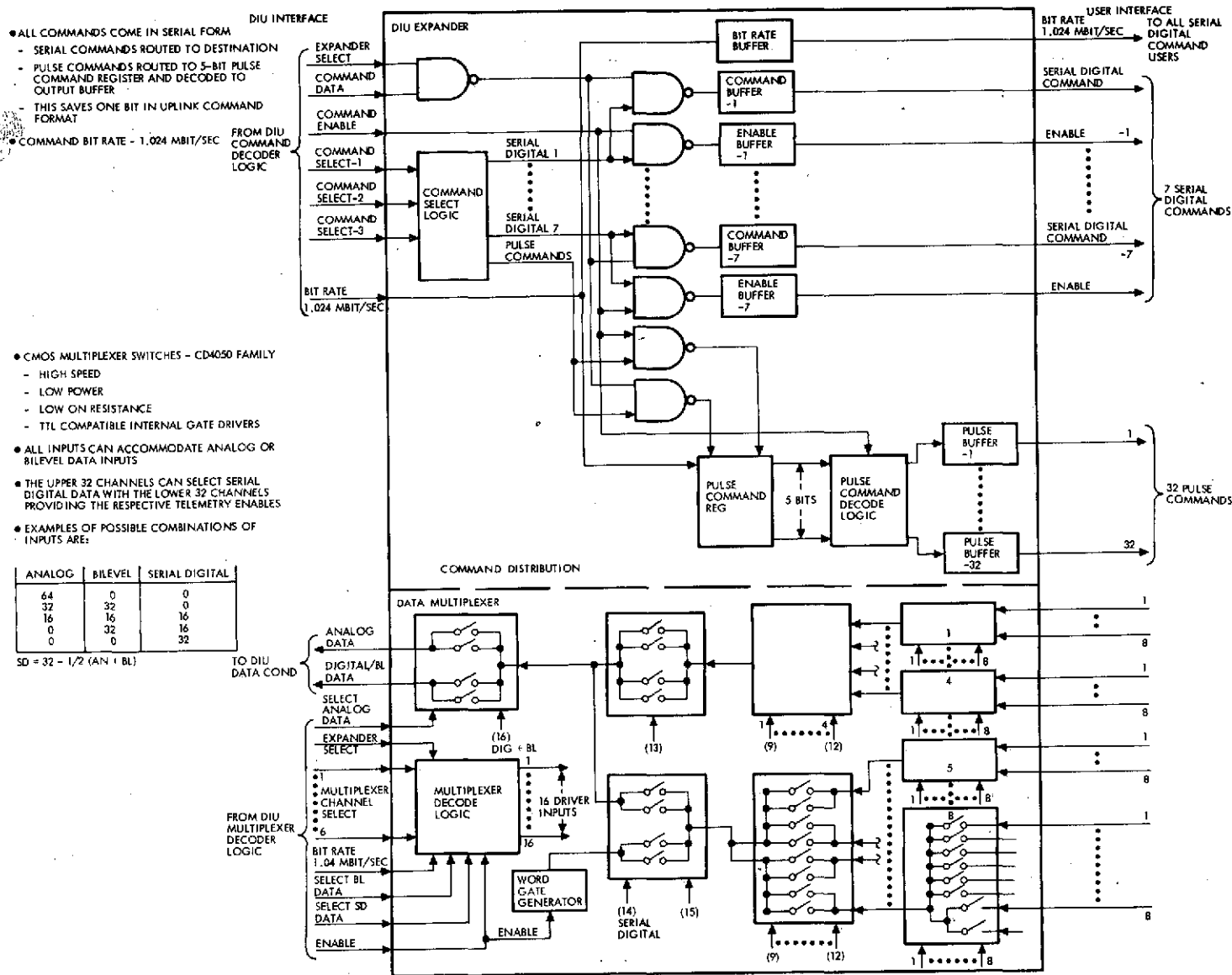


Figure 5-72. DIU Expander Block Diagram

investigated to determine if the message is to transmit a command or collect data and either the command decode or data multiplexer logic is enabled.

#### Timing Logic

The input timing logic block derives DIU synchronization from the detected bus clock rate, telemetry word rate and command decoding, multiplexer channel decoding, and the user modules. The inputs to the decoding logic are bit rates and command enable. The inputs to the multiplexer are bit rate and telemetry enable. The timing for command distribution and requests for data is given in Figures 5-73 and 5-74.

The inputs to the using module are bit rate, word rate, MF1, and MF2 to provide sufficient information for the user to arrange its telemetry sampling at times convenient to the telemetry format.

#### Command Decoding Logic

Figure 5-73 presents the command decoding timing. When the input decoding logic signals that a local command message is to be processed, the 6 bits of command address information is parallel transferred into the command address register. This register is decoded to determine the expander and command output selected, a 16-bit enable signal is issued, and the incoming command data is gated to the selected command channel. Figure 5-66 shows the block of the command logic and its interface with the DIU command select logic and output buffers. Each DIU slice has a set of seven serial digital output commands and 32 pulse commands. For using modules needing more commands, the addition of expanders can augment the capability in increments of 7 and 32 per expander to up to 56 serial digital commands and 256 pulse commands for seven additional expanders. Of the 6-bit command channel select address, the first three select the expander and the second three the serial digital channel. One of the serial digital channels is contained in the DIU to be decoded into 32 pulse command outputs. Figure 5-72 shows the implementation of the command distribution function.

If the pulse commands need conditioning for relay driving or other functions the using module may require a signal conditioner to provide proper shaping and drive to the pulse command.

# CMD/ADD BUS MESSAGE

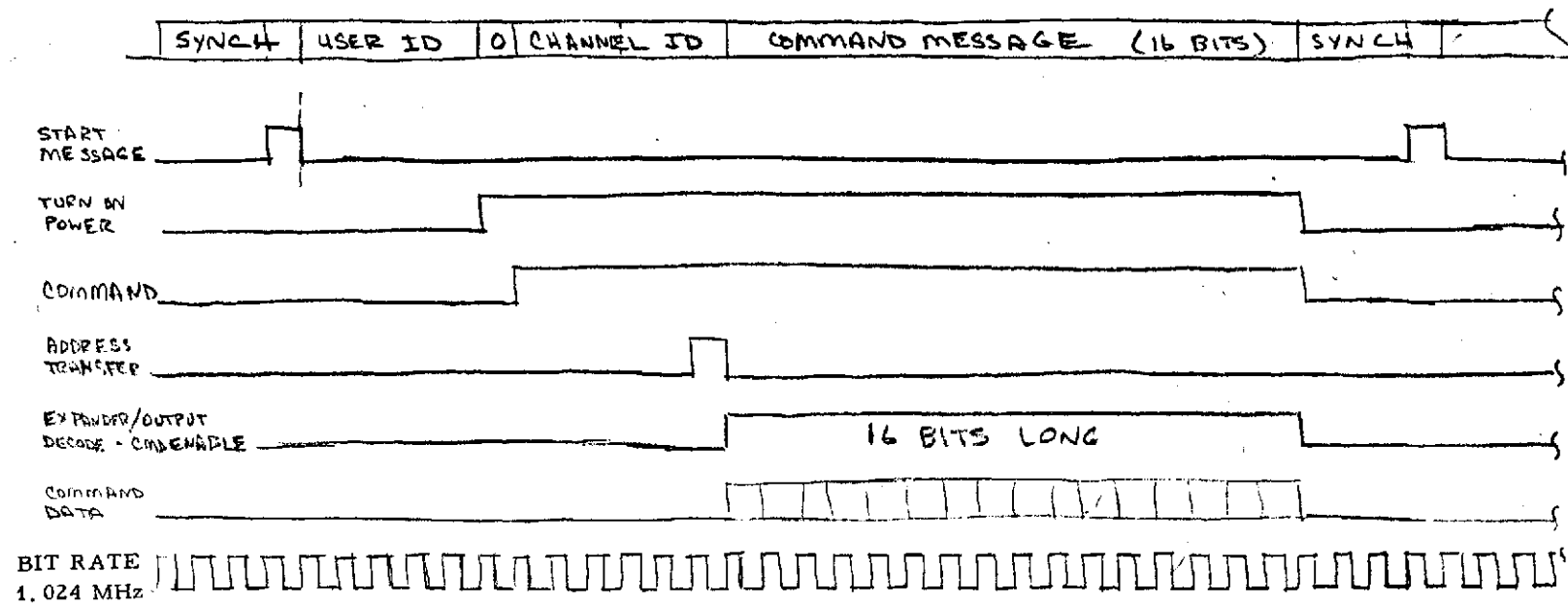


Figure 5-73. DIU Timing - Command Message

### Multiplexer Decoding Logic

Figure 5-74 presents the multiplexer decoding timing. When the input decoding logic signals that a request for data is being received the 9 bits of multiplexer channel is parallel transferred into the multiplexer decode register. This register is decoded to determine the expander and multiplexer channel. The next 2 bits are examined to determine data type requested: analog, bilevel, telemetry serial digital, or computer serial digital. The computer serial digital word is 16 bits long, the others are 8 bits long. Figure 5-74 shows the time for the 8 and 16 bit words.

The data multiplexer has 64 input data channels. (See Figure 5-72.) Each data input can handle analog and bilevel inputs. For each 64-input multiplexer the upper 32 channels can handle serial digital inputs and the lower 32 channels supply the corresponding word gate outputs. Figure 5-72 shows the features of the CMOS multiplexer and examples of combinations of input types.

Bilevel signals are sampled by a counting scheme. When a bilevel data group of 8 bits is identified they are sequentially sampled in bit times 1 through 8 and their contents serially shifted back on the digital data path.

Analog inputs are converted to digital form by the 8-bit successive approximation A/D converter in the DIU. This conversion also can be handled in 8-bit times as shown in Figure 5-74.

### DIU Packaging

To minimize complexity, parts count, size, weight, and cost of the DIU which will be repeated several times per system, two LSI chips can be used for most of the DIU. The demodulator, modulator, timing, input decoding, and command/multiplexer decoding can be contained on one chip and the A/D converter and output register on the other chip. The receiver/transformer AC coupling, the command distribution, and data multiplexer would be discrete SSI and MSI components.

The DIU can be contained in a 6 x 8 x 1 inch slice with two boards; one for the power converter and one for logic functions. The interconnects will be 125 pins which can be handled by three 50-pin connectors.



# CMD/ADD BUS MESSAGE

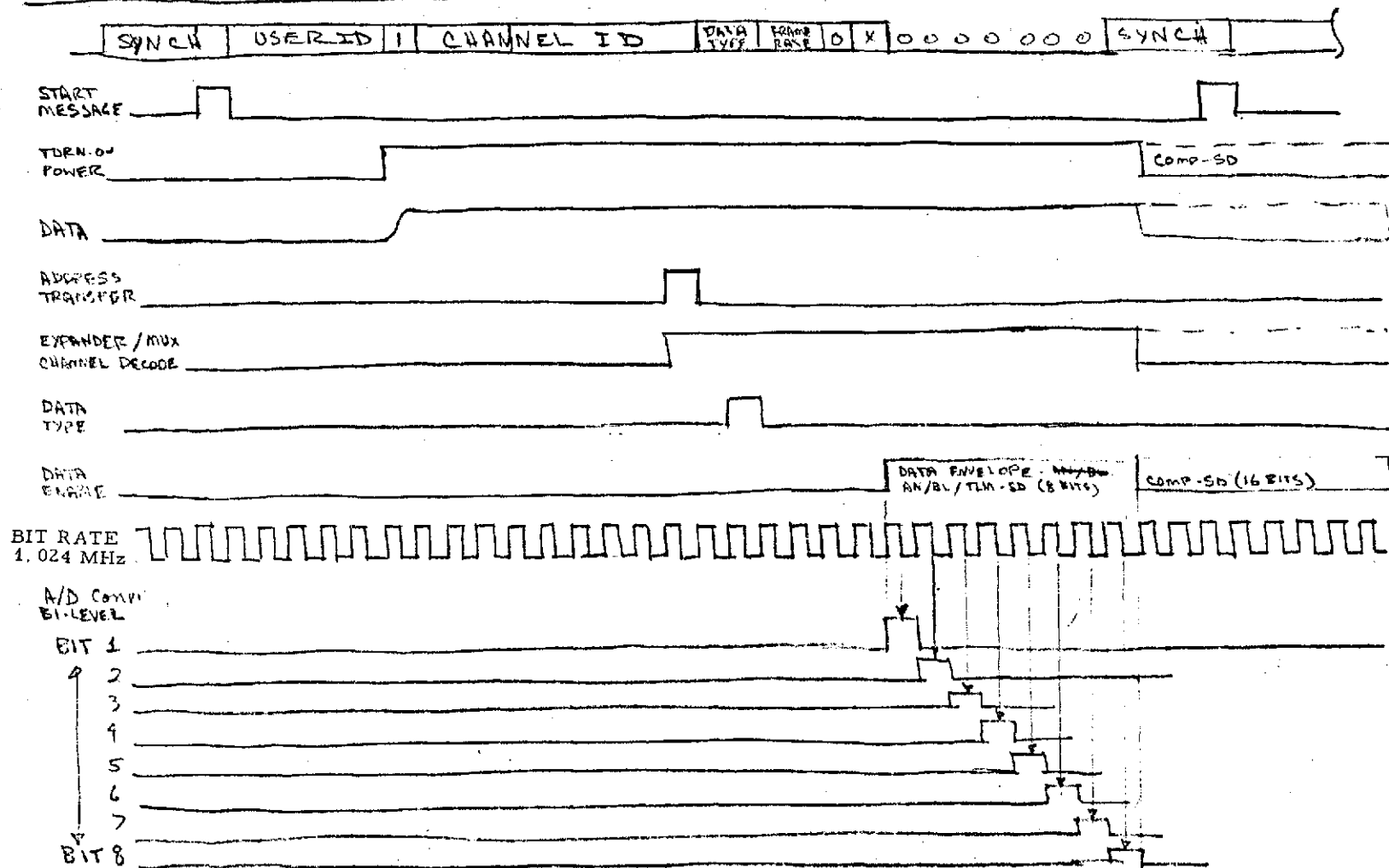


Figure 5-74. Multiplexer Decoding Timing

The DIU expander, including command distribution and input data multiplexer, can be contained in a one board 6 x 8 x 1 inch slice with 135 pins handled by three 50-pin connectors.

Because of the similarity of functions and the I/O of DIU and DIU expanders, much of the product design and documentation of the two slice types can be identical.

#### 5.1.7.2.3 Redundancy and Reliability

##### a. Baseline-Minimum Redundancy

The baseline data handling system presented in Figure 5-66 is non-redundant. The system has built-in features to enhance reliability and provide fault isolation diagnostics using downlink telemetry.

##### 1. Backup Format Generator

The BCU contains a backup telemetry format generator which is commandable by the demodulator/decoder should the computer format program operation fail. This backup format is a full-fixed format that interrogates all spacecraft subsystems and experiments including the computer. If the computer has failed then with the backup format, its failure will be detected, and under the resupply option it can be replaced.

##### 2. Channel Cross-Strapping (Super Commutation) - Data Inputs

The DIU design is such that the data channels are sampled in groups of eight. If a given input is critical then it can be cross-strapped to another input in a different group of eight inputs to improve the probability of the signal getting through. The flexible computer telemetry program format can be arranged to sample only one of the data channels unless it is suspected to fail; then the program can be changed to interrogate an alternate input.

##### 3. Power Bus Redundancy

The C and DH module converter receives power from both the A and B primary power buses protected from single internal failure or bus failure. If an external failure occurs on one bus line the converter can still be powered by the other.

#### 4. Computer Memory Dump

A regular telemetry channel interrogates the computer memory. The computer may run test programs to exercise different segments of operation and read out the results on the computer dump channel. In this way, the health of the computer can be monitored continually.

##### b. Nominal Redundancy

Figure 5-75 shows the data handling system for the nominal redundant configuration with all units redundant and using a dual-baseband assembly. The features discussed in a. pertain to the redundant system with the following additional features:

- Data Inputs. The data inputs to the redundant halves would not cross-strapped with the corresponding channel per DIU. Because of the high rates, the multiplexer inputs must be kept separate to preserve encoding accuracy.
- Cross-strapped Commands. Commands will be hardware cross-strapped with open collector outputs in each DIU driving the using inputs.
- Power On/Off. Figure 5-75 shows the power on/off controls for the units in the data handling systems. The special commands in each redundant demodulator/decoder are able to switch the converters in each redundant computer, and each redundant BCU. The DIU's have power switched internally (DIU-A switches DIU-A, and DIU-B switches DIU-B) and externally (DIU-A switches DIU-B and DIU-B switches DIU-A). The order of all switching will be to start within the order of the portion being switched (decoder/demodulator A switches OBC-A or BCU-A, and DIU-A switches DIU-A). If that order fails, then the cross-switching can be used.

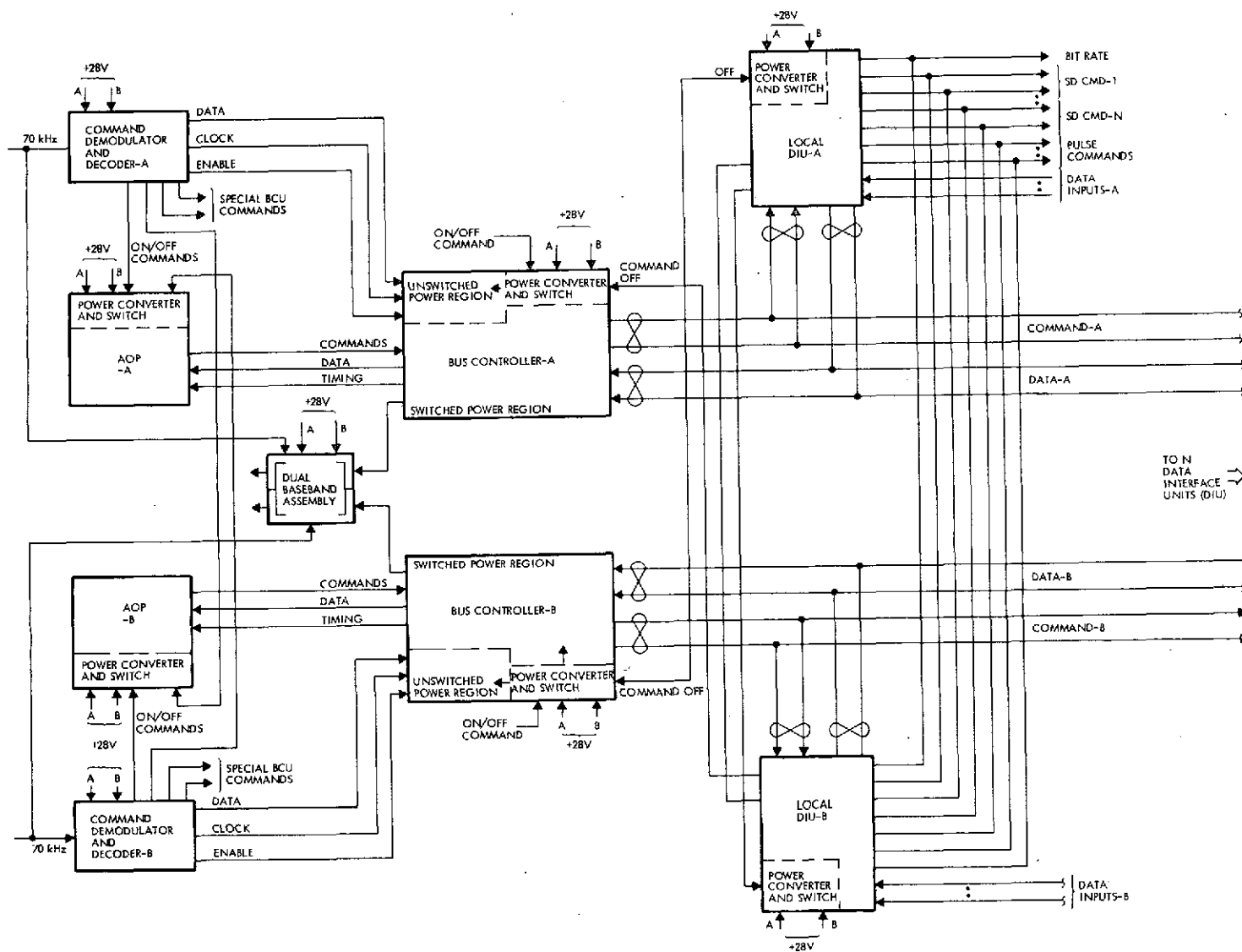


Figure 5-75. Nominal Redundant Data Handling System